

CONTENTS

Preface

xxv

1 The Atmosphere

1

- 1.1 History and Evolution of the Earth's Atmosphere 1
- 1.2 Climate 4
- 1.3 The Layers of the Atmosphere 6
- 1.4 Variation of Pressure with Height in the Atmosphere 9
- 1.5 Large-Scale Motion of the Atmosphere 10
 - 1.5.1 The General Circulation 10
 - 1.5.2 Troposphere–Stratosphere Transport 14
- 1.6 Temperature and Water Vapor 16
- 1.7 Expressing the Amount of a Substance in the Atmosphere 18
- 1.8 Composition of the Atmosphere 21
- 1.9 Radiation 23
 - 1.9.1 Solar and Terrestrial Radiation 26
 - 1.9.2 Absorption of Radiation by Gases 29
- 1.10 Energy Balance for Earth and Atmosphere 33
 - 1.10.1 Solar Variability 37
 - 1.10.2 Earth's Energy Balance 38
- 1.11 Spatial and Temporal Scales of Atmospheric Processes 40
- Appendix 1 Derivation of the Geostrophic Wind Speed 43
- References 47
- Problems 47

2 Atmospheric Composition, Global Cycles, and Lifetimes

49

- 2.1 Atmospheric Residence Times 50
 - 2.1.1 Residence Time 51
- 2.2 Sulfur-Containing Compounds 55
 - 2.2.1 Dimethyl Sulfide (CH_3SCH_3) 61
 - 2.2.2 Carbonyl Sulfide (OCS) 62
 - 2.2.3 Sulfur Dioxide (SO_2) 63
 - 2.2.4 The Atmospheric Sulfur Cycle 63
- 2.3 Nitrogen-Containing Compounds 67
 - 2.3.1 Nitrous Oxide (N_2O) 67
 - 2.3.2 Nitrogen Oxides ($\text{NO}_x = \text{NO} + \text{NO}_2$) 70
 - 2.3.3 Reactive Odd Nitrogen (NO_y) 71

2.3.4	Ammonia (NH ₃)	74
2.4	Carbon-Containing Compounds	75
2.4.1	Classification of Hydrocarbons	75
2.4.2	Methane	78
2.4.3	Volatile Organic Compounds	80
2.4.4	Biogenic Hydrocarbons	82
2.4.5	Carbon Monoxide	85
2.4.6	Carbon Dioxide	86
2.5	Halogen-Containing Compounds	86
2.6	Atmospheric Ozone	91
2.6.1	Stratospheric Ozone	92
2.6.2	Ozone Flux from the Stratosphere to the Troposphere	93
2.6.3	Tropospheric Ozone	94
2.7	Particulate Matter (Aerosols)	97
2.7.1	Stratospheric Aerosol	98
2.7.2	Chemical Components of Tropospheric Aerosol	98
2.7.3	Cloud Condensation Nuclei (CCN)	99
2.7.4	Sizes of Atmospheric Particles	100
2.7.5	Sources of Atmospheric Particulate Matter	100
2.7.6	Carbonaceous Particles	103
2.8	Emissions Inventories	103
2.9	Biomass Burning	104
2.10	Air Pollution Legislation	104
2.11	Hazardous Air Pollutants (Air Toxics)	107
Appendix 2	Compartmental Models of Global Biogeochemical Cycles	108
2.A.1	Relation Between Atmospheric Mass and Volume Mixing Ratio	114
2.A.2	Application of the Compartment Model to Methyl Chloroform (CH ₃ CCl ₃)	115
References		117
Problems		121

3 Atmospheric Photochemistry and Chemical Kinetics

125

3.1	Radiative Flux in the Atmosphere	125
3.1.1	Solar Radiation Received on Earth	127
3.1.2	Earth Geometry for Solar Radiation	129
3.2	Absorption Coefficient and Absorption Cross Section	133
3.3	Actinic Flux	135
3.4	Atmospheric Photochemistry	140
3.5	Chemical Kinetics	152
3.5.1	The Pseudo-Steady-State Approximation	154
3.5.2	Pressure Dependence of Reactions	157

References 160

Problems 161

4 Chemistry of the Stratosphere

- 4.1 Chapman Mechanism 164
- 4.2 HO_x Cycles 171
- 4.3 NO_x Cycles 173
 - 4.3.1 N₂O Stratospheric Source of NO_x 173
 - 4.3.2 NO_x Cycles 175
- 4.4 ClO_x Cycles 177
- 4.5 Reservoir Species and Coupling of the Cycles 180
- 4.6 Stratospheric Species Observations and Predictions 184
 - 4.6.1 Upper Stratosphere 184
 - 4.6.2 Lower Stratosphere 186
- 4.7 Ozone Hole 189
 - 4.7.1 Polar Stratospheric Clouds 192
 - 4.7.2 PSCs and the Ozone Hole 194
 - 4.7.3 Antarctic Ozone Hole Measurements 198
 - 4.7.4 Arctic Ozone Hole 199
 - 4.7.5 Summary 202
- 4.8 Heterogeneous (Nonpolar) Stratospheric Chemistry 203
 - 4.8.1 Heterogeneous Hydrolysis of N₂O₅ 203
 - 4.8.2 Effect of Volcanoes on Stratospheric Ozone 207
 - 4.8.3 Summary of Midlatitude and Tropical Stratospheric Ozone Chemistry 210
- 4.9 Transport Between the Tropical and Midlatitude Stratosphere 210
- 4.10 Ozone-Depleting Potential of Halocarbons 212
- 4.11 Effect of Aircraft Emissions on Stratospheric Ozone 215
- 4.12 Carbonyl Sulfide (OCS) and the Stratospheric Aerosol Layer 216
 - 4.12.1 Atmospheric Chemistry of OCS and OCS Lifetime 217
 - 4.12.2 Stratospheric Aerosol Layer 217
- 4.13 Projections of Future Ozone Change 218
- Appendix 4 Sensitivity/Uncertainty Analysis of Atmospheric Chemical Mechanisms 219
 - 4.A.1 Sensitivity Coefficients 222
 - 4.A.2 The Direct Decoupled Method 223
 - 4.A.3 Adjoint Methods 224
 - 4.A.4 Green's Function Methods 224
- References 226
- Problems 230

5 Chemistry of the Troposphere

- 5.1 Basic Photochemical Cycle of NO₂, NO, and O₃ 235
- 5.2 Atmospheric Chemistry of Carbon Monoxide and NO_x 239
- 5.3 Atmospheric Chemistry of Formaldehyde and NO_x 244

- 5.4 Chemistry of the Background Troposphere 245
 - 5.4.1 Ozone Photolysis 246
 - 5.4.2 Methane Oxidation 246
 - 5.4.3 Hydrogen Peroxide 249
- 5.5 The Hydroxyl Radical 250
- 5.6 The Nitrate Radical 253
- 5.7 The Ozone Budget of the Troposphere and the Role of NO_x 254
 - 5.7.1 Tropospheric Sinks of Ozone 255
 - 5.7.2 Tropospheric Source of Ozone 257
 - 5.7.3 Fate of NO_x 259
 - 5.7.4 Ozone Budget of the Troposphere 261
 - 5.7.5 Climatology of Regional Tropospheric Ozone 262
- 5.8 Chemistry of Nonmethane Organic Compounds in the Troposphere 264
 - 5.8.1 Alkanes 264
 - 5.8.2 Alkenes 268
 - 5.8.3 Aromatics 277
 - 5.8.4 Aldehydes 281
 - 5.8.5 Peroxyacyl Nitrates (PANs) 282
 - 5.8.6 Ketones 284
 - 5.8.7 α, β -Unsaturated Carbonyls 286
 - 5.8.8 Ethers 286
 - 5.8.9 Alcohols 286
 - 5.8.10 Acids 287
- 5.9 Atmospheric Chemistry of Biogenic Hydrocarbons 288
 - 5.9.1 Isoprene 289
 - 5.9.2 Other Biogenic Hydrocarbons 292
- 5.10 Summary of Organic/ NO_x Chemistry 292
 - 5.10.1 Generalized Organic/ NO_x Chemistry 292
 - 5.10.2 Behavior of Generalized Mechanism 297
 - 5.10.3 Effect of Temperature on Ozone Formation in Urban and Rural Environments 298
- 5.11 Relative Roles of VOC and NO_x in Ozone Formation 299
 - 5.11.1 Importance of the VOC/ NO_x Ratio 299
 - 5.11.2 Ozone Isoleth Plot 300
 - 5.11.3 Relation of $[\text{O}_3]$ to $[\text{NO}_y]$ 302
- 5.12 Origin and Behavior of the Radical Pool in Photochemical Ozone Formation 303
- 5.13 Organic Reactivity with Respect to Ozone Formation 309
 - 5.13.1 OH Reactivity 309
 - 5.13.2 Incremental Reactivity 311
- 5.14 Atmospheric Chemistry of Reduced Nitrogen Compounds 313
 - 5.14.1 Amines 313
 - 5.14.2 Nitriles 313
 - 5.14.3 Nitrites 314

5.15	Atmospheric Chemistry (Gas Phase) of Sulfur Compounds	314
5.15.1	Sulfur Oxides	314
5.15.2	Reduced Sulfur Compounds (Dimethyl Sulfide)	315
5.16	Tropospheric Chemistry of Halogen Compounds	317
5.16.1	Chemical Cycles of Halogen Species	318
5.16.2	Tropospheric Chemistry of CFC Replacements: Hydrofluorocarbons (HFCs) and Hydrochlorofluorocarbons (HCFCs)	319
	References	323
	Problems	331
6	Chemistry of the Atmospheric Aqueous Phase	337
6.1	Liquid Water in the Atmosphere	337
6.1.1	Cloud Types and Liquid Water Content	338
6.2	Absorption Equilibria and Henry's Law	340
6.2.1	Gas/Aqueous-Phase Distribution Factor	343
6.3	Aqueous-Phase Chemical Equilibria	344
6.3.1	Water	344
6.3.2	Carbon Dioxide/Water Equilibrium	345
6.3.3	Sulfur Dioxide	348
6.3.4	Ammonia/Water Equilibrium	353
6.3.5	Nitric Acid/Water Equilibrium	355
6.3.6	Equilibrium of Other Important Atmospheric Gases	356
6.4	Aqueous-Phase Reaction Rates	361
6.5	S(IV) to S(VI) Transformation and Sulfur Chemistry	363
6.5.1	Oxidation of S(IV) by Dissolved O ₃	363
6.5.2	Oxidation of S(IV) by Hydrogen Peroxide	366
6.5.3	Oxidation of S(IV) by Organic Peroxides	367
6.5.4	Uncatalyzed Oxidation of S(IV) by O ₂	368
6.5.5	Oxidation of S(IV) by O ₂ Catalyzed by Iron and Manganese	369
6.5.6	S(IV) Oxidation by the OH Radical	372
6.5.7	Oxidation of S(IV) by Oxides of Nitrogen	374
6.5.8	Reaction of Dissolved SO ₂ with HCHO	376
6.5.9	Comparison of Aqueous-Phase S(IV) Oxidation Paths	378
6.6	Aqueous-Phase Nitrite and Nitrate Chemistry	380
6.6.1	NO _x Oxidation	380
6.6.2	Nitrogen Radicals	381
6.7	Aqueous-Phase Organic Chemistry	381
6.8	Oxygen and Hydrogen Chemistry	383
6.9	Dynamic Behavior of Solutions with Aqueous-Phase Chemical Reactions	384
6.9.1	Closed System	385

6.9.2 Calculation of Concentration Changes in a Droplet
with Aqueous-Phase Reactions 387

Appendix 6 Thermodynamic and Kinetic Data 391

References 399

Problems 404

7 Properties of the Atmospheric Aerosol

7.1 The Size Distribution Function 408

7.1.1 The Number Distribution $n_N(D_p)$ 411

7.1.2 The Surface Area, Volume, and Mass Distributions 414

7.1.3 Distributions Based on $\ln D_p$ and $\log D_p$ 416

7.1.4 Relating Size Distributions Based on Different
Independent Variables 418

7.1.5 Properties of Size Distributions 419

7.1.6 The Log-Normal Distribution 421

7.1.7 Plotting the Log-Normal Distribution 424

7.1.8 Properties of the Log-Normal Distribution 425

7.1.9 Other Aerosol Distributions 426

7.2 Ambient Aerosol Size Distributions 429

7.2.1 Urban Aerosols 429

7.2.2 Marine Aerosols 433

7.2.3 Rural Continental Aerosols 435

7.2.4 Remote Continental Aerosols 435

7.2.5 Free Tropospheric Aerosols 436

7.2.6 Polar Aerosols 437

7.2.7 Desert Aerosols 438

7.3 Aerosol Chemical Composition 440

7.4 Vertical Variation 444

References 446

Problems 448

8 Dynamics of Single Aerosol Particles

8.1 Continuum and Noncontinuum Dynamics 452

8.1.1 The Mean Free Path 453

8.2 The Drag on a Single Particle: Stokes' Law 459

8.2.1 Corrections to Stokes' Law: The Drag Coefficient 462

8.2.2 Stokes' Law and Noncontinuum Effects:
Slip Correction Factor 463

8.3 Gravitational Settling of an Aerosol Particle 465

8.3.1 Settling of Particles for Any Re 467

8.4 Motion of an Aerosol Particle in an External Force Field 469

8.4.1 Motion of a Charged Particle in an Electric Field 469

8.5 Brownian Motion of Aerosol Particles 470

8.5.1 Particle Diffusion 473

8.5.2	Aerosol Mobility and Drift Velocity	475
8.5.3	Mean Free Path of an Aerosol Particle	478
8.6	Phoretic Effects	480
8.6.1	Thermophoresis	480
8.6.2	Diffusiophoresis	483
8.6.3	Photophoresis	483
8.7	Aerosol and Fluid Motion	484
8.7.1	Motion of a Particle in an Idealized Flow (90° Corner)	485
8.7.2	Stop Distance and Stokes Number	486
8.8	Diameters of Nonspherical Particles	488
	References	488
	Problems	489

9 Thermodynamics of Aerosols

491

9.1	Thermodynamic Principles	491
9.1.1	Internal Energy and Chemical Potential	491
9.1.2	The Gibbs Free Energy, G	493
9.1.3	Conditions for Chemical Equilibrium	495
9.1.4	Chemical Potentials of Ideal Gases and Ideal Gas Mixtures	499
9.1.5	Chemical Potential of Solutions	501
9.1.6	The Equilibrium Constant	506
9.2	Aerosol Liquid Water Content	507
9.2.1	Chemical Potential of Water in Atmospheric Particles	508
9.2.2	Temperature Dependence of the DRH	510
9.2.3	Deliquescence of Multicomponent Aerosols	514
9.2.4	Crystallization of Single and Multicomponent Salts	519
9.3	Equilibrium Vapor Pressure Over a Curved Surface: The Kelvin Effect	519
9.4	Thermodynamics of Atmospheric Aerosol Systems	523
9.4.1	The $\text{H}_2\text{SO}_4\text{-H}_2\text{O}$ System	523
9.4.2	The Sulfuric Acid–Ammonia–Water System	529
9.4.3	The Ammonia–Nitric Acid–Water System	531
9.4.4	The Ammonia–Nitric Acid–Sulfuric Acid–Water System	537
9.4.5	Other Inorganic Aerosol Species	539
	References	541
	Problem	543

10 Nucleation

545

10.1	Classical Theory of Homogeneous Nucleation: Kinetic Approach	547
10.1.1	The Forward Rate Constant β_i	550
10.1.2	The Reverse Rate Constant γ_i	551

10.1.3	Derivation of the Nucleation Rate	551
10.2	Classical Homogeneous Nucleation Theory: Constrained Equilibrium Approach	556
10.2.1	Free Energy of <i>i</i> -mer Formation	556
10.2.2	Constrained Equilibrium Cluster Distribution	558
10.2.3	The Evaporation Coefficient γ_i	560
10.2.4	Nucleation Rate	561
10.2.5	Recapitulation	563
10.3	Experimental Measurement of Nucleation Rates	565
10.3.1	Upward Thermal Diffusion Cloud Chamber	565
10.3.2	Fast Expansion Chamber	566
10.3.3	Turbulent Mixing Chambers	567
10.3.4	Experimental Evaluation of Classical Homogeneous Nucleation Theory	567
10.4	Modifications of the Classical Theory and More Rigorous Approaches	568
10.5	Binary Homogeneous Nucleation	570
10.6	Binary Nucleation in the H ₂ SO ₄ -H ₂ O System	575
10.7	Nucleation in the Presence of a Preexisting Aerosol	579
10.7.1	Homogeneous-Homomolecular Nucleation	579
10.7.2	Effect of a Preexisting Aerosol on H ₂ SO ₄ -H ₂ O Binary Nucleation	582
10.8	Heterogeneous Nucleation	585
10.8.1	Nucleation on an Insoluble Foreign Surface	585
10.8.2	Ion-Induced Nucleation	586
10.9	Nucleation from Chemical Reaction	589
Appendix 10	The Law of Mass Action	591
References		593
Problems		595

Mass Transfer Aspects of Atmospheric Chemistry

596

11.1	Mass and Heat Transfer to Atmospheric Particles	596
11.1.1	The Continuum Regime	596
11.1.2	The Kinetic Regime	600
11.1.3	The Transition Regime	601
11.1.4	The Accommodation Coefficient	605
11.2	Mass Transport Limitations in Aqueous-Phase Chemistry	607
11.2.1	Characteristic Time for Gas-Phase Diffusion to a Particle	610
11.2.2	Characteristic Time to Achieve Equilibrium in the Gas-Particle Interface	611
11.2.3	Characteristic Time of Aqueous Dissociation Reactions	614
11.2.4	Characteristic Time of Aqueous-Phase Diffusion in a Droplet	616

11.2.5	Characteristic Time for Aqueous-Phase Chemical Reactions	617
11.3	Mass Transport and Aqueous-Phase Chemistry	617
11.3.1	Gas-Phase Diffusion and Aqueous-Phase Reactions	618
11.3.2	Aqueous-Phase Diffusion and Reaction	620
11.3.3	Interfacial Mass Transport and Aqueous-Phase Reactions	621
11.3.4	Application to the S(IV)–Ozone Reaction	623
11.3.5	Application to the S(IV)–Hydrogen Peroxide Reaction	626
11.3.6	Calculation of Aqueous-Phase Reaction Rates	627
11.3.7	An Aqueous-Phase Chemistry/Mass Transport Model	634
11.4	Mass Transfer to Falling Drops	635
11.5	Characteristic Time for Atmospheric Aerosol Equilibrium	636
11.5.1	Solid Aerosol Particles	636
11.5.2	Aqueous Aerosol Particles	638
Appendix 11	Solution of the Transient Gas-Phase Diffusion Problem Equations (11.4) to (11.7)	641
References		643
Problems		645

12 Dynamics of Aerosol Populations

648

12.1	Mathematical Representations of the Aerosol Size Distributions	648
12.1.1	Discrete Distribution	648
12.1.2	Continuous Distribution	649
12.2	Condensation	649
12.2.1	Solution of the Condensation Equation	652
12.3	Coagulation	656
12.3.1	Brownian Coagulation	656
12.3.2	Coagulation in Laminar Shear Flow	664
12.3.3	Coagulation in Turbulent Flow	665
12.3.4	Coagulation from Gravitational Settling	665
12.3.5	Brownian Coagulation and External Force Fields	666
12.3.6	The Coagulation Equation	672
12.3.7	Solution of the Coagulation Equation	676
12.4	The Discrete General Dynamic Equation	680
12.5	The Continuous General Dynamic Equation	682
12.6	Evolution of an Aerosol Size Distribution During Gas-to-Particle Conversion	684
12.6.1	Diffusion-Controlled Growth	685
12.6.2	Surface Reaction-Controlled Growth	686
12.6.3	Volume Reaction-Controlled Growth	688
12.6.4	Dimensionless Size Spectra Evolution	689

Appendix 12 Solution of (12.92) 693

References 695

Problems 696

13 Organic Atmospheric Aerosols

700

13.1 Organic Aerosol Components 700

13.2 Elemental Carbon 700

13.2.1 Formation of Soot and Elemental Carbon 700

13.2.2 Emission Sources of Elemental Carbon 702

13.2.3 Ambient Elemental Carbon Concentrations 705

13.2.4 Ambient Elemental Carbon Size Distribution 707

13.2.5 Degree of Mixing of EC in Ambient Aerosols 708

13.2.6 Heterogeneous Chemistry of Carbonaceous
Particles 708

13.3 Organic Carbon 709

13.3.1 Ambient Aerosol Organic Carbon Concentrations 709

13.3.2 Primary Versus Secondary Organic Carbon 711

13.4 Primary Organic Carbon 712

13.4.1 Sources 712

13.4.2 Chemical Composition 714

13.4.3 Primary OC Size Distribution 723

13.5 Secondary Organic Carbon 724

13.5.1 Overview of Secondary Organic Aerosol
Formation Pathways 724

13.5.2 Dissolution and Gas/Particle Partitioning of
Organic Compounds 727

13.5.3 Adsorption and Gas/Particle Partitioning of
Organic Compounds 735

13.5.4 Precursor Gases 738

13.5.5 Physical Properties 742

13.6 Polycyclic Aromatic Hydrocarbons (PAHs) 743

13.6.1 Emission Sources 744

13.6.2 Size Distributions 745

13.6.3 Atmospheric Chemistry 745

13.6.4 Partitioning Between the Gas and Aerosol
Phases 747

13.7 Biogenics 748

Appendix 13 Measurement of Elemental and Organic Carbon 749

References 751

Problems 764

14 Meteorology of Air Pollution

766

14.1 Temperature in the Lower Atmosphere 767

14.1.1 Pressure and Temperature Relationships in the
Lower Atmosphere 767

14.1.2	Temperature Changes of a Rising (or Falling) Parcel of Air	770
14.2	Atmospheric Stability	772
	Problems	775
15	Cloud Physics	777
15.1	Properties of Water and Water Solutions	777
15.1.1	Specific Heat of Water and Ice	778
15.1.2	Latent Heats of Evaporation and of Melting for Water	778
15.1.3	Water Surface Tension	779
15.2	Water Equilibrium in the Atmosphere	780
15.2.1	Equilibrium of a Flat Pure Water Surface with the Atmosphere	780
15.2.2	Equilibrium of a Pure Water Droplet	781
15.2.3	Equilibrium of a Flat Water Solution	783
15.2.4	Atmospheric Equilibrium of an Aqueous Solution Drop	784
15.2.5	Atmospheric Equilibrium of an Aqueous Solution Drop Containing an Insoluble Substance	790
15.3	Cloud and Fog Formation	793
15.3.1	Isobaric Cooling	794
15.3.2	Adiabatic Cooling	795
15.3.3	Cooling with Entrainment	798
15.3.4	A Simplified Mathematical Description of Cloud Formation	799
15.4	Growth Rate of Individual Cloud Droplets	801
15.5	Growth of a Droplet Population	805
15.6	Cloud Condensation Nuclei	809
15.7	Cloud Processing of Aerosols	812
15.7.1	Nucleation Scavenging of Aerosols by Clouds	813
15.7.2	Chemical Composition of Cloud Droplets	814
15.7.3	Nonraining Cloud Effects on Aerosol Concentrations	816
15.7.4	Interstitial Aerosol Scavenging by Cloud Droplets	821
15.7.5	Aerosol Nucleation Near Clouds	823
15.8	Other Forms of Water in the Atmosphere	823
15.8.1	Ice Clouds	824
15.8.2	Rain	828
15.9	Cloud Climatology	832
	References	834
	Problems	839
16	Micrometeorology	841
16.1	Basic Equations of Atmospheric Fluid Mechanics	841
16.2	Turbulence	847
16.3	Equations for the Mean Quantities	849

- 16.4 Mixing-Length Models for Turbulent Transport 851
- 16.5 Variation of Wind with Height in the Atmosphere 855
 - 16.5.1 Mean Velocity in the Surface Layer in Adiabatic Conditions 856
 - 16.5.2 Effects of Temperature on the Surface Layer 859
 - 16.5.3 Wind Profiles in the Nonadiabatic Surface Layer 867
 - 16.5.4 Determination of the Friction Velocity u_* 870
 - 16.5.5 Empirical Formula for the Mean Wind Speed 870
- 16.6 The Pasquill Stability Classes 873
- 16.7 The Convective Boundary Layer 873
- 16.8 Meteorological Measurements 875
- References 876
- Problems 877

17 Atmospheric Diffusion Theories

- 17.1 Eulerian Approach 880
- 17.2 Lagrangian Approach 883
- 17.3 Comparison of Eulerian and Lagrangian Approaches 884
- 17.4 Equations Governing the Mean Concentration of Species in Turbulence 885
 - 17.4.1 Eulerian Approaches 885
 - 17.4.2 Conditions for Validity of the Atmospheric Diffusion Equation 886
 - 17.4.3 Lagrangian Approaches 889
- 17.5 Solution of the Atmospheric Diffusion Equation for an Instantaneous Source 892
- 17.6 Mean Concentration from Continuous Sources 893
 - 17.6.1 Lagrangian Approach 893
 - 17.6.2 Eulerian Approach 898
 - 17.6.3 Summary of Continuous Point Source Solutions 899
- 17.7 Statistical Theory of Turbulent Diffusion 901
 - 17.7.1 Qualitative Features of Atmospheric Diffusion 901
 - 17.7.2 Motion of a Single Particle Relative to a Fixed Axis 903
- 17.8 Summary of Atmospheric Diffusion Theories 907
- Appendix 17 Further Solutions 908
 - 17.A.1 Solution of (17.47) to (17.49) 908
 - 17.A.2 Solution of (17.68) and (17.69) 910
 - 17.A.3 Solution of (17.77) to (17.79) 911
- References 912
- Problems 912

**18 Analytical Solutions for Atmospheric Diffusion:
The Gaussian Plume Equation and Others**

- 18.1 Gaussian Concentration Distributions 916
- 18.2 Derivation of the Gaussian Plume Equation as a Solution of the Atmospheric Diffusion Equation 918

18.3	Summary of Gaussian Point Source Diffusion Formulas	923
18.4	Dispersion Parameters in Gaussian Models	926
18.4.1	Correlations for σ_y and σ_z Based on Similarity Theory	926
18.4.2	Correlations for σ_y and σ_z Based on Pasquill Stability Classes	929
18.5	Plume Rise	931
18.6	Analytical Properties of the Gaussian Plume Equation	933
18.7	Functional Forms of Mean Wind Speed and Eddy Diffusivities	938
18.7.1	Mean Wind Speed	938
18.7.2	Vertical Eddy Diffusion Coefficient K_{zz}	938
18.7.3	Horizontal Eddy Diffusion Coefficients K_{xx} and K_{yy}	942
18.8	Solutions of the Steady-State Atmospheric Diffusion Equation	943
18.8.1	Diffusion from a Point Source	943
18.8.2	Diffusion from a Line Source	944
	References	947
	Problems	949
19	Dry Deposition	958
19.1	Deposition Velocity	958
19.2	Resistance Model for Dry Deposition	960
19.2.1	Aerodynamic Resistance	962
19.2.2	Quasi-Laminar Resistance	963
19.2.3	Surface of Canopy Resistance	965
19.2.4	Relative Magnitudes of r_a , r_b , and r_c	968
19.3	Dry Deposition of Particles	969
19.4	A Model for Dry Deposition Calculations	971
19.5	Measurement of Dry Deposition	977
19.5.1	Direct Methods	978
19.5.2	Indirect Methods	979
19.5.3	Comparison of Methods	980
19.6	Some Comments on Modeling and Measurement of Dry Deposition	980
19.7	Interaction Between Equilibration Processes and Dry Deposition	982
19.7.1	Solution of the Model Equations	987
19.7.2	The Deposition Ratio	988
19.7.3	Effects of Equilibration Processes on Dry and Wet Deposition	989
	References	993
	Problems	995
20	Wet Deposition	997
20.1	General Representation of Atmospheric Wet Removal Processes	997

20.1.1	Parameters Used in Wet Deposition Studies	1000
20.2	Below-Cloud Scavenging of Gases	1003
20.2.1	Below-Cloud Scavenging of an Irreversibly Soluble Gas	1003
20.2.2	Below-Cloud Scavenging of a Reversibly Soluble Gas	1010
20.3	Precipitation Scavenging of Particles	1016
20.3.1	Raindrop–Aerosol Collision Efficiency	1018
20.3.2	Scavenging Rates	1021
20.4	In-Cloud Scavenging	1027
20.5	Cloud Processes and Wet Deposition	1027
20.6	Acid Deposition	1030
20.6.1	Acid Rain Overview	1030
20.6.2	Current Acid Rain Data and Trends	1033
20.6.3	Effects of Acid Deposition	1045
20.6.4	Cloudwater Deposition	1046
20.6.5	Fogs and Wet Deposition	1047
20.6.6	Source–Receptor Relationships	1048
20.6.7	Linearity	1051
20.7	Acid Deposition Process Synthesis	1056
20.7.1	Chemical Species Involved in Acid Deposition	1056
20.7.2	Dry Versus Wet Deposition	1057
20.7.3	Chemical Pathways for Sulfate and Nitrate Production	1057
20.7.4	Acid Rain Chemistry	1059
	References	1066
	Problems	1069

21 Atmospheric Chemistry and Climate

1075

21.1	Global Temperature Record and Solar Variability	1078
21.1.1	The Global Temperature Record	1078
21.1.2	Solar Variability	1082
21.2	Possible Effects of Global Warming	1086
21.3	Carbon Dioxide	1087
21.4	Atmospheric Chemistry and Climate Change	1093
21.4.1	Direct Radiative Impacts	1094
21.4.2	Indirect Chemical Impacts	1096
21.4.3	Atmospheric Lifetimes and Adjustment Times	1098
21.5	Radiative Effects of Clouds	1100
21.6	Radiative Forcing and Climate Sensitivity	1101
21.7	Relative Radiative Forcing Indices	1104
	References	1108
	Problems	1110

22	Radiative Effects of Atmospheric Aerosols: Visibility and Climate	
22.1	Scattering and Absorption of Light by Small Particles	1114
22.1.1	Rayleigh Scattering Regime	1120
22.1.2	Geometric Scattering Regime	1122
22.1.3	Scattering Phase Function	1123
22.1.4	Extinction by an Ensemble of Particles	1123
22.2	Visibility	1126
22.3	Scattering, Absorption, and Extinction Coefficients from Mie Theory	1131
22.4	Calculated Visibility Reduction Based on Atmospheric Data	1135
22.5	Direct Effect of Aerosols on Climate	1139
22.5.1	Optical Depth	1143
22.5.2	Upscatter Fraction	1146
22.5.3	Scattering Model of an Aerosol Layer	1147
22.5.4	Cooling Versus Heating of an Aerosol Layer	1152
22.5.5	Scattering Model of an Aerosol Layer for a Nonabsorbing Aerosol	1154
22.5.6	Direct Aerosol Forcing of Climate by Sulfate Aerosols	1156
22.5.7	Effect of Mineral Dust on Radiative Forcing of Climate	1160
22.5.8	Effect of Carbonaceous Aerosols on Radiative Forcing of Climate	1166
22.5.9	Internal and External Mixtures	1166
22.6	Indirect Effect of Aerosols on Climate	1170
22.6.1	Radiative Model for a Cloudy Atmosphere	1173
22.6.2	Sensitivity of Cloud Albedo to Cloud Drop Number Concentration	1175
22.6.3	Relation of Cloud Drop Number Concentration to Aerosol Concentrations	1177
22.6.4	Estimates of Indirect Radiative Forcing of Aerosols	1179
22.7	Summary: Estimates of Contributions to Radiative Forcing	1180
22.8	Climate Response to Anthropogenic Aerosol Forcing	1182
Appendix 22	Calculation of Scattering and Extinction Coefficients by Mie Theory	1184
	References	1185
	Problems	1190
23	Atmospheric Chemical Transport Models	
23.1	Introduction	1193
23.1.1	Model Types	1194
23.1.2	Types of Atmospheric Chemical Transport Models	1195

- 23.2 Box Models 1197
 - 23.2.1 The Eulerian Box Model 1197
 - 23.2.2 A Lagrangian Box Model 1200
- 23.3 Three-Dimensional Atmospheric Chemical Transport Models 1203
 - 23.3.1 Coordinate System—Uneven Terrain 1204
 - 23.3.2 Initial Conditions 1206
 - 23.3.3 Boundary Conditions 1206
- 23.4 One-Dimensional Lagrangian Models 1208
- 23.5 Other Forms of Chemical Transport Models 1211
 - 23.5.1 Atmospheric Diffusion Equation Expressed in Terms of Mixing Ratio 1211
 - 23.5.2 Pressure-Based Coordinate System 1215
 - 23.5.3 Spherical Coordinates 1216
- 23.6 Numerical Solution of Chemical Transport Models 1217
 - 23.6.1 Coupling Problem—Operator Splitting 1218
 - 23.6.2 Chemical Kinetics 1223
 - 23.6.3 Diffusion 1229
 - 23.6.4 Advection 1229
- 23.7 Applications of Atmospheric Chemical Transport Models 1234
 - 23.7.1 Los Angeles Basin Photochemical Smog 1234
 - 23.7.2 Acid Deposition in North America 1236
 - 23.7.3 Global Sulfur 1238
- 23.8 Model Evaluation 1238
- References 1240
- Problems 1242

24 Statistical Models

1245

- 24.1 Receptor Modeling Methods 1245
 - 24.1.1 Chemical Mass Balance (CMB) 1248
 - 24.1.2 Factor Analysis 1258
 - 24.1.3 Empirical Orthogonal Function Receptor Models 1263
- 24.2 Probability Distributions for Air Pollutant Concentrations 1265
 - 24.2.1 The Log-Normal Distribution 1267
 - 24.2.2 The Weibull Distribution 1268
- 24.3 Estimation of Parameters in the Distributions 1269
 - 24.3.1 Method of Quantiles 1269
 - 24.3.2 Method of Moments 1270
- 24.4 Order Statistics of Air Quality Data 1273
 - 24.4.1 Basic Notions and Terminology of Order Statistics 1273
 - 24.4.2 Extreme Values 1274
- 24.5 Exceedances of Critical Levels 1275
 - 24.5.1 Distribution of Exceedances 1275
 - 24.5.2 Expected Return Period or Waiting Time 1276

24.6	Alternative Forms of Air Quality Standards	1277
24.6.1	Evaluation of Alternative Forms of the Ozone Air Quality Standard with 1971 Pasadena, California, Data	1279
24.6.2	Selection of the Averaging Time	1281
24.7	Relating Current and Future Air Pollutant Statistical Distributions	1281
	References	1283
	Problems	1285
Appendix A	Units and Physical Constants	1289
A.1	SI Base Units	1289
A.2	SI Derived Units	1289
A.3	Fundamental Physical Constants	1292
A.4	Properties of the Atmosphere and Water	1293
A.5	Units for Representing Chemical Reactions	1294
A.6	Concentrations in the Aqueous Phase	1295
A.7	Symbols for Concentration	1295
	References	1295
Appendix B	Rate Constants of Atmospheric Chemical Reactions	1297
	References	1307
Index		1309

PREFACE

The study of atmospheric chemistry as a scientific discipline goes back to the 18th century, when the principal issue was identifying the major chemical components of the atmosphere, nitrogen, oxygen, water, carbon dioxide, and the noble gases. In the late 19th and early 20th centuries attention turned to the so-called trace gases, species present at less than 1 part per million parts of air by volume ($1 \mu\text{mol}$ per mole). We now know that the atmosphere contains a myriad of trace species, some at levels as low as 1 part per trillion parts of air. The role of trace species is disproportionate to their atmospheric abundance; they are responsible for phenomena ranging from urban photochemical smog, to acid deposition, to stratospheric ozone depletion, to potential climate change. Moreover, the composition of the atmosphere is changing; analysis of air trapped in ice cores reveals a record of striking increases in the long-lived so-called greenhouse gases, carbon dioxide (CO_2), methane (CH_4), and nitrous oxide (N_2O). Within the last century, concentrations of tropospheric ozone (O_3), sulfate (SO_4^{2-}), and carbonaceous aerosols in the Northern Hemisphere have increased significantly. There is evidence that all these changes are altering the basic chemistry of the atmosphere.

Atmospheric chemistry occurs within a fabric of profoundly complicated atmospheric dynamics. The results of this coupling of dynamics and chemistry are often unexpected: witness the unique combination of dynamical forces that lead to a wintertime polar vortex over Antarctica, with the concomitant formation of polar stratospheric clouds that serve as sites for heterogeneous chemical reactions involving chlorine compounds resulting from anthropogenic chlorofluorocarbons—all leading to the near total depletion of stratospheric ozone over the South Pole each spring; witness the nonlinear, and counterintuitive, dependence of the amount of ozone generated by reactions involving hydrocarbons and oxides of nitrogen (NO_x) at the urban and regional scale—although both hydrocarbons and NO_x are ozone precursors, situations exist where continuing to emit more and more NO_x actually leads to less ozone.

The chemical constituents of the atmosphere do not go through their life cycles independently; the cycles of the various species are linked together in a complex way. Thus a perturbation of one component can lead to significant, and nonlinear, changes to other components and to feedbacks that can amplify or damp the original perturbation.

In many respects, at once both the most important and the most paradoxical trace gas in the atmosphere is ozone (O_3). High in the stratosphere ozone screens living organisms from biologically harmful solar ultraviolet radiation; ozone at the surface, in the troposphere, can produce adverse effects on human health and plants when present at levels elevated above natural. At the urban and regional scale, significant policy issues concern how to decrease ozone levels by controlling the ozone precursors—hydrocarbons and oxides of nitrogen. At the global scale, understanding both the natural ozone chemistry of the troposphere and the causes of continually increasing background tropospheric ozone levels is a major goal.

Aerosols are particles suspended in the atmosphere. They arise directly from emissions of particles and from the conversion of certain gases to particles in the atmosphere. At elevated levels they inhibit visibility and are a human health hazard. There is a growing body of epidemiological data that suggests that increasing levels of aerosols may cause a significant increase in human mortality. For many years it was thought that atmospheric aerosols did not interact in any appreciable way with the cycles of trace gases. We now know that particles in the air affect climate and interact chemically in heretofore unrecognized ways with atmospheric gases. Volcanic aerosols in the stratosphere, for example, participate in the catalytic destruction of ozone by chlorine compounds, not directly, but through the intermediary of NO_x chemistry. Aerosols reflect solar radiation back to space and, in so doing, cool the Earth. Aerosols are also the nuclei around which clouds droplets form—no aerosols, no clouds. Clouds are one of the most important elements of our climate system, so the effect of increasing global aerosol levels on the Earth's cloudiness is a key problem in climate.

Historically the study of urban air pollution and its effects occurred more or less separately from that of the chemistry of the Earth's atmosphere as a whole. Similarly, in its early stages, climate research focused exclusively on CO_2 , without reference to effects on the underlying chemistry of the atmosphere and their feedbacks on climate itself. It is now recognized, in quantitative scientific terms, that the Earth's atmosphere is a continuum of spatial scales in which the urban atmosphere, the remote troposphere, the marine boundary layer, and the stratosphere are but points from the smallest turbulent eddies and the fastest time scales of free radical chemistry to global circulations and the decadal time scales of the longest-lived trace gases.

The object of this book is to provide a rigorous, comprehensive treatment of the chemistry of the atmosphere, including the formation, growth, dynamics, and properties of aerosols, the meteorology of air pollution, the transport, diffusion, and removal of species in the atmosphere, the formation and chemistry of clouds, the interaction of atmospheric chemistry and climate, the radiative and climatic effects of gases and particles, and the formulation of mathematical chemical/transport models of the atmosphere. Each of these elements is covered in detail in the present volume. In each area the central results are developed from first principles. In this way, the reader will gain a significant understanding of the science underlying the description of atmospheric processes and will be able to extend theories and results beyond those for which we have space here.

The book assumes that the reader has had introductory courses in thermodynamics, transport phenomena (fluid mechanics and/or heat and mass transfer), and engineering mathematics (differential equations). Thus the treatment is aimed at the senior or first-year graduate level in typical engineering curricula as well as in meteorology and atmospheric science programs.

The book is intended to serve as a textbook for a course in atmospheric science that might vary in length from one quarter or semester to a full academic year. Aside from its use as a course textbook the book will serve as a comprehensive reference book for professionals as well as for those from traditional engineering and science disciplines. Two types of appendices are given: those of a general nature appear at the end of the book and are designated by letters; those of a nature specific to a certain chapter appear with that chapter and are numbered according to the associated chapter.

Numerous problems are provided to enable the reader to evaluate his or her understanding of the material. In many cases the problems have been chosen to extend the results given in the chapter to new situations. The problems are coded with a "degree of difficulty"

for the benefit of the student and the instructor. The designation (A) indicates a problem that involves a straightforward application of material in the text. Those problems denoted (B) require some extension of the ideas in the text. Problems designated (C) encourage the reader to apply concepts from the book to current problems in atmospheric science and go somewhat beyond the level of (B) problems. Finally, those problems denoted (D) are of a degree of difficulty corresponding to (C) but generally require development of a computer program for their solution.

This book is a successor to John H. Seinfeld's *Atmospheric Chemistry and Physics of Air Pollution* (Wiley, 1986), which has been widely used for a decade. Substantial additions have been made in virtually all areas covered by the earlier book, reflecting the significant increase in our understanding of atmospheric processes that has emerged over the last decade and reflecting the truly global scope of the science of atmospheric chemistry and physics.

We extend sincere appreciation to Marta Goodman and Laura Shaheen who provided so much valuable assistance in making this book a reality and to Cecilia Lin who drafted the figures so skillfully.

JOHN H. SEINFELD

SPYROS N. PANDIS

1 The Atmosphere

1.1 HISTORY AND EVOLUTION OF THE EARTH'S ATMOSPHERE

It is generally believed that the solar system condensed out of an interstellar cloud of gas and dust, referred to as the "primordial solar nebula," about 4.6 billion years ago. The atmospheres of the Earth and the other terrestrial planets, Venus and Mars, are thought to have formed as a result of the release of trapped volatile compounds from the planet itself. The early atmosphere of the Earth is believed to have been a mixture of carbon dioxide (CO_2), nitrogen (N_2), and water vapor (H_2O), with trace amounts of hydrogen (H_2), a mixture similar to that emitted by present day volcanoes.

The composition of the present atmosphere bears little resemblance to the composition of the early atmosphere. Most of the water vapor that outgassed from the Earth's interior condensed out of the atmosphere to form the oceans. The predominance of the CO_2 that outgassed formed sedimentary carbonate rocks after dissolution in the ocean. It is estimated that for each molecule of CO_2 presently in the atmosphere, there are about 10^5 CO_2 molecules incorporated as carbonates in sedimentary rocks. Since N_2 is chemically inert, non-water soluble, and noncondensable, most of the outgassed N_2 accumulated in the atmosphere over geologic time to become the atmosphere's most abundant constituent.

The early atmosphere of the Earth was a mildly reducing chemical mixture, whereas the present atmosphere is strongly oxidizing. The dramatic rise of oxygen (O_2) as an atmospheric constituent over time was the result of the production of O_2 as a by-product of photosynthetic activity. It has been estimated that the current level of O_2 in the atmosphere was achieved approximately 400 million years ago (Cloud, 1983). The present level of O_2 is maintained by a balance between production from photosynthesis and removal through respiration and decay of organic carbon. If O_2 were not replenished by photosynthesis, the reservoir of surface organic carbon would be completely oxidized in about 20 years, at which time the amount of O_2 in the atmosphere would have decreased by less than 1% (Walker, 1977). In the absence of surface organic carbon to be oxidized, weathering of sedimentary rocks would consume the remaining O_2 in the atmosphere, but it would take approximately 4 million years to do so.

The Earth's atmosphere is composed primarily of the gases N_2 (78%), O_2 (21%), and Ar (1%), whose abundances are controlled over geologic time scales by the biosphere, uptake and release from crustal material, and degassing of the interior. Water vapor is the next most abundant constituent; it is found mainly in the lower atmosphere and its concentration is highly variable, reaching concentrations as high as 3%. Evaporation and precipitation control its abundance. The remaining gaseous constituents, the *trace gases*, comprise less than 1% of the atmosphere. These trace gases play a crucial role in the Earth's radiative

balance and in the chemical properties of the atmosphere. The trace gas abundances have changed rapidly and remarkably over the last two centuries.

The study of atmospheric chemistry can be traced back to the 18th century when chemists such as Joseph Priestley, Antoine-Laurent Lavoisier, and Henry Cavendish attempted to determine the chemical components of the atmosphere. Largely through their efforts, as well as those of a number of 19th century chemists and physicists, the identity and major components of the atmosphere, N_2 , O_2 , water vapor, CO_2 , and the rare gases, were established. In the late 19th and early 20th century focus shifted from the major atmospheric constituents to trace constituents, that is, those having mole fractions below 10^{-6} , 1 part per million (ppm) by volume. It has become clear that the atmosphere contains a myriad of trace species. The presence of these species can be traced to geological, biological, chemical, and anthropogenic processes.

Spectacular innovations in instrumentation in the last quarter of the 20th century have enabled identification of atmospheric trace species down to levels of almost 10^{-12} parts per part of air, 1 part per trillion (ppt) by volume. Observations have shown that the composition of the atmosphere is changing on the global scale. Present-day measurements coupled with analyses of ancient air trapped in bubbles in ice cores provide a record of dramatic, global increases in the concentrations of gases such as CO_2 , methane (CH_4), nitrous oxide (N_2O), and various halogen-containing compounds. These "greenhouse gases" act as atmospheric thermal insulators. They absorb infrared radiation from the Earth's surface and reradiate a portion of this radiation back to the surface. These gases include CO_2 , O_3 , CH_4 , N_2O , and halogen-containing compounds. The emergence of the Antarctic ozone hole provides striking evidence of the ability of emissions of trace species to perturb large-scale atmospheric chemistry. Observations have documented the essentially complete disappearance of ozone in the Antarctic stratosphere during the austral spring, a phenomenon that has been termed the "Antarctic ozone hole." Observations have also documented less dramatic decreases over the Arctic and over the northern and southern midlatitudes. Whereas stratospheric ozone levels have been eroding, those at ground level in the Northern Hemisphere have, over the past century, been increasing. Paradoxically, whereas ozone in the stratosphere protects living organisms from harmful solar ultraviolet radiation, ozone in the lower atmosphere can have adverse effects on human health and plants. Ozone also has effects on climate. Climate is most sensitive to changes in ozone near the tropopause; information on ozone levels in this region, and for the rest of the troposphere above ground level as well, is limited to a few locations globally where balloon-borne measurements have been made for about 30 years.

Quantities of airborne particles in industrialized regions of the Northern Hemisphere have increased markedly since the Industrial Revolution. Atmospheric particles (aerosols) arise both from direct emissions and from gas-to-particle conversion of vapor precursors. Aerosols can affect climate and stratospheric ozone concentrations and have been implicated in human morbidity and mortality in urban areas. The climatic role of atmospheric aerosols arises from their ability to reflect solar radiation back to space and from their role as cloud condensation nuclei. Estimates of the cooling effect resulting from the reflection of solar radiation back to space by aerosols indicate that the cooling effect may be sufficiently large to mask the warming effect of greenhouse gas increases over industrialized regions of the Northern Hemisphere.

The atmosphere is the recipient of many of the products of our technological society. These effluents include products of combustion of fossil fuels and of the development of new synthetic chemicals. Historically these emissions can lead to unforeseen consequences in the atmosphere. Classical examples include the realization in the 1950s that motor vehicle emissions could lead to urban smog and the realization in the 1970s that emissions of chlorofluorocarbons from aerosol spray cans and refrigerators could cause the depletion of stratospheric ozone.

The chemical fates of trace atmospheric species are often intertwined. The life cycles of the trace species are inextricably coupled through the complex array of chemical and physical processes in the atmosphere. As a result of these couplings, a perturbation in the concentration of one species can lead to significant changes in the concentrations and lifetimes of other trace species and to feedbacks that can either amplify or damp the original perturbation. An example of this coupling is provided by methane. Methane is the predominant organic molecule in the troposphere and it is the second most important greenhouse gas after CO_2 . Methane sources such as rice paddies and cattle can be estimated and are increasing. Methane is removed from the atmosphere by reaction with the hydroxyl (OH) radical, at a rate that depends on the atmospheric concentration of OH . But, the OH concentration depends on the amount of carbon monoxide (CO), which itself is a product of CH_4 oxidation as well as a result of fossil fuel combustion and biomass burning. The hydroxyl concentration also depends on the concentration of ozone and oxides of nitrogen. Change in CH_4 can affect the total amount of ozone in the troposphere, so methane itself affects the concentration of the species, OH , that governs its removal.

Depending on their atmospheric lifetime, trace species can exhibit an enormous range of spatial and temporal variability. Relatively long-lived species have a spatial uniformity such that a handful of strategically located sampling sites around the globe are adequate to characterize their spatial distribution and temporal trend. As species lifetimes become shorter, their spatial and temporal distributions become more variable. Urban areas, for example, can require tens of monitoring stations over an area of hundreds of square kilometers in order to characterize the spatial and temporal distribution of their atmospheric components.

The extraordinary pace of the recent increases in atmospheric trace gases can be seen when current levels are compared with those of the distant past. Such comparisons can be made for CO_2 and CH_4 , whose histories can be reconstructed from their concentrations in bubbles of air trapped in ice in such perpetually cold places as Antarctica and Greenland. With gases that are long-lived in the atmosphere and therefore distributed rather uniformly over the globe, such as CO_2 and CH_4 , polar ice core samples reveal global average concentrations of previous eras. Analyses of bubbles in ice cores show that CO_2 and CH_4 concentrations remained essentially unchanged from the end of the last ice age some 10,000 years ago until roughly 300 years ago, at mixing ratios close to 260 ppm by volume and 0.7 ppm by volume, respectively. (See Section 1.4 for discussion of units.) About 300 years ago methane levels began to climb, and about 100 years ago levels of both gases began to increase markedly. Before the large-scale production of chlorofluorocarbons the natural level of chlorine in the stratosphere was 0.6 part per billion (ppb) by volume; now it is 3 ppb, a factor of 5 increase.

Activities of humans account for most of the rapid changes in the trace gases over the past 200 years—combustion of fossil fuels (coal and oil) for energy and transportation, in-

dustrial and agricultural activities, biomass burning (the burning of vegetation), and deforestation. For CO_2 , for example, the sources are mainly fossil-fuel combustion and deforestation in the tropics; for CH_4 , mainly rice cultivation, cattle breeding, biomass burning, microbial activity in municipal landfills, and leakage of gas during the recovery of coal, oil, and natural gas.

1.2 CLIMATE

Viewed from space, the Earth is a multicolored marble; clouds and snow-covered regions of white, blue oceans, and brown continents. The white areas make Earth a bright planet; about 30% of the Sun's radiation is reflected immediately back to space. Solar energy that does not reflect off clouds and snow is absorbed by the atmosphere and the Earth's surface. As the surface warms, it sends infrared radiation back to space. The atmosphere, however, absorbs much of the energy radiated by the surface and reemits its own energy, but at much lower temperatures. Aside from gases in the atmosphere, clouds play a major climatic role. Some clouds cool the planet by reflecting solar radiation back to space; others warm the Earth by trapping energy near the surface. On balance, clouds exert a significant cooling effect on Earth, although in some areas, such as the tropics, heavy clouds can markedly warm the regional climate.

The temperature of the Earth adjusts so that solar energy reaching the Earth is balanced by that leaving the planet. Whereas the radiation budget must balance for the entire Earth, it does not balance at each particular point on the globe. Very little solar energy reaches the white, ice-covered polar regions, especially during the winter months. The Earth absorbs most solar radiation near its equator. Over time, though, energy absorbed near the equator spreads to the colder regions of the globe, carried by winds in the atmosphere and by currents in the oceans. This global heat engine, in its attempt to equalize temperatures, generates the climate with which we are all familiar. It pumps energy into storm fronts and powers hurricanes. In the colder seasons, low-pressure and high-pressure cells push each other back and forth every few days. Energy is also transported over the globe by masses of wet and dry air. Through evaporation, air over the warm oceans absorbs water vapor and then travels to colder regions and continental interiors where water vapor condenses as rain or snow, a process that releases heat into the atmosphere. In the oceans, salt helps drive the heat engine. Over some areas, like the arid Mediterranean, water evaporates from the sea faster than rain or river flows can replace it. As seawater becomes increasingly salty, it grows denser. In the North Atlantic, cool air temperatures and excess salt cause the surface water to sink, creating a current of heavy water that spreads throughout the world's oceans. By redistributing energy in this way, the oceans act to smooth out differences in temperature and salinity. Whereas the atmosphere can respond in a few days to a warming or cooling in the ocean, it takes the sea surface months or longer to adjust to changes in energy coming from the atmosphere.

Solar radiation, clouds, ocean currents, and the atmospheric circulation weave together in a complex and chaotic way to produce our climate. Until recently, climate was assumed to change on a time scale much much longer than our lifetimes and those of our children. Evidence is mounting, however, that the release of trace gases to the atmosphere, the "greenhouse gases," has the potential to lead to an increase of the Earth's temperature by several degrees Celsius. The Earth's average temperature rose about 0.5°C over the past

century. It has been estimated that a doubling of CO₂ from its pre-Industrial Revolution mixing ratio of 280 ppm by volume could lead to a rise in average global temperature of 1.5 to 4.5°C. A 2°C warming would produce the warmest climate seen on Earth in 6000 years. A 4.5°C rise would place the world in a temperature regime last experienced in the Mesozoic Era—the age of dinosaurs.

Although an average global warming of a few degrees does not sound like much, it could create dramatic changes in climatic extremes. It has been estimated, for example, that, in the event of an average global warming of 1.7°C, the frequency of periods of 5 days or more exceeding 35°C (95°F) in the Corn Belt of the United States would increase threefold. Such conditions at critical stages of the growing season are known to harm corn and lead to reduced yields. With a doubling of CO₂, the number of days exceeding 38°C (100°F) and nights above 27°C (80°F) have been estimated to rise dramatically in many major American cities. Changes in the timing and amount of precipitation would almost certainly occur with a warmer climate. Soil moisture, critical during planting and early growth periods, will change. Some regions would probably become more productive, others less so. The North American Grain Belt, according to at least one climate model, will shift northward into Canada as warming produces hotter, drier conditions in the American Midwest.

Of all the effects of a global warming, perhaps none has captured more attention than the prospect of rising sea levels. This would result from the melting of land-based glaciers and volume expansion of ocean water as it warms. Prevailing opinion is that a sea level rise of about 0.5 m could occur by 2100. In the most dramatic scenario, the West Antarctic ice sheet, which rests on land that is below sea level, could slide into the sea if the buttress of floating ice separating it from the ocean were to melt. This would raise the average sea level 5 to 6 m (Bentley, 1997). Even a 0.3 m (1 foot) rise would have major effects on the erosion of coastlines, salt water intrusion into the water supply of coastal areas, flooding of marshes, and inland extent of surges from large storms.

To systematically approach the complex subject of climate, the scientific community has divided the problem into two major parts, climate *forcings* and climate *responses*. Climate *forcings* are changes in the energy balance of the Earth that are imposed upon it; forcings are measured in units of heat flux—watts per square meter ($W\ m^{-2}$). An example of a forcing is a change in energy output from the sun. *Responses* are the meteorological results of these forcings, reflected in temperatures, rainfall, extremes of weather, sea level height, and so on.

Much of the variation in the predicted magnitude of potential climate effects resulting from the increase in greenhouse gas levels hinges on estimates of the size and direction of various feedbacks that may occur in response to an initial perturbation of the climate. Negative feedbacks have an effect that damps the warming trend; positive feedbacks reinforce the initial warming. One example of a greenhouse warming feedback mechanism involves water vapor. As air warms, each cubic meter of air can hold more water vapor. Since water vapor is a greenhouse gas, this increased concentration of water vapor further enhances greenhouse warming. In turn, the warmer air can hold more water, and so on. This is an example of a positive feedback, providing a physical mechanism for multiplying the original impetus for change beyond its initial amount.

Some mechanisms provide a negative feedback, which decreases the initial impetus. For example, increasing the amount of water vapor in the air may lead to forming more clouds. Low-level, white clouds reflect sunlight, thereby preventing sunlight from reaching the

earth and warming the surface. Increasing the geographical coverage of low-level clouds would reduce greenhouse warming, whereas increasing the amount of high, convective clouds could enhance greenhouse warming. This is because high, convective clouds absorb energy from below at higher temperatures than they radiate energy into space from their tops, thereby effectively trapping energy. It is not known with certainty whether increased temperatures would lead to more low-level clouds or more high, convective clouds.

Another feedback uncertainty involves the response of plants to rising CO₂ levels. Some studies indicate that agricultural crops grow faster in a high-CO₂ environment, pulling more carbon out of the atmosphere and storing it in plant tissues. Little is known about the response of the forests, grasslands, and tundra that cover much of the Earth.

Probably of even greater significance than the feedback involving terrestrial plants and soils are the immense and very complex ocean–atmosphere interactions. Without human influence, the flows of carbon between the atmosphere, plants, and ocean would be roughly balanced. Fossil-fuel combustion today adds about 5×10^9 metric tons per year (5 Gt yr^{-1}) of carbon to the atmosphere. (1 metric ton, Mt, equals 10^6 g.) About half of the 5 Gt yr^{-1} remains in the atmosphere as rising CO₂ levels. The rest is absorbed by plants and oceans but uncertainty exists as to just how much goes to each reservoir. Deforestation is adding up to 4 Gt of carbon to the atmosphere annually. Thus, of the 5 to 9 Gt yr⁻¹ added to the atmosphere by humans, 2.5 Gt remains in the atmosphere and 2.5 to 6.5 Gt yr⁻¹ is absorbed by plants and the oceans. Accepting the higher end of the range of estimates for deforestation and the lower end of the range of estimates for plant uptake, plants can serve as a net source, rather than a sink, for CO₂.

The oceans contain 55 times as much carbon as does the atmosphere and 20 times as much as do land plants. Thus small changes in the oceans' capacity to store carbon can have a large effect on atmospheric concentrations. In most areas, atmospheric CO₂ interacts only with the top 100 m or so of seawater and moves downward slowly because of thermal gradients that separate the surface layer from deeper waters. However, the only effective way for the oceans to buffer the atmospheric increase in CO₂ is to pump the carbon into the deep ocean, either as dissolved gaseous CO₂ or as carbonate particles that settle in the sediments at the ocean floor. CO₂ may be drawn into the deep ocean in a few locations, like the North Atlantic, where cold surface waters sink to the bottom. Some have speculated that global warming could cause the oceans' currents to become more sluggish, reducing their ability to take up CO₂ and exacerbating the warming.

1.3 THE LAYERS OF THE ATMOSPHERE

In the most general terms, the atmosphere is divided into lower and upper regions. The lower atmosphere is generally considered to extend to the top of the stratosphere, an altitude of about 50 kilometers (km). Study of the lower atmosphere is known as *meteorology*; study of the upper atmosphere is called *aeronomy*.

The Earth's atmosphere is characterized by variations of temperature and pressure with height. In fact, the variation of the average temperature profile with altitude is the basis for distinguishing the layers of the atmosphere. The regions of the atmosphere are (Figure 1.1):

Troposphere. The lowest layer of the atmosphere, extending from the Earth's surface up to the tropopause, which is at 10 to 15 km altitude depending on latitude and time of year; characterized by decreasing temperature with height; rapid vertical mixing.

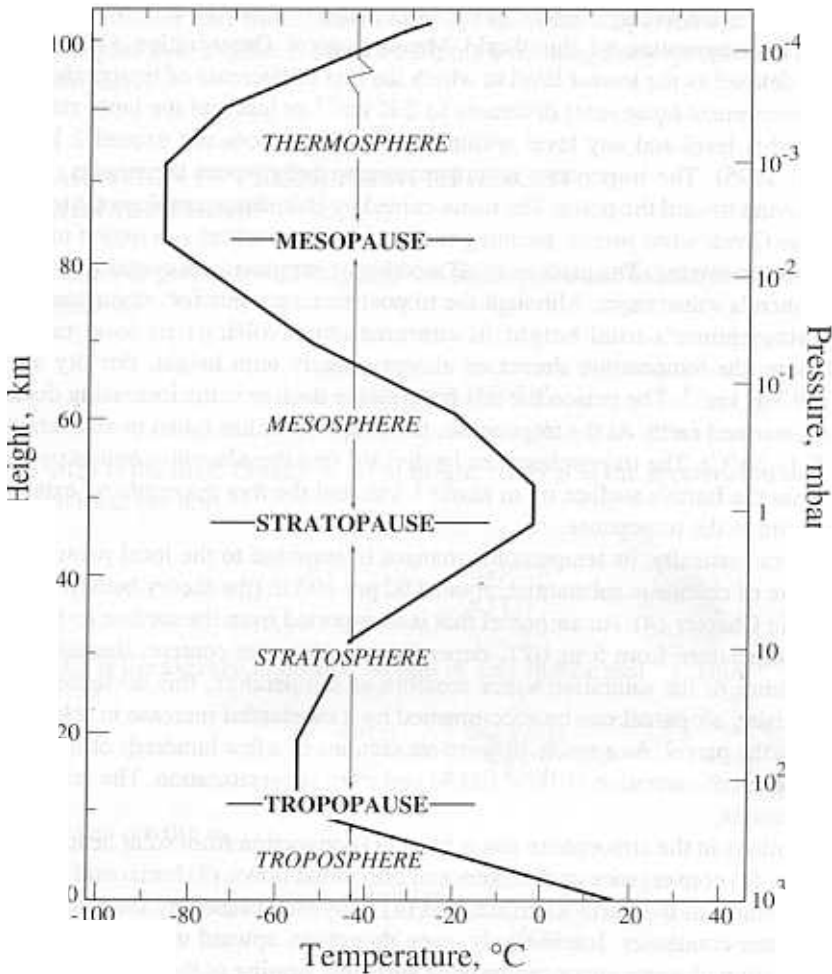


FIGURE 1.1 Layers of the atmosphere.

Stratosphere. Extends from the tropopause to the stratopause (~45 to 55 km altitude); temperature increases with altitude, leading to a layer in which vertical mixing is slow.

Mesosphere. Extends from the stratopause to the mesopause (~80 to 90 km altitude); temperature decreases with altitude to the mesopause, which is the coldest point in the atmosphere; rapid vertical mixing.

Thermosphere. The region above the mesopause; characterized by high temperatures as a result of absorption of short wavelength radiation by N_2 and O_2 ; rapid vertical mixing. The *ionosphere* is a region of the upper mesosphere and lower thermosphere where ions are produced by photoionization.

Exosphere. The outermost region of the atmosphere (>500 km altitude) where gas molecules with sufficient energy can escape from the Earth's gravitational attraction.

Over the equator the average height of the tropopause is about 18 km; over the poles about 8 km. By convention of the World Meteorological Organization (WMO), the tropopause is defined as the lowest level at which the rate of decrease of temperature with height (the *temperature lapse rate*) decreases to 2 K km^{-1} or less and the lapse rate averaged between this level and any level within the next 2 km does not exceed 2 K km^{-1} (Holton et al., 1995). The tropopause is at a maximum height over the tropics, sloping downward moving toward the poles. The name coined by British meteorologist, Sir Napier Shaw, from the Greek word *tropos*, meaning turning, the troposphere is a region of ceaseless turbulence and mixing. The caldron of all weather, the troposphere contains almost all of the atmosphere's water vapor. Although the troposphere accounts for only a small fraction of the atmosphere's total height, it contains about 80% of its total mass. In the troposphere, the temperature decreases almost linearly with height. For dry air the lapse rate is 9.7 K km^{-1} . The reason for this progressive decline is the increasing distance from the sun-warmed earth. At the tropopause, the temperature has fallen to an average of about 217 K (-56°C). The troposphere can be divided into the *planetary boundary layer*, extending from the Earth's surface up to about 1 km, and the *free troposphere*, extending from about 1 km to the tropopause.

As air moves vertically, its temperature changes in response to the local pressure. For dry air, this rate of change is substantial, about 1°C per 100 m (the theory behind this will be developed in Chapter 14). An air parcel that is transported from the surface to 1 km can decrease in temperature from 5 to 10°C depending on its water content. Because of the strong dependence of the saturation vapor pressure on temperature, this decrease of temperature of a rising air parcel can be accompanied by a substantial increase in relative humidity (RH) in the parcel. As a result, upward air motions of a few hundreds of meters can cause the air to reach saturation ($\text{RH} = 100\%$) and even supersaturation. The result is the formation of clouds.

Vertical motions in the atmosphere result from (1) convection from solar heating of the Earth's surface, (2) convergence or divergence of horizontal flows, (3) horizontal flow over topographic features at the Earth's surface, and (4) buoyancy caused by the release of latent heat as water condenses. Interestingly, even though an upward moving parcel of air cools, condensation of water vapor can provide sufficient heating of the parcel to maintain the temperature of the air parcel above that of the surrounding air. When this occurs, the parcel is buoyant and accelerates upward even more, leading to more condensation. Cumulus clouds are produced in this fashion, and updraft velocities of meters per second can be reached in such clouds. Vertical convection associated with cumulus clouds is, in fact, a principal mechanism for transporting air from close to the Earth's surface to the mid- and upper-troposphere.

The stratosphere, extending from about 11 km to about 50 km, was discovered at the turn of the 20th century by the French meteorologist, Léon Philippe Teisserenc de Bort. Sending up temperature-measuring devices in balloons, he found that, contrary to the popular belief of the day, the temperature in the atmosphere did not steadily decrease to absolute zero with increasing altitude, but stopped falling and remained constant at 11 km or so. He named the region the stratosphere from the Latin word *stratum* meaning layer. Although an isothermal region does exist from about 11 to 20 km at midlatitudes, temperature progressively increases from 20 to 50 km, reaching 271 K at the stratopause, a temperature not much lower than the average of 288 K at the Earth's surface. The vertical thermal structure of the stratosphere is a result of the presence of ozone in the stratosphere.

Absorption of solar ultraviolet radiation by O_3 causes the temperature in the stratosphere to be much higher than expected, based on simply extending the troposphere's lapse rate into the stratosphere.

1.4 VARIATION OF PRESSURE WITH HEIGHT IN THE ATMOSPHERE

The variation of pressure with height in the atmosphere can be addressed with the hydrostatic equation,¹

$$\frac{dp(z)}{dz} = -\rho(z)g \quad (1.1)$$

where $\rho(z)$ is the mass density of air at height z and g is the acceleration due to gravity. From the ideal gas law,

$$\rho(z) = \frac{M_{\text{air}}p(z)}{RT(z)} \quad (1.2)$$

where M_{air} is the average molecular weight of air (28.97 g mol^{-1}). Thus

$$\frac{dp(z)}{dz} = -\frac{M_{\text{air}}gp(z)}{RT(z)} \quad (1.3)$$

which we can rewrite as

$$\frac{d \ln p(z)}{dz} = -\frac{1}{H(z)} \quad (1.4)$$

where $H(z) = RT(z)/M_{\text{air}}g$ is a characteristic length scale for decrease of pressure with height.

The temperature in the atmosphere varies by less than a factor of 2, while the pressure changes by six orders of magnitude (see Table A.8). If the temperature can be taken to be approximately constant, just to obtain a simple approximate expression for $p(z)$, then the

¹*Units of pressure.* Because instruments for measuring pressure, such as the manometer, often contain mercury, commonly used units for pressure are based on the height of the mercury column (in millimeters) that the gas pressure can support. The unit mm Hg is often called the *Torr* in honor of the scientist, Evangelista Torricelli. A related unit for pressure is the standard atmosphere (abbreviated atm):

$$1 \text{ standard atmosphere} = 1 \text{ atm} = 760 \text{ mm Hg} = 760 \text{ Torr}$$

The unit of pressure in the International System of Units (SI) is newtons per meter squared (N m^{-2}), which is called the *pascal* (Pa). In terms of pascals, the standard atmosphere is $1.01325 \times 10^5 \text{ Pa}$. Another commonly used unit of pressure in atmospheric science is the millibar (mbar), which is equivalent to the hPa (see Tables A.5 and A.8). The standard atmosphere is 1013.25 mbar

pressure decrease with height is approximately exponential,

$$\frac{p(z)}{p_0} = e^{-z/H} \quad (1.5)$$

where $H = RT/M_{\text{air}}g$ is called the scale height.

The concept of scale height can be applied individually to atmospheric species, $H_i = RT/M_i g$, with $p_i(z)$ the partial pressure of species i . A species with a molecular weight M_i less than that of air will have a correspondingly larger scale height. On this basis high molecular mass gases like Xe and Kr would tend to be concentrated close to the Earth's surface and lighter gases, He and H₂, would extend to a greater altitude. Because of the overwhelming effect of turbulent mixing in the atmosphere, however, this separation based on molecular masses does not occur in the lower atmosphere. Only above about 120 km do the lightest components (H and He) tend to "rise to the top" and the heavy components (⁴⁰Ar, Xe, Kr) fall off rapidly with height.

In the lower atmosphere, the scale height H is about 8 km at $T = 273$ K. It is sometimes stated that the e -folding length scale for pressure in the lower atmosphere is approximately 8 km (actually ± 1 km).

The variation of pressure and temperature with altitude in the so-called standard atmosphere is given in Table A.8. The SI pressure unit used in Table A.8 is the hectopascal, hPa, which is equivalent to the millibar. Because the millibar (mbar) is the unit most commonly used in the meteorological literature, we will use it when discussing pressure at various altitudes in the atmosphere. Mean surface pressure at sea level is 1013 mbar; global mean surface pressure, calculated over both land and ocean, is estimated as 984 mbar. The lower value reflects the effect of surface topography; over the highest mountains, which reach an altitude of over 8000 m, the pressure may be as low as 300 mbar. The 850 mbar level, which, as we see from Table A.8, is at about 1.5 km altitude, is often used for representation of atmospheric quantities, such as temperature, as the first standard meteorological level above much of the topography and a level at which a considerable quantity of heat is located as well as transported.

1.5 LARGE-SCALE MOTION OF THE ATMOSPHERE

1.5.1 The General Circulation

The large-scale motion of the atmosphere comprises the winds, the global structure of which is referred to as the general circulation. Moisture, momentum, and energy are exchanged between the atmosphere and the underlying ocean and land. Little mass and momentum are exchanged with space, although the atmosphere absorbs directly a portion of the solar radiation. The total dry mass of the atmosphere, calculated as an annual mean, is estimated to be 5.13×10^{18} kg (Trenberth and Guillemot, 1994).

Even though the total input and output of radiant energy to and from the Earth are essentially in balance, they are not in balance at every point on the Earth. The amount of energy reaching the Earth's surface depends, in part, on the nature of the surface (e.g., land versus sea) and the degree of cloudiness, as well as on the latitude of the point. For example, at lower solar angles, in the polar regions the same amount of solar energy as radiated

to the tropics must pass through more atmosphere and intercept a larger surface area. The uneven distribution of energy resulting from latitudinal variations in insolation and from differences in absorptivity of the Earth's surface leads to the large-scale air motions of the Earth. In particular, the tendency to transport energy from the tropics toward the polar regions, thereby redistributing energy inequalities on the Earth, is the overall factor governing the general circulation of the atmosphere.

In order to visualize the nature of the general circulation of the atmosphere, we can think of the atmosphere over either hemisphere as a fluid enclosed within a long, shallow container, heated at one end and cooled at the other. Because the horizontal dimension of the "container" is so much greater than its vertical dimension, the curvature of the Earth can be neglected, and the container can be considered to be rectangular. If such a container were constructed in the laboratory and the ends differentially heated as described above, one would observe a circulation of the fluid, consisting of rising motion along the heated wall and descending motion along the cooled wall, flow in the direction of warm to cold at the top of the box, and flow in the direction of cold to warm along the bottom of the box. In the atmosphere, then, the tendency is for warm tropical air to rise and cold polar air to sink, with poleward and equatorward flows to complete the circulation.

However, the general circulation of the atmosphere is not as simple as just described. Another force arises because of the motion of the Earth, the Coriolis force. At the Earth's surface an object at the equator has a greater tangential velocity than one in the temperate zones. Air moving toward the south cannot acquire an increased eastward (the Earth rotates from west to east) tangential velocity as it moves south and thus, *to an observer on the Earth*, appears to acquire a velocity component in the westward direction. Thus air moving south in the Northern Hemisphere appears to lag behind the Earth. To an observer on the Earth it appears that the air has been influenced by a force in the westward direction. To an observer in space, it would be clear that the air is merely trying to maintain straight-line motion while the Earth turns below it. Friction between the wind and the ground diminishes this effect in the lower atmosphere.

From the standpoint of air motion, the atmosphere can be segmented vertically into two layers. Extending from the ground up to about 1000 m is the *planetary boundary layer*, the zone in which the effect of the surface is felt and in which the wind speed and direction are governed by horizontal pressure gradients, shear stresses, and Coriolis forces. Above the planetary boundary layer is the *geostrophic layer*, in which only horizontal pressure gradients and Coriolis forces influence the flow.

To predict the general pattern of macroscale air circulation on the Earth we must consider both the tendency for thermal circulation and the influence of Coriolis forces. Figure 1.2 shows the nature of the general circulation of the atmosphere. At either side of the equator is a thermal circulation, in which warm tropical air rises and cool northern air flows toward the equator. The circulation does not extend all the way to the poles because radiative cooling of the upper northward flow causes it to subside (fall) at about 30° N and S latitude. The Coriolis force acting on these cells leads to easterly winds, called the trade winds. The same situation occurs in the polar regions, in which warm air from the temperate zones moves northward in the upper levels, eventually cooling by radiation and subsiding at the poles. The result is the polar easterlies.

In the temperate regions, between 40° and 55° latitude, influences of both tropical and polar regions are felt. The major feature of the temperate regions is large-scale weather systems, which results in the circulation shown in Figure 1.2. The surface winds in the Northern Hemisphere are westerlies because of the Coriolis force.

sometimes represented as transfers among well-mixed compartments. Prather et al. (1987) employed a three-dimensional chemical tracer model to study the horizontal and vertical exchanges within and among the major atmospheric compartments. Interhemispheric exchanges occur mainly in the upper troposphere. Dispersion of material occurs more efficiently in the summer by horizontal winds, while in the winter, vertical transport tends to predominate. Characteristic times for exchanges between atmospheric compartments are (Salstein, 1995):

Northern troposphere/southern troposphere	0.7–1.8	1.0
Troposphere/stratosphere	0.8–2.0	1.4
Northern stratosphere/southern stratosphere	3–6	4.0

Whereas it takes about 1 to 2 months to mix a species throughout a hemisphere, 1 to 2 years are needed to mix a species through the entire Earth's lower atmosphere. The relatively long time for mixing between the Northern and Southern Hemispheres arises from the presence of the *intertropical convergence zone* at the equator. Because air rises in this zone, the region has considerable cloudiness and rain and no strong north–south winds that would tend to mix gases between the Northern and Southern Hemispheres.

1.5.2 Troposphere–Stratosphere Transport

Transport of chemical species between the stratosphere and troposphere is a key process in atmospheric chemistry. For example, anthropogenic species transported from the troposphere into the stratosphere initiate the chemistry responsible for stratospheric ozone depletion. Conversely, downward transport from the stratosphere represents a significant source of ozone into the troposphere and constitutes the ultimate removal mechanism for many stratospheric species, including those involved in ozone depletion. As noted above, the phenomenon that most distinguishes the troposphere from the stratosphere is the disparity in vertical mixing timescales; vertical transport of air and chemical species throughout the depth of the troposphere can occur on timescales as short as a few hours via strong convective updrafts associated with large cumulus formation, whereas vertical transport over a similar altitude range in the stratosphere takes months to a year or more. We mentioned above that the troposphere and stratosphere are sometimes regarded as isolated compartments. The relatively long timescale for vertical transport in the stratosphere, however, and the vertical inhomogeneity in the chemical and radiative environment in the stratosphere imply that the concept of the stratosphere as a well-mixed box is not really valid. Thus describing stratosphere–troposphere exchange by a single mass transport rate between two boxes has only limited utility. What is really of interest is to describe the rate at which tropospheric species are supplied to and removed from regions of the stratosphere.

Figure 1.3 depicts dynamical aspects of stratosphere–troposphere exchange. Transport across the tropopause occurs both ways as large latitudinal displacements of the tropopause occur. The shading in Figure 1.3 shows the region within the lower stratosphere most directly affected by these large-scale motions. In the tropics moist convection strongly transports material vertically. The traditional view of tropical troposphere-to-stratosphere

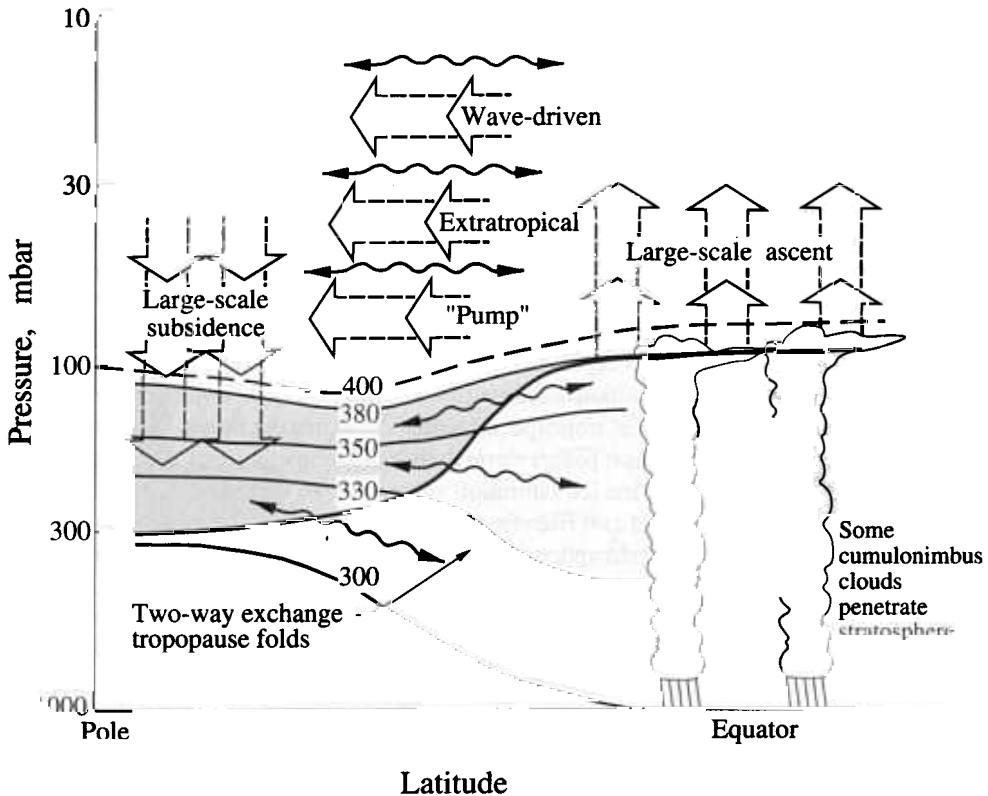


FIGURE 1.3 Dynamical aspects of stratosphere-troposphere exchange (Holton et al., 1995). The tropopause is shown by the thick line. Thin lines are surfaces of constant potential temperature (in kelvin units). (Potential temperature will be defined and developed in Chapter 14. For now, these surfaces can be thought of as those on which horizontal transport occurs.) The shaded region of the stratosphere is that within which so-called tropopause folding occurs. (Tropopause folding is a process whereby a thin band of stratospheric air intrudes into the troposphere along strongly tilted isentropes. Part of the stratospheric air in the fold returns reversibly to the stratosphere and part is drawn irreversibly into the troposphere.) The region of the stratosphere above about 380 K potential temperature does not have direct stratosphere-troposphere exchange in the midlatitudes. The broad arrows indicate transport by the global-scale circulation, which is driven by the "extratropical pump." The extratropical stratosphere acts persistently on the tropical lower stratosphere as a kind of global-scale suction pump, the strength of which varies seasonally and interannually and in which air is gradually withdrawn from the tropical stratosphere and pushed poleward and ultimately downward.

exchange is that air is forced into the stratosphere by tropical cumulus convective turrets. More consistent, however, is that the net flux from the tropical troposphere to the stratosphere is actually a result of the wave-driven pumping from the extratropical stratosphere (the large horizontal arrows in Figure 1.3). It is this pumping that is the cause of the steady ascent of air in the tropical stratosphere (Holton et al., 1995). The shaded region of the stratosphere, the lowermost stratosphere, is the only part of the stratosphere that can receive material from the troposphere by transport along surfaces of constant tem-

perature.² Stratospheric air above this region cannot reach the troposphere without first slowly descending, as shown. Exchange between the shaded region of the stratosphere and the troposphere can be significantly faster than that between the stratosphere overlaying this region and the shaded region. Much of the ozone transport from the lowermost stratosphere into the troposphere is believed to occur in connection with tropopause folding events.

Long-lived chemical species with nearly uniform tropospheric mixing ratios, such as CH₄, N₂O and the chlorofluorocarbons, are observed to have their largest stratospheric mixing ratios immediately above the tropical tropopause, matching tropospheric values. These mixing ratios extend well up into the tropical stratosphere, reflecting plumes of air rising from deep moist convection in the tropical troposphere. One would expect a similar behavior to be exhibited by water vapor, but the water vapor mixing ratio actually exhibits a minimum of a few parts per million within a few kilometers of the tropical tropopause. This value is far lower than typical tropospheric water vapor mixing ratios. Water vapor is effectively frozen out of the air as it passes through the cold temperature of the tropopause, with its mixing ratio reduced to the ice saturation value. (As we will see in Chapter 4, this air gradually becomes moistened as it rises from the tropopause as a result of the oxidation of methane that occurs in the stratosphere.) Water vapor mixing ratios of air entering the tropical stratosphere vary seasonally with the annual cycle of tropopause temperature. The minimum saturation mixing ratio is “recorded” on each layer of air moving upward (Holton et al., 1995). Since horizontal transport between the tropical and extratropical stratosphere is relatively slow, layers of air passing upward through the tropical tropopause retain their water vapor signature for many months. The imprint of the seasonally varying saturation mixing ratio of the tropical tropopause is observable as alternating layers of low and high water vapor mixing ratios that propagate upward at the speed of the large-scale circulation. The annually varying mixing ratio signal produced by freeze drying of water at the tropopause remains noticeable for as long as two years, well into the middle stratosphere. The implied ascent rates just above the tropical tropopause are 0.2 mm s⁻¹ in northern summer to 0.4 mm s⁻¹ in northern winter (Holton et al., 1995).

Simultaneous *in situ* measurements of CO₂ and water vapor in the lower stratosphere in November 1992 and May 1993, for example, were analyzed to infer a mean transport time of 4 to 6 months from the tropical tropopause (~16 km) to ~18.5 to 19 km at midlatitudes (Boering et al., 1995). It takes many years for a species to reach the upper levels of the stratosphere from the time it crosses the tropopause.

1.6 TEMPERATURE AND WATER VAPOR

Temperature in the atmosphere varies with location on the surface and elevation. Figure 1.4 shows the mean temperature over the period 1980 to 1989 between 1000 mbar and 50 mbar averaged around a latitude band. Highest values occur in the tropics; at the 1000 mbar level

²Potential temperature is defined for an ideal gas as $\theta = T(p_0/p)^{R/c_p}$, where T is temperature, p is pressure, $p_0 = 1000$ hPa, and R and c_p are the gas constant and specific heat of dry air, respectively. θ is the temperature that an air parcel would attain if it were adiabatically compressed from pressure p and temperature T to pressure p_0 . Potential temperature is conserved by air parcels when the motion is adiabatic. Since diabatic processes occur on timescales of weeks in the stratosphere, on shorter timescales parcels move essentially on surfaces of constant θ . We will return to potential temperature in Chapter 14.

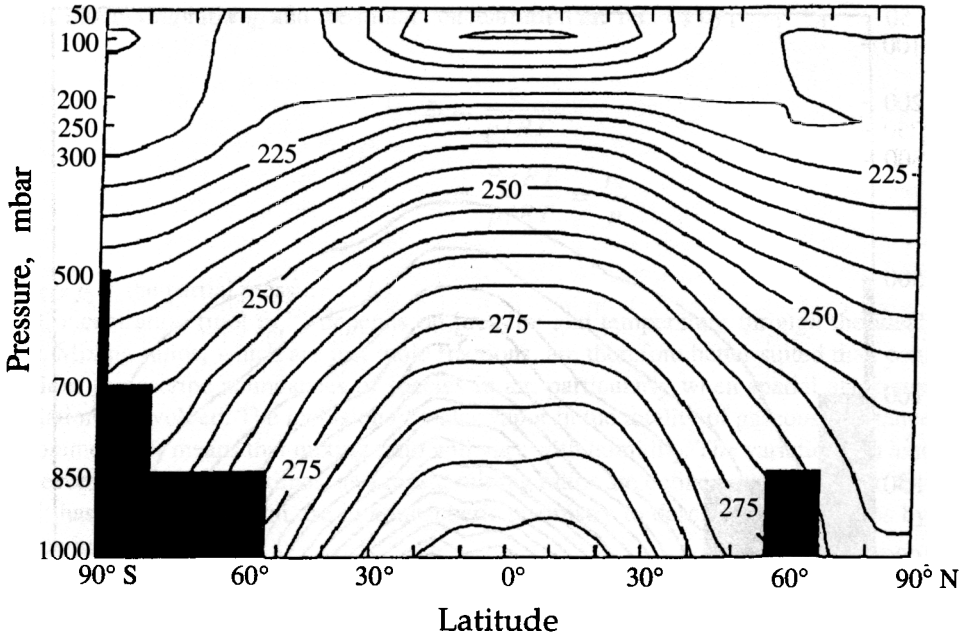


FIGURE 1.4 Mean atmospheric temperature over the period 1980 to 1989 between 1000 mbar and 50 mbar averaged around a latitude band (Salstein, 1995). Data not available in blackened areas.

the average temperature exceeds 295 K. The annual mean temperature structure is largely symmetric about the equator (although the highest temperature occurs at about 10° N), with the difference in mean surface temperature between the tropics and the poles about 35°C. At the top of the troposphere, about the 200 mbar level, the meridional temperature gradient begins to reverse; at 100 mbar, for example, temperature increases poleward by about 20°C.

Water vapor is distributed throughout the lower troposphere, at highly variable levels. The water vapor content of the atmosphere can be expressed in a variety of ways:

1. Mole (or volume) mixing ratio—moles of water vapor per mole of air (see Section 1.7).
2. Amount of water vapor to dry air by mass [$\text{g H}_2\text{O (kg dry air)}^{-1}$].
3. Specific humidity—proportion of water vapor to total air [$\text{g H}_2\text{O (kg air)}^{-1}$].
4. Relative humidity—ratio of the specific humidity to the maximum specific humidity possible at a given temperature and pressure (dimensionless). (See Section 1.7.)
5. Mass concentration $\text{g H}_2\text{O (m}^3 \text{ air)}^{-1}$.
6. Mass mixing ratio $\text{g H}_2\text{O (g air)}^{-1}$.

Figure 1.5 shows the zonal mean specific humidity for the period 1980 to 1989. Maximum specific humidities are reached in the tropics, about 16 g kg^{-1} . By the 500 mbar altitude, the value over the tropics has decreased to 2 g kg^{-1} . This value of 2 g kg^{-1} also holds in the northern and southern polar regions.

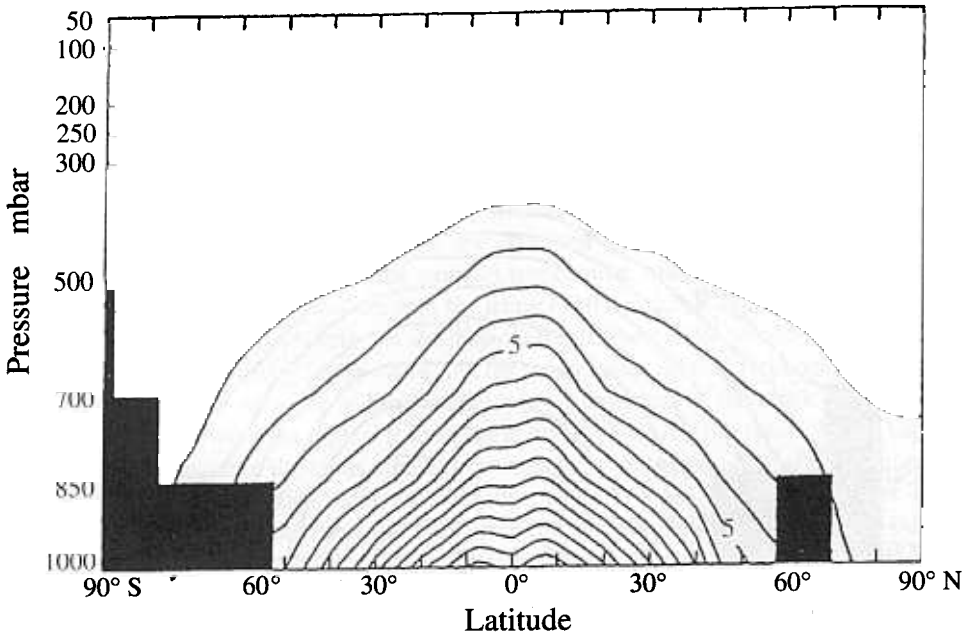


FIGURE 1.5 Zonal mean specific humidity [$\text{g H}_2\text{O (kg air)}^{-1}$] for the period 1980 to 1989 (Salstein, 1995). Isolines are spaced every $1 \text{ g (kg dry air)}^{-1}$.

1.7 EXPRESSING THE AMOUNT OF A SUBSTANCE IN THE ATMOSPHERE

The SI unit for the amount of a substance is the mole (mol). The number of atoms or molecules in 1 mol is Avogadro's number, $N_A = 6.022 \times 10^{23} \text{ mol}^{-1}$. Concentration is the amount (or mass) of a substance in a given volume divided by that volume. *Mixing ratio* in atmospheric chemistry is defined as the ratio of the amount (or mass) of the substance in a given volume to the total amount (or mass) of all constituents in that volume. In this definition for a gaseous substance the sum of all constituents includes all gaseous substances, including water vapor, but *not* including particulate matter or condensed phase water. Thus mixing ratio is just the fraction of the total amount (or mass) contributed by the substance of interest.

The volume mixing ratio for a species i is

$$\xi_i = \frac{c_i}{c_{\text{total}}} \quad (1.6)$$

where c_i is the molar concentration of i and c_{total} is the total molar concentration of air. From the ideal gas law the total molar concentration at any point in the atmosphere is

$$c_{\text{total}} = \frac{N}{V} = \frac{p}{RT} \quad (1.7)$$

Thus the mixing ratio ξ_i and the molar concentration are related by

$$\begin{aligned}\xi_i &= \frac{c_i}{p/RT} \\ &= \frac{P_i/RT}{p/RT} = \frac{p_i}{p}\end{aligned}\quad (1.8)$$

where p_i is the partial pressure of i .

Concentration (mol m^{-3}) depends on pressure and temperature through the ideal gas law. Mixing ratios, which are just mole fractions, are therefore better suited than concentrations to describe abundances of species in air, particularly when spatial and temporal variation is involved. The inclusion of water vapor in the totality of gaseous substances in a volume of air means that mixing ratio will vary with humidity. The variation can amount to several percent. Sometimes, as a result, mixing ratios are defined with respect to dry air.

It has become common use in atmospheric chemistry to describe mixing ratios by the following units:

parts per million (ppm)	10^{-6}	$\mu\text{mol mol}^{-1}$
parts per billion (ppb)	10^{-9}	nmol mol^{-1}
parts per trillion (ppt)	10^{-12}	pmol mol^{-1}

These quantities are sometimes distinguished by an added v (for volume) and m (for mass), that is,

ppmv	parts per million by volume
ppmm	parts per million by mass

Unless noted otherwise, we will always use mixing ratios by volume and not use the added v. The parts per million, parts per billion, and parts per trillion measures are not SI units; the SI versions are, as given above, $\mu\text{mol mol}^{-1}$, nmol mol^{-1} , and pmol mol^{-1} .

The concentration of air molecules at any temperature and pressure can be computed from the ideal gas law (1.7). At $T = 298 \text{ K}$ and $p = 1 \text{ atm}$, for example, the concentration, expressed in molecules cm^{-3} , is

$$\begin{aligned}c &= \frac{.01325 \times 10^5 \text{ N/m}^2}{\left(8.314 \frac{\text{Nm}}{\text{mol K}}\right) (298 \text{ K})} \\ &= 40.897 \frac{\text{mol}}{\text{m}^3} \\ &= \left(\frac{\text{mol}}{\text{m}^3}\right) \left(\frac{\text{m}^3}{10^6 \text{ cm}^3}\right) \left(\frac{6.022 \times 10^{23} \text{ molecules}}{\text{mol}}\right) \\ &= 2.463 \times 10^{19} \frac{\text{molecules}}{\text{cm}^3}\end{aligned}$$

Thus, at $T = 298 \text{ K}$ and $p = 1 \text{ atm}$, the following mixing ratios and their corresponding concentrations are:

1 ppm	$2.463 \times 10^{13} \text{ molecules cm}^{-3}$
1 ppb	$2.463 \times 10^{10} \text{ molecules cm}^{-3}$
1 ppt	$2.463 \times 10^7 \text{ molecules cm}^{-3}$

In carrying out calculations in atmospheric chemistry it is frequently necessary to have the concentration of water vapor in units of either $\mu\text{g m}^{-3}$ or ppm. For a given ambient temperature T , relative humidity RH is defined as the ratio of the partial pressure of water to its saturation vapor pressure at the same temperature,

$$\text{RH} = 100 \frac{p_{\text{H}_2\text{O}}}{p_{\text{H}_2\text{O}}^\circ} \quad (1.9)$$

where the factor of 100 is used because RH is usually expressed in percent. Alternatively, RH is the ratio of the actual mole fraction of water vapor y to that at saturation y_s ,

$$\text{RH} = 100 \frac{y}{y_s} \quad (1.10)$$

Since the mole fraction is equivalent to the volume fraction, the water vapor mixing ratio in ppm is given by

$$[\text{H}_2\text{O}] = 10^6 y = 10^4 \text{ RH } y_s \text{ (ppm)} \quad (1.11)$$

This equation can be written in terms of $p_{\text{H}_2\text{O}}^\circ$ and the atmospheric pressure p ,

$$[\text{H}_2\text{O}] = 10^4 \text{ RH} \frac{p_{\text{H}_2\text{O}}^\circ}{p} \text{ (ppm)} \quad (1.12)$$

Example 1.1 Conversion from Mixing Ratio to $\mu\text{g m}^{-3}$ Atmospheric species concentrations are sometimes expressed in terms of mass per volume, most frequently as $\mu\text{g m}^{-3}$. Given a concentration m_i , in $\mu\text{g m}^{-3}$, the molar concentration of species i , in mol m^{-3} , is

$$c_i = \frac{10^{-6} m_i}{M_i}$$

where M_i is the molecular weight of species i .

Noting that the total molar concentration of air at pressure p and temperature T is $c = p/RT$, then

$$\text{Mixing ratio of } i \text{ in ppm} = \frac{RT}{p M_i} \times \text{Concentration of } i \text{ in } \mu\text{g m}^{-3}$$

If T is in K and p in Pa (see Table A.6 for the value of the molar gas constant, R)

$$\text{Mixing ratio of } i \text{ in ppm} = \frac{8.314T}{p M_i} \times \text{Concentration of } i \text{ in } \mu\text{g m}^{-3}$$

As an example, let us determine the concentration in $\mu\text{g m}^{-3}$ for O_3 corresponding to a mixing ratio of 120 ppb at $p = 1 \text{ atm}$ and $T = 298 \text{ K}$. The 120 ppb corresponds to 0.12 ppm. Then

$$\begin{aligned} \text{Concentration in } \mu\text{g m}^{-3} &= \frac{p M_i}{8.314 T} \times \text{Mixing ratio in ppm} \\ &= \frac{(1.0133 \times 10^5)(48)}{8.314(298)} \times 0.12 \\ &= 235.6 \mu\text{g m}^{-3} \end{aligned}$$

Now let us convert $365 \mu\text{g m}^{-3}$ of SO_2 to ppm at the same temperature and pressure:

$$\begin{aligned} \text{Mixing ratio in ppm} &= \frac{(8.314)(298)}{(1.0133 \times 10^5)(64)} \times 365 \\ &= 0.139 \text{ ppm} \end{aligned}$$

1.8 COMPOSITION OF THE ATMOSPHERE

The atmosphere is composed primarily of nitrogen, oxygen, and several noble gases, the concentrations of which have remained remarkably fixed over time. Also present are a number of trace gases that occur in relatively small and sometimes highly variable amounts.

In spite of its apparent unchanging nature, the atmosphere is in reality a dynamic system, with its gaseous constituents continuously being exchanged with vegetation, the oceans, and biological organisms. The so-called cycles of the atmospheric gases involve a number of physical and chemical processes. Gases are produced by chemical processes within the atmosphere itself, by biological activity, volcanic exhalation, radioactive decay, and human industrial activities. Gases are removed from the atmosphere by chemical reactions in the atmosphere, by biological activity, by physical processes in the atmosphere (such as particle formation), and by deposition and uptake by the oceans and earth. The average lifetime of a gas molecule introduced into the atmosphere can range from seconds to millions of years, depending on the effectiveness of the removal processes. Most of the species considered air pollutants (in a region in which their concentrations exceed substantially the normal background levels) have natural as well as man-made sources. Therefore, in order to assess the effect man-made emissions may have on the atmosphere as a whole, it is essential to understand the atmospheric cycles of the trace gases, including natural and anthropogenic sources as well as predominant removal mechanisms.

The important atmospheric gases are listed in Table 1.1 arranged according to the nature of their global cycles. The total quantity of a species both in the atmosphere and dissolved

TABLE 1.1 Atmospheric Gases

	Molecular Weight	Average Mixing Ratio (ppm)	Cycle	Status
Ar	39.948	9340	} No cycle	} Accumulation during Earth's history
Ne	20.179	18		
Kr	83.80	1.1		
Xe	131.30	0.09		
N ₂	28.013	780,840	} Biological and microbiological	}
O ₂	32	209,460		
CH ₄	16.043	1.72	Biogenic and chemical	} Quasi-steady-state or equilibrium
CO ₂	44.010	355	Anthropogenic and biogenic	
CO	28.010	0.12 (NH) 0.06 (SH)	Anthropogenic and chemical	
H ₂	2.016	0.58	Biogenic and chemical	
N ₂ O	44.012	0.311	Biogenic and chemical	
SO ₂	64.06	10 ⁻⁵ -10 ⁻⁴	Anthropogenic, biogenic, chemical	
NH ₃	17	10 ⁻⁴ -10 ⁻³	Biogenic and chemical	
NO	30.006	10 ⁻⁶ -10 ⁻²	Anthropogenic, biogenic, chemical	
NO ₂	46.006			
O ₃	48	10 ⁻² -10 ⁻¹	Chemical	
H ₂ O	18.015	Variable	} Physicochemical	
He	4.003	5.2		

in the oceans, say, M_g , and that deposited on the earth as sediment, say, M_s , must equal that which has been exhaled from the earth's interior over time, M_i . Thus $M_i = M_g + M_s$. If $M_g > M_s$, most of the constituent has remained in the atmosphere and, for that reason, it can be called an *accumulative* gas. If, on the other hand, $M_g < M_s$, only a small amount of the gas is in the atmosphere and its concentration level is determined by processes resulting in quasi-steady-state conditions. Such gases can be called nonaccumulative or *quasi-equilibrium* gases. The ratio M_g/M_s for the noble gases and N₂ is greater than 1. From CO₂ on down Table 1.1, the ratio $M_g/M_s \leq 10^{-3}$, clearly establishing these species as equilibrium gases.

The processes that govern the abundance of the equilibrium gases vary for different gases. The water composition of the atmosphere is controlled by the variation of the vapor pressure of water with temperature. Ozone abundance is determined, as we shall see, by chemical processes in the upper and lower atmosphere. Methane, nitrous oxide, and carbon monoxide levels are controlled by atmospheric chemical reactions as well as by biological processes. It is estimated that only $\frac{1}{1000}$ of all CO₂ released to the Earth's surface by exhalation has remained in the atmosphere-ocean system, with most existing as carbonate sediments on the land and in water. The processes actually governing the atmospheric CO₂ content have not been clearly determined, although it is most likely that these represent a combination of chemical equilibrium with the oceans and geochemical cycles. For oxygen, the estimated range of M_g/M_s lies between 1/50 and 1/12. Most of the Earth's oxygen is believed to have been produced by photosynthesis. Oxygen is consumed by oxidation of min-

erals at the Earth's surface. Thus the oxygen concentration in the atmosphere is probably a result of both accumulation and geochemical cycles.

While in the air, a substance can be chemically altered in one of two ways. First, the sunlight itself may contain sufficient energy to break the molecule apart, a so-called photochemical reaction. The more frequently occurring chemical alteration, however, takes place when two molecules interact and undergo a chemical reaction to produce new species. Atmospheric chemical transformations can occur homogeneously or heterogeneously. Homogeneous reactions occur entirely in one phase; heterogeneous reactions involve more than one phase, such as a gas interacting with a liquid or with a solid surface.

During transport through the atmosphere, all but the most inert substances are likely to participate in some form of chemical reaction. This process can transform a chemical from its original state, the physical (gas, liquid, or solid) and chemical form in which it first enters the atmosphere, to another state that may have either similar or very different characteristics. Transformation products can differ from their parent substance in their chemical properties, toxicity, and other characteristics. These products may be removed from the atmosphere in a manner very different from that of their precursors. For example, when a substance that was originally emitted as a gas is transformed into a particle, the overall removal is usually hastened since particles often tend to be removed from the air more rapidly than gases.

In spite of the fact that the atmosphere is composed predominantly of relatively inert molecules such as N_2 and O_2 , it is actually a rather efficient oxidizing medium. One reason for the atmosphere's oxidizing capacity arises because the atmosphere contains minute amounts of very reactive molecular fragments, called free radicals. The most important free radical in the chemistry of the troposphere is the hydroxyl (OH) radical, which reacts with nearly every molecular species in the atmosphere. In addition, the atmosphere contains trace amounts of species less reactive than free radicals but nonetheless reactive enough to attack a variety of airborne compounds. Ozone (O_3) is one important oxidizer, which also participates in the formation of the hydroxyl radical.

Once emitted, species are converted at various rates into substances generally characterized by higher chemical oxidation states than their parent substances. Frequently this oxidative transformation is accompanied by an increase in polarity (and hence water solubility) or other physical and chemical changes from the precursor molecule. An example is the conversion of sulfur dioxide (SO_2) into sulfuric acid (H_2SO_4). Sulfur dioxide is moderately water soluble, but its oxidation product, sulfuric acid, is so water soluble that even single molecules of sulfuric acid in air immediately become associated with water molecules. The demise of one substance through a chemical transformation can become another species *in situ* source. In general, then, a species emitted into the air can be transformed by a chemical process to a product that may have markedly different physicochemical properties and a unique fate of its own.

1.9 RADIATION

Basically all the energy that reaches the Earth comes from the Sun. The absorption and loss of radiant energy by the Earth and the atmosphere are almost totally responsible for the Earth's weather, both on a global and local scale. The average temperature on the Earth re-

mains fairly constant, indicating that the Earth and the atmosphere on the whole lose as much energy by reradiation back into space as is received by radiation from the Sun. The accounting for the incoming and outgoing radiant energy constitutes the Earth's energy balance. The atmosphere, although it may appear to be transparent to radiation, plays a very important role in the energy balance of the Earth. In fact, the atmosphere controls the amount of solar radiation that actually reaches the surface of the Earth and, at the same time, controls the amount of outgoing terrestrial radiation that escapes into space.

Radiant energy, arranged in order of its wavelengths λ , is called the *spectrum* of radiation. The electromagnetic spectrum is shown in Figure 1.6. The Sun radiates over the entire electromagnetic spectrum, although, as we will see, most of the energy is concentrated near the visible portion of the spectrum, the narrow band of wavelengths from 400 to 700 nm (0.4 to 0.7 μm). Our interest will be confined to the so-called optical region, which extends over the near ultraviolet, the visible, and the near infrared, the wavelength range from 200 nm to 100 μm . This range covers most of the solar radiation and that emitted by the Earth's surface and atmosphere. Three interrelated measures are used to specify the location in the electromagnetic spectrum, the wavelength λ , the frequency ν , and the wavenumber $\tilde{\nu} = \lambda^{-1}$. Frequency ν and wavelength λ are related by $\nu = c/\lambda$, where c is the speed of light. In the ultraviolet and visible portion of the spectrum it is common to characterize radiation by its wavelength, expressed either in nanometers (nm) or micrometers (μm). In the infrared part of the spectrum, the wavenumber (cm^{-1}) is frequently used.

Radiation is emitted from matter when an electron drops to a lower level of energy. The difference in energy between the initial and final level, $\Delta\varepsilon$, is related to the frequency of the emitted radiation by

$$\Delta\varepsilon = h\nu = \frac{hc}{\lambda} \quad (1.13)$$

where Planck's constant, $h = 6.626 \times 10^{-34}$ J s, and the speed of light in vacuum, $c = 2.9979 \times 10^8$ m s⁻¹ (see Table A.6). When the energy difference $\Delta\varepsilon$ is large, the frequency of the excited photon is high (very small wavelength) and the radiation is in the X-ray or gamma-ray region. Equation (1.13) also applies to the absorption of a photon of energy by a molecule. Thus a molecule can absorb radiant energy only if the wavelength of the radiation corresponds to the difference between two of its energy levels. Since the spacing between energy levels is, in general, different for molecules of different composition and shape, the absorption of radiant energy by molecules of differing structure occurs in different regions of the electromagnetic spectrum.

The amount of energy radiated from a body depends largely on the temperature of the body. It has been demonstrated experimentally that at a given temperature there is a maximum amount of radiant energy that can be emitted per unit time per unit area of a body. This maximum amount of radiation for a certain temperature is called the *blackbody radiation*. A body that radiates, for every wavelength, the maximum possible intensity of radiation at a certain temperature is called a *blackbody*. This maximum is identical for every blackbody regardless of its constituency. Thus the intensity of radiation emitted by a blackbody is a function only of the wavelength, absolute temperature, and surface area. The term "blackbody" has no reference to the color of the body. A blackbody can also be characterized by the property that all radiant energy reaching its surface is absorbed.

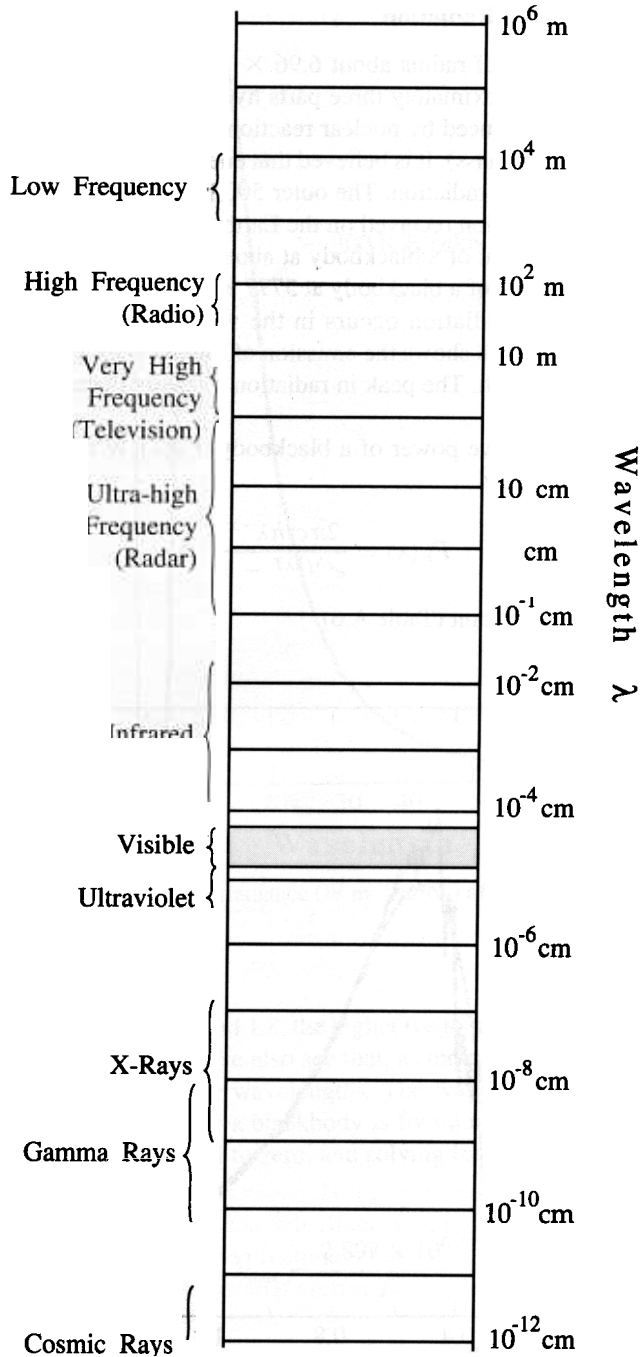


FIGURE 1.6 Electromagnetic spectrum.

1.9.1 Solar and Terrestrial Radiation

The Sun is a gaseous sphere of radius about 6.96×10^5 km and of mass about 1.99×10^{30} kg. It is made up of approximately three parts hydrogen and one part helium. In the core of the Sun energy is produced by nuclear reactions (fusion of four H atoms into one He atom, with a small loss of mass). It is believed that energy is transferred to the outer layers mainly by electromagnetic radiation. The outer 500 km of the Sun, called the *photosphere*, emits most of the radiation received on the Earth. Radiation emitted by the photosphere closely approximates that of a blackbody at about 6000 K. The energy spectrum of the Sun as compared with that of a blackbody at 5777 K is shown in Figure 1.7. The maximum intensity of incident radiation occurs in the visible spectrum at about 500 nm ($0.5 \mu\text{m}$). In contrast, Figure 1.8 shows the emission of radiant energy from a blackbody at 300 K, approximating the Earth. The peak in radiation intensity occurs at about $10 \mu\text{m}$ in the invisible infrared.

The monochromatic emissive power of a blackbody $F_B(\lambda)(\text{W m}^{-2} \text{m}^{-1})$ is related to temperature and wavelength by

$$F_B(\lambda) = \frac{2\pi c^2 h \lambda^{-5}}{e^{ch/k\lambda T} - 1} \quad (1.14)$$

where k is the Boltzmann constant (Table A.6).

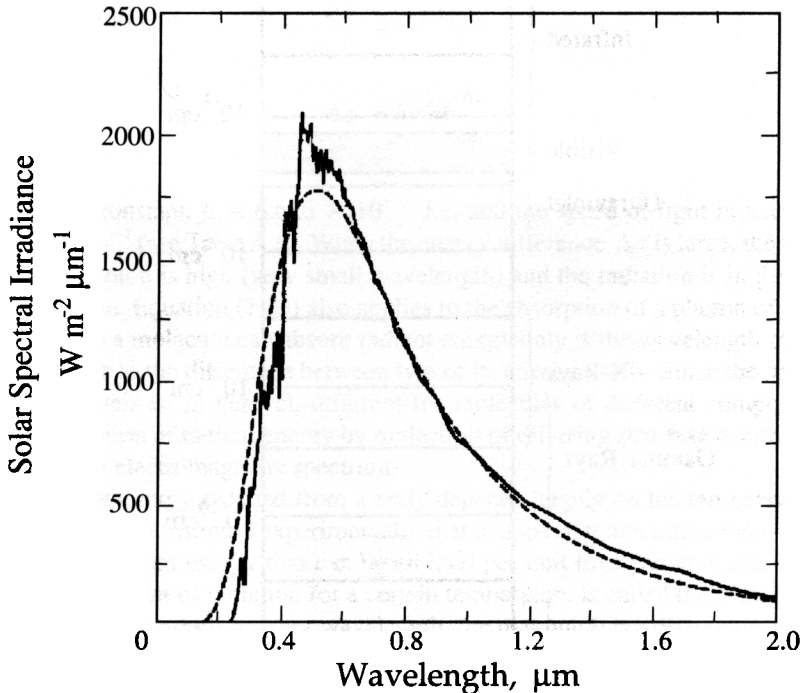


FIGURE 1.7 Solar spectral irradiance ($\text{W m}^{-2} \mu\text{m}^{-1}$) compared to that of a blackbody at 5777 K (dashed line) (Iqbal, 1983). Reprinted by permission of Academic Press.

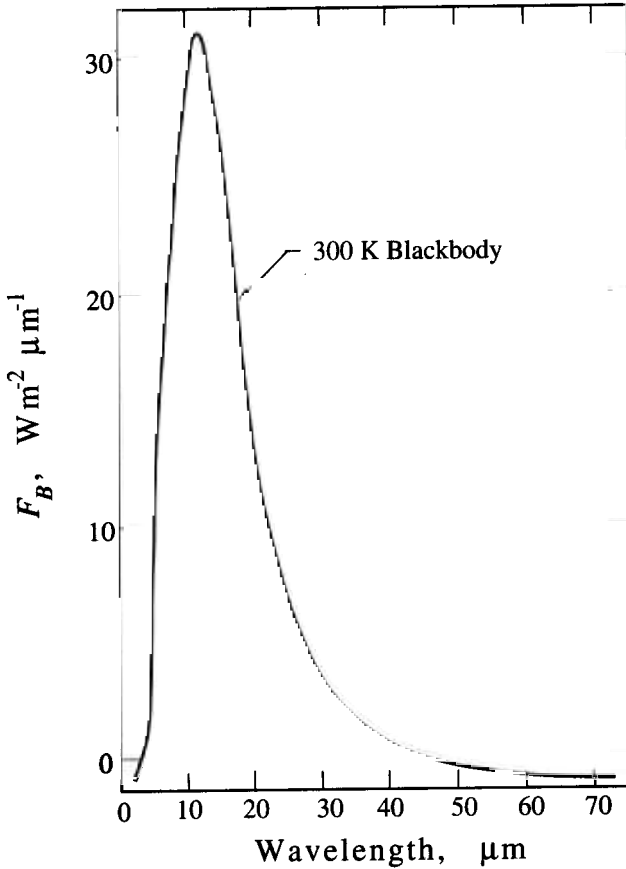


FIGURE 1.8 Spectral irradiance ($\text{W m}^{-2} \mu\text{m}^{-1}$) of a blackbody at 300 K.

As can be seen from Figures 1.7 and 1.8, the higher the temperature, the greater is the emissive power (at all wavelengths). We also see that, as temperature increases, the maximum value of $F_B(\lambda)$ moves to shorter wavelengths. The wavelength at which the maximum amount of radiation is emitted by a blackbody is found by differentiating (1.14) with respect to λ , setting the result equal to zero, and solving for λ . The result with λ expressed in nm and T in kelvin units is

$$\lambda_{\max} = \frac{2.897 \times 10^6}{T} \quad (1.15)$$

Thus hot bodies not only radiate more energy than cold ones, they do so at shorter wavelengths. The wavelengths for the maxima of solar and terrestrial radiation are 480 nm and about 10,000 nm, respectively. The Sun, with an effective surface temperature of about 6000 K, radiates about 2×10^5 more energy per square meter than the Earth at 300 K.

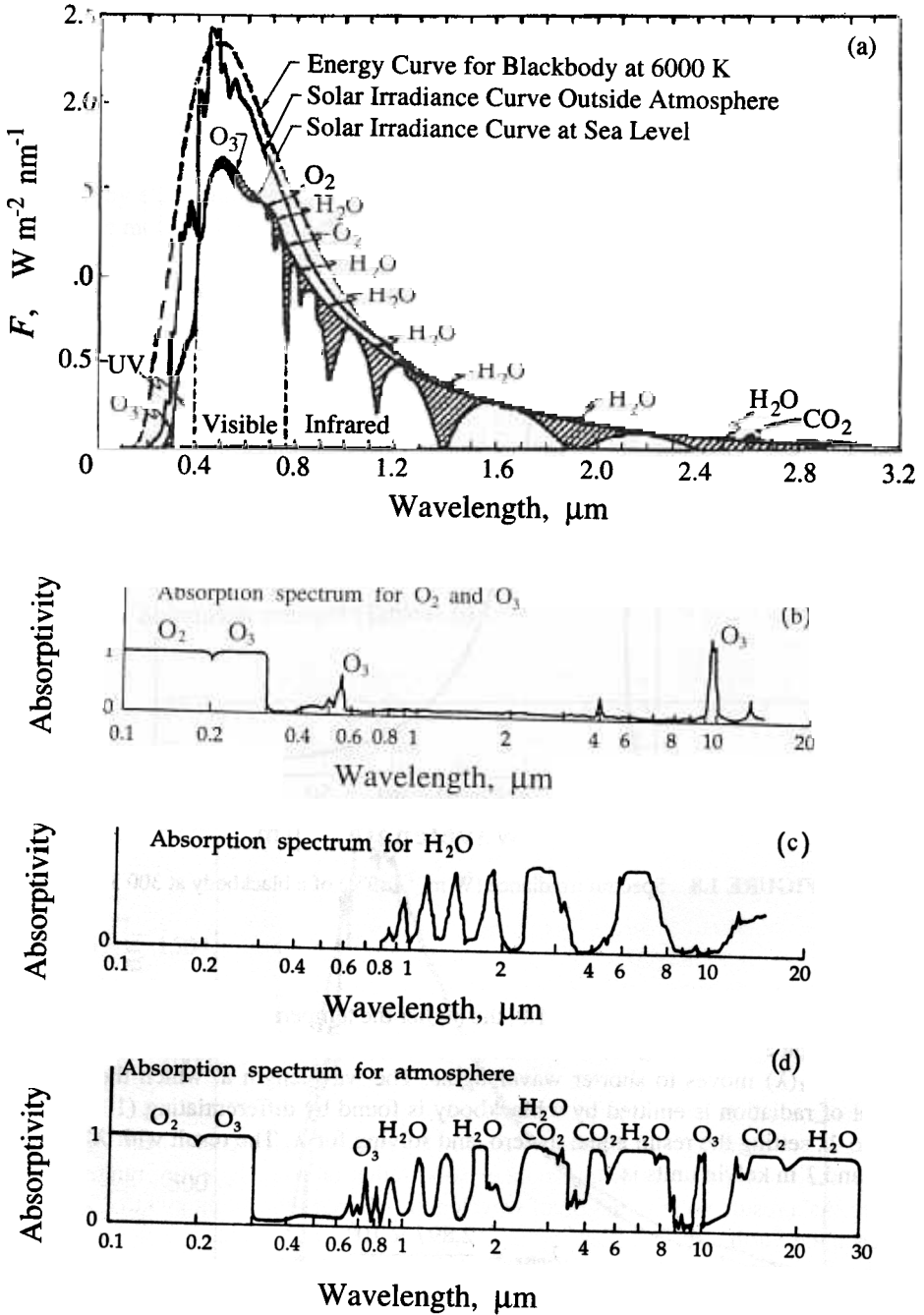


FIGURE 1.9 (a) Solar spectral irradiance at the top of the atmosphere and at sea level. Shaded regions indicate the molecules responsible for absorption. Absorption spectra for (b) molecular oxygen and ozone, (c) water vapor, and (d) the atmosphere, expressed on a scale of 0 to 1.

If (1.14) is integrated over all wavelengths, the total emissive power F_B (W m^{-2}) of a blackbody is found to be

$$F_B = \int_0^{\infty} F_B(\lambda) d\lambda = \sigma T^4 \quad (1.16)$$

where $\sigma = 5.671 \times 10^{-8} \text{ W m}^{-2} \text{ K}^{-4}$, the Stefan–Boltzmann constant.

1.9.2 Absorption of Radiation by Gases

Absorption of radiation by gases is one of the most important aspects of both global meteorology and atmospheric chemistry. The solar spectrum is radically altered by absorption as the radiation traverses the atmosphere. It is important to note that the molecules that are responsible for the most pronounced absorption of both solar and terrestrial radiation are the minor constituents of the atmosphere, not N_2 and O_2 . Thus ozone in the upper atmosphere effectively absorbs all solar radiation below 290 nm, whereas water vapor and carbon dioxide absorb much of the long-wave terrestrial radiation. The most significant absorbing gases in the atmosphere are O_2 , O_3 , H_2O , and CO_2 . Figure 1.9 shows the solar irradiance at the top of the atmosphere and that at sea level. The absorption spectra are quite complex, but they do indicate that absorption is so strong in some spectral regions that no solar energy in those regions reaches the surface of the Earth. For example, absorption by O_2 and O_3 is responsible for removal of practically all the incident radiation with wavelengths shorter than 290 nm. However, atmospheric absorption is not strong from 300 to about 800 nm, forming a “window” in the spectrum. About 40% of the solar energy is concentrated in the region of 400 to 700 nm. Water vapor absorbs in a complicated way, and mostly in the region where the Sun’s and Earth’s radiation overlap. From 300 to 800 nm, the atmosphere is essentially transparent. From 800 to 2000 nm, terrestrial long-wave radiation is moderately absorbed by water vapor in the atmosphere. Table 1.2 summarizes the attenuation of solar radiation by the atmosphere.

Figure 1.10 shows the penetration of radiation as a function of height in the atmosphere. Wavelengths shorter than about 100 nm are absorbed by O_2 and N_2 and do not penetrate below 100 km. O_2 absorbs strongly in the range 100 to 175 nm, the so-called Schumann–Runge continuum, and also in the range 175 to 200 nm, the Schumann–Runge bands. Wavelengths in the 200 to 245 nm range are absorbed in the stratosphere, mainly by O_2 (the weak Herzberg continuum). Wavelengths between 200 and 230 nm do penetrate as low as 30 km altitude. Ultraviolet absorption by ozone, which peaks near 254 nm (the Hartley band of O_3 absorption), attenuates solar radiation over the entire range of 230 to 300 nm. As a result, solar radiation of wavelengths shorter than about 290 to 300 nm does not reach the Earth’s surface.

Why molecules absorb in particular regions of the spectrum can be determined only through quantum chemical calculations. In general, the geometry of the molecule explains, for example, why H_2O , CO_2 , and O_3 interact strongly with radiation above 400 nm but N_2 and O_2 do not. In H_2O , for instance, the center of the negative charge is shifted toward the oxygen nucleus and the center of positive charge toward the hydrogen nuclei, leading to a separation between the centers of positive and negative charge, a so-called electric dipole moment. Molecules with dipole moments interact strongly with electromagnetic radiation

TABLE 1.2 Attenuation of Solar Radiation by the Atmosphere as a Function of Altitude

Wavelength Regions									Altitude	
0.12 to 0.20 μm	0.20 to 0.29 μm	0.29 to 0.32 μm	0.32 to 0.35 μm	0.35 to 0.55 μm	0.55 to 0.9 μm	0.9 to 2.5 μm	2.5 to 7 μm	7 to 20 μm		
O ₂ Absorbs almost completely			Solar irradiation intensity approximates extra-atmospheric; attenuation by scattering increases markedly toward shorter wavelengths.							Above 60 km
	0.20 to 0.21 μm absorption by O ₂ ; absorption by O ₃ appreciable	O ₃ absorption not important					Energy small	Energy very small	60 km to 33 km	
	No radiation penetrates below about 11 km	O ₃ absorption attenuates more than loss by scattering	O ₃ absorption significantly attenuates radiation	Irradiation diminished mostly by scattering by permanent gases in atmosphere	H ₂ O responsible for major absorption; CO ₂ absorbs slightly at 2 μm ; water vapor (or ice crystals) is found up to about 20 km			Strong O ₃ absorption at 9.6 μm ; strong CO ₂ absorption at 12–17 μm	33 km to 11 km	
			Highly variable aerosol responsible for attenuation in regions 0.32 to 0.7 μm		Energy transmitted with small loss down to 2 km		Energy penetrates to sea level only through “windows” at approximately 1.2, 1.6 and 2.2 μm	No significant penetration below 2 km except in “windows” at approximately 3.8 and 4.9 μm	11 km to 2 km	
		Appreciable penetration through “clear” atmosphere to sea level About 7% About 30%	Penetration through “clear” atmosphere to sea level about 40%	Dust scattering and absorption				Energy transmitted with moderate loss; many absorption bands due to atmospheric gases	2 km to sea level	

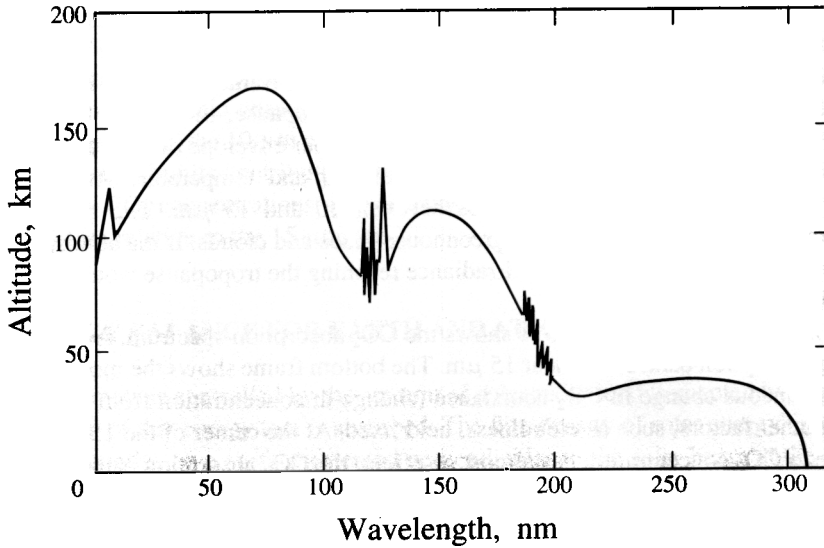


FIGURE 1.10 Depth of penetration of solar radiation through the atmosphere. Altitudes correspond to an attenuation of $1/e$ (Kluwer Academic Publishers *Aeronomy of the Middle Atmosphere*, 1984, Brasseur, G. and Solomon, S. with kind permission from Kluwer Academic Publishers).

because the electric field of the wave causes oppositely directed forces and therefore accelerations on electrons and nuclei at one end of the molecule as compared with the other. Similar arguments hold for ozone; however, nitrogen and oxygen are symmetric and thus are not strongly affected by radiation above 400 nm. The CO_2 molecule is linear but can easily be bent, leading to an induced dipole moment. A transverse vibrational mode exists for CO_2 at $15 \mu\text{m}$, just where the Earth emits most of its infrared radiation.

Considering the outgoing long-wave infrared radiation, the spectral region from about 7 to $13 \mu\text{m}$ is also a window region; nearly 80% of the radiation emitted by the Earth in this region escapes to space. Most of the non- CO_2 greenhouse gases, including O_3 , CH_4 , N_2O , and the chlorofluorocarbons, all have strong absorption bands in this window region. For this reason, relatively small changes in the concentrations of these gases can produce a significant change in the net radiative flux. As the concentration of a greenhouse gas continues to increase, it can absorb more of the radiation in its energy bands. Once an absorption wavelength becomes saturated, further increases in the concentration of the gas have less and less effect on radiative flux. This is called the band saturation effect. For CO_2 , for example, the $15 \mu\text{m}$ band is already close to saturated. In addition, if a gas absorbs at wavelengths that are also absorbed by other gases, then the effect of increasing concentrations on radiative flux is less than in the absence of band overlap. For example, there is significant overlap between some of the absorption bands of CH_4 and N_2O ; this overlap must be carefully accounted for when calculating the effect of these gases on radiative fluxes.

Even with the band saturation effect, it is incorrect to conclude that because there is already so much CO_2 in the atmosphere, more CO_2 can have no additional effect on absorption of outgoing radiation. When gases are present in small concentrations, doubling the concentration of the gas will approximately double its absorption. When an absorbing gas is present in high concentration the effect of further addition is not one-to-one but it is not

zero either. For example, doubling the concentration of CO_2 from its present-day value leads to a 10 to 20% increase in its total greenhouse effect (IPCC, 1995). Where this increase comes from can be explained as follows. The top frame of Figure 1.11 shows the spectral variation in the infrared radiance at the tropopause, in $\text{W m}^{-2} (\text{cm}^{-1})^{-1}$. The Planck function (1.14) determines the shape of the upper envelope of the curve, the maximum energy that can be emitted at a given wavelength and temperature. At typical atmospheric temperatures the maximum lies between 10 and 15 μm . The notches in the spectrum result from the presence of greenhouse gases and clouds. If the atmosphere were transparent to infrared radiation, the irradiance reaching the tropopause would be the same as that leaving the surface.

The middle frame of Figure 1.11 shows the CO_2 absorption spectrum. As noted earlier, a strong absorption band exists near 15 μm . The bottom frame shows the modeled effect of an instantaneous change in CO_2 abundance (change in concentration from 1980 to 1990) with all other factors, such as cloudiness, held fixed. At the center of the 15 μm band, the increase in CO_2 concentration has almost no effect; the CO_2 absorption is indeed saturated

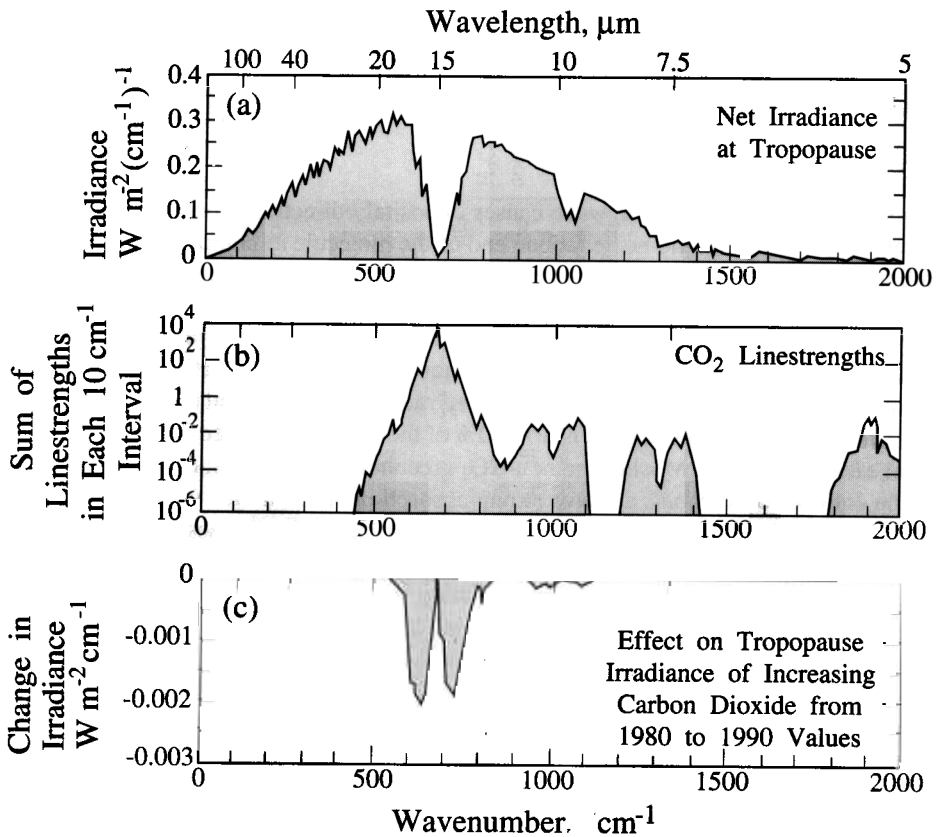


FIGURE 1.11 Effect of CO_2 : (a) net infrared irradiance ($\text{W m}^{-2} (\text{cm}^{-1})^{-1}$) at the tropopause; (b) representation of the strength of the spectral lines of CO_2 in the thermal infrared (note the logarithmic scale); and (c) change in net irradiance at the tropopause as a result of increasing the CO_2 concentration from its 1980 to 1990 levels, holding all other parameters fixed (IPCC, 1995).

in this portion of the spectrum. Away from this band, however, where CO_2 is less strongly absorbing, the increase in CO_2 does have an effect. As more and more CO_2 is added to the atmosphere, more of its spectrum will become saturated, but there will always be regions of the spectrum that remain unsaturated and thus capable of continuing to absorb infrared radiation. For example, the $10\ \mu\text{m}$ absorption band is about 10^6 times weaker than the peak of the $15\ \mu\text{m}$ band, but its contribution to the irradiance change in the lower frame is important. And as CO_2 concentrations increase, the importance of the $10\ \mu\text{m}$ band will continue to increase relative to the $15\ \mu\text{m}$ band.

1.10 ENERGY BALANCE FOR EARTH AND ATMOSPHERE

The Earth's climate is controlled by the amount of solar radiation intercepted by the planet and the fraction of that energy that is absorbed. The flux density of solar energy, integrated over all wavelengths, on a surface oriented perpendicular to the solar beam at the Earth's orbit is about $1370\ \text{W m}^{-2}$. This is called the *solar constant*.³ Let the solar constant be denoted by $S_0 = 1370\ \text{W m}^{-2}$. The cross-sectional area of the Earth that intercepts the solar beam is πR^2 , where R is the Earth's radius. The surface area of the Earth that receives the radiation is $4\pi R^2$. Thus the fraction of the solar constant received per unit area of the Earth is $(\pi R^2/4\pi R^2) = 1/4$ of the solar constant, about $343\ \text{W m}^{-2}$. Of this incoming solar radiation, a fraction is reflected back to space; that fraction, which we can denote by R_p , is the global mean planetary reflectance or *albedo*. R_p is about 0.3 (Ramanathan, 1987; Ramanathan et al., 1989). Contributing to R_p are clouds, scattering by air molecules, scattering by atmospheric aerosol particles, and reflection from the surface itself, the surface albedo (the surface albedo is denoted as R_s). The fraction $1 - R_p$ represents that fraction of solar short-wave radiation that is absorbed by the Earth-atmosphere system. For $R_p = 0.3$, this corresponds to about $240\ \text{W m}^{-2}$. This amount is matched, on an annual and global average basis, by the long-wave infrared radiation emitted from the Earth-atmosphere system to space (Figure 1.12). The infrared radiative flux emitted at the surface of the Earth, about $390\ \text{W m}^{-2}$, substantially exceeds the outgoing infrared flux of $240\ \text{W m}^{-2}$ at the top of the atmosphere. Clouds, water vapor, and the greenhouse gases (GHGs) both absorb and emit infrared radiation. Since these atmospheric constituents are at temperatures lower than that at the Earth's surface, they emit infrared radiation at a lower intensity than if they were at the temperature of the Earth's surface and therefore are net absorbers of energy.

The equilibrium temperature of the Earth can be estimated by a simple model that equates incoming and outgoing energy (Figure 1.13). Incoming solar energy at the surface of the Earth is

$$F_S = \frac{S_0}{4}(1 - R_p) \quad (1.17)$$

³Since the late 1970s, regular satellite measurements of the solar constant have been performed (Mecherikunnel et al., 1988). Maximum differences in the value of S_0 among the instruments is about $2\ \text{W m}^{-2}$, corresponding to a little more than 0.1% of the value of S_0 . Over the period 1980 to 1986 the so-called SMM/ACRIM instrument measured an average value of S_0 of about $1386\ \text{W m}^{-2}$, whereas that on NIMBUS-7 reported an average S_0 of about $1370\ \text{W m}^{-2}$.

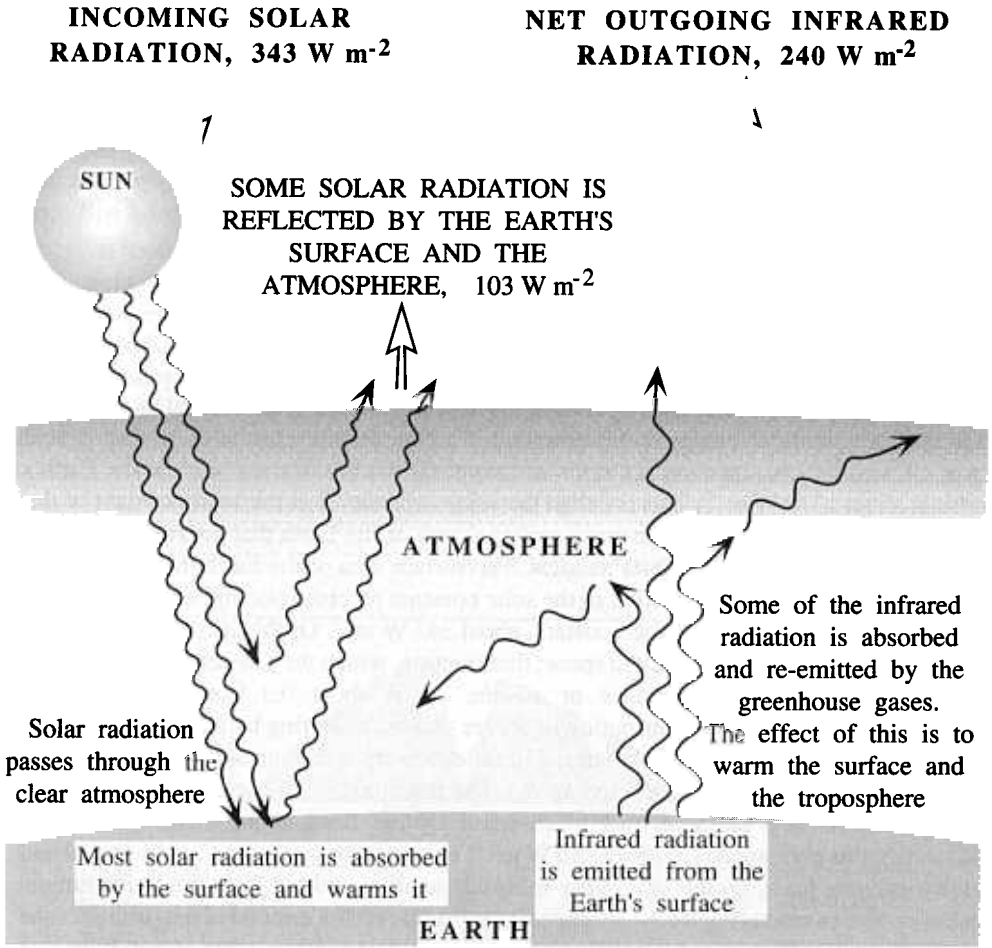


FIGURE 1.12 Earth's overall energy balance (IPCC, 1995). Net input of solar radiation ($\sim 240 \text{ W m}^{-2}$) must be balanced by net output of infrared radiation. About one-third ($\sim 103 \text{ W m}^{-2}$) of incoming solar radiation is reflected and the remainder is mostly absorbed by the surface.

For an average blackbody temperature of the Earth–atmosphere system, T_e , defined on the basis of (1.16), the long-wave emitted flux averaged over the globe is

$$F_L = \sigma T_e^4 \tag{1.18}$$

Equating F_S and F_L yields the following expression for T_e ,

$$T_e = \left(\frac{(1 - R_p) S_0}{4\sigma} \right)^{1/4} \tag{1.19}$$

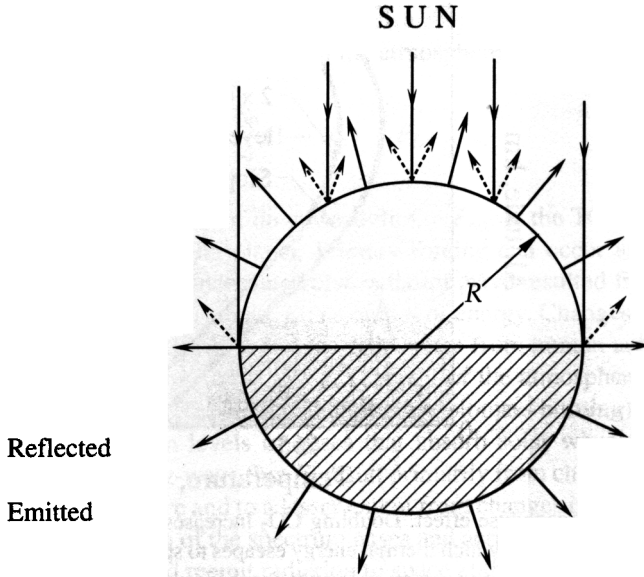


FIGURE 1.13 Global radiative equilibrium.

For $R_p = 0.30$, this equation gives $T_e \approx 255$ K. If the Earth were totally devoid of clouds, then the global albedo would be about $R_p = 0.15$. With this value of R_p , the equilibrium temperature $T_e = 268$ K. This simple equation predicts that T_e varies about 0.5 K for a 10 W m^{-2} (0.7%) variation in the solar constant, or for a reflectance variation around $R_p = 0.3$ of $\Delta R_p = 0.005$.

The net radiative energy input, $F_{\text{net}} = F_S - F_L$, is zero at equilibrium. If a perturbation occurs then the change in net energy input is related to the changes in both solar and long-wave components by

$$= \Delta F_S - \Delta F_L \quad (1.20)$$

To reestablish equilibrium, a temperature change ΔT_e results, which can be related to ΔF_{net} by a parameter λ_0 ,

$$\Delta T_e = \lambda_0 \Delta F_{\text{net}} \quad (1.21)$$

where λ_0 , having units $\text{K (W m}^{-2})^{-1}$ is called the *climate sensitivity factor*. If we neglect any feedbacks in the climate system, λ_0 can be estimated as $(\partial F_e / \partial T_e)^{-1}$,

$$\lambda_0 = \frac{T_e}{4\sigma T_e^3} = \frac{T_e}{4F_L} \quad (1.22)$$

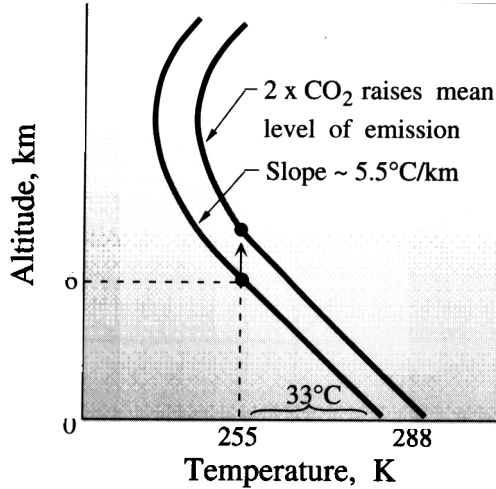


FIGURE 1.14 Greenhouse effect. Doubling CO_2 increases infrared absorption, raising by about 200 m the mean level from which thermal energy escapes to space. Because it is colder, the higher up one goes in the troposphere, the energy emitted to space is temporarily reduced and the Earth radiates less energy than it absorbs. The surface temperature must rise by 1.2 K to restore the energy balance, if the temperature gradient and other factors are held constant.

and $\lambda_0 \simeq 0.3 \text{ K (W m}^{-2}\text{)}^{-1}$. A doubling of the CO_2 abundance from the preindustrial level is estimated to produce $\Delta F_L = 4.6 \text{ W m}^{-2}$. With $\lambda_0 = 0.3 \text{ K (W m}^{-2}\text{)}^{-1}$, this would lead to an increase in the global mean temperature of $\Delta T_e = 1.4 \text{ K}$. This temperature increase is less than what climate models predict because of feedbacks that act to enhance warming. As noted earlier, such feedbacks include, for example, the fact that a warmer atmosphere contains more water vapor, and hence an enhanced infrared absorption.

The mean emitted power of the Earth–atmosphere system, 240 W m^{-2} , corresponds to a blackbody temperature of 255 K. The surface emission, 390 W m^{-2} , corresponds to a blackbody temperature of 288 K. The 33 K difference between the blackbody temperatures of the Earth’s surface and the Earth–atmosphere system is the so-called greenhouse effect. Increases in concentrations of CO_2 and other GHGs since the Industrial Revolution are estimated to have contributed about $+2.5 \text{ W m}^{-2}$ to the global and annual average radiation balance (IPCC, 1995).

Figure 1.14 shows another way to view the greenhouse effect. The mean atmospheric temperature profile is shown starting from the current mean surface temperature of 288 K. If we assume a global average rate of decrease of temperature with height of 5.5 K km^{-1} , the temperature of 255 K, the blackbody temperature corresponding to the mean emitted power of the Earth–atmosphere system, is reached at about 6 km altitude. A doubling of CO_2 from the preindustrial level diminishes the mean emitted power of the Earth–atmosphere system. The result is that the mean altitude from which thermal energy escapes to space rises by about 200 m. Because it is colder 200 m higher, the energy emitted to space is temporarily reduced and the Earth radiates less energy than it absorbs. The surface temperature must rise by 1.2 K to restore the energy balance, if the vertical temperature gradient and other factors are held fixed.

Global climate change is induced by a forcing that disturbs the equilibrium and leads to a nonzero average downward net flux at the top of the atmosphere (TOA),

$$-F_{\text{net}} = \frac{S_0}{4}(1 - R_p) - F_L \quad (1.23)$$

It is customary to write (1.23) in terms of downward flux, $-F_{\text{net}}$, at the TOA; an increase of $-F_{\text{net}}$ corresponds to heating of the planet. Primary forcing can occur as a result of changes of S_0 , R_p , or F_L . Changes in incoming solar radiation have resulted from changes in the Earth's orbit and from variations in the Sun's output of energy. Changes in the planetary albedo R_p can result from changes in surface reflectance from human activity (agriculture, deforestation), from changes in the aerosol content of the atmosphere from both natural (volcanoes) and anthropogenic (industrial emissions, biomass burning) causes, and to a lesser extent from changes in levels of gases that absorb solar wavelengths (e.g., ozone). Changes in the emitted long-wave flux F_L result primarily from changes (increases) of absorbing gases in the atmosphere and to a lesser extent from changes in aerosols. As we have seen, in the long-wave portion of the spectrum gases and aerosols absorb much of the radiation emitted by the surface and reemit radiation to space at their lower temperature.

1.10.1 Solar Variability

The amount of solar radiation reaching Earth and Earth's changing orientation to the Sun have been the major causes for climatic change throughout its history. If the Sun's radiation intensity declined 5 to 10% and there were no other compensating factors, ice would engulf the planet in less than a century. Although no theory exists to predict future changes in solar output, the effect of changes in Earth's orbit as it travels around the Sun is beginning to be understood. During the past million years, Earth has experienced 10 major and 40 minor episodes of glaciation. All appear to have been controlled by three so-called orbital elements that vary cyclically over time.

First, Earth's tilt changes from 22° to 24.5° and back again every 41,000 years. Second, the month when Earth is closest to the Sun also varies over cycles of 19,000 and 24,000 years. Currently, Earth is closest to the Sun in January. This month-of-closest-approach factor can make a difference of 10% in the amount of solar radiation reaching a particular location in a given season. Last, the shape of Earth's orbit varies from being nearly circular to being more elliptical with a period of 100,000 years. The climatic cycles caused by these orbital factors are called Milankovitch cycles after the Serbian mathematician Milutin Milankovitch, who first described them in 1920. Superimposed on the Milankovitch cycles are changes in the Sun that occur over days or months or a few years. Over the period 1979 to 1990, for example, total solar irradiance varied by about 0.1% (Hickey et al., 1988; Willson and Hudson, 1988).

Even though studies of ocean cores have shown that these orbital changes are the principal determinant of the times of glaciation, the exact mechanisms by which Earth responds to the orbital changes have not been established. Orbital changes alone appear not to have caused the vast climate shifts associated with glaciation and deglaciation. Feedbacks, such as changes in Earth's reflectivity, amount of particles in the atmosphere, and the carbon dioxide and methane content of the atmosphere, act together with orbital changes to enhance global warming and cooling. The levels of carbon dioxide and

methane, as shown in ice core measurements, decrease during times of glaciation and increase during warming periods, although it is not known exactly how or why their concentrations rise and fall.

The radiative forcing resulting from changing solar output can be obtained by multiplying the change in total solar irradiance by $(1 - R_p)/4$, where R_p is the Earth's albedo. For $R_p = 0.3$, $(1 - R_p)/4 = 0.175$. A 0.1% change in total solar irradiance (1.4 W m^{-2}) would be equivalent to a radiative forcing of about 0.2 W m^{-2} .

1.10.2 Earth's Energy Balance

The solar flux impinging on the Earth-atmosphere system, averaged over a year, can be represented as 100 units. (Based on a solar constant of 1370 W m^{-2} , the average solar flux at the top of the atmosphere is $\sim 343 \text{ W m}^{-2}$.) Figure 1.15 depicts the Earth's energy balance and contains three types of processes: the solar flux, the infrared or long-wave flux

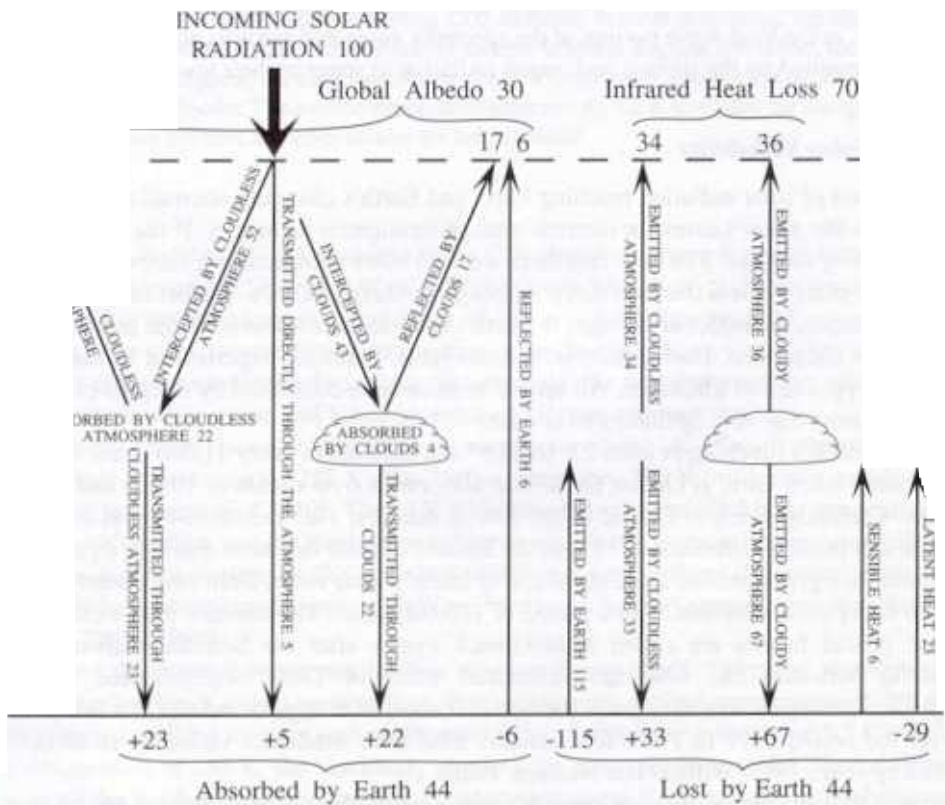


FIGURE 1.15 Energy balance of the Earth-atmosphere system. Incoming solar energy is taken to be 100 units, which must be balanced by reflected solar energy and thermal infrared heat loss. At the surface, the energy balance involves sensible and latent heat components. From *Radiation and Cloud Processes in the Atmosphere: Theory, Observation and Modeling* by Kuo-Nan Liou. Copyright © 1992 by Oxford University Press, Inc. Used by permission of Oxford University Press, Inc.

from the Earth, and nonradiative processes. Of the 100 units of incoming solar flux:

~26 units are absorbed within the atmosphere (~22 by cloud-free air and ~4 by clouds)

~30 units are reflected back to space⁴ (~7 from the cloud-free atmosphere, ~17 from the cloudy atmosphere, and ~6 from the Earth's surface)

~44 units absorbed by the Earth's surface

The Earth-atmosphere system emits thermal infrared radiation. The upward flux from the Earth's surface is ~115 units. The cloud-free atmosphere emits ~33 units back to the Earth's surface and ~34 units out to space. The cloudy atmosphere emits ~67 units back to Earth and ~36 units out to space. Thus ~70 units of infrared radiation leave the top of the atmosphere, balancing the net ~70 units of solar radiation penetrating the top of the atmosphere. The net upward flux of infrared radiation at the surface of the Earth is ~15 units, consisting of ~115 units emitted by the Earth and ~100 units radiated back to Earth by the cloud-free and cloudy atmosphere.

The incoming solar energy absorbed by the Earth is ~44 units; this is balanced by the net upward flux of infrared radiation of ~15 units, plus ~6 unit loss by sensible heat conduction, and ~23 unit loss by latent heat. The Earth emits ~115 units of infrared radiation to the atmosphere, whereas the atmosphere emits ~170 units of infrared radiation, a net deficit of ~55 units. Since the atmosphere absorbs ~26 units of solar radiation, the net radiative loss from the atmosphere is ~29 units; this is made up for by the sensible and latent heat fluxes. The net radiative cooling of the atmosphere is thus balanced by the latent heat of condensation released in precipitation processes and by the convection and conduction of sensible heat from the surface.

The average annual ratio of sensible to latent heat loss at the surface is called the Bowen ratio. With ~6 units of sensible heat loss and ~23 units of latent heat loss, the Bowen ratio is ~0.27.

Figure 1.16 shows the zonally annual averaged absorbed solar and emitted infrared fluxes, as observed from satellites. We note a net gain of radiative energy between about 40° N and 40° S, and a net loss of energy in the polar regions. This pattern results largely from the decrease in insolation to the polar regions in winter and from the high surface albedo in the polar regions. The outgoing infrared flux displays only a small latitudinal dependence. The tendency for the outgoing infrared flux to be greatest in the tropics where the surface temperature is largest is muted by the larger amount of atmospheric water vapor and the higher and colder clouds in the tropics. As a result of the net gain of radiative energy in the tropics and the net loss in the polar regions, an equator-to-pole temperature gradient is generated.

⁴The average value of the albedo, the incoming radiation that is reflected or scattered back to space without absorption, is usually taken to be somewhere in the range of 30 to 34%. It is important to note that the albedo varies considerably, depending on the surface of the Earth. For example, in the polar regions, which are covered by ice and snow, the reflectivity of the surface is very high. On the other hand, in the equatorial regions, which are largely covered with oceans, the reflectivity is low, and most of the incoming energy is absorbed by the surface.

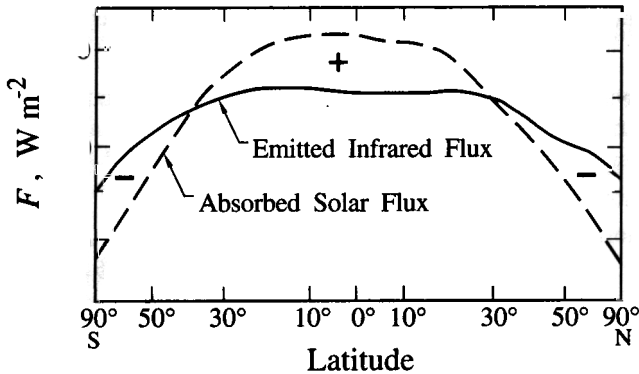


FIGURE 1.16 Zonally averaged components of the absorbed solar flux and emitted thermal infrared flux at the top of the atmosphere. The + and - signs denote energy gain and loss, respectively. From *Radiation and Cloud Processes in the Atmosphere: Theory, Observation and Modeling* by Kuo-Nan Liou. Copyright © 1992 by Oxford University Press, Inc. Used by permission of Oxford University Press, Inc.

As we discussed earlier, in the equatorial region, warm air expands upward and creates a poleward pressure gradient force at the upper altitudes, where air flows poleward from the equator. This air, as it moves poleward, cools and sinks in the subtropical high-pressure belts ($\sim 30^\circ$) and returns to the equator at the surface. This thermally driven circulation between the equator and the subtropics is referred to as the *Hadley cell*. In the polar regions, a similar thermally driven circulation occurs. An airflow exists at upper levels toward the equator and at lower levels toward the poles, producing a Hadley circulation between the poles and the subpolar low-pressure regions.

The large-scale circulation of the atmosphere results in a substantial transport of sensible and latent heat. The transport of latent heat by atmospheric circulation is coupled to the hydrologic cycle. Since the total water mass is conserved, total annual precipitation must be balanced by the total annual evaporation over the globe. There are, however, large imbalances in localized regions. In the subtropical belts of both hemispheres there is an excess of evaporation over precipitation. In the equatorial belt and at latitudes above 40° , precipitation exceeds evaporation. Thus the subtropical belts serve as source regions for water vapor, whereas equatorial regions and high-latitude areas are sinks for moisture in the atmosphere, resulting in the transport of latent heat.

1.11 SPATIAL AND TEMPORAL SCALES OF ATMOSPHERIC PROCESSES

The atmosphere can be likened to an enormous chemical reactor in which a myriad of species are continually being introduced and removed over a vast array of spatial and temporal scales. The atmosphere itself presents a range of spatial scales in its motions that spans eight orders of magnitude (Figure 1.17). The scales of motion in the atmosphere vary from tiny eddies of a centimeter or less in size to huge air mass movements of continental

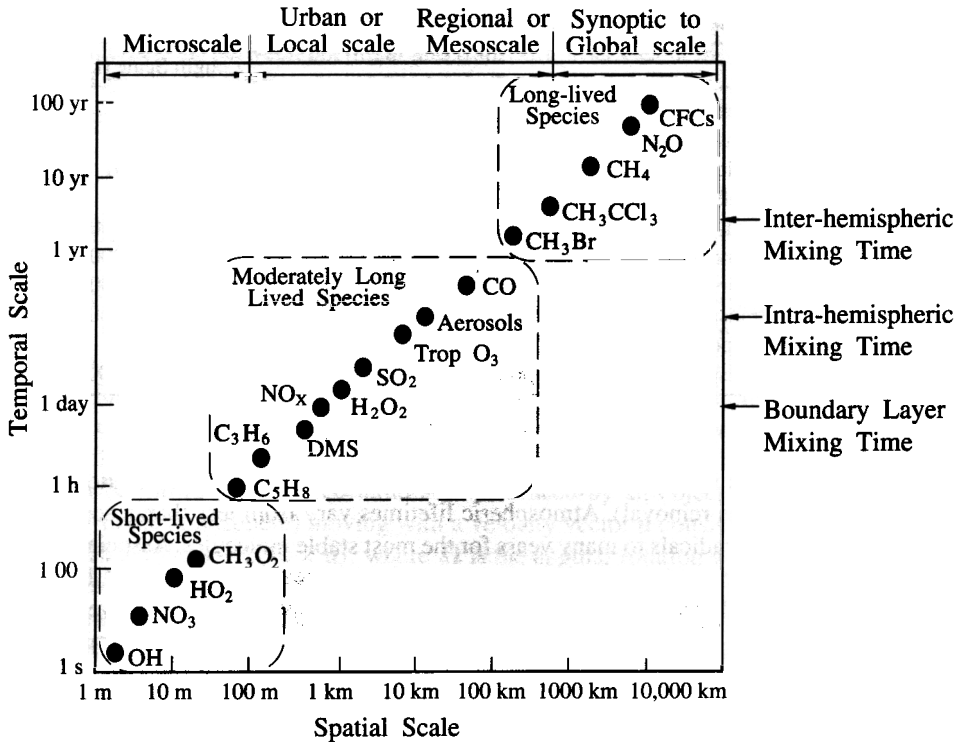


FIGURE 1.17 Spatial and temporal scales of variability for atmospheric constituents.

dimensions. Four rough categories have proved convenient to classify atmospheric scales of motion:

1. *Microscale*. Phenomena occurring on scales of the order of 0 to 100 m, such as the meandering and dispersion of a chimney plume and the complicated flow regime in the wake of a large building.
2. *Mesoscale*. Phenomena occurring on scales of tens to hundreds of kilometers, such as land-sea breezes, mountain-valley winds, and migratory high- and low-pressure fronts.
3. *Synoptic Scale*. Motions of whole weather systems, on scales of hundreds to thousands of kilometers.
4. *Global Scale*. Phenomena occurring on scales exceeding 5×10^3 km.

Spatial scales characteristic of various atmospheric chemical phenomena are given in Table 1.3. Many of the phenomena in Table 1.3 overlap; for example, there is more or less of a continuum between (1) urban and regional air pollution, (2) the aerosol haze associated with regional air pollution and aerosol/climate interactions, (3) greenhouse gas increases and stratospheric ozone depletion, and (4) tropospheric oxidative capacity and stratospheric ozone depletion. The lifetime of a species is the average time that a molecule

Phenomenon	Length Scale (km)
Urban air pollution	1–100
Regional air pollution	10–1000
Acid rain/deposition	100–2000
Toxic air pollutants	0.1–100
Stratospheric ozone depletion	1000–40,000
Greenhouse gas increases	1000–40,000
Aerosol–climate interactions	100–40,000
Tropospheric transport and oxidation processes	1–40,000
Stratospheric–tropospheric exchange	0.1–100
Stratospheric transport and oxidation processes	1–40,000

of that species resides in the atmosphere before removal (chemical transformation to another species counts as removal). Atmospheric lifetimes vary from less than a second for the most reactive free radicals to many years for the most stable molecules. Associated with each species is a characteristic spatial transport scale; species with very short lifetimes have comparably small characteristic spatial scales while those with lifetimes of years have a characteristic spatial scale equal to that of the entire atmosphere. With a lifetime of less than 0.01 s, the hydroxyl radical (OH) has a spatial transport scale of only about 1 cm. Methane (CH₄), on the other hand, with its lifetime of about 10 years, can become more or less uniformly mixed over the entire Earth.

The spatial scales of the various atmospheric chemical phenomena shown above result from an intricate coupling between the chemical lifetimes of the principal species and the

Gas	Urban	Acid Deposition	Visibility Impairment	Greenhouse Effect	Stratospheric O ₃ Depletion	Decreased Self-Cleaning of Atmosphere (Decreases OH)
	Air Pollution					(Decreases OH)
CO ₂					+/-	
CH ₄					+/-	+/-
CO						+
N ₂ O					+/-	
NO _x (NO + NO ₂)						
SO ₂						
CFCs				+		
O ₃				+		

*Plus signs indicate a contribution to the effect; minus signs indicate amelioration. Dual signs (+/-) indicate that the effect of the gas can vary. For example, CO₂, N₂O, and NO_x can either enhance or deplete stratospheric O₃ depending on altitude. CH₄ generally ameliorates stratospheric O₃ depletion, except in the polar ozone hole. The tendency of CH₄ to diminish the self-cleaning of the atmosphere by reducing OH abundance is different in the Northern (NH) and Southern Hemispheres (SH); CH₄ diminishes self-cleaning in the SH but has the opposite effect in the NH.

Source: Graedel and Crutzen (1989).

atmosphere's scales of motion. Much of this book will be devoted to understanding the exquisite interactions between chemical and transport processes in the atmosphere. In anticipation of much of the remainder of this book, Table 1.4 summarizes atmospheric effects of trace gases.

APPENDIX 1 DERIVATION OF THE GEOSTROPHIC WIND SPEED

The direction of winds in the geostrophic layer is determined by horizontal pressure gradients and Coriolis forces. As we have discussed, an air parcel moving southward in the Northern Hemisphere as a result of pressure gradients is accelerated toward the west by the Coriolis force. We can actually compute the wind speed and direction at any latitude as a function of the prevailing pressure gradient if we assume that only pressure and Coriolis forces influence the flow.

It can be shown that the acceleration experienced by an object on the surface of the Earth (or in the atmosphere) moving with a velocity vector \mathbf{u} consists of two components, $-\boldsymbol{\Omega} \times (\boldsymbol{\Omega} \times \mathbf{r})$ and $-2(\boldsymbol{\Omega} \times \mathbf{u})$, where $\boldsymbol{\Omega}$ is the angular rotation vector for the Earth and \mathbf{r} is the radius vector from the center of the Earth to the point in question. The first term is simply the centrifugal force, in a direction that acts normal to the Earth's surface and is counterbalanced by gravity. The second term, $\boldsymbol{\Omega} \times \mathbf{u}$, is the Coriolis force. This force arises only when an object, such as an air parcel, is moving; that is $\mathbf{u} \neq 0$. Even though the Coriolis force is of much smaller magnitude than the centrifugal force, only the Coriolis force has a horizontal component. Since the winds are horizontal in the geostrophic layer, the Coriolis acceleration is given by the horizontal component of the Coriolis term, namely, $2u_G\Omega \sin \phi$, where Ω is the rate of rotation of the Earth and ϕ is the latitude. The direction of the Coriolis force is perpendicular to the wind velocity, as shown in Figure 1.A.1. Wind speed u_G at latitude ϕ lies in the horizontal plane.

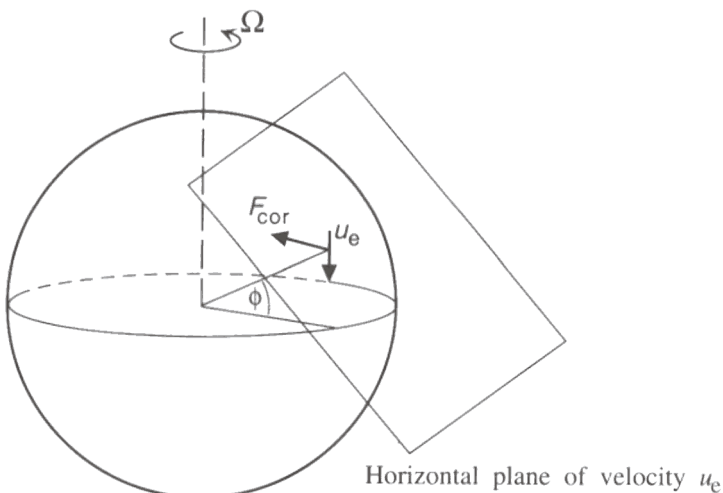


FIGURE 1.A.1 Direction of the Coriolis force in the Northern Hemisphere.

In the geostrophic layer it may be assumed that the atmosphere is inviscid (frictionless) and in laminar flow. The equations of continuity and motion for such a fluid are

$$\frac{\partial u}{\partial x} + \frac{\partial v}{\partial y} + \frac{\partial w}{\partial z} = 0 \tag{1.A.1}$$

and

$$\begin{aligned} \frac{\partial u}{\partial t} + u \frac{\partial u}{\partial x} + v \frac{\partial u}{\partial y} + w \frac{\partial u}{\partial z} &= -\frac{1}{\rho} \frac{\partial p}{\partial x} + F_x \\ \frac{\partial v}{\partial t} + u \frac{\partial v}{\partial x} + v \frac{\partial v}{\partial y} + w \frac{\partial v}{\partial z} &= -\frac{1}{\rho} \frac{\partial p}{\partial y} + F_y \\ \frac{\partial w}{\partial t} + u \frac{\partial w}{\partial x} + v \frac{\partial w}{\partial y} + w \frac{\partial w}{\partial z} &= -\frac{1}{\rho} \frac{\partial p}{\partial z} + F_z \end{aligned} \tag{1.A.2}$$

where u , v , and w are the three components of the velocity and F_x , F_y , and F_z are the three components of the external force.

Let the axes be fixed in the Earth, with the x axis horizontal and extending to the east, the y axis horizontal and extending to the north, and the z axis normal to the Earth's surface. As before, Ω is the angular velocity of rotation of the Earth and ϕ the latitude. The components of the Coriolis force in the x , y , and z directions on a particle are the components of $\mathbf{F}_c = -2(\boldsymbol{\Omega} \times \mathbf{u})$:

$$\begin{aligned} F_{cx} &= -2\Omega(w \cos \phi - v \sin \phi) \\ F_{cy} &= -2\Omega u \sin \phi \\ F_{cz} &= 2\Omega u \cos \phi \end{aligned} \tag{1.A.3}$$

At great heights, the vertical velocity component w can usually be neglected relative to the horizontal components u and v . Therefore, substituting (1.A.3) into (1.A.2), we obtain, for steady motion

$$\begin{aligned} u \frac{\partial u}{\partial x} + v \frac{\partial u}{\partial y} &= 2\Omega v \sin \phi - \frac{1}{\rho} \frac{\partial p}{\partial x} \\ u \frac{\partial v}{\partial x} + v \frac{\partial v}{\partial y} &= -2\Omega u \sin \phi - \frac{1}{\rho} \frac{\partial p}{\partial y} \end{aligned} \tag{1.A.4}$$

We see that the air moves so that a balance is achieved between the pressure gradient and the Coriolis force. Let us consider the situation in which the velocity vector is oriented in the x direction, and so $v = 0$; then

$$u \frac{\partial u}{\partial x} = -\frac{1}{\rho} \frac{\partial p}{\partial x} \tag{1.A.5}$$

$$0 = -2\Omega u \sin \phi - \frac{1}{\rho} \frac{\partial p}{\partial y} \tag{1.A.6}$$

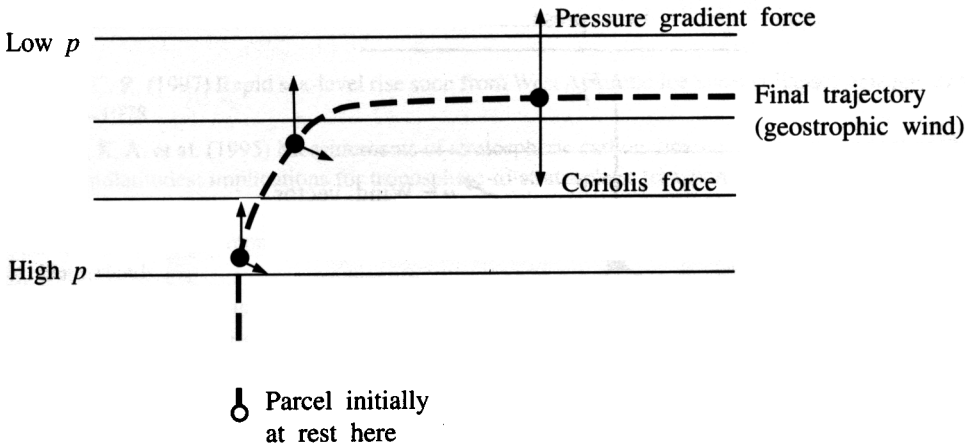


FIGURE 1.A.2 Approach to geostrophic equilibrium.

We usually denote $2\Omega \sin \phi$ by f , called the Coriolis parameter. From the continuity equation (1.A.1), we see that $\partial u / \partial x = 0$, since $v = w = 0$. Thus from (1.A.5) $\partial p / \partial x = 0$, and the direction of flow is perpendicular to the pressure gradient $\partial p / \partial y$. In addition, from (1.A.6), we see that the component of the Coriolis force, $-fu$, is exactly balanced by the pressure gradient, $(1/\rho) \partial p / \partial y$. Therefore the *geostrophic wind speed* u_G is given by

$$u_G = \frac{\partial p / \partial y}{2\rho\Omega \sin \phi} \quad (1.A.7)$$

The approach to the geostrophic equilibrium for an air parcel starting from rest, accelerated by the pressure gradient and then affected by the Coriolis force, is shown in Figure 1.A.2.

The geostrophic balance determines the wind direction at altitudes above about 500 m. In order to describe the air motions at lower levels we must take into account the friction of the Earth's surface. The presence of the surface induces a shear in the wind profile, as in a turbulent boundary layer over a flat plate generated in a laboratory wind tunnel. In analyzing the geostrophic wind speed we found that for steady flow a balance exists between the pressure force and the Coriolis force. Consequently, steady flow of air at levels near the ground leads to a balance of three forces: pressure force, Coriolis force, and friction force due to the Earth's surface. Thus, as shown in Figure 1.A.3, the net result of these three forces must be zero for a nonaccelerating air parcel. Since the pressure gradient force F_p must be directed from high to low pressure, and the frictional force F_f must be directed opposite to the velocity u , a balance can be achieved only if the wind is directed at some angle toward the region of low pressure. This angle between the wind direction and the isobars increases as the ground is approached since the frictional force increases. At the ground, over open terrain, the angle of the wind to the isobars is usually between 10° and 20° . Because of the relatively smooth boundary existing over this type of terrain, the wind speed at a 10 m height (the height at which the so-called surface wind is usually measured)

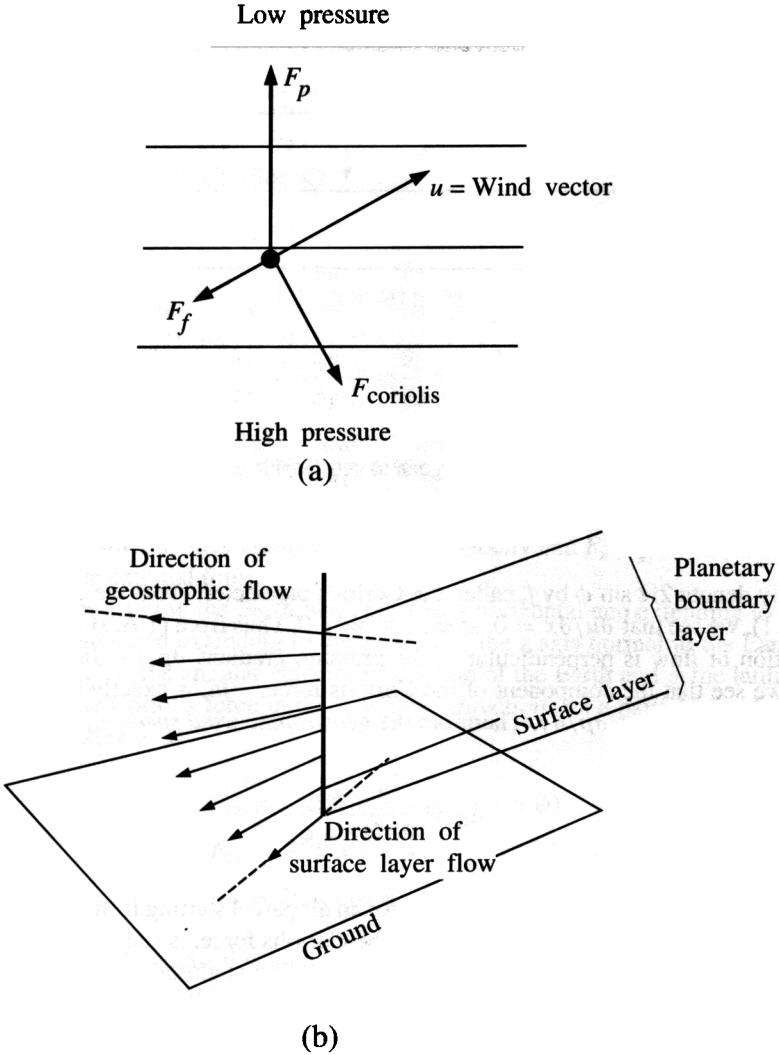


FIGURE 1.A.3 Variation of wind direction with altitude. (a) Balance of forces among pressure gradient, Coriolis force, and friction. (b) The Ekman spiral.

is already almost 90% of the geostrophic wind speed. Over built-up areas, on the other hand, the speed at a 10 m height may be only 50% of the geostrophic wind speed, owing to the mixing induced by the surface roughness. In this case the surface wind may be at an angle of 45° to the isobars.

As a result of these frictional effects, the wind direction commonly turns with height, as shown in Figure 1.A.3b. The variation of wind direction with altitude is known as the *Ekman spiral*. We defer a derivation of the Ekman spiral until Problem 16.2, when we have had the opportunity to discuss turbulent transport of momentum.

REFERENCES

- Bentley, C. R. (1997) Rapid sea-level rise soon from West Antarctic Ice Sheet collapse? *Science*, **275**, 1077–1078.
- Boering, K. A. et al. (1995) Measurements of stratospheric carbon dioxide and water vapor at northern midlatitudes: implications for troposphere-to-stratosphere transport, *Geophys. Res. Lett.*, **22**, 2737–2740.
- Brasseur, G., and Solomon, S. (1984) *Aeronomy of the Middle Atmosphere*. Reidel, Dordrecht, The Netherlands.
- Cloud, P. (1983). The biosphere. *Sci. Am.*, **249**, 176–189.
- Graedel, T. E., and Crutzen, P. J. (1989) The changing atmosphere, *Sci. Am.*, **261**, 58–68.
- Hickey, J. R., Alton, B. M., Kyle, H. L., and Hoyt, D. (1988) Total solar irradiance measurements by ERB/Nimbus-7: a review of nine years, *Space Sci. Rev.*, **48**, 321–342.
- Holton, J. R., Haynes, P. H., McIntyre, M. E., Douglass, A. R., Rood, R. B., and Pfister, L. (1995) Stratosphere–troposphere exchange, *Rev. Geophys.*, **33**, 403–439.
- Intergovernmental Panel on Climate Change (IPCC) (1995) *Climate Change 1994: Radiative Forcing of Climate Change and an Evaluation of the IPCC IS92 Emission Scenarios*. Cambridge University Press, Cambridge, UK.
- Iqbal, M. (1983) *An Introduction to Solar Radiation*. Academic Press, Toronto.
- Liou, K. N. (1992) *Radiation and Cloud Processes in the Atmosphere*. Oxford University Press, Oxford, UK.
- Mecherikunnel, A. T., Lee, R. B., Kyle, H. L., and Major, E. R. (1988) Intercomparison of solar total irradiance data from recent spacecraft measurements, *J. Geophys. Res.*, **93**, 9503–9509.
- Prather, M., McElroy, M., Wofsy, S., Russell, G., and Rind, D. (1987) Chemistry of the global troposphere: fluorocarbons as tracers of air motion, *J. Geophys. Res.*, **92**, 6579–6613.
- Ramanathan, V. (1987) The role of earth radiation budget studies in climate and general circulation research, *J. Geophys. Res.*, **92**, 4075–4095.
- Ramanathan, V., Cess, R. D., Harrison, E. F., Minnis, P., Barkstrom, B. R., Ahmad, E., and Hartmann, D. (1989) Cloud-radiative forcing and climate: results from the earth radiation budget experiment, *Science*, **243**, 57–63.
- Salstein, D. A. (1995) Mean properties of the atmosphere, in *Composition, Chemistry, and Climate of the Atmosphere*, edited by H. B. Singh. Van Nostrand Reinhold, New York, pp. 19–49.
- Trenberth, K. E., and Guillemot, C. J. (1994) The total mass of the atmosphere, *J. Geophys. Res.*, **99**, 23079–23088.
- Walker, J. C. G. (1977) *Evolution of the Atmosphere*. Macmillan, New York.
- Willson, R. C., and Hudson, H. S. (1988) Solar luminosity variations in solar cycle 21, *Nature*, **332**, 810–812.

PROBLEMS

- 1.1_A Calculate the concentration (in molecules cm^{-3}) and the mixing ratio (in ppm) of water vapor at ground level at $T = 298 \text{ K}$ at RH values of 50%, 60%, 70%, 80%, 90%, 95%, and 99%.

The vapor pressure of pure water as a function of temperature can be calculated with the following correlation:

$$p_{\text{H}_2\text{O}}^\circ(T) = p_s \exp[13.3185a - .976a^2 - 0.6445a^3 - 0.1299a^4]$$

where $p_s = 1013.25$ mbar and $a = 1 - (373.15/T)$. (An alternate correlation is given in Table 15.2.)

- 1.2_A Compute the total concentration of air molecules (in molecules cm^{-3}) at sea level, 1 km, 2 km, 5 km, 10 km, 15 km, and 25 km.
- 1.3_A Determine the concentration (in $\mu\text{g m}^{-3}$) for N_2O at a mixing ratio of 311 ppb at $p = 1$ atm and $T = 298$ K.
- 1.4_A A typical global concentration of hydroxyl (OH) radicals is about 10^6 molecules cm^{-3} . What is the mixing ratio corresponding to this concentration at sea level and 298 K?
- 1.5_A Measurements of dimethyl sulfide (CH_3SCH_3) during the Aerosol Characterization Experiment-1 (ACE-1) conducted November–December 1995 off Tasmania were in the range of 250 to 500 ng m^{-3} . Convert these values to mixing ratios in ppt at 298 K at sea level.
- 1.6_A For a global mean albedo of $R_p = 0.3$, show that the equilibrium temperature of the Earth (assuming no atmospheric absorption of outgoing infrared radiation) is about 255 K. For $R_p = 0.15$, show that the equilibrium temperature is 268 K. Calculate the variation in solar constant and in global albedo corresponding to a change of 0.5 K in temperature.

2 Atmospheric Composition, Global Cycles, and Lifetimes

Virtually every element in the periodic table is found in the atmosphere; however, when classifying atmospheric species according to chemical composition it proves to be convenient to use a small number of major groupings such as:

1. Sulfur-containing compounds.
2. Nitrogen-containing compounds.
3. Carbon-containing compounds.
4. Halogen-containing compounds.

Obviously these categories are not exclusive; many sulfur-containing compounds, for example, also include atoms of carbon. And virtually all the atmospheric halogens involve a carbon atom backbone. We do not include in the above list species of the general formula H_xO_y ; with the exception of water and hydrogen peroxide (H_2O_2), these are all radical species (e.g., hydroxyl, OH) that play key roles in atmospheric chemistry but do not necessarily require a separate category. Every substance emitted into the atmosphere is eventually removed so that a cycle of the elements in that substance is established. This is called the *biogeochemical cycle* of the element. The biogeochemical cycle of an element or a compound refers to the transport of that substance among atmospheric, oceanic, biospheric, and land compartments, the amounts contained in the different reservoirs, and the rate of exchange among them. The circulation of water among oceans, atmosphere, and continents is a prime example of a biogeochemical cycle. The term biogeochemical cycle is often used to describe the global or regional cycles of the "life elements," C, O, N, S, and P, with reservoirs including the atmosphere, the ocean, the sediments, and living organisms (Rodhe, 1992).

A condition of "air pollution" may be defined as a situation in which substances that result from anthropogenic activities are present at concentrations sufficiently high above their normal ambient levels to produce a measurable effect on humans, animals, vegetation, or materials. This definition could include any substance, whether noxious or benign; however, the implication is that the effects are undesirable. Traditionally, air pollution has been viewed as a phenomenon characteristic only of large urban centers and industrialized regions. It is now clear that dense urban centers are just "hotspots" in a continuum of trace species concentrations over the entire Earth. Both urban smogs and stratospheric ozone depletion by chlorofluorocarbons are manifestations of what might be termed in the broadest sense as air pollution.

The first recognized type of air pollution was that typified by high concentrations of sulfur compounds (SO_2 and sulfates) and particles, resulting from combustion of coal and high-sulfur-containing fuels. Cities with this characteristic type of air pollution are often in cold climates where electric power generation and domestic heating are major sources of emissions.

A second type of air pollution appeared only with the widespread use of gasoline as a motor fuel. Although automobile exhaust was recognized as a potential air pollutant as early as 1915, it was not until about 1945 that the first urban air pollution problem definitely attributable to automobile emissions appeared in Los Angeles. This type of air pollution, once exclusive to Los Angeles, now occurs worldwide in any metropolitan area in which there is a heavy use of automobiles; Tokyo, Athens, Mexico City, and Sao Paulo, Brazil are examples of some of the most afflicted cities. Although historically this second type of air pollution has been called "smog" (or "photochemical smog"), presumably borrowed from the English condensation of smoke and fog, it is, in fact, neither smoke nor fog but the reactants and products of complex chemistry that takes place when sunlight irradiates an atmosphere laden with organic gases and oxides of nitrogen. Photochemical smog occurs with high temperatures and bright sunlight. The main primary pollutants in photochemical smog are nitric oxide and organic compounds, which are rapidly converted to secondary pollutants, the most important of which is ozone, but also consisting of organic nitrates, oxidized hydrocarbons, and so-called photochemical aerosol. It is the secondary pollutants that are responsible for effects such as eye irritation and plant damage. Ozone is naturally present in the clean, background troposphere at mixing ratios ranging from 20 to 60 ppb; levels in urban atmospheres have reached values as high as 500 ppb.

2.1 ATMOSPHERIC RESIDENCE TIMES

Imagine that we could follow all the individual molecules of a substance emitted into the air. Some might be removed close to their point of emission by contact with airborne droplets or the Earth's surface. Others might get carried high into the atmosphere and be transported a great distance before they ultimately are removed. Averaging the life histories of all molecules of a substance yields an average lifetime or average *residence time* for that substance. This residence time tells us on average how long a representative molecule of the substance will stay in the atmosphere before it is removed. The atmosphere presents two ultimate exits: precipitation and the surface of the Earth itself. Species released into the air must sooner or later leave by one of these two routes.

Atmospheric species removal processes can be conveniently grouped into two categories: dry deposition and wet deposition. Dry deposition denotes the direct transfer of species, both gaseous and particulate, to the Earth's surface and proceeds without the aid of precipitation. Wet deposition, on the other hand, encompasses all processes by which airborne species are transferred to the Earth's surface in aqueous form (i.e., rain, snow, or fog): (1) dissolution of atmospheric gases in airborne droplets, for example, cloud drops, rain, or fog; (2) removal of atmospheric particles when they serve as nuclei for the condensation of atmospheric water to form a cloud or fog droplet and are subsequently incorporated in the droplet; and (3) removal of atmospheric particles when the particle collides with a droplet both within and below clouds.

It is important to note that even though a gas or particle is scavenged by a droplet, that gas or particle may not actually be removed from the air if the droplet evaporates rather than eventually falling to earth.

By "particulate matter" we refer to any substance, except pure water, that exists as a liquid or solid in the atmosphere under normal conditions and is of microscopic or submicroscopic size but larger than molecular dimensions. Among atmospheric constituents, particulate matter is unique in its complexity. Airborne particulate matter results not only

from direct emissions of particles but also from emissions of certain gases that either condense as particles directly or undergo chemical transformation to a species that condenses as a particle. A full description of atmospheric particles requires specification of not only their concentration but also their size, chemical composition, phase (i.e., liquid or solid), and morphology.

Once particles are in the atmosphere, their size, number, and chemical composition are changed by several mechanisms until ultimately they are removed by natural processes. Some of the physical and chemical processes that affect the "aging" of atmospheric particles are more effective in one regime of particle size than another. In spite of the specific processes that affect particulate aging, the usual residence time of particles in the lower atmosphere does not exceed several weeks. Very close to the ground, the main mechanisms for particle removal are settling and dry deposition on surfaces; whereas at altitudes above about 100 m, precipitation scavenging is the predominant removal mechanism.

As air rises through a cloud and becomes slightly supersaturated with water vapor (i.e., as its relative humidity exceeds 100%), cloud droplets form on condensation nuclei—usually soluble aerosol particles (e.g., microscopic particles of various salts) that exist in the atmosphere at concentrations of 100 to 3000 cm^{-3} —and grow by condensation of water vapor. As the droplets grow and collide with each other they become raindrops, which grow rapidly as they fall and accrete cloud droplets.

2.1.1 Residence Time

The fundamental physical principle governing the behavior of a chemical in the atmosphere is conservation of mass. In any imaginary cube of air the following balance must hold:

$$\begin{array}{rcccl} \text{Rate of the} & \text{Rate of the} & \text{Rate of intro-} & \text{Rate of} & \text{Rate of accumu-} \\ \text{species} & \text{species} & \text{duction (emis-} & \text{removal of} & \text{lation of the} \\ \text{flowing in} & \text{flowing out} & \text{sion) of the} & \text{the species} & \text{species in the} \\ & & \text{species} & & \text{imaginary volume} \\ & & & & \\ & & + & - & = \end{array}$$

This balance must hold from the smallest cube of air all the way up to the entire atmosphere.

If we let Q denote the total mass of the substance in the volume of air, F_{in} and F_{out} the mass flow rates of the substance in and out of the air volume, respectively, P the rate of introduction of the species from sources, and R the rate of removal of the species, then conservation of mass can be expressed mathematically as

$$\frac{dQ}{dt} = (F_{\text{in}} - F_{\text{out}}) + (P - R) \quad (2.1)$$

If the amount Q of the substance in the volume or reservoir is not changing with time, then Q is a constant and $dQ/dt = 0$. In order for Q to be unchanging, all the sources of the substance to the reservoir must be precisely balanced by the sinks of the substance. This means that

$$F_{\text{in}} + P = F_{\text{out}} + R \quad (2.2)$$

In such a case *steady-state* conditions are said to hold.

If the volume we are referring to is the entire atmosphere, then $F_{\text{in}} = 0$ and $F_{\text{out}} = 0$, and for a substance at steady-state conditions, its rate of injection from sources must equal its rate of removal, $P = R$. The average residence time τ , in terms of the quantities introduced earlier, is

$$\tau = \frac{Q}{R + F_{\text{out}}} \quad (2.3)$$

Since at steady-state conditions $R + F_{\text{out}} = P + F_{\text{in}}$, the residence time is also given by

$$\tau = \frac{Q}{P + F_{\text{in}}} \quad (2.4)$$

If the entire atmosphere is taken as the reservoir, then under steady-state conditions

$$\tau = \frac{Q}{R} = \frac{Q}{P} \quad (2.5)$$

As an illustration of the concept of residence time, consider all sulfur-containing compounds in the troposphere. If the average mixing ratio of these compounds is 1 part per billion by mass (ppbm) and a steady state is assumed to exist, then with the mass of the troposphere about 4×10^{21} g, the total mass of sulfur-containing compounds in the troposphere is $Q = 4 \times 10^{12}$ g. If natural and anthropogenic sources of sulfur contribute to give a total P of about 200×10^{12} g yr⁻¹, the residence time of sulfur compounds in the troposphere is estimated to be

$$\tau = \frac{4 \times 10^{12} \text{ g}}{200 \times 10^{12} \text{ g yr}^{-1}} = 1 \text{ week}$$

Note that a more accurate estimate of sulfur fluxes will be given shortly.

Calculations of residence times can be useful in estimating how far from its source a species is likely to remain airborne before it is removed from the atmosphere.

If we consider a particular region of the atmosphere, say, the volume of air over a city or the volume of air in the Northern Hemisphere or the entire stratosphere, we can define a characteristic mixing time for that volume as the time needed to thoroughly mix a chemical in that volume of air. Call the characteristic mixing time τ_M . A reservoir is poorly mixed for a particular species if the characteristic mixing time, τ_M , is not small compared with the species residence time, τ . Note that this means that a particular reservoir can be well mixed for some species and poorly mixed for others, depending on the residence time of each species. Furthermore, as we have seen, the mixing times in the atmosphere are different for different directions. For example, as we have noted, the characteristic vertical mixing time in the troposphere, the time required to mix a species uniformly from the ground up to the tropopause, is about one week; whereas the troposphere's horizontal mixing time, the time required to mix a constituent thoroughly around the globe in the troposphere, is about one year. Thus the troposphere can be considered well mixed for ⁸⁵Kr, which has a residence time of 10 years; but for sulfur compounds, which are estimated to have a residence time of about one week, the troposphere is not even well mixed vertically.

The stratosphere can be considered well mixed vertically only for atmospheric species with residence times greatly exceeding 50 years. In fact, one of the only examples of such a long-lived species is He, which has its source at the Earth's surface and its sink as escape through the very top of the atmosphere into space. Thus the stratosphere is poorly mixed vertically for essentially all atmospheric trace constituents.

Frequently the rate at which a chemical is removed from the atmosphere is proportional to its concentration (first-order loss)—the more that is present, the faster its rate of removal. This is generally the case for both dry deposition at the Earth's surface and scavenging by cloud droplets. Consider a species for which steady-state conditions hold and which is removed at a rate proportional to its concentration with a proportionality constant λ . Such a species is ^{85}Kr , the only significant removal process for which is radioactive decay. For ^{85}Kr , then

$$\tau = \frac{Q}{\lambda Q} = \frac{1}{\lambda}$$

Thus to estimate the residence time of ^{85}Kr does not even require knowledge of its atmospheric abundance Q , but only of the radioactive decay constant. Consequently, it does not matter whether ^{85}Kr is uniformly mixed throughout the entire atmosphere or not to estimate its lifetime. In a case where the removal process is first order, then even for a poorly mixed species a simple and accurate estimate for its residence time can be obtained provided that its removal rate constant can be accurately estimated.

Now consider a species with mass Q in the atmosphere that is removed by two independent processes, the first at a rate $k_1 Q$ and the second at a rate $k_2 Q$, where k_1 and k_2 are the first-order removal coefficients. Its overall residence time is given by

$$\tau = \frac{Q}{k_1 Q + k_2 Q} = \frac{1}{k_1 + k_2}$$

or

$$\frac{1}{\tau} = k_1 + k_2$$

Process 1, for example, could be dry deposition and process 2 cloud scavenging. We can actually associate time constants with the two individual removal processes,

$$\tau_1 = \frac{1}{k_1} \quad \tau_2 = \frac{1}{k_2}$$

where τ_1 can be thought of as the residence time of the species if the only removal process is process 1, which is also true for τ_2 . From (2.8) and (2.9) we can express the overall residence time τ in terms of the two individual removal times τ_1 and τ_2 by

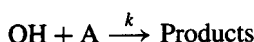
$$\frac{1}{\tau} = \frac{1}{\tau_1} + \frac{1}{\tau_2} \quad (2.10)$$

Equation (2.10) shows that separate removal paths add together to give a total residence time, like electrical resistances in parallel add to give a total resistance that is even smaller than the smallest resistance. From (2.10)

$$\tau = \frac{\tau_1 \tau_2}{\tau_1 + \tau_2} \quad (2.11)$$

If $\tau_1 \gg \tau_2$, the residence time associated with removal by process 1 is much longer than that associated with process 2, process 2 is the more effective removal mechanism, and $\tau \simeq \tau_2$. Thus, when there are several competing removal paths, in order to estimate the overall residence time of a species, focus should always be on improving estimates for the fastest removal rate.

Removal in the troposphere of those compounds that react with the hydroxyl radical occurs according to the chemical reaction



The parameter k is the rate constant for the reaction, such that the rate of the reaction is $k[\text{OH}][\text{A}]$, where the brackets denote the concentration of the species contained therein.

From the analysis of atmospheric residence times, if Q is the total quantity of species A in the troposphere and its rate of removal is $R = k[\text{OH}]Q$, then the compound's residence time is, from (2.6),

$$\begin{aligned} \tau &= \frac{Q}{k[\text{OH}]Q} \\ &= \frac{1}{k[\text{OH}]} \end{aligned} \quad (2.12)$$

where $[\text{OH}]$ is an appropriate globally averaged tropospheric concentration of OH radicals.

Let us develop the equations governing the total moles of a species i in the atmosphere Q_i . The dynamic material balance can be written as

$$\frac{dQ_i}{dt} = P_i - R_i \quad (2.13)$$

where P_i and R_i represent the source and loss rates. The terms P_i and R_i consist of the following contributions:

$$P_i \begin{cases} P_i^n & \text{natural emissions} \\ P_i^a & \text{anthropogenic emissions} \\ P_i^c & \text{chemical reactions} \end{cases}$$

$$R_i \begin{cases} R_i^d & \text{dry deposition} \\ R_i^w & \text{wet deposition} \\ R_i^c & \text{chemical reactions} \\ R_i^t & \text{transport to the stratosphere} \end{cases}$$

The loss processes are usually represented as first order; for example, $R_i^d = k_i^d Q_i$, where the first-order rate constants, which we will denote by k 's, must be specified. Thus (2.13) becomes

$$\frac{dQ_i}{dt} = P_i^n + P_i^a + P_i^c - (k_i^d + k_i^w + k_i^c + k_i^l) Q_i \quad (2.14)$$

If the concentration of the species is not changing, then a steady state may be presumed in which

$$P_i^n + P_i^a + P_i^c - (k_i^d + k_i^w + k_i^c + k_i^l) Q_i = 0$$

The mean residence time of species i can be calculated by either

$$\tau_i = \frac{Q_i}{k_i^d + k_i^w + k_i^c + k_i^l}$$

or

$$\tau_i = \frac{Q_i}{P_i^n + P_i^a + P_i^c} \quad (2.17)$$

To use (2.16) the individual first-order rate constants for removal must be estimated, whereas in (2.17), estimates for the total number of moles in the troposphere, which can be derived from a concentration measurement, and for the source strength terms are needed. If the k_i values are difficult to specify, mean residence times are often estimated from (2.17).

2.2 SULFUR-CONTAINING COMPOUNDS

Sulfur is present in the Earth's crust at a mixing ratio of less than 500 parts per million by mass and in the Earth's atmosphere at a total volume mixing ratio of less than 1 ppm. Yet, sulfur-containing compounds exert a profound influence on the chemistry of the atmosphere and, likely, on climate. The main questions that we will seek to answer with respect to sulfur compounds, and indeed for all classes of atmospheric compounds, are:

1. What are the species present in the atmosphere? What are their natural and anthropogenic sources?
2. What chemical reactions do they undergo in the atmosphere? How fast are these reactions?
3. What are the products of atmospheric transformations?
4. What effect does the presence of the compound and its chemical transformation products have on the atmosphere?

In this chapter we focus on the first question.

Table 2.1 lists atmospheric sulfur compounds. The principal sulfur compounds in the atmosphere are H_2S , CH_3SCH_3 , CS_2 , OCS , and SO_2 . Sulfur occurs in five oxidation states in the atmosphere.¹ Chemical reactivity of atmospheric sulfur compounds is inversely related to their sulfur oxidation state. Reduced sulfur compounds, those with oxidation state -2 or -1 , are rapidly oxidized by the hydroxyl radical and, to a lesser extent, by other species, with resulting atmospheric lifetimes of a few days. The water solubility of sulfur species increases with oxidation state; reduced sulfur species occur preferentially in the gas phase, whereas the $\text{S}(+6)$ compounds often tend to be found in particles or droplets. Once converted to compounds in the $\text{S}(+6)$ state, sulfur species residence times are determined by removal by wet and dry deposition.

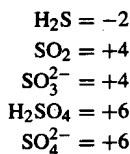
Table 2.2 presents estimates of total sulfur emissions to the atmosphere, both anthropogenic and natural, including estimated division between Northern and Southern

¹The oxidation states of atoms in covalent compounds are obtained by arbitrarily assigning the electrons to particular atoms. For a covalent bond between two identical atoms, the electrons are split equally between the two. When two different atoms are involved, the shared electrons are assigned completely to the atom that has the stronger attraction for the electrons. In the water molecule, for example, oxygen has a greater attraction for electrons than hydrogen, so in assigning the oxidation states of oxygen and hydrogen in H_2O , it is assumed that the oxygen atom possesses all the electrons. This gives the oxygen an excess of two electrons, and its oxidation state is -2 . Each hydrogen has no electrons, and the oxidation state of each hydrogen is $+1$.

Rules for assigning oxidation states are:

1. The oxidation state of an atom in an element is 0.
2. The oxidation state of a monatomic ion is the same as its charge.
3. Oxygen is assigned an oxidation state of -2 in its covalent compounds, such as CO , CO_2 , SO_2 , and SO_3 . An exception to this rule occurs in peroxides, where each oxygen is assigned an oxidation state of -1 .
4. In its covalent compounds with nonmetals, hydrogen is assigned an oxidation state of $+1$. Examples include HCl , H_2O , NH_3 , and CH_4 .
5. In its compounds fluorine is always assigned an oxidation state of -1 .
6. The sum of the oxidation states must be zero for an electrically neutral compound. For an ion, the sum must equal the charge of the ion. For example, the sum of oxidation states for the nitrogen and hydrogen atoms in NH_4^+ is $+1$, and the oxidation state of nitrogen is -3 . For NO_3^- , the sum of oxidation states is -1 . Since oxygen has an oxidation state of -2 , nitrogen must have an oxidation state of $+5$. Sometimes, oxidation states are indicated with roman numerals, for example, the sulfur atom in SO_4^{2-} is $+VI$.

Oxidation states of sulfur in various compounds of atmospheric importance are as follows:



Oxidation states of nitrogen in atmospheric species are as follows:

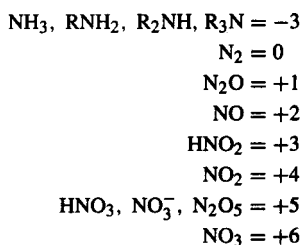


TABLE 2.1 Atmospheric Sulfur Compounds

Oxidation State	Compound		Chemical Structure	Usual Atmospheric State
	Name	Formula		
	Hydrogen sulfide	H ₂ S	H—S—H	Gas
	Dimethyl sulfide (DMS)	CH ₃ SCH ₃	CH ₃ —S—CH ₃	Gas
	Carbon disulfide	CS ₂	S=C=S	Gas
	Carbonyl sulfide	OCS	O=C=S	Gas
	Methyl mercaptan	CH ₃ SH	CH ₃ —S—H	Gas
	Dimethyl disulfide	CH ₃ SSCH ₃	CH ₃ —S—S—CH ₃	Gas
0	Dimethyl sulfoxide	CH ₃ SOCH ₃	$\begin{array}{c} \text{O} \\ \\ \text{CH}_3-\text{S}-\text{CH}_3 \end{array}$	Gas
4	Sulfur dioxide	SO ₂	O=S=O	Gas
	Bisulfite ion	HSO ₃ ⁻		Aqueous
	Sulfite ion	SO ₃ ²⁻		Aqueous
6	Sulfuric acid	H ₂ SO ₄	$\begin{array}{c} \text{O} \\ \\ \text{HO}-\text{S}-\text{OH} \\ \\ \text{O} \end{array}$	Gas aqueous/aerosol
	Bisulfate ion	HSO ₄ ⁻	$\begin{array}{c} \text{O} \\ \\ \text{HO}-\text{S}-\text{O}^- \\ \\ \text{O} \end{array}$	Aqueous/aerosol
	Sulfate ion	SO ₄ ²⁻	$\begin{array}{c} \text{O} \\ \\ \text{O}-\text{S}-\text{O}^- \\ \\ \text{O} \end{array}$	Aqueous/aerosol

TABLE 2.1 (Continued)

Oxidation State	Compound		Chemical Structure	Usual Atmospheric State
	Name	Formula		
6	Methane sulfonic acid (MSA)	$\text{CH}_3\text{SO}_3\text{H}$	$\begin{array}{c} \text{O} \\ \\ \text{CH}_3-\text{S}-\text{OH} \\ \\ \text{O} \end{array}$	Gas/aqueous
	Dimethyl sulfone	$\text{CH}_3\text{SO}_2\text{CH}_3$	$\begin{array}{c} \text{O} \\ \\ \text{CH}_3-\text{S}-\text{CH}_3 \\ \\ \text{O} \end{array}$	Gas
	Hydroxymethane sulfonic acid (HMSA)	$\text{HOCH}_2\text{SO}_3\text{H}$	$\begin{array}{c} \text{O} \\ \\ \text{HOCH}_2-\text{S}-\text{OH} \\ \\ \text{O} \end{array}$	Aqueous

TABLE 2.2 Global Sulfur Emissions Estimates (Tg(S) yr⁻¹)

Source	H ₂ S	DMS	CS ₂	OCS ^d	SO ₂	SO ₄	Total ^a
Fossil-fuel combustion + industry							71–77 (mid-1980s) (68/6)
Biomass burning	<0.01?	—	<0.01?	0.075	2.8	0.1	2.2–3.0 (1.4/1.1)
Oceans	<0.3	15–25	0.08	3.08	—	40–320	15–25 (8.4/11.6) ^b
Wetlands	0.006–1.1	0.003–0.68	0.0003–0.06	—	—	—	0.01–2 (0.8/0.2)
Plants + soils	0.17–0.53	0.05–0.16	0.02–0.05	—	—	2–4	0.25–0.78 (0.3/0.2) ^c
Volcanoes	0.5–1.5	—	—	0.01	7–8	2–4	9.3–11.8 (7.6/3.0)
Anthropogenic (total)							73–80
Natural (total, without sea salt and soil dust)							25–40
Total							98–120

^aNumbers in parentheses are fluxes from Northern Hemisphere/Southern Hemisphere.

^bExcluding sea-salt contributions.

^cExcluding soil dust contributions.

^dAndreae and Crutzen (1997)

Source: Berresheim et al. (1995).

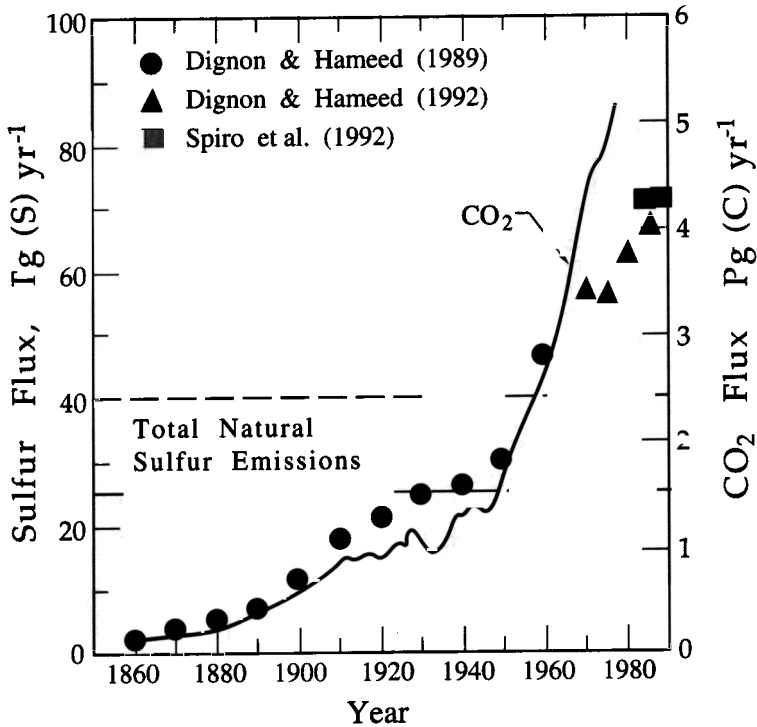


FIGURE 2.1 Global anthropogenic SO_2 and CO_2 emissions since 1860 (Berresheim et al., 1995). Data are from Dignon and Hameed (1989; circles), Hameed and Dignon (1992; triangles), and Spiro et al. (1992; squares). CO_2 emissions (solid curve) are shown for reference. Dashed lines indicate the estimated range for the global natural sulfur flux (excluding seasalt sulfate).

Hemisphere. Current estimates place total global emissions (excluding seasalt) in the range of 98 to 120 Tg(S) yr^{-1} . At present, anthropogenic emissions account for about 75% of total sulfur emissions, and 90% of the anthropogenic emissions occur in the Northern Hemisphere.

Figure 2.1 shows estimated global emissions of SO_2 since 1860, based on data of Dignon and Hameed (1989), Hameed and Dignon (1992), and Spiro et al. (1992).² The dashed lines indicate the estimated range of the natural global sulfur flux. Hameed and Dignon estimate that Asia has become the leading sulfur-emitting continent since about 1981 ($>20 \text{ Tg(S) yr}^{-1}$ in 1986, as compared with $<15 \text{ Tg(S) yr}^{-1}$ for North America). One reason for the growth of sulfur emissions from Asia is the increased use of coal combustion in China. Table 2.3 summarizes observed mixing ratios of H_2S , CH_3SCH_3 , CS_2 , OCS , and SO_2 .

²Units of atmospheric emission rates and fluxes. Fluxes of sulfur and other species into the atmosphere are expressed in yearly amounts, using the prefixes given in Table A.5. Sulfur fluxes, for example, as shown in Figure 2.1, are usually expressed as multiples of Tg yr^{-1} ($1 \text{ Tg} = 10^{12} \text{ g}$). An alternative is to employ the metric ton ($1 \text{ t} = 10^6 \text{ g} = 10^3 \text{ kg}$). CO_2 fluxes, as shown on the right-hand side of Figure 2.1, are often expressed as multiples of gigatons, Gt ($1 \text{ Gt} = 10^9 \text{ t} = 10^{15} \text{ g} = 1 \text{ Pg}$).

TABLE 2.3 Observed Mixing Ratios of Atmospheric Sulfur Gases

Compound and Location	Average Mixing Ratio (ppt)
H₂S	
Marine surface layer	3.6–7.5
Coastal regions	65
Forests	35–60
Wetlands	450–840
Urban areas	365
Free troposphere (2–5 km)	6–8.5
CH₃SCH₃	
Marine surface layer	80–110
Continental surface layer	8–60
Free troposphere (2–5 km)	1.5–15
CS₂	
Marine surface layer	2–18
Continental surface layer	35–120
Free troposphere (2–5 km)	5–7
OCS	
Total troposphere	500
Marine surface layer	500
Continental surface layer	545
SO₂	
Marine surface layer	20
Free troposphere (>5 km)— Europe/North Sea/Arctic	50
North America clean continental	160
Coastal Europe	260
Polluted continental air	1500

Source: Berresheim et al. (1995) (detailed references given by the authors).

2.2.1 Dimethyl Sulfide (CH₃SCH₃)

Dimethyl sulfide (DMS) is the dominant sulfur compound emitted from the world's oceans. DMS was discovered in the surface ocean by Lovelock et al. (1972), who suggested that DMS may be the biogenic sulfur species that was needed at the time to balance the global sulfur budget.

DMS is produced in oceanic waters by both benthic and planktonic marine organisms (Dacey and Wakeham, 1986), suggesting that it may be ubiquitous in the surface ocean (Barnard et al., 1982). It is thought to originate from the decomposition of dimethyl-sulfiniopropionate produced by marine organisms, in particular, phytoplankton (Andreae, 1990). Its concentration in the upper layer of the ocean varies between a few nanograms of S per liter to a few micrograms of S per liter (Lovelock et al., 1972; Barnard et al., 1982; Andreae and Raemdonck, 1983; Cline and Bates, 1983; Nguyen et al., 1984, 1988). The DMS surface seawater concentration is highly nonuniform; its average concentration is approximately 100 nanograms (ng) of S per liter. It has been observed that the concentration of DMS is dependent on diurnal (Andreae and Barnard, 1984) and seasonal variations (Turner and Liss, 1985), and on depth and location (Andreae and Raemdonck, 1983).

Based on DMS concentrations in the atmosphere and its Henry's law constant in seawater (see Chapter 6), oceanic DMS concentrations are greatly in excess of those that would be in equilibrium with atmospheric values (Andreae, 1990). The result of this lack of equilibrium is a flux of DMS from the ocean to the atmosphere.

Once the importance of DMS to the global sulfur cycle was established, numerous measurements of DMS concentrations in the marine atmosphere have been conducted. The average DMS mixing ratio in the marine boundary layer (MBL) is in the range of 80 to 110 ppt but can reach values as high as 1 ppb over entrophic (e.g., coastal, upwelling) waters. As indicated in Table 2.3, DMS mixing ratios fall rapidly with altitude to a few parts per trillion in the free troposphere. After transfer across the air-sea interface into the atmosphere, DMS reacts predominantly with the hydroxyl radical and also with the nitrate (NO_3) radical. Hydroxyl radical reaction predominates in the marine atmosphere. Because the OH radical has a photochemical source, DMS is removed more effectively during daylight hours rather than at night when the NO_3 reaction could be important. As a result, marine boundary layer DMS concentrations exhibit a diel cycle, with a nighttime maximum and daytime minimum. Yvon et al. (1996) report shipboard measurements of atmospheric DMS levels in the tropical Pacific marine boundary layer (12° S , 135° W) for 6 days during March 1992, and consistent diel cycles of DMS were observed with an amplitude of approximately 85 ppt. (These investigators found the mean atmospheric DMS mixing ratio during this period to be 453 ± 93 ppt, considerably higher than the range of mixing ratios given in Table 2.3.) Oxidation of DMS is the exclusive source of methane sulfonic acid (MSA) in the atmosphere, and the dominant source of SO_2 in the marine atmosphere. We will return to the atmospheric chemistry of DMS in Chapter 5.

2.2.2 Carbonyl Sulfide (OCS)

Carbonyl sulfide is the most abundant sulfur gas in the global background atmosphere because of its low reactivity in the troposphere and its correspondingly long residence time. It is the only sulfur compound that survives to enter the stratosphere. (An exception is the direct injection of SO_2 into the stratosphere in volcanic eruptions.) In fact, the input of OCS into the stratosphere is considered to be responsible for the maintenance of the normal stratospheric sulfate aerosol layer. Measurements of atmospheric OCS mixing ratios and surface fluxes have been reviewed by Chin and Davis (1995). OCS exhibits an average tropospheric mixing ratio of about 500 ppt.

A recent analysis of the global OCS cycle led to the following estimates of sources and sinks (all in $\text{Tg}(\text{OCS})\text{yr}^{-1}$) (Andreae and Crutzen, 1997):

<u>Sources</u>	<u>Sinks</u>
CS ₂ oxidation	Plant uptake
Ocean emission	OH reaction
Biomass burning	Soil uptake
Other	Other
<u>0.73</u>	<u>0.90</u>

Given the uncertainty of the estimates, this budget can be considered to be roughly in balance. On the basis of atmospheric measurements, Chin and Davis (1995) estimated the total quantity of OCS in the atmosphere to be 5.2 Tg, of which 4.63 Tg is in the troposphere

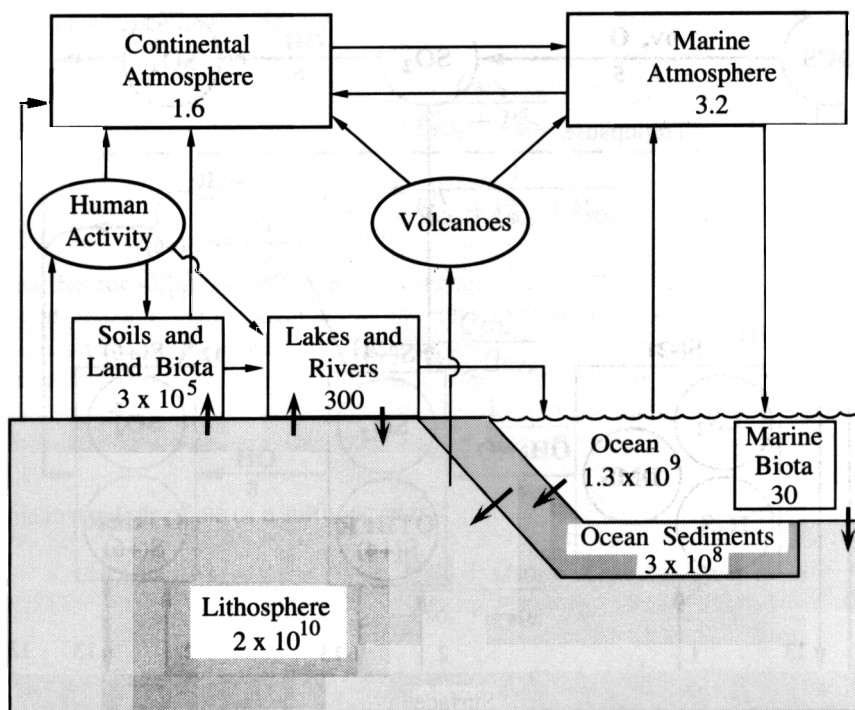


FIGURE 2.2 Major reservoirs and burdens of sulfur, in Tg(S) (Charlson et al., 1992). Reprinted by permission of Academic Press.

and 0.57 Tg in the stratosphere. Based on the estimated global OCS source strength of 0.73 Tg yr^{-1} , the global atmospheric lifetime of OCS is estimated to be about 7 years. We will return to the global cycle and chemistry of OCS in Chapter 4 in connection with the stratospheric aerosol layer.

2.2.3 Sulfur Dioxide (SO_2)

Sulfur dioxide is the predominant anthropogenic sulfur-containing air pollutant. Mixing ratios of SO_2 in continental background air range from 20 ppt to over 1 ppb; in the unpolluted marine boundary layer levels range between 20 and 50 ppt. Urban SO_2 mixing ratios can attain values of several hundred parts per billion. We will consider the atmospheric chemistry of SO_2 in Chapter 5.

2.2.4 The Atmospheric Sulfur Cycle

Figure 2.2 depicts the major reservoirs in the biogeochemical cycle of sulfur, with estimated quantities (in Tg(S)) in each reservoir. Directions of fluxes between the reservoirs are indicated by arrows. The major pathways of sulfur compounds in the atmosphere are depicted in Figure 2.3. The numbers on each arrow refer to the description of the process given in the caption to the figure (not to fluxes). All the processes indicated schematically in Figure 2.3 will be studied later in this book.

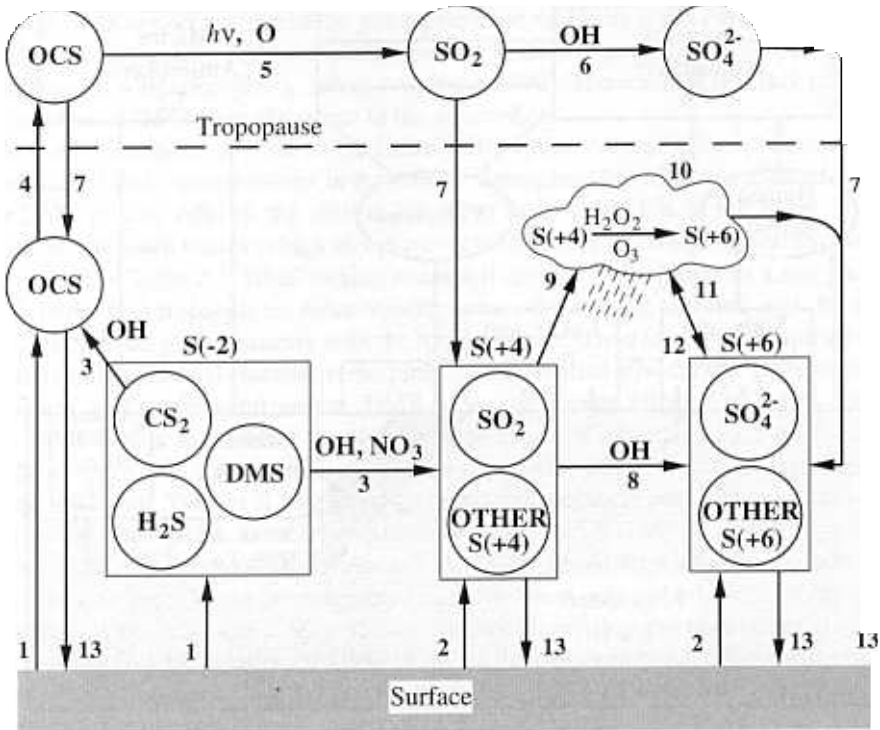


FIGURE 2.3 Major pathways of sulfur compounds in the atmosphere (Berresheim et al., 1995). The paths are labeled according to the processes: (1) emission of DMS, H₂S, CS₂, and OCS; (2) emission of S(+4) and S(+6); (3) oxidation of DMS, H₂S, and CS₂ by OH, and DMS, by NO₃ in the troposphere; (4) transport of OCS into the stratosphere; (5) photolysis of OCS or reaction with O atoms to form SO₂ in the stratosphere; (6) oxidation of SO₂ in the stratosphere; (7) transport of stratospheric OCS, SO₂, and sulfate back into the troposphere; (8) oxidation of SO₂ and other S(+4) products by OH in the troposphere; (9) absorption of S(+4), mainly SO₂, into hydrosols (cloud/fog/rain droplets, moist aerosol particles); (10) liquid phase oxidation of S(+4) by H₂O₂(aq) in hydrosols (and by O₂ in the presence of elevated levels of catalytic metal ions); (11) absorption/growth of S(+6) aerosol—mainly sulfate—into hydrosols; (12) evaporation of cloud-water leaving residual S(+6) aerosol; (13) deposition of OCS, S(+4), and S(+6).

We wish now to analyze that portion of the global sulfur cycle involving SO₂ and sulfate shown in Figure 2.3. We will denote the natural and anthropogenic emissions of SO₂ as $P_{\text{SO}_2}^n$ and $P_{\text{SO}_2}^a$, respectively. $P_{\text{SO}_2}^n$ includes a contribution from the oxidation of reduced sulfur species to SO₂. SO₂ is removed by dry and wet deposition and oxidized to sulfate by chemical reaction. Sulfate is also removed from the atmosphere by dry and wet deposition. Our goal is to obtain estimates for the lifetimes of SO₂ and SO₄²⁻.

Writing (2.15) for both SO₂ and SO₄²⁻, we obtain

$$P_{\text{SO}_2}^n + P_{\text{SO}_2}^a - (k_{\text{SO}_2}^a + k_{\text{SO}_2}^w + k_{\text{SO}_2}^c) Q_{\text{SO}_2} = 0 \quad (2.18)$$

$$k_{\text{SO}_2}^c Q_{\text{SO}_2} - (k_{\text{SO}_4}^a + k_{\text{SO}_4}^w) Q_{\text{SO}_4} = 0 \quad (2.19)$$

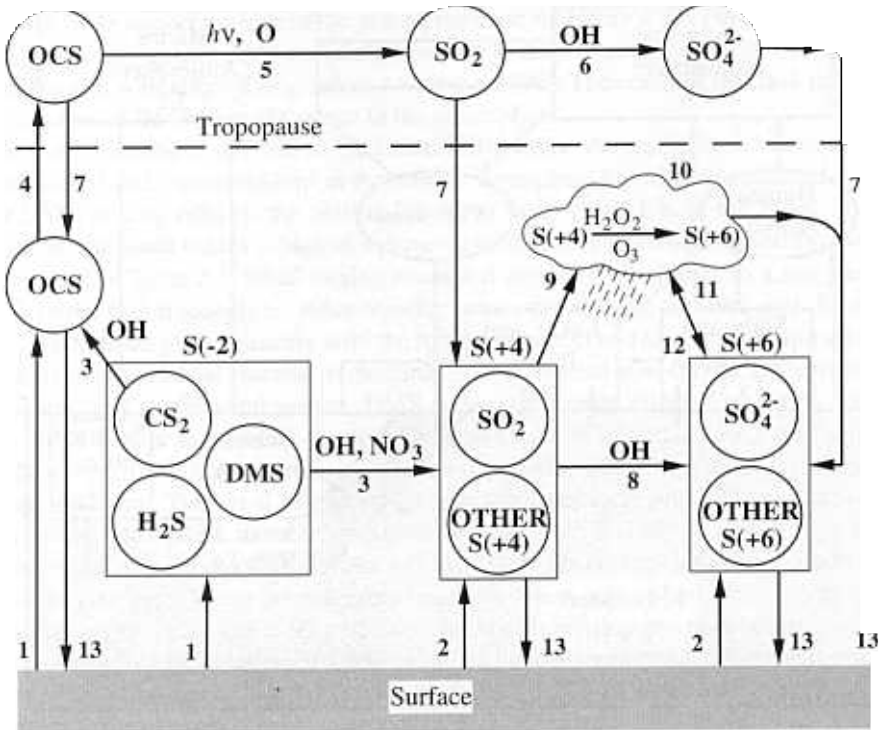


FIGURE 2.3 Major pathways of sulfur compounds in the atmosphere (Berresheim et al., 1995). The paths are labeled according to the processes: (1) emission of DMS, H₂S, CS₂, and OCS; (2) emission of S(+4) and S(+6); (3) oxidation of DMS, H₂S, and CS₂ by OH, and DMS, by NO₃ in the troposphere; (4) transport of OCS into the stratosphere; (5) photolysis of OCS or reaction with O atoms to form SO₂ in the stratosphere; (6) oxidation of SO₂ in the stratosphere; (7) transport of stratospheric OCS, SO₂, and sulfate back into the troposphere; (8) oxidation of SO₂ and other S(+4) products by OH in the troposphere; (9) absorption of S(+4), mainly SO₂, into hydrosols (cloud/fog/rain droplets, moist aerosol particles); (10) liquid phase oxidation of S(+4) by H₂O₂(aq) in hydrosols (and by O₂ in the presence of elevated levels of catalytic metal ions); (11) absorption/growth of S(+6) aerosol—mainly sulfate—into hydrosols; (12) evaporation of cloud-water leaving residual S(+6) aerosol; (13) deposition of OCS, S(+4), and S(+6).

We wish now to analyze that portion of the global sulfur cycle involving SO₂ and sulfate shown in Figure 2.3. We will denote the natural and anthropogenic emissions of SO₂ as $P_{\text{SO}_2}^n$ and $P_{\text{SO}_2}^a$, respectively. $P_{\text{SO}_2}^n$ includes a contribution from the oxidation of reduced sulfur species to SO₂. SO₂ is removed by dry and wet deposition and oxidized to sulfate by chemical reaction. Sulfate is also removed from the atmosphere by dry and wet deposition. Our goal is to obtain estimates for the lifetimes of SO₂ and SO₄²⁻.

Writing (2.15) for both SO₂ and SO₄²⁻, we obtain

$$P_{\text{SO}_2}^n + P_{\text{SO}_2}^a - (k_{\text{SO}_2}^d + k_{\text{SO}_2}^w + k_{\text{SO}_2}^c) Q_{\text{SO}_2} = 0 \quad (2.18)$$

$$k_{\text{SO}_2}^c Q_{\text{SO}_2} - (k_{\text{SO}_4}^d + k_{\text{SO}_4}^w) Q_{\text{SO}_4} = 0 \quad (2.19)$$

The mean residence time of SO_2 is

$$\tau_{\text{SO}_2} = \frac{Q_{\text{SO}_2}}{P_{\text{SO}_2}^n + P_{\text{SO}_2}^a} \frac{1}{k_{\text{SO}_2}^d + k_{\text{SO}_2}^w + k_{\text{SO}_2}^c}$$

whereas that for sulfate is

$$\tau_{\text{SO}_4} = \frac{Q_{\text{SO}_4}}{k_{\text{SO}_4}^c Q_{\text{SO}_2}} \frac{1}{k_{\text{SO}_4}^d + k_{\text{SO}_4}}$$

The mean residence time of a sulfur atom is

$$\tau_S = \frac{Q_{\text{SO}_2} + Q_{\text{SO}_4}}{P_{\text{SO}_2}^n + P_{\text{SO}_2}^a}$$

which can be expressed in terms of the two previous mean residence times as

$$\tau_S = \tau_{\text{SO}_2} + b\tau_{\text{SO}_4} \quad (2.23)$$

where

$$b = \frac{k_{\text{SO}_2}^c Q_{\text{SO}_2}}{P_{\text{SO}_2}^n + P_{\text{SO}_2}^a} \quad (2.24)$$

the fraction of S converted to SO_4^{2-} before being removed.

We can also define individual characteristic times such as

$$\tau_{\text{SO}_2}^d = (k_{\text{SO}_2}^d)^{-1} \quad \tau_{\text{SO}_2}^w = (k_{\text{SO}_2}^w)^{-1} \quad \tau_{\text{SO}_4}^d = (k_{\text{SO}_4}^d)^{-1}$$

so that

$$\frac{1}{\tau_{\text{SO}_2}} = \frac{1}{\tau_{\text{SO}_2}^d} + \frac{1}{\tau_{\text{SO}_2}^w} + \frac{1}{\tau_{\text{SO}_2}^c}$$

$$\frac{1}{\tau_{\text{SO}_4}} = \frac{1}{\tau_{\text{SO}_4}^d} + \frac{1}{\tau_{\text{SO}_4}^w}$$

We can also define the mean residence time of a sulfur atom before surface removal or precipitation scavenging by

$$\tau_S^{d,w} = \frac{Q_{\text{SO}_2} + Q_{\text{SO}_4}}{k_{\text{SO}_2}^{d,w} Q_{\text{SO}_2} + k_{\text{SO}_4}^{d,w} Q_{\text{SO}_4}}$$

so that using

$$\frac{P_{SO_2}^n + P_{SO_2}^a}{Q_{SO_2} + Q_{SO_4}} = (k_{SO_2}^d + k_{SO_2}^w) \frac{Q_{SO_2}}{Q_{SO_2} + Q_{SO_4}} + (k_{SO_4}^a + k_{SO_4}^w) \frac{Q_{SO_4}}{Q_{SO_2} + Q_{SO_4}} \tag{2.28}$$

we get

$$\frac{1}{\tau_S} = \frac{1}{\tau_S^d} + \frac{1}{\tau_S^w} \tag{2.29}$$

The mean residence times for a sulfur atom before surface removal (or precipitation scavenging) can be related to the mean surface removal residence times for SO₂ and SO₄²⁻ as follows. Noting that

$$\begin{aligned} \tau_S^d &= \frac{Q_{SO_2} + Q_{SO_4}}{k_{SO_2}^d Q_{SO_2} + k_{SO_4}^d Q_{SO_4}} \\ &= \frac{Q_{SO_2} + Q_{SO_4}}{\frac{Q_{SO_2}}{\tau_{SO_2}^d} + \frac{Q_{SO_4}}{\tau_{SO_4}^d}} \\ &= \frac{Q_{SO_2}}{Q_{SO_2} + Q_{SO_4}} \frac{1}{\tau_{SO_2}^d} + \frac{Q_{SO_4}}{Q_{SO_2} + Q_{SO_4}} \frac{1}{\tau_{SO_4}^d} \end{aligned}$$

we have

$$\frac{1}{\tau_S^d} = \frac{c}{\tau_{SO_2}^d} + \frac{(1-c)}{\tau_{SO_4}^d}$$

where

$$c = \frac{b(k_{SO_2}^d + k_{SO_2}^w + k_{SO_2}^c)}{k_{SO_4}^d + k_{SO_4}^w} \tag{2.32}$$

By virtue of (2.31), *c* is the fraction of the total sulfur that is SO₂.

Rodhe (1978) has estimated values of the sulfur residence times (in hours):

60	100	80	25	>400	80	80
----	-----	----	----	------	----	----

Assuming *c* = 0.5, the sulfur atom residence times are (in hours):

τ_S^d	τ_S^w	τ_S
120	90	50

Because of the uneven spatial distribution of anthropogenic sources and the relatively short residence time of sulfur in the atmosphere, global averages do not provide an accurate description of human influence on the sulfur cycle in populated parts of the world.

2.3 NITROGEN-CONTAINING COMPOUNDS

Aside from N_2 , which is extremely stable chemically and is not involved in the chemistry of the troposphere or stratosphere, the important nitrogen-containing trace species in the atmosphere are nitrous oxide (N_2O), nitric oxide (NO), nitrogen dioxide (NO_2), nitric acid (HNO_3), and ammonia (NH_3). The first of these, nitrous oxide (N_2O), is a colorless gas that is emitted almost totally by natural sources, principally by bacterial action in the soil. The gas is employed as an anesthetic and is commonly referred to as “laughing gas.” The second, nitric oxide (NO), is emitted by both natural and anthropogenic sources. Nitrogen dioxide (NO_2) is emitted in small quantities from combustion processes along with NO and is also formed in the atmosphere by oxidation of NO. The sum of NO and NO_2 is usually designated as NO_x . Nitric oxide is the major oxide of nitrogen formed during high-temperature combustion, resulting from both the interaction of nitrogen in the fuel with oxygen present in the air and the chemical conversion of atmospheric nitrogen and oxygen at the high temperatures of combustion. Other oxides of nitrogen, such as NO_3 and N_2O_5 , exist in the atmosphere in relatively low concentrations but nonetheless participate importantly in atmospheric chemistry. Nitric acid is an oxidation product of NO_2 in the atmosphere. Ammonia (NH_3) is emitted primarily by natural sources. Finally, nitrate and ammonium salts are not emitted in any significant quantities but result from the atmospheric conversion of NO, NO_2 , and NH_3 .

Nitrogen is an essential nutrient for all living organisms. The primary source of this nitrogen is the atmosphere. However, N_2 is not useful to most organisms until it is “fixed” or converted to a form that can be chemically utilized by the organisms. (Nitrogen fixation refers to the chemical conversion of N_2 to any other nitrogen compound.) The “natural” fixation of N_2 occurs by two types of processes. One is the action of a comparatively few microorganisms that are capable of converting N_2 to ammonia, ammonium ion (NH_4^+), and organic nitrogen compounds. The other natural nitrogen fixation process occurs in the atmosphere by the action of ionizing phenomena, such as cosmic radiation or lightning, on N_2 . This process leads to the formation of nitrogen oxides in the atmosphere, which are ultimately deposited on the Earth’s surface as biologically useful nitrates.

In addition to natural nitrogen fixation, human activities have led to biological and industrial fixation and fixation by combustion. Humans have increased the cultivation of legumes, which have a symbiotic relationship with certain microorganisms capable of nitrogen fixation. Legumes provide an increase in the soil nitrogen and serve as a valuable food crop. Industrial nitrogen fixation consists primarily of the production of ammonia for fertilizer use. Combustion can also lead to the fixation of nitrogen as NO_x . In the process of nitrification, ammonium is oxidized to NO_2^- and NO_3^- by microbial action. N_2O and NO are by-products of nitrification; the result is the release of N_2O and NO to the atmosphere. Reduction of NO_3^- to N_2 , NO_2 , N_2O , or NO is called denitrification. Denitrification is accomplished by a number of bacteria and is the process that continually replenishes the atmosphere’s N_2 . Figure 2.4 depicts the atmospheric nitrogen cycle.

2.3.1 Nitrous Oxide (N_2O)

Nitrous oxide (N_2O) is an important atmospheric gas that is emitted predominantly by biological sources in soils and water. Although by comparison to CO_2 and H_2O , N_2O has a far lower concentration, it is an extremely influential greenhouse gas. This is a result of its long

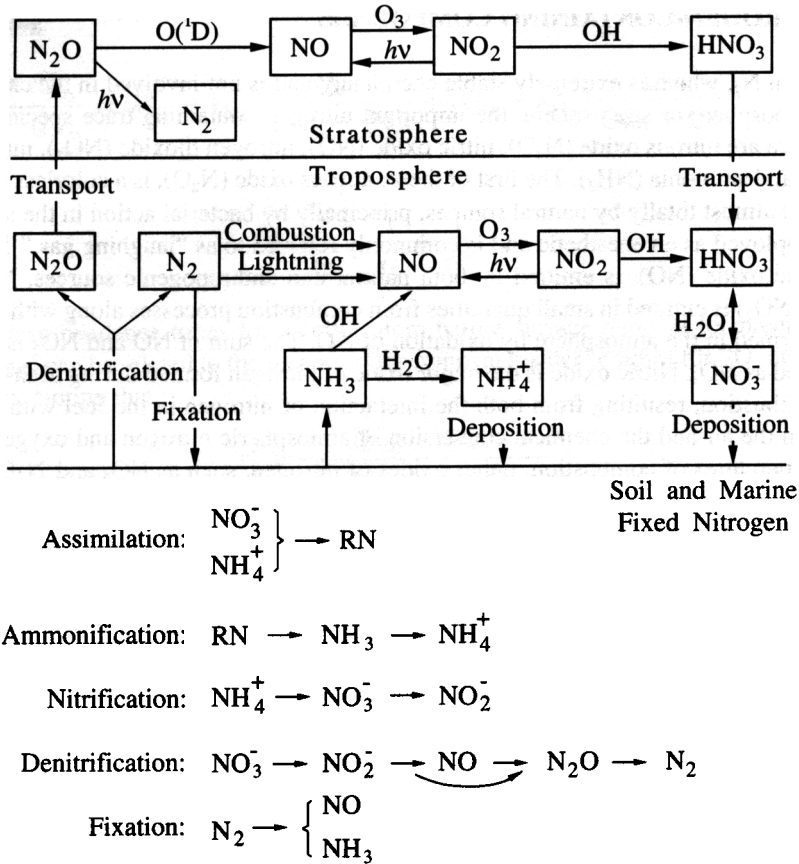


FIGURE 2.4 Processes in the atmospheric cycle of nitrogen compounds. A species written over an arrow signifies reaction with the species from which the arrow originates.

residence time and its relatively large energy absorption capacity per molecule. Per unit mass the global warming potential of N_2O (see Chapter 21) is about 300 times that of CO_2 . Tropical soils are the most important source of N_2O to the atmosphere; this source is estimated at 4 Tg(N) yr^{-1} (Table 2.4). N_2O is also emitted in smaller quantities by a large number of other sources, such as biomass burning, degassing of irrigation water, agricultural activities, and industrial processes, although the quantities of emission from these sources are difficult to estimate (Bouwman et al., 1995). The oceans are significant N_2O sources. The total preindustrial N_2O source was approximately 9 Tg(N) yr^{-1} (range 6 to 12). The current flux of N_2O into the atmosphere that results from anthropogenic activities is 3.7 to $7.7 \text{ Tg(N) yr}^{-1}$.

Nitrous oxide is inert in the troposphere; its major atmospheric sink is photodissociation in the stratosphere (about 90%) and reaction with excited atomic oxygen atoms, $\text{O}(^1\text{D})$ (about 10%). Oxidation of N_2O by $\text{O}(^1\text{D})$ yields NO , providing the major input of NO to

TABLE 2.4 Estimated Sources and Sinks of N₂O Typical of the Last Decade

Sources	Range (Tg(N) yr ⁻¹)	Likely (Tg(N) yr ⁻¹)
NATURAL		
Oceans	1-5	3
<i>Tropical soils</i>		
Wet forests	2.2-3.7	3
Dry savannas	0.5-2.0	1
<i>Temperate soils</i>		
Forests	0.1-2.0	
Grasslands	0.5-2.0	
Total natural sources		9
ANTHROPOGENIC		
Cultivated soils	1.8-5.3	3.5
Biomass burning	0.2-1.0	0.5
Industrial sources	0.7-1.8	1.3
Cattle and feedlots	0.2-0.5	0.4
SINKS		
Stratosphere	9-16	12.3
Soils	?	
Total sinks	9-16	12.3
Implied total sources (atmospheric increase + total sinks) ^a		

^aThe observed atmospheric increase implies that sources exceed sinks by 3.9 Tg(N) yr⁻¹.

Source: IPCC (1995).

the stratosphere. We will return to this process in Chapter 4. Sources of N₂O exceed estimated sinks by 2.4 Tg(N) yr⁻¹.

Estimates for the atmospheric lifetime of N₂O come from stratospheric chemical transport models that have been tested against observed N₂O distributions. The best current estimate for the lifetime of N₂O is 120 ± 30 years. Because of its long lifetime N₂O exhibits more or less uniform concentrations throughout the troposphere. Ice core records of N₂O show a preindustrial mixing ratio of about 276 ppb. N₂O levels have risen approximately 15% since preindustrial times, reaching 311 ppb in 1992 (IPCC, 1995; Machida et al., 1995) (Figure 2.5). This observed atmospheric increase is consistent with a difference of 3.9 Tg(N) yr⁻¹ excess of sources over sinks, which is in reasonable agreement, given the uncertainties, with the mismatch based on attempting to estimate sources and sinks independently.

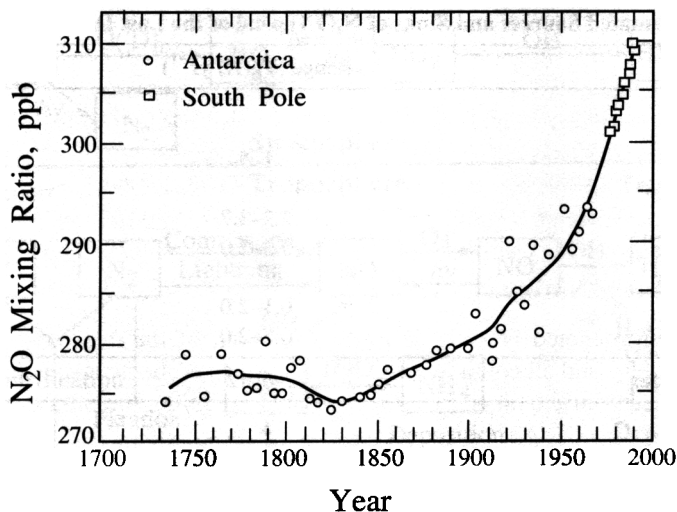


FIGURE 2.5 Atmospheric N_2O mixing ratios over the last 250 years obtained from ice core data (Machida et al., 1995). Annual mean values at the South Pole for the period 1977 to 1991 are given by squares. Solid curve is a fit to the data.

2.3.2 Nitrogen Oxides ($\text{NO}_x = \text{NO} + \text{NO}_2$)

The oxides of nitrogen, NO and NO_2 , are among the most important molecules in atmospheric chemistry. We will devote in this book considerable attention to their chemistry. Estimated global emissions of NO_x typical of the last decade are given in Table 2.5. Estimated global emissions of NO_x from fossil-fuel combustion increased from $18.1 \text{ Tg(N) yr}^{-1}$ in 1970 to $24.3 \text{ Tg(N) yr}^{-1}$ in 1986 (Hameed and Dignon, 1992). Aircraft emissions are listed separately in Table 2.5 because they are released predominantly in the free troposphere at altitudes of 8 to 12 km rather than at the surface, and although such emissions are only a small fraction of the total combustion source, they are potentially responsible for a large fraction of the NO_x found at those altitudes at northern midlatitudes (Ehhalt et al., 1992).

TABLE 2.5 Estimated Global Emissions of NO_x Typical of the Last Decade

	Magnitude (Tg(N) yr^{-1})	Comments
Fossil-fuel combustion	24	Surface source; >95% NH
Soil release (natural and anthropogenic)	12	Continental surface source
Biomass burning	8	Tropical surface source
Lightning	5	Free tropospheric source
NH_3 oxidation	3	Tropospheric source
Aircraft	0.5	6–12 km source; 95% NH
Transport from stratosphere	0.1 (0.6 total NO_x)	Free tropospheric source

Source: IPCC (1995).

Detailed emissions inventories are available for Canada, the United States, and western Europe that describe the spatial patterns of NO_x emissions from combustion of fossil fuels and from industrial processes (Lubkert and Zierock, 1989; Placet et al., 1990). Between 40 and 45% of all NO_x emissions in the United States are estimated to come from transportation, 30 to 35% from power plants, and about 20% from industrial sources. About half the NO_x emissions associated with transportation come from light-duty gasoline trucks and cars and approximately one-quarter are from heavy-duty gasoline and diesel vehicles.³

2.3.3 Reactive Odd Nitrogen (NO_y)

Reactive nitrogen, denoted NO_y , is defined as the sum of the two oxides of nitrogen ($\text{NO}_x = \text{NO} + \text{NO}_2$) and all compounds that are products of the atmospheric oxidation of NO_x . These include nitric acid (HNO_3), nitrous acid (HONO), the nitrate radical (NO_3), dinitrogen pentoxide (N_2O_5), peroxyxynitric acid (HNO_4), peroxyacetyl nitrate (PAN) (RC(O)OONO_2) and its homologues, alkyl nitrates (RONO_2), and peroxyalkyl nitrates (ROONO_2). Nitric acid (HNO_3) is the major oxidation product of NO_x in the atmosphere. Because of its extreme water solubility, HNO_3 is rapidly deposited on surfaces and in water droplets. Also, in the presence of NH_3 , HNO_3 can form an ammonium nitrate (NH_4NO_3) aerosol. The nitrate radical (NO_3) is an important constituent in the chemistry of the troposphere, especially at night. NO_3 is present at night at mixing ratios ranging up to 300 ppt in the boundary layer. Nitrous oxide (N_2O) and ammonia (NH_3) are not considered in this context as reactive nitrogen compounds.

Measurement of total NO_y in the atmosphere provides an important measure of the total oxidized nitrogen content. Concentrations of individual NO_y species relative to the total indicate the extent of interconversion among species. NO_y is indeed closer to a conserved quantity than any of its constituent species (Roberts, 1995).

There is a sizable body of data on the concentrations of NO_x in the atmosphere, but caution must be exercised in drawing conclusions from these measurements. Many measurements of NO_x have been made by devices that convert NO_2 to NO , which is then measured by the phenomenon of chemiluminescence. Comparison of these measurements with more specific techniques suggests that surface converters that can convert NO_2 to NO also convert other reactive nitrogen oxide species, such as peroxyacetyl nitrate (PAN), to NO , thereby causing interference. In urban locations, where the local NO sources are typically large, NO and NO_2 are probably the dominant constituents of the total reactive nitrogen NO_y . Thus, in urban areas, interference from PAN and other oxides of nitrogen is believed to be relatively small. In rural and remote locations, however, the interference can be substantial. For this reason, all nonurban NO_x measurements made with surface converters must be considered upper limits (biased toward a high measurement).

Given the dominant role of anthropogenic emissions in the budget of atmospheric NO_x and the fact that the sources of these emissions tend to be located in or near urban areas, elevated concentrations of NO_x are to be expected in these locations. Observations of NO_x support this expectation. The range and variability of NO_x measurements are reflected in measurements made in 29 cities across the eastern and southern United States during the

³It is estimated that in 1994 there were 147,000,000 light-duty motor vehicles in the United States, 48,000,000 trucks (85% light-duty), and 676,000 buses. Total vehicle miles traveled were estimated as 235×10^{12} , with 1.4×10^{11} gallons of gasoline consumed.

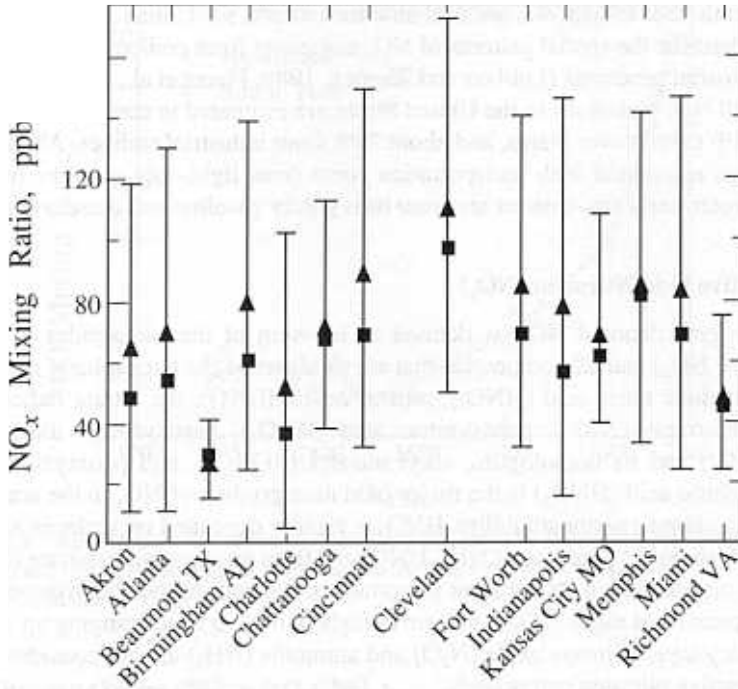


FIGURE 2.6 NO_x mixing ratios measured in urban areas in the United States during the summer of 1984 (National Research Council, 1991). All measurements were made between 6:00 a.m. and 9:00 a.m. daylight savings time. The triangles are the averages for each site, the squares are the medians, and the bars show the standard deviations of the means. Originally adapted from Baugues (1986).

summers of 1984 and 1985 (Baugues, 1986) (Figure 2.6). NO_x measurements were made in 10 of the cities in both years. The measurements were made during the morning rush hour, 6:00 a.m. and 9:00 a.m. Figure 2.6 shows the average and median NO_x mixing ratios and the standard deviations for each city. The average for all the cities studied varied between 18 ppb in Texas City, Texas, and 114 ppb in Cleveland, Ohio.

Because urban areas have concentrated sources of NO_x , urban measurements allow study of the rate of temporal and spatial decline of the NO_x concentration with distance downwind of a source. From a number of observational studies, it has been estimated that the characteristic time for conversion of NO_x to other NO_y species is 4 to 20 hours. The ratio of NO_x to NO_y reflects the chemical processing that occurs in an air mass after the initial introduction of NO_x . Thus this quantity is indicative of the oxidation that has occurred in the air mass. Because urban areas have large sources of NO_x and because it takes several hours to convert NO_x to other NO_y compounds, NO_y concentrations in urban locations are generally dominated by NO_x .

Only during the past decade or so have techniques been available with sufficient sensitivity and range of detectability to measure NO_x in nonurban locales (NO_x concentrations below 1 ppb), and as a result the size and reliability of the database needed to define nonurban NO_x concentrations are limited. Measurements taken at isolated rural sites in the United States tend to be significantly lower than concentrations measured at less-isolated

TABLE 2.6 Typical Boundary Layer NO_x Mixing Ratios

Region	NO _x (ppb)
Urban-suburban	
Rural	
Remote tropical forest	
Remote marine	

Source: National Research Council (1991).

rural sites and generally range from a few tenths to 1 ppb. Measurements of NO_x in the atmospheric boundary layer and lower free troposphere in remote maritime locations have generally yielded mixing ratios of 0.02 to 0.04 ppb (20 to 40 ppt). Although the database is still quite sparse, mixing ratios in remote tropical forests (not under the direct influence of biomass burning) appear to range from 0.02 to 0.08 ppb (20 to 80 ppt); the somewhat higher NO_x concentrations found in remote tropical forests, as compared with those observed in remote marine locations, could result from biogenic NO_x emissions from soil.

A summary of the NO_x measurements made in the four regions of the globe mentioned above is presented in Table 2.6. It can be seen that NO_x concentrations decrease sharply as one moves from urban and suburban to rural sites in the United States and then to remote sites over the ocean and tropical forests. The striking difference of three orders of magnitude or more between NO_x concentrations in urban-suburban areas and remote locations is compelling evidence for the dominant role of anthropogenic emissions of NO_x over strong anthropogenic source regions such as North America. Because the ability to measure NO_y was developed only recently, the rural and remote NO_y database is even more limited than that for NO_x. However, there are enough data to establish a rough indication of the NO_y distribution. Average NO_y concentrations observed at many sites in the United States are quite similar; median mixing ratio values range from 3 to 10 ppb. These are somewhat lower than NO_x mixing ratios typically observed in urban and suburban locations, which range from 10 to 1000 ppb.

The contrast in NO_x concentrations found in rural areas of the continental United States with those observed in the remote troposphere is illustrated in Figure 2.7. The measurement sites are Scotia, Pennsylvania, a rural site in the eastern United States; Niwot Ridge, Colorado, an isolated inland site in the western United States; Point Arena, California, a site on the West Coast that often receives air from the Pacific Ocean; and Mauna Loa, Hawaii, a remote maritime site. Two of the sites, Mauna Loa and Niwot Ridge, are at high elevations (approximately 3 km), and thus the air sampled there is not necessarily representative of the boundary layer. There is a progressive decrease in the contribution of NO_x to NO_y as one moves toward more remote regions. On average, NO_x at Scotia accounted for 59% of the observed NO_y. At Niwot Ridge in 1987, NO_x accounted for 32% of the NO_y, and at Mauna Loa, NO_x accounted for only 15% of the NO_y. Because NO_y enters the atmosphere as NO_x, the decrease in the ratio of NO_x to NO_y as one moves to more remote sites can be understood in terms of the increasing chemical conversion of NO_x to organic nitrates (principally PAN) and to inorganic nitrates (principally HNO₃) with increasing distance of the site from major anthropogenic sources. The most remote sites are characterized by the lowest ratios of NO_x/NO_y. Those sites at high altitudes have the largest ratio of

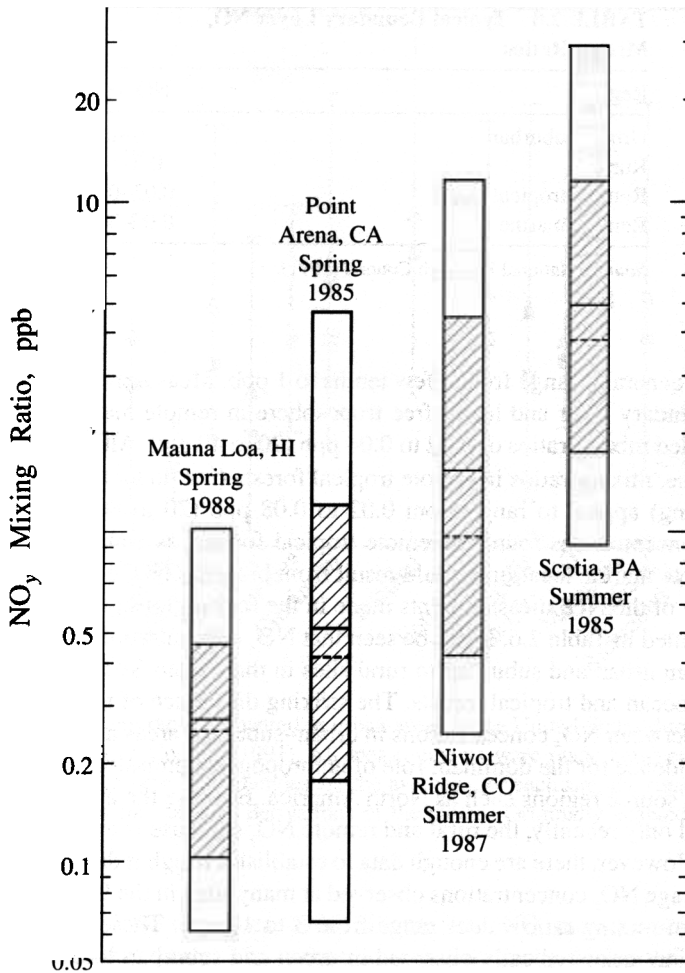


FIGURE 2.7 NO_y measurements in the continental United States and Hawaii (National Research Council, 1991). Bars show the range of data. Dashed line is median of values; solid line is mean; shaded area is central 68% of data. Original data sources are given in National Research Council (1991).

PAN/NO_y , a fact that we will return to later when we discuss tropospheric chemistry. Indeed, PAN is the most abundant NO_y species in the remote free troposphere.

On the basis of the estimated source strengths and concentrations, the mean tropospheric residence time for gaseous NO_x , including HNO_3 , is estimated to be in the range of 1 to 4 days and that for particulate nitrate, in the range of 3 to 9 days. Because of these relatively short atmospheric lifetimes, the major effects of emissions of nitrogen oxides are expected to be local or regional rather than global in nature.

2.3.4 Ammonia (NH_3)

Ammonia is the primary basic gas in the atmosphere and, after N_2 and N_2O , is the most abundant nitrogen-containing compound in the atmosphere. The significant sources of NH_3

TABLE 2.7 Estimated Global Ammonia Emissions

Source of Ammonia	Emission (Tg(N) yr ⁻¹)
ANTHROPOGENIC	
Dairy cattle	5.5
Beef cattle/buffalo	8.7
Pigs	2.8
Horses	1.2
Sheep/goats	2.5
Poultry	1.3
Fertilizer	6.4
Biomass burning	2.0
Subtotal	<u>30.4</u>
NATURAL	
Wild animals	2.5
Vegetation	5.1
Ocean	<u>7.0</u>
Subtotal	<u>14.6</u>
Total	<u>45.0</u>

Source: Dentener and Crutzen (1994).

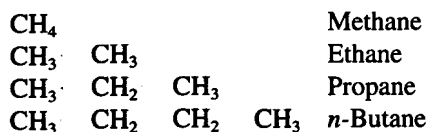
are animal waste, ammonification of humus followed by emission from soils, losses of NH₃-based fertilizers from soils, and industrial emissions (Table 2.7). The ammonium (NH₄⁺) ion is an important component of the continental tropospheric aerosol. Because NH₃ is readily absorbed by surfaces such as water and soil, its residence time in the lower atmosphere is expected to be quite short, about 10 days. Wet and dry deposition of NH₃ are the main atmospheric removal mechanisms for NH₃. In fact, deposition of atmospheric NH₃ and NH₄⁺ may represent an important nutrient to the biosphere in some areas. Atmospheric concentrations of NH₃ are quite variable, depending on proximity to a source-rich region. NH₃ mixing ratios over continents range typically between 0.1 and 10 ppb.

2.4 CARBON-CONTAINING COMPOUNDS

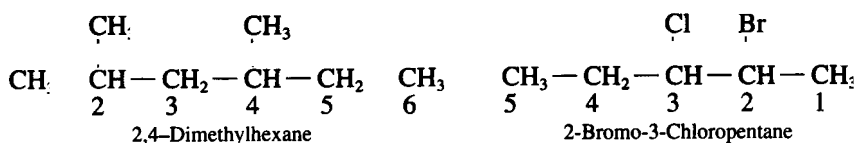
2.4.1 Classification of Hydrocarbons

Let us review briefly the classifications of carbon-containing compounds, particularly those of interest in atmospheric chemistry. The carbon atom has four valence electrons and can therefore share bonds with from one to four other atoms. The nature of the carbon-carbon bonding in a hydrocarbon molecule basically governs the properties (as well as the nomenclature) of the molecule.

In some sense the simplest hydrocarbon molecules are those in which all the carbon bonds are shared with hydrogen atoms except for a minimum number required for carbon-carbon bonds. Molecules of this type are referred to as *alkanes* or, equivalently, as paraffins. The general chemical formula of alkanes is C_nH_{2n+2} . The first four paraffins having a straight chain structure are:

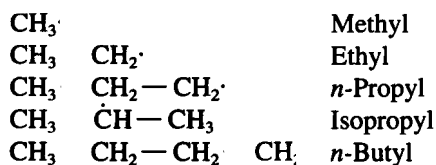


Alkanes need not have a straight chain structure. If a side carbon chain exists, the name of the longest continuous chain of carbon atoms is taken as the base name, which is then modified to include the type of group. Typical examples of substituted alkanes are (the numbering system is indicated below the carbon atoms):



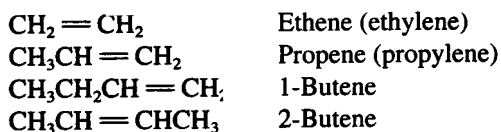
Alkanes may also be arranged in a ring structure, in which case the molecule is referred to as a cycloalkane.

Alkanes generally react by replacement of a hydrogen atom. Once a hydrogen atom is removed from an alkane, the involved carbon atom has an unpaired electron and the molecule becomes a free radical, in this case an alkyl radical. Examples of alkyl radicals are:

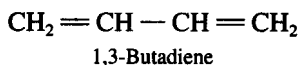


Alkyl radicals are often simply designated $R \cdot$, where R denotes the chemical formula for any member of the alkyl group. The unpaired electron in a free radical makes the species extremely reactive. As we have already noted, free radicals play an essential role in atmospheric chemistry.

The next class of carbon-containing compounds of interest in atmospheric chemistry is the *alkenes*. In this class two neighboring carbon atoms share a pair of electrons, a so-called double bond. Alkenes are also known as alkylenes or olefins. The location of the carbon atom nearest to the end of the molecule that is the first of the two carbon atoms sharing the double bond is often indicated by the number of the carbon atom. Examples of common alkenes are:

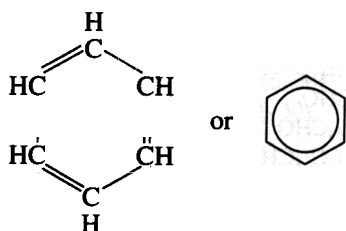


Molecules with two double bonds are called alkadienes, an example of which is

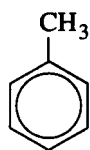


Molecules with a single triple bond are known as *alkynes*, the first in the series of which is acetylene, $\text{HC} \equiv \text{CH}$.

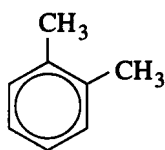
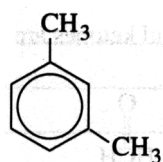
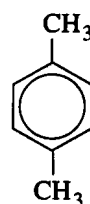
Double-bonded hydrocarbons may also be arranged in a ring structure. This class of molecules, of which the basic unit is benzene,



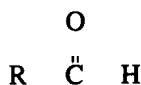
is called *aromatics*. Other common aromatics are



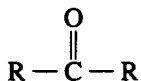
Toluene

*o*-Xylene*m*-Xylene*p*-Xylene

Hydrocarbons may acquire one or more oxygen atoms. Of the oxygenated hydrocarbons, two classes of *carbonyls* that are of considerable importance in the atmosphere are *aldehydes* and *ketones*. In each type of molecule, a carbon atom and an oxygen atom are joined by a double bond. Aldehydes have the general form



whereas ketones have the structure



Thus the distinction lies in whether the carbon atom is bonded to one or two alkyl groups.

TABLE 2.8 Some Atmospheric Organic Species

Alkanes	Methane	CH ₄	Microbial processes, natural gas	OH	1.7 ppb
	Ethane	C ₂ H ₆	Motor vehicles	OH	0–100 ppb
	Hexane	C ₆ H ₁₄	Motor vehicles	OH	0–30 ppb
Alkenes	Ethene	C ₂ H ₄	Motor vehicles, microbial processes	OH, O ₃	0–100 ppb
	Propene	C ₃ H ₆	Motor vehicles	OH, O ₃	0–50 ppb
	Isoprene	C ₅ H ₈	Vegetation	OH, O ₃	0.2–30 ppb
Alkynes	Acetylene	C ₂ H ₂	Motor vehicles	OH	0–100 ppb
Aromatics	Benzene	C ₆ H ₆	Motor vehicles	OH	
	Toluene	C ₇ H ₈	Motor vehicles	OH	
Aldehydes	Formaldehyde	HCHO	Motor vehicles	<i>hν</i> , OH	
	Acetaldehyde	CH ₃ CHO	Motor vehicles	<i>hν</i> , OH	
	Acrolein	CH ₂ CHCHO			
Ketones	Acetone	CH ₃ C(O)CH ₃		<i>hν</i> , OH	0–10 ppb
Acids	Formic acid	HCOOH		Rain	
	Acetic acid	CH ₃ COOH		Rain	
Alcohols	Methanol	CH ₃ OH		OH	

Examples of aldehydes and ketones are:

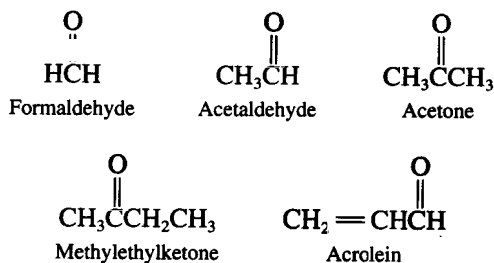


Table 2.8 lists a number of organic species found in the atmosphere.

2.4.2 Methane

Methane is the most abundant hydrocarbon in the atmosphere. Table 2.9 summarizes the global sources of CH₄, which are estimated at 535 Tg(CH₄) yr⁻¹ (range 410 to 660) (IPCC, 1995). Of the estimated global annual emissions, 160 Tg(CH₄) yr⁻¹ is attributed to natural sources, with the most prominent contribution being emissions from wetlands. Of the estimated 375 Tg(CH₄) yr⁻¹ from anthropogenic sources, 100 Tg(CH₄) yr⁻¹ comes from fossil fuel combustion, and the remainder from biospheric sources. Methane is removed from the atmosphere through reaction with hydroxyl radicals (OH) in the troposphere, estimated at 445 Tg(CH₄) yr⁻¹, and by reaction in the stratosphere, estimated at 40 Tg(CH₄) yr⁻¹. Microbial uptake in soils contributes an estimated 30 Tg(CH₄) yr⁻¹ removal rate. The im-

CARBON-CONTAINING COMPOUNDS

TABLE 2.9 Estimated Sources and Sinks of Methane ($\text{Tg}(\text{CH}_4) \text{ yr}^{-1}$)

Identified Sources	Individual Estimate	Total
NATURAL		
Wetlands	115 (55–150)	
Termites	20 (10–50)	
Oceans	10 (5–50)	
Other	15 (10–40)	
Total identified natural sources		160 (110–210)^a
ANTHROPOGENIC		
Fossil-fuel related sources		
Natural gas	40 (25–50)	
Coal mines	30 (15–45)	
Petroleum industry	15 (5–30)	
Coal combustion	? (1–30)	
Total fossil-fuel related		100 (70–120)^b
Biospheric carbon		
Enteric fermentation	85 (65–100)	
Rice paddies	60 (20–100)	
Biomass burning	40 (20–80)	
Landfills	40 (20–70)	
Animal waste	25 (20–30)	
Domestic sewage	25 (15–80)	
Total biospheric		275 (200–350)
Total identified anthropogenic sources		375 (300–450)^a
Total identified sources		
Sinks		
Tropospheric OH	445 (360–530)	
Stratosphere	40 (32–48)	
Soils	30 (15–45)	
Total sinks		515 (430–600)
Total global burden: 4850 Tg (CH_4)		

^aA preindustrial level of 700 ppb would have required a source of 210 $\text{Tg}(\text{CH}_4) \text{ yr}^{-1}$ if the lifetime has remained constant, and 280 $\text{Tg}(\text{CH}_4) \text{ yr}^{-1}$ if current tropospheric chemical feedbacks can be extrapolated back. The total anthropogenic emissions of CH_4 based on identified sources, 375 (300–450), is slightly higher than the inferred range from preindustrial levels, 270–340, but is well within the uncertainties.

^bFractional source from fossil carbon based on a measure of the atmospheric ratio of $^{14}\text{CH}_4$ to $^{12}\text{CH}_4$.

Note: The observed increases in methane show that sources exceed sinks by about 35 to 40 Tg each year. All data are rounded to the nearest 5 Tg.

Source: IPCC (1995).

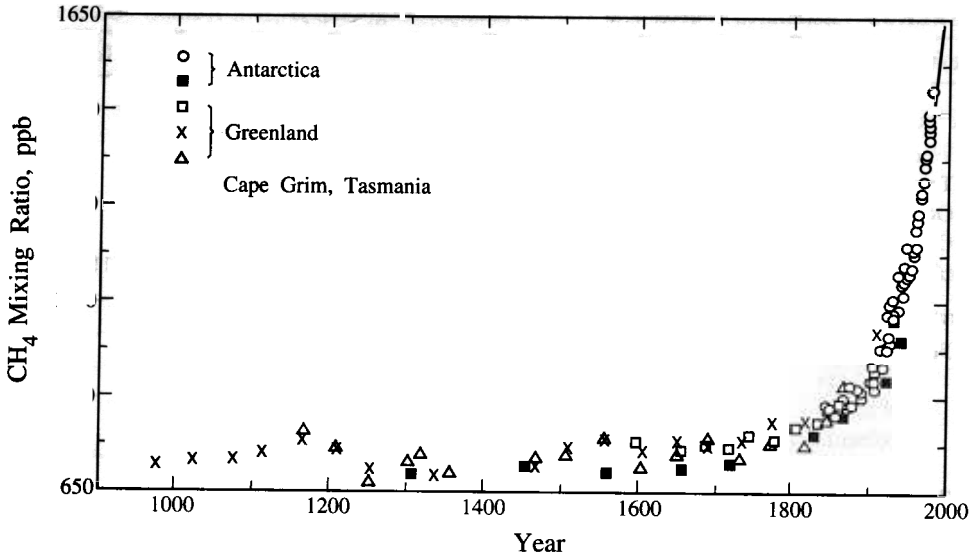


FIGURE 2.8 Methane mixing ratios over the last 1000 years as determined from ice cores from Antarctica and Greenland (IPCC, 1995). Different data points indicate different locations. Atmospheric data from Cape Grim, Tasmania, are included to demonstrate the smooth transition from ice core to atmospheric measurements.

balance between the current sources and sinks of CH_4 in Table 2.9 indicates that methane is accumulating in the atmosphere.

Atmospheric CH_4 concentrations have changed considerably over time. Figure 2.8 shows CH_4 mixing ratios over the past 1000 years. CH_4 has increased from a preindustrial mixing ratio near 700 ppb to a present-day value of 1720 ppb (Dlugokencky et al., 1994). The tropospheric concentration increase results from a source/sink imbalance of about 35 to 40 $\text{Tg}(\text{CH}_4) \text{yr}^{-1}$. Based on the observed rate of increase, the implied total source of CH_4 (atmospheric increase + total sinks) is about 550 $\text{Tg} \text{yr}^{-1}$. All the data points are based on CH_4 in air bubbles trapped in ice cores in Antarctica, with the exception of the solid curve, which is based on atmospheric measurements made at Cape Grim, Tasmania. Atmospheric CH_4 levels are about 6% lower in the Southern Hemisphere than in the Northern Hemisphere, which is explained by the fact that sources of CH_4 are essentially land based and exist predominantly in the Northern Hemisphere. This 6% difference corresponds to an excess Northern Hemisphere source of about 280 $\text{Tg}(\text{CH}_4) \text{yr}^{-1}$.

2.4.3 Volatile Organic Compounds

The term volatile organic compounds (VOCs) is used to denote the entire set of vapor-phase atmospheric organics excluding CO and CO_2 . VOCs are central to atmospheric chemistry from the urban to the global scale. Characterizing VOC emissions ideally requires not just total VOCs but the individual chemical compounds that constitute the entire mixture since the atmospheric behavior of individual species can vary enormously. The U.S. National Acid Precipitation Assessment Program (NAPAP) inventory of anthro-

TABLE 2.10 Estimated Global Anthropogenic Emissions of Nonmethane Volatile Organic Compounds

Activity	Emission (Tg yr ⁻¹)
FUEL PRODUCTION/DISTRIBUTION	
Petroleum	8
Natural gas	2
Oil refining	5
Gasoline distribution	2.5
FUEL CONSUMPTION	
Coal	3.5
Wood	25
Crop residues (including waste)	14.5
Charcoal	2.5
Dung cakes	3
Road transport	36
Chemical industry	2
Solvent use	20
Uncontrolled waste burning	8
OTHER	10
Total	142

Source: Middleton (1995).

pogenic VOC emissions included, for example, about 600 different compounds (Placet et al., 1990).

Motor vehicles are the dominant contributor to VOC emissions in the United States. VOCs emitted from motor vehicles are mainly hydrocarbons that result from the incomplete combustion of fuel or from its vaporization. These contributions are generally categorized and reported as exhaust and evaporative emissions. Within the exhaust emissions category are included the unburned and partially burned fuel and lubricating oil in the exhaust and gases that leak from the engine. The evaporative emissions category includes fuel vapor emitted from the engine and fuel system that can be attributed to several sources: vaporization of fuel as a result of the heating of the fuel tank, vaporization of fuel from the heat of the engine after it has been turned off (hot-soak emissions), vaporization of fuel from the fuel system while the vehicle is operating (running losses), fuel losses due to leaks and diffusion through containment materials (resting losses), and fuel vapor displacement as a result of filling fuel tanks (refueling losses). Motor vehicles are the major sources of alkane and aromatic emissions.

Estimates of global anthropogenic nonmethane VOC emissions in 1990 are given in Table 2.10. In general, a breakdown by chemical compound is not yet available for global anthropogenic VOC emissions. As seen in Table 2.10, transportation is the largest source of VOC emissions worldwide, with solvent use following as the second largest source.

As an illustration of the large number of organic compounds identified in the atmosphere, Table 2.11 lists the median concentrations of the 25 most abundant nonmethane organic species measured in the 1987 Southern California Air Quality Study.

TABLE 2.11 Median Mixing Ratio of the 25 Most Abundant Nonmethane Organic Compounds Measured in the Summer 1987 Southern California Air Quality Study

	Median Mixing Ratio in Parts per Billion of Carbon ^a
Ethane	27.1
Ethene	22.3
Acetylene	17.3
Propane	56.0
Propene	7.8
<i>i</i> -Butane	19.4
Butane	42.0
<i>i</i> -Pentane	52.4
Pentane	24.0
2-Methylpentane	16.0
3-Methylpentane	11.8
Hexane	10.8
Methylcyclopentane	10.1
Benzene	17.0
3-Methylhexane	7.4
Heptane	6.0
Methylcyclohexane	7.0
Toluene	49.1
Ethylbenzene	7.6
<i>m</i> - and <i>p</i> -Xylenes	25.2
<i>o</i> -Xylene	10.0
1,2,4-Trimethylbenzene	8.2
Formaldehyde	9.1
Acetaldehyde	14.8
Acetone	22.4

^aParts per billion of carbon (ppbC) is the parts per billion of carbon atoms in the molecule. It is simply the volume mixing ratio of the compound multiplied by the number of carbon atoms in the molecule.

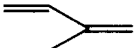
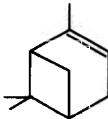
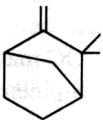
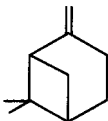

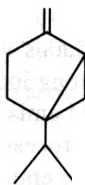
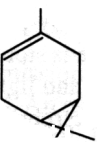
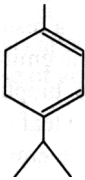
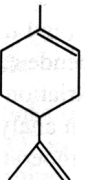
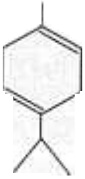

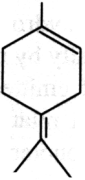
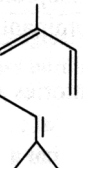
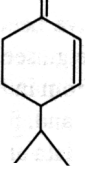

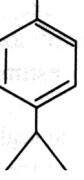
Source: Lurmann and Main (1992).

2.4.4 Biogenic Hydrocarbons

Vegetation naturally releases organic compounds to the atmosphere. In 1960, Went (1960) first proposed that natural foliar emissions of VOCs from trees and other vegetation could have a significant effect on the chemistry of the Earth's atmosphere. Since that study, numerous researchers have investigated the speciation of natural VOCs (Rasmussen and Went, 1965; Rasmussen, 1970), their rate of emission (Tingey et al., 1991; Zimmerman, 1979; Arnts and Meeks, 1981; Guenther et al., 1995; Lamb et al., 1985, 1986, 1987, 1993; Zimmerman et al., 1988; Monson et al., 1992), and the distribution of these compounds and their oxidation products in the atmosphere (Isodorov et al., 1985; Fehsenfeld et al., 1992; Montzka et al., 1993, 1995; Yokouchi, 1994).

Measurements in wooded and agricultural areas coupled with emission studies from selected individual trees and agricultural crops have demonstrated the ubiquitous nature of biogenic emissions and the variety of organic compounds that can be emitted. Table 2.12

TABLE 2.12 Organic Compounds Emitted by Vegetation^a

Isoprene		α -Pinene	
Camphene		β -Pinene	
2-Carene		Sabinene	
Δ^3 -Carene		α -Terpinene	
<i>d</i> -Limonene		γ -Terpinene	
Myrcene		Terpinolene	
Ocimene		β -Phellandrene	
α -Phellandrene		<i>p</i> -Cymene	

^aIn the simplified molecular structures here bonds between carbon atoms are shown. Vertices represent carbon atoms. Hydrogen atoms bonded to the carbons are not explicitly indicated.

shows the chemical structures of some of the common biogenic hydrocarbons. Each of the compounds shown in Table 2.12 is characterized by an olefinic double bond that renders the molecule highly reactive in the atmosphere, with the result that the lifetimes of these molecules tend to be quite short. One compound typically emitted by deciduous trees is isoprene (C_5H_8); conifers typically emit terpenes such as α -pinene and β -pinene (Rasmussen and Went, 1965). Often half or more of the VOC mass emitted by vegetation is made up of compounds other than isoprene and α - and β -pinene (Isodorov et al., 1985; Winer et al., 1989; Singh and Zimmerman, 1990; Placet et al., 1990).

Isoprene (2-methyl-1,3-butadiene, C_5H_8) is unique among the biogenic hydrocarbons in its relationship to photosynthetic activity in a plant. It is emitted from a wide variety of mostly deciduous vegetation in the presence of photosynthetically active radiation, exhibiting a strong increase in emission as temperature increases. Not only do the isoprene and terpenoid emissions vary considerably among plant species, but the biochemical and biophysical processes that control the rate of these emissions also appear to be quite distinct. Isoprene emissions appear to be a species-dependent by-product of photosynthesis, photorespiration, or both; there is no evidence that isoprene is stored within or metabolized by plants. As a result, isoprene emissions are temperature and light dependent; essentially no isoprene is emitted without illumination. By contrast, terpenoid emissions seem to be triggered by biophysical processes associated with the amount of terpenoid material present in the leaf oils and resins and the vapor pressure of the terpenoid compounds. As a result, terpene emissions do not depend strongly on light (and they typically continue at night), but they do vary with ambient temperature. The dependence of natural isoprene and terpenoid emissions on temperature can result in a large variation in the rate of production of biogenic VOCs over the course of a growing season. An analysis of emissions data by Lamb et al. (1987) indicates that an increase in ambient temperature from 25 to 35°C can result in a factor of 4 increase in the rate of natural VOC emissions from isoprene-emitting deciduous trees and in a factor of 1.5 increase from terpene-emitting conifers. Thus, all other factors being equal, natural VOC emissions are generally highest on hot summer days.

Biogenic hydrocarbon emission rates from individual plant species have been estimated experimentally by placing small plants or branches in enclosures and measuring the accumulation of emitted compounds. Extensive emission rate measurements have been reported for a relatively limited number of compounds: isoprene and a number of the dominant monoterpenes. Isoprene does appear to be the dominant compound emitted from vegetation.

There have been a number of efforts to compile inventories of biogenic hydrocarbon emissions (e.g., see Lamb et al., 1987, 1993; and Guenther et al., 1995). Emission rate measurements from individual plant species are used with empirical algorithms that account for temperature and, for isoprene, light effects to scale up to entire geographical regions, based on land use data and biomass density factors. Biomass density, expressed in $g\ m^{-2}$ of area, is required to convert individual plant species emission rates, expressed in $mg\ g^{-1}\ min^{-1}$, to emission fluxes, in $mg\ m^{-2}\ min^{-1}$, which are then multiplied by vegetation class land coverage, in m^2 , to yield total emissions. Uncertainties in these inventories are large; Lamb et al. (1993) estimated total U.S. biogenic hydrocarbon emissions ranging from 29 to 51 $Tg\ yr^{-1}$.

On a global scale, the largest biogenic hydrocarbon emissions occur in the tropics, with isoprene being the dominant emitted compound. These result from a combination of high temperatures and large biomass densities. During summer months, the maximum flux of

TABLE 2.13 Global Biogenic VOC Emission Rate Estimates by Source and Class of Compound (Tg yr⁻¹)

Source	Isoprene	Monoterpenes	ORVOC ^a	Total VOC ^b
				821
				120
				194
				5
				9
		127	260	

^aOther reactive biogenic VOCs (ORVOC).

^bThese totals include additional non-reactive VOCs not reflected in the columns to the left.

Source: Guenther et al. (1995).

biogenic hydrocarbon emissions in the southeastern United States is predicted to be as large as that in the tropics. An estimate of global biogenic VOC emissions appears in Table 2.13. On a global basis, biogenic hydrocarbon emissions far exceed those of anthropogenic hydrocarbons.

2.4.5 Carbon Monoxide

The global sources and sinks of CO are given in Table 2.14. Methane oxidation (by OH) is a major source of CO, as are technological processes (combustion and industrial processes), biomass burning, and the oxidation of nonmethane hydrocarbons. Uncertainties in each of these estimated sources are large. It is estimated that about two-thirds

TABLE 2.14 Estimated Sources and Sinks of CO Typical of the Last Decade

Sources	Range (Tg(CO) yr ⁻¹)
Technological	
Biomass burning	
Biogenics	
Oceans	
Methane oxidation	
NMHC oxidation	
Sinks	

of the CO comes from anthropogenic activities, including oxidation of anthropogenically derived CH₄. The major sink for CO is reaction with OH radicals, with soil uptake and diffusion into the stratosphere being minor routes.

Tropospheric CO mixing ratios range from 40 to 200 ppb. Carbon monoxide has a chemical lifetime of 30 to 90 days on the global scale of the troposphere. Measurements indicate that there is more CO in the Northern Hemisphere than in the Southern Hemisphere with the maximum values being found near the surface at northern midlatitudes. In general, the CO mixing ratio decreases with altitude in the Northern Hemisphere to a free tropospheric average value of about 120 ppb near 45° N. In the Southern Hemisphere CO tends to be more nearly uniformly mixed vertically with a mixing ratio of about 60 ppb near 45° S. Seasonal variations have been established to be about ±40% about the mean in the Northern Hemisphere and ±20% about the mean in the Southern Hemisphere. The maximum concentration is observed to occur during the local spring and the minimum is found during the late summer or early fall.

2.4.6 Carbon Dioxide

Atmospheric CO₂ levels have increased from about 280 ppm in 1800 to 356 ppm in 1993. The current rate of increase of about 1.5 ppm yr⁻¹ is the result of combustion of fossil fuels, cement production, and land use conversion. Because of the critical role played by CO₂ in climate, we will consider the global cycle of CO₂ in Chapter 21.

2.5 HALOGEN-CONTAINING COMPOUNDS

Atmospheric halogen-containing compounds are referred to by a variety of names:

Halocarbons—a general term referring to halogen-containing organic compounds

Chlorofluorocarbons (CFCs)—the collective name given to a series of halocarbons containing carbon, chlorine, and fluorine atoms

Hydrochlorofluorocarbons (HCFCs)—halocarbons containing atoms of hydrogen, in addition to carbon, chlorine, and fluorine

Hydrofluorocarbons (HFCs)—halocarbons containing atoms of hydrogen, in addition to carbon and fluorine

Perhalocarbons—halocarbons in which every available carbon bond contains a halogen atom (compounds saturated with halogen atoms)

Halons—bromine-containing halocarbons, especially used as fire extinguishing agents

The earliest interest in halogens in the atmosphere arose from sea salt as a source of gaseous halogens (Eriksson, 1959). Synthetic halocarbons have been known for the past century. Chlorofluorocarbons (CFCs) were first synthesized in the late 19th century and their properties as refrigerants were recognized over 50 years ago. Halocarbons have achieved widespread industrial use as refrigerants, propellants, and solvents. Global emissions to the atmosphere of all man-made halocarbons grew from virtually negligible quantities in 1940 to about 2.5 Tg yr⁻¹ in 1990 (Singh, 1995). The global average chlorine level in the atmosphere in 1945 was about 1 ppb, of which about 25% was man-made; by 1995 the total chlorine loading had increased to 3.5 ppb, 85% of which was anthropogenic.

As a group of atmospheric chemicals, halogen-containing compounds have a wide variety of anthropogenic and natural sources. They are produced by biological processes in the oceans, from sea salt, from biomass burning, and from industrial synthesis. Their atmospheric lifetimes vary considerably depending on their mechanism of removal, ranging from a few days to several centuries.

Table 2.15 lists atmospheric halogenated organic species with global average concentrations, atmospheric burdens, lifetimes, sources, and sinks.⁴ Of the exclusively man-made organic halogenated species, the chlorofluorocarbons are used as refrigerants (CFC-12, HCFC-22), blowing agents (CFC-11, HCFC-22), and cleaning agents (CFC-113). Methyl chloroform (CH_3CCl_3), methylene chloride (CH_2Cl_2), and tetrachloroethene (C_2Cl_4) are used as degreasers and as dry cleaning and industrial solvents. Methyl bromide (CH_3Br) is a widely used agricultural and space fumigant. All the monomethyl halides in Table 2.15 have natural sources. Methyl chloride (CH_3Cl) and CH_3Br are also products of biomass burning.

Lovelock (1971) first detected SF_6 and CFCl_3 in the atmosphere using the electron capture detector. In landmark work in atmospheric chemistry for which they received the 1995 Nobel Prize in Chemistry, Molina and Rowland (1974) showed that CFCs that are immune to removal in the troposphere could decompose photolytically in the stratosphere to release Cl atoms capable of catalytic destruction of stratospheric ozone. The very lack of chemical reactivity that makes chlorofluorocarbon molecules so intrinsically useful also allows them to survive unchanged in most commercial applications and eventually to be released to the atmosphere in their original gaseous form. The usual tropospheric sinks of oxidation, photodissociation, and wet and dry deposition are ineffective with the chlorofluorocarbons. The only important sink for CFCl_3 and CF_2Cl_2 is photodissociation in the mid-stratosphere (25 to 40 km) by solar ultraviolet radiation with wavelengths shorter than 230 nm. These same CFCs that lead to stratospheric ozone depletion are efficient absorbers of infrared radiation and potentially important greenhouse gases.

There is a sharp demarcation in atmospheric behavior between fully halogenated halocarbons and those containing one or more atoms of hydrogen. Halocarbons containing at least one hydrogen atom, such as CF_2HCl , CHCl_3 , and CH_3CCl_3 , are effectively broken down in the troposphere by reaction with the hydroxyl radical before they can reach the stratosphere. Atmospheric lifetimes of these species range from months to decades. Some of these gases also react with seawater; it is estimated that 5 to 10% of the removal of CH_3CCl_3 occurs by absorption into the ocean. The hydrohalogenated species such as

⁴The term hydrochlorofluorocarbons is the collective name given to a series of chemicals with varying number of carbon, hydrogen, chlorine, and fluorine atoms. The somewhat arcane system of numbering these compounds was proposed by the American Society of Heating and Refrigeration Engineers in 1957. For the simpler hydrochlorofluorocarbons, the numbering system may be summarized as follows:

1. The first digit on the right is the number of fluorine (F) atoms in the compound.
2. The second digit from the right is one more than the number of hydrogen (H) atoms in the compound.
3. The third digit from the right, plus one, is the number of carbon (C) atoms in the compound. When this digit is zero (i.e., only one carbon atom in the compound), it is omitted from the number.
4. The number of chlorine (Cl) atoms in the compound is found by subtracting the sum of the fluorine and hydrogen atoms from the total number of atoms that can be connected to the carbon atoms.

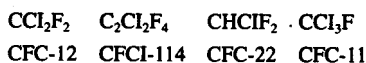


TABLE 2.15 Atmospheric Halogens

	Generic Name	1992 Mixing Ratio (ppb)	Atmospheric Burden (Tg)	Lifetime (yr)		Sinks ^b
CFCl ₃	CFC-11	0.268	6.2	50 ± 5	A	Strat. <i>hν</i>
CF ₂ Cl ₂	CFC-12	0.503	10.3	102	A	Strat. <i>hν</i>
CF ₂ ClCFCl ₂	CFC-113	0.082	2.6	85	A	Strat. <i>hν</i>
CF ₂ ClCF ₂ Cl	CFC-114	0.020		300	A	Strat. <i>hν</i>
CCl ₄	Carbon tetrachloride	0.132	3.4	42	A	Strat. <i>hν</i>
CH ₃ CCl ₃	Methyl chloroform	0.160	3.5	5.4 ± 0.6	A	Trop. OH
CH ₃ Cl	Methyl chloride	0.6	5.0	1.5	N(O),BB	Trop. OH
CF ₂ HCl	HCFC-22	0.105	1.5	13.3	A	Trop. OH
CH ₃ Br	Methyl bromide	0.012	0.15	1.3	N(O),A,BB	Trop. OH
CF ₃ Br	H-1301	0.002	0.05	65	A	Strat. <i>hν</i>
CF ₄	Perfluoromethane	0.070	0.9	50,000	A	Meso. <i>hν</i>
SF ₆	Sulfur hexafluoride	0.0025		3200	A	Meso. electron
CF ₃ CHCl ₂	HCFC-123			1.4	A	Trop. OH
CF ₃ CHFCl	HCFC-124			5.9	A	Trop. OH
CH ₃ CFCl ₂	HCFC-141b			9.4	A	Trop. OH
CH ₃ CF ₂ Cl	HCFC-142b	0.0035		19.5	A	Trop. OH
CF ₃ CF ₂ CHCl ₂	HCFC-225ca			2.5	A	Trop. OH
CClF ₂ CF ₂ CHClF	HCFC-225cb			6.6	A	Trop. OH
CHCl ₃	Chloroform			0.55	A,N(O)	Trop. OH
CH ₂ Cl ₂	Methylene chloride			0.41	A	Trop. OH
CF ₃ CF ₂ Cl	CFC-115	<0.01		1700	A	Strat. O(¹ D)
C ₂ Cl ₄	Tetrachloroethene	0.002		0.4	A	Trop. OH

^aA = anthropogenic; N(O) = natural (oceanic); BB = biomass burning.

^bStrat *hν* = photolysis in stratosphere; Trop OH = hydroxyl radical reaction in troposphere; Meso. electrons = mesosphere electron impact; Strat O(¹D) = reactions in stratosphere with excited atomic oxygen.

Source: IPCC (1995) and Singh (1995).

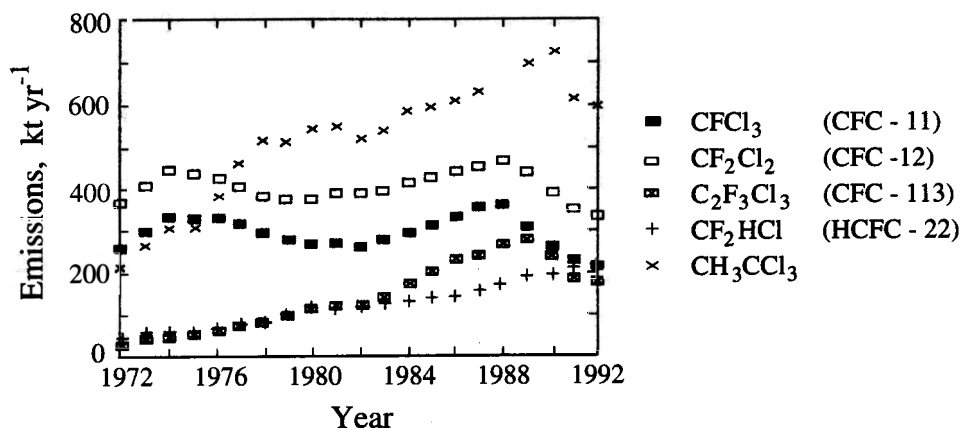


FIGURE 2.9 Annual emissions of industrially important halocarbons from 1972 to 1992 (IPCC, 1995).

methyl chloroform (CH_3CCl_3) and the HCFCs are also significant infrared absorbers but their shorter atmospheric lifetimes reduce their radiative impact relative to the fully halogenated CFCs.

Discovery of the stratospheric ozone-depleting potential of CFCs in the mid-1970s led to a ban in the United States (announced in 1976 and effective in 1978) on the use of CFCs as aerosol propellants and to similar restrictions in Canada and Scandinavia. When the Antarctic ozone hole was discovered, subsequently, an international protocol outlining proposed actions to protect the stratospheric ozone layer was signed in Montreal in September 1987. The so-called Montreal Protocol specifies a 20% reduction from 1986 emissions of fully halogenated CFCs by 1994 and a further 30% reduction by 1999. Global emissions of CFCl_3 , CF_2Cl_2 , $\text{C}_2\text{F}_3\text{Cl}_3$, CF_2HCl , and CH_3CCl_3 up to 1992 are shown in Figure 2.9. The turn-down in emission rates reflects the results of the Montreal Protocol.

Atmospheric levels of CF_2Cl_2 , CFCl_3 , and CH_3CCl_3 from 1978 to 1992 are shown in Figure 2.10. Mixing ratios increased steadily until about 1990. Methyl chloride (CH_3Cl), at an atmospheric abundance of about 600 ppt, is the dominant halogen compound in the atmosphere. To maintain the steady-state CH_3Cl concentration, with an atmospheric lifetime of order 2 years, requires a source strength of about 3.5 Tg yr^{-1} , most of which comes from the ocean. Southern Hemisphere (SH) CFC concentrations lag behind those in the Northern Hemisphere (NH) by about 1 year, reflecting the predominant source of CFCs in the NH and the approximate 1 year mixing time between the NH troposphere and the SH troposphere.

At present, the atmosphere contains approximately 20 ppt of bromine, about half of which is methyl bromide (CH_3Br). Methyl bromide is an ubiquitous component of the atmosphere, arising from both man-made and natural sources. A calculated atmospheric lifetime of 1.7 to 1.9 years, based solely on removal by reaction with OH radicals, is consistent with a global source of 90 to $110 \text{ Gg} (10^9 \text{ g}) \text{ yr}^{-1}$ (Singh and Kanakidou, 1993). A shorter lifetime of about 1.3 years (see Table 2.15) results if deposition/hydrolysis losses are also considered. Available data provide an estimate of global sources of CH_3Br that divide 35% (20 to 50%) man-made and 65% (80 to 50%) natural. Oceans are supersaturated with CH_3Br and constitute the major natural source of CH_3Br of about 60 Gg yr^{-1} , which could

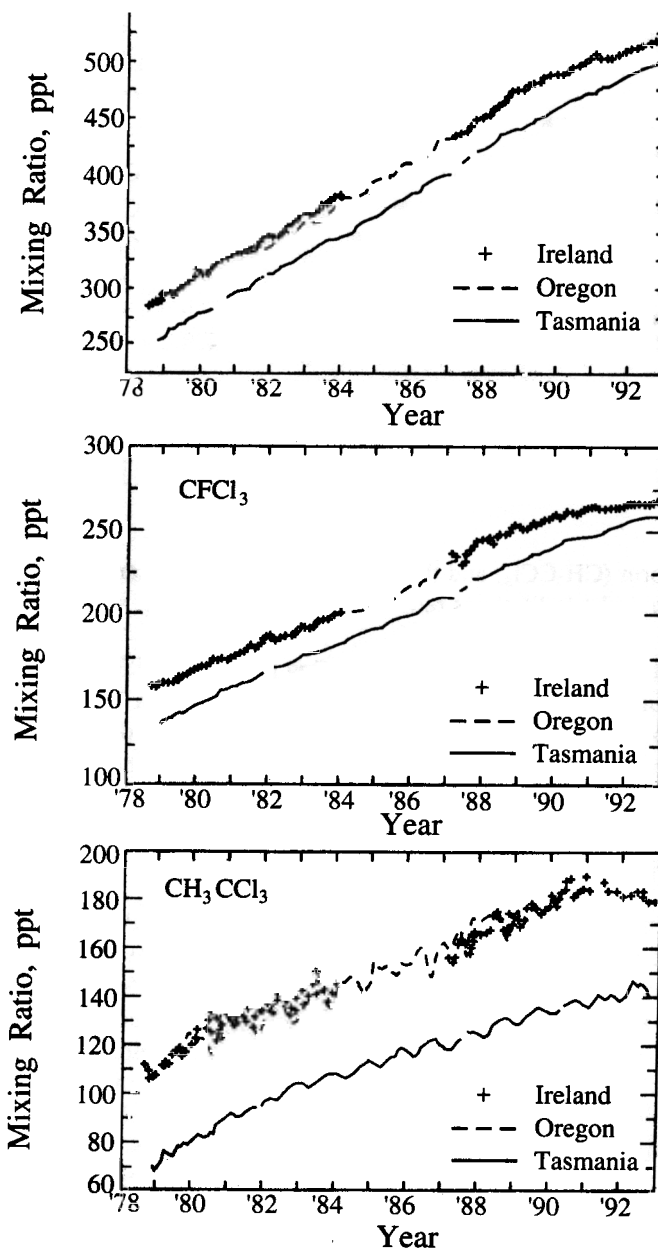


FIGURE 2.10 Atmospheric abundances of CF_2Cl_2 , CFCl_3 , and CH_3CCl_3 from 1978 to 1992 (IPCC, 1995). Monthly mean clean air values are shown for three sites: Ireland, Oregon, and Tasmania.

range from 40 to 80 Gg yr⁻¹. CH₃Br mixing ratios in the Northern Hemisphere around 1992 were about 14 ppt, with a ratio of NH to SH mixing ratios varying between 1.2 and 1.4 depending on season. The seasonal variation is a result of source strength and OH variations. CH₃Br levels have been increasing at a rate of 0.1 to 0.2 ppt yr⁻¹. Despite the fact that CH₃Br is largely removed in the troposphere by OH reaction, enough survives to enter the stratosphere and contribute to halogen-induced stratospheric ozone depletion.

2.6 ATMOSPHERIC OZONE

Ozone (O₃) is a reactive oxidant gas produced naturally in trace amounts in the Earth's atmosphere. Ozone was discovered by C. F. Schönbein in the middle of the last century; he also was first to detect ozone in air (Schönbein, 1840, 1854). Schönbein (1840) suggested the presence of an atmospheric gas having a peculiar odor (the Greek word for "to smell" is *ozein*). Spectroscopic studies in the late 19th century showed that ozone is present at a higher mixing ratio in the upper atmospheric layers than close to the ground. Attempts to explain the chemical basis of existence of ozone in the upper atmosphere began nearly 70 years ago. Within the last 30 years, however, while increased understanding of the role of other trace atmospheric species in stratospheric ozone was unfolding, it became apparent that anthropogenically emitted substances have the potential to seriously deplete the natural levels of ozone in the stratosphere. At about the same period, ironically, it was realized that anthropogenic emissions could lead to ozone *increases* in the troposphere. Whereas stratospheric ozone is essential for screening of solar ultraviolet radiation, ozone at ground level can, at elevated concentrations, lead to respiratory effects in humans. This paradoxical dual role of ozone in the atmosphere has, on occasion, led to the dubbing of stratospheric ozone as "good" ozone and tropospheric ozone as "bad" ozone.

Most of the Earth's atmospheric ozone (about 90%) is found in the stratosphere where it plays a critical role in absorbing ultraviolet radiation emitted by the Sun. Figure 2.11

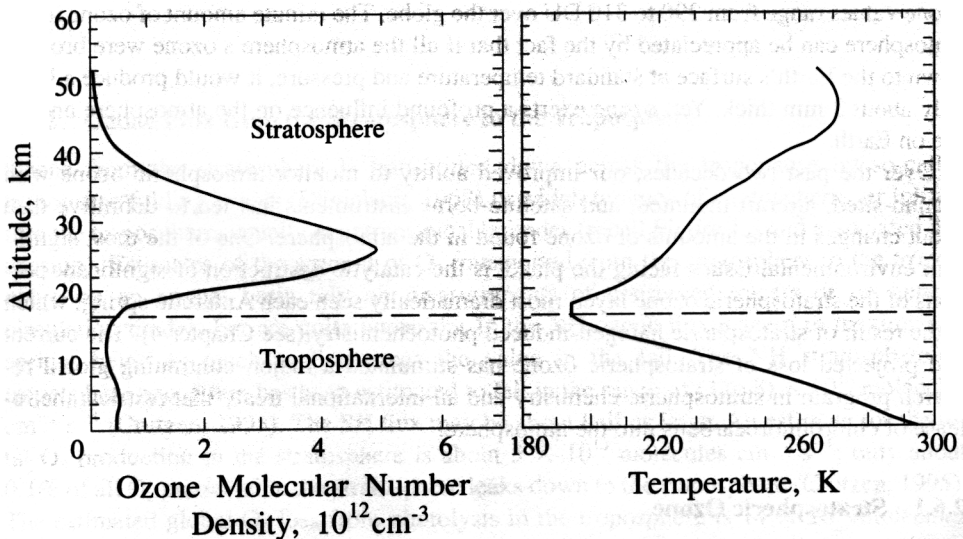


FIGURE 2.11 Stratospheric ozone layer over Natal, Brazil (5° S), March 25 to April 15, 1985 (Barnes et al. 1987)

shows the stratospheric ozone layer over Natal, Brazil (5° S), March 25 to April 15, 1985. The peak in ozone molecular number density (concentration) occurs in the region of 20 to 30 km. The so-called stratospheric ozone layer absorbs virtually all of the solar ultraviolet radiation of wavelengths between 240 and 290 nm. Such radiation is harmful to unicellular organisms and to surface cells of higher plants and animals. In addition, ultraviolet radiation in the wavelength range 290 to 320 nm, so-called UV-B, is biologically active. A reduction in stratospheric ozone leads to increased levels of UV-B at the ground, which can lead to increased incidence of skin cancer in susceptible individuals. (An approximate rule-of-thumb is that a 1% decrease in stratospheric ozone leads to a 2% increase in UV -B.) The stratospheric temperature profile (see Figure 1.1) is the result of ozone absorption of radiation. Stratospheric chemistry centers around the chemical processes influencing the abundance of ozone.

As compared with the stratosphere, natural concentrations of tropospheric ozone are small—usually a few tens of parts per billion (ppb) in mixing ratio (molecules of O₃/molecules of air; 10 ppb = 2.5×10^{11} molecules cm⁻³ at sea level and 298 K) versus peak stratospheric mixing ratios of more than 10,000 ppb (10 ppm). Since the atmospheric molecular number density thins out exponentially with altitude, the peak in ozone mixing ratio occurs at a higher altitude than does its peak in concentration. (See Problem 2.2 at the end of this chapter.) Still, a significant amount of naturally occurring ozone, about 10 to 15% of the atmospheric total, is found in the troposphere (Fishman et al., 1990). The total amount of O₃ in the atmosphere, stratosphere and troposphere combined, is extremely small. In the pristine, unpolluted troposphere ozone mixing ratios are in the range of 10 to 40 ppb with somewhat higher mixing ratios in the upper troposphere. Ozone reaches a maximum mixing ratio of about 10 ppm at an altitude of 25 to 30 km in the stratosphere.

The total column integrated ozone, that is, the total amount of O₃ integrated from the surface of the Earth to the top of the atmosphere, is often expressed in terms of *Dobson units* (DU). One DU is the thickness, measured in units of hundredths of a millimeter, that the ozone column would occupy at standard temperature and pressure (273 K and 1 atmosphere). 1 Dobson unit = 10^{-3} atm cm $\approx 2.69 \times 10^{16}$ molecules cm⁻². Total column ozone values range from 290 to 310 DU over the globe. The minute amount of ozone in the atmosphere can be appreciated by the fact that if all the atmosphere's ozone were brought down to the Earth's surface at standard temperature and pressure, it would produce a layer only about 3 mm thick. Yet, ozone exerts a profound influence on the atmosphere and on life on Earth.

Over the past two decades, our improved ability to monitor atmospheric ozone with ground-sited, aircraft-mounted, and satellite-borne instruments has led to definitive data about changes in the amounts of ozone found in the atmosphere. One of the most significant environmental issues facing the planet is the catalytic destruction of significant portions of the stratospheric ozone layer, most dramatically seen each Antarctic spring, which is the result of stratospheric halogen-induced photochemistry (see Chapter 4). The current and projected loss of stratospheric ozone has stimulated a major, continuing global research program in stratospheric chemistry and an international treaty that restricts the release of chlorofluorocarbons into the atmosphere.

2.6.1 Stratospheric Ozone

Stratospheric ozone levels over northern midlatitudes (30° N to 60° N) have decreased since around 1970. The losses are greatest in winter and spring. Satellite measurements

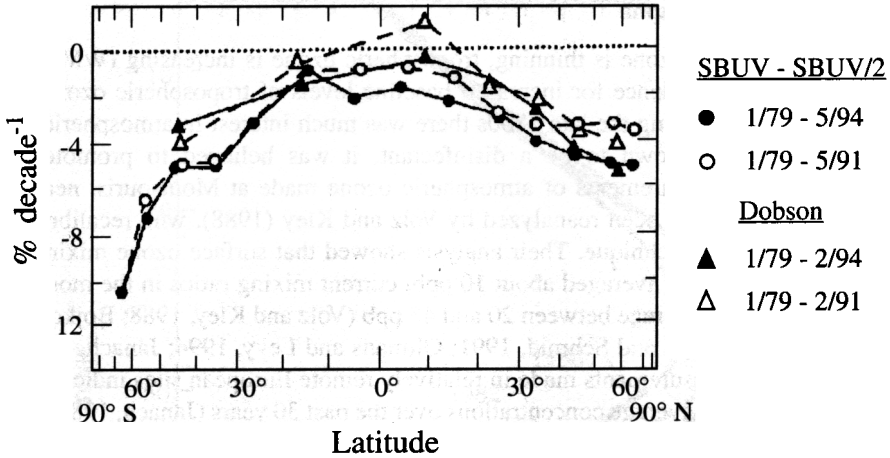


FIGURE 2.12 Annual latitudinal variation of the total ozone from January 1979 to May 1991 or February 1994, as indicated (IPCC, 1995).

from 1979 to 1991 have shown that broadly similar midlatitude losses have also occurred at equivalent latitudes in the Southern Hemisphere (IPCC, 1995). Figure 2.12 shows the annual, latitudinal variation of the total ozone trends calculated from the Dobson ground-based measurement record and satellite observations. The effect of the Antarctic ozone hole is seen in the data from 60° S to 90° S. Analysis of the total ozone mapping spectrometer (TOMS) data over the period 1979 to 1989 between 69° S and 69° N reveals a total global average ozone decrease of 3.5% over that 11 year period (Herman et al., 1991). Statistically significant decreases in total ozone are now being observed in all seasons in both the Northern and Southern Hemispheres at middle and high latitudes (Stolarski et al., 1992).

2.6.2 Ozone Flux from the Stratosphere to the Troposphere

Ozone from the stratosphere is transported down across the tropopause by so-called tropopause folding events (Danielson, 1968) in which tongues of stratospheric air intrude into the troposphere, usually at extratropical latitudes (recall Figure 1.3 and associated discussion). Estimates of the amount of O₃ transported from the stratosphere to the troposphere on an annual basis rely on measurements of conserved tracers or on general circulation models but are quite uncertain. In the NH ozone fluxes seem to maximize in spring, being as much as five times the value in the fall. The NH stratosphere-to-troposphere ozone flux has been estimated to fall in the range of $(3 \text{ to } 8) \times 10^{10}$ molecules $\text{cm}^{-2} \text{ s}^{-1}$ (Crutzen, 1995). The SH flux may be about half as large. An estimate for the total O₃ production in the stratosphere is about 5×10^{13} molecules $\text{cm}^{-2} \text{ s}^{-1}$; only about 0.1% of all O₃ produced in the stratosphere leaks down to the troposphere (Crutzen, 1995). The estimated global O₃ loss from photolysis in the troposphere is 14×10^{10} molecules $\text{cm}^{-2} \text{ s}^{-1}$, which generously exceeds the amount of O₃ from stratosphere-to-troposphere exchange.

2.6.3 Tropospheric Ozone

Whereas stratospheric ozone is thinning, tropospheric ozone is increasing (WMO, 1986, 1990). Much of the evidence for increased baseline levels of tropospheric ozone comes from Europe, where during the late 1800s there was much interest in atmospheric ozone. Because ozone was known to be a disinfectant, it was believed to promote health (Warneck, 1988). Measurements of atmospheric ozone made at Montsouris, near Paris, from 1876 to 1910 have been reanalyzed by Volz and Kley (1988), who recalibrated the original measurement technique. Their analysis showed that surface ozone mixing ratios near Paris 100 years ago averaged about 10 ppb; current mixing ratios in the most unpolluted parts of Europe average between 20 and 45 ppb (Volz and Kley, 1988; Bojkov, 1988; Crutzen, 1988; Staehelin and Schmid, 1991; Oltmans and Levy, 1994; Janach, 1989). An analysis of ozone measurements made in relatively remote European sites indicates a 1 to 2% annual increase in average concentrations over the past 30 years (Janach, 1989) (Figure 2.13).⁵ Based on Total Ozone Mapping Spectrometer (TOMS) data between the high Andes and the Pacific Ocean, from 1979 to 1992 tropospheric ozone concentrations in the tropical Pacific South America apparently increased by 1.48% per year (Jiang and Yung, 1996). The integrated ozone column in the troposphere can be determined from the difference of the measurements of two satellite instruments, TOMS and SAGE, which detect total column ozone and stratospheric ozone, respectively (Fishman et al., 1990, 1992). Tropospheric ozone column densities average about 30 DU, but there is significant variation with season and hemisphere.

Global ozone measurements indicate a general increase of O₃ mixing ratios with altitude, indicative of stratosphere-to-troposphere exchange and more efficient O₃ production in the upper troposphere (e.g., see Fehsenfeld and Liu, 1993). Data also indicate higher O₃ concentrations in the NH than in the SH, consistent with a larger stratospheric influx in the NH and larger photochemical production as a result of higher NO_x emissions in the NH. Biomass burning, however, a major source of nonmethane hydrocarbons and NO, is a source of O₃ production that is predominant in the SH (Delaney et al., 1985; Browell et al., 1988; Andreae et al., 1992).

The database of ground-level ozone observations for urban and suburban areas in North America and Europe is fairly extensive. At most rural surface sites, ozone concentrations have been found to vary over a diurnal cycle with a minimum in the early morning hours before dawn and a maximum in the late afternoon (Figure 2.14). This pattern results from daytime photochemical production or downward transport of ozone-rich air from above, combined with ozone loss by dry deposition and reaction with nitric oxide (NO) at night, when photochemical production ceases and vertical transport is inhibited by an inversion of the normal temperature profile. In locations near large sources of NO, the nighttime minimum in ozone can be quite pronounced because of the rapid reaction between ozone and NO. In fact, in many urban areas the NO source is strong enough to cause the complete nighttime disappearance of ozone. In addition to variations over a diurnal cycle, ozone concentrations at a given location also can vary significantly from one day to the next. It is not uncommon for the daily maximum ozone concentration at an urban site, for instance, to vary by a factor of 2 or 3 from day to day as local meteorological conditions change. In and

⁵If stratospheric ozone concentrations remained constant, the 10% increase in tropospheric ozone would increase the total column abundance of ozone by about 1%. Thus the additional tropospheric ozone is believed to have counteracted only a small fraction of the stratospheric loss, even if the trends observed over Europe are representative of the entire northern midlatitude region.

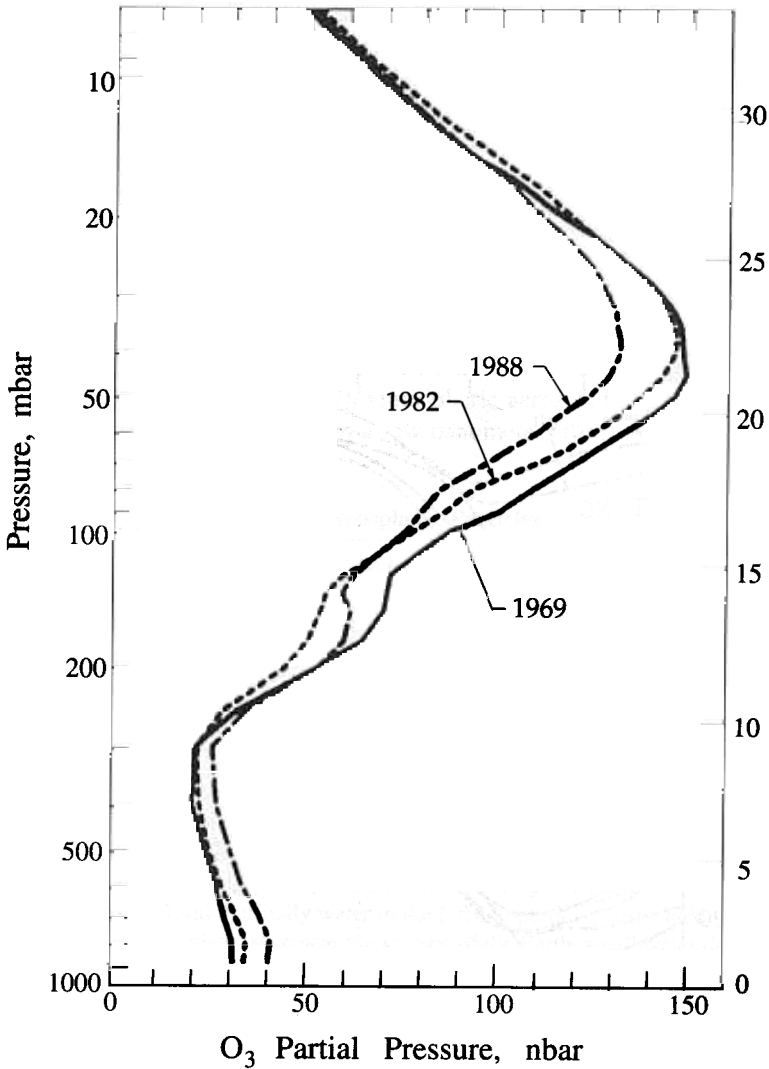


FIGURE 2.13 Selected annual means of ozone balloon soundings over Payerne, Switzerland (Stachelin and Schmid, 1991). The annual mean altitude of the tropopause at Payerne is about 10 km, varying from about 8 km in winter to 12 km in summer. (Reprinted from *Atmos. Environ.*, **25A**, Staehelin, J. and Schmid, W., Trend analysis of tropospheric ozone concentrations utilizing the 20-year data set of balloon soundings over Payerne (Switzerland), p. 1739, 1991, with kind permission from Elsevier Science Ltd, The Boulevard, Langford Lane, Kidlington OX5 1GB, UK.)

downwind of large urban areas, under certain meteorological conditions, emissions of NO_x and VOCs can result in ozone concentrations as high as 200 to 400 ppb. Such production of ozone and related oxidant species is called photochemical air pollution; it was first recognized in the Los Angeles basin in the 1940s. The database of ozone observations suggests a systematic pattern of decreasing daily maximum concentrations as one moves from urban-suburban locations to rural locations and then to remote locations. Daily maximum ozone concentrations within the atmospheric boundary layer tend to be largest in the

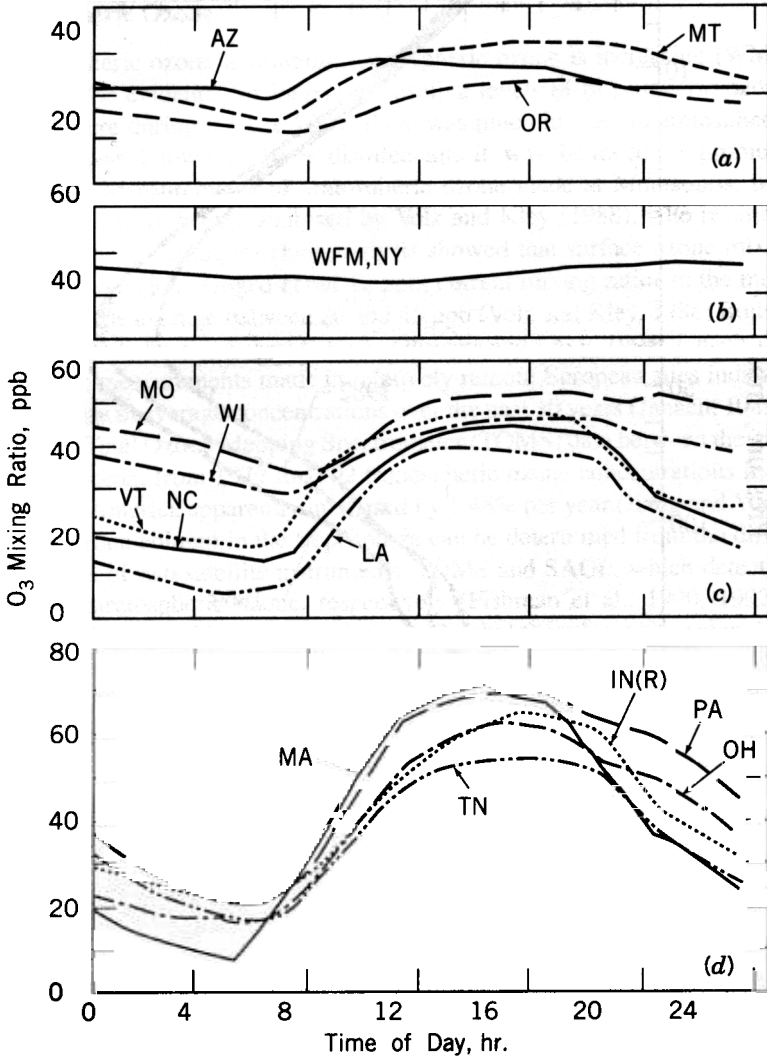


FIGURE 2.14 Diurnal behavior of ozone at rural sites in the United States in July (Logan, 1989). Sites are identified by the state in which they are located. (WFM refers to Whiteface Mountain, New York, located at 1.5 km above sea level.)

TABLE 2.16 Typical Summertime Daily Maximum Ozone Concentrations

Region	
Urban-suburban	100-400
Rural	50-120
Remote tropical forest	20-40
Remote marine	20-40

Source: National Research Council (1991).

urban–suburban atmosphere, where maxima well above 200 ppb have been observed (Table 2.16). Ozone concentrations in rural areas tend to be more moderate and rarely exceed 150 ppb. In remote locations, ozone concentrations typically range from 20 to 40 ppb.

2.7 PARTICULATE MATTER (AEROSOLS)

Particles in the atmosphere arise from natural sources, such as windborne dust, sea spray, and volcanoes, and from anthropogenic activities, such as combustion of fuels. Whereas an aerosol is technically defined as a suspension of fine solid or liquid particles in a gas, common usage refers to the aerosol as the particulate component only (Table 2.17). Emitted directly as particles (primary aerosol) or formed in the atmosphere by gas-to-particle conversion processes (secondary aerosol), atmospheric aerosols are generally considered to be the particles that range in size from a few nanometers (nm) to tens of micrometers

TABLE 2.17 Terminology Relating to Atmospheric Particles

Aerosols, aerocolloids, aerodisperse systems	Tiny particles dispersed in gases
Dusts	Suspensions of solid particles produced by mechanical disintegration of material such as crushing, grinding, and blasting. $D_p > 1 \mu\text{m}$.
Fog	A loose term applied to visible aerosols in which the dispersed phase is liquid. Usually, a dispersion of water or ice, close to the ground. The solid particles generated by condensation from the vapor state, generally after volatilization from melted substances, and often accompanied by a chemical reaction such as oxidation. Often the material involved is noxious. $D_p < 1 \mu\text{m}$. An aerosol that impedes vision and may consist of a combination of water droplets, pollutants, and dust. $D_p < 1 \mu\text{m}$.
Mists	Liquid, usually water in the form of particles suspended in the atmosphere at or near the surface of the Earth; small water droplets floating or falling, approaching the form of rain, and sometimes distinguished from fog as being more transparent or as having particles perceptibly moving downward. $D_p > 1 \mu\text{m}$.
Particle	An aerosol particle may consist of a single continuous unit of solid or liquid containing many molecules held together by intermolecular forces and primarily larger than molecular dimensions ($> 0.001 \mu\text{m}$). A particle may also be considered to consist of two or more such unit structures held together by interparticle adhesive forces such that it behaves as a single unit in suspension or upon deposit. A term derived from smoke and fog, applied to extensive contamination by aerosols. Now sometimes used loosely for any contamination of the air. Small gas-borne particles resulting from incomplete combustion, consisting predominantly of carbon and other combustible material, and present in sufficient quantity to be observable independently of the presence of other solids. $D_p \geq 0.01 \mu\text{m}$.
Soot	Agglomerations of particles of carbon impregnated with “tar,” formed in the incomplete combustion of carbonaceous material.

(μm) in diameter. Once airborne, particles can change their size and composition by condensation of vapor species or by evaporation, by coagulating with other particles, by chemical reaction, or by activation in the presence of water supersaturation to become fog and cloud droplets. Particles smaller than $1 \mu\text{m}$ diameter generally have atmospheric concentrations in the range from around ten to several thousand per cm^3 ; those exceeding $1 \mu\text{m}$ diameter are usually found at concentrations less than 1cm^{-3} .

Particles are eventually removed from the atmosphere by two mechanisms: deposition at the Earth's surface (dry deposition) and incorporation into cloud droplets during the formation of precipitation (wet deposition). Because wet and dry deposition lead to relatively short residence times in the troposphere, and because the geographical distribution of particle sources is highly nonuniform, tropospheric aerosols vary widely in concentration and composition over the Earth. Whereas atmospheric trace gases have lifetimes ranging from less than a second to a century or more, residence times of particles in the troposphere vary only from a few days to a few weeks.

2.7.1 Stratospheric Aerosol

The stratospheric aerosol is composed of an aqueous sulfuric acid solution of 60 to 80% sulfuric acid for temperatures from -80 to -45°C , respectively (Shen et al., 1995). The source of the globally distributed, unperturbed background stratospheric aerosol is oxidation of carbonyl sulfide (OCS), which has its sources at the Earth's surface. OCS is chemically inert and water insoluble and has a long tropospheric lifetime. It diffuses into the stratosphere where it dissociates by solar ultraviolet radiation to eventually form sulfuric acid, the primary component of the natural stratospheric aerosol. Other surface-emitted sulfur-containing species, for example, SO_2 , DMS, and CS_2 , do not persist long enough in the troposphere to be transported to the stratosphere.

A state of unperturbed background stratospheric aerosol may be relatively rare, however, as frequent volcanic eruptions inject significant quantities of SO_2 directly into the lower and midstratosphere. Recent major eruptions include Agung in 1963, El Chichón in 1982, and Pinatubo in 1991. The subsequent sulfuric acid aerosol clouds can, over a period of months, be distributed globally at optical densities that overwhelm the natural background aerosol. The stratosphere's relaxation to background conditions has a characteristic time on the order of years, so that, given the frequency of volcanic eruptions, the stratospheric aerosol is seldom in a state that is totally unperturbed by volcanic emissions. With an estimated aerosol mass addition of 30 Tg to the stratosphere, the June 1991 eruption of Mt. Pinatubo was the largest in the 20th century and led to enhanced stratospheric aerosol levels for over 2 years.

2.7.2 Chemical Components of Tropospheric Aerosol

A significant fraction of the tropospheric aerosol is anthropogenic in origin. Tropospheric aerosols contain sulfate, ammonium, nitrate, sodium, chloride, trace metals, carbonaceous material, crustal elements, and water. The carbonaceous fraction of the aerosols consists of both elemental and organic carbon. Elemental carbon, also called black carbon, graphitic carbon, or soot, is emitted directly into the atmosphere, predominantly from combustion processes. Particulate organic carbon is emitted directly by sources or can result from atmospheric condensation of low-volatility organic gases. Anthropogenic emissions leading

TABLE 2.18 Mass Concentrations and Composition of Tropospheric Aerosols

Region	Mass ($\mu\text{g m}^{-3}$)	C (elem)	Percentage Composition			
			C (org)	NH ₄ ⁺	NO ₃ ⁻	SO ₄ ²⁻
Remote (11 areas) ^a						
Nonurban continental (14 areas) ^a	15	5	24	11	4	37
Urban (19 areas) ^a	32	9	31	8	6	28
Rubidoux, California ^b (1986 annual average)	87.4		18	6	20	6

^aHeintzenberg (1989).^bSolomon et al. (1989).

to atmospheric aerosol have increased dramatically over the past century and have been implicated in human health effects (Dockery et al., 1993), in visibility reduction in urban and regional areas (see Chapter 22), in acid deposition (see Chapter 20), and in perturbing the Earth's radiation balance (see Chapter 22).

Table 2.18 presents data summarized by Heintzenberg (1989) and Solomon et al. (1989) on aerosol mass concentrations and composition in different regions of the troposphere. It is interesting to note that average total fine particle mass (that associated with particles of diameter less than about 2 μm) in nonurban continental, (i.e., regional) aerosols is only a factor of 2 lower than urban values. This reflects the relatively long residence time of particles. Correspondingly, the average compositions of nonurban continental and urban aerosols are roughly the same. The average mass concentration of remote aerosols is a factor of 3 lower than that of nonurban continental aerosols. The elemental carbon component, a direct indicator of anthropogenic combustion sources, drops to 0.3% in the remote aerosols, but sulfate is still a major component. This is attributable to a global average concentration of non-sea-salt sulfate of about 0.5 $\mu\text{g m}^{-3}$. Rubidoux, California, located about 100 km east of downtown Los Angeles, routinely experiences some of the highest particulate matter concentrations in the United States.

2.7.3 Cloud Condensation Nuclei (CCN)

Aerosols are essential to the atmosphere as we know it; if the Earth's atmosphere were totally devoid of particles, clouds could not form. Particles that can become activated to grow to fog or cloud droplets in the presence of a supersaturation of water vapor are termed cloud condensation nuclei (CCN). At a given mass of soluble material in the particle there is a critical value of the ambient water vapor supersaturation below which the particle exists in a stable state and above which it spontaneously grows to become a cloud droplet of 10 μm or more diameter. The number of particles from a given aerosol population that can act as CCN is thus a function of the water supersaturation. For marine stratiform clouds, for which supersaturations are in the range of 0.1 to 0.5%, the minimum CCN particle diameter is 0.05 to 0.14 μm . CCN number concentrations vary from fewer than 100 cm^{-3} in re-

mote marine regions to many thousand cm^{-3} in polluted urban areas. An air parcel will spend, on average, a few hours in a cloud followed by a few days outside clouds. The average lifetime of a CCN is about 1 week, so that an average CCN will experience 5 to 10 cloud activation/cloud evaporation cycles before actually being removed from the atmosphere in precipitation.

2.7.4 Sizes of Atmospheric Particles

Atmospheric aerosols consist of particles ranging in size from a few tens of angstroms (\AA) to several hundred micrometers. Particles less than $2.5 \mu\text{m}$ in diameter are generally referred to as “fine” and those greater than $2.5 \mu\text{m}$ diameter as “coarse.” The fine and coarse particle modes, in general, originate separately, are transformed separately, are removed from the atmosphere by different mechanisms, require different techniques for their removal from sources, have different chemical composition, have different optical properties, and differ significantly in their deposition patterns in the respiratory tract. Therefore the distinction between fine and coarse particles is a fundamental one in any discussion of the physics, chemistry, measurement, or health effects of aerosols.

The phenomena that influence particle sizes are shown in an idealized schematic in Figure 2.15, which depicts the typical distribution of surface area of an atmospheric aerosol. Fine particles can often be divided roughly into two modes: the *nuclei mode* and the *accumulation mode*. The *nuclei mode*, extending from about 0.005 to $0.1 \mu\text{m}$ diameter, accounts for the preponderance of particles by number; because of their small size, these particles rarely account for more than a few percent of the total mass of airborne particles. Particles in the nuclei mode are formed from condensation of hot vapors during combustion processes and from the nucleation of atmospheric species to form fresh particles. They are lost principally by coagulation with larger particles. The *accumulation mode*, extending from 0.1 to about $2.5 \mu\text{m}$ diameter, usually accounts for most of the aerosol surface area and a substantial part of the aerosol mass. The source of particles in the accumulation mode is the coagulation of particles in the nuclei mode and from condensation of vapors onto existing particles, causing them to grow into this size range. The accumulation mode is so named because particle removal mechanisms are least efficient in this regime, causing particles to accumulate there. The *coarse mode*, from $>2.5 \mu\text{m}$ diameter, is formed by mechanical processes and usually consists of man-made and natural dust particles. Coarse particles have sufficiently large sedimentation velocities that they settle out of the atmosphere in a reasonably short time. Because removal mechanisms that are efficient at the small and large particle extremes of the size spectrum are inefficient in the accumulation range, particles in the accumulation mode tend to have considerably longer atmospheric residence times than those in either the nuclei or coarse mode.

2.7.5 Sources of Atmospheric Particulate Matter

Significant natural sources of particles include soil and rock debris (terrestrial dust), volcanic action, sea spray, biomass burning, and reactions between natural gaseous emissions. Table 2.19 presents a range of emission estimates of particles generated from natural and anthropogenic sources, on a global basis. Emissions of particulate matter attributable to the activities of humans arise primarily from four source categories: fuel combustion, industrial processes, nonindustrial fugitive sources (roadway dust from paved and unpaved

mote marine regions to many thousand cm^{-3} in polluted urban areas. An air parcel will spend, on average, a few hours in a cloud followed by a few days outside clouds. The average lifetime of a CCN is about 1 week, so that an average CCN will experience 5 to 10 cloud activation/cloud evaporation cycles before actually being removed from the atmosphere in precipitation.

2.7.4 Sizes of Atmospheric Particles

Atmospheric aerosols consist of particles ranging in size from a few tens of angstroms (\AA) to several hundred micrometers. Particles less than $2.5 \mu\text{m}$ in diameter are generally referred to as “fine” and those greater than $2.5 \mu\text{m}$ diameter as “coarse.” The fine and coarse particle modes, in general, originate separately, are transformed separately, are removed from the atmosphere by different mechanisms, require different techniques for their removal from sources, have different chemical composition, have different optical properties, and differ significantly in their deposition patterns in the respiratory tract. Therefore the distinction between fine and coarse particles is a fundamental one in any discussion of the physics, chemistry, measurement, or health effects of aerosols.

The phenomena that influence particle sizes are shown in an idealized schematic in Figure 2.15, which depicts the typical distribution of surface area of an atmospheric aerosol. Fine particles can often be divided roughly into two modes: the *nuclei mode* and the *accumulation mode*. The *nuclei mode*, extending from about 0.005 to $0.1 \mu\text{m}$ diameter, accounts for the preponderance of particles by number; because of their small size, these particles rarely account for more than a few percent of the total mass of airborne particles. Particles in the nuclei mode are formed from condensation of hot vapors during combustion processes and from the nucleation of atmospheric species to form fresh particles. They are lost principally by coagulation with larger particles. The *accumulation mode*, extending from 0.1 to about $2.5 \mu\text{m}$ diameter, usually accounts for most of the aerosol surface area and a substantial part of the aerosol mass. The source of particles in the accumulation mode is the coagulation of particles in the nuclei mode and from condensation of vapors onto existing particles, causing them to grow into this size range. The accumulation mode is so named because particle removal mechanisms are least efficient in this regime, causing particles to accumulate there. The *coarse mode*, from $>2.5 \mu\text{m}$ diameter, is formed by mechanical processes and usually consists of man-made and natural dust particles. Coarse particles have sufficiently large sedimentation velocities that they settle out of the atmosphere in a reasonably short time. Because removal mechanisms that are efficient at the small and large particle extremes of the size spectrum are inefficient in the accumulation range, particles in the accumulation mode tend to have considerably longer atmospheric residence times than those in either the nuclei or coarse mode.

2.7.5 Sources of Atmospheric Particulate Matter

Significant natural sources of particles include soil and rock debris (terrestrial dust), volcanic action, sea spray, biomass burning, and reactions between natural gaseous emissions. Table 2.19 presents a range of emission estimates of particles generated from natural and anthropogenic sources, on a global basis. Emissions of particulate matter attributable to the activities of humans arise primarily from four source categories: fuel combustion, industrial processes, nonindustrial fugitive sources (roadway dust from paved and unpaved

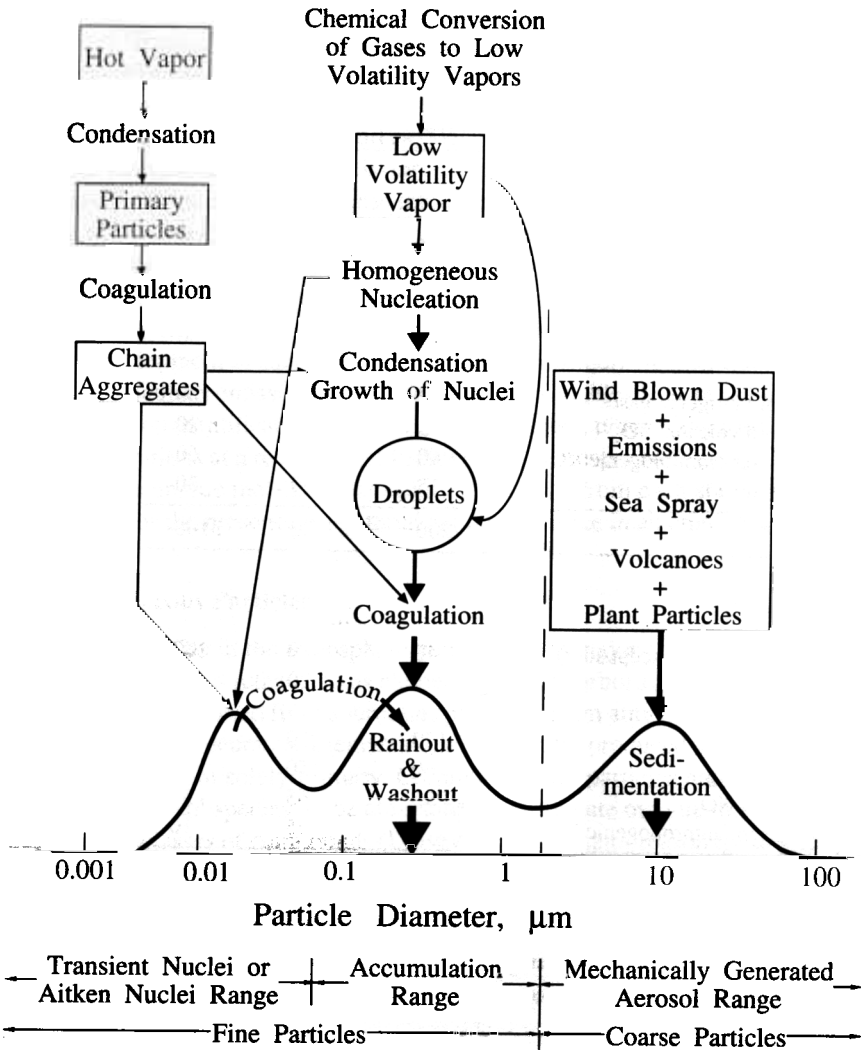


FIGURE 2.15 Idealized schematic of the distribution of particle surface area of an atmospheric aerosol (Whitby and Cantrell, 1976). Principal modes, sources, and particle formation and removal mechanisms are indicated.

roads, wind erosion of cropland, construction, etc.), and transportation sources (automobiles, etc.).

Fugitive particles are those not emitted from a definable point such as a stack. Industrial fugitive dust emissions result from wind erosion of storage piles and unpaved plant roads and from vehicular traffic over plant roads. Fugitive process emissions result from industry-related operations such as materials handling, loading, and transfer operations. Three broad categories account for nearly all of the potential process fugitive emissions—mineral products, food and agriculture, and primary metals. Nonindustrial fugitive particulate emissions, commonly termed *fugitive dust*, are caused by traffic entrainment of dust from

TABLE 2.19 Global Emission Estimates for Major Aerosol Types in the 1980s

Source	Estimated Flux (Tg yr ⁻¹)			Particle Size Category ^a
	Low	High	Best	
NATURAL				
Primary				
Soil dust (mineral aerosol)	1000	3000	1500	Mainly coarse
Sea salt	1000	10000	1300	Coarse
Volcanic dust	4	10000	30	Coarse
Biological debris	26	80	50	Coarse
Secondary				
Sulfates from biogenic gases				Fine
Sulfates from volcanic SO ₂				Fine
Organic matter from biogenic VOC				Fine
Nitrates from NO _x				Fine and coarse
Total natural	2200	23500	3100	
ANTHROPOGENIC				
Primary				
Industrial dust, etc. (except soot)	40	130	100	Fine and coarse
Soot	5	20	10	Mainly fine
Secondary				
Sulfates from SO ₂			190	Fine
Biomass burning			90	Fine
Nitrates from NO _x			50	Mainly coarse
Organics from anthropogenic VOC			10	Fine
Total anthropogenic				
Total	2500	24000	3600	

^aCoarse and fine size categories refer to mean particle diameter above and below 1 μm, respectively.

Note: Sulfates and nitrates are assumed to occur as ammonium salts. Flux unit: Tg yr⁻¹ (dry mass).

Source: Kiehl and Rodhe (1995).

paved and unpaved roads, agricultural operations, construction, and fires. Except for the last, all these sources entail dust entrainment by the interaction of machinery with materials and by the forces of wind on materials. While it is estimated that fugitive dust emissions exceed particulate emissions from stationary point sources in most areas, their impact is limited because the emissions are mostly large particles that settle a short distance from the source, and fugitive dust sources exist mainly in rural areas.

Transportation source emissions occur in two categories: (1) vehicle exhaust and (2) vehicle-related particles from tire, clutch, and brake wear. Engine-related particulate emissions are composed primarily of lead halides, sulfates, and carbonaceous matter and are mostly smaller than 1 μm in diameter. About 40% of particles from tire wear are less than 10 μm (about 20% are less than 1 μm) and are primarily carbon. Particles from brake linings are less than 1 μm and are composed mainly of asbestos and carbon.

Atmospheric particulate matter samples can be analyzed routinely for more than 50 trace elements. Trace element emissions arise from a large number of different source types in urban areas. For example, motor vehicles burning leaded fuel, electric arc steel furnaces, Kraft recovery boilers, and secondary lead smelters contribute to atmospheric lead concentrations. The wide spectrum of sources, together with the fact that trace metals often are only a minor fraction of the mass emissions from each source, obscure the relative importance of the contributors to atmospheric trace element levels.

As with all atmospheric species, trace metal emissions undergo atmospheric transport and dilution before they reach a particular receptor site. Mathematical models can be constructed based on the fundamentals of atmospheric chemistry and physics that will track the contributions from many emission sources as they undergo atmospheric transport. Indeed, the development of such models will receive considerable attention in this book. In the case of particulate emissions, an alternative is available. It is possible to attack the source contribution identification problem in reverse order, proceeding from measured particulate concentrations at a receptor site backward to the responsible emission sources (see Chapter 24). The unique metals content of the emissions from each source type is viewed as a fingerprint for the presence of material from that source in an ambient aerosol sample.

2.7.6 Carbonaceous Particles

Carbonaceous particles in the atmosphere consist of two major components—graphitic or black carbon (sometimes referred to as elemental or free carbon) and organic material. The latter can be directly emitted from sources or produced from atmospheric reactions involving gaseous organic precursors. Elemental carbon can be produced only in a combustion process and is therefore solely primary. Graphitic carbon particles are the most abundant light-absorbing aerosol species in the atmosphere. Particulate organic matter is a complex mixture of many classes of compounds (Daisey, 1980). A major reason for the study of particulate organic matter has been the possibility that such compounds pose a health hazard. Specifically, certain fractions of particulate organic matter, especially those containing polycyclic aromatic hydrocarbons (PAHs), have been shown to be carcinogenic in animals and mutagenic in *in vitro* bioassays.

2.8 EMISSIONS INVENTORIES

An estimate of emissions of a species from a source is based on a technique that uses “emission factors,” which are based on source-specific emission measurements as a function of activity level (e.g., amount of annual production at an industrial facility) with regard to each source. For example, suppose one wants to sample a power plant’s emissions of SO₂ or NO_x at the stack. The plant’s boiler design and its BTU (British thermal unit) consumption rate are known. The sulfur and nitrogen content of fuel burned can be used to calculate an emissions factor of kilograms (kg) of SO₂ or NO_x emitted per metric ton (Mg) of fuel consumed.

The U.S. Environmental Protection Agency (EPA) has compiled emission factors for a variety of sources and activity levels (such as production or consumption), reporting the results since 1972 in “AP-42 Compilation of Air Pollutant Emission Factors,” for which supplements are issued regularly. Emission factors currently in use are developed from only a

limited sampling of the emissions source population for any given category, and the values reported are an average of those limited samples and might not be statistically representative of the population. For example, 30 source tests of coal-fueled, tangentially fired boilers led to calculations of emission factors that range approximately from 5 to 11 kg NO_x per metric ton of coal burned (Placet et al., 1990). The sample population was averaged and the emission factor for this source type was reported as 7.5 kg NO_x per metric ton of coal. The uncertainties associated with emission factor determinations can be considerable.

The formulation of emission factors for mobile sources, the major sources of VOCs and NO_x, is based on rather complex emission estimation models used in conjunction with data from laboratory testing of representative groups of motor vehicles. Vehicle testing is performed with a chassis dynamometer, which determines the exhaust emission of a vehicle as a function of a specified ambient temperature and humidity, speed, and load cycle. The current specified testing cycle is called the Federal Test Procedure (FTP). Based on results from this set of vehicle emissions data, a computer model has been developed to simulate for specified speeds, temperatures, and trip profiles, for example, the emission factors to be applied for the national fleet average for all vehicles or any specified distribution of vehicle age and type. These data are then incorporated with activity data on vehicle miles traveled as a function of spatial and temporal allocation factors to estimate emissions.

2.9 BIOMASS BURNING

The intentional burning of land results in a major source of combustion products to the atmosphere. Most of this burning occurs in the tropics. Emissions from burning vegetation are typical of those from any uncontrolled combustion process and include CO₂, CO, NO_x, CH₄ and nonmethane hydrocarbons, and elemental and organic particulate matter. The quantity and type of emissions from a biomass fire depend not only on the type of vegetation, but on its moisture content, ambient temperature, humidity, and local wind speed. Estimates of global emissions of trace gases from biomass burning have already been given in many of the tables in this chapter. For CH₄, for example, it is estimated that 40 Tg yr⁻¹ out of a total anthropogenic flux of 375 Tg yr⁻¹ (Table 2.9) is a result of biomass burning. For CO, a biomass burning source of 300 to 700 Tg yr⁻¹ out of a total source of 1800 to 2700 Tg yr⁻¹ is estimated (Table 2.14). For NO_x, biomass burning is estimated to contribute globally one-third of that from fossil-fuel burning (Table 2.5). The effect of emissions from biomass burning on atmospheric chemistry and climate, particularly in the tropics, is critically important. Large-scale savanna burning in the dry season in Africa leads to regional-scale ozone levels that approach those characteristic of urban industrialized regions (60 to 100 ppb) (Andreae et al., 1992; Fishman et al., 1990, 1992).

2.10 AIR POLLUTION LEGISLATION

The legislative basis for air pollution abatement in the United States is the 1963 Clean Air Act and its amendments. The Clean Air Act was the first modern environmental law enacted by the U.S. Congress. The original act was signed into law in 1963, and major amendments were made in 1970, 1977, and 1990. The act establishes the federal-state re-

lationship that requires the U.S. Environmental Protection Agency (EPA) to develop National Ambient Air-Quality Standards (NAAQS) and empowers the states to implement and enforce regulations to attain them. The act also requires the EPA to set NAAQS for common and widespread pollutants after preparing criteria documents summarizing scientific knowledge of their detrimental effects. The EPA has established NAAQS for each of six criteria pollutants: sulfur dioxide, particulate matter, nitrogen dioxide, carbon monoxide, ozone, and lead. At certain concentrations and length of exposure these pollutants are anticipated to endanger public health or welfare. The NAAQS are threshold concentrations based on a detailed review of the scientific information related to effects. Concentrations below the NAAQS are expected to have no adverse effects for humans and the environment. Table 2.20 presents the U.S. national primary and secondary ambient air-quality standards for ozone, carbon monoxide, nitrogen dioxide, sulfur dioxide, suspended particulate matter, and lead.

In the Clean Air Act Amendments of 1970, Congress set 1975 as the deadline for meeting the NAAQS. By 1977, 2 years after this deadline, many areas were still in violation of the ozone NAAQS. The 1977 amendments to the Clean Air Act delayed compliance with the ozone and carbon monoxide NAAQS until 1982, and areas that demonstrated they could not meet the 1982 deadline were given extensions until 1987. The 1990 amendments classify nonattainment areas according to degree of noncompliance with the NAAQS. The classifications are extreme, severe, serious, moderate, or marginal, depending on the area's ozone design value and the percentage by which the value is greater than the NAAQS. Ozone design values are ozone concentrations that are statistically determined from air-quality measurements for each nonattainment area. If monitoring data for an area are complete, the design value is the fourth highest monitor reading over the past 3 years. Design values are used to determine the extent of control needed for an area to reach attainment.

The 1990 amendments of the Clean Air Act establish an interstate ozone transport region extending from the Washington, DC metropolitan area to Maine. In this densely populated region, ozone violations in one area are caused, at least in part, by emissions in upwind areas. A transport commission is authorized to coordinate control measures within the interstate transport region and to recommend to the EPA when additional control measures should be applied in all or part of the region in order to bring any area in the region into attainment. Hence areas within the transport region that are in attainment of the ozone NAAQS might become subject to the controls required for nonattainment areas in that region.

The Clean Air Act requires each state to adopt a plan, a so-called State Implementation Plan (SIP), that provides for the implementation, maintenance, and enforcement of the NAAQS. It is, of course, emission reductions that will abate air pollution. Thus the states' plans must contain legally enforceable emission limitations, schedules, and timetables for compliance with such limitations. The control strategy must consist of a combination of measures designed to achieve the total reduction of emissions necessary for the attainment of the air-quality standards. The control strategy may include, for example, such measures as emission limitations, emission charges or taxes, closing or relocation of commercial or industrial facilities, periodic inspection and testing of motor vehicle emission control systems, mandatory installation of control devices on motor vehicles, means to reduce motor vehicle traffic, including such measures as parking restrictions and carpool lanes on freeways, and expansion and promotion of the use of mass transportation facilities.

TABLE 2.20 United States National Ambient Air Quality Standards

	National Standard ^b	Maximum Allowable Annual Mean Concentrations			Maximum Allowable Short-Period Concentrations and Averaging Times ^a			
		AAM ^c ($\mu\text{g m}^{-3}$)	AAM ^c (ppm)	AGM ^d ($\mu\text{g m}^{-3}$)	(mg m ⁻³)			
						Averaging Times		
Ozone	Primary ^f				240	0.12	1 hour	
	Secondary				240	0.12	1 hour	
Carbon monoxide	Primary ^e					10	9	8 hours
						40	35	1 hour
	Secondary					10	9	8 hours
						40	35	1 hour
Nitrogen dioxide	Primary	100	0.05					
	Secondary	100	0.05					
Sulfur dioxide	Primary	80	0.03		365	0.14	24 hours	
	Secondary				1300	0.50	3 hours	
Particulate matter	Primary ^f			75	260		24 hours	
	Secondary			60	150		24 hours	
Lead	Primary				1.5		Quarterly	
	Secondary				1.5		Average	

^aNot to be exceeded more than once per year (for ozone, the average number of days per year above the standard must be less than or equal to 1).

^bNational Air Quality Standards as presented in the code of Federal Regulations, 40, Protection of Environment, Part 50, Sec. 50.4 to 50.11, July 1, 1974, U.S. Government Printing Office, Washington, DC, 1974. Primary Standard—necessary to protect the public health (Sec. 50.2). Secondary Standard—necessary to protect the public welfare and the environment from known or anticipated adverse effects of a pollutant (Sec. 50.2).

^cAAM = annual arithmetic mean.

^dAGM = annual geometric mean.

^eBoth the 8-hour and 1-hour standard must be met.

^fThe U.S. Environmental Protection Agency announced in the December 13, 1996 *Federal Register* (vol. 61, no. 241, pp. 65763–65778) proposed new ozone and particulate matter air quality standards. The O₃ standard would be changed to 0.08 ppm over an 8-hour averaging time. The revised particulate matter standard is directed toward particles of diameter $\leq 2.5 \mu\text{m}$, denoted PM_{2.5}, and would be set at 15 $\mu\text{g m}^{-3}$, annual mean, and 50 $\mu\text{g m}^{-3}$, 24-hour average.

2.11 HAZARDOUS AIR POLLUTANTS (AIR TOXICS)

Hazardous air pollutants or toxic air contaminants (“air toxics”) refer to any substances that may cause or contribute to an increase in mortality or in serious illness, or that may pose a present or potential hazard to human health. Title III of the Clean Air Act Amendments of 1990 completely overhauled the existing hazardous air emission program. Section 112 of the Amendments defines a new process for controlling air toxics that includes the listing of 189 substances, the development and promulgation of Maximum Achievable Control Technology (MACT) standards, and the assessment of residual risk after the implementation of MACT. Any stationary source emitting in excess of 10 tons yr⁻¹ of any listed hazardous substance, or 25 tons yr⁻¹ or more of any combination of hazardous air contaminants, is a major source for the purpose of Title III and is subject to regulation. Congress established a list of 189 hazardous air pollutants in the CAA itself. It includes organic chemicals, pesticides, metals, coke-oven emissions, fine mineral fibers, and radionuclides (including radon). This initial list may be revised by the EPA to either add or remove substances. The EPA is required to add pollutants to the list if they are shown to present, through inhalation or other routes of exposure, a threat of adverse human health effects or adverse environmental effects, whether through ambient concentrations, bioaccumulation, deposition, or otherwise.

Congress directed the EPA to list by 15 November 1995, the categories and subcategories of sources that represent 90% of the aggregate emissions of:

- Alkylated lead compounds
- Polycyclic organic matter
- Hexachlorobenzene
- Mercury
- Polychlorinated biphenyls
- 2,3,7,8-Tetrachlorodibenzofuran
- 2,3,7,8-Tetrachlorodibenzo-*p*-dioxin

Congress further directed the EPA to establish and promulgate emissions standards for such sources by 15 November 2000. The emissions standards must effect the maximum degree of reduction in the listed substance, including the potential for a prohibition on such emissions, taking into consideration costs, any non-air-quality health and environmental impacts, and energy requirements. In establishing these emissions standards, the EPA may also consider health threshold levels, which may be established for particular hazardous air pollutants. Each state may develop and submit to the EPA for approval a program for the implementation and enforcement of emission standards and other requirements for hazardous air pollutants or requirements for the prevention and mitigation of accidental releases of hazardous substances.

The California Air Resources Board (ARB) (1989) has developed a list of substances of concern in California, called “Status of Toxic Air Contaminant Identification.” This list and the organization of substances within it are subject to periodic revision, as needed. The February 1989 Status List groups substances into three categories. Category I includes identified toxic air contaminants: asbestos, benzene, cadmium, carbon tetrachloride, chlorinated dioxins and dibenzofurans (15 species), chromium (VI), ethylene dibromide and

ethylene dichloride, and ethylene oxide. Category IIA contains nine substances already in the formal review process (1,3-butadiene, chloroform, formaldehyde, inorganic arsenic, methylene chloride, nickel, perchloroethylene, trichloroethylene, and vinyl chloride). Category IIB contains 23 substances not yet reviewed (acetaldehyde, acrylonitrile, beryllium, coke-oven emissions, dialkylnitrosamines, *p*-dichlorobenzene, di(2-ethylhexyl)-phthalate, 1,4-dioxane, dimethyl sulfate, environmental tobacco smoke, ethyl acrylate, hexachlorobenzene, inorganic lead, mercury, 4,4'-methylenedianiline, *N*-nitrosomorpholine, PAHs, PCBs, propylene oxide, radionuclides, styrene, toluene diisocyanates, and 2,4,6-trichlorophenol). Category III includes substances for which additional health information is needed prior to review. These are acrolein, allyl chloride, benzyl chloride, chlorobenzene, chlorophenols/phenol, chloroprene, glycol ethers, maleic anhydride, manganese, methyl bromide, methyl chloroform, nitrobenzene, vinylidene chloride, and xylenes. Available information on these compounds is summarized in Table 2.21.

APPENDIX 2 COMPARTMENTAL MODELS OF GLOBAL BIOGEOCHEMICAL CYCLES

Consider Figure 2.A.1 in which four natural atmospheric reservoirs are depicted, the NH and SH troposphere and the NH and SH stratosphere.⁶ We use this model of four interconnected atmospheric compartments as a vehicle to derive balance equations from which global biogeochemical cycles can be analyzed.

We will assume that the substance of interest is removed by different first-order processes in the troposphere and stratosphere, characterized by first-order rate constants, k_T and k_S . Thus the rates of removal of the substance in the two tropospheres are $k_T Q_{NH}^T$ and $k_T Q_{SH}^T$; the rates of removal in the two stratospheres are $k_S Q_{NH}^S$ and $k_S Q_{SH}^S$. k_T could represent, for example, OH reaction in the troposphere and k_S could represent photolysis in the stratosphere. k_T can also include removal at the Earth's surface.

A dynamic balance on the mass of substance in the NH troposphere component is

$$\begin{aligned} \frac{dQ_{NH}^T}{dt} = & k_{SH/NH}^T Q_{SH}^T - k_{NH/SH}^T Q_{NH}^T && \text{(exchange between NH and SH tropospheres)} \\ & + k_{S/T}^{NH} Q_{NH}^S - k_{T/S}^{NH} Q_{NH}^T && \text{(exchange between NH tropospheres and stratosphere)} \\ & - k_T^{NH} Q_{NH}^T && \text{(removal in troposphere)} \\ & + P_{NH} && \text{(source emission into NH troposphere)} \end{aligned} \quad (2.A.1)$$

⁶While the division of the troposphere into two compartments, the NH and SH, is reasonable from the point of view of estimating lifetimes of relatively long-lived tropospheric constituents, such a division is less applicable in the stratosphere. In the case of stratospheric transport and mixing, a better compartmental division would be between the tropical and midlatitude stratosphere (Volk et al., 1996). With such a division, the stratosphere would actually be represented by three compartments, the tropical stratosphere and the NH and SH midlatitude to polar stratospheres. The development in this appendix can be extended to such a five-compartment model, if desired.

TABLE 2.21 Substances Either Confirmed or Under Study as Hazardous to Human Health by State of California Air Resources Board (1989)

Substance	Qualitative Health Assessment ^a	Manner of Usage/ Major Sources	Atmospheric Residence Time	Concentrations	
				Ambient Average ^b	Hotspot
	Human carcinogen			4.6 ppb (SoCAB) ^c	
Ethylene dibromide	Probable carcinogen	Gasoline, pesticides	50 days	7.4 ppt (SoCAB)	
Ethylene dichloride	Probable carcinogen	Gasoline, solvents, pesticides	42 days	19–110 ppt	
Hexavalent chromium	Human carcinogen	Chrome plating, corrosion inhibitor		0.5 ng m ⁻³ (SoCAB)	
Dioxins	Probable carcinogen	Combustion product	1 yr in soil	1.0 pg m ⁻³	—
Asbestos	Human carcinogen	Milling, mining	Unknown; removed by deposition	8–80 fibers m ⁻³	50–500 fibers m ⁻³
Cadmium	Probable carcinogen	Secondary smelters, fuel combustion	7 days; removed by deposition	2.5 ng m ⁻³	40 ng m ⁻³
Carbon tetrachloride	Probable carcinogen	CCl ₄ production, grain fumigant	42 yr	0.13 ppb	0.63 ppb
Ethylene oxide	Probable carcinogen	Sterilization agent, manufacture of surfactants	200 days	50 ppt (SoCAB)	17 ppb
Vinyl chloride	Human carcinogen	Landfill by-product	2 days	—	0.08–0.34 ppb
Inorganic arsenic	Human carcinogen	Fuel combustion, pesticides	Unknown; removed by deposition	2.4 ng m ⁻³ (SoCAB)	200 ng m ⁻³
Methylene chloride	Probable carcinogen	Solvent	0.41 yr	1.1–2.4 ppb	10.7 ppb
Perchloroethylene	Probable carcinogen	Solvent, chemical intermediate	0.4 yr	0.71 ppb	22 ppb
Trichloroethylene	Probable carcinogen	Solvent, chemical	5–8 days	0.22 ppb	

Continued

TABLE 2.21 (Continued)

	Qualitative Health Assessment ^a	Manner of Usage/ Major Sources	Atmospheric Residence Time	Concentrations	
Nickel	Probable carcinogen	Alloy, plating ceramics, dyes intermediate	Unknown, removed by deposition	7.3 ng m ⁻³	23 ng m ⁻³
Chloroform	Probable carcinogen	Solvent, chemical intermediate	0.55 yr	0.006–0.13 ppb	10 ppb
Formaldehyde	Probable carcinogen	Chemical	3.8–8.6 hours	2–39 ppb	
1,3-Butadiene	Probable carcinogen	Chemical feedstock, resin production	< 1 day		0.016 ppb
Acetaldehyde	Probable carcinogen	Motor vehicles	9 hour		35 ppb
Acrylonitrile	Probable carcinogen	Feedstock, resins, rubber	5.6 days		
Beryllium	Probable carcinogen	Metals alloys, fuel combustion	10 days to be removed by deposition	0.11–0.22 ng m ⁻³	
Dialkylnitrosamines	Probable carcinogen	Chemical feedstock	9.6 hours		0.3 ppb
<i>p</i> -Dichlorobenzene	Probable carcinogen	Room deodorant, moth repellent	39 days		105–1700 µg m ⁻³
Di-(2-ethylhexyl) phthalate	Probable carcinogen	Plasticizer, resins	1.3–13 hours (urban)	2 µg m	
1,4-Dioxane	Probable carcinogen	Solvent stabilizer, feedstock	3.9 days		
Dimethyl sulfate	Probable carcinogen	Chemical reagent			
Ethyl acrylate	Possible carcinogen	Chemical intermediates	12 hours		
Hexachlorobenzene	Probable carcinogen	Solvent, pesticide	4 yr in soils		

Continued

TABLE 2.21 (Continued)

Substance	Qualitative Health Assessment ^a	Manner of Usage/ Major Sources	Atmospheric Residence Time	Concentrations	
				Ambient Average ^b	Hotspot
Lead	Blood system toxic, neurotoxicity	Auto exhaust, fuel additive	7–30 days removed by deposition		
Mercury	Neurotoxic	Electronics, paper pulp manufacture	0.3–2 yr removed by deposition	0.37–0.49 ppb	1.2 ppb
4,4'-Methylenedianiline	Possible carcinogen	Chemical intermediate	6.4 hours	—	—
N-Nitrosomorpholine	Probable carcinogen	Detergents, corrosion inhibitor	< 9.6 hours	0.025 ng m ⁻³	0.1 ng m ⁻³
PAHs	Probable carcinogen	Fuel combustion	0.4–40 days removed by deposition	0.46 ng m ⁻³	
PCBs	Probable carcinogen	Electronics	3–1700 days removed by deposition	0.5–14 ng m ⁻³	
Propylene oxide	Probable carcinogen	Resin manufacture, surfactant	6 days		
Styrene	Probable carcinogen	Chemical feedstock	—	10 ppb	—
Toluene diisocyanates	Possible carcinogen	Raw material	26 hours	—	—
2,4,6-Trichlorophenol	Probable carcinogen	Herbicide, wood preservative			

^a*Human carcinogen* = sufficient evidence in humans (Intern. Agency for Research on Cancer). *Probable human carcinogen* = limited human or sufficient animal evidence using IARC criteria or EPA guidelines for carcinogen risk assessment. *Possible human carcinogen* = limited animal evidence using IARC criteria or EPA guidelines for carcinogen risk assessment.

^bValues presented by the California ARB relevant to California.

^cSouth Coast Air Basin of California (Los Angeles metropolitan area).

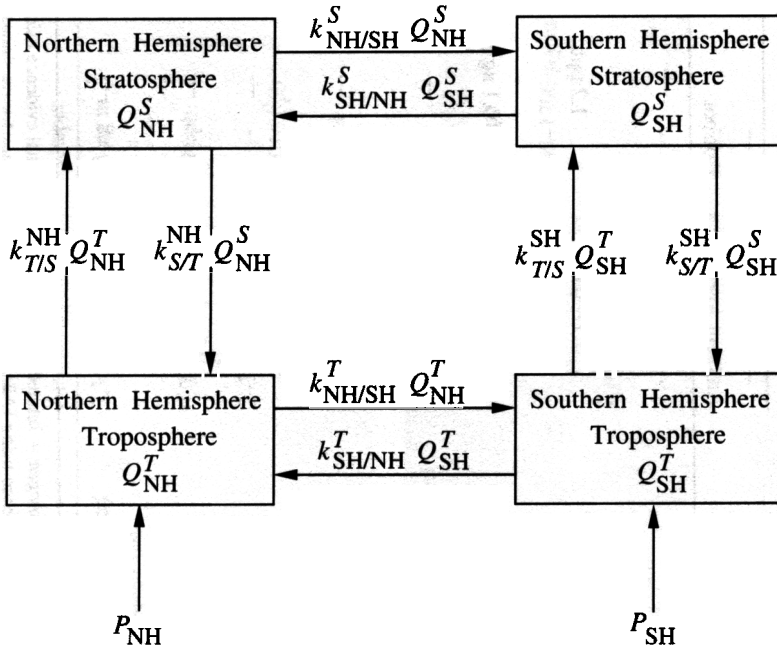


FIGURE 2.A.1 Four-compartment model of the atmosphere (NH = Northern Hemisphere, SH = Southern Hemisphere, S = stratosphere, T = troposphere). P_{NH} and P_{SH} are source emission rates of the compound in the NH and SH troposphere, respectively. The quantities of the species of interest in the four reservoirs are denoted Q_{NH}^T , Q_{NH}^S , Q_{SH}^T , and Q_{SH}^S . The fluxes between the reservoirs are proportional to the content of the compound in the reservoir where the flux originates. The flux of material from the NH troposphere to the SH troposphere is $k_{NH/SH}^T Q_{NH}^T$ and the reverse flux is $k_{SH/NH}^T Q_{SH}^T$. Other intercompartmental fluxes are defined similarly.

At steady state, the sources and sinks balance,

$$0 = k_{SH/NH}^T Q_{SH}^T - k_{NH/SH}^T Q_{NH}^T + k_{S/T}^{NH} Q_{NH}^S - k_{T/S}^{NH} Q_{NH}^T - k_{T/S}^{NH} Q_{NH}^T + P_{NH} \quad (2.A.2)$$

which can be rearranged as

$$0 = -\left(k_{NH/SH}^T + k_{T/S}^{NH} + k_{T}^{NH}\right) Q_{NH}^T + k_{SH/NH}^T Q_{SH}^T + k_{S/T}^{NH} Q_{NH}^S + P_{NH} \quad (2.A.3)$$

A similar steady-state balance on the SH troposphere yields

$$0 = -\left(k_{SH/NH}^T + k_{T/S}^{SH} + k_{T}^{SH}\right) Q_{SH}^T + k_{NH/SH}^T Q_{NH}^T + k_{S/T}^{SH} Q_{SH}^S + P_{SH} \quad (2.A.4)$$

Comparable balances on the two stratosphere compartments yield

$$0 = -\left(k_{\text{NH/SH}}^S + k_{S/T}^{\text{NH}} + k_S^{\text{NH}}\right) Q_{\text{NH}}^S + k_{\text{SH/NH}}^S Q_{\text{SH}}^S + k_{T/S}^{\text{NH}} Q_{\text{NH}}^T \quad (2.A.5)$$

$$0 = -\left(k_{\text{SH/NH}}^S + k_{S/T}^{\text{SH}} + k_S^{\text{SH}}\right) Q_{\text{SH}}^S + k_{\text{NH/SH}}^S Q_{\text{NH}}^S + k_{T/S}^{\text{SH}} Q_{\text{SH}}^T \quad (2.A.6)$$

Equations (2.A.3) to (2.A.6) constitute four equations in the four unknowns Q_{NH}^T , Q_{SH}^T , Q_{NH}^S , and Q_{SH}^S . It is useful to rewrite these equations as

$$0 = -\alpha_1 Q_1 + \alpha_2 Q_2 + \alpha_3 Q_3 + P_1 \quad (2.A.7)$$

$$0 = -\alpha_4 Q_2 + \alpha_5 Q_1 + \alpha_6 Q_4 + P_2 \quad (2.A.8)$$

$$0 = -\alpha_7 Q_3 + \alpha_8 Q_4 + \alpha_9 Q_1 \quad (2.A.9)$$

$$0 = -\alpha_{10} Q_4 + \alpha_{11} Q_3 + \alpha_{12} Q_2 \quad (2.A.10)$$

where $Q_1 = Q_{\text{NH}}^T$, $Q_2 = Q_{\text{SH}}^T$, $Q_3 = Q_{\text{NH}}^S$, $Q_4 = Q_{\text{SH}}^S$, $P_1 = P_{\text{NH}}$, and $P_2 = P_{\text{SH}}$. Also,

$$\begin{aligned} \alpha_1 &= k_{\text{NH/SH}}^T + k_{T/S}^{\text{NH}} + k_T^{\text{NH}} & \alpha_2 &= k_{\text{SH/NH}}^T & \alpha_3 &= k_{S/T}^{\text{NH}} \\ \alpha_4 &= k_{\text{SH/NH}}^T + k_{T/S}^{\text{SH}} + k_T^{\text{SH}} & \alpha_5 &= k_{\text{NH/SH}}^T & \alpha_6 &= k_{S/T}^{\text{SH}} \\ \alpha_7 &= k_{\text{NH/SH}}^S + k_{S/T}^{\text{NH}} + k_S^{\text{NH}} & \alpha_8 &= k_{\text{SH/NH}}^S & \alpha_9 &= k_{T/S}^{\text{NH}} \\ \alpha_{10} &= k_{\text{SH/NH}}^S + k_{S/T}^{\text{SH}} + k_S^{\text{SH}} & \alpha_{11} &= k_{\text{NH/SH}}^S & \alpha_{12} &= k_{T/S}^{\text{SH}} \end{aligned}$$

Equations (2.A.9) and (2.A.10) can be solved simultaneously to obtain Q_3 and Q_4 in terms of Q_1 and Q_2 ,

$$Q_3 = \beta_1 Q_2 + \beta_2 Q_1 \quad (2.A.11)$$

$$Q_4 = \beta_3 Q_2 + \beta_4 Q_1 \quad (2.A.12)$$

where

$$\begin{aligned} \beta_1 &= \frac{\frac{\alpha_8 \alpha_{12}}{\alpha_7 \alpha_{10}}}{1 - \frac{\alpha_8 \alpha_{11}}{\alpha_7 \alpha_{10}}} & \beta_2 &= \frac{\frac{\alpha_9}{\alpha_7}}{1 - \frac{\alpha_8 \alpha_{11}}{\alpha_7 \alpha_{10}}} \\ \beta_3 &= \frac{\frac{\alpha_{11} \alpha_8 \alpha_{12}}{\alpha_{10} \alpha_7 \alpha_{10}} + \frac{\alpha_{12}}{\alpha_{10}}}{1 - \frac{\alpha_8 \alpha_{11}}{\alpha_7 \alpha_{10}}} & \beta_4 &= \frac{\frac{\alpha_9 \alpha_{11}}{\alpha_7 \alpha_{10}}}{1 - \frac{\alpha_8 \alpha_{11}}{\alpha_7 \alpha_{10}}} \end{aligned}$$

The resulting equations for Q_1 and Q_2 are

$$0 = (\alpha_3 \beta_2 - \alpha_1) Q_1 + (\alpha_2 + \alpha_3 \beta_1) Q_2 + P_1 \quad (2.A.13)$$

$$0 = (\alpha_5 + \alpha_6 \beta_4) Q_1 + (\alpha_6 \beta_3 - \alpha_4) Q_2 + P_2 \quad (2.A.14)$$

the solutions of which are

$$Q_1 = \frac{(\alpha_2 + \alpha_3\beta_1)P_2 - (\alpha_6\beta_3 - \alpha_4)P_1}{(\alpha_3\beta_2 - \alpha_1)(\alpha_6\beta_3 - \alpha_4) - (\alpha_5 + \alpha_6\beta_4)(\alpha_2 + \alpha_3\beta_1)} \quad (2.A.15)$$

$$Q_2 = \frac{(\alpha_5 + \alpha_6\beta_4)P_1 - (\alpha_3\beta_2 - \alpha_1)P_2}{(\alpha_3\beta_2 - \alpha_1)(\alpha_6\beta_3 - \alpha_4) - (\alpha_5 + \alpha_6\beta_4)(\alpha_2 + \alpha_3\beta_1)} \quad (2.A.16)$$

Equations (2.A.15) and (2.A.16) give the steady-state concentrations of the substance in the NH and SH troposphere, respectively ($Q_1 = Q_{\text{NH}}^T$ and $Q_2 = Q_{\text{SH}}^T$), as a function of the source rates into the two hemispheres and all the transport and removal parameters of the four compartments. Steady-state concentrations in the two stratospheric reservoirs, $Q_3 = Q_{\text{NH}}^S$ and $Q_4 = Q_{\text{SH}}^S$, are then obtained from (2.A.11) and (2.A.12). These equations provide a general, steady-state analysis of a four-compartment model of a substance that is emitted into the troposphere and removed by separate first-order processes in each of the four compartments.

The mass of the substance in the entire atmosphere is the sum of the masses in the four compartments,

$$Q_{\text{total}} = Q_{\text{NH}}^T + Q_{\text{SH}}^T + Q_{\text{NH}}^S + Q_{\text{SH}}^S \quad (2.A.17)$$

The overall average residence time of a molecule of the substance in the atmosphere can be obtained by dividing its total quantity in the atmosphere by its total rate of introduction from sources,

$$\tau = \frac{Q_{\text{total}}}{P_{\text{NH}} + P_{\text{SH}}} \quad (2.A.18)$$

Average residence times in any of the four compartments can be calculated from the quantity in the compartment divided by the net source rate in that compartment.

The foregoing analysis can be simplified to fewer than four atmospheric compartments. For a substance that is completely removed in the troposphere, only the two tropospheric hemispheric components need be considered. If the lifetime of such a substance is shorter than the time needed to mix throughout the entire global troposphere, then a two-compartment model, NH troposphere and SH troposphere, is called for. If the substance's lifetime is long compared to the interhemispheric mixing time, then the entire troposphere can be considered as a single compartment. Because horizontal mixing in the stratosphere is so much faster than vertical mixing, for many substances that reach the stratosphere, the stratosphere can be considered as a single compartment.

2.A.1 Relation Between Atmospheric Mass and Volume Mixing Ratio

The Q 's in the foregoing equations have units of mass (g). What is frequently available for a substance is its average mixing ratio ξ . To relate the mixing ratio to the mass in a reservoir one needs the total mass of air in the reservoir. For this purpose we use

$$\begin{aligned} W_{\text{air}}^T &= \text{mass of air in the troposphere} \\ &= 4.56 \times 10^{21} \text{ g} \end{aligned}$$

$$\begin{aligned} W_{\text{air}}^S &= \text{mass of air in the stratosphere} \\ &= 0.72 \times 10^{21} \text{ g} \end{aligned}$$

It can be assumed that these masses divide equally between the NH and SH. With the average molecular weight of air, $M_{\text{air}} = 28.9 \text{ g mol}^{-1}$, the tropospheric mass of a substance of molecular weight M that has a tropospheric mixing ratio of ξ^T is

$$Q^T = \frac{W_{\text{air}}^T}{M_{\text{air}}} \xi^T M \quad (2.A.19)$$

Similarly, for the stratosphere,

$$Q^S = \frac{W_{\text{air}}^S}{M_{\text{air}}} \xi^S M \quad (2.A.20)$$

Thus the total mass of the substance in the atmosphere is

$$Q = Q^T + Q^S = \left(\frac{W_{\text{air}}^T}{M_{\text{air}}} \xi^T + \frac{W_{\text{air}}^S}{M_{\text{air}}} \xi^S \right) M \quad (2.A.21)$$

If the tropospheric mass is divided into Q_{NH}^T and Q_{SH}^T ,

$$Q_{\text{NH}}^T = \frac{W_{\text{air}}^T/2}{M_{\text{air}}} \xi_{\text{NH}}^T M \quad (2.A.22)$$

$$Q_{\text{SH}}^T = \frac{W_{\text{air}}^T/2}{M_{\text{air}}} \xi_{\text{SH}}^T M \quad (2.A.23)$$

As an example, the average mixing ratios of OCS in the troposphere and stratosphere are (Chin and Davis, 1995)

$$\xi_{\text{OCS}}^T = 490 \text{ ppt} = 490 \times 10^{-12}$$

$$\xi_{\text{OCS}}^S = 380 \text{ ppt} = 380 \times 10^{-12}$$

The total atmospheric mass of OCS is ($M_{\text{OCS}} = 60 \text{ g mol}^{-1}$):

$$\begin{aligned} Q &= \left(\frac{4.56 \times 10^{21}}{28.9} (490 \times 10^{-12}) + \frac{0.72 \times 10^{21}}{28.9} (380 \times 10^{-12}) \right) 60 \\ &= 4.63 \times 10^{12} \text{ g} + 0.57 \times 10^{12} \text{ g} \\ &= 4.63 \text{ Tg} + 0.57 \text{ Tg} \\ &= 5.2 \text{ Tg} \end{aligned}$$

2.A.2 Application of the Compartment Model to Methyl Chloroform (CH_3CCl_3)

Methyl chloroform is a man-made substance, the total emissions of which to the atmosphere are reasonably well known. Its atmospheric degradation occurs almost entirely by hydroxyl radical reaction. The CH_3CCl_3 mixing ratio in the atmosphere is well established;

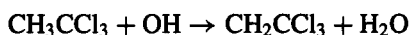
thus the global steady-state budget of CH_3CCl_3 can be used as a means of estimating a global average OH radical concentration. Such estimates are usually accomplished with a three-dimensional transport model (Prinn et al., 1992), but here we apply the simple four-compartment model to analyze the global budget of CH_3CCl_3 .

The following emissions data for CH_3CCl_3 are available (Prinn et al., 1992):

$$P_{\text{NH}} = 5.647 \times 10^{11} \text{ g yr}^{-1} \quad (1978 \text{ to } 1990 \text{ average})$$

$$P_{\text{SH}} = 2.23 \times 10^{10} \text{ g yr}^{-1}$$

CH_3CCl_3 is removed by OH reaction,



with a rate constant $k = 1.8 \times 10^{-12} \exp(-1550/T)$ (see Table B.1). To evaluate average values of the rate constant in the troposphere and stratosphere, we use the tropospheric average temperature of 277 K. An average temperature for the stratosphere is taken as that at 12 km in the U.S. Standard Atmosphere, $T = 216.7$ K. A global average tropospheric OH concentration is taken as 8.7×10^5 molecules cm^{-3} (Prinn et al., 1992). An average stratospheric OH mixing ratio in the midlatitude is 1 ppt (see Chapter 4), which translates, at 12 km, into a concentration of 6.48×10^6 molecules cm^{-3} . CH_3CCl_3 is also degraded by photolysis in the stratosphere, but at a rate almost 4000 times slower than OH reaction, so we will neglect it here. Finally, CH_3CCl_3 is lost by deposition to the Earth's surface with a first-order loss coefficient of 0.012 yr^{-1} (Prinn et al., 1992).

We need the exchange rates among the four atmospheric compartments. We use the following values:

$$k_{\text{SH/NH}}^T = k_{\text{NH/SH}}^T = 1.0 \text{ yr}^{-1}$$

$$k_{\text{SH/NH}}^S = k_{\text{NH/SH}}^S = 0.25 \text{ yr}^{-1}$$

$$k_{\text{S/T}}^{\text{NH}} = k_{\text{T/S}}^{\text{SH}} = 0.4 \text{ yr}^{-1} \quad (\text{van Velthoven and Kelder, 1996})$$

$$k_{\text{T/S}}^{\text{NH}} = k_{\text{S/T}}^{\text{SH}} = 0.063 \text{ yr}^{-1} \quad (\text{van Velthoven and Kelder, 1996})$$

The four-compartment model can be used, with the above parameter values and yearly emission rates, to estimate the steady-state mixing ratios of CH_3CCl_3 in the troposphere and stratosphere and the overall atmospheric residence time of CH_3CCl_3 . The results are given below.

	Calculated by Four-Compartment Model	
Tropospheric mixing ratio (ppt)	129 ppt	160 ppt ^b
Stratospheric mixing ratio (ppt)	75 ppt	
Atmospheric lifetime (yr)	5.0 yr ^a	

^aThe CH_3CCl_3 lifetime estimated by IPCC (1995) is 5.4 ± 0.6 years based on three-dimensional model calculations.

^bSee Table 2.15.

REFERENCES

- Andreae, M. O. (1990) Ocean—atmosphere interactions in the global biogeochemical sulfur cycle, *Marine Chem.*, **30**, 1–29.
- Andreae, M. O., and Barnard, W. R. (1984) The marine chemistry of dimethylsulfide, *Marine Chem.*, **14**, 267–279.
- Andreae, M. O., and Crutzen, P. J. (1997) Atmospheric aerosols: biogeochemical sources and role in atmospheric chemistry, *Science*, **276**, 1052–1058.
- Andreae, M. O., and Raemdonck, H. (1983) Dimethylsulfide in the surface ocean and the marine atmosphere: a global view, *Science*, **221**, 744–747.
- Andreae, M. O., et al. (1992) Ozone and aiken nuclei over equatorial Africa: airborne observations during DECAFE 88, *J. Geophys. Res.*, **97**, 6137–6148.
- Arnts, R. R., and Meeks, S. (1981) Biogenic hydrocarbon contribution to the ambient air of selected areas, *Atmos. Environ.*, **15**, 1643–1651.
- Barnard, W. R., Andreae, M. O., Watkins, W. E., Bingemer, H., and Georgii, H. W. (1982) The flux of dimethylsulfide from the oceans to the atmosphere, *J. Geophys. Res.*, **87**, 8787–8793.
- Barnes, R. A., Holland, A. C., and Kirchhoff, V. W. J. H. (1987) Equatorial ozone profiles from the ground to 52-km during the Southern Hemisphere autumn, *J. Geophys. Res.*, **92**, 5573–5583.
- Baugues, K. (1986) A review of NMOC, NO_x, and NMOC/NO_x ratios measured in 1984 and 1985. U.S. Environmental Protection Agency report EPA-450/4-86-015, Research Triangle Park, NC.
- Berresheim, H., Wine, P. H., and Davis, D. D. (1995) Sulfur in the atmosphere, in *Composition, Chemistry, and Climate of the Atmosphere*, edited by H. B. Singh. Van Nostrand Reinhold, New York, pp. 251–307.
- Bojkov, R. D. (1988) Ozone changes at the surface and in the free troposphere, in *Tropospheric Ozone*, edited by I. S. A. Isaksen. Reidel, Dordrecht, pp. 83–96.
- Bouwman, A. F., Van der Hoeck, K. W., and Olivier, J. G. J. (1995) Uncertainties in the global source distribution of nitrous oxide, *J. Geophys. Res.*, **100**, 2785–2800.
- Browell, E. V., Gregory, G. L., Harriss, R. C., and Kirchhoff, V. W. J. H. (1988) Tropospheric ozone and aerosol distributions across the Amazon. *J. Geophys. Res.*, **93**, 1431–1451.
- California Air Resources Board (1989) Information on substances for review as toxic air contaminants. Report No. ARB/SSD/89-01, Sacramento, CA.
- Charlson, R. J., Anderson, T. L., and McDuff, R. E. (1992) The sulfur cycle, in *Global Biogeochemical Cycles*, edited by S. S. Butcher, R. J. Charlson, G. H. Orians, and G. V. Wolfe. Academic Press, New York, pp. 285–300.
- Chin, M., and Davis, D. D. (1995) A reanalysis of carbonyl sulfide as a source of stratospheric background sulfur aerosol, *J. Geophys. Res.*, **100**, 8993–9005.
- Cline, J. D., and Bates, T. S. (1983) Dimethyl sulfide in the equatorial Pacific Ocean: a natural source of sulfur to the atmosphere, *Geophys. Res. Lett.*, **10**, 949–952.
- Crutzen, P. J., (1988) Tropospheric ozone: a review, in *Tropospheric Ozone*, edited by I. S. A. Isaksen. Reidel, Dordrecht, pp. 3–32.
- Crutzen, P. J. (1995) Ozone in the troposphere, in *Composition, Chemistry, and Climate of the Atmosphere*, edited by H. B. Singh. Van Nostrand Reinhold, New York, pp. 349–393.
- Dacey, J. W. H., and Wakeham, S. G. (1986) Oceanic dimethylsulfide: production during zooplankton grazing on phytoplankton, *Science*, **233**, 1314–1316.
- Daisey, J. M. (1980) Organic compounds in urban aerosols, *Ann. N. Y. Acad. Sci.*, **338**, 50–69.
- Danielson, E. F. (1968) Stratosphere–troposphere exchange based on radioactivity, ozone and potential vorticity. *J. Atmos. Sci.* **25**. 502–518.

- Delaney, A. C., Haagenson, P., Walters, S., Wartburg, A. F., and Crutzen, P. J. (1985) Photochemically produced ozone in the emission from large-scale tropical vegetation fires. *J. Geophys. Res.*, **90**, 2425–2429.
- Dentener, F. J., and Crutzen, P. J. (1994) A three-dimensional model of the global ammonia cycle. *J. Atmos. Chem.*, **19**, 331–369.
- Dignon, J., and Hameed, S. (1989) Global emissions of nitrogen and sulfur oxides from 1860 to 1980. *J. Air Pollut. Contr. Assoc.*, **39**, 180–186.
- Dlugokencky, E. J., Steele, L. P., Lang, P. M., and Mesarie, K. A. (1994) The growth rate and distribution of atmospheric CH₄. *J. Geophys. Res.*, **99**, 17021–17043.
- Dockery, D. W., Pope, C. A. III, Xu, X., Spengler, J. D., Ware, J. H., Fay, M. E., Ferris, B. G. Jr., and Speizer, F. E. (1993) An association between air pollution and mortality in six U.S. cities. *N. Engl. J. Med.*, **329**, 1753–1759.
- Ehhalt, D. H., Rohrer, F., and Wahner, A. (1992) Sources and distribution of NO_x in the upper troposphere at northern mid-latitudes. *J. Geophys. Res.*, **97**, 3725–3738.
- Eriksson, E. (1959) The yearly circulation of chloride and sulfur in nature. Meteorological, geochemical, and pedological implications. *Tellus*, **11**, 375–404.
- Fehsenfeld, F. C., and Liu, S. C. (1993) Tropospheric ozone: distribution and sources, in *Global Atmospheric Chemical Change*, edited by C. N. Hewitt and W. T. Sturgess. Elsevier, New York, pp. 169–231.
- Fehsenfeld, F. C., Calvert, J., Fall, R., Goldan, P., Guenther, A. B., Hewitt, C. N., Lamb, B., Liu, S., Trainer, M., Westberg, H., and Zimmerman, P. (1992) Emission of volatile organic compounds from vegetation and the implications for atmospheric chemistry. *Global Biogeochem. Cycles*, **6**, 389–430.
- Fishman, J., Watson, C. E., Larsen, J. C., and Logan, J. A. (1990) Distribution of tropospheric ozone determined from satellite data. *J. Geophys. Res.*, **95**, 3599–3617.
- Fishman, J., et al. (1992) Distribution of tropospheric ozone in the tropics from satellite and ozonesonde measurements. *J. Atmos. Terr. Phys.*, **54**, 589–597.
- Guenther, A., et al. (1995) A global model of natural volatile organic compound emissions. *J. Geophys. Res.*, **100**, 8873–8892.
- Hameed, S., and Dignon, J. (1992) Global emissions of nitrogen and sulphur oxides in fossil fuel combustion 1970–1986. *J. Air Waste Manage. Assoc.*, **42**, 159–163.
- Herman, J. R., McPeters, R., Stolarski, R., Larko, D., and Hudson, R. (1991) Global average ozone change from November 1978 to May 1990. *J. Geophys. Res.*, **90**, 17297–17305.
- Heintzenberg, J. (1989) Fine particles in the global troposphere—a review. *Tellus*, **41B**, 149–160.
- Intergovernmental Panel on Climate Change (IPCC) (1995) *Climate Change 1994: Radiative Forcing of Climate Change and an Evaluation of the IPCC IS92 Emission Scenarios*. Cambridge University Press, Cambridge, UK.
- Isodorov, V. A., Zenkevich, I. G., and Ioffe, B. V. (1985) Volatile atmospheric compounds in the atmosphere of forests. *Atmos. Environ.*, **19**, 1–8.
- Janach, W. E. (1989) Surface ozone: trend details, seasonal variations, and interpretation. *J. Geophys. Res.*, **94**, 18289–18295.
- Jiang, Y., and Yung, Y. L. (1996) Concentrations of tropospheric ozone for 1979 to 1992 over tropical Pacific South America from TOMS data. *Science*, **272**, 714–716.
- Kiehl, J. T., and Rodhe, H. (1995) Modeling geographical and seasonal forcing due to aerosols, in *Aerosol Forcing of Climate*, edited by R. J. Charlson and J. Heintzenberg. Wiley, New York, pp. 281–296.
- Lamb, B., Gay, D., Westberg, H., and Pierce, T. (1993) A biogenic hydrocarbon emission inventory for the U.S.A. using a simple forest canopy model. *Atmos. Environ.*, **27A**, 1673–1690.

- Lamb, B., Guenther, A., Gay, D., and Westberg, H. (1987) A national inventory of biogenic hydrocarbon emissions, *Atmos. Environ.*, **21**, 1695–1705.
- Lamb, B., Westberg, H., and Allwine, G. (1985) Biogenic hydrocarbon emissions from deciduous and coniferous trees in the United States, *J. Geophys. Res.*, **90**, 2380–2390.
- Lamb, B., Westberg, H., and Allwine, G. (1986) Isoprene emission fluxes determined by an atmospheric tracer technique, *Atmos. Environ.*, **20**, 1–8.
- Logan, J. A. (1989) Ozone in rural areas of the United States, *J. Geophys. Res.*, **94**, 8511–8532.
- Lovelock, J. E. (1971) Atmospheric fluorine compounds as indicators of air movements, *Nature*, **230**, 379.
- Lovelock, J. E., Maggs, R. J., and Rasmussen, R. A. (1972) Atmospheric dimethyl sulfide and the natural sulfur cycle, *Nature*, **237**, 452–453.
- Lubkert, B., and Zierock, K. H. (1989) European emission inventories—a proposal of international worksharing, *Atmos. Environ.*, **23**, 37–48.
- Lurmann, F. W., and Main, H. H. (1992) Analysis of the ambient VOC data collected in the Southern California Air Quality Study. Final Report. ARB Contract No. A832-130, California Air Resources Board, Sacramento, CA.
- Machida, T., Nakazawa, T., Fujii, Y., Aoki, S., and Watanabe, O. (1995) Increase in the atmospheric nitrous oxide concentration during the last 250 years, *Geophys. Res. Lett.*, **22**, 2921–2924.
- Middleton, P. (1995) Sources of air pollutants, in *Composition, Chemistry, and Climate of the Atmosphere*, edited by H. B. Singh. Van Nostrand Reinhold, New York, pp. 88–119.
- Molina, M. J., and Rowland, F. S. (1974) Stratospheric sink for chlorofluoromethanes: chlorine atom catalyzed destruction of ozone, *Nature*, **249**, 810–812.
- Monson, R., Jaeger, C., Adams, W., Driggers, E., Silver, G., and Fall, R. (1992) Relationships among isoprene emission rate, photosynthesis, and isoprene synthase activity as influenced by temperature, *Plant Physiol.*, **92**, 1175–1180.
- Montzka, S. A., Trainer, M., Angevine, W. M., and Fehsenfeld, F. C. (1995) Measurements of 3-methyl furan, methyl vinyl ketone, and methacrolein at a rural forested site in the southeastern United States, *J. Geophys. Res.*, **100**, 11393–11401.
- Montzka, S. A., Trainer, M., Goldan, P. D., Kuster, W. C., and Fehsenfeld, F. C. (1993) Isoprene and its oxidation products, methyl vinyl ketone and methacrolein, in the rural atmosphere, *J. Geophys. Res.*, **98**, 1101–1111.
- National Research Council (1991) *Rethinking the Ozone Problem in Urban and Regional Air Pollution*. National Academy Press, Washington, DC.
- Nguyen, B. C., Beloriso, S., Mihalopoulos, N., Gostan, J., and Nival, P. (1988) Dimethyl sulfide production during natural phytoplanktonic blooms, *Mar. Chem.*, **24**, 133–141.
- Nguyen, B. C., Bergeret, C., and Lambert, G. (1984) Exchange rates of dimethyl sulfide between ocean and atmosphere, in *Gas Transfer at Water Surfaces*, edited by W. Brunsart and G. H. Jirka. Reidel, Dordrecht, pp. 539–545.
- Oltmans, S. J., and Levy, H. II (1994) Surface ozone measurements from a global network, *Atmos. Environ.*, **28**, 9–24.
- Placet, M., Battye, R. E., Fehsenfeld, F. C., and Bassett, G. W. (1990) *Emissions Involved in Acidic Deposition Processes. State-of-Science/Technology Report 1. National Acid Precipitation Assessment Program*. U.S. Government Printing Office, Washington, DC.
- Prinn, R., et al. (1992) Global average concentration and trend for hydroxyl radicals deduced from ACE/GAGE trichloroethane (methyl chloroform) data from 1978–1990, *J. Geophys. Res.*, **97**, 2445–2461.
- Rasmussen, R. A. (1970) Isoprene: identified as a forest-type emission to the atmosphere, *Environ. Sci. Technol.*, **4**, 669–673.

- Rasmussen, R. A., and Went, F. W. (1965) Volatile organic material of plant origin in the atmosphere, *Proc. Natl. Acad. Sci. (USA)*, **53**, 215–220.
- Roberts, J. M. (1995) Reactive odd-nitrogen (NO_y) in the atmosphere, in *Composition, Chemistry, and Climate of the Atmosphere*, edited by H. B. Singh. Van Nostrand Reinhold, New York, pp. 176–215.
- Rodhe, H. (1978) Budgets and turn-over times of atmospheric sulfur compounds, *Atmos. Environ.*, **12**, 671–680.
- Rodhe, H. (1992) Modeling biogeochemical cycles, in *Global Biogeochemical Cycles*, edited by S. S. Butcher, R. J. Charlson, G. H. Orians, and G. V. Wolfe. Academic Press, San Diego, CA, pp. 55–72.
- Schönbein, C. F. (1840) Beobachtungen über den bei der elektrolyse des wassers und dem ausströmen der gewöhnlichen electricität aus spitzen eich entwicelnden geruch, *Ann. Phys. Chem.*, **50**, 616.
- Schönbein, C. F. (1854) Über verschiedene zustände des sauerstoffs, liebig's, *Ann. Chem.*, **89**, 257–300.
- Shen, T.-L., Wooldridge, P. J., and Molina, M. J. (1995) Stratospheric pollution and ozone depletion, in *Composition, Chemistry, and Climate of the Atmosphere*, edited by H. B. Singh. Van Nostrand Reinhold, New York, pp. 394–442.
- Singh, H. B. (1995) Halogens in the atmospheric environment, in *Composition, Chemistry, and Climate of the Atmosphere*, edited by H. B. Singh, Van Nostrand Reinhold, New York, pp. 216–250.
- Singh, H. B., and Zimmerman, P. (1990) Atmospheric distributions and sources of non-methane hydrocarbons, in *Advances in Environmental Science and Technology*, Vol. 24, edited by J. O. Nriagu. Wiley, New York, pp. 177–235.
- Singh, H. B., and Kanakidou, M. (1993) An investigation of the atmospheric sources and sinks of methyl bromide, *Geophys. Res. Lett.*, **20**, 133–136.
- Solomon, P. A., Fall, T., Salmon, L., Cass, G. R., Gray, H. A., and Davidson, A. (1989) Chemical characteristics of PM_{10} aerosols collected in the Los Angeles area. *J. Air Pollut. Control Assoc.*, **39**, 154–163.
- Spiro, P. A., Jacob, D. J., and Logan, J. A. (1992) Global inventory of sulfur emissions with $1^\circ \times 1^\circ$ resolution. *J. Geophys. Res.*, **97**, 6023–6036.
- Staehelin, J., and Schmid, W. (1991) Trend analysis of tropospheric ozone concentrations utilizing the 20-year data set of balloon soundings over Payerne (Switzerland), *Atmos. Environ.*, **25A**, 1739–1749.
- Stolarski, R., Bojkov, R., Bishop, L., Zerefos, C., Staehelin, J., and Zawodny, J. (1992) Measured trends in stratospheric ozone, *Science*, **256**, 342–349.
- Tingey, D., Turner, D., and Weber, J. (1991) Factors controlling the emissions of monoterpenes and other volatile organic compounds, in *Trace Gas Emissions by Plants*, edited by T. D. Sharkey, E. A. Holland, and H. A. Mooney. Academic Press, San Diego, CA, pp. 93–120.
- Turner, S. M., and Liss, P. S. (1985) Measurements of various sulfur gases in a coastal marine environment, *J. Atmos. Chem.*, **2**, 223–232.
- van Velthoven, P. F. J., and Kelder, H. (1996) Estimates of stratosphere—troposphere exchange: sensitivity to model formulation and horizontal resolution. *J. Geophys. Res.*, **101**, 1429–1434.
- Volk, C. M., et al. (1996) Quantifying transport between the tropical and mid-latitude lower stratosphere, *Science*, **272**, 1763–1768.
- Volz, A., and Kley, D. (1988) Evaluation of the Montsouris series of ozone measurements made in the nineteenth century, *Nature*, **332**, 240–242.
- Warneck, P. (1988) *Chemistry of the Natural Atmosphere*. Academic Press, New York.

- Went, F. W. (1960) Organic matter in the atmosphere and its possible relation to petroleum formation, *Proc. Natl. Acad. Sci. (USA)*, **46**, 212–221.
- Whitby, K. T., and Cantrell, B. (1976) Fine particles, in International Conference on Environmental Sensing and Assessment, Las Vegas, NV, Institute of Electrical and Electronic Engineers.
- Winer, A. M., Arey, J., Aschmann, S. M., Atkinson, R., Long, W. D., Morrison, L. C., and Olszyk, D. M. (1989) Hydrocarbon emissions from vegetation found in California's Central Valley. Final Report. Contract No. A732-155. California Air Resources Board, Sacramento, CA.
- World Meteorological Organization (WMO) (1986) *Atmospheric Ozone 1985*. Global Ozone Research and Monitoring Project: Report No. 16, Geneva.
- World Meteorological Organization (WMO) (1990) Report of the International Ozone Trends Panel: 1988. Global Ozone Research and Monitoring Project: Report No. 18, Geneva.
- Yokouchi, Y. (1994) Seasonal and diurnal variation of isoprene and its reaction products in a semi-rural area. *Atmos. Environ.*, **28**, 2651–2658.
- Yvon, S. A., Saltzman, E. S., Cooper, D. J., Bates, T. S., and Thompson, A. M. (1996) Atmosphere sulfur cycling in the tropical Pacific marine boundary layer (12° S, 135° W): a comparison of field data and model results I. Dimethylsulfide, *J. Geophys. Res.*, **101**, 6899–6909.
- Zimmerman, P. (1979) Testing of hydrocarbon emissions from vegetation, leaf litter and aquatic surfaces, and development of a method for compiling biogenic emission inventories. U.S. Environmental Protection Agency Report, EPA-450-4-70-004, Research Triangle Park, NC.
- Zimmerman, P., Greenberg, J., and Westberg, C. (1988) Measurements of atmospheric hydrocarbons and biogenic emission fluxes in the Amazon boundary layer, *J. Geophys. Res.*, **93**, 1407–1416.

PROBLEMS

- 2.1_A In the simplified calculation of the atmospheric sulfur cycle in Section 2.2.4, if the value of c , the SO₂ fraction of the total sulfur, is taken as 0.5, a sulfur atom residence time of 50 hours is estimated. What is the value of b , the fraction of sulfur converted to SO₄²⁻ before being removed, that is consistent with this choice of c ?
- 2.2_A Prepare a plot of ozone mixing ratio versus altitude from ground level to 50 km. Total molecular number density of air can be obtained from Table A.8, and O₃ molecular number density is given in Figure 2.11. Why do the molecular number density and mixing ratio peak at different altitudes?
- 2.3_A One Dobson unit corresponds to 2.69×10^{16} molecules O₃ cm⁻² integrated over a vertical column to the top of the atmosphere. Show how vertical ozone column data can be converted to Dobson units.
- 2.4_A Calculate the change in total ozone column, as measured in Dobson units, between 1969 and 1988 for the ozone profiles in Figure 2.13.
- 2.5_A Confirm the calculations presented in Section 2.A.2 on the concentration and lifetime of methyl chloroform.
- 2.6_B Derive the balance equations for a substance that is completely removed in the troposphere, but for which two tropospheric reservoirs should be considered (see Appendix 2). Apply the balance to CO using the source and sink data from Table 2.14. As a first approximation, assume that anthropogenic sources are totally concentrated in the Northern Hemisphere and that biomass burning sources are totally in the

Southern Hemisphere. The CH_4 oxidation source can be apportioned according to the NH/SH ratio of CH_4 concentration. NMHC oxidation can be assumed to be entirely in the NH. Biogenic CO sources can be equally apportioned between the NH and SH, and the ocean source according to a 2 : 1 ratio SH to NH. Soil uptake can be apportioned in the reverse ratio. The NH/SH exchange rates in Section 2.A.2 can be used. A global mean OH concentration of 8.7×10^5 molecules cm^{-3} can be assumed, and the CO–OH reaction rate constant is given in Table B.1. Calculate the CO mixing ratios in the NH and SH, using the mean values of the ranges in Table 2.14 and compare with those observed.

2.7_c Consider a species that is totally man-made and that was first emitted to the atmosphere at a time, say, $t = 0$. If the fractional rate of removal from the atmosphere by all processes is $p \text{ yr}^{-1}$, let us calculate the fraction f of the total amount of the compound produced up to time t still remaining in the atmosphere at any time t . Let us assume that mixing between the Northern and Southern Hemispheres is fast enough to provide a homogeneous concentration in the troposphere.

- a. Let the emission rate of the species be given by $P(t) = P_0 e^{rt}$. If $M(t)$ is the total mass in the atmosphere at time t , show that M is governed by

$$\frac{dM}{dt} = P_0 e^{rt} - pM \quad M(0) = 0$$

and that the solution is

$$M(t) = \frac{P_0}{r + p} (e^{rt} - e^{-pt})$$

Show that the total quantity produced in time t is

$$Q(t) = \frac{P_0}{r} (e^{rt} - 1)$$

so the fraction f still in the atmosphere at time t is

$$f = \frac{M(t)}{Q(t)} = \frac{r + p}{r} \left(\frac{e^{rt} - e^{-pt}}{e^{rt} - 1} \right)$$

The mean residence time, τ , can be estimated if necessary from the relation for f . A value of f can be estimated from the measured atmospheric concentration of the compound and the total quantity emitted. Knowing f and r , p can be determined and τ can be calculated as $1/p$. For $rt \gg 1$, $f \simeq r/(r + p)$.

- b. As an application of the foregoing theory, let us estimate the atmospheric residence times of the three species in Table 2.P.1, which presents atmospheric mixing ratios, together with values of f estimated from total production data (assuming that each species is of anthropogenic origin only). As noted above, the

atmospheric residence time $\tau = p^{-1}$. Given values of f and r , p can be calculated from $f = r/(r + p)$ since these species have been emitted long enough so that $rt \gg 1$. Plot f versus p (and τ) for $r = 0.15 \text{ yr}^{-1}$ showing points corresponding to the three compounds.

- c. Let us now assume that the troposphere can be divided into Northern and Southern Hemispheres with an interhemispheric fractional mixing rate of $m \text{ yr}^{-1}$. The rate of removal from the atmosphere, $p \text{ yr}^{-1}$, is assumed to be the same in both hemispheres. If all the manufacture and release of the compound are assumed to occur in the Northern Hemisphere, then let us find the ratio of concentrations, R , between the Northern and Southern Hemispheres at any time t . Let

M_N = mass of species in Northern Hemisphere

M_S = mass of species in Southern Hemisphere

Show that the hemispheric material balances are

$$\frac{dM_N}{dt} = P_0 e^{rt} - pM_N + m(M_S - M_N)$$

$$\frac{dM_S}{dt} = m(M_N - M_S) - pM_S$$

$$M_N(0) = M_S(0) = 0$$

$$M_N + M_S = \frac{P_0}{r + p} (e^{rt} - e^{-pt})$$

show that

$$M_S(t) = \frac{mP_0}{r + p} \left[\frac{e^{rt}}{r + p + 2m} - \frac{e^{-pt}}{\left(\frac{1}{2m} - \frac{1}{r + p + 2m} \right)} e^{-(p+2m)t} \right]$$

$$R = \frac{M_N(t)}{M_S(t)} = \frac{2(r + p + m)e^{rt} - (r + p + 2m)e^{-pt} - (r + p)e^{-(2m+p)t}}{2me^{rt} - (r + p + 2m)e^{-pt} + (r + p)e^{-(2m+p)t}}$$

For $e^{rt} \gg$

$$R \simeq 1 + \frac{r + p}{m}$$

- d. An independent calculation of atmospheric residence times can be made by performing the global balance over both Northern and Southern Hemispheres. Using the data in Table 2.P.1 as rough estimates of the thoroughly mixed background concentration in each hemisphere, estimate the values of p (yr^{-1}) by preparing a plot of R versus p for $r = 0.15 \text{ yr}^{-1}$ and $m = 0.2, 0.4, \text{ and } 0.7$.

Using the value $R = 1.4$ from Table 2.P.1 for A, and $r = 0.15 \text{ yr}^{-1}$ with $p = 0.02 \text{ yr}^{-1}$, the most appropriate value for m is 0.4 yr^{-1} . For the error ranges given by $R = 1.4 \pm 0.2$, $r = 0.13 \pm 0.03$, and $p = 0.03 \pm 0.01$, the extreme range in m values can be determined. The estimates of p are independent of the approximations of relative production rates used in the first calculation. On the other hand, the direct release of compounds in the Southern Hemisphere systematically leads to lower measured values of R , a high estimate of m from A data, and low estimates of p for a given choice of r .

Assuming a reasonable approximate value of $r = 0.15 \text{ yr}^{-1}$, show that satisfactory agreement between both methods of calculation can be obtained for $m \approx 0.4 \text{ yr}^{-1}$, $p_B = 0.3 \text{ yr}^{-1}$, and $p_C = 2 \text{ yr}^{-1}$. While these estimates could readily be in error by a factor of 2 or 3, it is clear that the atmospheric residence time of C is less than 1 year, and that of B is not more than about 5 or 6 years.

TABLE 2.P.1 Atmospheric Mixing Ratios of Three Species

	Atmospheric Mixing Ratios (ppt)			
	Hemisphere			
	N	S		
A	80 ± 5	57	69	0.87
B	65 ± 17	20 ± 5	43	0.37
C	15 ± 12	1.5	8	0.07

3 Atmospheric Photochemistry and Chemical Kinetics

3.1 RADIATIVE FLUX IN THE ATMOSPHERE

The essential energy flux in atmospheric chemistry is the flux of solar radiation. The *radiant flux density* F is the radiant energy flux across any surface element, without consideration of the direction; F is measured in watts per square meter (W m^{-2}). The radiant flux density is called the *irradiance* E when the radiation is received on a surface. Thus F and E are often used interchangeably. We will use F in general and E when we are referring specifically to the radiant flux density on a surface. The *radiance* L is the radiant flux as a function of the solid angle $d\omega$ crossing a surface perpendicular to the axis of the radiation beam; L is measured in watts per square meter per steradian ($\text{W m}^{-2} \text{sr}^{-1}$). The radiance as a function of direction gives a complete description of the radiative field.

Consider a beam of radiation of radiance L crossing a surface dS with the beam axis making an angle θ to the normal to dS (Figure 3.1). dS projects as $dS \cos \theta$ perpendicular to the beam axis of the radiation, and the radiant flux density dF on dS is

$$dF = L \cos \theta d\omega$$

The radiant flux density, or irradiance, on the surface dS is obtained by integrating the radiance over all angles,

$$E = \int L \cos \theta d\omega$$

When the radiance L is independent of direction, the radiative field is called *isotropic*. In this case, (3.2) can be integrated over the half space, $\Omega = 2\pi$, and the relation between the irradiance and the radiance is

$$E = \pi L$$

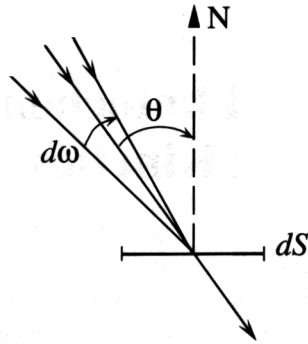


FIGURE 3.1 Relation between radiance and radiant flux density.

The irradiance upon a horizontal surface is obtained from the incoming radiance by integrating the radiance over the spherical coordinates θ and ϕ ,

$$E = \int_0^{2\pi} \int_0^\pi L(\theta, \phi) \cos \theta \sin \theta \, d\theta \, d\phi \quad (3.4)$$

where the direction of the incoming beam is characterized by the angle θ (see Figure 3.2).

The *monochromatic* or *spectral radiant flux density*, $F(\lambda)$, is the radiant flux density per unit wavelength interval, expressed in watts per square meter per nanometer ($\text{W m}^{-2} \text{nm}^{-1}$). Equivalently, when considering radiation incident upon a surface, the *spectral irradiance*, $E(\lambda)$, is expressed as $\text{W m}^{-2} \text{nm}^{-1}$.

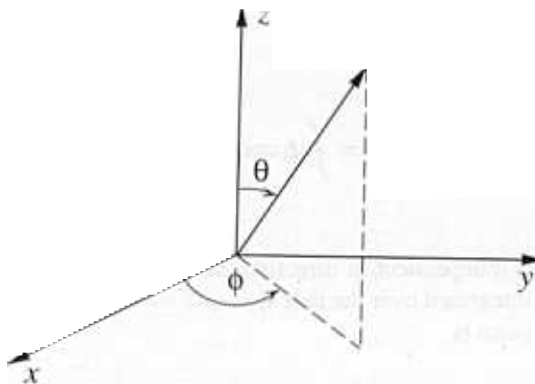


FIGURE 3.2 Coordinates for radiative calculations.

Sometimes the spectral radiant flux density is expressed as a function of frequency ν , that is, $F(\nu)$. Because the frequency ν of radiation is related to its wavelength by (1.13), $\nu = c/\lambda$, $F(\lambda)$ and $F(\nu)$ can be interrelated. Since the flux of energy in a small interval of wavelength $d\lambda$ must be equal to that in a small interval of corresponding frequency $d\nu$,

$$F(\lambda) d\lambda = F(\nu) d\nu$$

Since $d\nu = (c/\lambda^2) |d\lambda|$,

$$F(\lambda) = \left(\frac{c}{\lambda^2}\right) F(\nu)$$

$$\left(\frac{\nu^2}{c}\right) F(\nu)$$

Generally we will deal with wavelength as the variable rather than frequency, although they can easily be interrelated as indicated in (3.6).

3.1.1 Solar Radiation Received on Earth

Light absorption and scattering by atmospheric constituents attenuate the solar radiation as it passes through the atmosphere. The amount of attenuation depends on the nature and concentration of gases and particles and on the pathlength through which the solar beam passes. The pathlength is a function of the angle of the Sun, which depends on time of day, latitude, and date. Also, reflection of radiation from the Earth's surface contributes to the radiation at any point in the atmosphere.

Table 3.1 gives the solar spectral irradiance, normalized to a solar constant of 1367 W m^{-2} . Solar UV radiation, expressed in units of photons $\text{cm}^{-2} \text{ s}^{-1} \text{ nm}^{-1}$, at the surface (0 km), 20, 30, 40, and 50 km is shown in Figure 3.3. (A discussion of the processes that lead to the progressive attenuation of radiation was given in Chapter 1 in association with Figure 1.9.) Usually radiative transfer through the atmosphere is calculated by radiative transfer models that divide the atmosphere into layers and the radiative spectrum into wavelength intervals (Goody and Yung, 1989; Liou, 1992; Lenoble, 1993). The vertical distribution of trace gases and particles and the surface albedo serve as inputs to such models. Near the Earth's surface the spectral distribution shows a steep cutoff, when moving from longer to shorter wavelengths, beginning at about 320 nm. Radiation below 290 nm does not reach the Earth's surface; as noted in Chapter 1, this cutoff is the result of absorption of solar radiation by stratospheric ozone. There is no overlap between the absorption cross section of the major atmospheric gases, N_2 , O_2 , CO_2 , and H_2O , and the solar spectrum at the Earth's surface. Overlap does exist, however, with a number of trace gases that are

TABLE 3. Solar Spectral Irradiance, Normalized to a Solar Constant of 1367 W m^{-2}

λ (nm)	$F(\lambda)$ ($\text{W m}^{-2} \text{ nm}^{-1}$)	$\int_0^\lambda F(\lambda') d\lambda'$ (W m^{-2})	λ (nm)	$F(\lambda)$ ($\text{W m}^{-2} \text{ nm}^{-1}$)	$\int_0^\lambda F(\lambda') d\lambda'$ (W m^{-2})
250.5	0.059	2.092	490.5	2.009	276.7
255.5	0.089	2.387	495.5	1.928	286.4
260.5	0.102	2.967	500.5	1.859	296.1
265.5	0.280	3.921	510.5	1.949	315.3
270.5	0.293	5.257	520.5	1.833	333.5
275.5	0.200	6.245	530.5	1.954	352.3
280.5	0.112	7.111	540.5	1.772	371.1
285.5	0.141	8.364	550.5	1.864	389.8
290.5	0.623	10.44	560.5	1.845	408.4
295.5	0.548	13.19	570.5	1.772	426.7
300.5	0.403	15.51	580.5	1.840	445.2
305.5	0.580	18.26	590.5	1.815	463.3
310.0	0.495	20.54	600.5	1.748	481.1
315.2	0.695	24.03	610.5	1.705	498.7
320.0	0.712	27.46	620.5	1.736	515.7
325.2	0.646	31.15	631.0	1.641	535.0
330.0	1.144	35.86	641.0	1.616	551.4
335.5	0.982	41.69	651.0	1.608	567.5
340.5	0.992	46.17	661.0	1.573	582.8
345.5	0.967	50.77	671.0	1.518	598.2
350.5	1.119	55.52	681.0	1.494	613.3
355.5	1.058	60.69	691.0	1.450	627.9
360.5	0.979	65.26	701.0	1.388	642.2
365.5	1.263	70.56	711.0	1.387	656.1
370.5	1.075	76.52	721.0	1.332	669.7
375.5	1.141	81.75	731.0	1.327	683.0
380.5	1.289	87.77	741.0	1.259	696.0
385.5	0.954	92.27	751.0	1.263	708.8
390.5	1.223	97.67	761.0	1.238	721.3
395.5	1.378	103.0	771.0	1.205	733.4
400.5	1.649	109.5	781.0	1.188	745.3
405.5	1.672	118.0	791.0	1.159	757.1
410.5	1.502	126.3	801.0	1.143	768.5
415.5	1.736	135.1	821.0	1.081	790.6
420.5	1.760	143.8	841.0	1.045	811.8
425.5	1.697	152.3	861.0	0.997	831.6
430.5	1.136	159.8	881.0	0.960	850.9
435.5	1.725	168.3	901.0	0.905	869.7
440.5	1.715	177.1	921.0	0.830	887.1
445.5	1.823	186.7	941.0	0.800	903.5
450.5	2.146	196.8	961.0	0.767	919.1
455.5	2.036	206.9	981.0	0.762	934.3
460.5	2.042	217.1	1002.5	0.745	952.8
465.5	2.044	227.3	1052.5	0.661	987.9
470.5	1.879	237.1	1102.5	0.608	1019
475.5	2.018	247.3	1152.5	0.545	1048
480.5	2.037	257.4	1202.5	0.496	1074
485.5	1.832	267.4	1252.5	0.474	1098

Continued

TABLE 3.1 (Continued)

λ (nm)	$F(\lambda)$ ($\text{W m}^{-2} \text{nm}^{-1}$)	$\int_0^\lambda F(\lambda') d\lambda'$ (W m^{-2})	λ (nm)	$F(\lambda)$ ($\text{W m}^{-2} \text{nm}^{-1}$)	$\int_0^\lambda F(\lambda') d\lambda'$ (W m^{-2})
	0.438	1120		0.066	1313
	0.387	1140		0.054	1319
	0.353	1159		0.047	1325
	0.323	1176		0.041	1329
	0.296	1191		0.036	1332
	0.273	1205		0.031	1336
	0.247	1218		0.024	1342
	0.234	1230		0.019	1346
	0.217	1241		0.015	1349
	0.187	1251		0.012	1353
	0.169	1260		0.010	1355
	0.148	1267		0.008	1357
	0.133	1274		0.005	1360
	0.126	1281		0.003	1362
	0.116	1287		0.002	1364
	0.093	1298		0.001	1366
	0.075	1307		0.000	1367

Source: Fröhlich and London (1986).

important in tropospheric chemistry. In spite of its stratospheric absorption, a sufficient overlap exists between the solar UV spectrum at the Earth's surface and the absorption cross section of ozone that O_3 photolysis is also important in tropospheric chemistry.

3.1.2 Earth Geometry for Solar Radiation

Because of the rotation of the Earth around the Sun and its daily rotation around itself, the solar irradiance actually received at a given location on Earth depends on the location on the Earth, the date of the year, and the time of day. The Earth describes an ellipse around the Sun. The shortest distance between the Earth and Sun, occurring around January 3, is 1.471×10^8 km, and the largest distance, around July 4, is 1.521×10^8 km. The mean distance, the average of the two extremes, is 1.496×10^8 km.

The Earth rotates in an eastward direction around the polar axis, which is inclined at $23^\circ 27'$ from the normal to the ecliptic plane. The line joining the center of the Earth to the center of the Sun makes an angle Δ with the equatorial plane, which is called the *Sun declination* with the equatorial plane. Δ reaches its maximum value of $+23^\circ 27'$ at the summer solstice around June 21; it reaches its minimum value of $-23^\circ 27'$ at the winter solstice, around December 21, and is zero at the spring and fall equinoxes. Δ can be computed at any day of the year by Δ (in radians) = $-0.4 \cos[2\pi(d_n + 10)/365]$, where $d_n = 1$ for January 1, 2 for January 2, and so on.

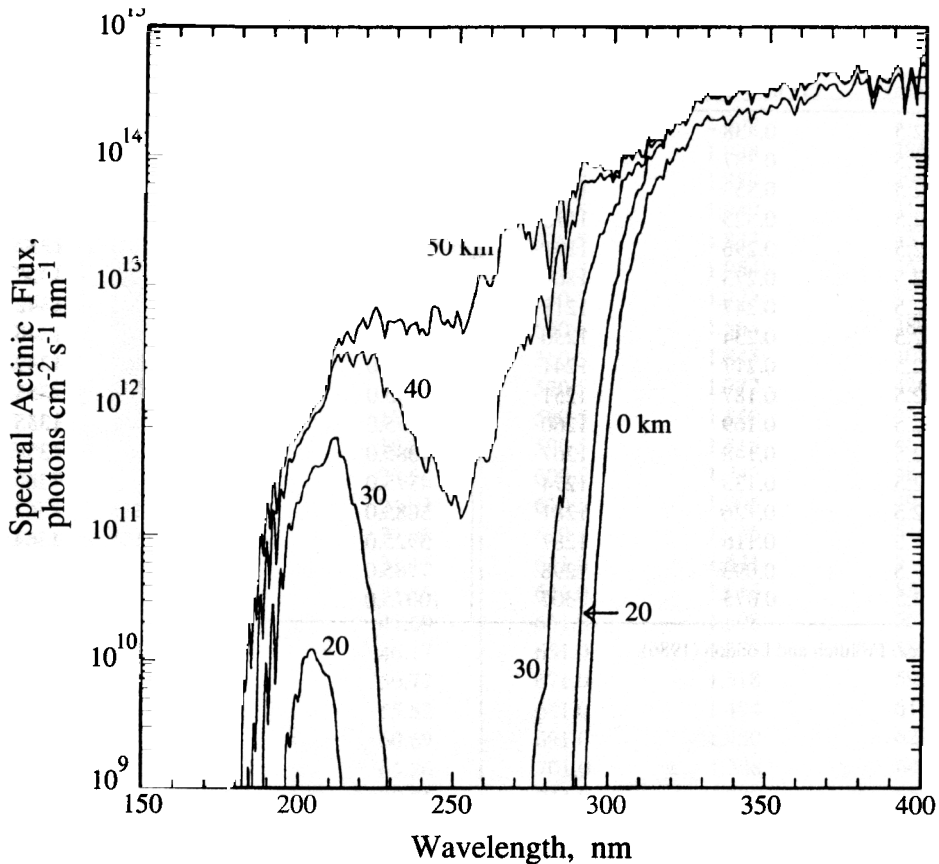


FIGURE 3.3 Solar spectral actinic flux ($\text{photons cm}^{-2} \text{s}^{-1} \text{nm}^{-1}$) at various altitudes and at the Earth's surface (DeMore et al., 1994).

A point on the Earth is characterized by its *latitude* ϕ and its *longitude* L (Figure 3.4). The latitude ϕ is the angle between the local vertical and the equatorial plane, measured in degrees from the equator (0°) to the pole ($\pm 90^\circ$), positive in the Northern Hemisphere and negative in the Southern Hemisphere. The longitude L is the angle between the local meridian, defined by the polar axis and the local vertical, and the Greenwich (United Kingdom) meridian. L is measured between 0° and 180° , positive eastward of Greenwich and negative westward.

The horizontal coordinates of the Sun are shown in Figure 3.5. The solar *zenith angle* θ_0 is the angle of the Sun's direction with respect to the local upward vertical, measured in degrees from 0° (overhead Sun) to 90° (Sun on horizon). The larger the solar zenith angle, the longer is the pathlength of solar radiation through the atmosphere and the greater the reduction in intensity by absorption and scattering by atmospheric constituents. The *azimuth angle* ϕ_0 (not to be confused with latitude ϕ) is the angle between the vertical plane of the Sun and a vertical plane of reference that is generally taken toward the geographic south. ϕ_0 is measured from the south, positive between 0° and 180° eastward and negative between 0° and -180° westward.

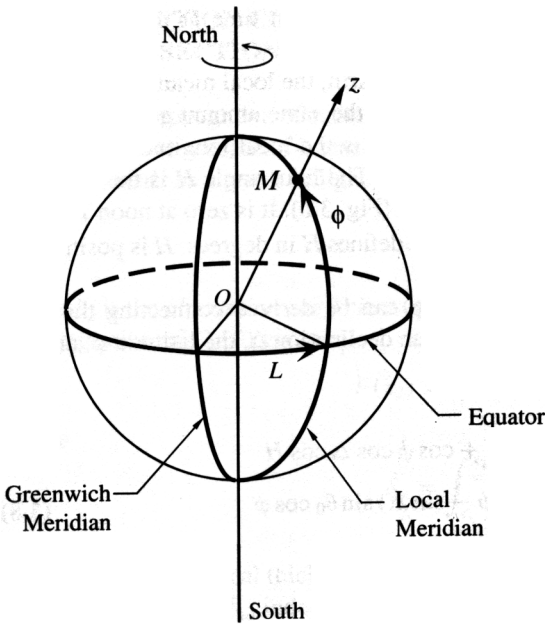


FIGURE 3.4 Definition of latitude and longitude of a point M on the Earth. Oz is the local vertical.

The period of the Earth's rotation is constant and is measured by the interval of time between two successive passages of a star in the observer's meridian. This is called the *sidereal day*. The interval of time between two successive passages of the Sun in the observer's meridian, the *solar day*, is slightly longer (by about 4 minutes) than the sidereal day. Also, because of the ellipticity of the orbit and the inclination of the axis, the solar day is not constant throughout the year. For practical purposes, we use a mean solar day divided into 24 hours. Local mean time (LMT) noon is defined on this basis. The real Sun passes in the meridian either earlier or later than the average Sun. The passage of the real Sun in the observer's meridian defines the local true solar time (TST) noon. The difference between the true solar time and the local mean time is $ET = TST - LMT$, which varies between ± 15

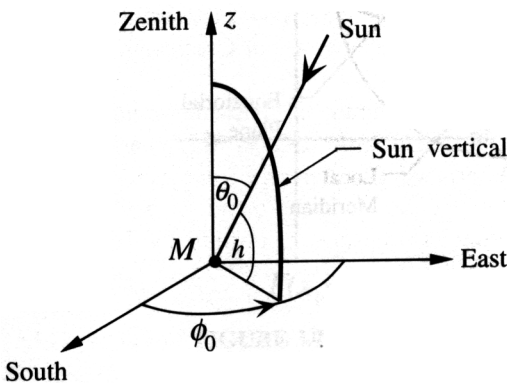


FIGURE 3.5 Horizontal coordinates of the Sun: θ_0 = solar zenith angle; h = altitude angle; ϕ_0 = azimuthal angle.

minutes. The Greenwich mean time (GMT) is the local mean time at the meridian of Greenwich, United Kingdom.

Since 24 hours corresponds to 360° rotation of the Earth, the local mean time increases by 4 minutes per 1° of longitude east and decreases by the same amount going west. The true solar time is $TST = GMT + 4L + ET$, where L is the local longitude in degrees, counted positively east from the Greenwich meridian. The hour angle H is the angle between the observer's meridian and the solar meridian (Fig. 3.6). It is zero at noon TST and changes by 15° per hour, $H = 15(12 - TST)$, which defines H in degrees. H is positive before noon and negative thereafter.

Based on spherical trigonometry, a relationship can be derived connecting the solar zenith angle θ_0 and the azimuthal angle ϕ_0 to the sun declination Δ , the latitude ϕ , and the hour angle H :

$$\cos \theta_0 = \sin \phi \sin \Delta + \cos \phi \cos \Delta \cos H$$

$$\cos \phi_0 = (\cos \theta_0 \sin \phi - \sin \Delta) \sin \theta_0 \cos \phi$$

At local noon TST ($H = 0$), the solar zenith angle is

$$\theta_0 = |\phi - \Delta|$$

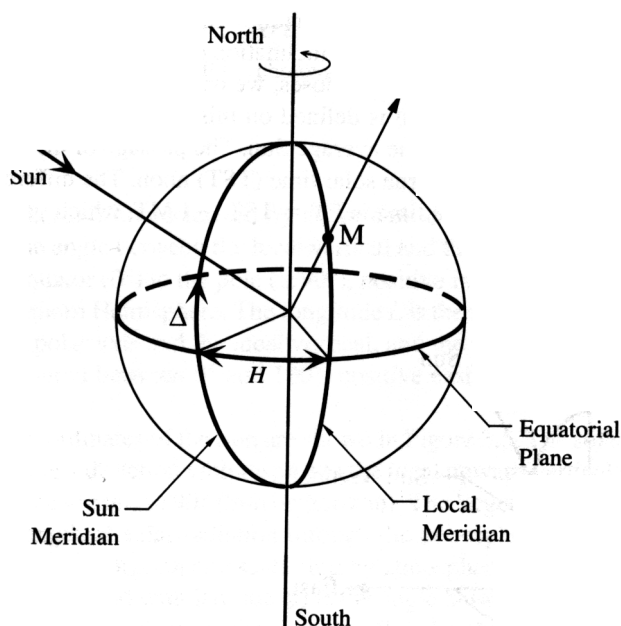


FIGURE 3.6 Hour angle of the Sun.

3.2 ABSORPTION COEFFICIENT AND ABSORPTION CROSS SECTION

Consider the propagation of radiation through a medium and select a layer of thickness dx perpendicular to a beam of intensity F (Figure 3.7). The loss of intensity F over the infinitesimal slice dx as a result of light absorption is

$$dF = -b_a F dx \tag{3.10}$$

where b_a is the *absorption coefficient* (m^{-1}) of the medium. For a finite path between x_1 and x_2 , integration of (3.10) gives

$$F(x_2) = F(x_1) \exp(-\delta_a)$$

where

$$\delta_a = \int_{x_1}^{x_2} b_a(x) dx \tag{3.12}$$

is the absorption optical thickness (dimensionless) between x_1 and x_2 . If the medium is homogeneous, $b_a(x) = b_a$, independent of x , and

$$F(x_2) = F(x_1) \exp[-b_a(x_2 - x_1)] \tag{3.13}$$

This result is known as the *Beer-Lambert law of extinction*. When x is measured vertically in the atmosphere the optical thickness is called the *optical depth*.

The *transmittance* of the layer between x_1 and x_2 along the direction of propagation is defined by

$$\tau = \frac{F(x_2)}{F(x_1)} = \exp(-\delta_a)$$

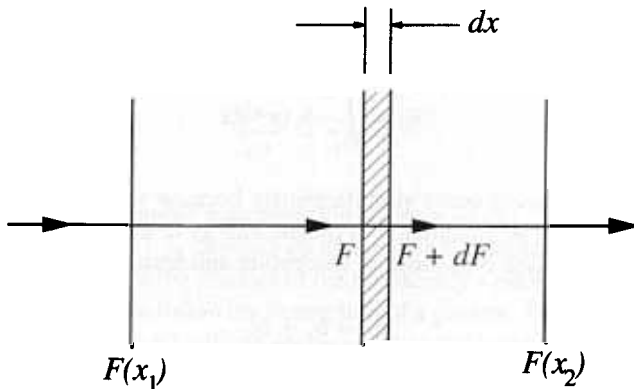


FIGURE 3.7 Propagation of radiation through a medium.

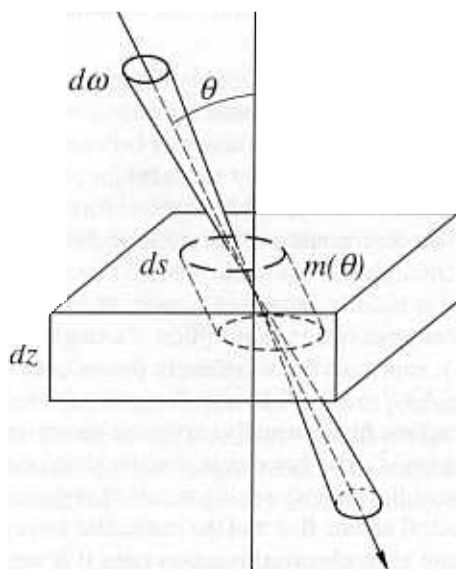


FIGURE 3.8 Interception of radiation emanating from a solid angle $d\omega$ on a surface element of area ds on an atmospheric layer of thickness dz . Pathlength through the layer is $m(\theta)$.

photons absorbed in time dt in wavelength range $d\lambda$ as

$$\sigma_A(\lambda)n_A m(\theta)L(\lambda, \theta, \phi) \cos \theta ds d\omega dt d\lambda$$

where $\sigma_A(\lambda)$ is the absorption cross section (cm^{-2}) of a molecule of A and $m(\theta)$ is the pathlength shown in Figure 3.8. $m(\theta) = dz/\cos \theta$. For each photon absorbed, the probability that the molecule will dissociate is $\phi_A(\lambda)$. (This is called the *quantum yield*.) Thus the number of molecules dissociated in time dt in wavelength range $d\lambda$ is

$$\phi_A(\lambda)\sigma_A(\lambda)n_A L(\lambda, \theta, \phi) ds dz d\omega dt d\lambda$$

The total number of dissociations dN_A occurring in the volume in a time interval dt is obtained by integrating over all solid angles, over the upper surface of the layer, and over all wavelengths,

$$dN_A = - \left[dz \int_s ds \right] (n_A dt) \int_{\lambda} \phi_A(\lambda)\sigma_A(\lambda) \left(\int_{\omega} L(\lambda, \theta, \phi) d\omega \right) d\lambda$$

The first factor on the right-hand side (R.H.S.) is just the total volume of the layer, which can be brought to the left-hand side (L.H.S.) along with dt to produce

$$\frac{dn_A}{dt} = -n_A \int_{\lambda} \underbrace{\phi_A(\lambda)\sigma_A(\lambda) \left(\int_{\omega} L(\lambda, \theta, \phi) d\omega \right)}_{J_{\lambda}} d\lambda$$

As indicated, the quantity on the R.H.S. multiplying n_A is j_A . The spectral actinic flux is then the radiative quantity that drives the photodissociation, that is, the quantity that multiplies $\phi_A(\lambda)\sigma_A(\lambda)$ to produce a product that when integrated over all wavelengths produces the photodissociation rate coefficient.

The spectral actinic flux $I(\lambda)$ is then

$$\begin{aligned} I(\lambda) &= \int_{\omega} L(\lambda, \theta, \phi) d\omega \\ &= \int_{\phi} \int_{\theta} L(\lambda, \theta, \phi) \sin \theta d\theta d\phi \end{aligned} \quad (3.23)$$

The spectral irradiance $E(\lambda)$ is the radiant energy crossing a surface (per unit surface area, time, and wavelength) and is calculated from $L(\lambda, \theta, \phi)$ by (3.4),

$$E(\lambda) = \iint_{\phi \theta} L(\lambda, \theta, \phi) \cos \theta \sin \theta d\theta d\phi \quad (3.24)$$

The factor $\cos \theta$ reflects the change in the projected area of the surface as the angle of incidence is varied. This factor does not appear in the expression for the actinic flux because the projected area and the pathlengths offset exactly. As the angle of incidence is changed from overhead ($\theta = 0^\circ$) to nearly glancing ($\theta \rightarrow 90^\circ$), the energy (irradiance) incident upon the layer decreases, but the actinic flux remains unchanged because the lower intensity is exactly compensated for by the longer pathlength of light through the layer.

Two special cases exist, collimated and isotropic light, in which simple relationships exist between actinic flux and irradiance (Madronich, 1987). These two limiting cases often can be used to approximate atmospheric situations. Collimated light can be considered to be parallel, having originated from a very small solid angle $\Delta\omega_0$. An example is the direct solar beam, which subtends $\Delta\omega_0 \approx 7 \times 10^{-5}$ sr at the Earth. Over this small solid angle the radiance may be taken as constant, while at all other solid angles it equals zero: $L(\theta, \phi) = L_0 = \text{constant}$ over the solid angle $\Delta\omega_0$ centered about (θ_0, ϕ_0) . In this case (3.23) and (3.24) become

$$I_0 = L_0 \Delta\omega_0 \quad (3.25)$$

$$E_0 = L_0 \cos \theta_0 \Delta\omega_0 \quad (3.26)$$

Thus, if L_0 is the extraterrestrial solar radiance, E_0 is the solar irradiance at the top of the atmosphere.

The other special case is that of isotropic radiation, $L(\theta, \phi) = L_1 = \text{constant}$. In this case

$$I = 2\pi L_1 \quad (3.27)$$

$$E = \pi L_1 \quad (3.28)$$

Equation (3.28) is identical to (3.3).

Example 3.1 Effect of a Reflecting Surface on the Radiance, Irradiance, and Actinic Flux (Madronich, 1987) Consider both collimated and isotropic light incident from above onto a horizontal surface that reflects a fraction R_p of the incoming energy back into the overhead atmosphere. We wish to calculate the radiance, irradiance, and actinic flux associated with this reflected light (L_\uparrow , E_\uparrow , I_\uparrow) in terms of the incident collimated beam (L_0 , E_0 , I_0) and the incident isotropic values (L_\downarrow , E_\downarrow , I_\downarrow). By definition of the albedo R_p ,

$$E_\uparrow = R_p(E_0 + E_\downarrow) \quad (3.29)$$

Using (3.23) and (3.24),

$$E_\uparrow = R_p(E_0 + E_\downarrow) = \int L_\uparrow(\theta, \phi) \cos \theta \, d\omega \quad (3.30)$$

$$I_\uparrow = \int L_\uparrow(\theta, \phi) \, d\omega \quad (3.31)$$

To evaluate the integrals one must know $L_\uparrow(\theta, \phi)$. A good approximation is that the surface is *Lambertian*, that is, the upward radiance is isotropic,

$$L_\uparrow(\theta, \phi) = L_\uparrow = \text{constant}$$

Then

$$L_\uparrow = R_p(L_0 \cos \theta_0 \Delta\omega_0/\pi + L_\downarrow) \quad (3.32)$$

$$E_\uparrow = R_p(E_0 + E_\downarrow) \quad (3.33)$$

$$I_\uparrow = R_p(2 \cos \theta_0 I_0 + I_\downarrow) \quad (3.34)$$

The total actinic flux is the sum of the downward and upward components,

$$\begin{aligned} I_{\text{total}} &= I_0 + I_\downarrow + I_\uparrow \\ &= I_0(1 + 2R_p \cos \theta) + I_\downarrow(1 + R_p) \end{aligned} \quad (3.35)$$

The interpretation of the two terms in (3.35) is as follows:

$$I_{\text{total}} = \underbrace{I_0(1 + 2R_p \cos \theta)}_{\substack{\text{When a collimated beam} \\ \text{is converted to isotropic} \\ \text{light, the actinic flux is} \\ \text{multiplied by a factor} \\ 2R_p \cos \theta}} + \underbrace{I_\downarrow(1 + R_p)}_{\substack{\text{With Lambertian} \\ \text{reflection of} \\ \text{isotropic light,} \\ \text{only the factor} \\ \text{of } R_p \text{ is incurred}}}$$

If the surface is totally reflecting, $R_p = 1$; in this case, for an overhead Sun ($\theta_0 = 0^\circ$) and a purely collimated incoming beam,

$$\begin{aligned} I_{\text{total}} &= I_0 + I_\uparrow \\ &= 3I_0 \end{aligned} \quad (3.36)$$

TABLE 3.2 Relation Between the Slant Path Optical Depth m and $\sec \theta_0$ for a Standard Rayleigh Atmosphere

θ_0	$\sec \theta_0$	m
0	1.00	1.00
30	1.15	1.15
60	2.00	1.99
70	2.92	2.90
75	3.86	3.81
80	5.76	5.59
85	11.47	10.32
87	19.11	15.16
89	57.30	26.26
90	∞	38.09

Source: Kasten and Young (1989).

Thus a highly reflecting Lambertian surface can increase the actinic flux by as much as a factor of 3 relative to the actinic flux from direct sunlight alone.

If $F_\infty(\lambda)$ is the spectral radiant flux density at the top of the atmosphere (TOA), that at ground level on a plane perpendicular to the solar beam can be determined from an extension of (3.11),

$$F(\lambda) = F_\infty(\lambda) \exp[-m\delta(\lambda)] \quad (3.37)$$

where $\delta(\lambda)$ is the total atmospheric optical depth at wavelength λ , and m is the ratio between the slant path optical depth for the actual solar zenith angle θ_0 and the overhead Sun optical depth (Figure 3.8). When the Sun is directly overhead ($\theta_0 = 0^\circ$), $m = 1.0$ and atmospheric attenuation is at its minimum. As the Sun approaches the horizon, θ_0 increases toward 90° , m increases and the attenuation of sunlight increases as a result of the increased pathlength. When the sphericity of the Earth can be neglected,

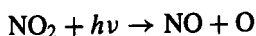
$$m = \frac{1}{\cos \theta_0} = \sec \theta_0 \quad (3.38)$$

This relation holds for θ_0 less than about 75° . For larger values of θ_0 , m has to be computed, taking into account the path through the spherical atmospheric layers, the vertical profile of absorbing and scattering species, and the curvature of the optical rays as a result of refraction. Values of m are given in Table 3.2 for the molecular atmosphere, that is, the Rayleigh scattering optical depth.²

²The TOA radiative flux can be estimated by measuring $E(\lambda)$ on a surface at ground level for various solar zenith angles θ_0 and plotting $\ln E(\lambda)$ versus m and extrapolating to $m = 0$. The slope of the best-fit straight line is $\delta(\lambda)$. This method of calculating $E_\infty(\lambda)$ is called the Bouguer–Langley method. Integrating $E_\infty(\lambda)$ over all wavelengths produces the solar constant S_0 .

3.4 ATMOSPHERIC PHOTOCHEMISTRY

According to Planck's law, the energy of one photon of frequency ν is $h\nu$. In atmospheric photochemistry, the photon that is a reactant in a chemical reaction is written as $h\nu$, for example, for the photolysis of NO_2 ,



Photon energy can be expressed per mole of a substance by multiplying $h\nu$, by Avogadro's number, 6.022×10^{23} molecules mol^{-1} ,

$$\begin{aligned} \varepsilon &= 6.022 \times 10^{23} h\nu \\ &= 6.022 \times 10^{23} \frac{hc}{\lambda} \end{aligned} \quad (3.39)$$

The energy³ associated with a particular wavelength λ is, with λ in nm,

$$\varepsilon = \frac{1.19625 \times 10^5}{\lambda} \text{ kJ mol}^{-1} \quad (3.40)$$

Typical ranges of wavelengths and energies in the portion of the electromagnetic spectrum of interest in atmospheric chemistry are:

Name	Typical Wavelength or Range of Wavelengths (nm)	Typical Range of Energies (kJ mol^{-1})
Visible		
Red	700	170
Orange	620	190
Yellow	580	210
Green	530	230
Blue	470	250
Violet	420	280
Near ultraviolet	400–200	300–600
Vacuum ultraviolet	200–50	600–2400

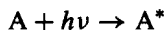
Photon energies can be compared with bond energies of molecules. The energy contained in photons of wavelengths near the red end of the visible spectrum is comparable to the bond energies of rather loosely bound chemical species. For example, in the ozone molecule, the $\text{O}-\text{O}_2$ bond energy is about 105 kJ mol^{-1} ; in NO_2 , the $\text{O}-\text{NO}$ bond energy is about 300 kJ mol^{-1} (which corresponds to a wavelength of about 400 nm). The lowest energy photons that are capable of promoting chemical reaction lie in the visible region of the electromagnetic spectrum. Wavelengths at which chemical change can occur correspond roughly to the energies at which electronic transitions in molecules take place. Absorption

³A traditional unit used by chemists for expressing energies associated with molecules is kcal mol^{-1} . The conversion factor between kJ mol^{-1} and kcal mol^{-1} is $(\text{kJ mol}^{-1}) \times 0.2390 = \text{kcal mol}^{-1}$

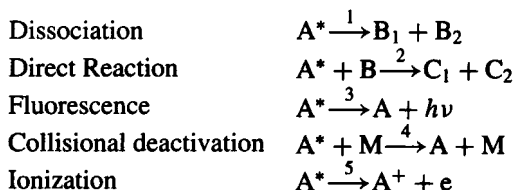
of radiation can only occur if an upper energy level of the molecule exists that is separated from the lower level by an energy equal to that of the incident photon. Small molecules generally exhibit intense electronic absorption at wavelengths shorter than do larger molecules. For example, N_2 and H_2 absorb significantly at wavelengths less than 100 nm, while O_2 absorbs strongly for $\lambda < 200$ nm, H_2O for $\lambda < 180$ nm, and CO_2 for $\lambda < 165$ nm.

As radiation penetrates deeper into the atmosphere the shorter wavelengths are progressively removed (recall Figure 1.10; also Figure 3.3). Photochemistry in the troposphere is confined to molecules that absorb radiation of wavelengths exceeding about 290 nm.

The primary step of a photochemical reaction may be written



where A^* is an electronically excited state of the molecule A . The excited molecule A^* may subsequently partake in:



The *quantum yield* for a specific process involving A^* is defined as the ratio of the number of molecules of A^* undergoing that process to the number of photons absorbed. Since the total number of A^* molecules formed equals the number of photons absorbed, the quantum yield ϕ_i for a specific process i , say, dissociation, is just the fraction of the A^* molecules that participate in path i . The sum of the quantum yields for all possible processes must equal 1.

The rate of formation of A^* is equal to the rate of photon absorption and is written⁴

$$\frac{d[A^*]}{dt} = j_A [A] \quad (3.41)$$

where j_A , having units s^{-1} , is the first-order rate constant for photolysis or the so-called specific absorption rate; j_A is normally taken to be independent of $[A]$. The rate of formation of B_1 in step 1 is

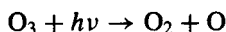
$$\frac{d[B_1]}{dt} = \phi_1 j_A [A] \quad (3.42)$$

where ϕ_1 is the quantum yield of step 1.

Photodissociation of a molecule can occur when the energy of the incoming photon exceeds the binding energy of the particular chemical bond. Thus the excited species A^* can lie energetically above the dissociation threshold of the molecule. One or more of the prod-

⁴In writing chemical reaction rate equations we will generally use $[A]$ to denote the concentration of species A , rather than c .

ucts of photodissociation may themselves be electronically excited. Consider the photolysis of ozone,



Various combinations of electronic states are possible for the products O and O₂ depending on the wavelength of incident radiation. The lowest energy pair of excited products is O(¹D) + O₂(¹Δ_g), which form at an expected threshold wavelength of about 310 nm. The singlet-D oxygen atom, O(¹D), is the most important electronically excited species in the atmosphere. (Henceforth we will have no need to distinguish electronically excited states of molecular oxygen; we will simply indicate all oxygen molecules emerging from photodissociation of O₃ as O₂.) The reaction of O(¹D) with water vapor is a source of OH radicals in the entire atmosphere, and O(¹D) reaction with N₂O is the principal source of NO_x in the stratosphere.

To calculate the rate of a photochemical reaction we need to know the number of photons absorbed per unit volume of air containing a given concentration [A] (molecules cm⁻³) of an absorbing molecule A. The absorption cross section of A, σ_A (cm² molecule⁻¹), was defined in (3.16). (It will not be necessary to retain the subscript "a" on σ, as in (3.16); rather we indicate the molecular identity by subscript to σ.)

The number of photons absorbed by a molecule A in a wavelength region λ to λ + dλ is the product of its absorption cross section σ_A(λ) (cm² molecule⁻¹), the spectral actinic flux I(λ) (photons cm⁻² s⁻¹ nm⁻¹), and the number concentration of A (molecules cm⁻³),

$$\sigma_A(\lambda)I(\lambda) d\lambda [A] \quad \text{photons cm}^{-3} \text{ s}^{-1}$$

To calculate the rate of photolysis of A we need to multiply the above expression by the quantum yield for photolysis, φ_A(λ). Thus the rate of photolysis in the wavelength region λ to λ + dλ is

$$\sigma_A(\lambda)\phi_A(\lambda)I(\lambda) d\lambda [A] \quad (3.43)$$

The total photolysis rate of A is the integral of this expression over all possible wavelengths,

$$\left[\int_{\lambda_1}^{\lambda_2} \sigma_A(\lambda)\phi_A(\lambda)I(\lambda) d\lambda \right] [A] \quad \text{molecules cm}^{-3} \text{ s}^{-1} \quad (3.44)$$

where λ₁ and λ₂ are, respectively, the shortest and longest wavelengths at which absorption occurs. For the troposphere, for example, λ₁ = 290 nm.

The quantity in brackets has already been identified as the first-order photolysis rate constant,

$$j_A = \int_{\lambda_1}^{\lambda_2} \sigma_A(\lambda, T)\phi_A(\lambda, T)I(\lambda) d\lambda \quad (3.45)$$

The integral in (3.45) is often approximated for computational purposes by a summation over small wavelength intervals,

$$j_A = \sum_i \bar{\sigma}_A(\lambda_i, T)\bar{\phi}_A(\lambda_i, T)\bar{I}(\lambda_i) \Delta\lambda_i \quad (3.46)$$

where the overbar denotes an average over a wavelength interval $\Delta\lambda_i$ centered at λ_i . The width of the wavelength intervals $\Delta\lambda_i$ is usually dictated by the available resolution for the actinic flux $I(\lambda)$. A typical size of $\Delta\lambda_i$ is 5 nm from 290 nm to over 400 nm, and 10 nm beyond 400 nm.⁵ Values of $\sigma(\lambda)$ and $\phi(\lambda)$ may not be available on precisely the same intervals as for $I(\lambda)$, so some interpolation may be necessary.

Table 3.3 summarizes important light-absorbing molecules in atmospheric chemistry. Photodissociation of molecular oxygen is key to stratospheric chemistry and will be ad-

TABLE 3.3 Some Photochemical Reactions of Importance in Atmospheric Chemistry^a

Reaction	Comments
$\text{O}_2 + h\nu \longrightarrow \text{O} + \text{O}({}^1\text{D}) > 50 \text{ km}$ $\longrightarrow \text{O} + \text{O}$	Photodissociation of molecular oxygen results primarily from absorption of solar radiation in the 200–220 nm wavelength region. The 185–200 nm region, the O ₂ Schumann–Runge band spectral range, is also important since solar radiation penetrates efficiently into the stratosphere at those wavelengths. Recommended absorption cross sections are given by DeMore et al. (1994).
$\text{O}_3 + h\nu \xrightarrow{1} \text{O}_2 + \text{O}$ $\xrightarrow{2} \text{O}_2 + \text{O}({}^1\text{D})$	<p>O₃ absorption cross sections are given in WMO Report No. 16 (1986) and DeMore et al. (1994). DeMore et al. (1994) present a polynomial expression for the quantum yield for O(¹D) production, $\phi(\text{O}^1\text{D})$, as a function of λ and T in the range 305–320 nm. The upper limiting value of $\phi(\text{O}^1\text{D})$ is taken as 0.95 at 305 nm. Discrepancies exist between published O(¹D) quantum yields, which can be separated into two groups: those that show ϕ to drop to zero at about 315 nm (DeMore et al., 1994) and those that exhibit a “tail” extending beyond 320 nm (Michelsen et al., 1994). In evaluating ambient data against both groups of quantum yields, Hofzumahaus et al. (1995) found that the ϕ data exhibiting a tail above 315 nm better represent observed data. As noted in the text, the implication of this finding is that solar photolysis of O₃ at wavelengths longer than 310 nm contributes significantly more to tropospheric O(¹D) formation than that based on the recommended correlation of DeMore et al. (1994).</p> <p style="text-align: center;">$j_2 = 10^{-3} \text{ s}^{-1}$ at 40 km</p> <p style="text-align: center;">$j_2 = 10^{-5} \text{ s}^{-1}$ at 10 km</p>

continued

⁵Madronich and Weller (1990) calculated tropospheric photolysis rate constants for NO₂, O₃, HONO, HCHO, and CH₃CHO using high spectral resolution ($\Delta\lambda = 0.1$ nm) and compared these to values calculated with $\Delta\lambda = 1, 2, 4, 6, 8,$ and 10 nm. Depending on the molecule, substantial errors were found to be introduced with the coarser resolution calculations.

TABLE 3.3 (Continued)

Reaction	Comments
$\text{H}_2\text{O}_2 + h\nu \longrightarrow \text{OH} + \text{OH}$	Absorption cross sections of H_2O_2 over the range 190–350 nm are presented by DeMore et al. (1994).
$\text{NO}_2 + h\nu \longrightarrow \text{NO} + \text{O}$	Photodissociation of NO_2 producing the oxygen atom leads to the only <i>in situ</i> chemical source of ozone in the troposphere and thus is an extremely important reaction. Absorption cross sections over the wavelength range 202–422 nm have been recommended by DeMore et al. (1994). Even more recent absorption cross sections have been reported by Mérienne et al. (1995). Quantum yields are also presented by DeMore et al. (1994). $j_{\text{NO}_2} = 8 \times 10^{-3} \text{ s}^{-1}$ at surface $= 10^{-2} \text{ s}^{-1}$ at 30 km
$\text{NO}_3 + h\nu \xrightarrow{1} \text{NO} + \text{O}_2$ $\xrightarrow{2} \text{NO}_2 + \text{O}$	Absorption cross sections for NO_3 in the wavelength range 600–670 nm are given by DeMore et al. (1994). Quantum yields, ϕ_1 and ϕ_2 , have been reviewed by DeMore et al. (1994) and Wayne (1991). DeMore et al. (1994) recommend the following photodissociation rate constants for overhead Sun at the Earth's surface: $j_1 = 0.016 \text{ s}^{-1}$ $j_2 = 0.19 \text{ s}^{-1}$
$\text{N}_2\text{O} + h\nu \longrightarrow \text{N}_2 + \text{O}(^1\text{D})$	DeMore et al. (1994) present absorption cross sections for N_2O in the wavelength range 173–240 nm over 194–320 K. The quantum yield for photodissociation is unity.
$\text{N}_2\text{O}_5 + h\nu \longrightarrow \text{NO}_2 + \text{NO}_3$	Absorption cross sections of N_2O_5 over the wavelength range 200–280 nm are presented by DeMore et al. (1994). NO_3 is produced with unit quantum yield.
$\text{HONO} + h\nu \longrightarrow \text{OH} + \text{NO}$	Photodissociation of HONO is a source of OH radicals in the atmosphere. Absorption cross sections over the wavelength range 310–396 nm are given by DeMore et al. (1994).
$\text{HNO}_3 + h\nu \xrightarrow{1} \text{OH} + \text{NO}_2$ $\xrightarrow{2} \text{O} + \text{HONO}$	Nitric acid absorption cross sections over the range 190–350 nm are given by DeMore et al. (1994). The quantum yield for the $\text{OH} + \text{NO}_2$ channel is near unity down to 222 nm. By 193 nm the $\text{O} + \text{HONO}$ path has a quantum yield of about 0.8.

continued

TABLE 3.3 (Continued)

Reaction	Comments
$\text{HCHO} + h\nu \xrightarrow{1} \dot{\text{H}} + \text{HCO}$ $\xrightarrow{2} \text{H}_2 + \text{CO}$	Formaldehyde photolysis is a significant source of free radicals in the troposphere. Absorption cross sections for HCHO are given by DeMore et al. (1994). DeMore et al. (1994) give quantum yields, ϕ_1 and ϕ_2 , from 301 to 356 nm. Channel 1 predominates at shorter wavelengths and channel 2 at longer wavelengths.
$\text{CH}_3\text{OOH} + h\nu \longrightarrow \text{products}$	Absorption cross sections for CH_3OOH from 210 to 360 nm are given by DeMore et al. (1994).
$\text{Cl}_2 + h\nu \longrightarrow \text{Cl} + \text{Cl}$	Absorption cross sections for Cl_2 from 260 to 470 nm are given by DeMore et al. (1994).
$\text{ClOO} + h\nu \longrightarrow \text{ClO} + \text{O}$	Absorption cross sections for ClOO from 220 to 280 nm are given by DeMore et al. (1994).
$\text{OCIO} + h\nu \longrightarrow \text{O} + \text{ClO}$	Absorption cross sections for OCIO from 272 to 475 nm are given by DeMore et al. (1994).
$\text{HOCl} + h\nu \longrightarrow \text{OH} + \text{Cl}$	Absorption cross sections for HOCl from 200 to 380 nm are given by DeMore et al. (1994).
$\text{ClONO}_2 + h\nu \xrightarrow{1} \text{Cl} + \text{NO}_3$ $\xrightarrow{2} \text{ClO} + \text{NO}_2$	Absorption cross sections for ClONO ₂ from 196 to 414 nm are given by DeMore et al. (1994). The preferred quantum yield values are $\phi_1 = 0.6$ ($\lambda < 308$ nm), $\phi_1 = 1.0$ ($\lambda > 364$ nm), and $\phi_2 = 1 - \phi_1$.
$\text{CCl}_3\text{F} + h\nu \longrightarrow \text{products}$	Absorption cross sections for CCl ₃ F from 170 to 260 nm are given by DeMore et al. (1994).
$\text{CCl}_2\text{F}_2 + h\nu \longrightarrow \text{products}$	Absorption cross sections for CCl ₂ F ₂ from 170 to 240 nm are given by DeMore et al. (1994).
$\text{OCS} + h\nu \longrightarrow \text{CO} + \text{S}$	Absorption cross sections for OCS from 186 to 296 nm are given by DeMore et al. (1994). The recommended quantum yield for photodissociation is 0.72.
$\text{CH}_3\text{CHO} + h\nu \xrightarrow{1} \text{CH}_4 + \text{CO}$ $\xrightarrow{2} \text{CH}_3 + \text{HCO}$	Absorption cross sections for acetaldehyde have been measured by Martinez et al. (1992) at 300 ± 2 K over the wavelength region 200–366 nm. Recommended quantum yields for channels 1 and 2 have been tabulated by Atkinson et al. (1992).
$\text{CH}_3\text{C(O)CH}_3 + h\nu \longrightarrow \text{CH}_3 + \text{CH}_3\text{CO}$	Absorption cross sections and quantum yields for acetone have been summarized by Atkinson et al. (1992). An average photodissociation quantum yield for CH ₃ CO formation is about 0.33 over the wavelength region 280–330 nm.

*Many of the rate constants for reactions important in atmospheric chemistry are surveyed periodically by a group organized through the Jet Propulsion Laboratory (JPL), Pasadena, CA. The latest report is that of De More et al. (1997) Evaluation No. 12, JPL Publication 97-4. Recommended values of rate constants, absorption cross sections, and quantum yields appear in these reports.

TABLE 3.4 Estimated Ground-Level Spectral Actinic Fluxes $I(\lambda)$ at 40° N Latitude

	$I(\lambda) \times 10^{-14}$ (photons $\text{cm}^{-2} \text{s}^{-1}$)	
	Noon	
	January	
290–295	0.0	0.0
295–300	0.0	0.031
300–305	0.021	0.335
305–310	0.196	1.25
310–315	0.777	2.87
315–320	1.45	4.02
320–325	2.16	5.08
325–330	3.44	7.34
330–335	3.90	7.79
335–340	4.04	7.72
340–345	4.51	8.33
345–350	4.62	8.33
350–355	5.36	9.45
355–360	5.04	8.71
360–365	5.70	9.65

Source: Finlayson-Pitts and Pitts (1986).

dressed in Chapter 4. Absorption of solar radiation by O_3 in the stratosphere effectively limits the short-wavelength limit of light reaching the troposphere to wavelengths longer than 290 nm and will also be discussed in Chapter 4. Table 3.4 gives estimated ground-level spectral actinic flux at 40° N latitude on January 1 and July 1.

Figure 3.9 shows the ozone absorption cross section at 273 K. Photolysis of ozone produces $\text{O}(^1\text{D})$ and O_2 with practically unit efficiency at wavelengths shorter than 300 nm. Near 310 nm the quantum yield for production of these species falls rapidly as the photolysis energy approaches the energetic limit for their production from ground-state O_3 . There has been controversy concerning the quantum yield of $\text{O}(^1\text{D})$ production at wavelengths longer than 310 nm (see Table 3.3). Figure 3.10 shows data summarized by Michelsen et al. (1994) for the quantum yield for $\text{O}(^1\text{D})$ production. Quantum yield curves such as Figure 3.10 do not exhibit a perfect step change at a discrete wavelength corresponding to a particular electronic transition because energy contained in internal vibrations and rotations can interact with the photon energy in causing dissociation. The quantum yield–wavelength curve is also temperature dependent. The critical role of wavelength in photolysis can be seen by comparing Figures 3.9 and 3.10, the O_3 absorption cross section and the quantum yield for $\text{O}(^1\text{D})$ production, respectively. From $\lambda = 304$ nm to $\lambda = 320$ nm, the absorption cross section drops by a factor of 10, and the quantum yield for $\text{O}(^1\text{D})$ formation drops from 0.9 to almost zero. Thus the $\sigma_{\text{O}_3}(\lambda, T)\phi_{\text{O}(^1\text{D})}(\lambda, T)$ product changes rapidly with λ , so the actual rate of production of $\text{O}(^1\text{D})$ is critically dependent on how $I(\lambda)$ varies with λ . At the surface of the Earth, the spectral actinic flux increases by about an order of magnitude between $\lambda = 300$ nm and $\lambda = 320$ nm (see Table 3.4).

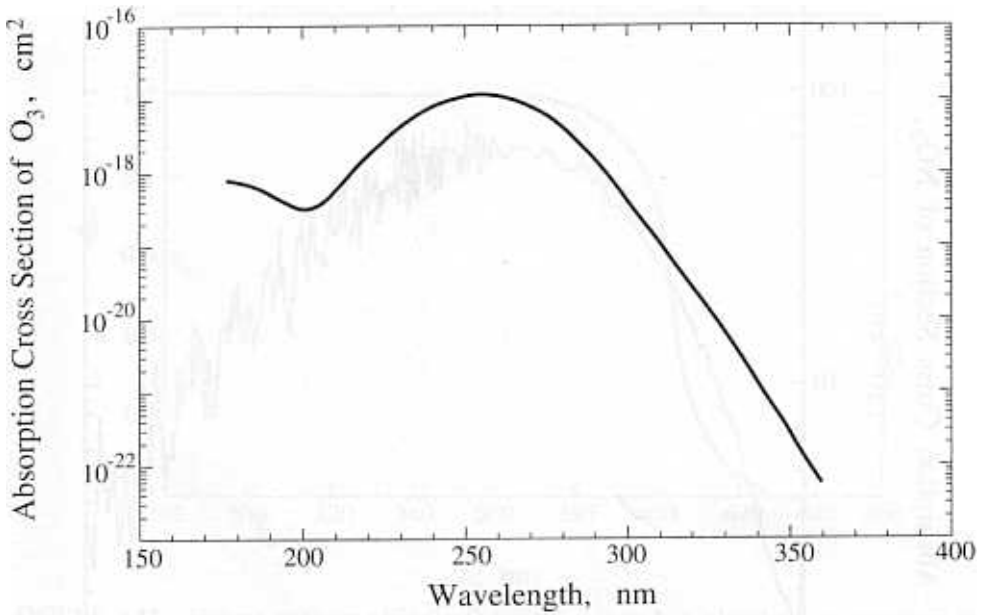


FIGURE 3.9 Absorption cross section for O₃ at 273 K based on data given in DeMore et al. (1994).

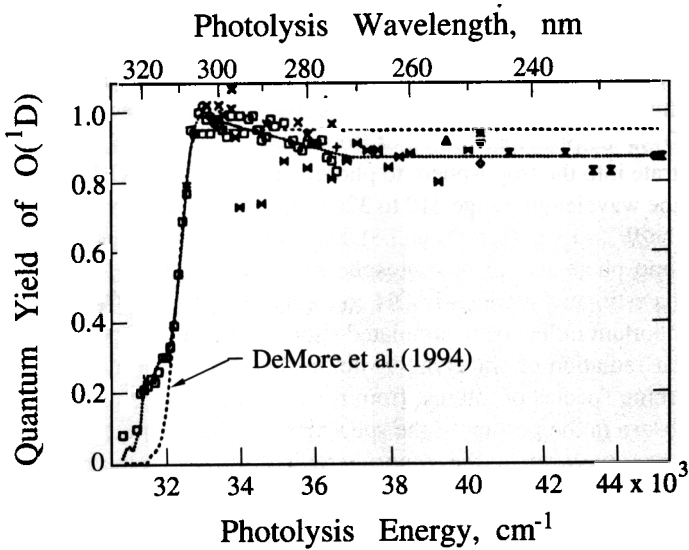


FIGURE 3.10 Primary quantum yield for O(¹D) formation from O₃ photolysis at 298 K. Summary of data presented by Michelsen et al. (1994).

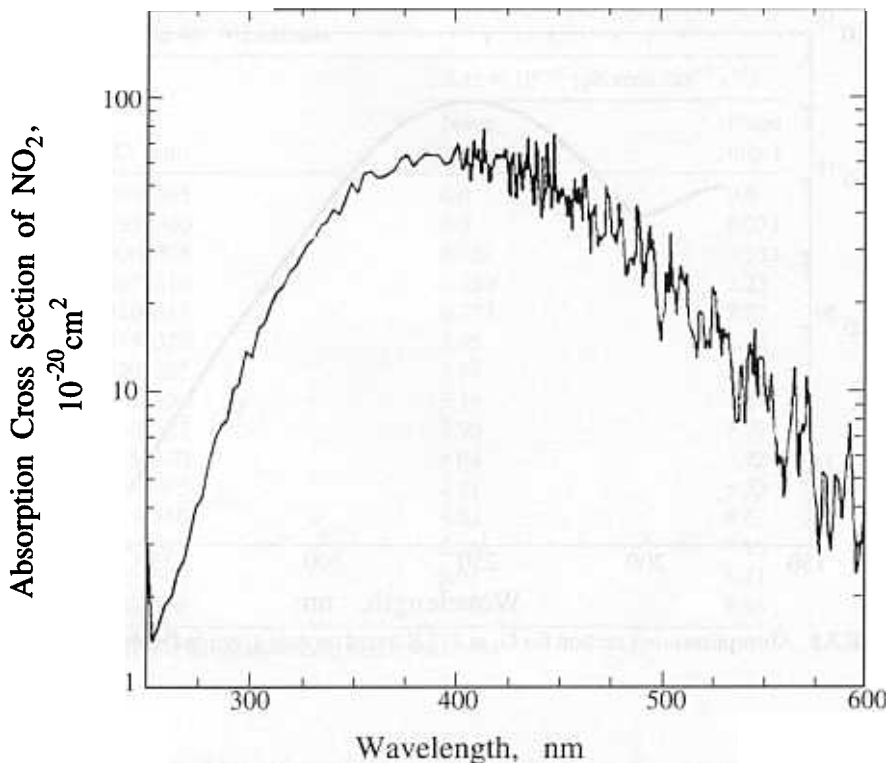


FIGURE 3.11 Absorption cross section for NO₂ at 298 K

The precise quantum yield of O(¹D) production for wavelengths between 310 and 320 nm is extremely important to atmospheric chemistry. This is because, as we will see in Chapter 5, O(¹D) is the principal source of tropospheric OH radicals, and wavelengths in this range penetrate into the troposphere to photolyze O₃, forming O(¹D). A quantum yield of 0.2 to 0.3 in the wavelength range 310 to 320 nm, rather than the value close to zero recommended by the JPL survey (see Table 3.3), leads to a calculated increase of O(¹D) by up to 40% in the troposphere and lower stratosphere (Michelsen et al., 1994). This increase in O(¹D) leads to an estimated increase in OH concentration of 15%. Changes of this magnitude exert an important influence in simulated stratospheric and tropospheric chemistry.

Since no solar radiation of wavelength shorter than about 290 nm reaches the troposphere, the absorbing species of interest from the point of view of tropospheric chemistry are those that absorb in the portion of the spectrum above 290 nm. Nitrogen dioxide is an extremely important molecule in the troposphere; it absorbs over the entire visible and ultraviolet range of the solar spectrum in the lower atmosphere (Figure 3.11). Between 300 and 370 nm over 90% of the NO₂ molecules absorbing will dissociate into NO and O (Figure 3.12). Above 370 nm this percentage drops off rapidly and above about 420 nm dissociation does not occur. As noted earlier, the bond energy between O and NO, about 300 kJ mol⁻¹, corresponds to the energy contained in wavelengths near 400 nm. At longer

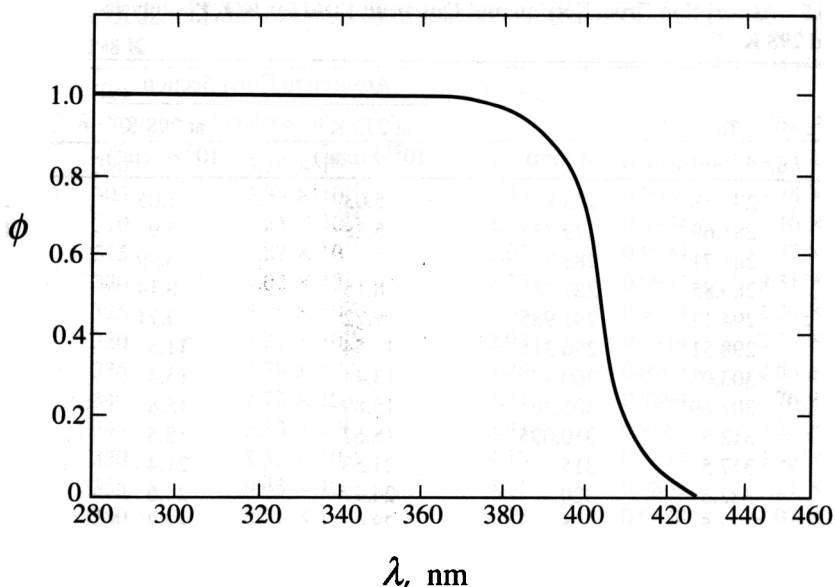


FIGURE 3.12 Primary quantum yield for O formation from NO_2 photolysis, as correlated by Demerjian et al. (1980).

wavelengths, there is insufficient energy to promote bond cleavage. The point at which dissociation fails to occur is not sharp because the individual molecules of NO_2 do not possess a precise amount of ground-state energy prior to absorption. The gradual transition area (370 to 420 nm) corresponds to a variation in ground-state energy of about 40 kJ mol^{-1} . This transition curve can be shifted slightly to longer wavelengths by increasing the temperature and therefore increasing the ground-state energy of the system. Table 3.5 gives tabulated values of the NO_2 absorption cross section and quantum yield at 273 and 298 K, and Table 3.6 illustrates the calculation of the photolysis rate j_{NO_2} for noon, July 1, at 40°N .

Example 3.2 Atmospheric Heating Rates: The Chapman Function The nature of the attenuation that occurs as radiation penetrates the atmosphere can be seen by considering the Beer-Lambert law of light absorption for a single absorbing component,

$$dF(\lambda) = -\sigma(\lambda)NF(\lambda) dx \quad (3.47)$$

where $\sigma(\lambda)$ is the absorption cross section ($\text{cm}^2 \text{ molecule}^{-1}$), N is the concentration of the species (molecules cm^{-3}), $F(\lambda)$ is the spectral radiant flux density at wavelength λ ($\text{W m}^{-2} \text{ nm}^{-1}$), and dx is an increment of optical path. If the absorbing species is uniformly mixed in the atmosphere, that is, it has a uniform mixing ratio, its concentration can be written as

$$N = N_t \xi \quad (3.48)$$

TABLE 3.5 Absorption Cross Section and Quantum Yield for NO₂ Photolysis at 273 and 298 K

From: λ (nm)	Absorption Cross Section		at 273 K $10^{20}\sigma$ (cm ²)	at 298 K $10^{20}\sigma$ (cm ²)	ϕ
273.97	277.78	275.875	5.03	5.05	
277.78	281.69	279.735	5.88	5.9	1
281.69	285.71	283.7	7	6.99	1
285.71	289.85	287.78	8.15	8.14	0.999
289.85	294.12	291.985	9.72	9.71	0.9986
294.12	298.51	296.315	11.54	11.5	0.998
298.51	303.03	300.77	13.44	13.4	0.997
303.03	307.69	305.36	15.89	15.8	0.996
307.69	312.5	310.095	18.67	18.5	0.995
312.5	317.5	315	21.53	21.4	0.994
317.5	322.5	320	24.77	24.6	0.993
322.5	327.5	325	28.07	27.8	0.992
327.5	332.5	330	31.33	31	0.991
332.5	337.5	335	34.25	33.9	0.99
337.5	342.5	340	37.98	37.6	0.989
342.5	347.5	345	40.65	40.2	0.988
347.5	352.5	350	43.13	42.8	0.987
352.5	357.5	355	47.17	46.7	0.986
357.5	362.5	360	48.33	48.1	0.984
362.5	367.5	365	51.66	51.3	0.983
367.5	372.5	370	53.15	52.9	0.981
372.5	377.5	375	55.08	54.9	0.979
377.5	382.5	380	56.44	56.2	0.9743
382.5	387.5	385	57.57	57.3	0.969
387.5	392.5	390	59.27	59	0.96
392.5	397.5	395	58.45	58.3	0.92
397.5	402.5	400	60.21	60.1	0.695
402.5	407.5	405	57.81	57.7	0.3575
407.5	412.5	410	59.99	59.7	0.138
412.5	417.5	415	56.51	56.5	0.0603
417.5	422.5	420	58.12	57.8	0.0188

where N_t is the total gas concentration and ξ is the species mixing ratio (mole fraction). The total gas concentration as a function of altitude in the atmosphere is given approximately by (see (1.5))

$$N_t = N_t^0 \exp(-z/H) \quad (3.49)$$

where N_t^0 is the total concentration at the Earth's surface and H is the scale height for pressure. Then (3.47) becomes

$$dF(\lambda) = -\sigma(\lambda)F(\lambda)N_t^0\xi \exp(-z/H)m dz \quad (3.50)$$

where m given by (3.38) accounts for the slant path of the Sun. To obtain $F(\lambda)$ at any height z in the atmosphere, (3.50) can be integrated from $z = \infty$, the top of the atmosphere, to z ,

TABLE 3.6 Calculation of the Photolysis Rate of NO₂ at Ground Level, July 1, Noon, 40° N, 298 K

From: λ (nm)	To: λ (nm)	I^a (photons cm ⁻² s ⁻¹)	$10^{19} \sigma_{\text{NO}_2}$ (cm ²)	ϕ	j_{NO_2} (s ⁻¹)
		3.14×10^{12}	1.22	0.9976	
		3.35×10^{13}	1.43	0.9966	
		1.24×10^{14}	1.74	0.9954	
		2.87×10^{14}	2.02	0.9944	
		4.02×10^{14}	2.33	0.9934	
		5.08×10^{14}	2.65	0.9924	
		7.34×10^{14}	2.97	0.9914	
		7.79×10^{14}	3.28	0.9904	
		7.72×10^{14}	3.61	0.9894	
		8.33×10^{14}	3.91	0.9884	
		8.32×10^{14}	4.18	0.9874	
		9.45×10^{14}	4.51	0.9864	
		8.71×10^{14}	4.75	0.9848	
		9.65×10^{14}	5.00	0.9834	
		1.19×10^{15}	5.23	0.9818	
		1.07×10^{15}	5.41	0.9798	
		1.20×10^{15}	5.57	0.9762	
		9.91×10^{14}	5.69	0.9711	
		1.09×10^{15}	5.84	0.9636	
		1.13×10^{15}	5.86	0.9360	
		1.36×10^{15}	5.93	0.7850	
		1.64×10^{15}	5.86	0.4925	
		1.84×10^{15}	5.89	0.2258	
		1.94×10^{15}	5.78	0.0914	
		1.97×10^{15}	5.73	0.0354	
		9.69×10^{14}	5.78	0.0188	
					Total $j_{\text{NO}_2} = 8.14 \times 10^{-3} \text{ s}^{-1}$
					$j_{\text{NO}_2} = 0.488 \text{ min}^{-1}$

^aActinic flux from Finlayson-Pitts and Pitts (1986).

assuming the scale height H is constant, to obtain

$$F(z; \lambda) = F_{\infty}(\lambda) \exp[-\sigma(\lambda)HN_i^0\xi m \exp(-z/H)] \quad (3.51)$$

The rate at which energy is removed from the incident radiation is the decrease in intensity per unit path traversed.

$$\begin{aligned} P(z; \lambda) &= \frac{dF}{dx} = \frac{1}{m} \frac{dF}{dz} \\ &= F_{\infty}(\lambda)N_i^0\xi\sigma(\lambda) \exp\left[-\frac{z}{H} - N_i^0\sigma(\lambda)\xi Hm \exp\left(-\frac{z}{H}\right)\right] \end{aligned} \quad (3.52)$$

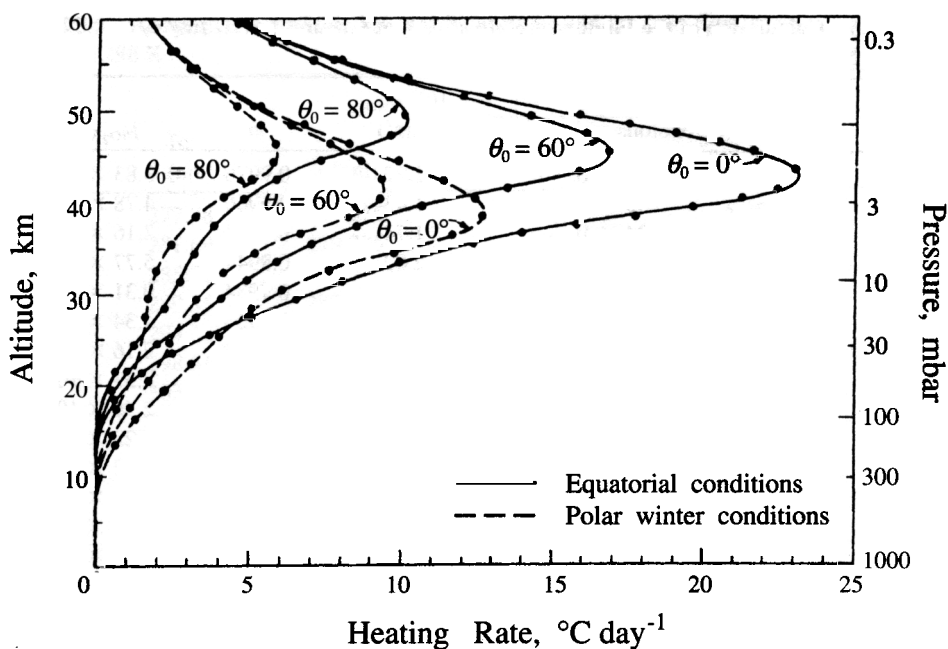


FIGURE 3.13 Heating rate from absorption of solar radiation by ozone for solar zenith angles $\theta_0 = 0^\circ, 60^\circ, 80^\circ$. The solid curve is for an ozone distribution representative of equatorial conditions; the dashed curve is representative of polar winter conditions. This calculation accounts for the change in ozone mixing ratio with altitude, whereas the analytical formula (3.52) assumes mixing ratio is constant with altitude.

$P(z; \lambda)$ exhibits a maximum at a certain altitude z , reflecting a balance between high light intensity but low number density at high altitudes and lower light intensity but higher number density at lower altitudes. Equation (3.52) is sometimes called a *Chapman function* in recognition of Chapman who first derived such a function in relation to the formation of an ozone layer in the stratosphere (see Chapter 4). If we apply (3.52) to O_3 , and consider $\lambda = 220$ nm, the maximum in energy removal, which varies only mildly with solar zenith angle, is predicted to occur at an altitude of about 35 km. As solar zenith angle increases, the altitude of the maximum in absorption increases and the magnitude of the maximum decreases (Figure 3.13).

3.5 CHEMICAL KINETICS

Gas molecules can react only when they come close enough to one another for direct energy exchange that can lead to bond breaking. From elementary kinetic theory, the frequency of collisions per unit volume of gas of molecules of type i of mass m_i with molecules of type j of mass m_j is (Benson, 1976)

$$Z_{ij} = \left(\frac{8kT}{\pi m_{ij}} \right)^{1/2} \pi \sigma_{ij}^2 N_i N_j \quad \text{cm}^{-3} \text{ s}^{-1} \quad (3.53)$$

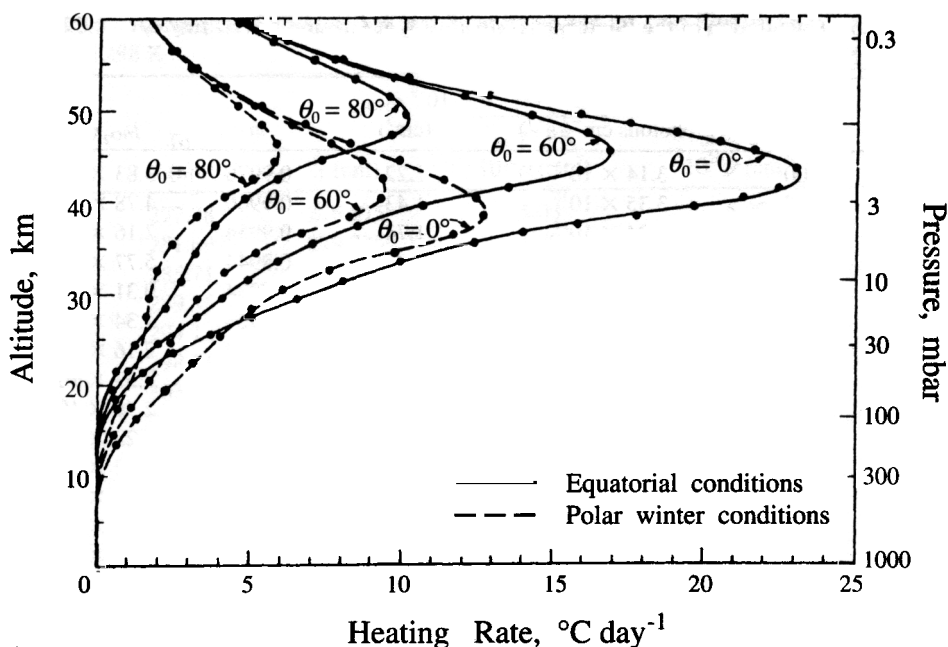


FIGURE 3.13 Heating rate from absorption of solar radiation by ozone for solar zenith angles $\theta_0 = 0^\circ, 60^\circ, 80^\circ$. The solid curve is for an ozone distribution representative of equatorial conditions; the dashed curve is representative of polar winter conditions. This calculation accounts for the change in ozone mixing ratio with altitude, whereas the analytical formula (3.52) assumes mixing ratio is constant with altitude.

$P(z; \lambda)$ exhibits a maximum at a certain altitude z , reflecting a balance between high light intensity but low number density at high altitudes and lower light intensity but higher number density at lower altitudes. Equation (3.52) is sometimes called a *Chapman function* in recognition of Chapman who first derived such a function in relation to the formation of an ozone layer in the stratosphere (see Chapter 4). If we apply (3.52) to O_3 , and consider $\lambda = 220$ nm, the maximum in energy removal, which varies only mildly with solar zenith angle, is predicted to occur at an altitude of about 35 km. As solar zenith angle increases, the altitude of the maximum in absorption increases and the magnitude of the maximum decreases (Figure 3.13).

3.5 CHEMICAL KINETICS

Gas molecules can react only when they come close enough to one another for direct energy exchange that can lead to bond breaking. From elementary kinetic theory, the frequency of collisions per unit volume of gas of molecules of type i of mass m_i with molecules of type j of mass m_j is (Benson, 1976)

$$Z_{ij} = \left(\frac{8kT}{\pi m_{ij}} \right)^{1/2} \pi \sigma_{ij}^2 N_i N_j \quad \text{cm}^{-3} \text{ s}^{-1} \quad (3.53)$$

where N_i is the number concentration of species i (cm^{-3}), $(8kT/\pi m_{ij})^{1/2}$ is the root-mean-square relative speed of the i and j molecules, k is the Boltzmann constant, $m_{ij} = m_i m_j / (m_i + m_j)$ is the reduced mass, and $\pi \sigma_{ij}^2$ is the so-called collision cross section of molecules i and j . The characteristic time during which molecules in thermal motion in a gas are close enough to interact is brief, on the order of 10^{-12} to 10^{-13} s. At ambient temperature and pressure the mean time between molecular collisions can be shown from (3.53) to be on the order of 10^{-9} s. Thus collisions are short in duration compared to the time between collisions.

Whereas the collision of two molecules is a necessary condition for reaction, sufficient energy must be available to break chemical bonds. Theory indicates that the fraction of collisions involving energy greater than a required energy E is given by $\exp(-E/kT)$. In this form E has units of energy per molecule. More commonly, E is expressed in terms of energy per mole, and we use $\exp(-E/RT)$, where R is the universal gas constant. The rate of reaction is expressed in a form that accounts for both the frequency of collisions and the fraction that exceed the required energy,

$$r = A(T) \exp\left(-\frac{E}{RT}\right) c_i c_j \quad (3.54)$$

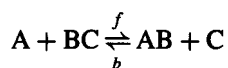
The preexponential factor $A(T)$ may depend on temperature since the translational kinetic energy and internal degrees of freedom of the molecules influence the probability of reaction in any collision event.

The rate of reaction is usually written as $r = kc_i c_j$, where the parameter k is called the *rate constant*,⁶

$$k = A(T) \exp\left(-\frac{E}{RT}\right) \quad (3.55)$$

If $A(T)$ is independent of T , we have the *Arrhenius form*, $k = A \exp(-E/RT)$. The maximum possible value of the rate constant of a bimolecular reaction is achieved if every molecular collision between molecules of i and j results in reaction. This is called the *gas-kinetic collision rate*, and the corresponding value of the second-order rate constant k at room temperature is about $2 \times 10^{-10} \text{ cm}^3 \text{ molecule s}^{-1}$. Most reactions have rate constants less than this. First, the activation energy E must be overcome for the reaction to proceed. Second, molecules that are geometrically complex may have to be aligned properly at the point of collision for reaction to take place and perfect alignment is not achieved in every collision.

Consider the potential energy surface for the bimolecular reaction (most elementary reactions can be considered to be reversible)



⁶The rate constant k is not to be confused with the Boltzmann constant. The latter will always appear as a product with T in this context.

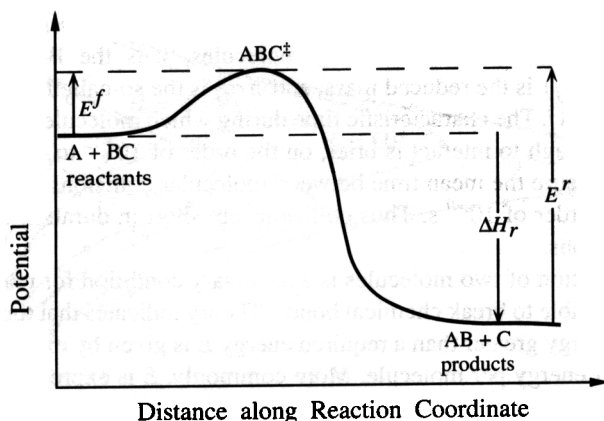


FIGURE 3.14 Potential energy surface along the reaction coordinate for a bimolecular reaction.

as shown in Figure 3.14. As the two reactant molecules approach each other, the energy of the reaction system rises. A point is reached, denoted by ABC^\ddagger , beyond which the energy starts to decrease again. ABC^\ddagger , sometimes called the activated complex, is a short-lived intermediate through which the reactants must pass if the encounter is to lead to reaction. By estimating the structure of this transition state the activation energy E may be estimated (Benson, 1976). This point is a saddle point in the potential energy surface of the system. Figure 3.14 shows the relationship between the energies of the process. The activation energy for the forward reaction is E^f ; that for the reverse reaction is E^r . The enthalpy of reaction is ΔH_r . Note that

$$E^f - E^r = \Delta H_r \quad (3.56)$$

The forward reaction (left to right) sketched in Figure 3.14 is exothermic, and $\Delta H_r = H_{\text{products}} - H_{\text{reactants}}$ is negative. The reverse reaction (right to left) is endothermic and must have an activation energy, E^r , at least as large as ΔH_r . It is customary to identify the activation energy E in (3.55) with E^f (or E^r .) Many atmospheric free radical reactions have a zero activation energy.

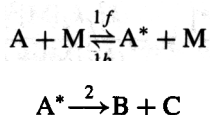
3.5.1 The Pseudo-Steady-State Approximation

Many chemical reactions involve very reactive intermediate species such as free radicals, which, as a result of their high reactivity, are consumed virtually as rapidly as they are formed and consequently exist at very low concentrations. The pseudo-steady-state approximation⁷ (PSSA) is a fundamental way of dealing with such reactive intermediates when deriving the overall rate of a chemical reaction mechanism.

It is perhaps easiest to explain the PSSA by way of an example. Consider the unimolecular reaction $A \rightarrow B + C$, whose elementary steps consist of the activation of A by collision with a background molecule M (a reaction chaperone) to produce an energetic A

⁷The word *pseudos* in Greek means "lie." As we will see shortly, the PSSA is a "lie" for a certain time period, and only after that period is it close to the truth.

molecule denoted by A^* , followed by decomposition of A^* to give $B + C$,



Note that A^* may return to A by collision and transfer of its excess energy to an M . The rate equations for this mechanism are

$$\frac{d[A]}{dt} = -k_{1f}[A][M] + k_{1b}[A^*][M]$$

$$\frac{d[A^*]}{dt} = k_{1f}[A][M] - k_{1b}[A^*][M] - k_2[A^*]$$

The reactive intermediate in this mechanism is A^* . The PSSA states that the rate of generation of A^* is equal to its rate of disappearance; physically, what this means is that A^* is so reactive that, as soon as an A^* molecule is formed, it reacts by one of its two paths. Thus the PSSA gives

$$k_{1f}[A][M] - k_{1b}[A^*][M] - k_2[A^*] = 0 \quad (3.59)$$

From this we find the concentration of A^* in terms of the concentrations of the stable molecules A and M ,

$$[A^*] = \frac{k_{1f}[A][M]}{k_{1b}[M] + k_2}$$

This expression can be used in (3.57) to give

$$\frac{d[A]}{dt} = -\frac{k_{1f}k_2[M][A]}{k_{1b}[M] + k_2} \quad (3.61)$$

We see that the single overall reaction $A \rightarrow B + C$ with a rate given by (3.61) depends on the concentration of M . If the background species M is in such excess that its concentration is effectively constant, the overall rate can be expressed as $d[A]/dt = -k[A]$, where $k = k_{1f}k_2[M]/(k_{1b}[M] + k_2)$ is a constant. If $k_{1b}[M] \gg k_2$ then $d[A]/dt = -k[A]$, with $k = k_{1f}k_2/k_{1b}$. On the other hand, if $k_{1b}[M] \ll k_2$, then $d[A]/dt = -k_{1f}[M][A]$, and the rate of the reaction depends on the concentration of M .

One comment is in order. The PSSA is based on the presumption that the rates of formation and disappearance of a reactive intermediate are equal. A consequence of this statement is that $d[A^*]/dt = 0$ from (3.58). This should not, however, be interpreted to mean that $[A^*]$ does not change with time. $[A^*]$ is at steady state with respect to $[A]$ and $[M]$. We can, in fact, compute $d[A^*]/dt$. It is

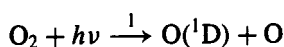
$$\frac{d[A^*]}{dt} = \frac{d}{dt} \frac{k_{1f}[A][M]}{k_{1b}[M] + k_2} \quad (3.62)$$

which, if $[M]$ is constant, is

$$\frac{d[A^*]}{dt} = -\frac{k_{1f}^2 k_2 [M]^2 [A]}{(k_{1b} [M] + k_2)^2} \quad (3.63)$$

To reconcile $d[A^*]/dt = 0$ from (3.58) with (3.63), we note that (3.60) is valid only after a short initial time interval needed for the rates of formation and disappearance of A^* to equilibrate so as to establish the steady state. After that time $[A^*]$ adjusts slowly on the timescale associated with changes in $[A]$ so as to maintain that balance. That slow adjustment is given by (3.63).

Let us consider, as an example, the steady-state concentration of oxygen atoms in the upper atmosphere (Wayne, 1991). In the upper atmosphere (~ 80 km), $O(^1D)$ is formed by O_2 photolysis,



and quenched by collision with N_2 or O_2 ,



Reaction 1 occurs at a rate R_1 . The rate equation for $O(^1D)$ formation is

$$\frac{d[O(^1D)]}{dt} = R_1 - k_2 [O(^1D)][M]$$

the solution of which for radiation that begins at $t = 0$, and constant R_1 and $[M]$ is

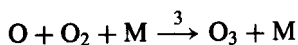
$$[O(^1D)] = \frac{R_1}{k_2 [M]} (1 - \exp(-k_2 [M] t))$$

If $O(^1D)$ is in a steady state, then

$$[O(^1D)]_{ss} = R_1 / k_2 [M]$$

(In a case in which the formation step is a photochemical reaction, we can refer to the steady state as a *photostationary state*.) For $t \gg 1/k_2 [M]$, $[O(^1D)]$ is at its steady-state value. At 80 km altitude, $[M] \approx 3 \times 10^{14}$ molecules cm^{-3} and $k_2 [M] \approx 3 \times 10^{-11}$ cm^3 molecule $^{-1}$ s $^{-1}$. As long as t is greater than about 10^{-4} s, the steady-state expression applies. What this means is that if R_1 or $[M]$ is changing, as long as they change over timescales that are longer than about 10^{-3} s, the steady-state approximation for $O(^1D)$ will hold at any instant.

Now let us consider the ground-state oxygen atom formed in reaction 1. (Its formation from reaction 2 can be neglected as a contribution to the rate of formation.) The major loss process is



The time behavior of O following irradiation beginning at $t = 0$ is

$$[\text{O}] = \frac{R_1}{k_3[\text{O}_2][\text{M}]} (1 - \exp(-k_3[\text{O}_2][\text{M}]t)) \quad (3.64)$$

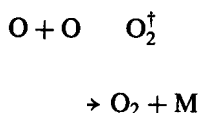
At 80 km, $T \approx 200$ K, at which $k_3 \approx 1.4 \times 10^{-33} \text{ cm}^6 \text{ molecule}^{-2} \text{ s}^{-1}$. The exponential term in (3.64) is < 0.01 for $t \geq 1.8 \times 10^5 \text{ s}$ (50 h). Thus the time needed for O to establish a steady-state concentration is much longer than that over which the solar intensity varies, and O is never in steady state at this altitude in the atmosphere. The reason why, at this altitude, O(¹D) achieves a steady state and O does not, is based on the relative rates of the removal reactions. That for O(¹D) is sufficiently fast; that for O is too slow to “keep up with” the formation step. In the lower regions of the atmosphere, where the pressure is large, and hence the concentration of third bodies, M, is large, removal reactions for both O and O(¹D) are, under all conditions, sufficiently fast that steady states are rapidly established for both species.

3.5.2 Pressure Dependence of Reactions

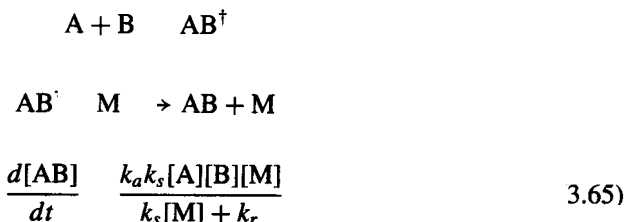
Certain reactions have an order that is variable with pressure; they are third order at low pressure and second order at high pressure. Consider, for example, the combination of two oxygen atoms (O(³P) in the triplet-P ground state, which we will denote simply by O) to form O₂. Upon collision the newly formed O₂ molecule possesses the combination energy of O + O. Unless some energy is removed within the time of one vibrational period, the freshly formed O₂ will decompose back to O + O. The excess energy is removed by the third body, M. The overall reaction is written as



But the elementary steps are



where the dagger denotes vibrational excitation. The rate of formation of a product AB in the general system



If the newly formed molecule is larger than diatomic, there are several vibrational modes into which the bond combination energy can be converted. In such a case, the lifetime of the newly formed molecule can extend over several vibrational periods before the critical

bond is broken. With a sufficiently large product molecule, the lifetime can be so great that collisional removal of the excess energy by a third molecule M is no longer rate determining.

From (3.65), if $k_r \gg k_s [M]$, the reaction is third order,

$$\frac{d[AB]}{dt} = \frac{k_a k_s}{k_r} [A][B][M] \quad (3.66)$$

If $k_r \ll k_s [M]$, then the reaction is second order,

$$\frac{d[AB]}{dt} = k_a [A][B] \quad (3.67)$$

As the product molecule AB becomes more complex, the value of k_r decreases because the combination energy is distributed among more and more vibrational modes. The concentration of the third body, [M], is usually related directly to the pressure since in the atmosphere M is the sum of N_2 and O_2 . The concentration of M at which the reaction rate behavior changes from third order to second order is lower the more complex the product molecule. Combination of two hydrogen atoms to form H_2 is third order all the way up to 10^4 atm. On the other hand, addition of the OH radical to the alkene, 1-butene, C_4H_8 , is second order at all tropospheric pressures. Two reactions of significant atmospheric importance,



and



lie just at the point where both second- and third-order kinetics are exhibited in the atmospheric pressure range.

The rate equation (3.65) can be written as pseudo-second order,

$$\frac{d[AB]}{dt} = k[A][B] \quad (3.68)$$

where k can be expressed in terms of the high- and low-pressure limiting values,

$$k_\infty = k_a \quad (3.69)$$

$$k_0 = \frac{k_a k_s}{k_r} [M] \quad (3.70)$$

as

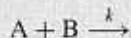
$$k = \frac{k_0 k_\infty}{k_0 + k_\infty} \quad (3.71)$$

Actual experimental data on the pressure variation of the pseudo-second-order rate constant k do not conform with (3.71). The reason is that the elementary rate constants k_a , k_r , and k_s should have been defined for each individual quantized vibrational level of AB^\ddagger , and the individual rates summed to give the total rate. Also, vibrations and rotations can interconvert in the newly formed molecule. A widely used modification of the treatment of pressure-dependent reactions is due to Troe (1983). In the Troe theory, the right-hand side of (3.71) is multiplied by a broadening factor F that is itself a function of k_0/k_∞ ,

$$k = \frac{k_0 k_\infty}{k_0 + k_\infty} F \quad (3.72)$$

Third-order reactions often exhibit decreasing rate with increasing temperature. The higher the temperature, the larger the thermal kinetic energy possessed by the reactants A and B, and the larger the internal vibrational energy stored in the AB^\ddagger molecule. The larger this energy, the higher the chance of recombination and the larger the value of k_r . The rate constants k_a and k_s do not depend strongly on temperature, so in the low-pressure regime since k_r increases as T increases, the overall rate constant decreases. This temperature dependence of k_0 is frequently represented empirically by a factor T^n in the overall rate constant (see Appendix B).

Example 3.3 Chemical Reaction Rate Constants Expressed in Terms of Mixing Ratios In the cgs unit system the rate constant k for a second-order chemical reaction,



is normally expressed as $\text{cm}^3 \text{ molecule}^{-1} \text{ s}^{-1}$. When A and B are expressed in mixing ratios (e.g., ppm), the appropriate units of k used are $\text{ppm}^{-1} \text{ min}^{-1}$. The conversion between the two systems can be accomplished as follows. At standard temperature and pressure (STP) condition $p_s = 1 \text{ atm}$, $T_s = 273 \text{ K}$, 6.022×10^{23} molecules occupy a volume (V_s) of 22.4 L. A mole of the same gas at any other temperature and pressure occupies a volume V of

$$V = V_s \left(\frac{p_s}{p} \right) \left(\frac{T}{T_s} \right)$$

So the number of molecules per cm^3 is given by ($V_s = 22.4 \text{ L}$)

$$\frac{\text{molecules}}{\text{cm}^3} = \frac{6.022 \times 10^{23}}{22.4(1/p)(T/273) \times 1000} = 7.34 \times 10^{21} (p/T)$$

The conversion between the two units for rate constants is given by

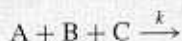
$$\begin{aligned} \frac{\text{cm}^3}{\text{molecule s}} &= \frac{60 \text{ s}}{\text{min}} \times 7.34 \times 10^{21} \left(\frac{p}{T} \right) \frac{\text{molecules}}{\text{cm}^3} \times \frac{1}{10^6 \text{ ppm}} \\ &= 4.40 \times 10^{17} \left(\frac{p}{T} \right) \frac{1}{\text{ppm min}} \end{aligned}$$

Thus

$$k(\text{ppm}^{-1} \text{ min}^{-1}) = 4.40 \times 10^{17} \left(\frac{P}{T}\right) k(\text{cm}^3 \text{ molecule}^{-1} \text{ s}^{-1})$$

At 298 K, $p = 1$ atm, the conversion factor is 1.47×10^{15} .

The rate constant for a third-order reaction



is expressed in cgs units as $\text{cm}^6 \text{ molecule}^{-2} \text{ s}^{-1}$ and in ppm min units as $\text{ppm}^{-2} \text{ min}^{-1}$. The conversion from $\text{cm}^6 \text{ molecule}^{-2} \text{ s}^{-1}$ to $\text{ppm}^{-2} \text{ min}^{-1}$ is accomplished as follows:

$$\begin{aligned} \frac{\text{cm}^6}{\text{molecule}^2 \text{ s}} &= \frac{60 \text{ s}}{\text{min}} \times \left[7.34 \times 10^{21} \left(\frac{P}{T}\right) \right]^2 \frac{\text{molecules}^2}{\text{cm}^6} \times \frac{1}{(10^6 \text{ ppm})^2} \\ &= 3.23 \times 10^{33} \left(\frac{P}{T}\right)^2 \frac{1}{\text{ppm}^2 \text{ min}} \end{aligned}$$

Thus

$$k(\text{ppm}^{-2} \text{ min}^{-1}) = 3.23 \times 10^{33} \left(\frac{P}{T}\right)^2 k(\text{cm}^6 \text{ molecule}^{-2} \text{ s}^{-1})$$

At 298 K, $p = 1$ atm, the conversion factor is 3.64×10^{28} .

REFERENCES

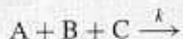
- Atkinson, R., Baulch, D. L., Cox, R. A., Hampson, R. F. Jr., Kerr, J. A., and Troe, J. (1992) Evaluated kinetic and photochemical data for atmospheric chemistry: Supplement IV, *J. Phys. Chem. Ref. Data*, **21**, 1125–1568.
- Benson, S. W. (1976) *Thermochemical Kinetics*, 2nd ed. Wiley, New York.
- Demerjian, K. L., Schere, K. L., and Peterson, J. T. (1980) Theoretical estimates of actinic (spherically integrated) flux and photolytic rate constants of atmospheric species in the lower troposphere, *Adv. Environ. Sci. Technol.*, **10**, 369–459.
- DeMore, W. G., Sander, S. P., Golden, D. M., Hampson, R. F., Kurylo, M. J., Howard, C. J., Ravishankara, A. R., Kolb, C. E. and Molina, M. J. (1994) *Chemical Kinetics and Photochemical Data for Use in Stratospheric Modeling*. Evaluation No. 11, JPL Publication 94-26. Jet Propulsion Laboratory, Pasadena, CA.
- Finlayson-Pitts, B. J., and Pitts, J. N. Jr. (1986) *Atmospheric Chemistry: Fundamentals and Experimental Techniques*. Wiley, New York.
- Fröhlich, C., and London, J. (eds.) (1986) *Revised Instruction Manual on Radiation Instruments and Measurements*, World Climate Research Program (WCRP) Publication Series No. 7. World Meteorological Organization/TD No. 149, Geneva.
- Goody, R. M., and Yung, Y. L. (1989) *Atmospheric Radiation*, 2nd ed. Oxford University Press, Oxford, UK.

Thus

$$k(\text{ppm}^{-1} \text{ min}^{-1}) = 4.40 \times 10^{17} \left(\frac{p}{T}\right) k(\text{cm}^3 \text{ molecule}^{-1} \text{ s}^{-1})$$

At 298 K, $p = 1 \text{ atm}$, the conversion factor is 1.47×10^{15} .

The rate constant for a third-order reaction



is expressed in cgs units as $\text{cm}^6 \text{ molecule}^{-2} \text{ s}^{-1}$ and in ppm min units as $\text{ppm}^{-2} \text{ min}^{-1}$. The conversion from $\text{cm}^6 \text{ molecule}^{-2} \text{ s}^{-1}$ to $\text{ppm}^{-2} \text{ min}^{-1}$ is accomplished as follows:

$$\begin{aligned} \frac{\text{cm}^6}{\text{molecule}^2 \text{ s}} &= \frac{60 \text{ s}}{\text{min}} \times \left[7.34 \times 10^{21} \left(\frac{p}{T}\right) \right]^2 \frac{\text{molecules}^2}{\text{cm}^6} \times \frac{1}{(10^6 \text{ ppm})^2} \\ &= 3.23 \times 10^{33} \left(\frac{p}{T}\right)^2 \frac{1}{\text{ppm}^2 \text{ min}} \end{aligned}$$

Thus

$$k(\text{ppm}^{-2} \text{ min}^{-1}) = 3.23 \times 10^{33} \left(\frac{p}{T}\right)^2 k(\text{cm}^6 \text{ molecule}^{-2} \text{ s}^{-1})$$

At 298 K, $p = 1 \text{ atm}$, the conversion factor is 3.64×10^{28} .

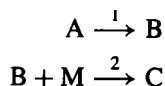
REFERENCES

- Atkinson, R., Baulch, D. L., Cox, R. A., Hampson, R. F. Jr., Kerr, J. A., and Troe, J. (1992) Evaluated kinetic and photochemical data for atmospheric chemistry: Supplement IV, *J. Phys. Chem. Ref. Data*, **21**, 1125–1568.
- Benson, S. W. (1976) *Thermochemical Kinetics*, 2nd ed. Wiley, New York.
- Demerjian, K. L., Schere, K. L., and Peterson, J. T. (1980) Theoretical estimates of actinic (spherically integrated) flux and photolytic rate constants of atmospheric species in the lower troposphere, *Adv. Environ. Sci. Technol.*, **10**, 369–459.
- DeMore, W. G., Sander, S. P., Golden, D. M., Hampson, R. F., Kurylo, M. J., Howard, C. J., Ravishankara, A. R., Kolb, C. E. and Molina, M. J. (1994) *Chemical Kinetics and Photochemical Data for Use in Stratospheric Modeling*. Evaluation No. 11, JPL Publication 94-26. Jet Propulsion Laboratory, Pasadena, CA.
- Finlayson-Pitts, B. J., and Pitts, J. N. Jr. (1986) *Atmospheric Chemistry: Fundamentals and Experimental Techniques*. Wiley, New York.
- Fröhlich, C., and London, J. (eds.) (1986) *Revised Instruction Manual on Radiation Instruments and Measurements*, World Climate Research Program (WCRP) Publication Series No. 7. World Meteorological Organization/TD No. 149, Geneva.
- Goody, R. M., and Yung, Y. L. (1989) *Atmospheric Radiation*, 2nd ed. Oxford University Press, Oxford, UK.

- Hofzumahaus, A., Kraus, A., and Müller, M. (1995) Comparison of tropospheric photolysis frequency data $J(\text{O}^1\text{D})$ measured simultaneously by chemical actinometry and spectroradiometry: test of laboratory O^1D quantum yield data, in *Tropospheric Oxidation Mechanisms*, edited by K. H. Becker. European Commission, Report EUR 16171EN, Luxembourg, pp. 71–76.
- Kasten, F., and Young, A. T. (1989) Revised optical air mass tables and approximation formula, *Appl. Opt.* **28**, 4735–4738.
- Lenoble, J. (1993) *Atmospheric Radiative Transfer*. A. Deepak Publishing, Hampton, VA.
- Liou, K. N. (1992) *Radiation and Cloud Processes in the Atmosphere*. Oxford University Press, Oxford, UK.
- Madronich, S. (1987) Photodissociation in the atmosphere 1. Actinic flux and the effects of ground reflections and clouds, *J. Geophys. Res.*, **92**, 9740–9752.
- Madronich, S., and Weller, G. (1990) Numerical integration errors in calculated tropospheric photodissociation rate coefficients, *J. Atmos. Chem.*, **10**, 283–300.
- Martinez, R. D., Buitrago, A. A., Howell, N. W., Hearn, C. H., and Joens, J. A. (1992) The near UV absorption-spectra of several aliphatic aldehydes and ketones, *Atmos. Environ.*, **26**, 785–792.
- Mérienne, M. F., Jenouvrier, A., and Coquart, B. (1995) The NO_2 absorption spectrum. I. Absorption cross-sections at ambient temperatures in the 300–500 nm region, *J. Atmos. Chem.*, **20**, 281–297.
- Michelsen, H. A., Salawitch, R. J., Wennberg, P. O., and Anderson, J. G. (1994) Production of O^1D from photolysis of O_3 , *Geophys. Res. Lett.*, **21**, 2227–2230.
- Troe, J. (1983) Specific rate constants $k(E, J)$ for unimolecular bond fissions, *J. Chem. Phys.*, **79**, 6017–6029.
- Wayne, R. P. (1991) *Chemistry of Atmospheres*, 2nd ed. Oxford University Press, Oxford, UK.
- World Meteorological Organization (WMO) (1986) *Atmospheric Ozone 1985*. Global Ozone Research and Monitoring Project, Report No. 16, Geneva.

PROBLEMS

3.1_B Consider the following reaction system:



Assume M is present in great excess, so that $[\text{M}] \simeq \text{constant}$. The concentrations of B and C are zero at $t = 0$.

- Derive analytical expressions for the exact dynamic behavior of this system over time. Show mathematically under what conditions the pseudo-steady-state approximation (PSSA) can be made for [B].
 - Use the PSSA to derive a simpler set of equations for the concentrations of A, B, and C.
- 3.2_B** The most important oxidizing species for tropospheric compounds is usually the hydroxyl (OH) radical. A standard way of determining the OH rate constant of a compound is to measure its decay in a reactor in the presence of OH relative to the decay of a second compound, the OH rate constant of which is known. Consider two compounds A and B, A being the one for which the OH rate constant is to be determined and B the reference compound for which its OH rate constant is known. Show that the

concentrations of A and B in such a reactor obey the following relation:

$$\ln \frac{[A]_0}{[A]_t} = \frac{k_A}{k_B} \ln \frac{[B]_0}{[B]_t}$$

where $[A]_0$ and $[B]_0$ are the initial concentrations, $[A]_t$ and $[B]_t$ are the concentrations at time t , and k_A and k_B are the OH rate constants. Thus, plotting

$$\ln \frac{[A]_0}{[A]_t} \quad \text{versus} \quad \ln \frac{[B]_0}{[B]_t}$$

yields a straight line with slope k_A/k_B . Knowing k_B allows one to calculate k_A from the slope.

- 3.3C Once released at the Earth's surface, a molecule diffuses upward into the troposphere and at any time may be removed by chemical reaction with other species, by absorption into particles and droplets, or by photodissociation. If the removal processes are rapid relative to the rate of diffusion, the species will not get mixed uniformly in the troposphere before it is removed. If, on the other hand, removal is slow relative to the rate of diffusion, the species may have a uniform tropospheric concentration.

Consider a species A whose removal from the atmosphere can be expressed as a first-order reaction, that is, $R_a = -k_A c_A$. If the removal of A is the result of reaction with background species B, then k_A can be a pseudo-first-order rate constant that includes the concentration of B in it. The intrinsic rate constant is given by the Arrhenius expression, $k_A = A_0 \exp(-E_a/RT)$.

Let us assume that the vertical concentration distribution of A can be represented generally as $c_A = c_{A0} \exp(-H_A z)$ by analogy to the exponential decrease of pressure with altitude, $p = p_0 \exp(-Hz)$. Show that the tropospheric lifetime of A over the tropospheric height H_T is given by

$$\tau_T = \frac{1 - e^{-H_A H_T}}{H_A \int_0^{H_T} k_A(T, z) \exp(-H_A z) dz}$$

The tropospheric temperature profile can be approximated by $T(z) = T_0 - \alpha z$, where $T_0 = 293$ K and $\alpha = 5.5$ K km⁻¹. Show that the ratio of the lifetime of species A at altitude z to that at the Earth's surface is

$$\frac{\tau_T}{\tau_0} = \frac{[1 - \exp(-H_A H_T)] \exp(-E_a/RT_0)}{H_A \int_0^{H_T} \exp[-E_a/R(T_0 - \alpha z)] \exp(-H_A z) dz}$$

Let us apply the foregoing theory to some trace atmospheric constituents whose principal removal reactions are with the OH radical. Consider CH₃Cl, CHF₂Cl, CH₃SCH₃, and H₂S. For the purpose of the calculation assume that the OH radical concentration is 10⁶ molecules cm⁻³, independent of height. Place the computed values of τ_T/τ_0 for these species on a plot of τ_T/τ_0 versus k_A at surface conditions. Discuss.

5 Chemistry of the Troposphere

The troposphere behaves as a chemical reservoir relatively distinct from the stratosphere. Transport of species from the troposphere into the stratosphere is much slower than mixing within the troposphere itself. A myriad of species are emitted at the Earth's surface and those with chemical lifetimes less than about a year or so are destroyed in the troposphere. Even though the most energetic solar wavelengths are removed in the stratosphere, sufficiently energetic wavelengths penetrate into the troposphere to promote significant photochemical reactions in the troposphere. A factor important in tropospheric chemistry is the relatively high concentration of water vapor. The chemistry of the stratosphere involves the reactions that form and destroy ozone; ozone formation and removal is, likewise, central to the chemistry of the troposphere.

The gas-phase chemistry of the troposphere involves the oxidation of organic molecules in the presence of oxides of nitrogen under the action of sunlight. Like a flame, atmospheric oxidation proceeds via chains of free radical reactions. For organic molecules these chains can be long and complex. Unlike combustion, however, atmospheric oxidation involves a very dilute fuel, at mixing ratios of parts per million or even parts per billion. Because of these very low concentrations, an external source of energy is required to drive the reactions, and that energy is provided by solar radiation. The predominant hydrocarbon in the troposphere is methane, and the chemistry of the background troposphere is fueled by methane. In the urban and continental troposphere a large number of other anthropogenic and biogenic hydrocarbons and organic species are present. As a result of combustion emissions, greatly enhanced levels of NO_x over those in the background troposphere exist in urban and continental areas, and NO_x is key in the chemistry of the troposphere. The troposphere is an oxidative medium; the tendency is for species to be moved to a more oxidized state. Hydrocarbons are reacted to aldehydes, then to acids, and finally to CO_2 . Sulfur-containing compounds advance through the chain of oxidation states, starting with reduced sulfur compounds such as H_2S and CH_3SCH_3 , which are oxidized to SO_2 and then to H_2SO_4 . Correspondingly, NO is oxidized to NO_2 and finally to HNO_3 .

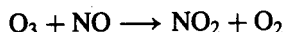
Ozone can be considered as the principal product of tropospheric chemistry. As noted in Chapter 4, the only ozone-forming reaction that occurs in the atmosphere is that between atomic and molecular oxygen. Because sunlight of wavelengths exceeding only about 290 nm reaches the troposphere, the source of the atomic oxygen in the troposphere cannot be O_2 , which only absorbs radiation of wavelengths shorter than this. That source is provided by nitrogen dioxide (NO_2). Though often present at levels of only a ppb or less, oxides of nitrogen play a central role in the chemistry of the troposphere. Their chemistry is, in fact, a good place to begin to study the chemistry of the troposphere.

5.1 BASIC PHOTOCHEMICAL CYCLE OF NO₂, NO, AND O₃

When NO and NO₂ are present in sunlight, ozone formation occurs as a result of the photolysis of NO₂ at wavelengths < 424 nm,



where M represents N₂ or O₂ or another third molecule that absorbs the excess vibrational energy and thereby stabilizes the O₃ molecule formed. There are no significant sources of ozone in the atmosphere other than reaction 5.2. Once formed, O₃ reacts with NO to regenerate NO₂,



Let us consider for a moment the dynamics of a system in which only these three reactions are taking place. Let us assume that known initial concentrations of NO and NO₂, [NO]₀ and [NO₂]₀, in air are placed in a reactor of constant volume at constant temperature and irradiated. The rate of change of the concentration of NO₂ after the irradiation begins is given by

$$\frac{d[\text{NO}_2]}{dt} = -j_{5.1}[\text{NO}_2] + k_{5.3}[\text{O}_3][\text{NO}]$$

Treating [O₂] as constant, there are four species in the system: NO₂, NO, O, and O₃. We could write the dynamic equations for NO, O, and O₃ just as we have done for NO₂. For example, the equation for [O] is

$$\frac{d[\text{O}]}{dt} = j_{5.1}[\text{NO}_2] - k_{5.2}[\text{O}][\text{O}_2][\text{M}]$$

However, if we were to evaluate the right-hand side numerically we would find that it is very close to zero. Physically, this means that the oxygen atom is so reactive that it disappears by reaction 5.2 virtually as fast as it is formed by reaction 5.1. In dealing with highly reactive species such as the oxygen atom, it is customary, as noted in Chapter 3, to invoke the pseudo-steady-state approximation (PSSA) and thereby assume that the rate of formation is exactly equal to the rate of disappearance, for example,

$$j_{5.1}[\text{NO}_2] = k_{5.2}[\text{O}][\text{O}_2][\text{M}]$$

The steady-state oxygen atom concentration in this system is then given by

$$[\text{O}]_{\text{ss}} = \frac{j_{5.1}[\text{NO}_2]}{k_{5.2}[\text{O}_2][\text{M}]}$$

Note that $[O]_{ss}$ is not constant; rather it varies with $[NO_2]$ in such a way that at any instant a balance is achieved between its rate of production and loss. What this approximation really means is that the oxygen atom concentration adjusts to changes in the NO_2 concentration many orders of magnitude faster than the NO_2 concentration changes. Thus, on a timescale of the NO_2 dynamics, $[O]_{ss}$ always appears to satisfy (5.7).

However, from (5.4) and (5.5) we see that these three reactions will reach a point where NO_2 is destroyed and reformed so fast that a steady-state cycle is maintained. Let us compute the steady-state concentrations of NO , NO_2 , and O_3 achieved in this cycle. (The steady-state concentration of oxygen atoms is already given by (5.7).) The steady-state ozone concentration is given by

$$[O_3]_{ss} = \frac{j_{5.1}[NO_2]}{k_{5.3}[NO]} \quad (5.8)$$

This expression, resulting from the steady-state analysis of reactions 5.1 to 5.3, has been named the *photostationary state relation*. We note that the steady-state ozone concentration is proportional to the $[NO_2]/[NO]$ ratio. We now need to compute $[NO_2]$ and $[NO]$. These are obtained from conservation of nitrogen,

$$[NO] + [NO_2] = [NO]_0 + [NO_2]_0$$

and the stoichiometric reaction of O_3 with NO ,

$$[O_3]_0 - [O_3] = [NO]_0 - [NO]$$

Solving for $[O_3]$, we obtain the relation for the ozone concentration formed at steady state by irradiating any mixture of NO , NO_2 , O_3 , and excess O_2 (in which only reactions 5.1 to 5.3 are important),

$$[O_3]_{ss} = -\frac{1}{2} \left([NO]_0 - [O_3]_0 + \frac{j_{5.1}}{k_{5.3}} \right) + \frac{1}{2} \left\{ \left([NO]_0 - [O_3]_0 + \frac{j_{5.1}}{k_{5.3}} \right)^2 + \frac{4j_{5.1}}{k_{5.3}} ([NO_2]_0 + [O_3]_0) \right\}^{1/2} \quad (5.9)$$

If $[O_3]_0 = [NO]_0 = 0$, (5.9) reduces to

$$[O_3]_{ss} = \frac{1}{2} \left\{ \left[\left(\frac{j_{5.1}}{k_{5.3}} \right)^2 + \frac{4j_{5.1}}{k_{5.3}} [NO_2]_0 \right]^{1/2} \frac{j_{5.1}}{k_{5.3}} \right\} \quad (5.10)$$

We will see later that a typical value of $j_{5.1}/k_{5.3}$ expressed in mixing ratio units is 10 ppb, so we can compute the ozone mixing ratio attained as a function of the initial mix-

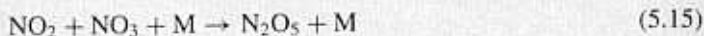
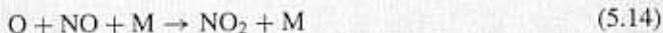
ing ratio of NO₂ with [O₃]₀ = [NO]₀ = 0:

[NO ₂] ₀ , (ppb)	[O ₃], (ppb)
100	
1000	

If, on the other hand, [NO₂]₀ = [O₃]₀ = 0, then [O₃] = 0. This is clear since with no NO₂ there is no means to produce atomic oxygen and therefore ozone. Thus the maximum steady-state ozone concentration would be achieved with an initial charge of pure NO₂. The mixing ratios of ozone attained in urban and regional atmospheres are often greater than those in the sample calculation. Since most of the NO_x emitted is in the form of NO and not NO₂, the concentration of ozone reached, if governed solely by reactions 5.1 to 5.3, would be far too low to account for the actual observed concentrations. It must be concluded that reactions other than 5.1 to 5.3 are important in tropospheric air in which relatively high ozone concentrations occur. Shortly we will see what those reactions are.

Example 5.1 Measurement of the Photolysis Rate of NO₂ The photolysis of NO₂ is a key atmospheric reaction. Its photodissociation rate can be calculated if the actinic flux $I(\lambda)$ is known. However, such measurements require specialized apparatus that is complex and expensive. A method that allows one to determine the NO₂ photodissociation rate, $j_{5.1}$, directly circumvents the need for elaborate measurements of the radiation intensity. By exposing a mixture of NO₂ and N₂ to sunlight one can determine the value of $j_{5.1}$ by comparing the measured NO₂ decay as a function of time with that obtained by integration of the rate equations. To integrate the rate equations it is necessary to assume a value for $j_{5.1}$. The desired value of $j_{5.1}$ is that which produces agreement between the observed and predicted NO₂ decay.

In the previous analysis we considered only reactions 5.1 to 5.3. There are several other reactions that occur in the NO_x-N₂ system that should be included for a more complete analysis. These are¹



¹ Actually in the presence of sunlight NO₃ photolyzes very rapidly (see Section 5.6) so that we do not expect daylight NO₃ levels to be appreciable. NO₃ is added to the mechanism at this point largely for completeness.

We now simply expand our analysis of the $\text{NO}_x\text{-N}_2$ system to include these six reactions. We assume that in addition to oxygen atoms and O_3 , NO_3 and N_2O_5 are in steady state. The PSSA applied to these two species yields $R_{5,12} - R_{5,13} = 0$ and $R_{5,15} - R_{5,16} = 0$, respectively. Using these relations and that derived for oxygen atoms, namely, $R_{5,1} = R_{5,2} + R_{5,11} + R_{5,12} + R_{5,14}$, we obtain

$$\frac{d[\text{NO}_2]}{dt} = -2k_{5,11}[\text{O}][\text{NO}_2] \quad (5.17)$$

Substituting the PSSA relation for $[\text{O}]$ into (5.17) and rearranging, we get

$$\frac{-2j_{5,1}}{d \ln[\text{NO}_2]/dt} = 1 + \frac{k_{5,12}[\text{M}]}{k_{5,11}} + \frac{k_{5,14}[\text{M}][\text{NO}]}{k_{5,11}[\text{NO}_2]} + \frac{k_{5,2}[\text{M}][\text{O}_2]}{k_{5,11}[\text{NO}_2]} \quad (5.18)$$

Equation (5.18) seems complex, but it can be interpreted. In the absence of any reactions except 5.1 and 5.11, all oxygen atoms formed would react with NO_2 to form NO and O_2 , giving an overall quantum yield of 2; that is, two molecules of NO_2 disappear for each photon absorbed. Thus, in that case,

$$-\frac{d \ln[\text{NO}_2]}{dt} = 2j_{5,1}$$

This result holds if the experiment were run without N_2 at low pressure ($[\text{M}] = 0$). In the actual situation, however, various species compete with NO_2 for the oxygen atoms. The effect of this competition is expressed in the last three terms of (5.18). These are the ratios of oxygen atom reaction rates by other pathways to the rate of reaction 5.11.

We can integrate (5.18) analytically under the assumption that most of the NO_x is either NO_2 or NO ,

$$[\text{NO}] = [\text{NO}]_0 + [\text{NO}_2]_0 - [\text{NO}_2]$$

The result of the integration is

$$j_{5,1} = \frac{1}{2t} \left[(1 + a_1 - a_2) \ln \frac{[\text{NO}_2]_0}{[\text{NO}_2]} + a_2 \left(\frac{[\text{NO}_2]_0}{[\text{NO}_2]} - 1 \right) + (a_2[\text{NO}]_0 + a_3[\text{O}_2]) \left(\frac{[\text{NO}_2]_0 - [\text{NO}_2]}{[\text{NO}_2]_0 [\text{NO}_2]} \right) \right] \quad (5.19)$$

where

$$a_1 = \frac{k_{5,12}[\text{M}]}{k_{5,11}} \quad a_2 = \frac{k_{5,14}[\text{M}]}{k_{5,11}} \quad a_3 = \frac{k_{5,2}[\text{M}]}{k_{5,11}}$$

Equation (5.19) may be simplified if the initial concentrations of NO and O_2 are zero:

$$j_{5,1} = \frac{1}{2t} \left[(1 + a_1 - a_2) \ln \frac{[\text{NO}_2]_0}{[\text{NO}_2]} + a_2 \left(\frac{[\text{NO}_2]_0}{[\text{NO}_2]} - 1 \right) \right] \quad (5.20)$$

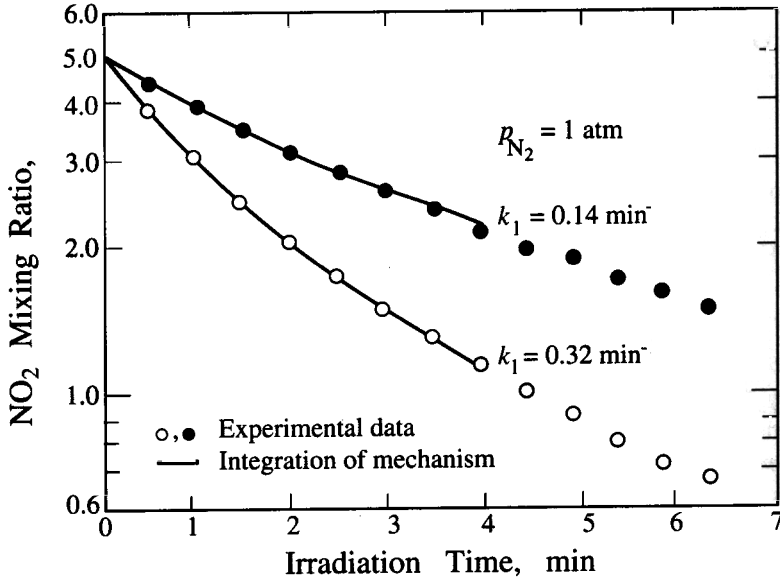


FIGURE 5.1 NO₂ mixing ratio as a function of time in a system initially comprising 5 ppm NO₂ in N₂. Experimental data and the predictions of the mechanism in the text are shown for two light intensities (Holmes et al., 1973).

Equation (5.20) can be used to compute $j_{5,1}$ from the measured [NO₂] versus time data in an irradiated system of NO₂ in N₂ by finding a value of $j_{5,1}$ that produces a fit of the data. Figure 5.1 shows NO₂ concentrations measured as a function of time for two different artificial light intensities. The curves represent (5.20) using the values of $j_{5,1}$ shown.

5.2 ATMOSPHERIC CHEMISTRY OF CARBON MONOXIDE AND NO_x

We noted that in order to explain frequently observed atmospheric ozone levels it is necessary that reactions other than 5.1 to 5.3 must be invoked. For these we must turn to the next major class of tropospheric compounds, carbon-containing species. In some respects the simplest atmospheric carbon-containing species is CO. Carbon monoxide does not, however, react readily with any of the species present in the NO_x-air system.

We already know from Section 4.2 that ozone photolysis to produce both ground-state (O) and excited singlet (O(¹D)) oxygen atoms is important in both the stratosphere and troposphere,



The ground-state O atom combines rapidly with O₂ by reaction 5.2 to reform O₃, so reaction 5.21a followed by reaction 5.2 has no net chemical effect. However, when O(¹D) is produced, since the O(¹D) → O transition is forbidden, it must react with another atmos-

pheric species. Most often $O(^1D)$ collides with N_2 or O_2 , removing the excess energy and quenching $O(^1D)$ to its ground state,



Since the oxygen atom then just reacts with O_2 to replenish O_3 , this path consisting of reactions 5.21b, 5.22, and 5.2 is just another null cycle. Occasionally, however, $O(^1D)$ collides with H_2O and produces two hydroxyl radicals (recall reaction 4.17),

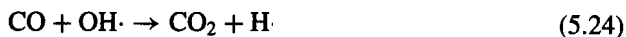


From this point on, for clarity, we will explicitly indicate radical species with the radical center "dot".

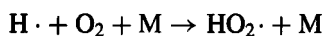
Because H_2O is present in the lower troposphere at mixing ratios up to 10^4 ppm (1%) and because reaction 5.23 has a rate constant about a factor of 10 larger than the quenching reaction 5.22 with $M = N_2$ or O_2 (see Table B.1), as much as 10% of the $O(^1D)$ produced reacts with H_2O to generate OH. Because two OH molecules are formed in reaction 5.23, this leads to an OH yield of approximately 0.2 molecule OH per O_3 molecule photolyzed.

The key to understanding tropospheric chemistry will turn out to lie in the reactions of the hydroxyl radical. This radical, unlike many molecular fragments formed from carbon-containing molecules, is unreactive toward oxygen, and, as a result, it survives to react with most atmospheric trace species.

Carbon monoxide will react with the hydroxyl radical formed in reaction 5.23,



and the hydrogen atom formed in reaction 5.24 combines so quickly with O_2 to form the hydroperoxyl radical $HO_2 \cdot$,



that, for all intents and purposes, we can simply write reaction 5.24 as

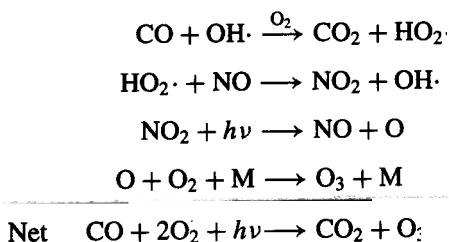


The addition of an H atom to O_2 weakens the O—O bond in O_2 , and the resulting HO_2 radical reacts much more freely than O_2 itself. When NO is present, the most important atmospheric reaction that the HO_2 radical undergoes is with NO,



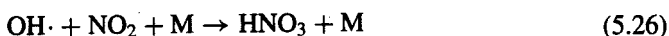
Again, we have already encountered this important reaction in the stratosphere (reaction 4.36).

The atmospheric oxidation of CO can be summarized as follows:



Note that neither OH nor HO₂ is consumed in this reaction cycle, which can be viewed as a catalytic oxidation of CO to CO₂. Net formation of O₃ occurs because the conversion of NO to NO₂ is accomplished by the HO₂ radical rather than by O₃ itself. This set of reactions can occur repeatedly until one of the molecules is removed in a termination reaction.

Termination of the chain can occur when OH and NO₂ react to form nitric acid,



Again, we have already encountered this reaction in the stratosphere. (Termination can also occur when HO₂ reacts with itself, but at this point we assume that NO_x concentrations are sufficiently large that the self-reaction of HO₂ is not favored.)

In analyzing this mechanism, the PSSA, as applied to this system, can be represented in terms of the rates of the nine reactions as²

$$\begin{aligned}
 [\text{O}]_{\text{ss}} \quad R_{5.1} - R_{5.2} + R_{5.22} &= 0 \\
 j_{5.1} [\text{NO}_2] - k_{5.2} [\text{O}] [\text{O}_2] [\text{M}] + k_{5.22} [\text{M}] [\text{O}({}^1\text{D})] &= 0 \\
 [\text{O}({}^1\text{D})]_{\text{ss}} \quad R_{5.21\text{b}} - R_{5.22} + R_{5.23} &= 0 \\
 k_{5.21\text{b}} [\text{O}_3] - k_{5.22} [\text{M}] [\text{O}({}^1\text{D})] - k_{5.23} [\text{H}_2\text{O}] [\text{O}({}^1\text{D})] &= 0 \\
 \left. \begin{aligned}
 [\text{OH}]_{\text{ss}} \quad 2R_{5.23} - R_{5.24} + R_{5.25} - R_{5.26} &= 0 \\
 [\text{HO}_2]_{\text{ss}} \quad R_{5.24} - R_{5.25} &= 0
 \end{aligned} \right\} \\
 2k_{5.23} [\text{H}_2\text{O}] [\text{O}({}^1\text{D})] - k_{5.26} [\text{OH}] [\text{NO}_2] &= 0 \\
 [\text{O}_3]_{\text{ss}} \quad R_{5.2} - R_{5.3} - R_{5.21} &= 0 \\
 k_{5.2} [\text{O}] [\text{O}_2] [\text{M}] - k_{5.3} [\text{O}_3] [\text{NO}] - k_{5.21\text{b}} [\text{O}_3] &= 0
 \end{aligned}$$

²In writing rate equations for reactions of the type $\text{A} + \text{B} + \text{M} \rightarrow \text{AB} + \text{M}$, for example, reaction 5.26, one must decide whether to express the rate of the reaction as $k[\text{A}][\text{B}][\text{M}]$ or $k[\text{A}][\text{B}]$. This is simply an issue of notation, since the value of the rate constant k will depend on the concentration of the third body M through its appropriate formula, as given in Appendix B. We will often choose not to explicitly indicate [M] in the rate equation for such three-body reactions, keeping in mind that the value of the rate constant will depend on [M] through its appropriate formula.

We have four equations with four unknowns. $[\text{HO}_2]_{\text{ss}}$ was eliminated by using $R_{5.24} - R_{5.25} = 0$ in the $[\text{OH}]_{\text{ss}}$ equation.) Solving the above equations we obtain

$$[\text{O}]_{\text{ss}} = \frac{j_{5.1} [\text{NO}_2] + k_{5.22} [\text{M}] [\text{O}({}^1\text{D})]}{k_{5.2} [\text{O}_2] [\text{M}]}$$

$$[\text{O}({}^1\text{D})]_{\text{ss}} = \frac{k_{5.21\text{b}} [\text{O}_3]}{k_{5.23} [\text{H}_2\text{O}]} a$$

$$[\text{OH}]_{\text{ss}} = \frac{2k_{5.23} [\text{H}_2\text{O}] [\text{O}({}^1\text{D})]}{k_{5.26} [\text{NO}_2]} = \frac{2k_{5.23} [\text{H}_2\text{O}] a}{k_{5.26} [\text{NO}_2]}$$

$$[\text{O}_3]_{\text{ss}} = \frac{k_{5.2} [\text{O}] [\text{O}_2] [\text{M}]}{k_{5.3} [\text{NO}] + k_{5.21\text{b}}} = \frac{j_{5.1} [\text{NO}_2]}{k_{5.3} [\text{NO}] + k_{5.21\text{b}} a}$$

where

$$a = \frac{k_{5.22} [\text{M}]}{1 + \frac{k_{5.22} [\text{M}]}{k_{5.23} [\text{H}_2\text{O}]}}$$

The rate equations for NO_2 , NO , and CO are

$$\frac{d[\text{NO}_2]}{dt} = -R_{5.1} + R_{5.3} + R_{5.25} - R_{5.26}$$

$$\frac{d[\text{NO}]}{dt} = R_{5.1} - R_{5.3} - R_{5.25}$$

$$\frac{d[\text{CO}]}{dt} = -R_{5.24}$$

Substituting the expressions for the rates into these equations and using the PSSA results for the free radical concentrations, we obtain

$$\frac{d[\text{NO}_2]}{dt} = \frac{j_{5.1} k_{5.21\text{b}} a [2k_{5.24} [\text{CO}] / k_{5.26} - 3[\text{NO}_2]]}{k_{5.3} [\text{NO}] + k_{5.21\text{b}} a}$$

$$\frac{d[\text{NO}]}{dt} = \frac{j_{5.1} k_{5.21\text{b}} a \{[\text{NO}_2] - 2k_{5.24} [\text{CO}] / k_{5.26}\}}{k_{5.3} [\text{NO}] + k_{5.21\text{b}} a}$$

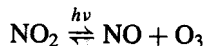
$$\frac{d[\text{CO}]}{dt} = -\frac{2j_{5.1} k_{5.21\text{b}} k_{5.24} a [\text{CO}] / k_{5.26}}{k_{5.3} [\text{NO}] + k_{5.21\text{b}} a}$$

Before we solve the rate equations let us examine the PSSA relation for ozone,

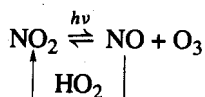
$$[\text{O}_3]_{\text{ss}} = \frac{j_{5.1} [\text{NO}_2]}{k_{5.3} [\text{NO}] + k_{5.21\text{b}} a}$$

As long as $k_{5.3} [\text{NO}] \gg k_{5.21\text{b}} a$, $[\text{O}_3]_{\text{ss}}$ reduces to the photostationary state relation (5.8).

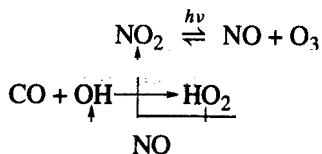
The qualitative features of the set of CO/NO_x reactions can be described as follows. Photolysis of NO₂ produces NO and O. The O atom immediately combines with an oxygen molecule to form O₃. Ozone then reacts mainly with NO to regenerate NO₂. The cycle of these three reactions can be represented concisely as (where O₂ is not indicated)



The characteristic time of this cycle is usually short enough relative to the competing reactions so that a steady state is achieved quickly. The concentration of O₃ at such a steady-state condition is given by the photostationary state relation (5.8). If we now consider the reactions resulting when CO is present, we see that the simple reversible cycle above is modified to be³



The HO₂ radical that converts NO back to NO₂ is converted in the process to OH, which then is available to react with another molecule of CO. Thus we obtain two interwoven cycles, a "fast" cycle and a "slow" cycle,



The CO/NO_x reaction mechanism is a chain reaction with OH as the chain carrier. The chain length L_c of such a reaction is defined as the number of propagation steps occurring for each termination step,

$$L_c = \frac{R_{5.25}}{R_{5.26}} = \frac{R_{5.24}}{R_{5.26}} = \frac{k_{5.24}[\text{CO}]}{k_{5.26}[\text{NO}_2]} \quad (5.31)$$

Since the steady-state O₃ concentration achieved in the fast cycle is proportional to the ratio of [NO₂] to [NO], the effect of the slow CO cycle is to slowly convert NO to NO₂ and therefore to increase the steady-state O₃ concentration. Thus, because of the rapidity of the NO₂/O₃ cycle, an independent path that changes the ratio of [NO₂] to [NO] indirectly controls the ozone concentration. It is common to refer to such oxidation chains that are driven by sunlight as *photooxidations*.

The basic reaction mechanism of the CO/NO_x system exhibits many of the key features of those involving much more complex organic molecules. In particular, the role of OH as

³ The presence of water is also necessary to provide a path for formation of hydroxyl radicals after ozone photolysis to give O(¹D).

the oxidizing species and the NO to NO₂ conversion by HO₂ are central to virtually every atmospheric organic/NO_x mechanism. It is useful to proceed to a molecule that is somewhat more complicated than CO to see how the similar chain reaction mechanism develops. For that purpose, formaldehyde (HCHO) is an ideal molecule to consider.

5.3 ATMOSPHERIC CHEMISTRY OF FORMALDEHYDE AND NO_x

Formaldehyde is emitted from sources and also is an oxidation product of hydrocarbons. It is an essential component of tropospheric chemistry. Thus the chemistry of formaldehyde is common to virtually all mechanisms of tropospheric chemistry. This section therefore serves both as a continuation of our discussion of ozone chemistry as well as an introduction to the chemistry of organic compounds.

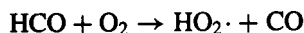
Formaldehyde undergoes two main reactions in the atmosphere, photolysis (see Table 3.3),



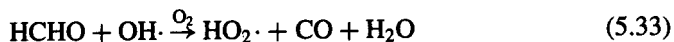
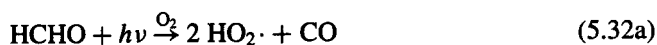
and reaction with OH,



As we have already noted, the hydrogen atom combines immediately with O₂ to yield HO₂. The formyl radical, HCO, also reacts very rapidly with O₂ to yield the hydroperoxyl radical and CO,



Because of the rapidity of this reaction, the formaldehyde reactions may be written concisely as



For overhead sun conditions 45% of the photolysis proceeds by reaction 5.32a and 55% by 5.32b (Rogers, 1990).

Applying the PSSA to reactions 5.32a, 5.32b, and 5.33, in addition to those in the CO system, we obtain

$$[\text{O}_3]_{\text{ss}} = \frac{j_{5.1}[\text{NO}_2]}{k_{5.3}[\text{NO}]}$$

$$[\text{OH}]_{\text{ss}} = \frac{2j_{5.32a}[\text{HCHO}]}{k_{5.26}[\text{NO}_2]}$$

$$[\text{HO}_2]_{\text{ss}} = 2j_{5.32a}[\text{HCHO}] \left\{ \frac{+ k_{5.33}[\text{HCHO}]/k_{5.26}[\text{NO}_2]}{k_{5.25}[\text{NO}]} \right\}$$

The rate equations for the photooxidation of a mixture of NO_2 , NO , and HCHO are, as a result,

$$\begin{aligned}\frac{d[\text{NO}_2]}{dt} &= \frac{2j_{5.32a}k_{5.33}[\text{HCHO}]^2}{k_{5.26}[\text{NO}_2]} \\ \frac{d[\text{NO}]}{dt} &= -2j_{5.32a} \left\{ 1 + \frac{k_{5.33}[\text{HCHO}]}{k_{5.26}[\text{NO}_2]} \right\} [\text{HCHO}] \\ \frac{d[\text{HCHO}]}{dt} &= - \left\{ j_{5.32a} + j_{5.32b} + 2j_{5.32a} \frac{k_{5.33}[\text{HCHO}]}{k_{5.26}[\text{NO}_2]} \right\} [\text{HCHO}]\end{aligned}$$

The chain length of the HCHO photooxidation is given by

$$\begin{aligned}L_c &= \frac{R_{5.25}}{R_{5.26}} \\ &= \frac{2j_{5.32a} + R_{5.33}}{R_{5.26}} \\ &= 1 + \frac{k_{5.33}[\text{HCHO}]}{k_{5.26}[\text{NO}_2]}\end{aligned}$$

We see that L_c is always greater than one as long as HCHO is present in the system. Each molecule of HCHO that photolyzes via reaction 5.32a leads to the conversion of two molecules of NO to NO_2 and at the same time generates two OH radicals. The HCHO-OH reaction, on the other hand, leads to one NO to NO_2 conversion and produces a single OH radical.

The reactivity of the system is controlled by the amount of HCHO . Upon photolysis, HCHO provides two HO_2 radicals on one path and none on the other. Since these paths are roughly comparable in rate, we can say approximately that each HCHO molecule leads to one HO_2 molecule. (It leads to exactly one in the OH reaction.) The conversion of NO to NO_2 and the formation of O_3 are therefore driven by HCHO through its production of HO_2 . Thus the theoretical maximum amount of O_3 that could be produced in this system is

$$[\text{O}_3] = [\text{HCHO}]_0 + [\text{NO}_2]_0$$

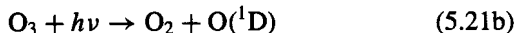
When all the NO_x is converted to HNO_3 , the system ceases reacting.

5.4 CHEMISTRY OF THE BACKGROUND TROPOSPHERE

We have begun a systematic development of the chemistry of the troposphere. We began with carbon monoxide since its atmospheric chemistry is the simplest, while exhibiting some of the essential elements of hydroxyl radical attack, formation of the hydroperoxyl radical, and conversion of NO to NO_2 . We then proceeded to formaldehyde, the atmospheric chemistry of which is slightly more complex than that of carbon monoxide. The next logical step would be to consider the simplest alkane, methane (CH_4), and that is, in fact, what we will now do. It turns out, moreover, that methane is the principal hydrocarbon species in the chemistry of the background troposphere. Thus, in studying the atmospheric chemistry of methane, we are led naturally to the chemistry of the background troposphere.

5.4.1 Ozone Photolysis

The reaction that can be considered to trigger background tropospheric chemistry is the photolysis of ozone at wavelengths < 319 nm to yield the electronically excited $O(^1D)$ atom, followed by $O(^1D)$ reaction with H_2O to generate two OH radicals,



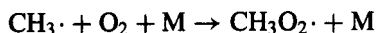
The O atoms formed directly in the photolysis of O_3 , reaction 5.21a, or formed from deactivation of $O(^1D)$ atoms, reaction 5.22, reform O_3 through reaction 5.2, leading to a null cycle with no chemical effect. As noted earlier, at room temperature and 50% relative humidity, 0.2 OH radicals are formed per $O(^1D)$ atom generated from the photolysis of ozone. Because the water vapor mixing ratio decreases with increasing altitude in the troposphere (World Meteorological Organization, 1992), and the ozone mixing ratio generally increases with increasing altitude, the OH radical concentration turns out, as a result, to be reasonably independent of altitude (Dentener and Crutzen, 1993). Although tropospheric ozone comprises only about 10% of all ozone in the atmosphere, through the formation of OH it determines the oxidizing or cleansing efficiency of the troposphere. In so doing, ozone ultimately maintains the chemical composition of the troposphere.

5.4.2 Methane Oxidation

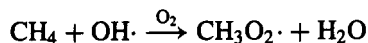
Hydroxyl radicals react with CH_4 ,



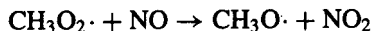
As in the case of the hydrogen atom, the methyl radical, $CH_3 \cdot$, reacts virtually instantaneously with O_2 to yield the methyl peroxy radical, $CH_3O_2 \cdot$,



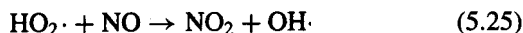
so that the CH_4 -OH reaction may be written concisely as



Under tropospheric conditions, the methyl peroxy radical can react with NO, NO_2 , and HO_2 radicals, and other organic peroxy (RO_2) radicals, with the reactions with NO and HO_2 radicals being the most important. The reaction with NO leads to the formation of the methoxy (CH_3O) radical,



Reaction of HO_2 with NO regenerates the OH radical,

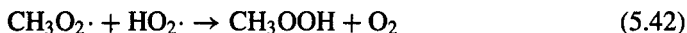


The methyl peroxy radical can also react with NO_2 ,

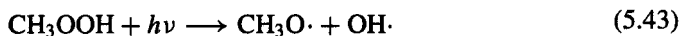


Methyl peroxyxynitrate, CH_3OONO_2 , thermally dissociates back to the reactants with a lifetime with respect to thermal decomposition of ~ 1 second at room temperature and atmospheric pressure, which increases to ~ 2 days for the temperature and pressure conditions in the upper troposphere (Atkinson et al., 1989; Atkinson, 1990). Methyl peroxyxynitrate can act as a temporary reservoir of NO_2 and CH_3O_2 radicals in the upper troposphere.

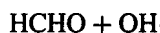
The reaction of CH_3O_2 with the HO_2 radical leads to the formation of methyl hydroperoxide,



which can photolyze or react with the OH radical

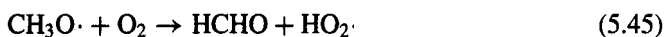


↓ fast



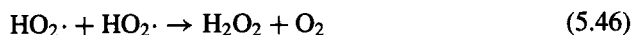
where the fractional splits indicated are those at 298 K. The lifetime of methyl hydroperoxide in the troposphere resulting from photolysis and reaction with the OH radical is calculated to be ~ 2 days. Methyl hydroperoxide is then a temporary sink of radicals, with its wet or dry deposition being a tropospheric loss process for radicals.

The only important reaction for the methoxy radical under tropospheric conditions is with O_2 to form formaldehyde and the HO_2 radical,



Formaldehyde is a "first-generation" product that reacts further, by photolysis by reactions 5.32a and 5.32b and with the OH radical, reaction 5.33. Formaldehyde is the first major product of CH_4 oxidation with a lifetime longer than a few seconds. The lifetimes of HCHO resulting from photolysis and OH radical reaction are ~ 4 hours and 1.5 days, respectively, leading to an overall lifetime of ~ 3 hours for overhead sun conditions.

Major chain-terminating steps in CH_4 oxidation include nitric acid and hydrogen peroxide formation,⁴



⁴ The recommended rate constant for reaction 5.46 is (Stockwell, 1995):

$$k_{5.46} = (k_c + k_p)f_w$$

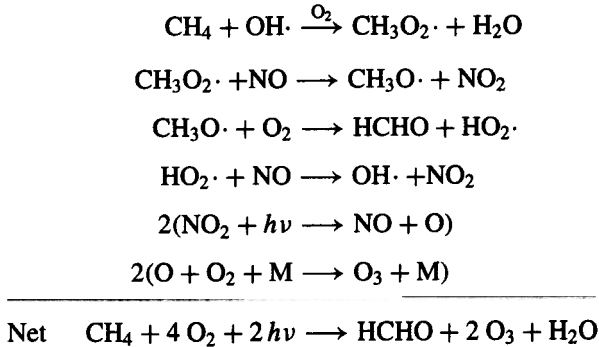
$$k_c = 2 \times 10^{-13} \exp(600/T)$$

$$k_p = 1.7 \times 10^{-33} [\text{M}] \exp(1000/T)$$

$$f_w = 1 + 1.4 \times 10^{-21} [\text{H}_2\text{O}] \exp(2200/T)$$

where T is in K and $[\text{M}]$ and $[\text{H}_2\text{O}]$ are in molecules cm^{-3} . k_c is the bimolecular term, k_p is the pressure-dependent term, and f_w is a water-vapor-dependent factor. Stockwell (1995) has shown that the contribution of the water-dependent term can be very important; at the surface the value of $k_{5.46}$ in air saturated with water vapor is over twice the value of $k_{5.46}$ in dry air. Above about 15 km the water-dependent contribution is negligible and above 25 km the reaction is almost completely bimolecular.

The overall reaction sequence leading to CO_2 formation, through the HCHO and CO intermediate "stable" products, is shown in Figure 5.2. When NO_x levels are sufficiently high that reaction of the peroxy radicals HO_2 and CH_3O_2 with NO predominates over peroxy radical self-reactions, the methane oxidation chain depicted in Figure 5.2 can be written as



Two molecules of ozone result from each CH_4 molecule. Further oxidation of formaldehyde leads to additional production of O_3 . Following the analysis of CO and HCHO oxi-

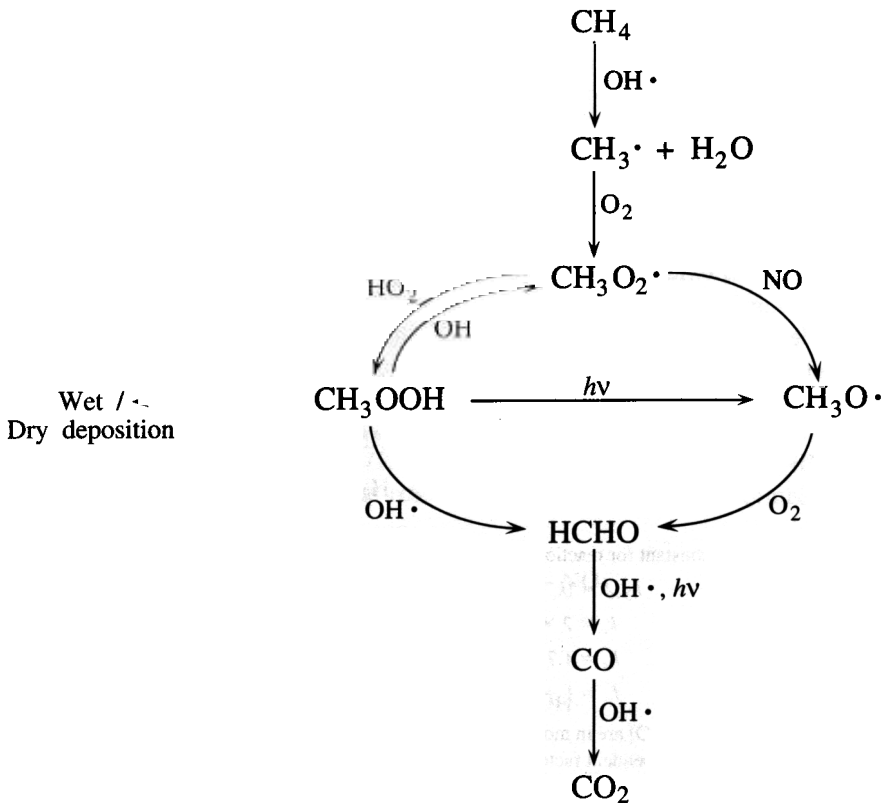


FIGURE 5.2 Atmospheric methane oxidation chain.

dition and assuming that the photostationary state holds at any instant, the local rate of formation of O_3 as a result of the above cycle is

$$P_{O_3} = \{k_{5.25}[HO_2] + k_{5.40}[CH_3O_2]\} [NO]$$

As a result of peroxy radical-NO reactions, the photostationary state relation must be adjusted to (Parrish et al., 1986; Ridley et al., 1992; Cantrell et al., 1993)

$$\frac{[NO_2]}{[NO]} = \frac{k_{5.3}[O_3] + k_{5.25}[HO_2] + k_{5.40}[CH_3O_2]}{j_{5.1}}$$

Measurements made during the spring of 1988 at Mauna Loa, Hawaii, indicated that peroxy radical mixing ratios of 60 ppt or so were required to account for observations of this ratio (Ridley et al., 1992).

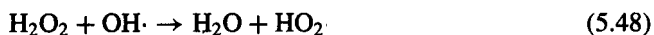
Production of O_3 in the CH_4 oxidation chain is interrupted if the peroxy radicals HO_2 and CH_3O_2 react with something other than NO, for example, themselves, NO_2 , or O_3 itself, or if NO_x is removed from the active cycle by reaction with OH to form HNO_3 . For the HO_2 radical, besides reaction 5.46, another important reaction is



Reaction 5.46 is the principal gas-phase source of H_2O_2 in the atmosphere.

5.4.3 Hydrogen Peroxide

Hydrogen peroxide is the dominant oxidant in clouds, fogs, or rain in the atmosphere. Photochemical activity largely determines the diurnal, seasonal, and latitudinal variations of the H_2O_2 concentration. H_2O_2 levels have been found to be higher in the afternoon, during the summer, and in the southern latitudes (Sakugawa et al., 1990). The major gas-phase destruction pathways for H_2O_2 are its reaction with OH and its photolysis,



The destruction of H_2O_2 in the aqueous phase, mainly by reacting with dissolved SO_2 , is considered in Chapter 6. Van Valin et al. (1990), Boatman et al. (1990), and Daum et al. (1990) reported continuous airborne measurements of H_2O_2 over the northeastern United States in June 1987. The range of H_2O_2 mixing ratios was < 0.2 to 37 ppb, with an average of 2 to 4 ppb. H_2O_2 concentrations are typically low near the surface, rise to a maximum at the top of the boundary layer, then slowly decrease with height. Photochemical model predictions indicate the H_2O_2 levels depend on whether the atmosphere is in a high or low NO_x regime, according to whether radical production is greater or less than the NO_x emission rate (Kleinman, 1991). In the low NO_x regime, more radicals are formed that can react with NO_x , and the "excess" radicals are removed by radical-radical reactions that are the source of peroxides (e.g., reaction 5.46). In this regime, peroxide formation is nearly proportional to the difference between radical source strength and NO_x emission rate. In the high NO_x regime, peroxide formation is suppressed.

5.5 THE HYDROXYL RADICAL

The hydroxyl radical does not react with any of the major constituents of the atmosphere, such as N_2 , O_2 , CO_2 , or H_2O , yet it is the most important reactive species in the troposphere. Indeed, OH reacts with most trace species in the atmosphere, and its importance derives from both its high reactivity toward other molecules and its relatively high concentration. Were OH simply to react with other species and not in some manner be regenerated, its concentration would be far too low, in spite of its high reactivity, to be an important player in tropospheric chemistry. The key is that, when reacting with atmospheric trace gases, OH is generated in catalytic cycles, leading to sustained concentrations on the order of 10^6 molecules cm^{-3} during daylight hours.

By using a chemical mechanism to simulate tropospheric chemistry, it is possible to estimate the atmospheric concentration of OH. Such calculations suggest a seasonally, diurnally, and globally averaged OH concentration of from 2×10^5 to 10^6 molecules cm^{-3} . Highest OH levels are predicted in the tropics, where high humidities and strong actinic fluxes lead to a high rate of OH production from O_3 photolysis to $O(^1D)$. In addition, OH levels are predicted to be about 20% higher in the Southern Hemisphere as a result of the large amounts of CO produced by human activities in the Northern Hemisphere that act to reduce OH through reaction with it. Hydroxyl radical levels are about a factor of 5 higher over the continents than over the oceans; it is estimated that a continental OH level is 7.5×10^6 molecules cm^{-3} , as opposed to a level of 1.5×10^6 molecules cm^{-3} over the remote Pacific Ocean. Since direct measurement of atmospheric OH levels is extremely difficult, confirmation of the levels predicted by the chemical mechanisms has usually been based on balancing budgets of species that are known to be consumed only by OH. For example, methyl chloroform (CH_3CCl_3) is removed from the atmosphere almost solely by reaction with OH, so the global average concentration of OH determines the mean residence time of CH_3CCl_3 . From the history of methyl chloroform emission, which is entirely anthropogenic and is known to reasonable accuracy, and its present atmospheric level, it is possible to infer its residence time and then to compare the OH level corresponding to that residence time to the level predicted theoretically from tropospheric chemical mechanisms. Using this method, Prinn et al. (1992) derived a 24 hour average OH radical concentration of $(8.1 \pm 0.9) \times 10^5$ molecules cm^{-3} (equivalent to a 12 hour daytime average of 1.6×10^6 molecules cm^{-3}). Measured and theoretical estimates of [OH] in the troposphere indicate the following ranges:

Daytime (summer)	$5-10 \times 10^6$ molecules cm^{-3}
Daytime (winter)	$1-5 \times 10^6$
Nighttime	$\leq 2 \times 10^5$

Methane is removed from the atmosphere by reaction with OH and by microbial oxidation in soil surface layers. Because of its relatively long lifetime, CH_4 is relatively well mixed over the globe, and, like CH_3CCl_3 , its lifetime can be determined from the global average distribution of OH. The OH rate constants of CH_3CCl_3 and CH_4 are (See Table B.1):

$$k_{CH_3CCl_3} = 1.8 \times 10^{-12} \exp(-1550/T) \text{ cm}^3 \text{ molecule}^{-1} \text{ s}^{-1}$$

$$k_{CH_4} = 2.65 \times 10^{-12} \exp(-1800/T) \text{ cm}^3 \text{ molecule}^{-1} \text{ s}^{-1}$$

Because the temperature dependences of these two rate constants are quite close, the atmospheric oxidation rate of CH_4 can be scaled to that of CH_3CCl_3 . An atmospheric CH_4 destruction rate of $440 \pm 50 \text{ Tg yr}^{-1}$ can be inferred in this way. From the current atmospheric loading of CH_4 of about 4850 Tg , a mean atmospheric lifetime of $11 (\pm 10\%)$ years is derived based solely on OH reaction. When loss in the stratosphere and removal in soils are also considered, the lifetime shortens to about 10 years.

Only in the past few years have reliable direct measurements been made of lower tropospheric OH radical concentrations (e.g., see, Felton et al., 1990; Eisele and Tanner, 1991; Hofzumahaus et al., 1991; Comes et al., 1992; Hard et al., 1992; Mount and Eisele, 1992; Eisele, 1995). These measurements show that, as expected, OH radical concentrations exhibit a diurnal profile, with daytime maximum concentrations of several $10^6 \text{ molecules cm}^{-3}$.

Ehhalt et al. (1991) have evaluated the extent of agreement between calculated and measured OH concentrations on May 20, 1983, 0908 to 1130 hours, at Deuselbach, a rural area in Germany, assuming that OH and HO_2 levels were governed by the CH_4 oxidation cycle. Figure 5.3 shows the calculated concentrations and fluxes between species. Since inter-

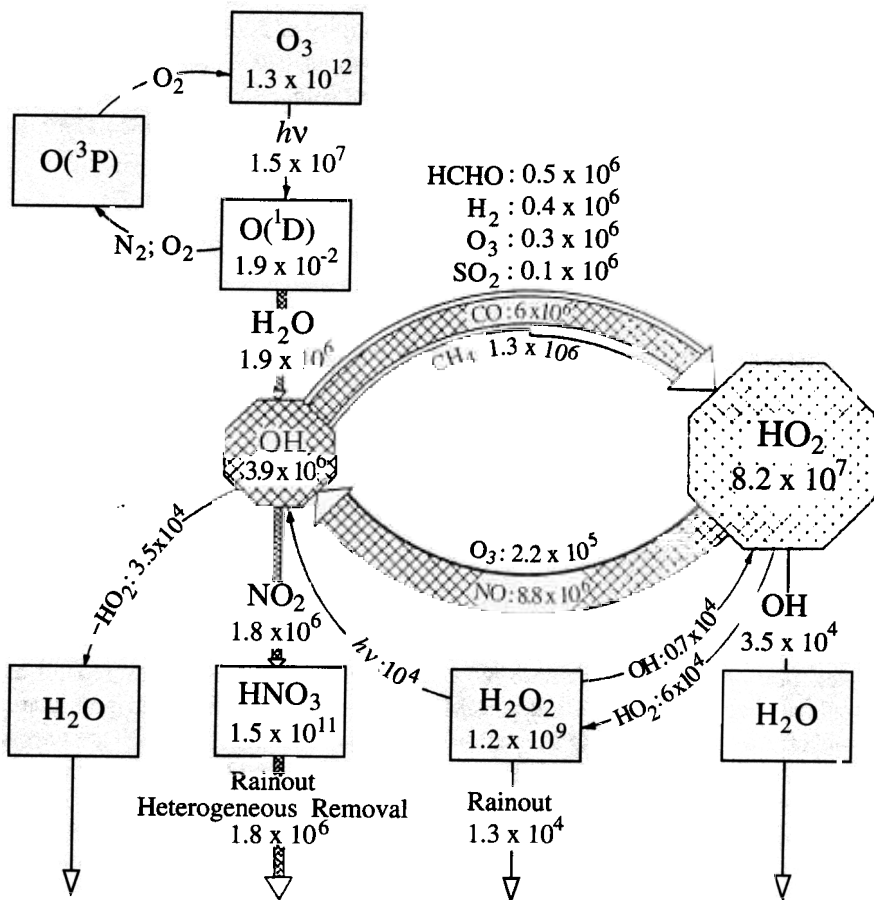
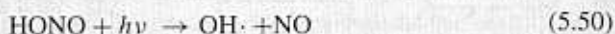


FIGURE 5.3 Concentrations and fluxes between OH and HO_2 (Ehhalt et al., 1991). The calculation simulates an air mass observed between 0908 and 1130 hours, May 20, 1983 at Deuselbach, Germany. Numbers in boxes are calculated concentrations (molecules cm^{-3}); numbers on arrows are conversion rates of OH and HO_2 (molecules $\text{cm}^{-3} \text{ s}^{-1}$).

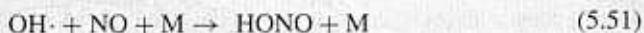
conversion rates between OH and HO₂ are nearly equal, the steady-state OH concentration can be estimated by equating its generation by O₃ photolysis to its removal by reaction with NO₂. Such an estimate leads to an OH concentration of 4.3×10^6 molecules cm⁻³. The OH-HO₂ interconversion rate is 9×10^6 molecules cm⁻³ s⁻¹. With the OH-NO₂ termination reaction occurring at a rate of 1.8×10^6 molecules cm⁻³ s⁻¹, an HO_x radical is cycled, on average, five times before it is removed by termination to form HNO₃. This amounts to a recycling of an HO_x radical every 9 seconds and an average lifetime of an HO_x radical of 45 seconds.

Example 5.2 Relative Importance of OH Production Routes in the Troposphere
Hydroxyl radicals are formed in the troposphere via the following processes:

- a. *Photolysis of O₃* At wavelengths less than 319 nm O₃ photodissociates to yield, in part, electronically excited oxygen atoms, O(¹D), by reaction 5.21b. Most of the excited O(¹D) atoms are physically quenched by N₂ and O₂ back to the ground state O(³P) by reaction 5.22. A small fraction of O(¹D) reacts with water vapor by reaction 5.23 to produce OH radicals. At a relative humidity of 50% at 298 K, about 0.2 OH radicals are formed for each O(¹D) atom formed.
- b. *Photolysis of Nitrous Acid* Nitrous acid, HONO, which is present during nighttime hours in urban atmospheres, is rapidly photolyzed at wavelengths ≤ 400 nm during daytime hours to yield OH radicals (Calvert et al., 1994),



Nitrous acid is formed from the reaction of OH radicals with NO⁵,



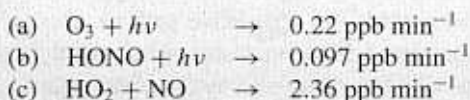
Since the principal removal process of HONO is photodecomposition, nitrous acid achieves its maximum concentrations during nighttime in the urban atmosphere. Typical nighttime urban mixing ratios range from about 1 ppb to maximum values approaching 10 ppb (Calvert et al., 1994). Values reported for remote areas are usually much lower than those for urban areas. The photodissociation lifetime of HONO ranges from about 10 minutes at high sun to about 1 hour for early morning sun. If HONO accumulates overnight, its photodissociation can be a significant early morning source of OH radicals before other sources become dominant.

- c. *Reaction of HO₂ Radicals with NO (Reaction 5.25)* Direct measurement of free radical concentrations in air, if possible at all, requires sophisticated instrumentation and careful analysis. Using a technique called fluorescence assay with gas expansion, Hard et al. (1992) determined HO₂ concentrations at two Oregon sites for continuous periods of 36 to 48 hours, one site characterized by clean marine air and an urban site. At both sites, maximum daily [HO₂] was in the range of $1\text{--}2 \times 10^8$ molecules cm⁻³ under clear-sky conditions. This range can be compared with levels predicted by photochemical models. Logan et al. (1981) predicted HO₂ concentrations of 3.3×10^8 molecules cm⁻³ (45° N latitude, surface, equinox) at the midday maximum and $1\text{--}10 \times 10^6$ molecules cm⁻³ at night. Madronich and Calvert (1990) pre-

⁵Nitrous acid can also be formed by the reaction of NO₂ and H₂O vapor (Jenkin et al., 1988).

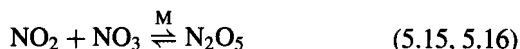
dicted noontime HO₂ concentrations of 3.2×10^8 molecules cm⁻³. Mihelcic et al. (1990) measured an HO₂ level of 8.3×10^8 molecules cm⁻³ at midday at a mountain site in Germany.

Under noontime conditions at 298 K, assuming [O₃] = 50 ppb (1.2×10^{12} molecules cm⁻³); [HO₂] = 4×10^{-3} ppb (1×10^8 molecules cm⁻³); [NO] = 40 ppb (9.8×10^{11} molecules cm⁻³); [HONO] = 1 ppb (2.5×10^{10} molecules cm⁻³), OH generation rates for pathways (a) to (c) are approximately as follows:



5.6 THE NITRATE RADICAL

We recall from Chapter 4 that the gaseous NO₃ radical is formed via the reactions (see Atkinson, 1991, Wayne et al., 1991, and Platt and Heintz, 1994, for comprehensive reviews of the nitrate radical),

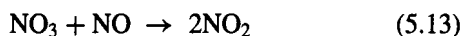


with N₂O₅ being in a relatively rapid (characteristic time to reach equilibrium ~1 minute at 298 K) equilibrium with NO₂ and the NO₃ radical. Nitrate radicals were first detected in the troposphere in 1980. NO₃ is a strong oxidizing agent and reacts with a number of other atmospheric species. The prerequisite for NO₃ radical production is the simultaneous presence of NO₂ and O₃ in the same air mass, as reaction 5.52 is the only primary source of NO₃ in the troposphere. The equilibrium with N₂O₅, reactions 5.15 and 5.16, is an important feature of NO₃ chemistry.

During daytime NO₃ radicals photolyze rapidly via two paths (see Table 3.3),

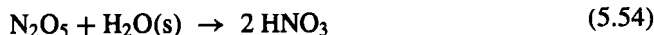


with a noontime lifetime of ~5 seconds, and react with NO,



sufficiently rapidly that NO and NO₃ cannot coexist at mixing ratios of a few parts per trillion (ppt) or higher. For typical daytime conditions of [NO₂] = 40 ppb, [O₃] = 50 ppb, and [NO] = 40 ppb, the maximum NO₃ mixing ratio will be 0.6 ppt. At nighttime, however, when NO concentrations drop near zero, due to reaction with O₃, the NO₃ mixing ratio can reach 100 ppt. Under conditions typical of rural areas in industrialized countries (NO₂ mixing ratio of ~1 ppb), NO₃ and N₂O₅ concentrations are roughly the same order of magnitude. Whereas homogeneous reactions of N₂O₅ with water vapor and other trace

gases are believed to be extremely slow, we have already seen the importance in the stratosphere of the heterogeneous (particle-phase) hydrolysis of N_2O_5 (reaction 4.27),



which occurs in aerosol particles or cloud droplets. This reaction is not expected to be important in daylight because NO_3 , the precursor to N_2O_5 via reaction 5.52, is rapidly photolyzed. Reaction 5.54 provides an alternative path to reaction 5.26 to convert NO_x into nitric acid. Indeed, reaction 5.54 is, in many cases, equal in importance to the “photochemical” conversion of NO_x to nitric acid by OH, reaction 5.26. Realization of the importance of the conversion of NO_x to HNO_3 via reaction 5.54 emerged after experimental verification of the presence of NO_3 radicals in the troposphere. Observed NO_3 lifetimes are a strong function of relative humidity (Platt and Heintz, 1994). Below $\text{RH} \simeq 50\%$, NO_3 lifetimes are the order of 40 minutes; above $\text{RH} \simeq 50\%$, observed NO_3 lifetimes drop to the order of a few minutes, most likely indicative of the water uptake of typical atmospheric aerosol particles around these humidities. These NO_3 lifetimes are most consistent with a loss of N_2O_5 , by reaction 5.54, which is in equilibrium with NO_3 . (If each reaction forming an N_2O_5 molecule would lead to irreversible loss of an NO_3 molecule, this would lead to much shorter NO_3 lifetimes than observed in the majority of cases. Thus it is more likely that an N_2O_5 molecule decomposes back to $\text{NO}_2 + \text{NO}_3$ than is lost irreversibly by reaction 5.54, but some fraction of N_2O_5 molecules are continuously lost to HNO_3 formation by reaction 5.54.)

5.7 THE OZONE BUDGET OF THE TROPOSPHERE AND THE ROLE OF NO_x

The fundamental question with respect to tropospheric ozone is: What are the sources and sinks of ozone, both locally and for the troposphere as a whole? Qualitatively, we know that at any location the sources are transport from the stratosphere and from other regions of the troposphere and local photochemical production, whereas the sinks are local photochemical destruction and wet and dry removal. Attempting to gain a quantitative understanding of the sources and sinks of ozone both locally and for the troposphere as a whole has occupied much of the research in tropospheric chemistry over the past decade.

In Chapter 2 we noted that intrusion of stratospheric air is a source of tropospheric ozone. Figure 5.4 shows a tropopause fold or break (recall Figure 1.3) at about 30°N during March and April 1987 as characterized by influx of stratospheric ozone into the troposphere. The approximate location of the tropopause is shown with crosses, and isopleths of constant O_3 mixing ratio are indicated. The measurements of O_3 in Figure 5.4 were taken via ozonesondes released from the research vessel *Polarstern* on a northern cruise in the Atlantic, mostly along 30°W . We also see that ozone levels decrease at lower altitudes from that in the upper troposphere, suggesting the presence of enhanced ozone removal processes near the surface. The observed decrease in O_3 as one goes from the NH to the SH suggests that the NH may be a source of SH ozone or that near-surface removal processes might be more effective in the SH.

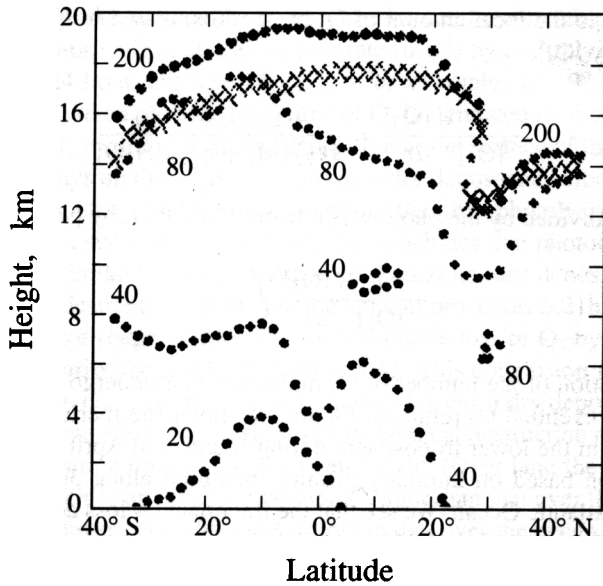


FIGURE 5.4 Meridional cross section of O₃ (in ppb) obtained during March and April 1987 via ozonesondes released from the research vessel *Polarstern* on a northern cruise in the Atlantic, mostly along 30° W. Approximate location of the tropopause is shown with crosses. (Figure presented in *Monthly Update*, Department of Energy Atmospheric Chemistry Program, originally presented by Smit et al., in *Ozone in the Atmosphere*, edited by R. D. Bojkov and P. Fabian, Deepak Publishing, 1989.)

5.7.1 Tropospheric Sinks of Ozone

The principal photochemical sink of O₃ in the troposphere is reactions 5.21b, 5.22, and 5.23. Because this removal path depends on the concentration of water vapor, it is most effective in low latitudes at low altitudes, where the radiation is intense and the humidity is high. An estimate of the magnitude of the local rate of O₃ destruction by reactions 5.21b, 5.22, and 5.23 can be obtained by assuming that [O(¹D))] is in a pseudo-steady state as a result of these three reactions. The pseudo-steady-state concentration of O(¹D)) is given by

$$[O(^1D)]_{ss} = \frac{j_{5.21b}[O_3]}{k_{5.22}[M] + k_{5.23}[H_2O]}$$

Ozone destruction occurs whenever an O(¹D)) reacts with H₂O, since this removes O(¹D)) from the system; otherwise O(¹D)) is just quenched back to O in reaction 5.22, and O immediately reforms O₃ by reaction 5.2. Thus the rate of O₃ removal by reactions 5.21b, 5.22, and 5.23 is

$$\begin{aligned} \frac{d[O_3]}{dt} &= -k_{5.23}[O(^1D)][H_2O] \\ &= -\frac{k_{5.23}[H_2O]j_{5.21b}[O_3]}{k_{5.22}[M] + k_{5.23}[H_2O]} \end{aligned}$$

A rate normalized to the local amount of O_3 present (expressed in s^{-1}) is obtained by dividing each side by $[O_3]$,

$$-\frac{1}{[O_3]} \frac{d[O_3]}{dt} = \frac{k_{5.23} [H_2O] j_{5.21b}}{k_{5.22} [M] + k_{5.23} [H_2O]}$$

If this rate is then divided by the photolysis rate constant of O_3 by path 5.21b,

$$\frac{1}{[O_3]} \frac{d[O_3]}{dt} \Big/ j_{5.21b}$$

we obtain the fraction of the number of O_3 molecules that undergo photolysis in reaction 5.21b that lead to eventual O_3 removal. Figure 5.5 shows the meridional cross section of fractional O_3 loss in the lower troposphere during March and April 1987, computed from the above equation based on humidity profiles measured along 30° W in the cruise of Figure 5.4 in the Atlantic Ocean. We see that the fractional O_3 loss decreases at the surface by a factor of ~ 3 from 10° N to 30° N and by almost an order of magnitude from close to the surface to an altitude of 5 km. At 5 km, about one O_3 molecule out of 100 that undergoes photolysis is ultimately destroyed; at the surface this is closer to one out of seven. This behavior is largely the result of the variation of H_2O vapor concentration with latitude and altitude.

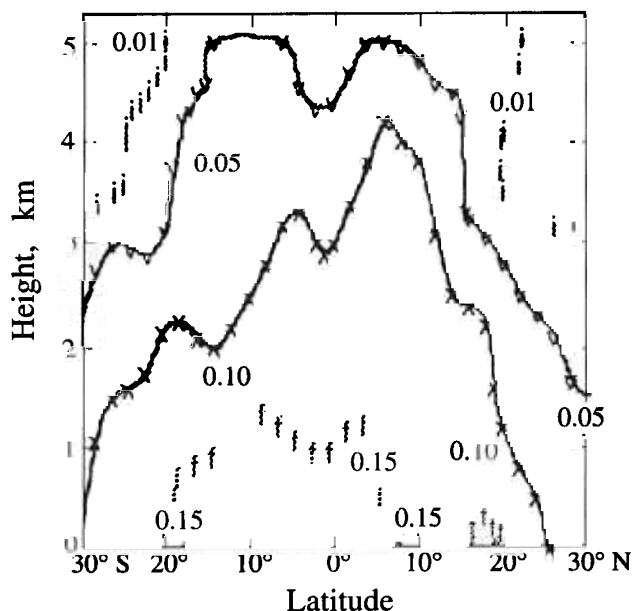
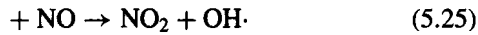


FIGURE 5.5 Meridional cross section of fractional photochemical ozone loss in the lower troposphere during March and April 1987, based on humidity profiles measured along 30° W above the Atlantic Ocean. Isolines represent the fraction of O_3 molecules undergoing photolysis to $O(^1D)$ that are ultimately lost through $O(^1D)$ reacting with water vapor. (Figure presented in *Monthly Update*, Department of Energy Atmospheric Chemistry Program, originally presented by Smit et al., in *Ozone in the Atmosphere*, edited by R. D. Bojkov and P. Fabian, Deepak Publishing, 1989.)

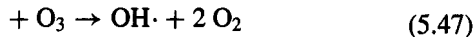
The fractional O₃ photochemical loss in Figure 5.5 can be converted into absolute 24-hour averages of the normalized O₃ destruction rate (in s⁻¹) by multiplying the fractions in Figure 5.5 by the 24-hour average of $j_{5.21b}$. For example, at 10° S at the surface, $j_{5.21b} \simeq 7 \times 10^{-6} \text{ s}^{-1}$, and a photolysis lifetime of O₃ is estimated as about 11 days. In contrast, the lifetime of O₃ resulting from dry deposition to the surface of the ocean can be estimated as about 35 days on the basis of assuming a dry deposition velocity of 0.05 cm s⁻¹ (see Chapter 19) (Smit et al., 1989). Since reactions other than photolysis also contribute to photochemical O₃ loss, such as reaction 5.47, one concludes that photochemistry is likely the major sink for O₃ in the boundary layer at 10° S and not dry deposition (Ayers et al., 1992). In fact, ozone destruction by the photochemical processes 5.21b, 5.22, and 5.23 is estimated to account for roughly 75% of the tropospheric loss of O₃ by gas-phase routes; the remainder is primarily the result of reaction 5.47. This conclusion is strengthened by the lack of observed O₃ decrease at night, which would occur if dry deposition to the ocean were having a noticeable effect on O₃, since photochemical destruction occurs only during daytime and dry deposition operates both day and night. (Over land the O₃ dry deposition velocity may be as much as an order of magnitude larger than that over the ocean, and with a nighttime boundary layer generally shallower than that over the ocean, dry deposition of ozone may compete effectively with chemical removal.)

5.7.2 Tropospheric Source of Ozone

The principal *in situ* chemical source of ozone in the troposphere is photochemical production through the methane oxidation chain. The level of NO is critical in this chain in dictating the fate of the HO₂ radical. Reaction 5.25,



leads to O₃ production; reaction 5.47,



destroys ozone. The *break-even concentration* of NO, below which O₃ is destroyed and above which it is produced, depends on the local O₃ concentration. Tropospheric air may be called NO_x rich when NO mixing ratios exceed those of O₃ by more than the ratio of the rate constants of reactions 5.47 and 5.25. The ratio of the rates of these two reactions is

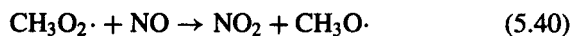
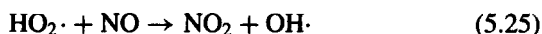
$$\frac{R_{5.47}}{R_{5.25}} = \frac{k_{5.47} [\text{O}_3]}{k_{5.25} [\text{NO}]}$$

The rate constant ratio, $k_{5.47}/k_{5.25} \simeq 2.5 \times 10^{-4}$. The O₃ mixing ratio near the Earth's surface in the remote continental troposphere is about 20 ppb. Then $R_{5.25} > R_{5.47}$ for NO mixing ratios exceeding about 5 ppt. This amount of NO is roughly equivalent to 15 to 20 ppt NO_x. A competition also exists between NO and the HO₂ radical for reaction with the CH₃O₂ radical, and the preferred route depends on the concentrations of HO₂ radicals and NO. The rate constants for the reaction of the CH₃O₂ radicals with NO (reaction 5.40) and HO₂ radicals (reaction 5.42) are of comparable magnitude (see Table B.1). Based on expected HO₂ radical concentrations in the troposphere, Logan et al. (1981) calculated that the reaction of the CH₃O₂ radical with NO dominates over that with HO₂ for NO mixing ra-

tios >30 ppt (equivalent to an NO concentration of 7×10^8 molecule cm^{-3} in the lower troposphere). For NO mixing ratios <30 ppt, the reaction of the CH_3O_2 radical with HO_2 dominates.

Because of the ozone depletion that occurs by photolysis, the NO_x break-even concentration at which net O_3 production occurs is somewhat larger than the value based just on the ratio of the rate constants of reactions 5.47 and 5.25. The approximate crossover point for NO_x between O_3 destruction and production is usually considered to be at about 30 ppt. Ozone mixing ratios in the planetary boundary layer over the remote Pacific Ocean are only about 5 to 6 ppb; NO_x levels are about 10 ppt. Thus, this region of the atmosphere is probably below the crossover point.

Net photochemical production of O_3 in the background troposphere can be estimated as follows. The rate-controlling reactions for O_3 production are 5.25 and 5.40,



where O_3 is produced from the photolysis of the NO_2 produced in these two reactions. Local photochemical destruction occurs by reactions 5.23 and 5.47. Thus the production and loss rates of O_3 are

$$P_{\text{O}_3} = \{k_{5.25} [\text{HO}_2] + k_{5.40} [\text{CH}_3\text{O}_2]\} [\text{NO}]$$

$$L_{\text{O}_3} = k_{5.23} [\text{O}(\text{D})] [\text{H}_2\text{O}] + k_{5.47} [\text{HO}_2] [\text{O}_3]$$

The local lifetime of ozone can be estimated on the basis of its local rate of either production or loss, as long as the local O_3 concentration is more or less in balance as a result of photochemical production and loss mechanisms. Thus we can use either

$$\tau_{\text{O}_3} = \frac{[\text{O}_3]}{P_{\text{O}_3}} \quad \text{or} \quad \tau_{\text{O}_3} = \frac{[\text{O}_3]}{L_{\text{O}_3}}$$

Which of the two expressions we choose to use depends on which of P_{O_3} or L_{O_3} can be more easily estimated.

Figure 5.6 shows calculated, 24-hour-average production and loss rates for the free troposphere above Hawaii during the MLOPEX (Mauna Loa Photochemistry Experiment) as a function of NO_x mixing ratio. The O_3 loss rate is seen to be almost independent of NO_x , at about 5×10^5 molecules $\text{cm}^{-3} \text{s}^{-1}$. For an O_3 mixing ratio of 40 ppb, this loss rate gives an O_3 lifetime of 17 days. Data for upper tropospheric concentrations over Hawaii indicate that $[\text{NO}_x]$ is typically ~30 ppt, with midday $[\text{NO}]$ at ~10 ppt (Ridley et al., 1992). From Figure 5.6 we see that at these levels O_3 production and loss are just about in balance, with loss predicted to be slightly greater. The difference between the loss and production rates is just about what is needed to destroy the expected amount of O_3 transported down from the stratosphere and to lead to an overall balance of O_3 in the background troposphere.

Ozone lifetimes in the troposphere vary significantly depending on altitude, latitude, and season. Lifetimes are shorter in the summer than in the winter as a result of the higher solar fluxes in the summer. Lifetimes are also shorter at the surface because of the higher water vapor concentration near the surface. At higher latitudes, lifetimes increase because

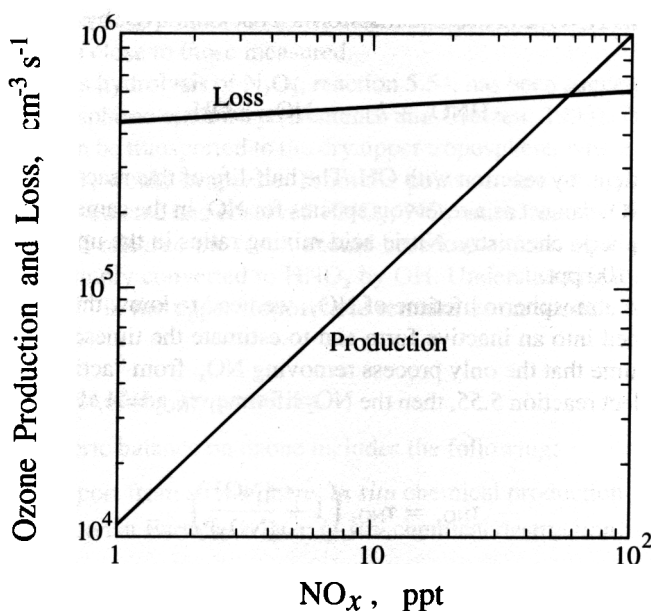


FIGURE 5.6 Calculated 24 hour average O₃ production and loss rates for the free troposphere above Hawaii during the MLOPEX as a function of the NO_x mixing ratio (Liu et al., 1992).

of the reduced solar intensity. At 20° N, for example, it is estimated that O₃ lifetimes at the surface are about 5 days in summer and 17 days in winter, whereas at 40° N these increase to 8 days in summer and 100 days in winter. At 20° N, at 10 km altitude, estimated summer and winter O₃ lifetimes are 30 days and 90 days, respectively, increasing by about a factor of 6 from those at the surface.

The key to understanding background tropospheric ozone is to determine whether a region is in a local O₃-producing or O₃-destroying condition. Because of the critical role played by NO_x, assessing the effect of anthropogenic NO_x emissions on background tropospheric NO_x is one of the major issues in tropospheric chemistry. Increasing NO_x weakens the net photochemical sink of O₃ in the background troposphere, leading to an overall increase of O₃.

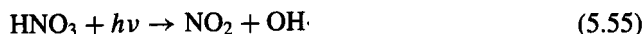
5.7.3 Fate of NO_x

At first glance it might appear that NO_x released in urban and regional areas will have a lifetime too short to permit its transport to the remote troposphere to influence background O₃. For typical OH levels, reaction 5.26,



leads to NO₂ lifetimes of a day or so, with HNO₃ subsequently removed by dry and wet deposition, typically in about a week. Because NO and NO₂ are relatively insoluble in precipitation, however, they can be vented to the upper troposphere by storms, where reaction 5.26 still occurs but the HNO₃ is not subject to dry deposition and generally not to wet de-

position either. This HNO_3 can itself be transformed back into NO_x by photolysis (see Table 3.3),



and, to a lesser extent, by reaction with OH. The half-life of this reaction at 10 km is about 23 days. Thus HNO_3 can act as a reservoir species for NO_x in the same vein as the reservoir species in stratospheric chemistry. Nitric acid mixing ratios in the upper troposphere vary from near zero to 100 ppt.

To estimate the atmospheric lifetime of NO_x , we need to know the processes by which NO_x is transformed into an inactive form and to estimate the timescale for that transformation. If we assume that the only process removing NO_x from "active" status is reaction 5.26, and we neglect reaction 5.55, then the NO_2 lifetime, $\tau_{\text{NO}_2} = 1/k_{5.26}[\text{OH}][\text{M}]$, and the NO_x lifetime is

$$\tau_{\text{NO}_x} = \tau_{\text{NO}_2} \left(1 + \frac{[\text{NO}]}{[\text{NO}_2]} \right)$$

Near the ground where OH levels are high and the NO/NO_2 ratio is small, τ_{NO_x} is on order of a day. In contrast, in the upper troposphere where the NO/NO_2 ratio can be large, τ_{NO_x} can be on the order of several days to a week.

Nitric acid is not the only NO_x -carrier important in tropospheric chemistry. The reactive nitrogen class, $\text{NO}_y = \text{NO}_x + \text{NO}_3 + 2\text{N}_2\text{O}_5 + \text{HONO} + \text{HNO}_3 + \text{PAN} + \text{RONO}_2 + \text{NO}_3^-$, includes the potential suite of such species. Of the components of NO_y , HNO_3 and $\text{CH}_3\text{C}(\text{O})\text{OONO}_2$ (PAN) (see Section 5.8.5) are likely the most important tropospheric NO_x -reservoir species (Sandholm et al., 1994). NO_2 sequestered in PAN, at the colder temperatures of the upper troposphere, is released in the thermal decomposition of PAN at the warmer temperatures of the lower troposphere.

Tropospheric chemical models, in attempting to simulate observed data, produce a ratio of predicted to observed $[\text{HNO}_3]/[\text{NO}_x]$ that is ~ 5 (Liu et al., 1992; Chatfield, 1994; Singh et al., 1996), that is, the models predict too much HNO_3 and not enough NO_x relative to what is measured. A variety of possible explanations for the discrepancy between gas-phase chemical theory and data for the HNO_3/NO_x ratio have been advanced. These include the following: (1) the absolute accuracy of HNO_3 measurements at remote tropospheric levels is unknown (Crosley, 1996); (2) HNO_3 predictions may be too high because of uncertainty in the absorption cross section for HNO_3 for reaction 5.55 (if the actual cross section is larger than that used, then both the predicted HNO_3 would be smaller and the predicted NO_2 would be larger, both of which would drive the predicted HNO_3/NO_x ratio smaller); (3) the predicted NO_2 concentration may be too low (if OH is overpredicted, NO_2 will be removed too rapidly via reaction 5.26); (4) a chemical mechanism exists that converts HNO_3 to HCOOH and NO_x (Chatfield, 1994; Folkins et al., 1995; Smythe et al., 1996); and (5) aircraft NO_x emissions might be responsible for some of the "missing" NO_x . Total annual NO_x emissions from aircraft are about $0.5 \text{ Tg}(\text{N}) \text{ yr}^{-1}$ (see Table 2.5) small relative to other NO_x sources, except that this amount is injected directly near the tropopause (peak emissions at 9 to 12 km), where residence times are long and removal is slow. It has been estimated that the amount of O_3 produced per unit of NO emitted may be 20 times greater at 10 km than at the surface (Johnson et al., 1992). The role of aircraft-injected NO_x on upper troposphere chemistry remains to be resolved. If wet re-

moval is indeed occurring, predicted HNO₃ concentrations and the HNO₃/NO_x ratio can be reduced to a value close to those measured.

The heterogeneous hydrolysis of N₂O₅, reaction 5.54, has been suggested to play an important role in tropospheric chemistry (Dentener and Crutzen, 1993). Particles on which HNO₃ has formed can be transported to the dry upper troposphere, where it is expected that most water and HNO₃ would evaporate. From the point of view of explaining the reason for the mismatch in predicted and observed HNO₃/NO_x ratios, reaction 5.54 does not help; if the HNO₃ is indeed released the result should be, more or less, equivalent to that if the original NO₂ were simply converted to HNO₃ by OH. Understanding the relationship between HNO₃ and NO_x in the upper troposphere remains as an outstanding problem in atmospheric chemistry.

5.7.4 Ozone Budget of the Troposphere

The global tropospheric balance on ozone includes the following:

Production: transport from stratosphere; *in situ* chemical production

Loss: dry deposition at Earth's surface; *in situ* chemical destruction

Transport from the stratosphere and dry deposition rates can be estimated. The estimated downward flux of O₃ from the stratosphere is $(3-8) \times 10^{10}$ molecules cm⁻² s⁻¹. Loss of O₃ by dry deposition on the Earth's surface is estimated at about 8×10^{10} molecules cm⁻² s⁻¹ (Galbally and Roy, 1980). The principal mechanism for *in situ* chemical destruction of O₃ is photolysis and subsequent reaction of O(¹D) with H₂O, estimated also to be about 8×10^{10} molecules cm⁻² s⁻¹ (Lelieveld et al., 1993). The most difficult term to estimate, of the four, is the average rate of *in situ* chemical production. We know that *in situ* production of O₃ on the global scale is driven by the oxidation of CO and CH₄. Thus a good starting point is to estimate the amount of O₃ that can be produced globally from the oxidation of CO and CH₄. Average destruction rates of CO and CH₄ by OH reaction are 3×10^{11} molecules cm⁻² s⁻¹ and 1×10^{11} molecules cm⁻² s⁻¹, respectively (Lelieveld et al., 1993). If all the CO and CH₄ oxidation were to occur in NO_x-rich environments, yielding one O₃ molecule per each CO and 2.7 O₃ molecules for each CH₄ (this number accounts for oxidation of the formaldehyde formed as a product of CH₄ oxidation), the average global production rate⁶ of O₃ would be $3 \times 10^{11} + 2.7 \times 10^{11} \simeq 6 \times 10^{11}$ molecules cm⁻² s⁻¹. This production rate exceeds substantially the amount of O₃ that can be destroyed by reactions 5.21b and 5.23 and that which can be removed by deposition at the Earth's surface. The conclusion one reaches is that large portions of the troposphere must contain so little NO_x that these regions lie below the NO crossover concentration with respect to O₃ formation. At present, the tropospheric O₃ budget can be calculated by global chemical models, but the validity of such calculations must be assessed by careful comparisons with field data that provide all important components of production and loss. Nonetheless, there is little doubt that production and loss of tropospheric ozone are dominated by *in situ* chemistry and not by downward transport of O₃ from the stratosphere.

Manzerall et al. (1996) have quantified the ozone budget over remote high northern latitudes in summer using chemical and meteorological measurements between 0 and 6 km

⁶Globally, the methane oxidation chain has been estimated to result in a net annual loss of about 0.22 molecules of OH for every CH₄ molecule destroyed (Tie et al., 1992). The associated average annual yield of CO from methane oxidation is about 0.82 molecule of CO per molecule of CH₄ destroyed. The global methane oxidation chain is estimated to produce, as a result, about 1.15 molecules of ozone for each molecule of CH₄ destroyed.

made during the 1990 Arctic Boundary Layer Expedition (ABLE 3B). They included all components of the O_3 budget: sinks (*in situ* photochemical loss and deposition) and sources (*in situ* photochemical production, advection of O_3 into the region, O_3 production in biomass wildfire plumes, and downward transport from the upper troposphere/stratosphere). *In situ* production and loss were calculated from a photochemical model. The net influx of O_3 from pollution sources was estimated from the enhancement ratio of $\Delta[O_3]/\Delta[C_2Cl_4]$, scaled by the net influx of C_2Cl_4 . The contribution of O_3 produced in biomass wildfire plumes was estimated from the enhancement ratio of $\Delta[O_3]/\Delta[CO]$ in aged fire plumes. Photochemical production and loss of O_3 in the 0 to 6 km column were found to be approximately equal. Of the overall sources of O_3 in the region, *in situ* photochemical production by background NO (at 5 to 10 ppt) accounted for 62%, influx of stratospheric O_3 , 27%, long-range transport, 9%, and production in wildfire plumes, only 2%. One should note, however, that long-range transport and fires may enhance the background NO_x and thereby promote the photochemical production of O_3 .

5.7.5 Climatology of Regional Tropospheric Ozone

Major regional episodes of high concentrations of ozone are associated with slow-moving, high-pressure weather systems. These systems are characterized by widespread sinking of air through most of the troposphere. The subsidence of air associated with large high-pressure systems creates a pronounced inversion of the normal temperature profile (normally temperature decreases with height in the troposphere), which serves as a strong lid to contain pollutants in a shallow layer in the troposphere. During an inversion, the temperature of the air in the lower troposphere increases with height, and the cooler air below does not mix with the warmer air above. Because winds associated with major high-pressure systems are generally light, there is a greater chance for precursors to accumulate in the atmospheric boundary layer. The often cloudless and warm conditions associated with large high-pressure systems also are favorable for the photochemical production of ozone.

In the eastern United States and Europe, the most severe regional ozone episodes occur when a slow-moving, high-pressure system develops in the summer (Logan, 1989). This is the time with the greatest amount of daylight, when solar radiation is most direct (the Sun is at a small zenith angle) and air temperatures become quite high. As the slow-moving air in the shallow boundary layer passes over major metropolitan areas, precursor concentrations rise, and, as the air slowly flows around the high-pressure system, photochemical production of ozone occurs at peak rates. Major high-pressure systems at the Earth's surface are associated with ridges of high-pressure surfaces in the middle and upper troposphere. High ozone episodes are often terminated by the passage of a front that brings cooler, cleaner air to the region.

Clouds play an important role in transporting pollutants from the atmospheric boundary layer into the lower, middle, and upper troposphere, a process known as *venting* (e.g., Gidel, 1983; Chatfield and Crutzen, 1984; Greenhut et al., 1984; Greenhut, 1986; Ching and Alkezweeny, 1986; Dickerson et al., 1987; Ching et al., 1988). The effect of clouds on vertical transport depends on their size and type. Although major high-pressure systems may be cloud-free, weaker systems may permit the formation of a variety of cloud types. Cumulonimbus clouds are convective clouds of significant height (often the entire height of the troposphere). Precipitation is important in their life cycle, organization, and energy transformation. The fundamental unit of a cumulonimbus is a cell, shown on radar as a region of concentrated precipitation, and characterized as a region of coherent updraft and

downdraft. Cumulonimbus clouds are classified by their cells, organization, and life cycles. Ordinary cumulonimbi contain a single cell that has a life cycle of 45 minutes to an hour. Many thunderstorms are composed of a number of cells, each having lifetimes of 45 to 60 minutes. These multicell storms can last for several hours and vertically redistribute large quantities of ozone and its precursors. Supercell storms, composed of a single steady cell, with strong updrafts and downdrafts, can last 2 to 6 hours and inject large quantities of pollutants into the upper troposphere (Dickerson et al., 1987; Pickering et al., 1989). Not all cases of convection cause such transport (e.g., convective clouds above a cold front; Pickering et al., 1988). Convective redistribution of ozone precursors may lead to an increase in the production rate of ozone averaged through the troposphere (Pickering et al., 1990).

Example 5.3 The Troposphere/Stratosphere Transition The transition from troposphere to stratosphere is traditionally defined based on the reversal of the atmospheric temperature profile. That transition is also dramatically reflected in how the concentrations of trace species vary with altitude below and above the tropopause. Of trace species, HO₂ and OH exhibit perhaps the most profound differences across the tropopause (Wennberg et al., 1995). In the lower stratosphere HO₂ and OH participate in HO_x Cycle 4, which is the predominant cycle involved in O₃ removal in that portion of the stratosphere. We saw in Chapter 4 that in the lower stratosphere the HO₂/OH ratio is described by

$$\frac{[\text{HO}_2]}{[\text{OH}]} = \frac{k_{4,11} [\text{O}_3]}{k_{4,36} [\text{NO}] + k_{4,14} [\text{O}_3]}$$

The presence of NO short-circuits HO_x Cycle 4 by reconverting HO₂ back to OH before it has a chance to react with O₃. This ratio varies from about 4 to 7 and decreases as [NO] increases. [OH] itself is essentially independent of [NO] and depends almost entirely on solar zenith angle. This independence of OH on NO is a result of the fact that the increase of OH that results from reaction 4.36 is offset almost exactly by a decrease of the rates of reactions that generate OH, reactions 4.14, 4.40, and 4.41. This occurs because the HO₂ that participates in reaction 4.36 is not otherwise available for reactions 4.14 and 4.40.

The behavior of HO₂ and OH in the upper troposphere is dominated by CO chemistry. (Because of its 1 to 3 month lifetime, CO is more or less uniformly mixed up to the tropopause. Above the tropopause, CO falls off with increasing altitude. Because of the much slower vertical transport rate in the stratosphere, the rate of the CO–OH reaction competes with the rate of vertical mixing.) Tropospheric CO oxidation proceeds according to reactions 5.24 and 5.25, coupled to reactions 5.1 to 5.3. (Note that 4.36 and 5.25 are the same reaction.) From Section 5.2 we can obtain an expression for the HO₂/OH ratio in the upper troposphere. Based on the steady-state relation for HO₂, we obtain

$$\frac{[\text{HO}_2]}{[\text{OH}]} = \frac{k_{5,24} [\text{CO}]}{k_{5,25} [\text{NO}]}$$

As one proceeds up in the troposphere, the NO₂/NO_x ratio decreases, achieving its lowest value at the tropopause, and then increases moving into the stratosphere. The increase of NO₂ relative to NO in the lower stratosphere is the result of reaction 4.36 (5.25). (The NO_x/NO₃ ratio is more or less constant in the upper troposphere, falling off as one goes

into the stratosphere. This fall off reflects the influence of the stratospheric aerosol layer in promoting the heterogeneous formation of HNO_3 .)

Hydroxyl radical levels in the upper troposphere vary from about 0.01 to 0.1 ppt. In the lower stratosphere OH depends on solar zenith angle and ranges up to about 1 ppt. As noted above, OH is essentially independent of NO in the lower stratosphere, whereas in the upper troposphere OH decreases as NO decreases. This fundamentally different behavior of OH with respect to changes in NO characterizes the troposphere/stratosphere transition.

5.8 CHEMISTRY OF NONMETHANE ORGANIC COMPOUNDS IN THE TROPOSPHERE

In the lower troposphere in all but the most pristine areas, and especially in urban areas, the chemical reactions of biogenic and anthropogenic VOC and anthropogenic NO_x emissions dominate over those of methane and its degradation products. Although, in principle, an extension of the chemistry of the clean, methane-dominated troposphere, the chemistry of the urban and regional troposphere is significantly more complicated because of the presence of many VOCs of various classes (alkanes, alkenes, and aromatic hydrocarbons) and the added complexities in the chemistry of these organic species.

5.8.1 Alkanes

Under tropospheric conditions, alkanes react with OH and NO_3 radicals with the latter process generally being of minor ($\leq 10\%$) importance as an atmospheric loss process under daytime conditions. Both reactions proceed via H-atom abstraction from C—H bonds,



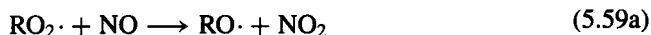
to produce the alkyl radical, R. Any H atom in the alkane is susceptible to OH attack. Generally, the OH radical will tend to abstract the most weakly bound hydrogen atom in the molecule. The overall rate constant reflects the number of available hydrogen atoms and the strengths of the C—H bonds for each of these. Correlations have been developed for calculating the OH rate constant of alkanes that account for the number of primary ($-\text{CH}_3$), secondary, ($-\text{CH}_2-$), and tertiary ($>\text{CH}$) hydrogen atoms in the molecule (Atkinson, 1987, 1994). Hydroxyl attack on a tertiary hydrogen atom is generally faster than that on a secondary H atom and is the slowest for primary H atoms. For propane, $\text{CH}_3\text{CH}_2\text{CH}_3$, for example, these structure-activity correlations predict that 70% of the OH reaction occurs by H-atom abstraction from the secondary carbon atom ($-\text{CH}_2-$) and 30% from the $-\text{CH}_3$ groups.

As with the methyl radical, the resulting alkyl (R) radical reacts rapidly, and exclusively, with O_2 under atmospheric conditions to yield an alkyl peroxy radical (RO_2) (see the comprehensive reviews of the chemistry of RO_2 radicals by Lightfoot et al., 1992, and Wallington et al., 1992):



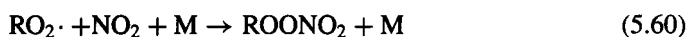
These alkyl peroxy radicals can be classed as primary, secondary, or tertiary depending on the availability of H atoms: $\text{RCH}_2\text{OO}\cdot$ (primary); $\text{RR}'\text{CHOO}\cdot$ (secondary); $\text{RR}'\text{R}''\text{COO}\cdot$ (tertiary). The alkyl radical- O_2 addition occurs with a room-temperature rate constant of $\geq 10^{-12} \text{ cm}^3 \text{ molecule}^{-1} \text{ s}^{-1}$ at atmospheric pressure. Given the high concentration of O_2 , the $\text{R} + \text{O}_2$ reaction can be considered as instantaneous relative to other reactions occurring such as those that form R in the first place. Henceforth, the formation of an alkyl radical will be considered to be equivalent to the formation of an alkyl peroxy radical.

Under tropospheric conditions, these alkyl peroxy (RO_2) radicals react with NO, via two pathways,



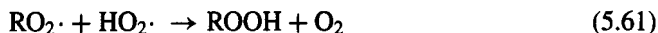
For alkyl peroxy radicals, reaction 5.59a can form the corresponding alkoxy ($\text{RO}\cdot$) radical together with NO_2 , or the corresponding alkyl nitrate, reaction 5.59b, with the yield of the alkyl nitrate increasing with increasing pressure and with decreasing temperature. For secondary alkyl peroxy radicals at 298 K and 760 Torr total pressure, the alkyl nitrate yields increase monotonically from <0.014 for a C_2 alkane up to ~ 0.33 for a C_8 alkane (Atkinson, 1990). The rate constant for the $\text{CH}_3\text{O}_2\cdot + \text{NO}$ reaction is (see Table B.1): $k_{5.40} = 4.2 \times 10^{-12} \exp(180/T) = 7.7 \times 10^{-12} \text{ cm}^3 \text{ molecule}^{-1} \text{ s}^{-1}$ at 298 K. Rate constants for higher ($\geq \text{C}_2$) alkyl peroxy radicals with NO are taken as (Atkinson, 1994): $k_{5.59} = 4.9 \times 10^{-12} \exp(180/T) = 8.9 \times 10^{-12} \text{ cm}^3 \text{ molecule}^{-1} \text{ s}^{-1}$ at 298 K.

Alkyl peroxy radicals react with NO_2 by combination to yield the peroxy nitrates (recall reaction 5.41),

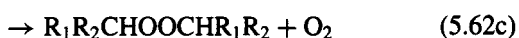
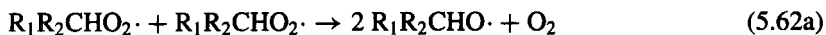


Limiting high pressure rate constants for $\geq \text{C}_2$ alkyl peroxy radicals are identical to that for the $\text{C}_2\text{H}_5\text{O}_2\cdot$ radical: $k_{5.60} = 9 \times 10^{-12} \text{ cm}^3 \text{ molecule}^{-1} \text{ s}^{-1}$, independent of temperature over the range 250 to 350 K.

Alkyl peroxy radicals also react with HO_2 radicals,



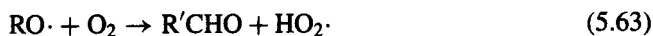
or with other RO_2 radicals. The self-reaction of $\text{RO}_2\cdot$ and $\text{RO}_2\cdot$ proceeds by the three pathways



Pathway 5.62b is not accessible for tertiary RO_2 radicals, and pathway 5.62c is expected to be of negligible importance. Under urban conditions, and indeed possibly for much of the lower troposphere in anthropogenically influenced continental regions, reaction with NO is the dominant reaction pathway for RO_2 radicals.

Alkoxy ($\text{RO}\cdot$) radicals are formed in the reaction of alkyl peroxy ($\text{RO}_2\cdot$) radicals with NO, reaction 5.59a. Subsequent reactions of alkoxy radicals determine to a large extent the

products resulting from the atmospheric oxidation of VOCs. Alkoxy radicals react under tropospheric conditions via a variety of processes: unimolecular decomposition, unimolecular isomerization, or reaction with O_2 . Alkoxy radicals with fewer than five carbon atoms are too short to undergo isomerization; for these the competitive processes are unimolecular decomposition versus reaction with O_2 . The general alkoxy radical- O_2 reaction involves abstraction of a hydrogen atom by O_2 to produce an HO_2 radical and a carbonyl species,



Rate constants for the $CH_3O\cdot + O_2$ and $C_2H_5O\cdot + O_2$ reactions are given in Table B.1. For primary ($RCH_2O\cdot$) and secondary ($R_1R_2CHO\cdot$) alkoxy radicals formed from the alkanes (Atkinson, 1994),⁷

$$\begin{aligned} k_{5.63}(RCH_2O\cdot + O_2) &= 6.0 \times 10^{-14} \exp(-550/T) \text{ cm}^3 \text{ molecule}^{-1} \text{ s}^{-1} \\ &= 9.5 \times 10^{-15} \text{ at } 298 \text{ K} \\ k_{5.63}(R_1R_2CHO\cdot + O_2) &= 1.5 \times 10^{-14} \exp(-200/T) \text{ cm}^3 \text{ molecule}^{-1} \text{ s}^{-1} \\ &= 8 \times 10^{-15} \text{ at } 298 \text{ K} \end{aligned}$$

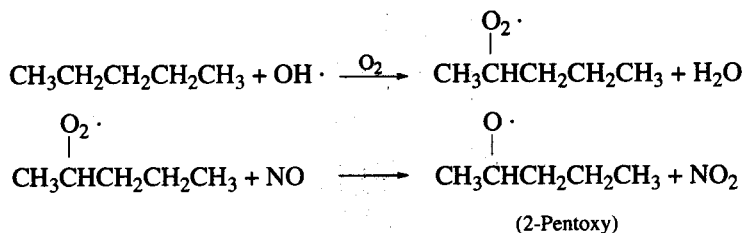
Tertiary alkoxy radicals are not expected to react with O_2 because of the absence of a readily available hydrogen atom.

Unimolecular decomposition, on the other hand, produces an alkyl radical and a carbonyl,



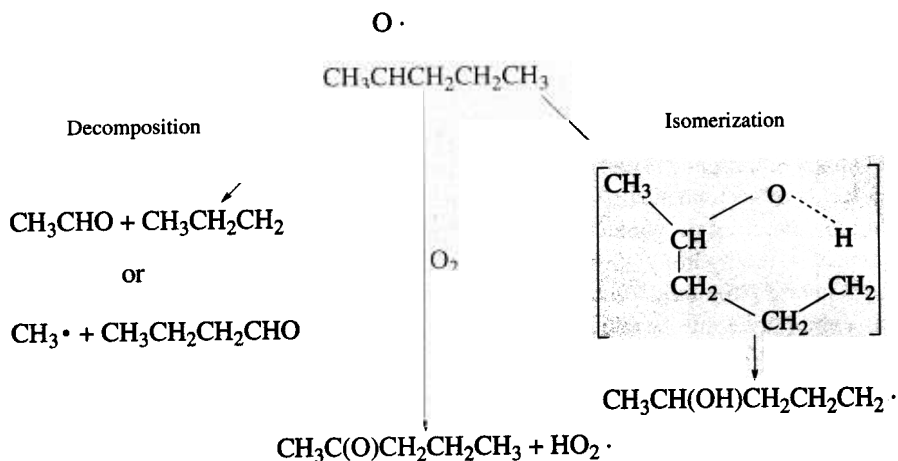
Atkinson (1994) presents a correlation that allows one to determine the relative importance of O_2 reaction and decomposition for a particular alkoxy radical. Generally, reaction with O_2 is the preferred path for primary alkoxy radicals that have C-atom chains of two or fewer C atoms in length attached to the carbonyl group.

To illustrate alkoxy radical isomerization, let us consider the OH reaction of *n*-pentane. The *n*-pentane-OH reaction proceeds as follows to produce the 2-pentoxy radical:



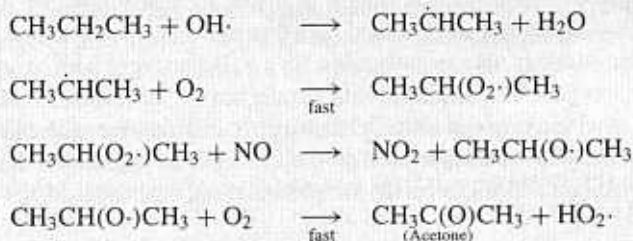
⁷Note a slight difference in the value of the preexponential factor between that in Table B.1 and that recommended by Atkinson (1994).

The 2-pentoxy radical can then react with O_2 , decompose, or isomerize:

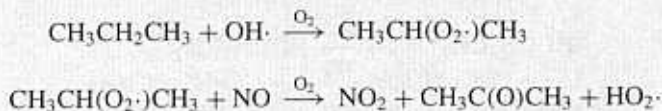


Rate constants for alkoxy radical isomerizations can be combined with rate constants for alkoxy radical decomposition and reaction with O_2 to predict the relative importance of the three pathways (Atkinson, 1994). Alkoxy radicals can also react with NO and NO_2 , but under ambient tropospheric conditions these reactions are generally of negligible importance.

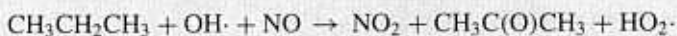
Example 5.4 Atmospheric Photooxidation of Propane To illustrate alkane chemistry, consider the atmospheric photooxidation of propane:



Internal H-atom abstraction predominates in the initial OH attack. As we have been doing, we can eliminate the fast reactions from the mechanism by combining them with the foregoing rate-determining step. Thus the above four reactions may be expressed more concisely as



If we further take the liberty of assuming that the $CH_3CH(O_2\cdot)CH_3$ radical is produced and consumed only in these two reactions, a good assumption in this case, these two reactions can be written as a single overall reaction,



where the reaction converts one molecule of NO to one molecule of NO₂. If we assume further that the sole fate of the HO₂ radical is reaction with NO, we can eliminate HO₂ from the right-hand side:

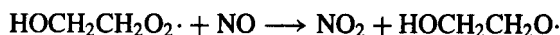
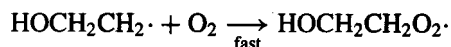
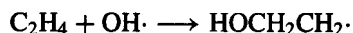


In writing the reaction this way, we can clearly see that the net effect of the hydroxyl radical attack on propane is conversion of two molecules of NO to NO₂, the production of one molecule of acetone, CH₃C(O)CH₃, and the regeneration of the hydroxyl radical. Thus the photooxidation of propane can be viewed as a chain reaction mechanism in which the active species, the hydroxyl radical, is regenerated. For larger alkanes, such as *n*-butane, the atmospheric photooxidation mechanisms become more complex, although they continue to exhibit the same essential features of the propane degradation path. Two important issues arise in the reaction mechanisms of the higher alkanes. The first is that some fraction of the peroxyalkyl-NO reactions lead to alkyl nitrates rather than NO₂ and an alkoxy radical. The second is that the larger alkoxy radicals may isomerize as well as react with O₂. Figure 5.7 shows the mechanism of the *n*-butane-OH reaction (Jungkamp et al., 1997).

5.8.2 Alkenes

We now proceed to the atmospheric chemistry of alkenes (or olefins). Alkenes are constituents of gasoline fuels and motor vehicle exhaust emissions. This class of organic compounds accounts for about 10% of the nonmethane organic compound concentration in the Los Angeles air basin (Lurmann and Main, 1992) and other U.S. cities (Chameides et al., 1992). Because of their high reactivity with respect to ozone formation, alkenes are important contributors to overall ozone formation in urban areas. By now we fully expect that alkenes will react with the hydroxyl radical, and that is indeed the case. Because of the double bonded carbon atoms in alkene molecules, they will also react with ozone, the NO₃ radical, and atomic oxygen. The reaction with ozone can be an important alkene oxidation path, whereas that with oxygen atoms is generally not competitive with the other paths because of the extremely low concentration of O atoms. Let us begin with the hydroxyl radical reaction mechanism and focus on the simplest alkene, ethene (C₂H₄).

a. OH Reaction We just saw that the initial step in OH attack on an alkane molecule is abstraction of a hydrogen atom to form a water molecule and an alkyl radical. In the case of alkenes, OH adds to the double bond rather than abstracting a hydrogen atom.⁸ The ethene-OH reaction mechanism is



⁸Hydrogen atom abstraction from —CH₃ groups accounts generally for <5% of the overall OH reaction of ethene and the methyl-substituted ethenes (propene, 2-methyl propene, the 2-butenes, 2-methyl-2-butene, and 2,3-dimethyl-2-butene). For alkenes with alkyl side chains, perhaps up to 10% of the OH reaction proceeds by H-atom abstraction, but we will neglect that path here.

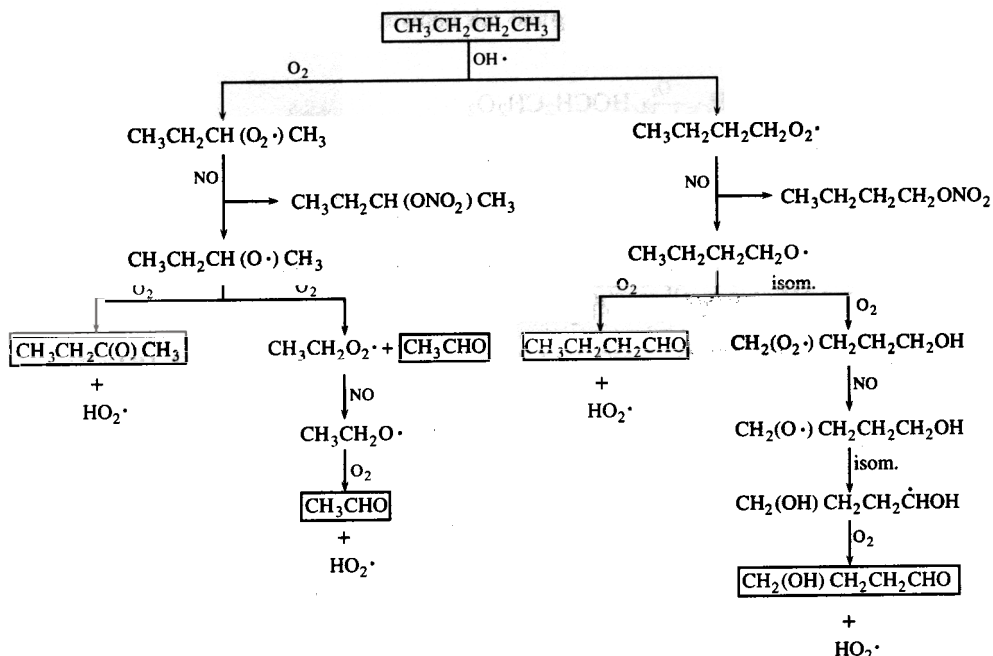
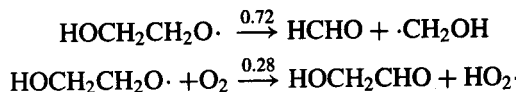
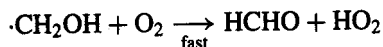


FIGURE 5.7 Atmospheric photooxidation mechanism for *n*-butane. The only significant reaction of *n*-butane is with the hydroxyl radical. Approximately 85% of that reaction involves H-atom abstraction from an internal carbon atom and 15% from a terminal carbon atom. In the terminal H-atom abstraction path, the $\text{CH}_3\text{CH}_2\text{CH}_2\text{CH}_2\text{O}\cdot$ alkoxy radical is estimated to react with O_2 25% of the time and isomerize 75% of the time. The second isomerization is estimated to be a factor of 5 faster than the first isomerization of the $\text{CH}_3\text{CH}_2\text{CH}_2\text{CH}_2\text{O}\cdot$ radical, so that competition with O_2 reaction is not considered at this step. The predominant fate of α -hydroxy radicals is reaction with O_2 . For example, $\cdot\text{CH}_2\text{OH} + \text{O}_2 \rightarrow \text{HCHO} + \cdot\text{HO}_2$, and $\text{CH}_3\dot{\text{C}}\text{HOH} + \text{O}_2 \rightarrow \text{CH}_3\text{CHO} + \cdot\text{HO}_2$. In the *n*-butane mechanism, the α -hydroxy radical, $\text{CH}_2(\text{OH})\text{CH}_2\text{CH}_2\dot{\text{C}}\text{HOH}$ reacts rapidly with O_2 to form 4-hydroxy-1-butanal, $\text{CH}_2(\text{OH})\text{CH}_2\text{CH}_2\text{CHO}$. In the internal H-atom abstraction path, the alkoxy radical $\text{CH}_3\text{CH}_2\text{CH}(\text{O}\cdot)\text{CH}_3$ reacts with O_2 to yield methyl ethyl ketone (MEK), $\text{CH}_3\text{CH}_2\text{C}(\text{O})\text{CH}_3$, and decomposes to form CH_3CHO and $\text{CH}_3\text{CH}_2\cdot$, which, after reaction with O_2 and NO and O_2 again, yields another molecule of CH_3CHO and $\cdot\text{HO}_2$.

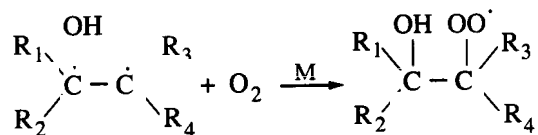
The $\text{HOCH}_2\text{CH}_2\text{O}\cdot$ radical then decomposes and reacts with O_2 :



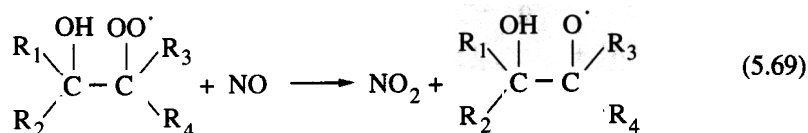
The numbers over the arrows indicate the fraction of the reactions that lead to the indicated products at 298 K. Finally, the $\cdot\text{CH}_2\text{OH}$ radical reacts with O_2 to give formaldehyde and a hydroperoxyl radical,



followed by rapid addition of O₂ to yield the corresponding β-hydroxyalkyl peroxy radicals,



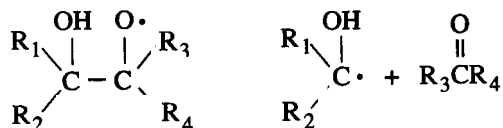
In the presence of NO, the β-hydroxyalkyl peroxy radical reacts with NO to form either the β-hydroxyalkoxy radical plus NO₂ or the β-hydroxynitrate:⁹



Rate constants for the reactions of β-hydroxyalkyl peroxy radicals with NO are essentially identical to those for the reaction of NO with more than C₂ alkyl peroxy radicals formed from alkanes (Atkinson, 1994).

The β-hydroxyalkoxy radicals can then decompose, react with O₂, or isomerize. Available data show that, apart from ethene, for which reaction of the HOCH₂CH₂O· radical with O₂ and decomposition are competitive, the β-hydroxyalkoxy radicals formed subsequent to OH addition to ≥C₃ alkenes undergo decomposition and the reaction with O₂ is negligible.

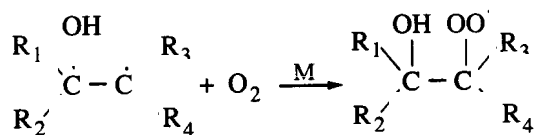
The decomposition reaction is



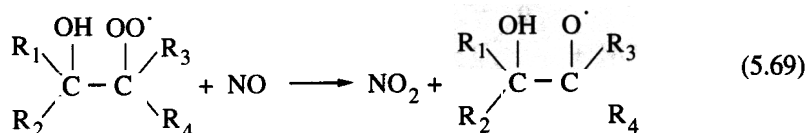
Carbonyl yields from alkene-OH reactions are summarized in Table 5.1. The yields of HCHO and RCHO arising from cleavage of the —C=C— bond of 1-alkenes RCH=CH₂ decrease monotonically from ≥0.90 for propene and 1-butene to 0.21 to 0.39 for 1-octene. H-atom abstraction from the CH₂ groups in the 1-alkenes is expected to account for an increasing fraction of the overall OH radical reaction as the carbon number of the 1-alkenes increases, with about 15% of the 1-heptene reaction being estimated to proceed by H-atom abstraction from the secondary CH₂ groups. The propene-OH reaction mechanism is shown in Figure 5.8.

⁹The β-hydroxynitrate formation pathway accounts for only ~1 to 1.5% of the overall NO reaction pathway at 298 K for propene (Shepson et al., 1985). The yields of β-hydroxynitrates from the propene-OH and 1-butene-OH reactions are about a factor of 2 lower than those of alkyl nitrates from the propane-OH and *n*-butane-OH reactions. These observations suggest that the formation yields of β-hydroxynitrates from the OH reaction with higher 1-alkenes could also be a factor of 2 lower than those from the reactions with the corresponding *n*-alkanes.

followed by rapid addition of O_2 to yield the corresponding β -hydroxyalkyl peroxy radicals,



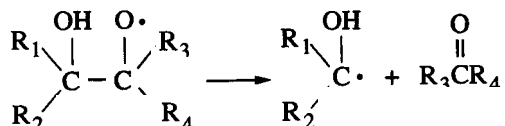
In the presence of NO, the β -hydroxyalkyl peroxy radical reacts with NO to form either the β -hydroxyalkoxy radical plus NO_2 or the β -hydroxynitrate:⁹



Rate constants for the reactions of β -hydroxyalkyl peroxy radicals with NO are essentially identical to those for the reaction of NO with more than C_2 alkyl peroxy radicals formed from alkanes (Atkinson, 1994).

The β -hydroxyalkoxy radicals can then decompose, react with O_2 , or isomerize. Available data show that, apart from ethene, for which reaction of the $HOCH_2CH_2O\cdot$ radical with O_2 and decomposition are competitive, the β -hydroxyalkoxy radicals formed subsequent to OH addition to $\geq C_3$ alkenes undergo decomposition and the reaction with O_2 is negligible.

The decomposition reaction is



Carbonyl yields from alkene-OH reactions are summarized in Table 5.1. The yields of HCHO and RCHO arising from cleavage of the $-C=C-$ bond of 1-alkenes $RCH=CH_2$ decrease monotonically from ≥ 0.90 for propene and 1-butene to 0.21 to 0.39 for 1-octene. H-atom abstraction from the CH_2 groups in the 1-alkenes is expected to account for an increasing fraction of the overall OH radical reaction as the carbon number of the 1-alkenes increases, with about 15% of the 1-heptene reaction being estimated to proceed by H-atom abstraction from the secondary CH_2 groups. The propene-OH reaction mechanism is shown in Figure 5.8.

⁹The β -hydroxynitrate formation pathway accounts for only ~ 1 to 1.5% of the overall NO reaction pathway at 298 K for propene (Shepson et al., 1985). The yields of β -hydroxynitrates from the propene-OH and 1-butene-OH reactions are about a factor of 2 lower than those of alkyl nitrates from the propane-OH and *n*-butane-OH reactions. These observations suggest that the formation yields of β -hydroxynitrates from the OH reaction with higher 1-alkenes could also be a factor of 2 lower than those from the reactions with the corresponding *n*-alkanes.

TABLE 5.1 Carbonyl Yields from 1-Alkene-OH Reactions

1-Alkene	Yield	
	HCHO	RCHO
Propene	0.86	0.98 (acetaldehyde)
1-Butene		0.94 (propanal)
1-Pentene	0.88	0.73 (butanal)
1-Hexene	0.57	0.46 (pentanal)
1-Heptene	0.49	0.30 (hexanal)
1-Octene	0.39	0.21 (heptanal)

Source: Atkinson et al. (1995b).

b. NO_3 Reaction Because of its strong oxidizing capacity and its relatively high nighttime concentrations, the NO_3 radical can play an important role in the nighttime removal of atmospheric organic species. Although the reaction of NO_3 with trace gases is significantly slower than that of OH, NO_3 can be present in much higher concentrations than OH, so that the overall reaction with many species is comparable for OH and NO_3 radicals. For example, from long-term observations at the coastal site of Kap Arkona, Germany, the average NO_3 level was found to be about 3 ppt, corresponding to about 8×10^7 molecules cm^{-3} (24 hour average). By comparison, the 24 hour average OH concentration is about 10^6 molecules cm^{-3} (Platt and Heintz, 1994). Since the reaction of OH with organic species is 10 to 1000 times faster than that of NO_3 , the oxidation potential of the two radicals is in the same ballpark.

Alkenes react with the nitrate radical (Barnes et al., 1990; Hjorth et al., 1990; Atkinson, 1991). As in OH-alkene reactions, NO_3 adds to the double bond and H-atom abstraction is relatively insignificant,

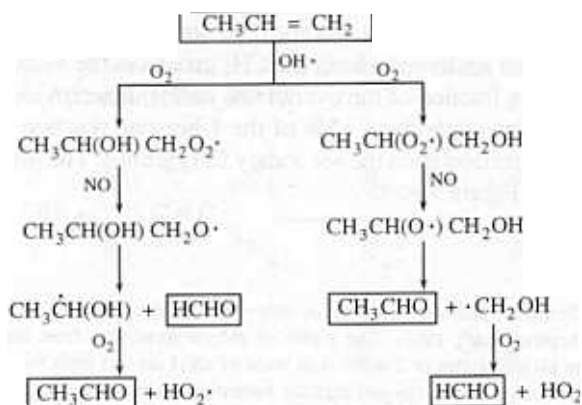
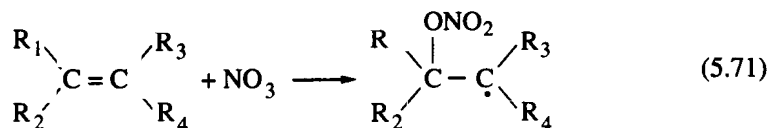
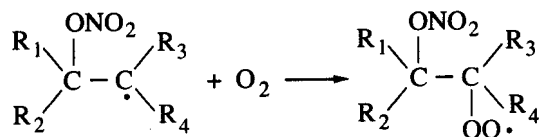
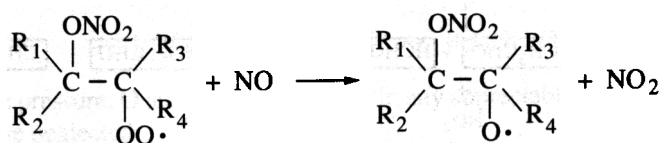


FIGURE 5.8 Propene-OH reaction mechanism.

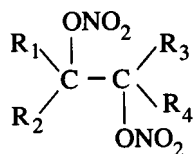
This is followed by rapid O₂ addition:



to produce the β -nitroalkyl peroxy radical, subsequent reactions of which are

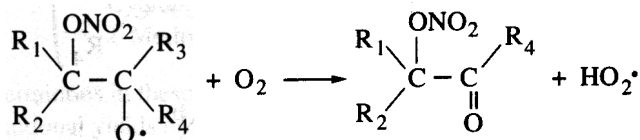


(5.73)

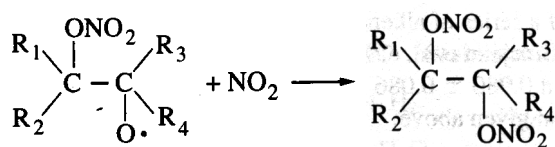
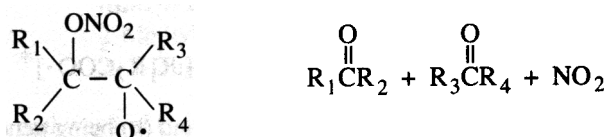


The latter reaction is expected to be minor.

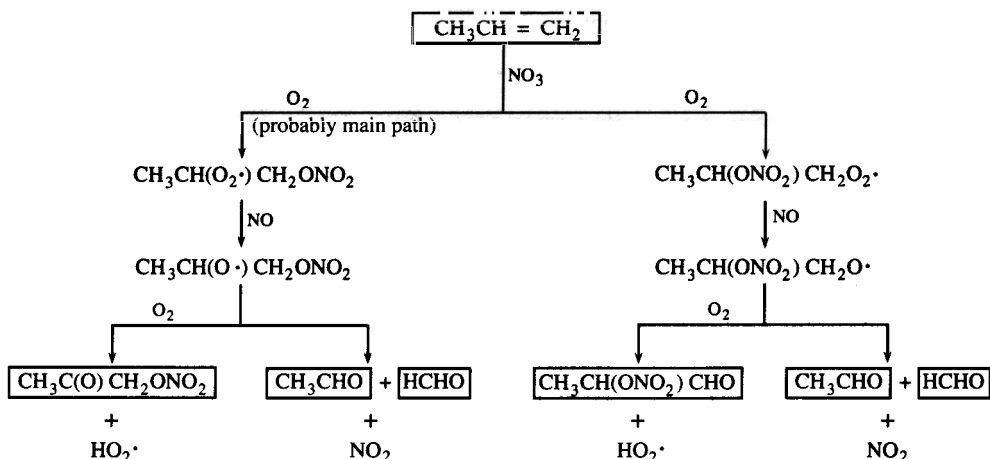
Further reactions of β -nitroalkoxy radicals include



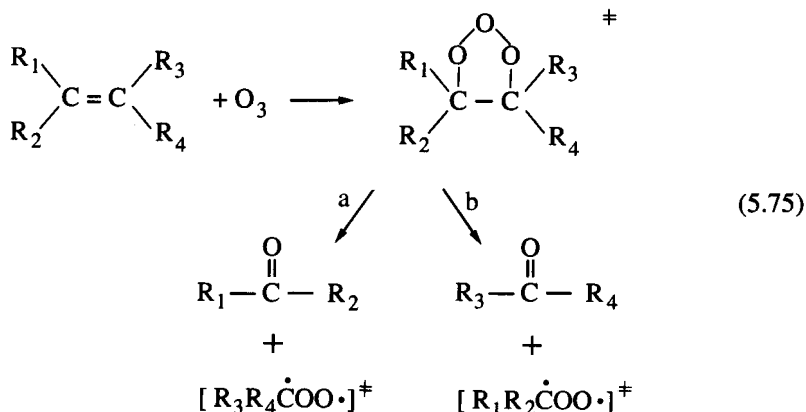
if R₃ = H



of which the last reaction is expected to be minor. Figure 5.9 shows the mechanism of the propene-NO₂ reaction.

FIGURE 5.9 Propene-NO₃ reaction mechanism.

c. Ozone Reaction The presence of the double bond renders alkenes susceptible to reaction with ozone. Reactions with ozone are, in fact, competitive with the daytime OH radical reactions and the nighttime NO₃ radical reaction as a tropospheric loss process for the alkenes. The ozone-alkene reaction proceeds via initial O₃ addition to the olefinic double bond, followed by rapid decomposition of the resulting molozonide:



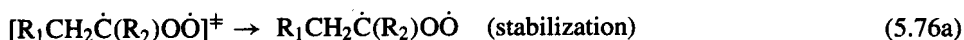
with the relative importance of the reaction pathways (a) and (b) being generally assumed to be approximately equal (Atkinson and Carter, 1984).

Atkinson et al. (1995a) and Grosjean et al. (1996) have measured the carbonyl product yields for the reaction of a series of alkenes with O₃. Yields of primary (from the initial O₃ attack) carbonyls from Grosjean et al. (1996) averaged 0.993 ± 0.141 (one standard deviation) for 22 alkenes and 0.980 ± 0.086 for styrene. These results are consistent with the initial alkene-O₃ reaction given above:



The kinetics and products of the gas-phase alkene-O₃ reaction have been studied extensively (Atkinson and Carter, 1984; Horie and Moortgat, 1991; Grosjean et al., 1994;

Atkinson, 1994; Horie et al., 1994 a, b; Neeb et al., 1995; Thomas et al., 1995; Neeb et al., 1996) and are reasonably well understood for a large number of the smaller alkenes. The major mechanistic issue concerns the fate, under atmospheric conditions, of the initially energy-rich Criegee biradical, which can be collisionally stabilized or can undergo unimolecular decomposition.



At atmospheric pressure, O atoms are not formed in any appreciable amount, so path 5.76b can generally be neglected.

Hydroxyl radicals have been observed to be formed from alkene-O₃ reactions, sometimes with close to a unit yield (1 molecule of OH per 1 molecule of alkene reacted) (Atkinson and Aschmann, 1993). Atkinson et al. (1995a) reported OH radical yields from a series of alkene-O₃ reactions:

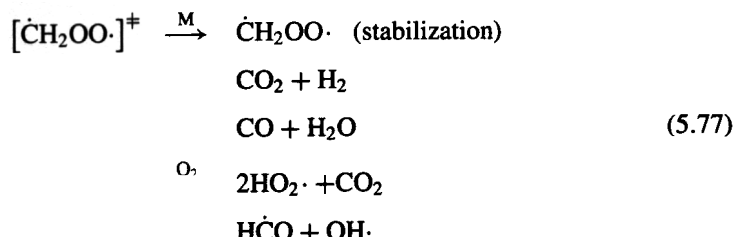
Alkene	OH Yield
1-Pentene	0.37
1-Hexene	0.32
1-Heptene	0.27
1-Octene	0.18
2,3-Dimethyl-1-butene	0.50
Cyclopentene	0.61
1-Methylcyclohexene	0.90

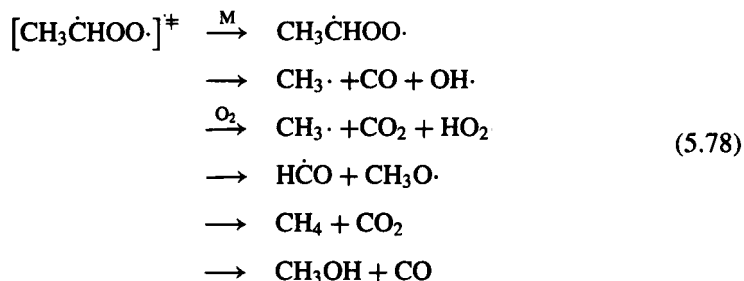
(Estimated uncertainties in these yields are a factor of ~1.5.)

At 1 atm, fractional yields of stabilized biradicals are estimated as (Atkinson, 1994):

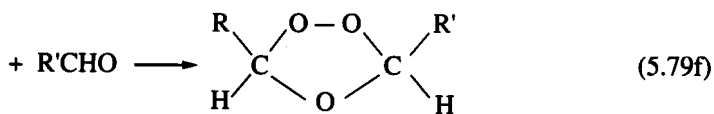
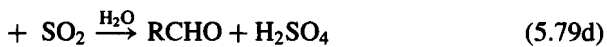
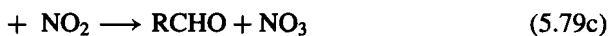
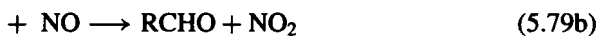
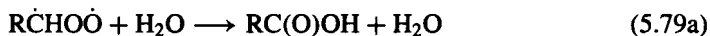
Ethene	0.37
Propene	0.275
<i>trans</i> -2-Butene	0.18
2-Methylpropene	0.174
2,-3-Dimethyl-2-butene	0.30

The reaction pathways of Criegee biradicals are generally well established for the first two compounds in the series although the exact fractions that proceed via each individual path are still open to question (Horie and Moortgat, 1991):

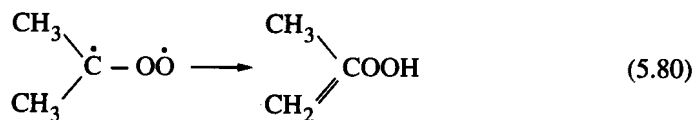




The stabilized biradicals can react with a number of species:



In addition, biradicals such as $(\text{CH}_3)_2\text{COO}\cdot$ may undergo unimolecular isomerization



Rate constants for reactions of $\dot{\text{C}}\text{H}_2\text{OO}\cdot$ radicals with the following species, relative to the reaction with SO_2 , are

HCHO	0.25
CO	0.0175
H ₂ O	0.00023
NO ₂	0.014

It appears that the reaction of stabilized biradicals with H₂O will predominate under atmospheric conditions (Atkinson, 1994).

5.8.3 Aromatics

Aromatic compounds are of great interest in the chemistry of the urban atmosphere because of their abundance in motor vehicle emissions and because of their reactivity with respect to ozone and organic aerosol formation. Understanding the atmospheric oxidation mechanisms of aromatics has long been cited as the most critical need in further development of reaction mechanisms for the urban and regional atmosphere (National Research Council, 1991). The major atmospheric sink for aromatics is reaction with the hydroxyl radical. Whereas rate constants for the OH reaction with aromatics have been well characterized (Atkinson, 1994), mechanisms of aromatic oxidation following the initial OH attack have been highly uncertain. Aromatic compounds of concern in urban atmospheric chemistry are given in Figure 5.10.

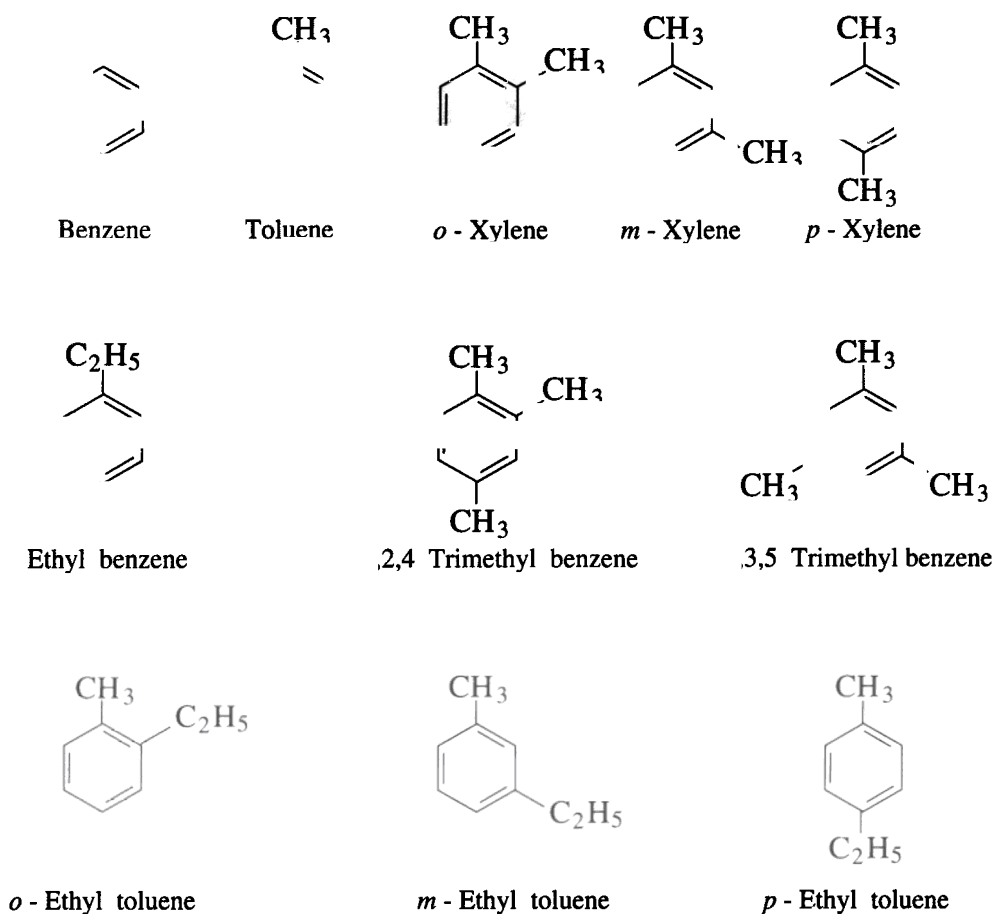
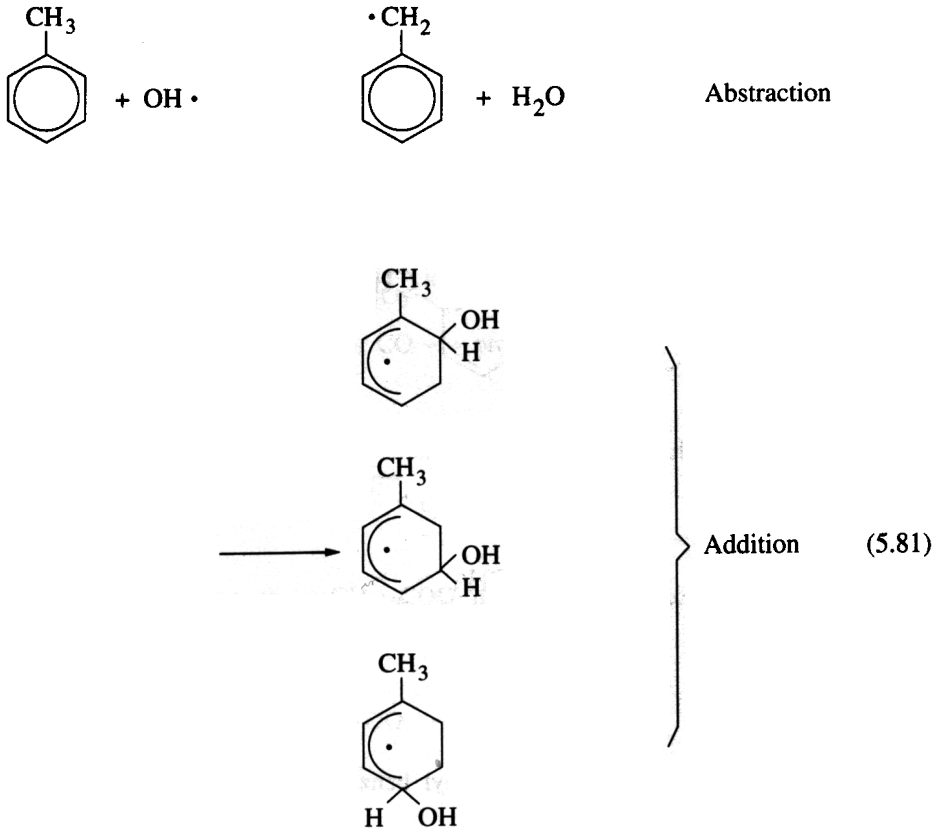
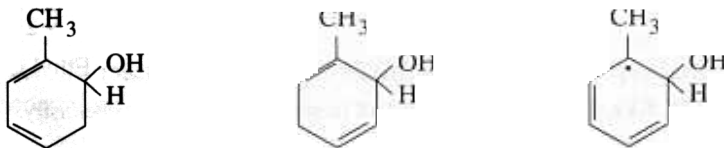


FIGURE 5.10 Aromatic compounds of interest in tropospheric chemistry.

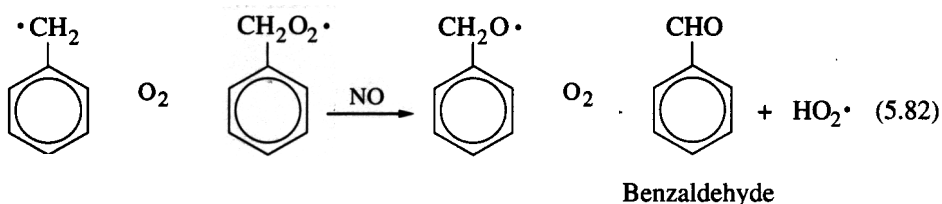
The aromatic-OH radical reaction proceeds via two pathways: (a) a minor one (of order 10%) involving H-atom abstraction from C—H bonds of, for benzene, the aromatic ring, or for alkyl-substituted aromatic hydrocarbons, the alkyl-substituent groups; and (b) a major reaction pathway (of order 90%) involving OH radical addition to the aromatic ring. For example, for toluene these reaction pathways are:



For the first addition product the structure above denotes the radicals,

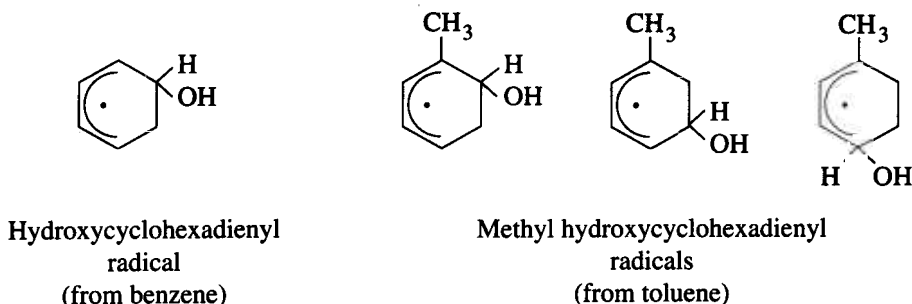


The H-atom abstraction pathway leads mainly to the formation of aromatic aldehydes

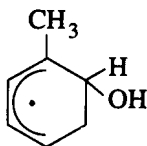


As noted above, this H-atom abstraction pathway is minor, accounting for <10% of the overall OH radical reaction for benzene and the alkyl-substituted aromatic hydrocarbons.

The radicals resulting from OH addition to the aromatic ring are named as follows:



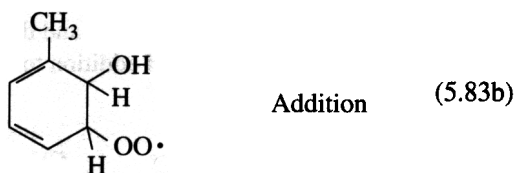
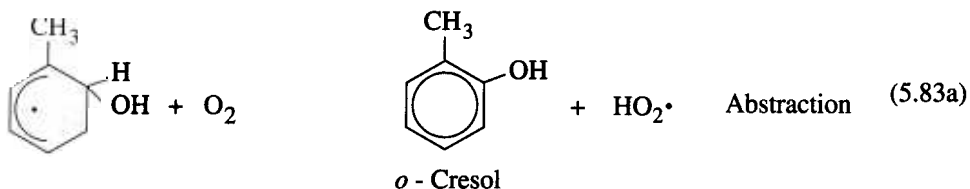
For toluene, and other aromatics, there are several possible sites of attack for the OH radical. Some sites are less sterically hindered than others or are favored because of stabilizations resulting from group interactions. Andino et al. (1996) have performed *ab initio* calculations to determine the most energetically favored structures resulting from OH addition to aromatic compounds. For toluene the most favored structure is that resulting from OH addition at the ortho position¹⁰:



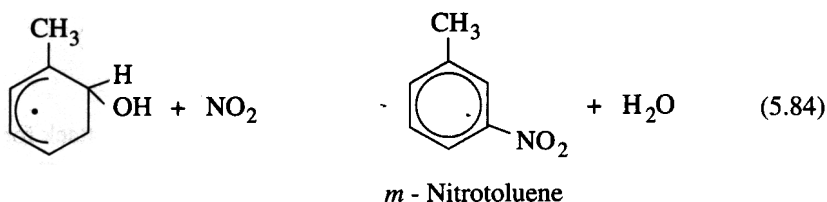
¹⁰OH addition to the meta and para positions of toluene yield structures that are only 1 to 2 kcal mol⁻¹ less favorable than addition at the ortho site and thus cannot be ruled out categorically. For our purposes, we will consider OH addition at the ortho site only.

(In general, the preferred place of OH addition to an aromatic is a position ortho to a substituent methyl group (Andino et al., 1996).)

Following formation of the OH adduct, the adduct can react with O_2 or NO_2 . The O_2 reaction path is

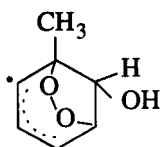


The location of O_2 addition in the product shown above is that most favored energetically (Andino et al., 1996). The H-atom abstraction reaction 5.83a to yield phenolic compounds, such as *o*-cresol, has been shown to be relatively minor, accounting for $\sim 16\%$ of the overall OH radical mechanism for toluene (Atkinson, 1990). The NO_2 reaction of the OH adduct leads to nitroaromatics:

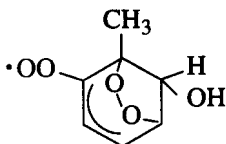


Rate constants for the methyl hydroxycyclohexadienyl radical with O_2 and NO_2 are $\sim 5 \times 10^{-16} \text{ cm}^3 \text{ molecule}^{-1} \text{ s}^{-1}$ and $\sim 3 \times 10^{-11} \text{ cm}^3 \text{ molecule}^{-1} \text{ s}^{-1}$, respectively (Knispel et al., 1990; Zetzsch et al., 1990; Goumri et al., 1992; Atkinson, 1994). Based on these rate constants, the NO_2 reaction with the toluene-OH adduct will be of significance for NO_2 concentrations exceeding about $9 \times 10^{12} \text{ molecules cm}^{-3}$ (300 ppb).

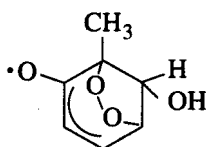
Alkyl peroxy radicals generally react with NO to form alkoxy radicals (assuming sufficient NO is present). Aromatic peroxy radicals, such as the product of reaction 5.83b, in contrast, are believed to cyclicize, forming bicyclic radicals. For the product of reaction 5.83b, the energetically favored bicyclic radical is



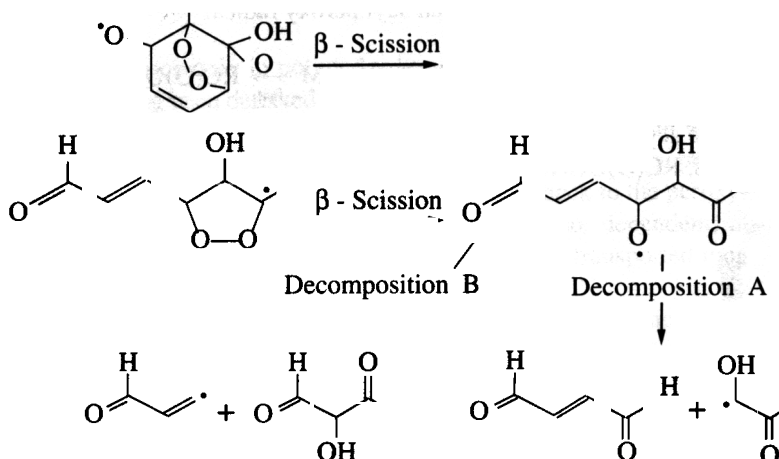
After bicyclic radical formation, O_2 rapidly adds to the radical, forming a bicyclic peroxy radical, for example,



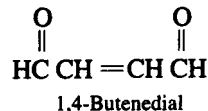
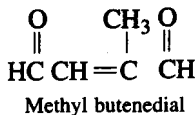
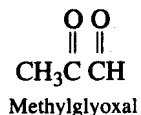
This radical is then expected to react with NO to form a bicyclic oxy radical and NO_2 , for example,



The only path for this bicyclic oxy radical is fragmentation via favorable β -scission reactions. For the above radical, such scission would produce



Observed ring-fragmentation products of the toluene-OH reaction include the following:



5.8.4 Aldehydes

Aldehydes are important constituents of atmospheric chemistry. We have already seen the role played by formaldehyde in the chemistry of the background troposphere. Aldehydes are formed in the atmosphere from the photochemical degradation of other organic com-

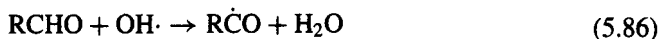
pounds. Aldehydes undergo photolysis, reaction with OH radicals, and reaction with NO₃ radicals. Reaction with NO₃ radicals is of relatively minor importance as a consumption process for aldehydes, thus the major loss processes involve photolysis and reaction with OH radicals.

Formaldehyde photolyzes by reactions 5.32a and 5.32b and reacts with OH by reaction 5.33. Recommended absorption cross sections and quantum yields are cited in Table 3.3. Acetaldehyde photolyzes by (Table 3.3)

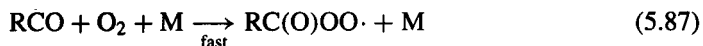


Data on absorption cross sections and quantum yields for higher aldehydes are summarized by Atkinson (1994).

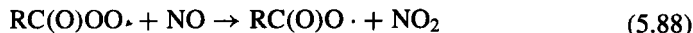
Hydroxyl radical reaction with aldehydes involves H-atom abstraction to produce the corresponding acyl (R $\dot{\text{C}}\text{O}$) radical,¹¹



that rapidly adds O₂ to yield an acyl peroxy radical

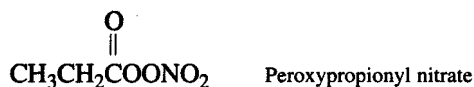
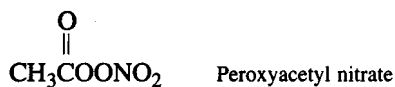


These acyl peroxy radicals then react with NO or NO₂, the latter leading to peroxyacyl nitrates, RC(O)OONO₂,



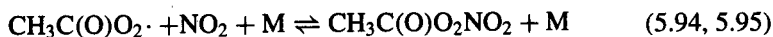
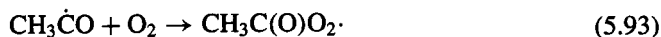
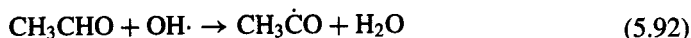
5.8.5 Peroxyacyl Nitrates (PANs)

The class of compounds of general formula RC(O)OONO₂ called peroxyacyl nitrates (PANs) was first discovered in the early 1950s as components of photochemical smog. The first two compounds in the series are



¹¹For glycolaldehyde (HOCH₂CHO), H-atom abstraction occurs from the C—H bonds of both the —CH₂— and —CHO groups in a 1:4 ratio at 298 K.

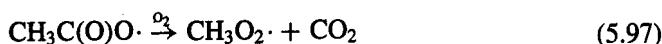
Peroxyacetyl nitrate, the first compound in the series of PANs, which itself is usually called PAN, is formed from the OH reaction with acetaldehyde,



Reaction 5.94 must compete with the NO-to-NO₂ conversion reaction



followed by



Peroxyacetyl nitrate does not absorb radiation above 290 nm so this class of compounds is not expected to photodissociate in the troposphere. Peroxyacetyl nitrate is not highly water soluble; it is more soluble than NO and NO₂ but considerably less soluble, for example, than nitric acid. Thus aqueous-phase scavenging is not expected to be an important tropospheric removal path for PANs.

Once thought to be of importance only in polluted urban atmospheres, PANs are now recognized to be ubiquitous, having been detected in urban, rural, and global environments (Roberts, 1990). By virtue of their photochemical inertness, relative insolubility in water, and low OH rate constant, PANs can have an appreciable atmospheric lifetime. The principal loss mechanism is thermal decomposition by reaction 5.91 or 5.95 back to the peroxyacetyl radical and NO₂. The thermal decomposition is highly temperature dependent; at temperatures of the upper troposphere PANs are quite stable and can be transported long distances.

The thermal decomposition rate constant for PAN, reaction 5.95, is both temperature and pressure dependent, being in the falloff region at room temperature at and below atmospheric pressure. Using the Troe falloff expression, over the temperature range 280 to 330 K,

$$k = \frac{k_0[\text{M}]}{1 + \frac{k_0[\text{M}]}{k_\infty}} F \left\{ \lg_{10} k_0[\text{M}]/k_\infty \right\}^2 \quad (5.98)$$

the specific values for PAN are

$$k_0 = 4.9 \times 10^{-3} \exp(-12100/T) \text{ cm}^3 \text{ molecule}^{-1} \text{ s}^{-1}$$

$$k_\infty = 4.0 \times 10^{16} \exp(-13600/T) \text{ s}^{-1}$$

$$F = 0.3$$

Thus $k_\infty = 6.1 \times 10^{-4} \text{ s}^{-1}$ at 298 K and $k_{5.95} = 5.2 \times 10^{-4} \text{ s}^{-1}$ at 298 K and 760 Torr total pressure. The decomposition rates of the higher peroxyacetyl nitrates are expected to be sim-

ilar to that for PAN, with the decomposition rate constants being closer to the high-pressure limit at a given pressure than for PAN.

PANs can be considered to exist in chemical equilibrium according to reactions 5.90 and 5.91. Thus the concentration of a PAN compound at any location and time will depend on the temperature and the local levels of NO_2 and NO , the latter molecule because of the competing reaction 5.96 that serves to remove peroxyacyl radicals from the PAN system.

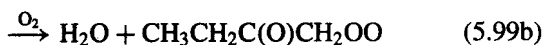
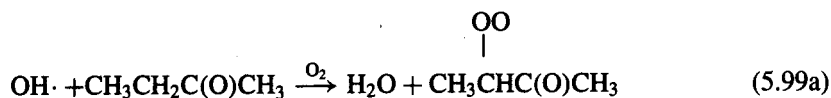
At night the thermal decomposition of PAN in an atmosphere with a relatively high mixing ratio of NO (e.g., 10 ppb) can initiate reaction 5.96 that converts NO to NO_2 and produces a methylperoxy radical, which itself may convert another NO to NO_2 and produce a molecule of formaldehyde, reaction 5.45. This sequence could lead to a reservoir of photochemically active species when the Sun rises.

The lifetime of peroxyacetyl nitrate is strongly temperature dependent and ranges from ~ 30 minutes at 298 K to ~ 8 hours at 273 K. At the temperatures of the upper troposphere, PAN lifetime from thermal decomposition is many months, so, in this region, OH reaction or photolysis will dominate as the PAN loss process. PAN therefore acts as a reservoir for NO_x , allowing for the long-range transport of NO_x . Under urban conditions at fairly warm temperatures the concentration of PAN is governed by the steady-state concentration of the peroxyacetyl radical, $\text{CH}_3\text{C}(\text{O})\text{OO}\cdot$. With PAN formation proportional to NO_2 and competitive with peroxyacetyl radical reaction with NO , the steady-state concentration of PAN is proportional to the NO_2/NO ratio. From the $\text{NO}_2/\text{NO}_2/\text{O}_3$ photostationary state relation (5.8), since the steady-state concentration of O_3 is also proportional to the NO_2/NO ratio, the steady-state PAN concentration is proportional to the O_3 concentration.

PAN mixing ratios in the vicinity of 100 ppt are present in the northern free troposphere, although its abundance is highly variable (Singh et al., 1995). Near the tropics mixing ratios near 10 ppt are often prevalent. PAN exhibits a strong vertical gradient, with mixing ratios in the marine boundary layer typically less than 2 ppt.

5.8.6 Ketones

This class of organic compounds is exemplified by acetone and its higher homologues. As for the aldehydes, photolysis and reaction with the OH radical are the major atmospheric loss processes (Atkinson, 1989). The limited experimental data available indicate that, with the exception of acetone (see Figure 5.11), photolysis is probably of minor importance. Reaction with the OH radical is then the major tropospheric loss process. For example, for methyl ethyl ketone the OH radical can attack any of the three carbon atoms that contain hydrogen atoms:



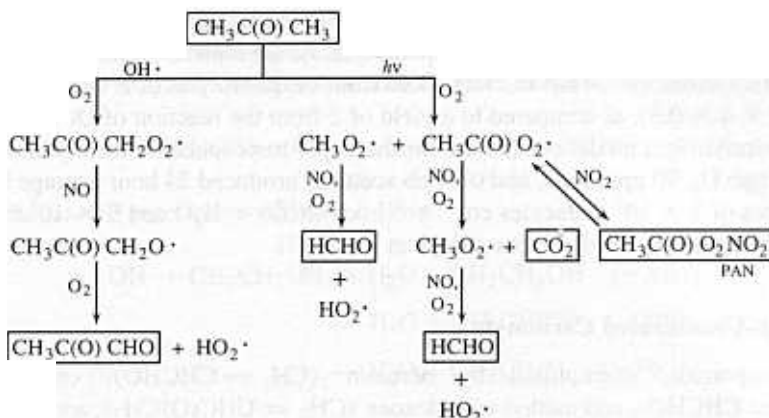
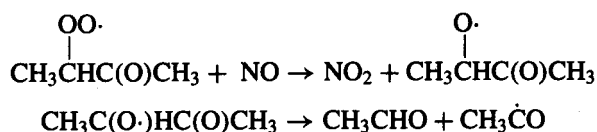


FIGURE 5.11 Atmospheric photooxidation mechanism for acetone.

with 5.99a being the major reaction pathway. Subsequent reaction of this particular radical with NO leads to



The major reaction products from the atmospheric reactions of the ketones are aldehydes and PAN precursors.

Acetone is an ubiquitous atmospheric species having a mixing ratio of about 1 ppb in rural sites in a variety of locations (Singh et al., 1994, 1995). Under extremely clean conditions, ground-level background mixing ratios of 550 ppt have been found throughout the NH troposphere. In the free troposphere, acetone mixing ratios on the order of 500 ppt are present at northern midlatitudes, declining to about 200 ppt at southern latitudes (Singh et al., 1995). From atmospheric data and three-dimensional photochemical models, a global acetone source of 40 to 60 Tg yr⁻¹ has been estimated, comprised of 51% secondary formation from the atmospheric oxidation of precursor hydrocarbons (principally propane, isobutane, and isobutene), 26% direct emission from biomass burning, 21% direct biogenic emissions, and 3% primary anthropogenic emissions (Singh et al., 1994). Atmospheric removal of acetone is estimated to result from photolysis (64%), OH reaction (24%), and deposition (12%). Acetone photolysis, which produces the PAN-precursor CH₃CO radical, is estimated to contribute 40 to 50 ppt of PAN in the middle and upper troposphere of the Northern Hemisphere. Based on tropospheric models, up to 50% of observed PAN may be formed by this mechanism. The average lifetime of acetone in the atmosphere is estimated to be 16 days (Singh et al., 1995).

By virtue of its photooxidation chemistry (Figure 5.11), acetone is a source of HO_x radicals in the upper troposphere. Under the dry conditions of the upper troposphere, where O(¹D) + H₂O is relatively slow, acetone makes an important additional contribution to

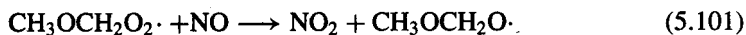
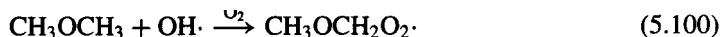
HO_x. Photolysis of acetone yields two HO₂ and two HCHO molecules (when [NO] >> [NO₂]), and 30% of the HCHO molecules photolyze via the radical-forming branch to yield two more HO₂ molecules. Thus the HO_x yield from the photolysis of acetone is ~3.2 (the result of 2 + 4 × 0.3), as compared to a yield of 2 from the reaction of O(¹D) + H₂O. A simple photochemical model calculation for the upper troposphere at the equinox (40° N, 11 km, 50 ppb O₃, 90 ppm H₂O, and 0.5 ppb acetone) produced 24 hour average HO_x production rates of 7 × 10³ molecules cm⁻³ s⁻¹ from O(¹D) + H₂O and 9 × 10³ molecules cm⁻³ s⁻¹ from photolysis of acetone (Singh et al., 1995).

5.8.7 α, β-Unsaturated Carbonyls

These compounds, exemplified by acrolein (CH₂ = CHCHO), crotonaldehyde (CH₃CH = CHCHO), and methyl vinyl ketone (CH₂ = CHC(O)CH₃), are known to react with ozone and with OH radicals. Photolysis and NO₃ radical reaction are of minor importance. Under atmospheric conditions the O₃ reactions are also of minor significance, leaving the OH radical reaction as the major loss process. For the aldehydes, OH radical reaction can proceed via two reaction pathways: OH radical addition to the double bond and H-atom abstraction from the—CHO group (Atkinson, 1989). These α,β-unsaturated aldehydes are expected to ultimately give rise to α-dicarbonyls such as glyoxal and methylglyoxal. For the α,β-unsaturated ketones such as methyl vinyl ketone the major atmospheric reaction with the OH radical occurs only by OH radical addition to the double bond. Again, α-dicarbonyls, together with aldehydes and hydroxyaldehydes, are formed as products.

5.8.8 Ethers

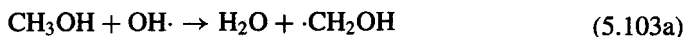
The aliphatic ethers, such as dimethyl ether and diethyl ether, react under atmospheric conditions essentially solely with the OH radical, via H-atom abstraction from C—H bonds (Wallington et al., 1988, 1989; Atkinson, 1989; Japar et al., 1990, 1991; Wallington and Japar, 1991). The reaction mechanism for dimethyl ether is



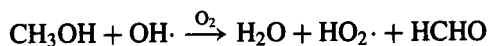
where the carbon-containing product in reaction 5.102 is methyl formate.

5.8.9 Alcohols

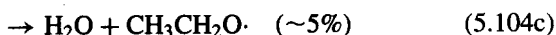
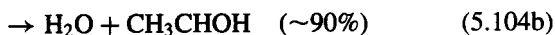
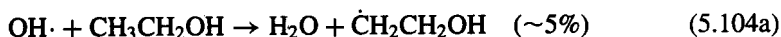
The reaction sequences for the simpler aliphatic alcohols under atmospheric conditions are known (Atkinson, 1989); these involve H-atom abstraction, mainly from the α C—H bonds. For example, the methanol—OH reaction is



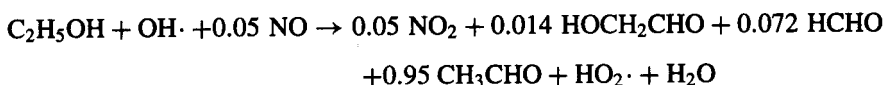
with the first reaction pathway accounting for ~85% of the overall reaction at 298 K. Since, as shown earlier, both the $\cdot\text{CH}_2\text{OH}$ and $\text{CH}_3\text{O}\cdot$ radicals react with O_2 to yield formaldehyde and HO_2 , the overall methanol-OH reaction can be written as



The ethanol-OH reaction proceeds as follows:



where the branching ratios are those at 298 K. The second two channels result in identical products under atmospheric conditions, $\text{HO}_2 + \text{CH}_3\text{CHO}$. The first channel forms the intermediate $\text{CH}_2\dot{\text{C}}\text{H}_2\text{OH}$, which, under atmospheric conditions, leads to the same products as the $\text{OH} + \text{ethene}$ reaction. Using the ethene-OH mechanism given earlier, the overall ethanol-OH reaction mechanism can be written as



with the principal products being acetaldehyde and the HO_2 radical.

Free tropospheric concentrations of methanol range from about 700 ppt at northern mid-latitudes to about 400 ppt at southern latitudes (Singh et al., 1995). In general, ethanol abundance in the free troposphere is an order of magnitude lower than that of methanol. Average lifetimes of CH_3OH and $\text{C}_2\text{H}_5\text{OH}$ in the atmosphere are on the order of 16 days and 4 days, respectively.

5.8.10 Acids

The atmospheric sources of formic and acetic acid are still open to question. In the Shenandoah Cloud and Photochemistry Experiment conducted during 1990 in the rural continental atmosphere at a mountaintop (1014 m) in Virginia, median mixing ratios for HCOOH and CH_3COOH were 5.4 and 2.1 ppb, respectively (Talbot et al., 1995). Formic acid mixing ratios often approached or exceeded 10 ppb. An observed lack of correlation between HCOOH and CH_3COOH with peroxide species argued against a significant source from permutation reactions of peroxy radicals (e.g., reaction 5.61). A strong correlation between the mixing ratios of both acids was suggestive of a common source, although combustion emissions could be ruled out. Correlation between the seasonal variation of the two acids and ambient temperature is consistent with a soil microbial source.

Together, the two acids contribute between 16 and 35% of the free acidity in North American precipitation and between 25 and 98% of the free acidity in precipitation in remote areas. Photochemical production of organic acids occurs in the gas phase from ozone-alkene reactions and in cloud water by the hydrolysis of aldehydes followed by aqueous-phase reaction with OH radicals (see Chapter 6). These routes can explain, in part,

7 Properties of the Atmospheric Aerosol

7.1 THE SIZE DISTRIBUTION FUNCTION

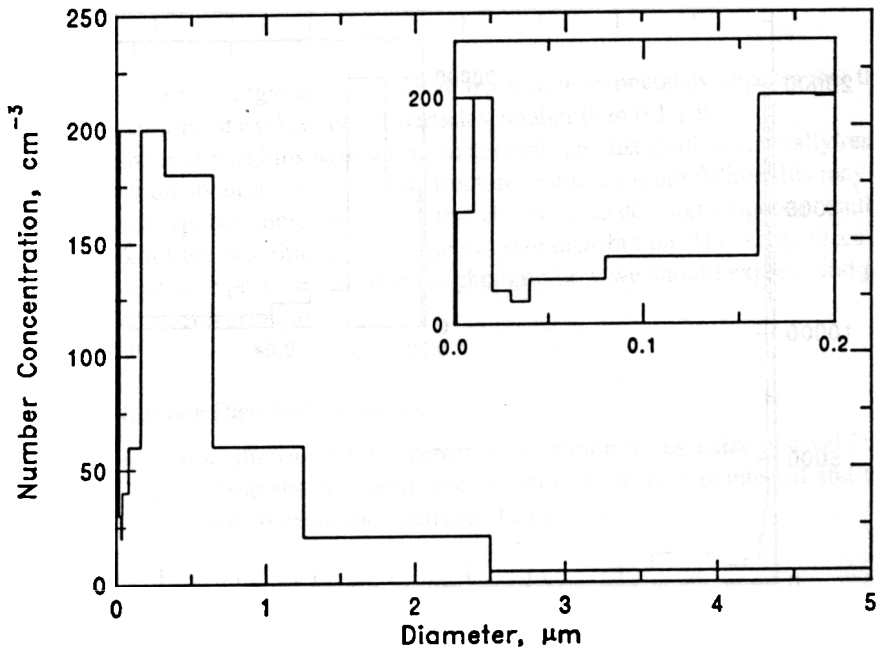
The atmosphere, whether in urban or remote areas, contains significant concentrations of aerosol particles sometimes as high as 10^7 to 10^8 cm^{-3} . The diameters of these particles span over four orders of magnitude, from a few nanometers to around $100 \mu\text{m}$. To appreciate this wide size range one just needs to consider that the mass of a $10 \mu\text{m}$ diameter particle is equivalent to the mass of one billion 10 nm particles. Combustion-generated particles, such as those from automobiles, power generation, and wood burning, can be as small as a few nanometers and as large as $1 \mu\text{m}$. Wind-blown dust, pollens, plant fragments, and sea salt are generally larger than $1 \mu\text{m}$. Material produced in the atmosphere by photochemical processes is mainly found in particles smaller than $1 \mu\text{m}$. The size of these particles affects both their lifetime in the atmosphere and their physical and chemical properties. It is therefore necessary to develop methods of mathematically characterizing aerosol size distributions. For the purposes of this chapter we neglect the effect of particle shape and consider only spherical particles.

An aerosol particle can be considered to consist of an integer number k of molecules or monomers. The smallest aerosol particle could be defined in principle as that containing two molecules. The aerosol distribution could then be characterized by the number concentration of each cluster, that is, by N_k , the concentration (per cm^3 of air) of particles containing k molecules. Although rigorously correct, this discrete method of characterizing the aerosol distribution cannot be used in practice because of the large number of molecules that comprise even the smallest aerosol particles. For example, a particle with a diameter of $0.01 \mu\text{m}$ contains approximately 10^4 molecules, and one with a diameter of $1 \mu\text{m}$ around 10^{10} .

A complete description of the aerosol size distribution can also include an accounting of the size of each particle. Even if such information were available, a list of the diameters of thousands of particles, that would vary as a function of time and space, would be cumbersome. A first step in simplifying the necessary accounting is division of the particle size range into discrete intervals and calculation of the number of particles in each size bin. Information for an aerosol size distribution using 12 size intervals is shown in Table 7.1. Such a summary of the aerosol size distribution requires only 25 numbers (the boundaries of the size sections and the corresponding concentrations) instead of the diameters of all the particles. This distribution is presented in the form of a histogram in Figure 7.1. Note that the enormous range of the aerosol particle sizes makes the presentation of the full size distribution difficult. The details of the size distribution lost by showing the whole range of diameters are illustrated in the inset of Figure 7.1.

TABLE 7.1 Example of Segregated Aerosol Size Information

Size Range (μm)	Concentration (cm^{-3})	Cumulative (cm^{-3})	Concentration ($\mu\text{m}^{-1} \text{cm}^{-3}$)
0.001–0.01	100	100	11111
0.01–0.02	200	300	20000
0.02–0.03	30	330	3000
0.03–0.04	20	350	2000
0.04–0.08	40	390	1000
0.08–0.16	60	450	750
0.16–0.32	200	650	1250
0.32–0.64	180	830	563
0.64–1.25	60	890	117
1.25–2.5	20	910	160
2.5–5.0	5	915	80
5.0–10.0	1	916	2

**FIGURE 7.1** Histogram of aerosol particle number concentrations versus the size range for the distribution of Table 7.1. The diameter range 0 to 0.2 μm for the same distribution is shown in the inset.

The size distribution of a particle population can also be described by using its cumulative distribution. The cumulative distribution value for a size section is defined as the concentration of particles that are smaller than or equal to this size range. For example, for the distribution of Table 7.1, the value of the cumulative distribution for the 0.03 to 0.04 μm size range indicates that there are 350 particles cm^{-3} that are smaller than 0.04 μm . The last value of the cumulative distribution indicates the total particle number concentration.

Use of size bins with different widths makes the interpretation of absolute concentrations difficult. For example, one may want to find out in which size range there are a lot of particles. The number concentrations in Table 7.1 indicate that there are 200 particles cm^{-3} in the range from 0.01 to 0.02 μm and another 200 particles cm^{-3} from 0.16 to 0.32 μm . However, this comparison of the concentration of particles covering a size range of 20 nm with that over a 160 nm range favors the latter. To avoid such biases, one often normalizes the distribution by dividing the concentration with the corresponding size range. The result is a concentration expressed in $\mu\text{m}^{-1} \text{cm}^{-3}$ (Table 7.1) and is illustrated in Figure 7.2. The distribution changes shape, but now the area below the curve is proportional to the number concentration. Figure 7.2 indicates that roughly half of the particles are smaller than 0.1 μm . A plot like Figure 7.1 may be misleading, as it indicates that almost all particles are larger than 0.1 μm . If a logarithmic scale is used for the diameter (Figure 7.3) both the

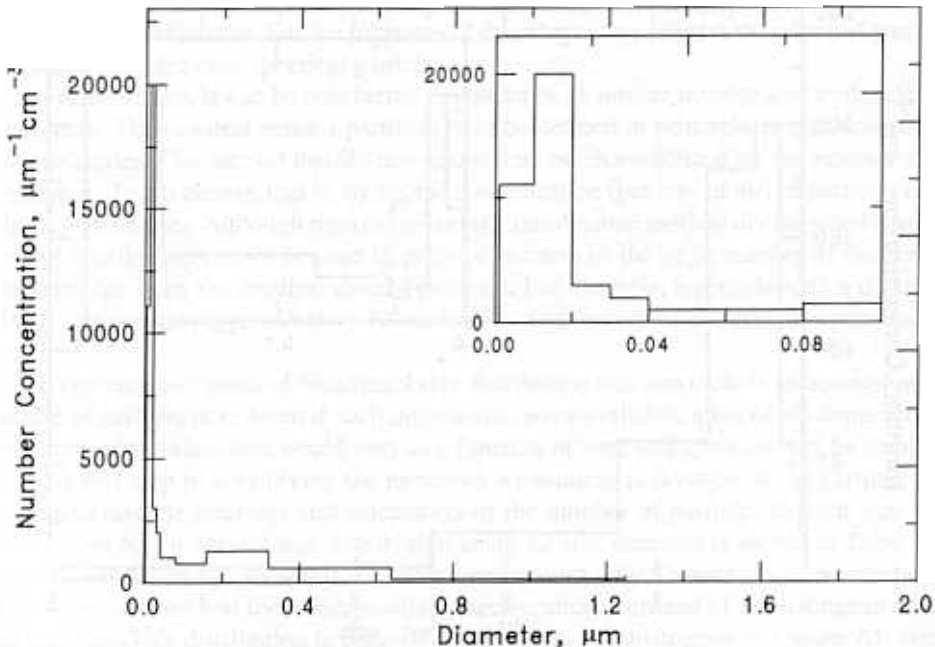


FIGURE 7.2 Aerosol number concentration normalized by the width of the size range versus size for the distribution of Table 7.1. The diameter range 0 to 0.1 μm for the same distribution is shown in the inset.

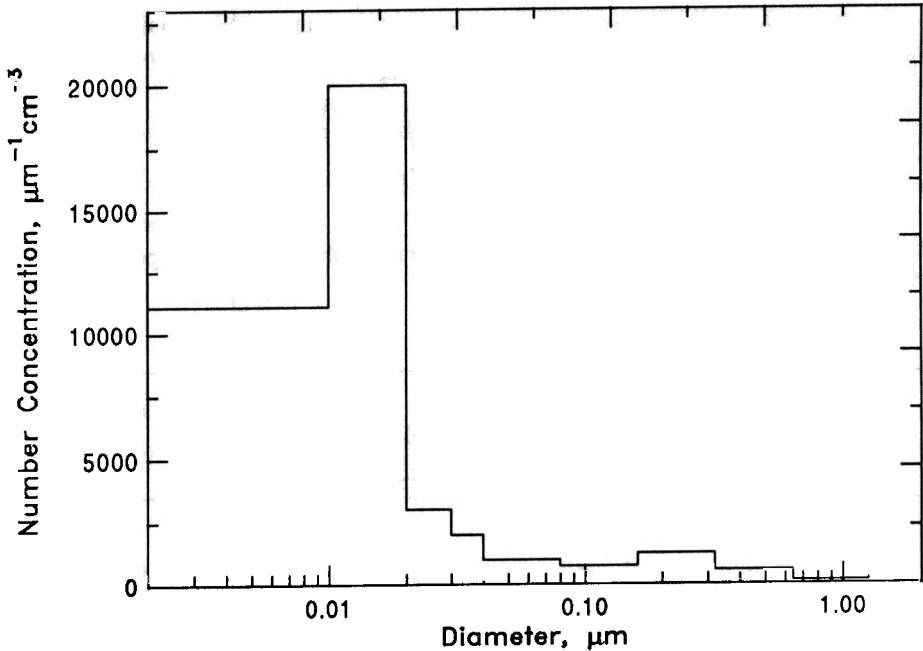


FIGURE 7.3 Same as Figure 7.2 but plotted versus the logarithm of the diameter.

large-and small-particle regions are depicted, but it now erroneously appears that the distribution consists almost exclusively of particles smaller than $0.1 \mu\text{m}$.

Using a number of size bins to describe an aerosol size distribution generally results in loss of information about the distribution structure inside each bin. While this may be acceptable for some applications, our goal in this chapter is to develop a rigorous mathematical framework for the description of the aerosol size distribution. The issues discussed in the preceding example provide valuable insights into how we should express and present ambient aerosol size distributions.

7.1.1 The Number Distribution $n_N(D_p)$

In the previous section, the value of the aerosol distribution n_i for a size interval i was expressed as the ratio of the absolute aerosol concentration N_i of this interval and the size range ΔD_p . The aerosol concentration can then be calculated by

$$N_i = n_i \Delta D_p$$

The use of arbitrary intervals ΔD_p can be confusing and makes the intercomparison of size distributions difficult. To avoid these complications and to maintain all the information regarding the aerosol distribution, one can use smaller and smaller size bins, effectively tak-

ing the limit $\Delta D_p \rightarrow 0$. At this limit, ΔD_p becomes infinitesimally small and equal to dD_p . Then one can define the size distribution function $n_N(D_p)$, as follows:

$$n_N(D_p) dD_p = \text{the number of particles per cm}^3 \text{ of air having diameters} \\ \text{in the range } D_p \text{ to } D_p + dD_p$$

The units of $n_N(D_p)$ are $\mu\text{m cm}^{-3}$ and the total number of particles per cm^{-3} , N , is then just

$$N = \int_0^{\infty} n_N(D_p) dD_p \quad (7.1)$$

By using the function $n_N(D_p)$ we implicitly assume that the number distribution is no longer a discrete function of the number of molecules, but a continuous function of the diameter D_p . This assumption of a continuous size distribution is valid beyond a certain number of molecules, say, around 100. In the atmosphere most of the particles have diameters smaller than $0.1 \mu\text{m}$ and the number distribution function $n_N(D_p)$ usually exhibits a narrow spike near the origin (Figure 7.4).

We can define a normalized size distribution function $\bar{n}_N(D_p)$ by $\bar{n}_N(D_p) = n_N(D_p)/N$, such that

$$\bar{n}_N(D_p) dD_p = \text{the fraction of the total number of particles per cm}^3 \text{ having diameters} \\ \text{in the range } D_p \text{ to } D_p + dD_p$$

The units of $\bar{n}_N(D_p)$ are μm^{-1} . The normalized size distribution function $\bar{n}_N(D_p)$ can also be viewed as the probability that a randomly selected particle has a diameter in the range $(D_p, D_p + dD_p)$; it is therefore equivalent to the normalized probability density of particle size.

If $dN = n_N(D_p) dD_p$ denotes the number of particles in the size range $(D_p, D_p + dD_p)$, then $n_N(D_p)$ can be written as

$$n_N(D_p) = \frac{dN}{dD_p} \quad (7.2)$$

Both sides of (7.2) represent the same aerosol distribution, and the notation dN/dD_p is often used instead of $n_N(D_p)$. To conform with the common notation we will also express the distributions in this manner.

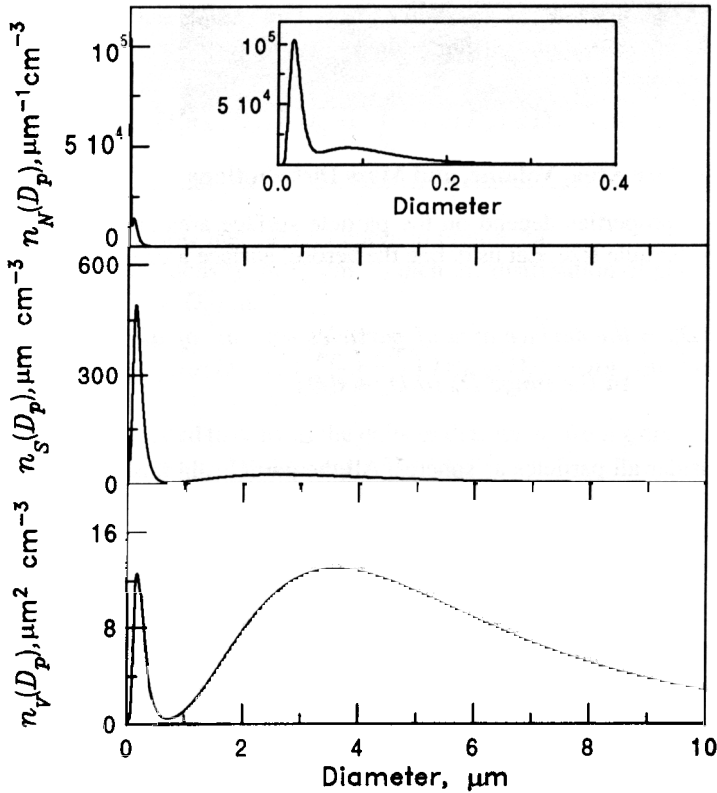


FIGURE 7.4 Atmospheric aerosol number, surface, and volume continuous distributions versus particle size. The diameter range 0 to 0.5 μm for the number distribution is shown as an inset.

Example 7.1 For the distribution of Figure 7.4, how many particles of diameter 0.1 μm exist?

According to the inset of Figure 7.4, $n_N(0.1 \mu\text{m}) = 13,000 \mu\text{m}^{-1} \text{cm}^{-3}$. However, this is not the number of particles of diameter 0.1 μm (it even has the wrong units). To calculate the number of particles we need to multiply n_N by the width of the size range ΔD_p . But if we are interested only in particles with $D_p = 0.1 \mu\text{m}$ this size range is zero and therefore there are zero particles of diameter exactly equal to 0.1 μm .

Let us try to rephrase the above question.

Example 7.2. For the distribution of Figure 7.4, how many particles with diameter in the range 0.1 to 0.11 μm exist?

The size distribution is practically constant over this narrow range with $n_N(0.1 \mu\text{m}) = 13,000 \mu\text{m}^{-1} \text{cm}^{-3}$. The width of the region is $0.11 - 0.1 = 0.01 \mu\text{m}$ and there are $0.01 \times 13,000 = 130$ particles cm^{-3} with diameters between 0.1 and 0.11 μm for this size distribution.

The above examples indicate that while n_N is a unique description of the aerosol size distribution (it does not depend on definitions of size bins, etc.), one should be careful with its physical interpretation.

7.1.2 The Surface Area, Volume, and Mass Distributions

Several aerosol properties depend on the particle surface area and volume distributions with respect to particle size. Let us define the aerosol surface area distribution $n_S(D_p)$ as

$n_S(D_p) dD_p =$ the surface area of particles per cm^3 of air having diameters
in the range D_p to $D_p + dD_p$

and let us consider all particles as spheres. All the particles in this infinitesimally narrow size range have effectively the same diameter D_p , and each of them has surface area πD_p^2 . There are $n_N(D_p) dD_p$ particles in this size range and therefore their surface area is $\pi D_p^2 n_N(D_p) dD_p$. But then by definition

$$n_S(D_p) = \pi D_p^2 n_N(D_p) \quad (\mu\text{m cm}^{-3}) \quad (7.3)$$

The total surface area S of the aerosol per cm^3 of air is then

$$S = \pi \int_0^\infty D_p^2 n_N(D_p) dD_p = \int_0^\infty n_S(D_p) dD_p \quad (\mu\text{m}^2 \text{cm}^{-3}) \quad (7.4)$$

and is equal to the area below the $n_S(D_p)$ curve in Figure 7.4. The aerosol volume distribution $n_V(D_p)$ can be defined as

$n_V(D_p) dD_p =$ the volume of particles per cm^3 of air having diameters
in the range D_p to $D_p + dD_p$

and therefore

$$n_V(D_p) = \frac{\pi}{6} D_p^3 n_N(D_p) \quad (\mu\text{m}^3 \text{cm}^{-3}) \quad (7.5)$$

The total aerosol volume per cm^3 of air, V , is

$$V = \frac{\pi}{6} \int_0^{\infty} D_p^3 n_N(D_p) dD_p = \int_0^{\infty} n_V(D_p) dD_p \quad (\mu\text{m}^3 \text{cm}^{-3}) \quad (7.6)$$

and is equal to the area below the $n_V(D_p)$ curve in Figure 7.4.

If the particles all have density ρ_p (g cm^{-3}) then the distribution of particle mass with respect to particle size, $n_M(D_p)$, is

$$n_M(D_p) = \left(\frac{\rho_p}{10^6}\right) n_V(D_p) = \left(\frac{\rho_p}{10^6}\right) \left(\frac{\pi}{6}\right) D_p^3 n_N(D_p) \quad (\mu\text{g } \mu\text{m}^{-1} \text{cm}^{-3}) \quad (7.7)$$

where the factor 10^6 is needed to convert the units of density ρ_p from g cm^{-3} to $\mu\text{g } \mu\text{m}^{-3}$, and to maintain the units for $n_M(D_p)$ as $\mu\text{g } \mu\text{m}^{-1} \text{cm}^{-3}$.

Because particle diameters in an aerosol population typically vary over several orders of magnitude, use of the distribution functions, $n_N(D_p)$, $n_S(D_p)$, $n_V(D_p)$, and $n_M(D_p)$, is often inconvenient. For example, all the structure of the number distribution depicted in Figure 7.4 occurs in the region from a few nanometers to $0.3 \mu\text{m}$ diameter, a small part of the 0 to $10 \mu\text{m}$ range of interest. To circumvent this scale problem the horizontal axis can be scaled in logarithmic intervals so that several orders of magnitude in D_p can be clearly seen (Figure 7.5). Plotting $n_N(D_p)$ on semilog axes gives, however, a somewhat dis-

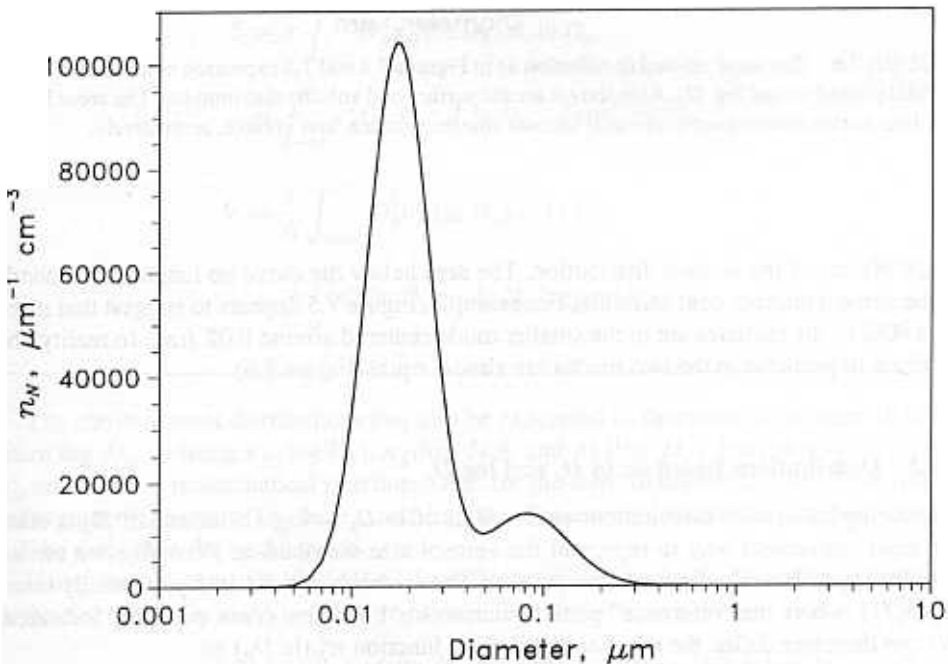


FIGURE 7.5 The same aerosol distribution as in Figure 7.4, plotted versus the logarithm of the diameter

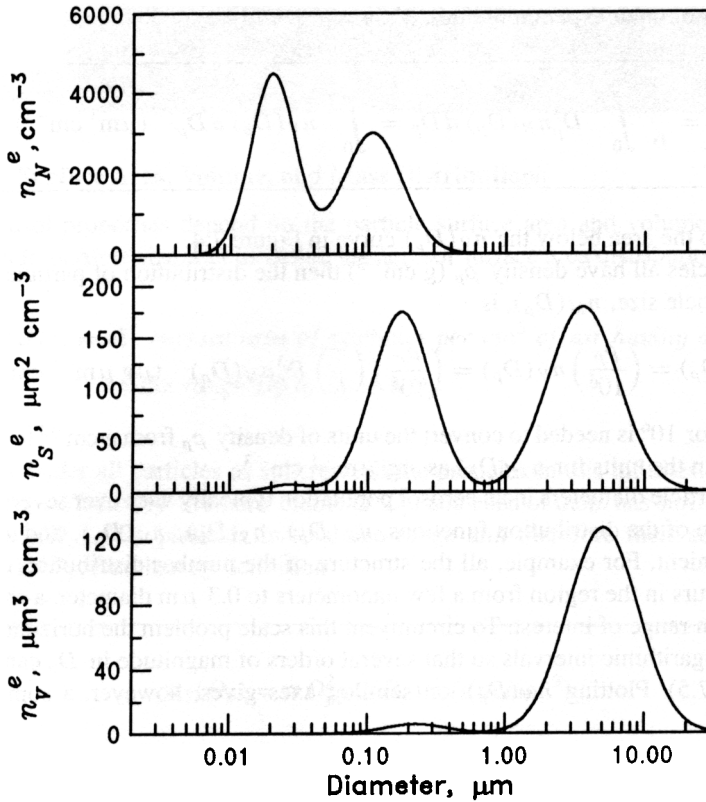


FIGURE 7.6 The same aerosol distribution as in Figures 7.4 and 7.5 expressed as a function of $\log D_p$ and plotted versus $\log D_p$. Also shown are the surface and volume distributions. The areas below the three curves correspond to the total aerosol number, surface, and volume, respectively.

torted picture of the aerosol distribution. The area below the curve no longer corresponds to the aerosol number concentration. For example, Figure 7.5 appears to suggest that more than 90% of the particles are in the smaller mode centered around $0.02 \mu\text{m}$. In reality, the numbers of particles in the two modes are almost equal (Figure 7.6).

7.1.3 Distributions Based on $\ln D_p$ and $\log D_p$

Expressing the aerosol distributions as functions of $\ln D_p$ or $\log D_p$ instead of D_p is often the most convenient way to represent the aerosol size distribution. Formally, we cannot take the logarithm of a dimensional quantity. Thus, when we write $\ln D_p$, we really mean $\ln(D_p/1)$, where the “reference” particle diameter is $1 \mu\text{m}$ and is not explicitly indicated. We can therefore define the number distribution function $n_N^e(\ln D_p)$ as

$$n_N^e(\ln D_p) d \ln D_p \quad \text{number of particles per cm}^3 \text{ of air in the size range } \ln D_p \text{ to } \ln D_p + d \ln D_p$$

The units of $n_N^e(\ln D_p)$ are cm^{-3} since $\ln D_p$ is dimensionless. The total number concentration of particles N is

$$N = \int_{-\infty}^{\infty} n_N^e(\ln D_p) d \ln D_p \quad (\text{cm}^{-3}) \quad (7.8)$$

The limits of integration in (7.8) are from $-\infty$ to ∞ as the independent variable is $\ln D_p$.

The surface area and volume distributions as functions of $\ln D_p$ can be defined similarly to those with respect to D_p ,

$$n_S^e(\ln D_p) = \pi D_p^2 n_N^e(\ln D_p) \quad (\mu\text{m}^2 \text{cm}^{-3}) \quad (7.9)$$

$$n_V^e(\ln D_p) = \frac{\pi}{6} D_p^3 n_N^e(\ln D_p) \quad (\mu\text{m}^3 \text{cm}^{-3}) \quad (7.10)$$

with

$$\begin{aligned} S &= \pi \int_{-\infty}^{\infty} D_p^2 n_N^e(\ln D_p) d \ln D_p \\ &= \int_{-\infty}^{\infty} n_S^e(\ln D_p) d \ln D_p \quad (\mu\text{m}^2 \text{cm}^{-3}) \end{aligned} \quad (7.11)$$

$$\begin{aligned} V &= \frac{\pi}{6} \int_{-\infty}^{\infty} D_p^3 n_N^e(\ln D_p) d \ln D_p \\ &= \int_{-\infty}^{\infty} n_V^e(\ln D_p) d \ln D_p \quad (\mu\text{m}^3 \text{cm}^{-3}) \end{aligned} \quad (7.12)$$

The above aerosol distributions can also be expressed as functions of the base 10 logarithm $\log D_p$, defining $n_N^{\circ}(\log D_p)$, $n_S^{\circ}(\log D_p)$, and $n_V^{\circ}(\log D_p)$. Note that n_N , n_N^e , and n_N° are different mathematical functions, and, for the same diameter D_p , they have different arguments, namely D_p , $\ln D_p$, and $\log D_p$. The expressions relating these functions will be derived in the next section.

Using the notation $dN/dS/dV$ = the differential number/surface/volume of particles in the size range D_p to $D_p + dD_p$ we have

$$dN = n_N(D_p) dD_p = n_N^e(\ln D_p) d \ln D_p = n_N^{\circ}(\log D_p) d \log D_p \quad (7.13)$$

$$dS = n_S(D_p) dD_p = n_S^e(\ln D_p) d \ln D_p = n_S^{\circ}(\log D_p) d \log D_p \quad (7.14)$$

$$dV = n_V(D_p) dD_p = n_V^e(\ln D_p) d \ln D_p = n_V^{\circ}(\log D_p) d \log D_p \quad (7.15)$$

Based on that notation, the various size distributions are

$$\begin{aligned}
 n_N(D_p) &= \frac{dN}{dD_p} & n_N^e(\ln D_p) &= \frac{dN}{d \ln D_p} & n_N^o(\log D_p) &= \frac{dN}{d \log D_p} \\
 n_S(D_p) &= \frac{dS}{dD_p} & n_S^e(\ln D_p) &= \frac{dS}{d \ln D_p} & n_S^o(\log D_p) &= \frac{dS}{d \log D_p} \\
 n_V(D_p) &= \frac{dV}{dD_p} & n_V^e(\ln D_p) &= \frac{dV}{d \ln D_p} & n_V^o(\log D_p) &= \frac{dV}{d \log D_p}
 \end{aligned} \quad (7.16)$$

7.1.4 Relating Size Distributions Based on Different Independent Variables

It is often necessary to relate a size distribution based on one independent variable, say, D_p , to one based on another independent variable, say, $\log D_p$. Such a relation can be derived based on (7.13). The number of particles dN in an infinitesimal size range D_p to $D_p + dD_p$ is the same regardless of the expression used for the description of the size distribution function. Thus in the particular case of $n_N(D_p)$ and $n_N^o(\log D_p)$

$$n_N(D_p) dD_p = n_N^o(\log D_p) d \log D_p \quad (7.17)$$

Since $d \log D_p = d \ln D_p / 2.303 = dD_p / 2.303D_p$, (7.17) becomes

$$n_N^o(\log D_p) = 2.303D_p n_N(D_p) \quad (7.18)$$

Similarly,

$$n_S^o(\log D_p) = 2.303D_p n_S(D_p) \quad (7.19)$$

$$n_V^o(\log D_p) = 2.303D_p n_V(D_p) \quad (7.20)$$

The distributions with respect to D_p are related to those with respect to $\ln D_p$ by

$$n_N^e(\ln D_p) = D_p n_N(D_p) \quad (7.21)$$

$$n_S^e(\ln D_p) = D_p n_S(D_p) \quad (7.22)$$

$$n_V^e(\ln D_p) = D_p n_V(D_p) \quad (7.23)$$

This procedure can be generalized to relate any two size distribution functions $n(u)$ and $n(v)$, where both u and v are related to D_p . The generalization of (7.17) is

$$n(u) du = n(v) dv \quad (7.24)$$

and dividing both sides by dD_p

$$n(u) = n(v) \frac{(dv/dD_p)}{(du/dD_p)} \quad (7.25)$$

7.1.5 Properties of Size Distributions

It is often convenient to summarize the features of an aerosol distribution using one or two of its properties (mean particle size, spread of distribution) than by using the full function $n_N(D_p)$. Growth of particles corresponds to a shifting of parts of the distribution to larger sizes or simply an increase of the mean particle size. These properties are called the *moments* of the distribution, and the two most often used are the mean and the variance.

Let us assume that we have a discrete distribution consisting of M groups of particles, with diameters D_k and number concentrations N_k , $k = 1, 2, \dots, M$. The number concentration of aerosols is therefore

$$N = \sum_{k=1}^M N_k \quad (7.26)$$

The mean particle diameter, \bar{D}_p , of the population is

$$\bar{D}_p = \frac{\sum_{k=1}^M N_k D_k}{N} = \frac{1}{N} \sum_{k=1}^M N_k D_k \quad (7.27)$$

The variance, σ^2 , a measure of the spread of the distribution around the mean diameter \bar{D}_p , is defined by

$$\sigma^2 = \frac{\sum_{k=1}^M N_k (D_k - \bar{D}_p)^2}{\sum_{k=1}^M N_k} = \frac{1}{N} \sum_{k=1}^M N_k (D_k - \bar{D}_p)^2 \quad (7.28)$$

A value of σ^2 equal to zero would mean that every one of the particles in the distribution has precisely diameter \bar{D}_p . An increasing σ^2 indicates that the spread of the distribution around the mean diameter \bar{D}_p is increasing.

We will usually deal with aerosol distributions in continuous form. Given the number distribution $n_N(D_p)$, (7.27) and (7.28) can be written in continuous form to define the

mean particle diameter of the distribution by

$$D_p = \frac{\int_0^\infty D_p n_N(D_p) dD_p}{\int_0^\infty n_N(D_p) dD_p} = \frac{1}{N} \int_0^\infty D_p n_N(D_p) dD_p \quad (7.29)$$

and the variance of the distribution by

$$\sigma^2 = \frac{\int_0^\infty (D_p - \bar{D}_p)^2 n_N(D_p) dD_p}{\int_0^\infty n_N(D_p) dD_p} = \frac{1}{N} \int_0^\infty (D_p - \bar{D}_p)^2 n_N(D_p) dD_p \quad (7.30)$$

Table 7.2 presents a number of other mean values that are often used in characterizing an aerosol size distribution.

TABLE 7.2 Mean Values Often Used in Characterizing an Aerosol Size Distribution

Property	Defining Relation	Description
Number mean diameter, \bar{D}_p	$\bar{D}_p = \int_0^\infty D_p n_N(D_p) dD_p$	Average diameter of the population
Median diameter, D_{med}	$\int_0^{D_{med}} n_N(D_p) dD_p = \frac{1}{2} N$	Diameter below which one-half the particles lie and above which one-half the particles lie
Mean surface area, \bar{S}	$\bar{S} = \frac{1}{N} \int_0^\infty n_S(D_p) dD_p$	Average surface area of the population
Mean, volume, \bar{V}	$\bar{V} = \frac{1}{N} \int_0^\infty n_V(D_p) dD_p$	Average volume of the population
Surface area mean diameter, D_S	$N\pi D_S^2 = \int_0^\infty n_S(D_p) dD_p$	Diameter of the particle whose surface area equals the mean surface area of the population
Volume mean diameter, D_V	$N\frac{\pi}{6} D_V^3 = \int_0^\infty n_V(D_p) dD_p$	Diameter of the particle whose volume equals the mean volume of the population
Surface area median diameter, D_{S_m}	$\int_0^{D_{S_m}} n_S(D_p) dD_p = \frac{1}{2} \int_0^\infty n_S(D_p) dD_p$	Diameter below which one-half the particle surface area lies and above which one-half the particle surface area lies
Volume median diameter, D_{V_m}	$\int_0^{D_{V_m}} n_V(D_p) dD_p = \frac{1}{2} \int_0^\infty n_V(D_p) dD_p$	Diameter below which one-half the particle volume lies and above which one-half the particle volume lies
Mode diameter, D_{mode}	$\left(\frac{dn_N(D_p)}{dD_p}\right)_{D_{mode}} = 0$	Local maximum of the number distribution

7.1.6 The Log-Normal Distribution

A measured aerosol size distribution can be reported as a table of the distribution values for dozens of diameters. For many applications carrying around hundreds or thousands of aerosol distribution values is awkward. In these cases it is often convenient to use a relatively simple mathematical function to describe the atmospheric aerosol distribution. These functions are semiempirical in nature and have been chosen because they match well observed shapes of ambient distributions (Hinds, 1982). Of the various mathematical functions that have been proposed, the log-normal distribution (Aitchison and Brown, 1957) often provides a good fit and is regularly used in atmospheric applications. A series of other distributions are discussed in the next section.

The normal distribution for a quantity u defined from $-\infty < u < \infty$ is given by

$$n(u) = \frac{N}{(2\pi)^{1/2}\sigma_u} \exp\left(-\frac{(u - \bar{u})^2}{2\sigma_u^2}\right) \quad (7.31)$$

where \bar{u} is the mean of the distribution, σ_u^2 is the variance, and

$$N = \int_{-\infty}^{\infty} n(u) du \quad (7.32)$$

The normal distribution has the characteristic bell shape, with a maximum at \bar{u} . The standard deviation, σ_u , quantifies the width of the distribution, and 68% of the area below the curve is in the range $\bar{u} \pm \sigma_u$.

A quantity u is *log-normally distributed* if its logarithm is normally distributed. Either the natural ($\ln u$) or the base 10 logarithm ($\log u$) can be used, but since the former is more common, we will express our results in terms of $\ln D_p$. An aerosol population is therefore log-normally distributed if $u = \ln D_p$ satisfies (7.31), or

$$n_N^e(\ln D_p) = \frac{dN}{d \ln D_p} = \frac{N}{(2\pi)^{1/2} \ln \sigma_g} \exp\left(-\frac{(\ln D_p - \ln \bar{D}_{pg})^2}{2 \ln^2 \sigma_g}\right) \quad (7.33)$$

where N is the total aerosol number concentration, and \bar{D}_{pg} and σ_g are for the time being the two parameters of the distribution. Shortly we will discuss the physical significance of these parameters. The distribution $n_N(D_p)$ is often used instead of $n_N^e(\ln D_p)$. Combining (7.21) with (7.33)

$$n_N(D_p) = \frac{dN}{dD_p} = \frac{N}{(2\pi)^{1/2} D_p \ln \sigma_g} \exp\left(-\frac{(\ln D_p - \ln \bar{D}_{pg})^2}{2 \ln^2 \sigma_g}\right) \quad (7.34)$$

A log-normal aerosol distribution with $\bar{D}_{pg} = 0.8 \mu\text{m}$ and $\sigma_g = 1.5$ is depicted in Figure 7.7.

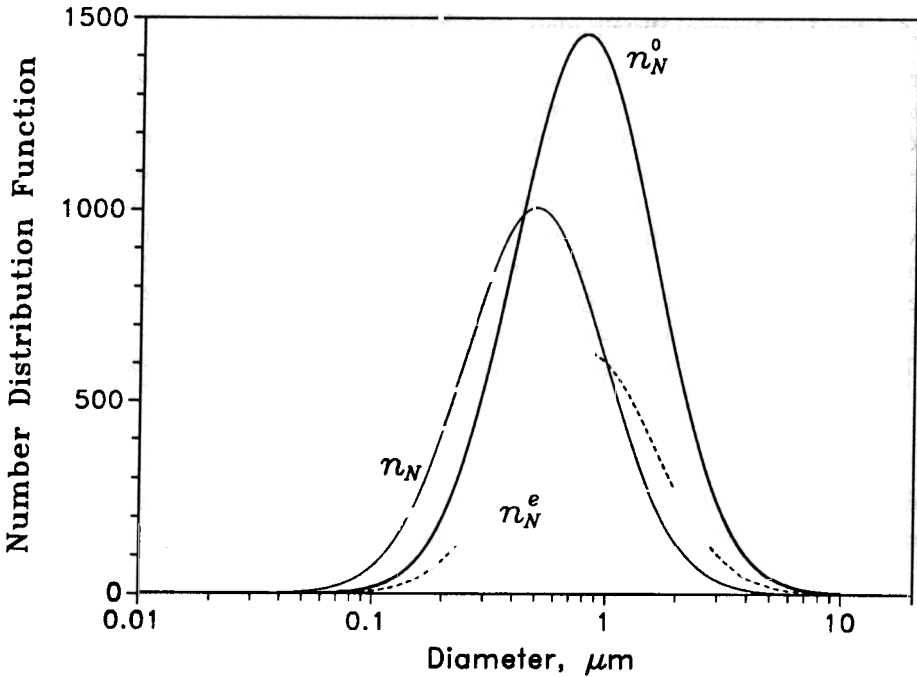


FIGURE 7.7 Aerosol distribution functions, $n_N(D_p)$, $n_N^0(\log D_p)$ and $n_N^e(\ln D_p)$ for a log-normally distributed aerosol distribution $\bar{D}_{pg} = 0.8 \mu\text{m}$ and $\sigma_g = 1.5$ versus $\log D_p$. Even if all three functions describe the same aerosol population, they differ from each other because they use a different independent variable. The aerosol number is the area below the $n_N^0(\log D_p)$ curve.

We now wish to examine the physical significance of the two parameters \bar{D}_{pg} and σ_g . To do so let us define the cumulative size distribution $F_N(D_p^*)$ as the concentration of particles in the population with diameters smaller than or equal to D_p^* , that is,

$$F_N(D_p^*) = \int_0^{D_p^*} n_N(D_p) dD_p \tag{7.35}$$

If the aerosol distribution is log-normal, $n_N(D_p)$ is given by (7.34) and therefore

$$F_N(D_p^*) = \frac{N}{(2\pi)^{1/2} \ln \sigma_g} \int_0^{D_p^*} \frac{1}{D_p} \exp \left[-\frac{(\ln D_p - \ln \bar{D}_{pg})^2}{2 \ln^2 \sigma_g} \right] dD_p \tag{7.36}$$

To evaluate this integral we let $\eta = (\ln D_p - \ln \bar{D}_{pg})/\sqrt{2} \ln \sigma_g$ and we obtain

$$F_N(D_p^*) = \frac{N}{\sqrt{\pi}} \int_{-\infty}^{(\ln D_p^* - \ln \bar{D}_{pg})/\sqrt{2} \ln \sigma_g} e^{-\eta^2} d\eta \tag{7.37}$$

The error function erf z is defined as

$$\text{erf } z = \frac{2}{\sqrt{\pi}} \int_0^z e^{-\eta^2} d\eta$$

and erf(0) = 0, erf(∞) = 1. If we divide the integral in (7.37) into one from $-\infty$ to 0 and the second from 0 to $(\ln D_p^* - \ln \bar{D}_{pg})/\sqrt{2} \ln \sigma_g$, then the first integral is seen to be equal to $\sqrt{\pi}/2$ and the second to $(\sqrt{\pi}/2)\text{erf}[(\ln D_p^* - \ln \bar{D}_{pg})/\sqrt{2} \ln \sigma_g]$. Thus for the log-normal distribution

$$F_N(D_p) = \frac{N}{2} + \frac{N}{2} \text{erf}\left(\frac{\ln(D_p/\bar{D}_{pg})}{\sqrt{2} \ln \sigma_g}\right) \tag{7.39}$$

For $D_p = \bar{D}_{pg}$, since erf(0) = 0

$$F(\bar{D}_{pg}) = \frac{N}{2}$$

and we see that $\bar{D}_{pg} = D_{\text{med}}$ is the *median diameter*, that is, the diameter for which exactly one-half of the particles are smaller and one-half are larger. To understand the role of σ_g let us consider the diameter $D_{p\sigma}$ for which $\sigma_g = D_{p\sigma}/\bar{D}_{pg}$. At that diameter, using (7.39),

$$F(D_{p\sigma}) = N \left[\frac{1}{2} + \frac{1}{2} \text{erf}\left(\frac{1}{\sqrt{2}}\right) \right] = 0.841N$$

Thus σ_g is the ratio of the diameter below which 84.1% of the particles lie to the median diameter and is termed the *geometric standard deviation*. A monodisperse aerosol population has $\sigma_g = 1$. For any distribution, 67% of all particles lie in the range from \bar{D}_{pg}/σ_g to $\bar{D}_{pg}\sigma_g$ and 95% of all particles lie in the range from $\bar{D}_{pg}/2\sigma_g$ to $2\bar{D}_{pg}\sigma_g$.

Let us calculate the mean diameter \bar{D}_p of a log-normally distributed aerosol. By definition, the mean diameter is found from

$$\bar{D}_p = \frac{1}{N} \int_0^\infty D_p n_N(D_p) dD_p \tag{7.42}$$

which we wish to evaluate in the case of $n_N(D_p)$ given by (7.34). Therefore

$$\bar{D}_p = \frac{1}{\sqrt{2\pi} \ln \sigma_g} \int_0^\infty \exp\left(-\frac{(\ln D_p - \ln \bar{D}_{pg})^2}{2 \ln^2 \sigma_g}\right) dD_p$$

After evaluating the integral one finds that

$$\bar{D}_p = \bar{D}_{pg} \exp\left(\frac{\ln^2 \sigma_g}{2}\right)$$

We see that the mean diameter of a log-normal distribution depends on both \bar{D}_{pg} and σ_g .

7.1.7 Plotting the Log-Normal Distribution

The cumulative distribution function $F_N(D_p)$ for a log-normally distributed aerosol population is given by (7.39). Defining the normalized cumulative distribution,

$$\bar{F}_N(D_p) = \frac{F_N(D_p)}{N} \quad (7.45)$$

one obtains

$$\bar{F}_N(D_p) = \frac{1}{2} + \frac{1}{2} \operatorname{erf} \left(\frac{\ln D_p - \ln \bar{D}_{pg}}{\sqrt{2} \ln \sigma_g} \right) \quad (7.46)$$

The cumulative distribution fraction $\bar{F}_N(D_p)$ can be plotted against the logarithm of particle diameter on special log-probability graph paper. In these diagrams the x axis is logarithmic and the y axis is scaled according to the error function. This scaling compresses the scale near the median (50% point) and expands the scale near the ends. Several computer graphics programs also allow the use of a probability axis. In these graphs the cumulative distribution function of a log-normal distribution is a straight line (Figure 7.8). The point at $\bar{F}_N(D_p) = 0.5$ occurs when $D_p = \bar{D}_{pg}$. Therefore the geometric mean, or median, of the distribution is the value of D_p where the straight line plot of \bar{F}_N crosses the 50th percentile. The point at $\bar{F}_N(D_p) = 0.84$ occurs for $\ln D_p = \ln \bar{D}_p + \ln \sigma_g$ or $D_p = \bar{D}_p \sigma_g$. The slope of the line is therefore related to the geometric standard deviation of the distribution. Log-normal distributions with the same standard deviation when plotted in log-probability coordinates are parallel to each other. A small standard deviation corresponds to a

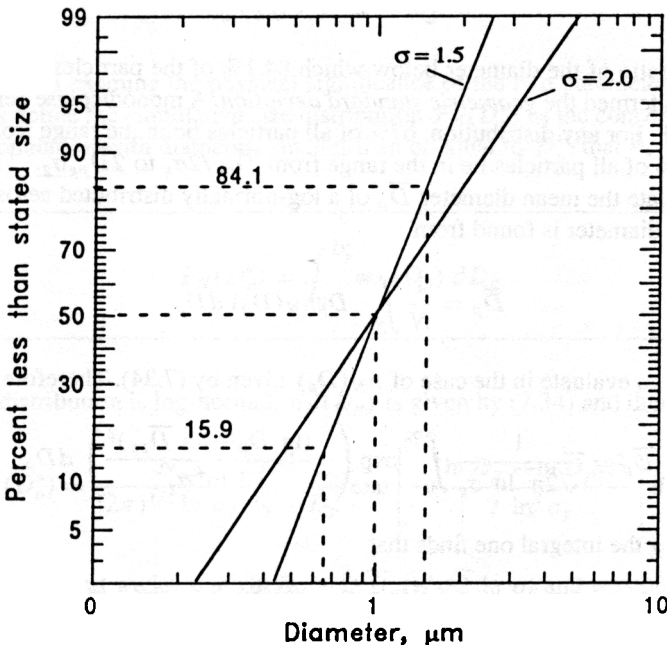


FIGURE 7.8 Cumulative log-normal aerosol number distributions plotted on log-probability paper. The distributions have mean diameter of $1 \mu\text{m}$ and $\sigma_g = 2$ and 1.5 , respectively.

narrow distribution and to a steep line in the log-probability graph (Figure 7.8). The geometric standard deviation can be calculated as the ratio of the diameter $D_{p+\sigma}$ for which $\bar{F}_N(D_{p+\sigma}) = 0.84$ to the mean diameter

$$\sigma_g = \frac{D_{p+\sigma}}{\bar{D}_p} \tag{7.47}$$

7.1.8 Properties of the Log-Normal Distribution

We have discussed the properties of the log-normal distribution for the number concentration. The next step is examination of the surface and volume distributions corresponding to a log-normal number distribution given by (7.34). Since $n_S(D_p) = \pi D_p^2 n_N(D_p)$ and $n_V(D_p) = (\pi/6) D_p^3 n_N(D_p)$, let us determine the forms of $n_S(D_p)$ and $n_V(D_p)$ when $n_N(D_p)$ is log-normal. From (7.34) one gets

$$n_S(D_p) = \frac{\pi D_p^2 N}{(2\pi)^{1/2} D_p \ln \sigma_g} \exp\left(- \frac{(\ln D_p - \ln \bar{D}_{pg})^2}{2 \ln^2 \sigma_g} \right)$$

By letting $D_p^2 = \exp(2 \ln D_p)$, expanding the exponential, and completing the square in the exponent, (7.48) becomes

$$n_S(D_p) = \frac{N}{(2\pi)^{1/2} D_p \ln \sigma_g} \exp(2 \ln \bar{D}_{pg} + 2 \ln^2 \sigma_g) \times \exp\left(- \frac{[\ln D_p - (\ln \bar{D}_{pg} + 2 \ln^2 \sigma_g)]^2}{2 \ln^2 \sigma_g} \right)$$

Thus we see that if the number distribution $n_N(D_p)$ is log-normal, the surface distribution $n_S(D_p)$ is also log-normal with the same geometric standard deviation σ_g as the parent distribution and with the surface median diameter given by

$$\ln \bar{D}_{pgS} = \ln \bar{D}_{pg} + 2 \ln^2 \sigma_g \tag{7.50}$$

The above calculations can be repeated for the volume distribution and one can show that

$$n_V(D_p) = \frac{\pi D_p^3 N}{6(2\pi)^{1/2} D_p \ln \sigma_g} \exp\left(- \frac{(\ln D_p - \ln \bar{D}_{pg})^2}{2 \ln^2 \sigma_g} \right)$$

or by letting $D_p^3 = \exp(3 \ln D_p)$, expanding the exponential, and completing the square in the exponent, (7.51) becomes

$$n_V(D_p) = \frac{N}{(2\pi)^{1/2} D_p \ln \sigma_g} \exp(3 \ln \bar{D}_{pg} + \frac{9}{2} \ln^2 \sigma_g) \times \exp\left(- \frac{[\ln D_p - (\ln \bar{D}_{pg} + 3 \ln^2 \sigma_g)]^2}{2 \ln^2 \sigma_g} \right) \tag{7.51a}$$

Therefore if the number distribution $n_N(D_p)$ is log-normal, the volume distribution $n_V(D_p)$ is also log-normal with the same geometric standard deviation σ_g as the parent distribution and with the volume median diameter given by

$$\ln \bar{D}_{pgV} = \ln \bar{D}_{pg} + 3 \ln^2 \sigma_g \quad (7.52)$$

The constant standard deviation for the number, surface, and volume distributions for any log-normal distribution is one of the great advantages of this mathematical representation.

Plotting the surface and volume distributions of a log-normal aerosol distribution on log-probability paper would also result in straight lines parallel to each other (same standard deviation). For the distribution shown in Figure 7.8 with $\bar{D}_{pg} = 1.0 \mu\text{m}$ and $\sigma_g = 2.0$, the resulting surface area and volume median diameters are approximately $2.6 \mu\text{m}$ and $4.2 \mu\text{m}$, respectively.

7.1.9 Other Aerosol Distributions

The Power-Law Distribution A series of other mathematical functions have been proposed for the description of atmospheric aerosol distributions. The power law, or Junge, distribution has often been used in atmospheric science (Pruppacher and Klett, 1980)

$$n_N^\circ(\log D_p) = \frac{C}{(D_p)^\alpha} \quad (7.53)$$

where C and α are constants. Plotting of the power-law distribution on log-log coordinates results in a straight line with slope $-\alpha$ and for $D_p = 1 \mu\text{m}$, $n_N^\circ = C$ (Figure 7.9). This distribution function assumes that the aerosol number concentration decreases monotonically with increasing particle size. This is not generally true in the atmosphere so the power-law distribution should be used with caution and only for specific size ranges (usually for $D_p > 0.1 \mu\text{m}$). The derived distributions are accurate only over a limited size range and extrapolation to smaller or larger sizes may introduce significant errors. Values of α from 2 to 5 have been suggested for ambient aerosol distributions (Pruppacher and Klett, 1980) (Figure 7.9). The corresponding volume distribution can be calculated using (7.10),

$$n_V^\circ(\log D_p) = \frac{\pi C}{6} D_p^{3-\alpha} \quad (7.54)$$

Leitch and Isaac (1991) proposed that, to a first approximation, most of the number distributions for the continental aerosol distributions can be represented by a -3 power-law function. However, important features of these distributions are clearly lost by such representation. On a log-diameter volume distribution plot, the corresponding -3 power-law

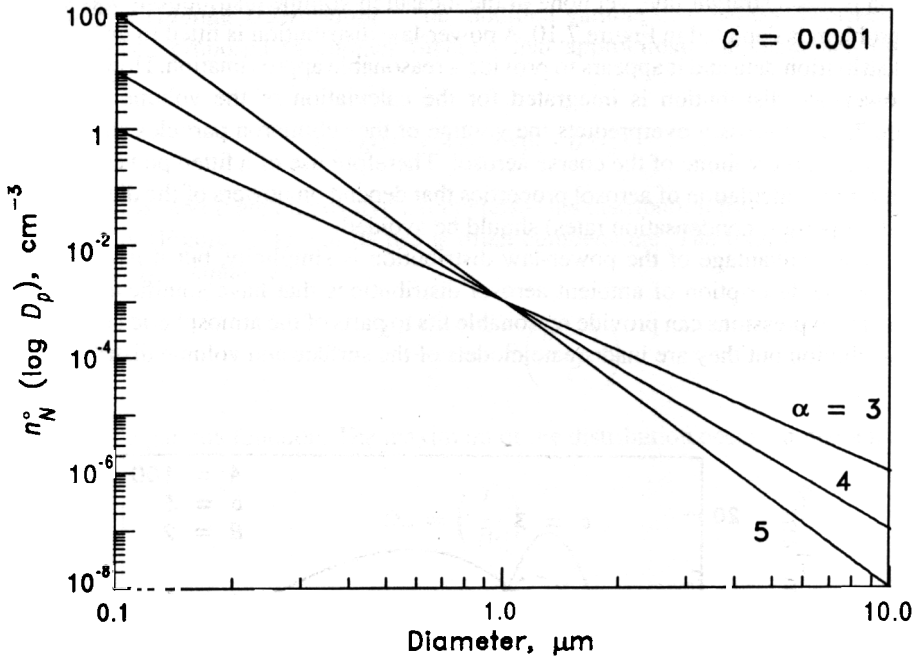


FIGURE 7.9 Power-law distributions for $C = 0.001$, and different values of α

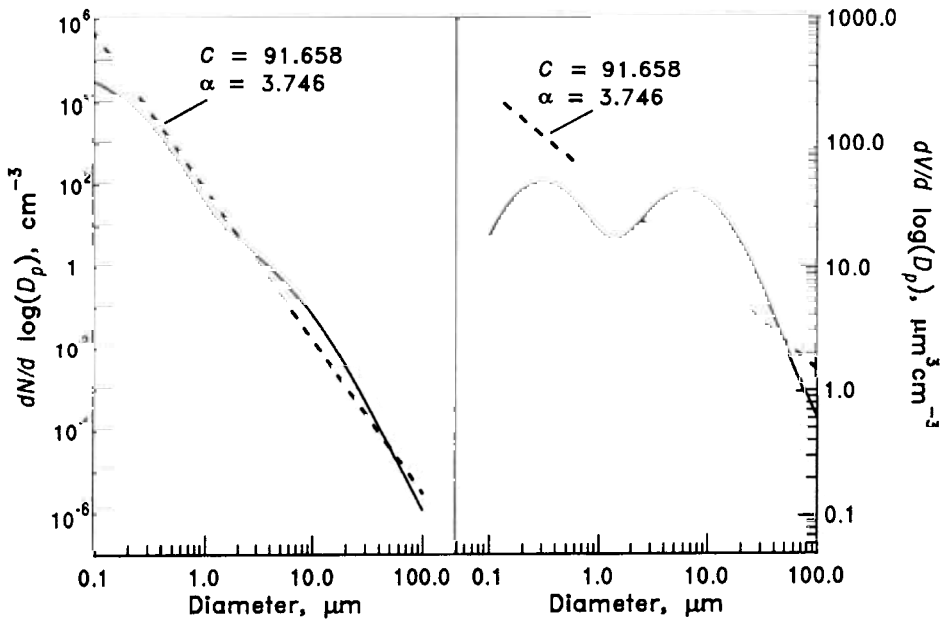


FIGURE 7.10 Fitting of an urban aerosol number distribution with a power-law distribution (left) and comparison of the corresponding volume distributions (right). Even if the power-law distribution appears to match the number distribution, it fails to reproduce the volume distribution.

function is just a straight line, yet none of the measured volume distributions was straight. This problem is depicted in Figure 7.10. A power-law distribution is fitted to urban aerosol size distribution data and it appears to provide a reasonable approximation. However, when the power-law distribution is integrated for the calculation of the volume distribution (Figure 7.10), it grossly overpredicts the volume of the submicron particles and seriously underpredicts the volume of the coarse aerosol. Therefore use of a fitted power-law distribution for the calculation of aerosol properties that depend on powers of the diameter (e.g., optical properties, condensation rates) should be avoided.

The main advantage of the power-law distribution is simplicity, but it is often inadequate for the description of ambient aerosol distributions that have significant structure. Power-law expressions can provide reasonable fits to parts of the atmospheric aerosol number distribution but they are inadequate models of the surface and volume distributions.

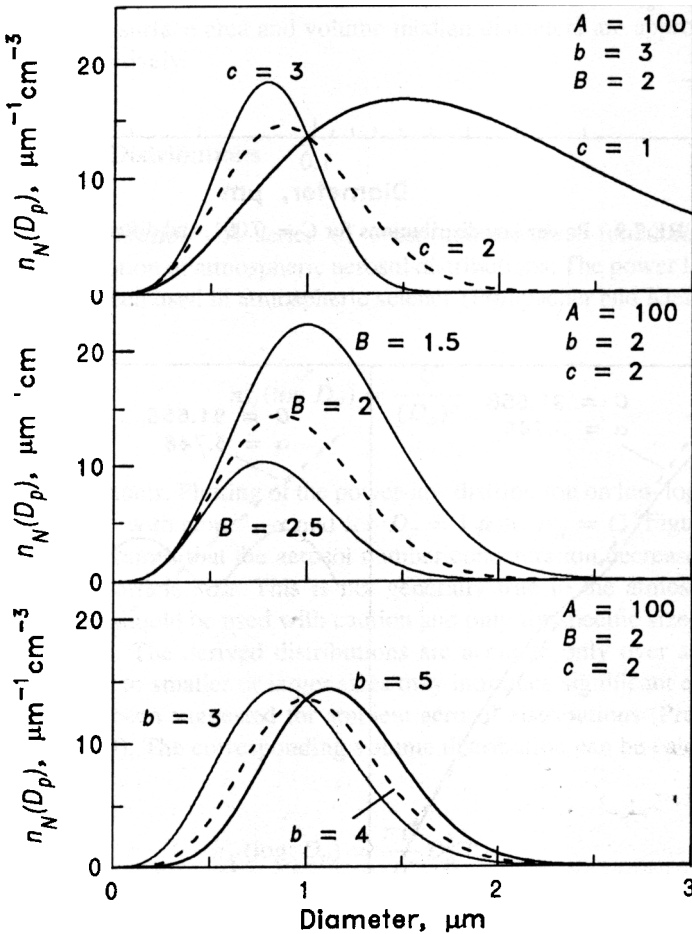


FIGURE 7.11 Modified gamma aerosol distributions for various combinations of the parameters A , b , B , and c .

The Modified Gamma Distribution The modified gamma distribution (Deirmendjian, 1969) has been proposed as another function that approximates ambient aerosol size distributions,

$$n_N(D_p) = A D_p^b \exp(-B D_p^c) \quad (7.55)$$

where A , b , B , and c are all positive parameters. This distribution form provides significant flexibility (Figure 7.11), but its use is often cumbersome. The total aerosol number concentration N is equal to

$$N = \frac{A B^{-(b+1)/c}}{c} \Gamma\left(\frac{b+1}{c}\right)$$

where Γ is the gamma function. The maximum of the distribution occurs at diameter D_m ,

$$D_m = \left(\frac{b}{Bc}\right)^{1/c}$$

7.2 AMBIENT AEROSOL SIZE DISTRIBUTIONS

Atmospheric aerosol size distributions are often described as the sum of n log-normal distributions,

$$n_N^{\circ}(\log D_p) = \sum_{i=1}^n \frac{N_i}{(2\pi)^{1/2} \log \sigma_i} \exp\left(-\frac{(\log D_p - \log \bar{D}_{pi})^2}{2 \log^2 \sigma_i}\right)$$

where N_i is the number concentration, \bar{D}_{pi} is the mean diameter, and σ_i is the standard deviation of the i^{th} log-normal mode. In this case $3n$ parameters are necessary for the description of the full aerosol distribution. Characteristics of model aerosol distributions are presented in Table 7.3 following the suggestions of Jaenicke (1993).

7.2.1 Urban Aerosols

Urban aerosols are mixtures of primary particulate emissions from industries, transportation, power generation, and natural sources and secondary material formed by gas-to-particle conversion mechanisms. The number distribution is dominated by particles smaller than $0.1 \mu\text{m}$, while most of the surface area is in the 0.1 to $0.5 \mu\text{m}$ size range. On the contrary, the aerosol mass distribution has usually two distinct modes, one in the submicron regime (referred to as the accumulation mode) and the other in the coarse particle regime (Figure 7.12).

The aerosol size distribution is quite variable in an urban area. Extremely high concentrations of fine particles (less than $0.1 \mu\text{m}$ in diameter) are found close to sources (e.g., highways), but their concentration decreases rapidly with distance from the source (Figure

TABLE 7.3 Parameters for Model Aerosol Distributions Expressed as the Sum of Three Log-Normal Modes

Type	Mode I			Mode II			Mode III		
	N (cm^{-3})	D_p (μm)	$\log \sigma$	N (cm^{-3})	D_p (μm)	$\log \sigma$	N (cm^{-3})	D_p (μm)	$\log \sigma$
Urban	9.93×10^4	0.013	0.245	1.11×10^3	0.014	0.666	3.64×10^4	0.05	0.337
Marine	133	0.008	0.657	66.6	0.266	0.210	3.1	0.58	0.396
Rural	6650	0.015	0.225	147	0.054	0.557	1990	0.084	0.266
Remote	3200	0.02	0.161	2900	0.116	0.217	0.3	1.8	0.380
continental									
Free troposphere	129	0.007	0.645	59.7	0.250	0.253	63.5	0.52	0.422
Polar	21.7	0.138	0.245	0.186	0.75	0.300	3×10^{-4}	8.6	0.291
Desert	726	0.002	0.247	114	0.038	0.770	0.178	21.6	0.433

Source: Jaenicke (1993)

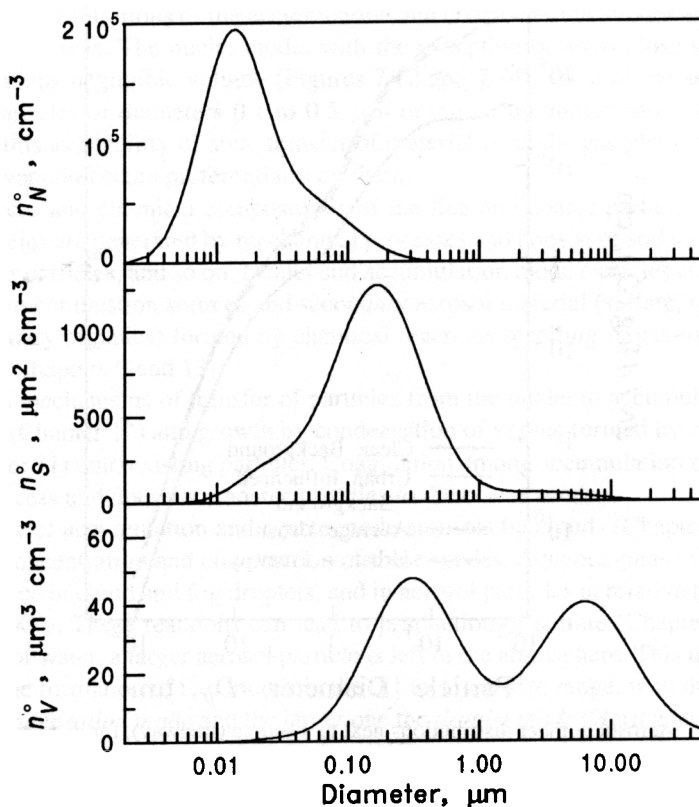


FIGURE 7.12 Typical urban aerosol number, surface, and volume distributions.

7.13). Figure 7.13 describes the number of particles as a function of their diameter (both in logarithmic scales) for a variety of environments. There are roughly an order of magnitude more particles close to the freeway compared to the average urban concentration. Figure 7.14 illustrates the corresponding volume distributions. These distributions show that most of the particles in an urban area are smaller than $0.1 \mu\text{m}$, while most of the particle mass is found in particles with diameters larger than $0.1 \mu\text{m}$.

An important feature of atmospheric aerosol size distributions is their multimodal character. Mass distributions, measured in urban centers, are characterized by three modes with a minimum between 1.0 and $3 \mu\text{m}$. The size range of particles larger than the minimum (supermicron particles) is termed "coarse," while the smaller particles are called "fine." The three modes present in the mass distribution of Figure 7.14 correspond to the nuclei mode (particles below $0.1 \mu\text{m}$), accumulation mode ($0.1 < D_p < 1 \mu\text{m}$), and coarse mode ($D_p > 1 \mu\text{m}$) (Whitby and Sverdrup, 1980). Thus the fine particles include both accumulation and nuclei modes. The boundaries between these sections are not precise (recall in Chapter 2 that we divided fine and coarse modes at $2.5 \mu\text{m}$ diameter). Note that our definition of modes has been based on the mass (or volume distribution). The location of modes may be different if they are based on the number or surface distribution.

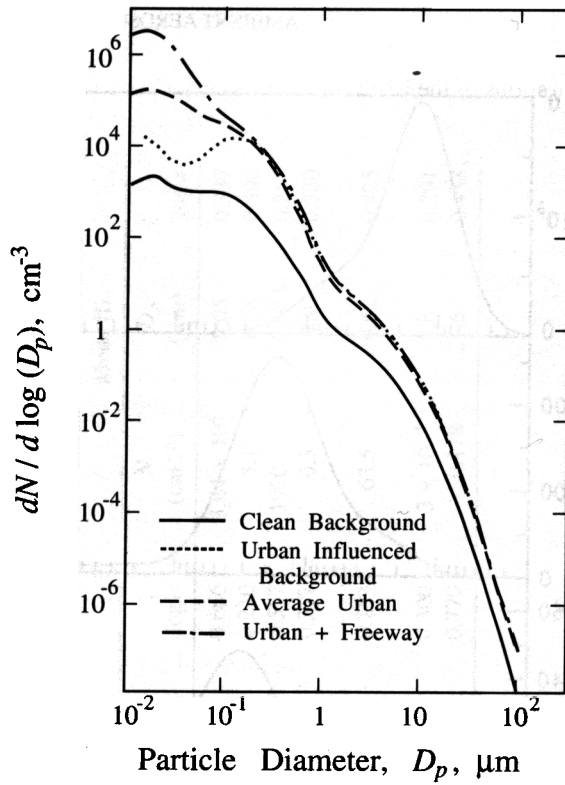


FIGURE 7.13 Aerosol number distributions next to a source (freeway), for average urban, for urban influenced background, and for background conditions.

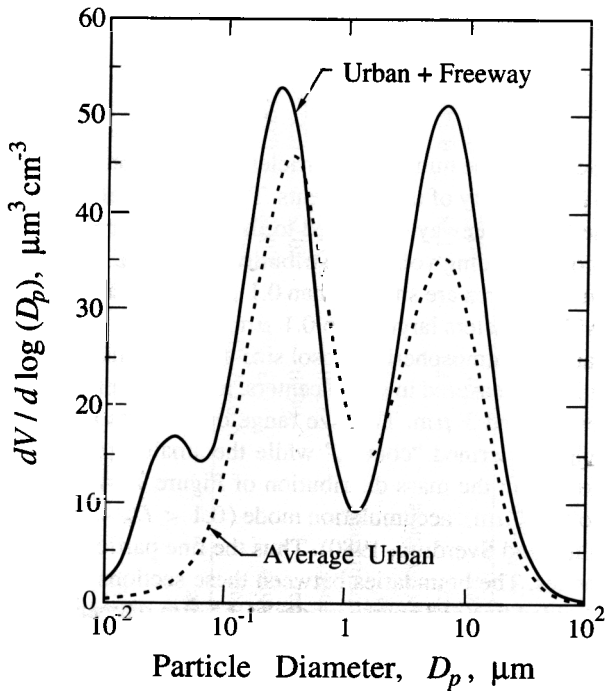


FIGURE 7.14 Aerosol volume distributions next to a source (freeway) and for average urban conditions.

The mass concentrations of the accumulation and coarse particle modes are comparable for most urban areas. The nuclei mode, with the exception of areas close to combustion sources, contains negligible volume (Figures 7.12 and 7.14). Most of the aerosol surface area is in particles of diameters 0.1 to 0.5 μm in the accumulation mode (Figure 7.12). Because of this availability of area, transfer of material from the gas phase during gas-to-particle conversion occurs preferentially on them.

The sources and chemical compositions of the fine and coarse particles are different. Coarse particles are generated by mechanical processes and consist of soil dust, sea salt, fly ash, tire wear particles, and so on. Nuclei and accumulation mode particles contain primary particles from combustion sources and secondary aerosol material (sulfate, nitrate, ammonium, secondary organics) formed by chemical reactions resulting in gas-to-particle conversion (see Chapters 9 and 13).

The main mechanisms of transfer of particles from the nuclei to accumulation mode is coagulation (Chapter 12) and growth by condensation of vapors formed by chemical reactions (Chapter 11) onto existing particles. Coagulation among accumulation mode particles is a slow process and does not transfer particles to the coarse mode.

Processing of accumulation and coarse mode aerosols by clouds (Chapter 15) can also modify the concentration and composition of these modes. Aqueous-phase chemical reactions take place in cloud and fog droplets, and in aerosol particles at relative humidities approaching 100%. These reactions can lead to production of sulfate (Chapter 6) and after evaporation of water, a larger aerosol particle is left in the atmosphere. This transformation can lead to the formation of two modes in the 0.1 to 1 μm size range, with the smaller one called the *condensation mode* and the larger one the *droplet mode* (Hering and Friedlander, 1982; John et al., 1990; Meng and Seinfeld, 1994).

Terms often used to describe the aerosol mass concentration include total suspended particulate matter (TSP) and PM_x (particulate matter with diameter smaller than x μm). TSP refers to the mass concentration of atmospheric particles smaller than 40 to 50 μm , while $\text{PM}_{2.5}$ and PM_{10} are routinely monitored. For a description of the sampling issues and problems related to the measurement of TSP, $\text{PM}_{2.5}$, and PM_{10} the reader is referred to the EPA Particulate Matter Criteria document (U.S. EPA, 1996).

7.2.2 Marine Aerosols

In the absence of significant transport of continental aerosols, particles over the remote oceans are largely of marine origin (Savoie and Prospero, 1989). Marine atmospheric particle concentrations are normally in the range of 100 to 300 cm^{-3} . Their size distribution is usually characterized by three modes (Figure 7.15): the nuclei ($D_p < 0.1$ μm) the accumulation ($0.1 < D_p < 0.6$ μm), and the coarse ($D_p > 0.6$ μm) (Fitzgerald, 1991). Typically, the coarse particle mode, comprising 95% of the total mass but only 5 to 10% of the particle number (Figure 7.16), results from the evaporation of sea spray produced by bursting bubbles or wind-induced wave breaking (Blanchard and Woodcock, 1957; Monahan et al., 1983). Typical sea-salt aerosol concentrations in the marine boundary layer (MBL) are around 5 to 30 cm^{-3} (Blanchard and Cipriano, 1987; O'Dowd and Smith, 1993).

Figures 7.15 and 7.16 show number and volume aerosol distributions in clean maritime air measured by several investigators (Mészáros and Vissy, 1974; Hoppel et al., 1989; Haaf and Jaenicke, 1980; De Leeuw, 1986) and a model marine aerosol size distribution. The dis-

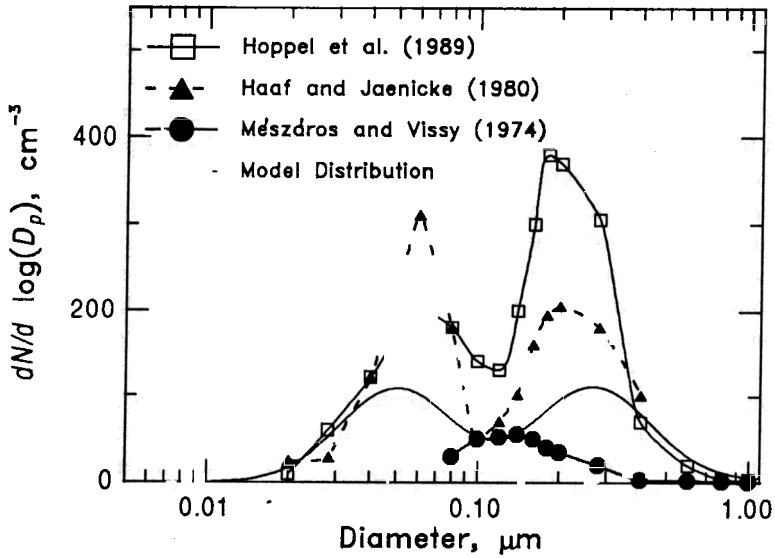


FIGURE 7.15 Measured marine aerosol number distributions and a model distribution used to represent average conditions.

tributions of Hoppel et al. (1989) and De Leeuw (1986) were obtained at wind speeds of less than 5 m s^{-1} in the subtropical and North Atlantic, respectively. The distribution of Mészáros and Vissy (1974) is an average of spectra obtained in the South Atlantic and Indian Oceans during periods when the average wind speed was 12 m s^{-1} . It is difficult to determine the extent to which the differences in these size distributions are the result of differences in sampling location and meteorological conditions such as wind speed (which af-

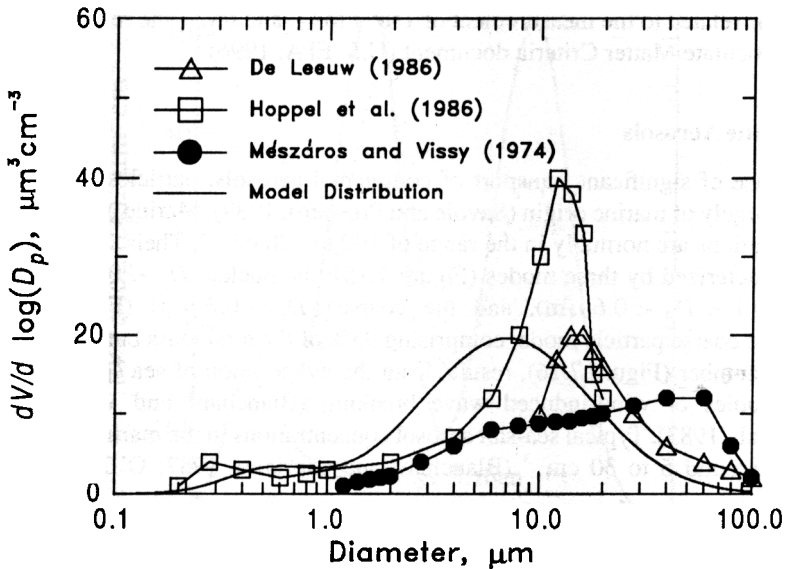


FIGURE 7.16 Measured marine aerosol volume distributions and a model distribution used to represent average conditions.

fects the concentrations of the larger particles), or to uncertainties inherent in the different measurement methods.

7.2.3 Rural Continental Aerosols

Aerosols in rural areas are mainly of natural origin but with a moderate influence of anthropogenic sources (Hobbs et al., 1985). The number distribution is characterized by two modes at diameters about 0.02 and 0.08 μm , respectively (Jaenicke, 1993), while the mass distribution is dominated by the coarse mode centered at around 7 μm (Figure 7.17). The mass distribution of continental aerosol not influenced by local sources has a small accumulation mode and no nuclei mode. The PM_{10} concentration of rural aerosols is around $20 \mu\text{g m}^{-3}$.

7.2.4 Remote Continental Aerosols

Primary particles (e.g., dust, pollens, plant waxes) and secondary oxidation products are the main components of remote continental aerosol (Deepak and Gali, 1991). Aerosol number concentrations average around 2000 to 10,000 cm^{-3} and PM_{10} concentrations are

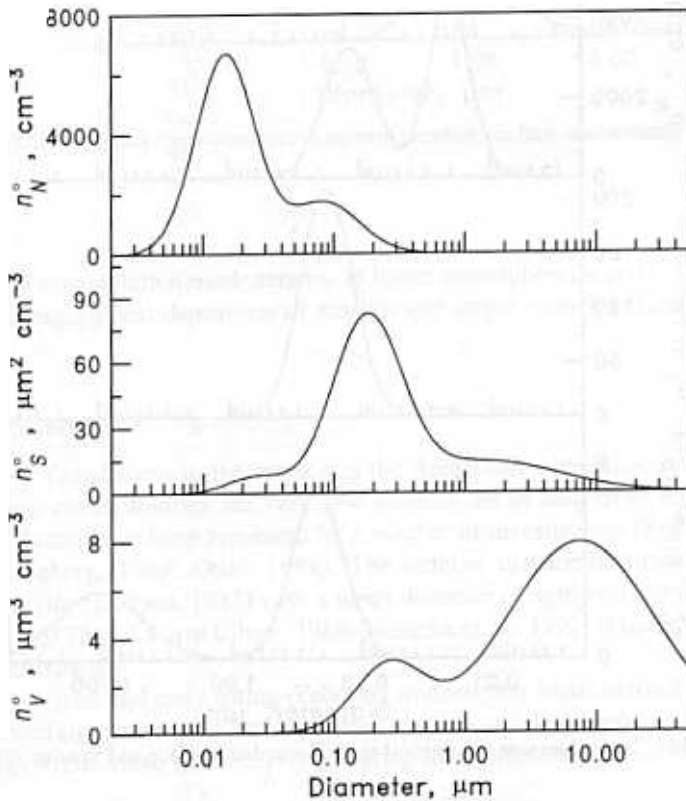


FIGURE 7.17 Typical rural continental aerosol number, surface, and volume distributions

around $10 \mu\text{g m}^{-3}$ (Bashurova et al., 1992; Koutsenogii et al., 1993; Koutsenogii and Jaenicke, 1994). For the continental United States PM_{10} concentrations in remote areas vary from 5 to $25 \mu\text{g m}^{-3}$ and $\text{PM}_{2.5}$ from 3 to $17 \mu\text{g m}^{-3}$ (U.S. EPA, 1996). Particles smaller than $2.5 \mu\text{m}$ in diameter represent 40 to 80% of the PM_{10} mass and consist mainly of sulfate, ammonium, and organics. The aerosol number distribution may be characterized by three modes at diameters 0.02, 0.1, and $2 \mu\text{m}$ (Jaenicke, 1993) (Figure 7.18).

7.2.5 Free Tropospheric Aerosols

Background free tropospheric aerosol is found in the mid- and upper troposphere above the clouds. Although it occupies a significant fraction of the tropospheric volume, it has received relatively little attention. Most measurements have been carried out at high-elevation ground sites or in subsiding airmasses reflecting midtropospheric conditions. The modes in the number distribution correspond to mean diameters of 0.01 and $0.25 \mu\text{m}$ (Jaenicke, 1993) (Figure 7.19). The middle troposphere spectra typically indicate more

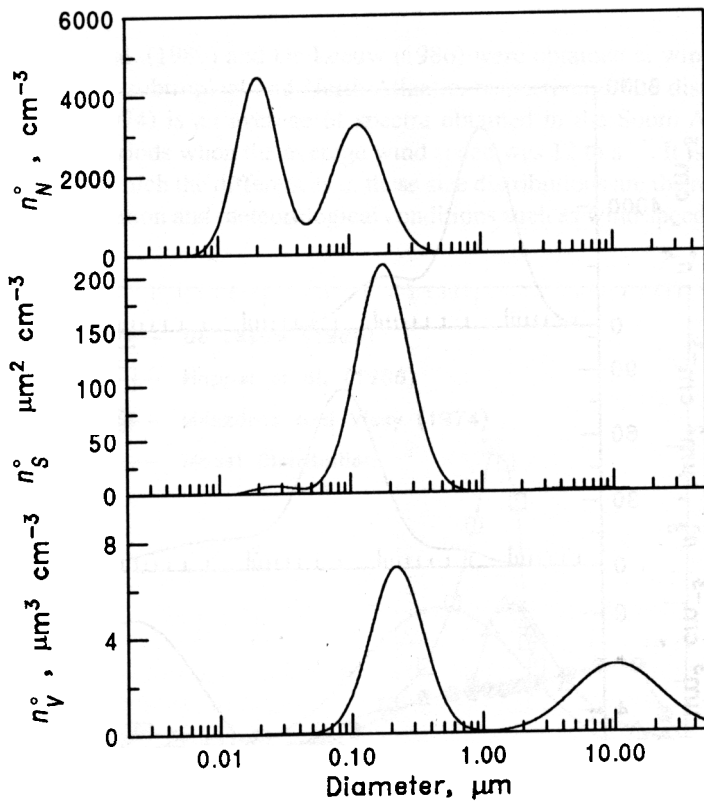


FIGURE 7.18 Typical remote continental aerosol number, surface and volume distributions.

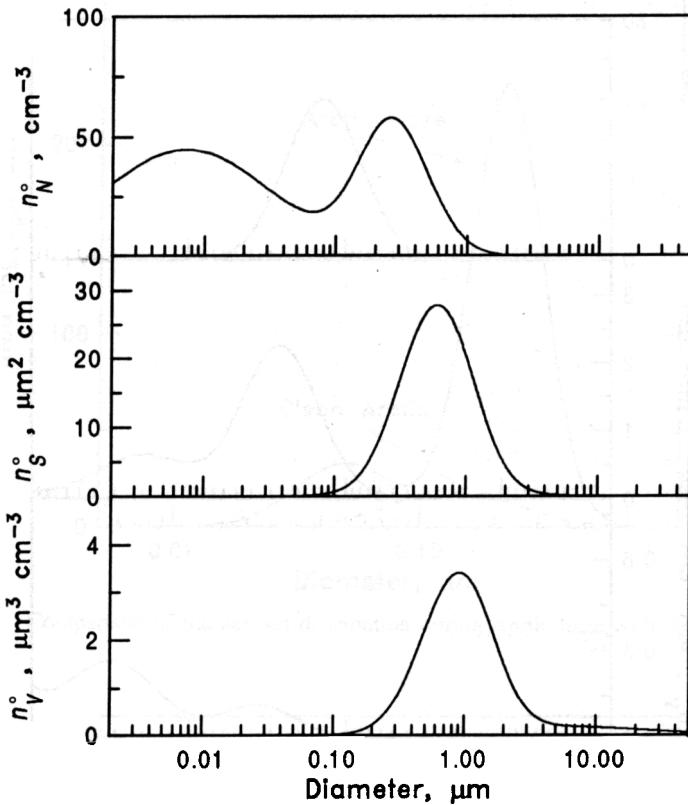


FIGURE 7.19 Typical free tropospheric aerosol number, surface, and volume distributions.

particles in the accumulation mode relative to lower tropospheric spectra, suggesting precipitation scavenging and deposition of smaller and larger particles (Leitch and Isaac, 1991).

7.2.6 Polar Aerosols

Polar aerosols, found close to the surface in the Arctic and Antarctica, reflect their aged character; their concentrations are very low. Collections of data from aerosol measurements in the Arctic have been presented by a number of investigators (Rahn, 1981; Shaw, 1985; Heintzenberg, 1989; Ottar, 1989). The number distribution appears practically monodisperse (Ito and Iwai, 1981) with a mean diameter of approximately $0.15 \mu\text{m}$; two more modes at 0.75 and $8 \mu\text{m}$ (Shaw, 1986; Jaenicke et al., 1992) (Figure 7.20) dominate the mass distribution.

During the winter and early spring (February to April) the Arctic aerosol has been found to be influenced significantly by anthropogenic sources, and the phenomenon is commonly referred to as Arctic Haze (Barrie, 1986). During this period the aerosol number concen-

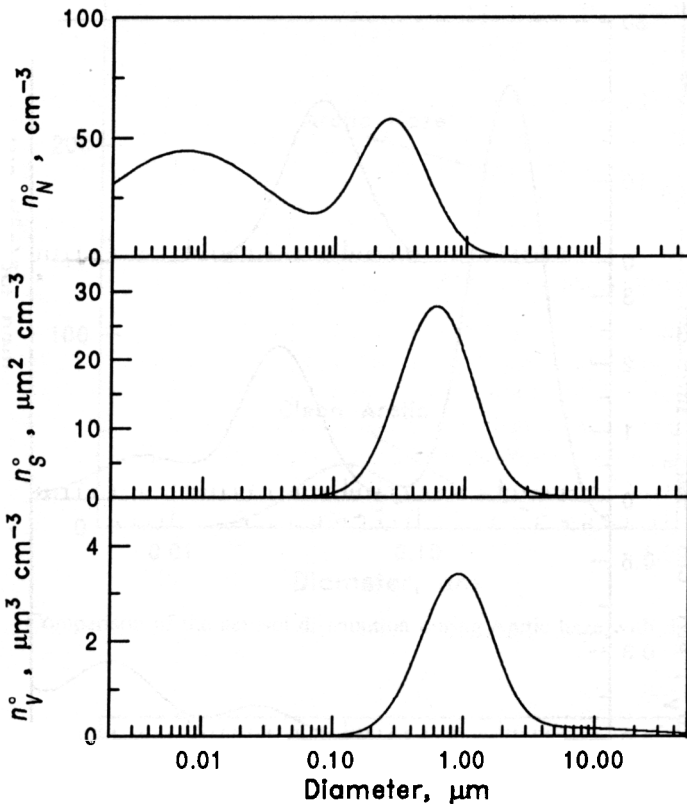


FIGURE 7.19 Typical free tropospheric aerosol number, surface, and volume distributions.

particles in the accumulation mode relative to lower tropospheric spectra, suggesting precipitation scavenging and deposition of smaller and larger particles (Leitch and Isaac, 1991).

7.2.6 Polar Aerosols

Polar aerosols, found close to the surface in the Arctic and Antarctica, reflect their aged character; their concentrations are very low. Collections of data from aerosol measurements in the Arctic have been presented by a number of investigators (Rahn, 1981; Shaw, 1985; Heintzenberg, 1989; Ottar, 1989). The number distribution appears practically monodisperse (Ito and Iwai, 1981) with a mean diameter of approximately $0.15 \mu\text{m}$; two more modes at 0.75 and $8 \mu\text{m}$ (Shaw, 1986; Jaenicke et al., 1992) (Figure 7.20) dominate the mass distribution.

During the winter and early spring (February to April) the Arctic aerosol has been found to be influenced significantly by anthropogenic sources, and the phenomenon is commonly referred to as Arctic Haze (Barrie, 1986). During this period the aerosol number concen-

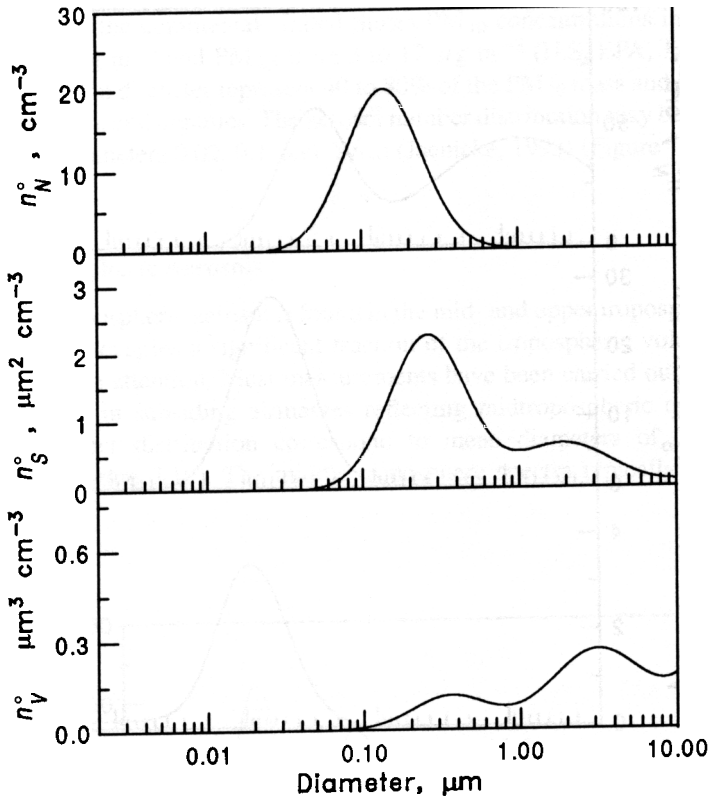


FIGURE 7.20 Typical polar aerosol number, surface, and volume distributions.

tration increases to over 200 cm^{-3} . The nucleation mode mean diameter is at $0.05 \text{ } \mu\text{m}$ and the accumulation mode at $0.2 \text{ } \mu\text{m}$ (Covert and Heintzenberg, 1993) (Figure 7.21). Similar measurements have been reported by Heintzenberg (1980), Radke et al. (1984), and (Shaw, 1984).

The polar aerosol contains carbonaceous material from midlatitude pollution sources, sulfate, sea salt from the surrounding ocean, and mineral dust from arid regions of the corresponding hemisphere. Aerosol PM_{10} concentrations in the polar regions are less than $5 \text{ } \mu\text{g m}^{-3}$ with sulfate representing roughly 40% of the mass.

7.2.7 Desert Aerosols

Desert aerosol, of course present over deserts, actually extends considerably over adjacent regions such as oceans (Jaenicke and Schutz, 1978; d'Almeida and Schutz, 1983; Li et al., 1996). The shape of its size distribution is similar to that of remote continental aerosol but depends strongly on the wind velocity. Its number distribution tends to exhibit three overlapping modes at diameters of $0.01 \text{ } \mu\text{m}$ or less, $0.05 \text{ } \mu\text{m}$, and $10 \text{ } \mu\text{m}$, respectively (Jaenicke, 1993) (Figure 7.22). An average composition of soils and crustal material is

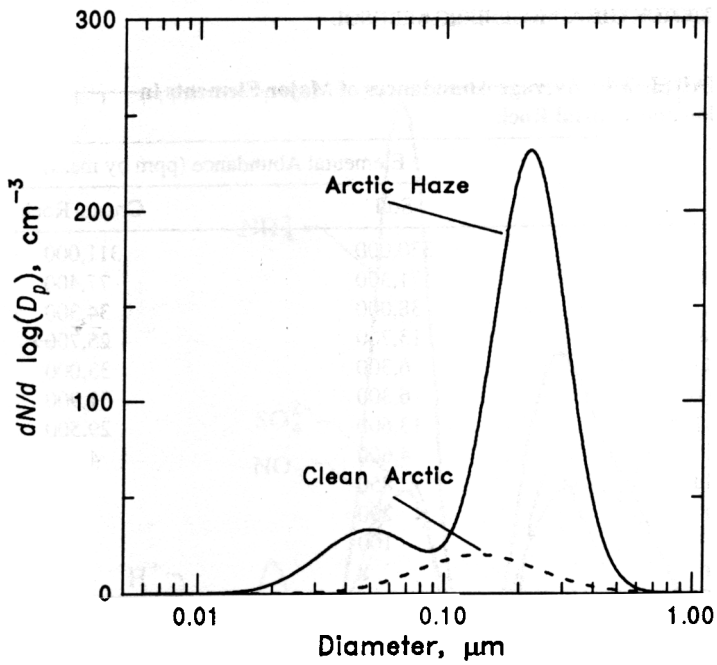


FIGURE 7.21 Comparison of the aerosol distribution during Arctic haze with the typical polar distribution.

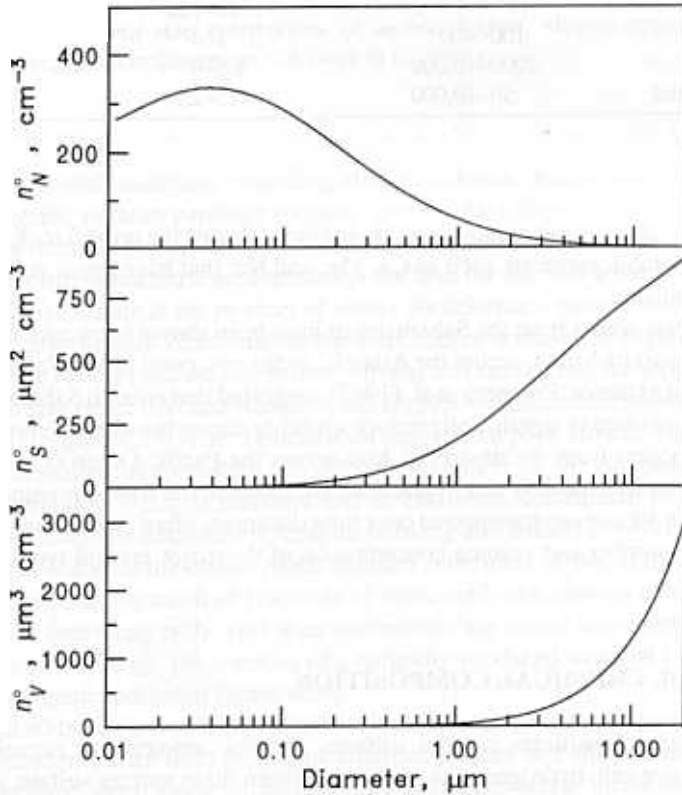


FIGURE 7.22 Typical desert aerosol number, surface, and volume distributions

TABLE 7.4 Average Abundances of Major Elements in Soil and Crustal Rock

Element	Elemental Abundance (ppm by mass)	
	Soil	Crustal Rock
Si	330,000	311,000
Al	71,300	77,400
Fe	38,000	34,300
Ca	13,700	25,700
Mg	6,300	33,000
Na	6,300	31,900
K	13,600	29,500
Ti	4,600	4,400
Mn	850	670
Cr	200	48
V	100	98
Co	8	12

Source: Warneck (1988).

TABLE 7.5 Properties of Atmospheric Aerosol Types

Type		PM ₁ ($\mu\text{g m}^{-3}$)	PM ₁₀ ($\mu\text{g m}^{-3}$)
Urban (polluted)	$10^5 - 4 \times 10^6$	30-150	100-300
Marine	100-400	1-4	10
Rural	2000-10,000	2.5-8	10-40
Remote continental	50-10,000	0.5-2.5	2-10

shown in Table 7.4. The soil composition is similar to that of the crustal rock, with the exception of the soluble elements such as Ca, Mg, and Na, that have lower relative concentrations in the soil.

Individual dust storms from the Sahara desert have been shown to transfer material from the northwest coast of Africa, across the Atlantic, to the east coast of the United States (Ott et al., 1991). For example, Prospero et al. (1987) suggested that enough Saharan dust is carried into the Miami area to significantly reduce visibility during the summer months. Similar dust transport occurs from the deserts of Asia across the Pacific Ocean (Prospero, 1995). While particles as large as $100 \mu\text{m}$ in diameter are found in the source regions, only particles smaller than $10 \mu\text{m}$ are transported over long distances, often further than 5000 km.

The average number and volume concentration of the major aerosol types are summarized in Table 7.5.

7.3 AEROSOL CHEMICAL COMPOSITION

Atmospheric aerosol particles contain sulfates, nitrates, ammonium, organic material, crustal species, sea salt, hydrogen ions, and water. From these species sulfate, ammonium, organic and elemental carbon, and certain transition metals are found predominantly in the

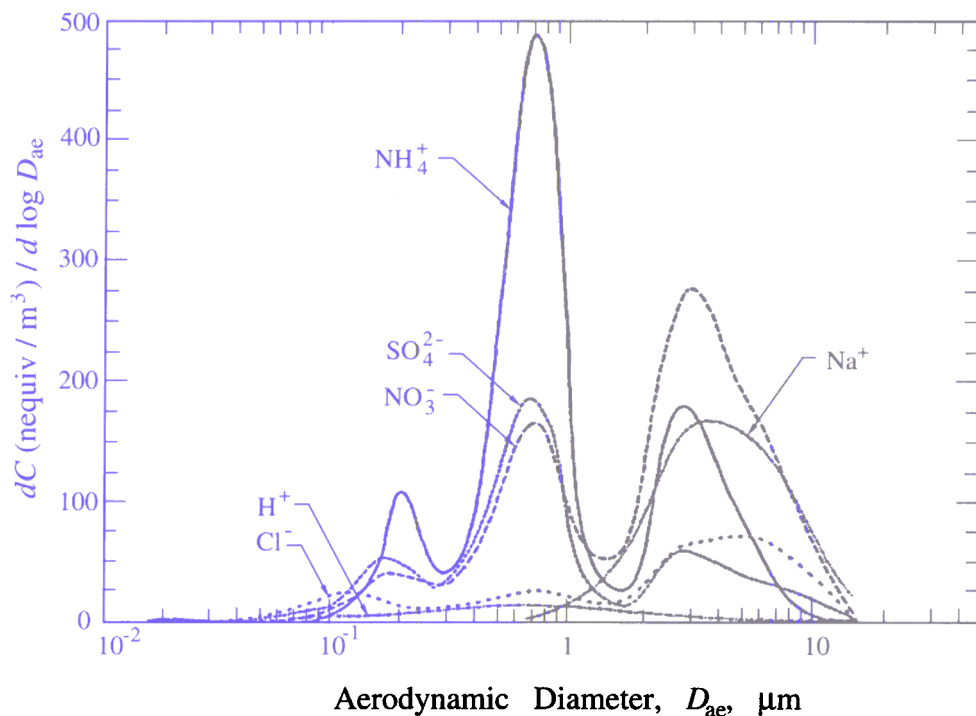


FIGURE 7.23 Measured size distributions of aerosol sulfate, nitrate, ammonium, chloride, sodium, and hydrogen ion in Claremont, CA (Wall et al., 1988).

fine particles. Crustal materials, including silicon, calcium, magnesium, aluminum, and iron, and biogenic organic particles (pollen, spores, plant fragments) are usually in the coarse aerosol fraction. Nitrate can be found in both the fine and coarse modes. Fine nitrate is usually the result of the nitric acid/ammonia reaction for the formation of ammonium nitrate, while coarse nitrate is the product of coarse particle/nitric acid reactions.

A typical urban aerosol size/composition distribution is shown in Figure 7.23 (Wall et al., 1988). These results indicate that sulfate, nitrate, and ammonium have two modes in the 0.1 to 1.0 μm size range (the condensation and droplet modes), and a third one over 1 μm (coarse mode) (Figure 7.24). The condensation mode has a peak around 0.2 μm and is the result of condensation of secondary aerosol components from the gas phase. The droplet mode peaks around 0.7 μm in diameter and its existence is attributed to heterogeneous, aqueous-phase reactions discussed in Chapter 6 (Meng and Seinfeld, 1994). More than half of the nitrate is found in the coarse mode together with most of the sodium and chloride. This coarse nitrate is the result of reactions of nitric acid with sodium chloride or aerosol crustal material (see Chapter 9). This is an interesting case where secondary aerosol matter (nitrate) is formed through the reaction of a naturally produced material (sea salt or dust) and an anthropogenic pollutant (nitric acid).

More than 40 trace elements are routinely found in atmospheric particulate matter samples. These elements arise from dozens of different sources including combustion of coal, oil, wood burning, steel furnaces, boilers, smelters, dust, waste incineration, and break wear. Depending on their sources, these elements can be found in either the fine or the

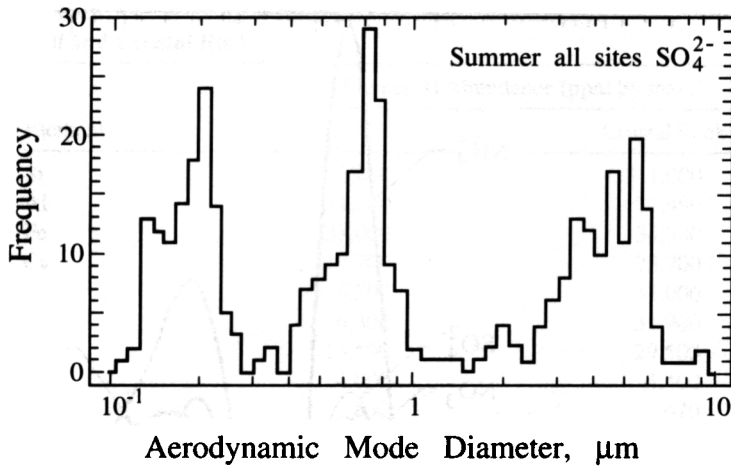


FIGURE 7.24 Frequency of observed occurrence of sulfate modes of various sizes as a function of mode diameter for Los Angeles during the summer of 1987 (John et al., 1990).

coarse mode. Concentrations of selected elements together with the size mode where these elements are usually found are shown in Table 7.6. The concentrations of these elements even for similar pollution levels vary over almost three orders of magnitude, indicating the strong effect of local sources. In general, elements such as lead, iron, and copper have the highest concentrations, while elements such as cobalt, mercury, and antimony are characterized by low concentrations. Elements produced during combustion usually exist in the

TABLE 7.6 Concentrations (ng m^{-3}) and Size Distribution of Various Elements Found in Atmospheric Particles

Element			Concentration (ng m^{-3})	
				Rural
Fe	F and C	0.6–4,200	55–14,500	130–13,800
Pb	F	0.01–65	2–1,700	30–90,000
Zn	F	0.03–450	10–400	15–8,000
Cd	F	0.01–1	0.4–1,000	0.2–7,000
As	F	0.01–2	1–28	2–2,500
V	F and C	0.01–15	3–100	1–1,500
Cu	F and C	0.03–15	3–300	3–5,000
Mn	F and C	0.01–15	4–100	4–500
Hg	—	0.01–1	0.05–160	1–500
Ni	F and C	0.01–60	1–80	1–300
Sb	F	0–1	0.5–7	0.5–150
Cr	F and C	0.01–10	1–50	2–150
Co	F and C	0–1	0.1–10	0.2–100
Se	F and C	0.01–0.2	0.01–30	0.2–30

*F = fine mode; C = coarse mode.

Source: Schroeder et al. (1987).

TABLE 7.7 Comparison of Ambient Fine and Coarse Particles

	Fine Particles	Coarse Particles
<i>Formation pathways</i>		
<i>Composition</i>		Resuspended dust Coal and oil fly ash Crustal element (Si, Al, Ti, Fe) oxides CaCO ₃ , NaCl Pollen, mold, spores Plant, animal debris Tire wear debris
<i>Solubility</i>	Largely soluble, hygroscopic Combustion (coal, oil, gasoline, diesel, wood) Gas-to-particle conversion of NO _x , SO ₂ , and VOCs Smelters, mills, etc.	Largely insoluble and non-hygroscopic
<i>Atmospheric lifetime</i>	Days to weeks	

Source: Adapted from Wilson and Shuh (1997) and U.S. EPA (1996).

form of oxides (e.g., Fe₂O₃, Fe₃O₄, Al₂O₃), but their chemical form is in general uncertain.

A summary of chemical information regarding the coarse and fine modes is presented in Table 7.7.

The composition of sea salt reflects the composition of seawater enriched in organic material (marine-derived sterols, fatty alcohols, and fatty acids) that exists in the surface layer of the oceans (Schneider and Gagosian, 1985). Seawater contains 3.5% by weight sea salt and when first emitted the sea salt composition is the same as that of seawater (Table 7.8). Reactions on sea salt particles modify its chemical composition; for example, sodium chloride reacts with sulfuric acid vapor to produce sodium sulfate and hydrochloric acid vapor



leading to an apparent "chloride deficit" in the marine aerosol.

TABLE 7.8 Composition of Sea-Salt^a

Species	Percent by Weight
Cl	55.04
Na	30.61
SO ₄ ²⁻	7.68
Mg	3.69
Ca	1.16
K	1.1
Br	0.19
C (noncarbonate)	3.5×10^{-3} – 8.7×10^{-3}
Al	4.6×10^{-4} – 5.5×10^{-3}
Ba	1.4×10^{-4}
I	1.4×10^{-4}
Si	1.4×10^{-4} – 9.4×10^{-3}
NO ₃ ⁻	3×10^{-6} – 2×10^{-3}
Fe	5×10^{-5} – 5×10^{-4}
Zn	1.4×10^{-5} – 4×10^{-5}
Pb	1.2×10^{-5} – 1.4×10^{-5}
NH ₄ ⁺	1.4×10^{-6} – 1.4×10^{-5}
Mn	2.5×10^{-6} – 2.5×10^{-5}
V	9×10^{-7}

^aBased on the composition of seawater and ignoring atmospheric transformations.

7.4 VERTICAL VARIATION

The vertical distribution of aerosol mass concentration typically shows an exponential decrease with altitude up to a height H_p and a rather constant profile above that altitude (Gras, 1991). The aerosol mass concentration as a function of height can then be expressed as

$$M(z) = M(0) \exp\left(-\frac{z}{H_p}\right) \quad (7.59)$$

where $M(0)$ is the surface concentration and H_p the scale height. Jaenicke (1993) proposed values of H_p equal to 900 m for the marine, 730 m for the remote continental, 2000 m for the desert, and 30,000 m for the polar aerosol types. The corresponding vertical aerosol mass concentration profiles are shown in Figure 7.25.

The aerosol number concentration may increase or decrease exponentially with altitude and one suggestion of a form of the profile is (Jaenicke, 1993)

$$N(z) = N(0) \left[\exp\left(\frac{-z}{|H'_p|}\right) + \left(\frac{N_B}{N(0)}\right)^n \right]^n \quad (7.60)$$

where

$$n = \frac{H'_p}{|H'_p|} \quad (7.61)$$

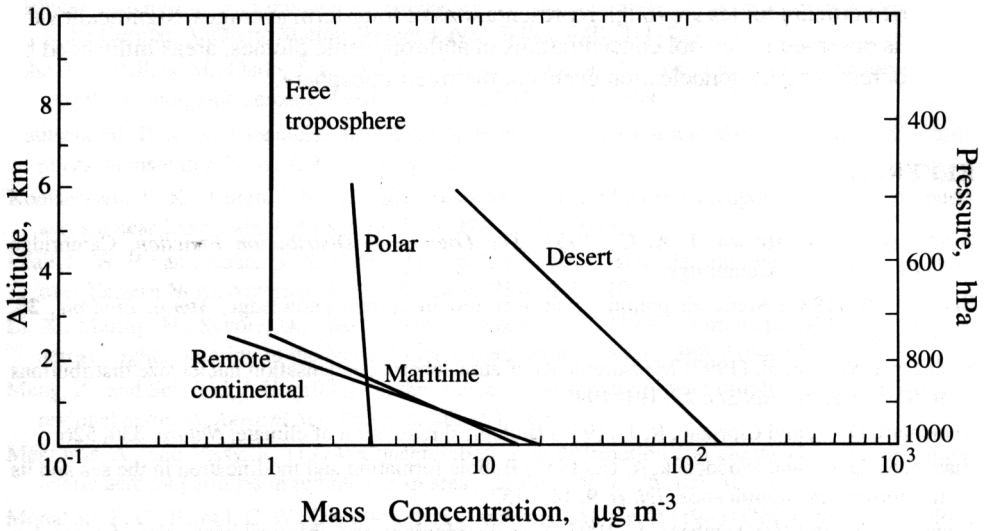


FIGURE 7.25 Representative vertical distribution of aerosol mass concentration (Jaenicke, 1993).

and N_B is the number concentration of the background aerosol aloft. For marine aerosol H'_p varies from -290 to 440 m. Note that if H'_p is negative $n = -1$, and (7.60) can be rewritten as

$$N(z) = N(0) \left[\exp\left(\frac{-z}{|H'_p|}\right) + \left(\frac{N(0)}{N_B}\right) \right]^{-1} \tag{7.62}$$

Because in this case $N(0) \ll N_B$, the equation has the correct limiting behavior both for $z \rightarrow 0$ and $z \rightarrow \infty$. Model vertical number concentration profiles are shown in Figure 7.26.

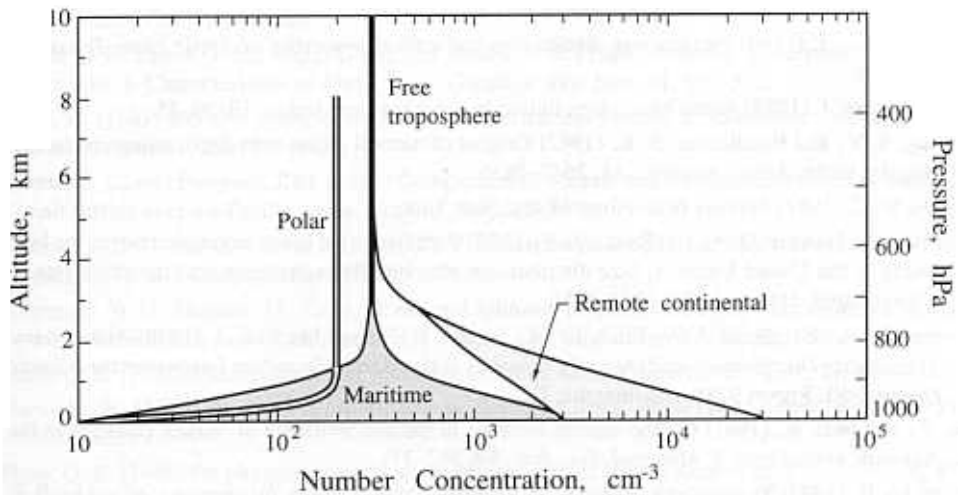


FIGURE 7.26 Representative vertical distribution of aerosol number concentration (Jaenicke, 1993). A range of concentrations is shown for marine and remote continental aerosols.

These vertical profiles are rough representations of long-term averages. Significant variability is observed in aerosol concentrations in anthropogenic plumes, areas influenced by local sources, or during nucleation events in the free troposphere.

REFERENCES

- Aitchison, J., and Brown, J. A. C. (1957) *The Lognormal Distribution Function*, Cambridge University Press, Cambridge.
- Barrie, L. A. (1986) Arctic air pollution: an overview of current knowledge, *Atmos. Environ.*, **20**, 643–663.
- Bashurova, V. S., et al. (1992) Measurements of atmospheric condensation nuclei size distributions in Siberia, *J. Aerosol Sci.* **23**, 191–199.
- Blanchard, D. C., and Cipriano, R. J. (1987) Biological regulation of climate, *Nature*, **330**, 526.
- Blanchard, D. C., and Woodcock, A. H. (1957) Bubble formation and modification in the sea and its meteorological significance, *Tellus*, **9**, 145–152.
- Covert, D. S., and Heintzenberg, J. (1993) Size distributions and chemical properties of aerosol at NY Ålesund, Svalbard, *Atmos. Environ.*, **27A**, 2989–2997.
- d'Almeida, G. A., and Schutz, L. (1983) Number, mass and volume distributions of mineral aerosol and soils of the Sahara, *J. Climate Appl. Meteorol.*, **22**, 233–243.
- Deepak, A., and Gali, G. (1991) *The International Global Aerosol Program (IGAP) Plan*. Deepak Publishing, Hampton, VA.
- Deirmendjian, D. (1969) *Electromagnetic Scattering on Spherical Polydispersions*, Elsevier, New York.
- De Leeuw, G. (1986) Vertical profiles of giant particles close above the sea surface, *Tellus*, **38B**, 51–61.
- Fitzgerald, J. W. (1991) Marine aerosols: a review, *Atmos. Environ.*, **25A**, 533–545.
- Gras, J. L. (1991) Southern hemisphere tropospheric aerosol microphysics, *J. Geophys. Res.*, **96**, 5345–5356.
- Haaf, W., and Jaenicke, R. (1980) Results of improved size distribution measurements in the Aitken range of atmospheric aerosols, *J. Aerosol Sci.*, **11**, 321–330.
- Heintzenberg, J. (1980) Particle size distribution and optical properties of Arctic haze, *Tellus*, **32**, 251–260.
- Heintzenberg, J. (1989) Arctic haze: air pollution in polar regions, *Ambio*, **18**, 50–55.
- Hering, S. V., and Friedlander, S. K. (1982) Origins of aerosol sulfur size distributions in the Los Angeles basin, *Atmos. Environ.*, **16**, 2647–2656.
- Hinds, W. C. (1982) *Aerosol Technology*, Wiley, New York.
- Hobbs, P. V., Bowdle, D. A., and Radke, L. F. (1985) Particles in the lower troposphere over the high plains of the United States. 1. Size distributions, elemental compositions, and morphologies, *J. Climate Appl. Meteorol.*, **24**, 1344–1356.
- Hoppel, W. A., Fitzgerald, J. W., Frick, G. M., Larson, R. E., and Mack, E. J. (1989) *Atmospheric Aerosol Size Distributions and Optical Properties in the Marine Boundary Layer over the Atlantic Ocean*. NRL Report 9188, Washington, DC.
- Ito, T., and Iwai, K. (1981) On the sudden increase in the concentration of aiten particles in the Antarctic atmosphere, *J. Meteorol. Soc. Jpn.*, **59**, 262–271.
- Jaenicke, R. (1993) Tropospheric aerosols, in *Aerosol–Cloud–Climate Interactions*, edited by P. V. Hobbs. Academic Press, San Diego, CA; pp. 1–31.
- Jaenicke, R., and Schutz, L. (1978) Comprehensive study of physical and chemical properties of the surface aerosol in the Cape Verde Islands region, *J. Geophys. Res.*, **83**, 3583–3599.

- Jaenicke R., Dreiling V., Lehmann E., Koutsenogii, P. K., and Stingl, J. (1992) Condensation nuclei at the German Antarctic Station Vonneymayer, *Tellus*, **44B**, 311–317
- John, W., Wall, S. M., Ondo, J. L., and Winklmayr, W. (1990) Modes in the size distributions of atmospheric inorganic aerosol, *Atmos. Environ.*, **24A**, 2349–2359.
- Koutsenogii, P. K., and Jaenicke, R. (1994) Number concentration and size distribution of atmospheric aerosol in Siberia, *J. Aerosol Sci.*, **25**, 377–383.
- Koutsenogii, P. K., Bufetov, N. S., and Drosdova, V. I. (1993) Ion composition of atmospheric aerosol near Lake Baikal, *Atmos. Environ.*, **27A**, 1629–1633.
- Leaitch, W. R., and Isaac, G. A. (1991) Tropospheric aerosol size distributions from 1982 to 1988 over Eastern North America, *Atmos. Environ.*, **25A**, 601–619.
- Li, X., Maring, H., Savoie, D., Voss, K., and Prospero, J. M. (1996) Dominance of mineral dust in aerosol light scattering in the North Atlantic trade winds, *Nature*, **380**, 416–419.
- Meng, Z., and Seinfeld, J. H. (1994) On the source of the submicrometer droplet mode of urban and regional aerosols, *Aerosol Sci. Technol.*, **20**, 253–265.
- Mészáros, A., and Vissy, K. (1974) Concentration, size distribution and chemical nature of atmospheric aerosol particles in remote ocean areas, *J. Aerosol Sci.*, **5**, 101–109.
- Monahan, E. C., Fairall, C. W., Davidson, K. L., and Jones-Boyle, P. (1983) Observed inter-relationships amongst 10-m-elevation winds, oceanic whitecaps, and marine aerosols, *Q. J. R. Meteorol. Soc.*, **109**, 379–392.
- O'Dowd, C. D., and Smith, M. H. (1993) Physicochemical properties of aerosols over the Northeast Atlantic: evidence for wind-speed related submicron sea-salt aerosol production, *J. Geophys. Res.*, **98**, 1137–1149.
- Ott, S. T., Ott, A., Martin, D. W., and Young, J. A. (1991) Analysis of trans-Atlantic saharan dust outbreak based on satellite and GATE data, *Mon. Weather Rev.*, **119**, 1832–1850.
- Ottar, B. (1989) Arctic air pollution: a Norwegian perspective, *Atmos. Environ.*, **23**, 2349–2356.
- Prospero, J. M. (1995) The atmospheric transport of particles to the ocean, in SCOPE Report: Particle Flux in the Ocean, Ittekkot, V., Honjo, S., Depetris, P. J. (Eds.), Wiley, New York, NY.
- Prospero, J. M., Nees, R. T., and Uematsu, M. (1987) Deposition rate of particulate and dissolved aluminum derived from sahara dust in precipitation in Miami, Florida, *J. Geophys. Res.*, **92**, 14723–14731.
- Pruppacher, H. R., and Klett, J. D. (1980) *Microphysics of Cloud and Precipitation*, D. Reidel, Dordrecht, The Netherlands.
- Radke, L. F., Lyons, J. H., Hegg, D. A., and Hobbs, P. V. (1984) Airborne observations of Arctic aerosols. I: Characteristics of Arctic haze, *Geophys. Res. Lett.*, **11**, 369–372.
- Rahn, K. (1981) Relative importance of North America and Eurasia as sources of Arctic aerosol, *Atmos. Environ.*, **15**, 1447–1456.
- Savoie, D. L., and Prospero, J. M. (1989) Comparison of oceanic and continental sources of non-sea-salt sulfate over the Pacific ocean, *Nature*, **339**, 685–687.
- Schneider, J. K., and Gagosian, R. B. (1985) Particle size distribution of lipids in aerosols off the coast of Peru, *J. Geophys. Res.*, **90**, 7889–7898.
- Schroeder, W. H., Dobson, M., Kane, D. M., and Johnson, N. D. (1987) Toxic trace elements associated with airborne particulate matter: a review, *J. Air Pollut. Cont. Assoc.*, **37**, 1267–1285.
- Shaw, G. E. (1984) Microparticle size spectrum of Arctic haze, *Geophys. Res. Lett.*, **11**, 409–412.
- Shaw, G. E. (1985) Aerosol measurements in Central Alaska 1982–1984, *Atmos. Environ.*, **19**, 2025–2031.
- Shaw, G. E. (1986) On physical properties of aerosols at Ross Island, Antarctica, *J. Aerosol Sci.*, **17**, 937–945.

- United States Environmental Protection Agency (1996) Air Quality Criteria for Particulate Matter, EPA/600/P-95/001, Research Triangle Park, NC.
- Wall, S. M., John, W., and Ondo, J. L. (1988) Measurement of aerosol size distributions for nitrate and major ionic species, *Atmos. Environ.*, **22**, 1649–1656.
- Warneck, P. (1988) *Chemistry of the Natural Atmosphere*, Academic Press, San Diego, CA.
- Whitby, K. T., and Sverdrup, G. M. (1980) California aerosols: their physical and chemical characteristics, in *The Character and Origins of Atmospheric Aerosols: A Digest of Results from the California Aerosol Characterization Experiment (ACHEX)*, Hidy, G. M., Mueller, P. K., Grosjean, D., Appel, B. R., and Wesolowski, J. J. (Eds.), pp. 477–517. *Advances in Environmental Science and Technology*, Vol. 9, Wiley, New York, NY.
- Wilson, W. E., and Shuh, H. H. (1997) Fine and coarse particles: concentration relationships relevant to epidemiological studies, *J. Air Waste Manage. Assoc.*, (in press).

PROBLEMS

Given the following data on the number of aerosol particles in the size ranges listed, tabulate and plot the normalized size distributions $\bar{n}_N(D_p) = n_N(D_p)/N$ and $\bar{n}_N^\circ(\log D_p) = n_N^\circ(\log D_p)/N$ as discrete histograms.

Size Interval (μm)	Mean of Size Interval (μm)	Number of Particles in Interval
0–0.2	0.1	10
0.2–0.4	0.3	80
0.4–0.6	0.5	132
0.6–0.8	0.7	142
0.8–1.0	0.9	138
1.0–1.2	1.1	112
1.2–1.4	1.3	75
1.4–1.6	1.5	65
1.6–1.8	1.7	52
1.8–2.1	1.95	65
2.1–2.7	2.4	62
2.7–3.6	3.15	32
3.6–5.1	4.35	35

For the data given in Problem 7.1, plot the surface area and volume distributions $n_S(D_p)$, $n_S^\circ(\log D_p)$, $n_V(D_p)$ and $n_V^\circ(\log D_p)$ in both non-normalized and normalized form as discrete histograms.

- 7.3_A You are given an aerosol size distribution function $n_M(m)$ such that $n_M(m) dm$ = aerosol mass per cm^3 of air contained in particles having masses in the range m to $m + dm$. It is desired to convert that distribution function to a mass distribution based on $\log D_p$. Show that

$$n_M^\circ(\log D_p) = 6.9 m n_M(m)$$

7.4_B Show that the variance of the size distribution of a log-normally distributed aerosol is

$$\overline{D}_p^2 [\exp(\ln^2 \sigma_g) - 1]$$

7.5_A Starting with semilogarithmic graph paper, construct a log-probability coordinate axis and show that a log-normal distribution plots as a straight line on these coordinates.

7.6_A The data given below were obtained for a log-normally distributed aerosol size distribution:

Size Interval (μm)	Geometric Mean of Size Interval (μm)	Number of Particles in Interval ^a
0.1–0.2	0.1414	50
0.2–0.4	0.2828	460
0.4–0.7	0.5292	1055
0.7–1.0	0.8367	980
1.0–2.0	1.414	1705
2.0–4.0	2.828	680
4.0–7.0	5.292	102
7.0–10	8.367	10
10–20	14.14	2

^aAssume that the particles are spheres with density $\rho = 1.5 \text{ g cm}^{-3}$.

- Complete the above table by computing the following quantities: $\Delta N_i / \Delta D_{pi}$, $\Delta N_i / N \Delta D_{pi}$, $\Delta S_i / \Delta D_{pi}$, $\Delta S_i / S \Delta D_{pi}$, $\Delta M_i / \Delta D_{pi}$, $\Delta M_i / M \Delta D_{pi}$, $\Delta N_i / \Delta \log D_{pi}$, $\Delta N_i / N \Delta \log D_{pi}$, $\Delta S_i / \Delta \log D_{pi}$, $\Delta S_i / S \Delta \log D_{pi}$, and $\Delta M_i / \Delta \log D_{pi}$, $\Delta M_i / M \Delta \log D_{pi}$, where M = particle mass.
 - Plot $\Delta N_i / \Delta \log D_{pi}$, $\Delta S_i / \Delta \log D_{pi}$, and $\Delta M_i / \Delta \log D_{pi}$ as histograms.
 - Determine the geometric mean diameter and geometric standard deviation of the log-normal distribution to which these data adhere and plot the continuous distributions on the three plots from part (b).
- 7.7_B For a log-normally distributed aerosol different mean diameters can be defined by

$$\overline{D}_{pv} = \overline{D}_{pg} \exp(v \ln^2 \sigma_g)$$

where v is a parameter that defines the particular mean diameter of interest. Show that

Diameter	v
Mode (most frequent value)	-1
Geometric mean or median	0
Number (arithmetic) mean	0.5
Surface area mean	1
Mass mean	1.5
Surface area median	2
Volume median	3

7.4_B Show that the variance of the size distribution of a log-normally distributed aerosol is

$$\overline{D}_p^2 [\exp(\ln^2 \sigma_g) - 1]$$

7.5_A Starting with semilogarithmic graph paper, construct a log-probability coordinate axis and show that a log-normal distribution plots as a straight line on these coordinates.

7.6_A The data given below were obtained for a log-normally distributed aerosol size distribution:

Size Interval (μm)	Geometric Mean of Size Interval (μm)	Number of Particles in Interval ^a
0.1–0.2	0.1414	50
0.2–0.4	0.2828	460
0.4–0.7	0.5292	1055
0.7–1.0	0.8367	980
1.0–2.0	1.414	1705
2.0–4.0	2.828	680
4.0–7.0	5.292	102
7.0–10	8.367	10
10–20	14.14	2

^aAssume that the particles are spheres with density $\rho = 1.5 \text{ g cm}^{-3}$.

- Complete the above table by computing the following quantities: $\Delta N_i / \Delta D_{pi}$, $\Delta N_i / N \Delta D_{pi}$, $\Delta S_i / \Delta D_{pi}$, $\Delta S_i / S \Delta D_{pi}$, $\Delta M_i / \Delta D_{pi}$, $\Delta M_i / M \Delta D_{pi}$, $\Delta N_i / \Delta \log D_{pi}$, $\Delta N_i / N \Delta \log D_{pi}$, $\Delta S_i / \Delta \log D_{pi}$, $\Delta S_i / S \Delta \log D_{pi}$, and $\Delta M_i / \Delta \log D_{pi}$, $\Delta M_i / M \Delta \log D_{pi}$, where M = particle mass.
 - Plot $\Delta N_i / \Delta \log D_{pi}$, $\Delta S_i / \Delta \log D_{pi}$, and $\Delta M_i / \Delta \log D_{pi}$ as histograms.
 - Determine the geometric mean diameter and geometric standard deviation of the log-normal distribution to which these data adhere and plot the continuous distributions on the three plots from part (b).
- 7.7_B For a log-normally distributed aerosol different mean diameters can be defined by

$$\overline{D}_{pv} = \overline{D}_{pg} \exp(v \ln^2 \sigma_g)$$

where v is a parameter that defines the particular mean diameter of interest. Show that

Diameter	v
Mode (most frequent value)	-1
Geometric mean or median	0
Number (arithmetic) mean	0.5
Surface area mean	1
Mass mean	1.5
Surface area median	2
Volume median	3

Plot a normalized log-normal particle size distribution over a range of D_p from 0 to $7 \mu\text{m}$ with $\bar{D}_{pg} = 1.0 \mu\text{m}$ and $\sigma_g = 2.0$ and identify each of the above diameters on the plot. *Hint:* You may find this integral of use:

$$\int_{L_1}^L e^{ru} \exp\left(-\frac{(u-\bar{u})^2}{2\sigma_u^2}\right) du$$

$$= (\pi/2)^{1/2} \sigma_u e^{r\bar{u}} e^{r^2\sigma_u^2/2} \left[\operatorname{erf}\left(\frac{L_2 - (\bar{u} + r\sigma_u^2)}{\sqrt{2}\sigma_u}\right) - \operatorname{erf}\left(\frac{L_1 - (\bar{u} + r\sigma_u^2)}{\sqrt{2}\sigma_u}\right) \right]$$

7.8_B Assume that an aerosol has a log-normal distribution with $\bar{D}_{pg} = 5.5 \mu\text{m}$ and $\sigma_g = 1.36$.

- Plot the number and volume distributions of this aerosol on log-probability paper.
- It is desired to represent this aerosol by a distribution of the form

$$F_V(D_p) = 1 - \exp(-cD_p^b)$$

where $F_V(D_p)$ is the fraction of the total aerosol volume in particles of diameter less than D_p . Determine the values of the constants c and b needed to match this distribution to the given aerosol.

7.9_B Given the following size frequency for a dust:

Size Interval (μm)	% by Number
7-17.5	10
17.5-21	10
21-25	10
25-28	10
28-30	10
30-33	10
33-36	10
36-41	10
41-49	10
49-70	10

- Plot the cumulative frequency distributions (in %) of the number, surface area, and mass on linear graph paper assuming all particles are spheres with $\rho_p = 1.6 \text{ g cm}^{-3}$.
- Is this a log-normally distributed dust?

14 Meteorology of Air Pollution

Meteorology is the study of the dynamics of the atmosphere. Meteorological scales of motion can be categorized as follows (see Section 1.11):

1. *Macroscale*. Phenomena occurring on scales of thousands of kilometers, such as semipermanent high- and low-pressure areas that reside over the oceans and continents. (The term *synoptic* is commonly used to denote macroscale.)
2. *Mesoscale*. Phenomena occurring on scales of hundreds of kilometers, such as land-sea breezes, mountain-valley winds, and migratory high- and low-pressure fronts.
3. *Microscale*. Phenomena occurring on scales of the order of 1 km, such as the meandering and dispersion of a chimney plume and the complicated flow regime in the wake of a large building.

Each of these scales of motion plays a role in air pollution, although over different periods of time. For example, micrometeorological effects take place over scales on the order of minutes to hours, whereas mesoscale phenomena influence transport and dispersal of pollutants over hours to days. Finally, synoptic scales of motion have characteristic times of days to weeks. The term "long-range transport" commonly refers to transport on the synoptic scale.

With respect to urban air pollution, the region of the atmosphere governing transport and dispersion is the so-called planetary boundary layer, roughly the lowest 1000 m. The planetary boundary layer represents the extent of influence of the Earth's surface on wind structure in the atmosphere. Within the planetary boundary layer, winds are influenced by the prevailing high-level flows and the frictional drag of the surface.

The atmospheric temperature profile (the variation of temperature with altitude) has an important effect on wind structure and turbulence in the lowest 1000 m. In the troposphere the temperature normally decreases with increasing altitude because of the decrease in pressure with height. The temperature profile against which all others are judged is that observed for a parcel of dry air as it moves upward in a hydrostatically stable atmosphere and expands slowly to lower pressure with no gain or loss of heat. If such a profile exists in the atmosphere, a parcel of air at any height is in neutral equilibrium; that is, it has no tendency either to rise or fall. The atmosphere is, however, very seldom in such delicate equilibrium; the influence of surface heating and large-scale phenomena usually results in a temperature profile different from this reference profile. If the temperature decreases faster with height than the reference profile, air parcels at any height are unstable; that is, if they are displaced either upward or downward, they will continue their movement in the direction in which they were displaced. Such a condition is referred to as unstable. On the other hand, if the temperature decreases more slowly with height than the reference profile (or even increases), air parcels are inhibited from either upward or downward motion and the situation

is referred to as stable. The stability condition of the atmosphere plays an important role in determining the rate of dispersal of material.

The phenomenon of direct interest in predicting the dispersion of air pollutants is turbulent diffusion. Actually, turbulent diffusion is something of a misnomer. The phrase refers to the observed spreading of a cloud of marked particles in a turbulent fluid at a rate many orders of magnitude greater than that from molecular diffusion alone. The spreading is really not due to a "diffusion" phenomenon such as results from molecular collisions but rather is a result of the rapid, irregular motion of macroscopic lumps of fluid (called eddies) in turbulence. Thus the scales of length in turbulent diffusion are much greater than in molecular diffusion, with the contribution of the latter to the dispersion of pollutants in turbulence being virtually negligible. The level of turbulence in the planetary boundary layer increases with increased wind speed, surface roughness, and instability. Turbulence therefore arises from both mechanical forces (shear, surface friction) and thermal forces (buoyancy).

Lower atmospheric temperature profiles determine in part the stability of the atmosphere or, in other words, the degree to which turbulence induced by wind, surface roughness, or buoyancy will propagate through the layer. Under strongly stable conditions, disturbances are highly damped and mixing of species is strongly suppressed. It is under such conditions that the worst air pollution episodes have occurred. The importance of winds to the atmospheric aspects of air pollution is clearly evident. Our discussion of winds in this chapter will be largely qualitative; in Chapter 16 we shall treat air motion in the lower atmosphere from a quantitative standpoint.

14.1 TEMPERATURE IN THE LOWER ATMOSPHERE

The layers of the atmosphere can be classified in a number of ways, such as by temperature, density, and chemical composition. From the standpoint of the dispersion of air pollutants, the most important classification is on the basis of temperature.

14.1.1 Pressure and Temperature Relationships in the Lower Atmosphere

We shall utilize the concept of an *air parcel*, a hypothetical mass of air that may deform as it moves vertically in the atmosphere. The concept of an air parcel is a tenable one as long as the parcel is of such a size that the exchange of air molecules across its boundary is small when compared with the total number of air molecules in the parcel. As such a parcel rises in the atmosphere, it expands to accommodate the lowering pressure; however, it does so in such a way that exchange of heat between the parcel and the surrounding air is negligible. As the parcel expands upon rising, its temperature decreases. The process of vertical mixing in the atmosphere can, for simplicity, be envisioned as one involving a large number of parcels rising and falling. If there is no heat exchange between the parcel and the surrounding air, the parcel and the surrounding air may be at different temperatures (but not different pressures). The relation of the parcel's temperature to that of the air determines whether the parcel will continue rising or falling or whether it will reach a point of equilibrium. Therefore the variation of temperature with altitude in the atmosphere is a key variable in determining the degree to which contaminant-bearing air parcels will mix vertically.

The variation of temperature with height for a rising parcel of dry air that cools adiabatically, that is, with no exchange of heat with its surroundings, is a basic property of the atmosphere. We now will derive the relation for this temperature change, as it will serve as a reference temperature profile against which to compare all actual profiles. To obtain the desired relation we need only the ideal gas law and the first law of thermodynamics.

The first law of thermodynamics is expressed as (9.1)

$$dU = dQ + dW \quad (14.1)$$

where dU is the change of internal energy of the system, dQ is the heat input to the system across its boundaries, and dW is the energy done on system by the surroundings as a result of work done to alter the volume of the system, namely, $-p dV$. The change in internal energy dU is equal to $C_v dT$, where C_v is the heat capacity of the system at constant volume.

Our intent is to apply the first law of thermodynamics to an air parcel whose volume is changing as it either ascends or descends in the atmosphere. Ultimately we will combine our result with (1.3), and so it is more convenient to work with pressure and temperature as the variables rather than with pressure and volume. Thus we convert $p dV$ to a form involving p and T . To do this, we express the ideal gas law as $pV = mRT/M_{\text{air}}$ for a mass m of air. Then

$$\begin{aligned} d(pV) &= \frac{mR dT}{M_{\text{air}}} \\ &= p dV + V dp \end{aligned} \quad (14.2)$$

Using this result, together with the adiabatic condition of $dQ = 0$, the first law of thermodynamics reduces to

$$\begin{aligned} C_v dT &= V dp - \frac{mR dT}{M_{\text{air}}} \\ &= \frac{mRT dp}{M_{\text{air}} p} - \frac{mR dT}{M_{\text{air}}} \end{aligned} \quad (14.3)$$

Rearranging, we obtain

$$\frac{dT}{dp} = \frac{mRT/M_{\text{air}}p}{C_v + mR/M_{\text{air}}} \quad (14.4)$$

Now we have two equations, (1.3) and (14.4), for the relation of T and p with z . Combining these we get

$$\begin{aligned} \frac{dT}{dz} &= -\frac{mg}{C_v + mR/M_{\text{air}}} \\ &= -\frac{g}{\hat{c}_v + R/M_{\text{air}}} \end{aligned} \quad (14.5)$$

for dry air. Since the saturation vapor pressure of water increases very markedly with temperature, the quantity dw_v/dz depends strongly on the temperature. Thus the wet adiabatic lapse rate is not a constant independent of z . In warm tropical air the wet adiabatic lapse rate is roughly one-third of the dry adiabatic lapse rate, whereas in cold polar regions there is little difference between the two.

14.1.2 Temperature Changes of a Rising (or Falling) Parcel of Air

The relationship between the temperatures and pressures at two heights in an atmosphere with an adiabatic profile is found by integrating (14.4) between any two points. Employing the ideal gas relation $\hat{c}_p = \hat{c}_v + R/M_{\text{air}}$, and the definition $\gamma = \hat{c}_p/\hat{c}_v$, the result of this integration is

$$\frac{T(z_2)}{T(z_1)} = \left[\frac{p(z_2)}{p(z_1)} \right]^{(\gamma-1)/\gamma} \quad (14.11)$$

For example, if z_1 is taken to be ground level, the temperature θ to which dry air originally in the state T, p would come if brought adiabatically to p_0 is given by

$$\theta = T \left(\frac{p}{p_0} \right)^{-(\gamma-1)/\gamma} \quad (14.12)$$

The temperature θ defined by (14.12) is called the *potential temperature*. We introduce the potential temperature because an actual atmosphere is seldom adiabatic and we want to relate the actual temperature profile to the adiabatic lapse rate. Adiabatic temperature profiles based on potential temperature are vertical on a plot of z versus θ , thereby facilitating such comparisons.

We can further interpret the potential temperature θ as follows. The gradient of θ with z may be expressed in terms of the gradient of absolute temperature T and the adiabatic lapse rate Γ . From (14.12) we see that

$$\frac{1}{\theta} \frac{d\theta}{dz} = \frac{1}{T} \frac{dT}{dz} - \frac{\gamma-1}{\gamma} \frac{1}{p} \frac{dp}{dz} = \frac{1}{T} \left(\frac{dT}{dz} + \Gamma \right) \quad (14.13)$$

At $z = 0$, $\theta = T$ if p_0 is taken as the surface pressure. Since, in magnitude, θ is quite close to T , (14.13) is often approximated by

$$\frac{d\theta}{dz} \simeq \frac{dT}{dz} + \Gamma \quad (14.14)$$

Thus $d\theta/dz$ is a measure of the departure of the actual temperature profile from adiabatic

conditions. Integrating (14.14) with respect to z gives

$$\theta \simeq T + \Gamma z \quad (14.15)$$

One might ask: Why does not the atmosphere always have an adiabatic lapse rate as its actual profile? The reason it does not is that other processes such as winds and solar heating of the Earth's surface lead to dynamic temperature behavior in the lowest layers of the atmosphere that is seldom adiabatic. These other processes exert a much stronger influence on the prevailing temperature profile than does the adiabatic rising and falling of air parcels.

Let us compute the temperature change with z of an isolated parcel of air (or possibly other gas) as it rises or falls adiabatically through an atmosphere that is not adiabatic. We assume that conduction or convection of heat across the boundary of the parcel will be slow compared with the rate of vertical motion. Thus an individual parcel is assumed to rise or fall adiabatically, even when the surrounding air is nonadiabatic.

Let T denote the temperature of the air parcel and T' the temperature of the surrounding air. At any height z , the pressure is the same in the parcel as in the atmosphere. The rate of change of T with p in the parcel is given by (14.4), and the rate of change of p with z is given by (1.3). Combining these two relations, we find that

$$\frac{dT}{dz} = -\Gamma \frac{T}{T'}$$

Therefore the rising air will cool at a greater or lesser rate than the adiabatic, depending on whether its temperature is higher or lower than that of the adjacent atmosphere.

If Λ is the actual lapse rate in the atmosphere, then at any height z

$$T'(z) = T'_0 - \Lambda z \quad (14.17)$$

Then, from (14.16) and (14.17),

$$\frac{dT}{dz} = -\Gamma \frac{T(z)}{T'_0 - \Lambda z} \quad (14.18)$$

Integrating (14.18) with $T(0) = T_0$, the surface temperature of the rising parcel

$$T(z) = T_0 \left(\frac{T'_0 - \Lambda z}{T'_0} \right)^{\Gamma/\Lambda}$$

so that, in general,

$$\frac{dT}{dz} = -\Gamma \left(\frac{T'_0 - \Lambda z}{T'_0} \right)^{(\Gamma-\Lambda)/\Lambda} \frac{T_0}{T'_0} \quad (14.20)$$

Of course, if $\Lambda = \Gamma$, then

$$\frac{dT}{dz} = -\Gamma \frac{T_0}{T_0'} \quad (14.21)$$

Thus, even if the atmosphere has an adiabatic lapse rate, a parcel of air introduced at the ground at a temperature $T_0 \neq T_0'$ will have a different rate of cooling than the adiabatic.

14.2 ATMOSPHERIC STABILITY

The lapse rate in the lower portion of the atmosphere has a great influence on the vertical motion of air. If the lapse rate is adiabatic, a parcel of air displaced vertically is always at equilibrium with its surroundings. Such a condition, in which vertical displacements are not affected by buoyancy forces, is called *neutral* stability. However, because of surface heating and local weather influences, the atmosphere seldom has an adiabatic temperature profile. The atmosphere is either:

Unstable—buoyancy forces enhance vertical motion.

Stable—buoyancy forces oppose vertical motion.

Let us suppose a warm parcel begins to rise in an atmosphere in which temperature decreases more rapidly with z than the adiabatic rate (its lapse rate exceeds the adiabatic lapse rate). The air parcel cools adiabatically, but the temperature difference between the rising parcel and the surroundings increases with z . If the density of the parcel is ρ and that of the air ρ' , the acceleration experienced by the parcel is

$$\begin{aligned} \text{Acceleration} &= g \left(\frac{\rho' - \rho}{\rho'} \right) \\ &= g \left(\frac{T - T'}{T'} \right) \end{aligned}$$

Thus the acceleration increases with z and the parcel continues to rise as long as $T > T'$. We can express the acceleration in terms of the two lapse rates Γ and Λ as follows, if $T_0 \simeq T_0'$:

$$\begin{aligned} \text{Acceleration} &= \frac{g(dT/dz - dT'/dz) dz}{T'} \\ &= g \frac{(\Lambda - \Gamma) dz}{T'} \end{aligned}$$

As long as $\Lambda > \Gamma$, the parcel continues to rise. Similarly, a parcel of air cooler than the surrounding air will continue to descend if its rate of adiabatic heating is less than the lapse rate in the atmosphere. Since vertical motion is enhanced by buoyancy, if $\Lambda > \Gamma$ the atmosphere is called *unstable*. Lapse rates Λ for which $\Lambda > \Gamma$ are called *superadiabatic*.

On the other hand, if $\Lambda < \Gamma$, a rising air parcel will cool more rapidly with height than the surroundings and a point will be reached at which the temperature of the parcel equals that of the surroundings. We see that, if $\Lambda < \Gamma$, the acceleration will oppose the motion of a parcel. Thus any fluctuations in the temperature of an air parcel will cause it to rise or fall, but only for a short distance. When $\Lambda < \Gamma$, the atmosphere is said to be *stable*. Summarizing, the conditions are:

- $\Lambda = \Gamma$, neutral stability
- $\Lambda > \Gamma$, unstable (vertical motions enhanced)
- $\Lambda < \Gamma$, stable (vertical motions suppressed)

These same arguments may be applied to the case of a moist atmosphere. Because of the release of the latent heat of vaporization, a saturated parcel cools on rising at a slower rate than a dry parcel, since

$$\Gamma_{\text{dry}} > \Gamma_{\text{wet}}$$

Thus a cloudy atmosphere is inherently *less* stable than a dry atmosphere, and a stable situation with reference to the dry adiabatic lapse rate may actually be unstable for upward displacements of a saturated air parcel.

Figure 14.1 summarizes the types of temperature profiles found in the lower atmosphere, and Figure 14.2 shows a typical diurnal variation of temperature near the ground. The air mass near the ground is adiabatic only under special circumstances. Adiabatic conditions are reached usually when the sky is heavy with clouds and there is a moderate to high wind. The clouds prevent radiation from reaching the surface and ensure that the temperature of the ground does not differ greatly from the air just above it. The wind serves to mix the air, thereby smoothing out temperature differences. Vertical movement is then a re-

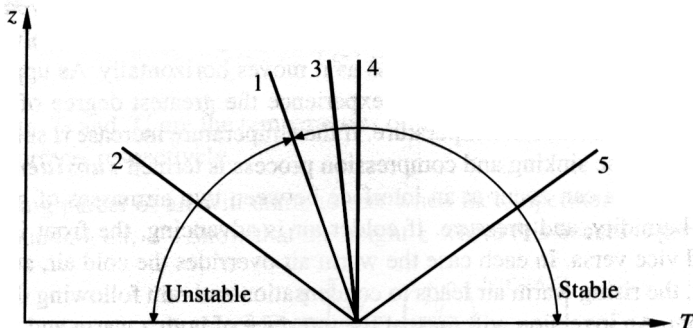


FIGURE 14.1 Temperature profiles in the atmosphere. (1) Adiabatic lapse rate (neutral stability, about 1°C per 100 m) T decreases with height such that any vertical movement imparted to an air parcel will result in the parcel maintaining the same T or density as the surrounding air. (2) Superadiabatic (unstable): a rising air parcel will be warmer than its environment so it becomes more buoyant and continues rising. (3) Subadiabatic (stable): a rising air parcel is cooler than its surroundings so it becomes less buoyant and subsides. (4) Isothermal (stable): temperature is constant with height. (5) Inversion (extremely stable): temperature *increases* with height.

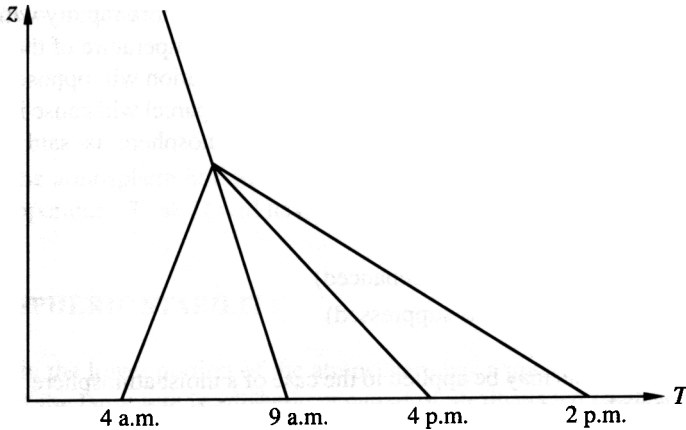


FIGURE 14.2 Typical diurnal variation of temperatures near the ground. At 4 a.m. radiation from the earth to black sky cools the ground to a lower temperature than the air, producing a ground-based inversion. At 9 a.m. the ground is heated rapidly after sunrise (slightly subadiabatic). At 2 p.m. there is continued heating (superadiabatic). At 4 p.m. the cooling in the afternoon returns the temperature profile to near adiabatic.

sult of mechanical forces, not buoyancy. From an air pollution standpoint, situations in which the temperature increases with height, so-called inversion conditions, are of great importance. Under these conditions the air is very stable, and little mixing of material takes place.

Inversions, as shown in Figure 14.1, form in one of two ways, through cooling from below or heating from above. Inversions often form, particularly at night, because of radiation cooling at the ground. Horizontal movement of an airmass from above a warm surface (land) to above a cool surface (water) also produces an inversion. (Note that at night the land surface may be cooler than the water.) Such inversions are termed *ground-based* or *surface* inversions. Inversions that are the result of heating from above involve the spreading, sinking, and compression of an airmass as it moves horizontally. As upper layers undergo the greatest elevation change, they experience the greatest degree of compression and thus the greatest increase in temperature. If the temperature increase is sufficient, an inversion will result. The sinking and compression process is termed *subsidence*.

A *frontal inversion* can occur at an interface between two airmasses of quite different temperatures, humidity, and pressure. If colder air is advancing, the front is known as a cold front, and vice versa. In each case the warm air overrides the cold air, and in the case of a cold front, the rising warm air leads to condensation and rain following the position of the surface front. An inversion will exist at the interface of both a warm and a cold front.

An *advective inversion* is formed when warm air flows over a cold surface or colder air. The inversion can be surface-based, as when warm air flows over cold plains, or elevated, as in the case when a cool sea breeze is overlaid by a warm land breeze.

A *radiational inversion* occurs frequently when the ground cools at night by radiation. The presence of nocturnal radiational inversions prevents the ventilation of emissions during the night in a city. At night in cities, buildings and streets cool slowly, often resulting in an unstable temperature profile for the first hundred meters or so. But this shallow mixing layer is usually topped by a more stable layer.

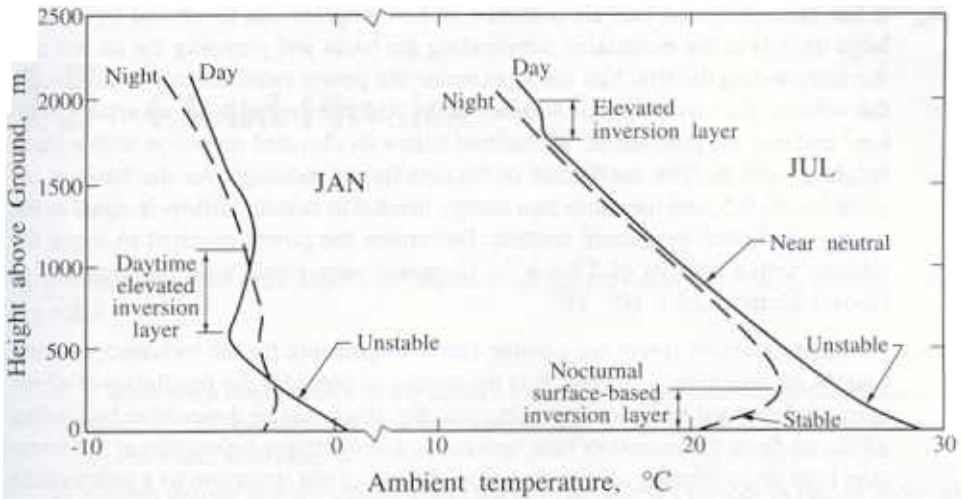


FIGURE 14.3 Monthly average diurnal and seasonal variations of the vertical thermal structure of the planetary boundary layer at a rural site near St. Louis, MO, based on 1976 data for January and July.

Figure 14.3 shows monthly average diurnal and seasonal variations of the vertical thermal structure of the planetary boundary layer at rural site near St. Louis, Missouri.

PROBLEMS

- 14.1_A Show that if the atmosphere is isothermal the temperature change of a parcel of air rising adiabatically is

$$T(z) = T_0 e^{-\Gamma z / T_0'}$$

Where T_0 and T_0' are the temperatures of the parcel at the surface and of the air at the surface, respectively.

- 14.2_A A rising parcel of air will come to rest when its temperature T equals that of the surrounding air, T' . Show that the height z where this occurs is given by

$$z = \frac{1}{\Lambda} \left[\left(\frac{T_0'}{T_0} \right)^{\Lambda / (\Gamma - \Lambda)} \right]$$

What condition must hold for this result to be valid?

- 14.3_A Show that the condition that the density of the atmosphere does not change with height is

$$\frac{dT}{dz} = -3.42 \times 10^{-2} \text{ } ^\circ\text{C m}^{-1}$$

- 14.4_B** It has been proposed that air pollution in Los Angeles can be abated by drilling large tunnels in the mountains surrounding the basin and pumping the air out into the surrounding deserts. You are to examine the power requirements in displacing the volume of air over the Los Angeles basin. Assume the basin has an area of 4000 km^2 and that the polluted air is confined below an elevated inversion with a mean height of 400 m. The coefficient of friction for air moving over the basin is assumed to be 0.5, and the minimum energy needed to sustain airflow is equal to the energy dissipated by ground friction. Determine the power required to move the air mass with a velocity of 7 km h^{-1} . Compare your result with the capacity of Hoover Dam: $1.25 \times 10^6 \text{ kW}$.
- 14.5_B** Elevated inversion layers are a prime factor responsible for the incidence of community air pollution problems. It is interesting to consider the feasibility of eliminating an elevated inversion layer. In principle, this could be done either by cooling all the air from the inversion base upward to a temperature below that at the inversion base or by heating all the air below the top of the inversion to a temperature higher than that at the inversion top.

Show that the energy E required to destroy an elevated inversion by heating from below is given by

$$E = \rho c_p [\Gamma(H_T - H_B) + (T_T - T_B)] \frac{H_T + H_B}{2}$$

where

ρ = average density of air

c_p = heat capacity of air

H_B, H_T = heights of base and top of inversion

T_B, T_T = temperatures of base and top of inversion

Assume that the lapse rate below the base of the inversion is adiabatic and that the rate of temperature increase with height in the inversion is linear.

Estimate the value of E for typical September conditions at Long Beach, California, at 7 a.m. Use

$$H_B = 475\text{m} \quad T_B = 14.1^\circ\text{C}$$

$$H_T = 1055\text{m} \quad T_T = 22.4^\circ\text{C}$$

If the area of the Los Angeles basin is 4000 km^2 and the energy produced by oil burning with 100% efficiency is $1.04 \times 10^7 \text{ cal/kg(oil)}^{-1}$, what is the amount of oil required in order to destroy the inversion over the entire basin?

15 Cloud Physics

Clouds are one of the most significant elements of the atmospheric system, playing several key roles.

1. Clouds are a major factor in the Earth's radiation budget, reflecting sunlight back to space or blanketing the lower atmosphere and trapping infrared radiation emitted by the Earth's surface.
2. Clouds deliver water from the atmosphere to the Earth's surface as rain or snow and are thus a key step in the hydrologic cycle.
3. Clouds scavenge gaseous and particulate materials and return them to the surface (wet deposition).
4. Clouds provide a medium for aqueous-phase chemical reactions and production of secondary species.
5. Clouds affect significantly vertical transport in the atmosphere. Updrafts and downdrafts associated with clouds determine in a major way the vertical redistribution of trace species in the atmosphere.

Despite their great importance, clouds still remain one of the least understood components of the weather and climate system. We begin our discussion of clouds by summarizing the properties of their basic constituent, water. We then investigate the formation of droplets in a cooling air parcel. The microphysics of a droplet population and the dynamics of cloud formation are then examined. Finally, we revisit the chemical processes taking place in clouds and fogs using the material already developed in Chapter 6. A comprehensive discussion of cloud physics, beyond the scope of this book, can be found in Pruppacher and Klett (1980).

15.1 PROPERTIES OF WATER AND WATER SOLUTIONS

Liquid water, H_2O , is characterized by the strong hydrogen bonds between its molecules, which give rise to a number of unique properties. Because of the strength of these bonds, a relatively large amount of energy is required to evaporate a unit mass of water. Similarly, the latent heat of freezing is also relatively large, as a result of further strong bonding in ice crystals. The surface tension (surface free energy) is also large. Table 15.1 summarizes these physical properties of water. In the following sections we discuss the atmospherically relevant properties of water and its solutions.

TABLE 15.1 Properties of Water

Property	Phase/Temperature		Value
Specific heat at constant pressure	Vapor	\hat{c}_{pv}	1.952 J g ⁻¹ K ⁻¹
	Liquid (0°C)	\hat{c}_{pw}	4.218 J g ⁻¹ K ⁻¹
Specific heat at constant volume	Vapor	\hat{c}_{vv}	1.463 J g ⁻¹ K ⁻¹
	0°C	ΔH_v	2.5 kJ g ⁻¹
Latent heat of evaporation	100°C		2.25 kJ g ⁻¹
	0°C	ΔH_m	0.33 kJ g ⁻¹
Latent heat of fusion	0°C		
Surface tension	water/air (20°C)	σ_{wo}	0.073 J m ⁻²

15.1.1 Specific Heat of Water and Ice

The specific heat of liquid water, \hat{c}_{pw} , varies with temperature and can be described by the semiempirical relationships

$$\hat{c}_{pw} = 4.218 + 3.47 \times 10^{-4}(T - 273)^2, \quad 233 \leq T \leq 273 \quad (15.1)$$

$$\begin{aligned} \hat{c}_{pw} &= 4.175 + 1.3 \times 10^{-5}(T - 308)^2 \\ &\quad + 1.6 \times 10^{-8}(T - 308)^4, \quad 273 \leq T \leq 308 \end{aligned} \quad (15.2)$$

where T is in K and \hat{c}_{pw} is in J g⁻¹ K⁻¹.

The above heat capacity refers to pure water. Most ions lower the heat capacity of water, but this change is negligible for solute concentrations smaller than 0.1 M. Therefore, for cloud applications, we will assume that the heat capacity of water is independent of the droplet concentration and depends only on temperature.

15.1.2 Latent Heats of Evaporation and of Melting for Water

Empirical fits to the specific latent heats of evaporation, ΔH_v , and of melting, ΔH_m , are as follows for temperature T in K,

$$\Delta H_v(\text{kJ g}^{-1}) = 2.5 \left(\frac{273.15}{T} \right)^{0.167 + 3.67 \times 10^{-4} T} \quad (15.3)$$

and

$$\Delta H_m(\text{J g}^{-1}) = 333.5 + 2.03 T - 0.0105 T^2 \quad (15.4)$$

The above enthalpies refer to pure water phase changes and are expected to differ for solutions. However, even at NaCl concentrations of 5 M, the enthalpy of evaporation changes by less than 0.2% (Pruppacher and Klett, 1980). Thus, for our purposes, these enthalpies will also be assumed to depend on temperature only.

15.1.3 Water Surface Tension

The surface tension of water decreases with increasing temperature. Pruppacher and Klett (1980) recommend use of the following function:

$$\sigma_{wo} = 0.0761 - 55 \times 10^{-4}(T - 273)$$

for the temperature range -40 to 40°C , where σ_{wo} is in J m^{-2} . The surface tension of water is $76.1 \times 10^{-3} \text{ J m}^{-2}$ at 0°C , and decreases by $1.55 \times 10^{-3} \text{ J m}^{-2}$ for every 10°C . Note that these values can be used for supercooled water also, that is, liquid water existing at temperatures below 0°C .

The dissolution of other compounds in water alters its surface tension. Experimental values of the variation of water solution surface tension with the solution concentration are tabulated in the *Handbook of Physics and Chemistry*. For salts like NaCl and $(\text{NH}_4)_2\text{SO}_4$ the dependence of the solution surface tension, σ_w , on the solution molarity is practically linear over the range of atmospheric interest:

$$\begin{aligned}\sigma_w(m_{\text{NaCl}}, T) &= \sigma_{wo}(T) + 1.62 \times 10^{-3} m_{\text{NaCl}} \\ \sigma_w(m_{(\text{NH}_4)_2\text{SO}_4}, T) &= \sigma_{wo}(T) + 2.17 \times 10^{-3} m_{(\text{NH}_4)_2\text{SO}_4}\end{aligned}$$

where $\sigma_{wo}(T)$ is the surface tension of pure water and m_{NaCl} and $m_{(\text{NH}_4)_2\text{SO}_4}$ are the molarities of NaCl and $(\text{NH}_4)_2\text{SO}_4$ in M, respectively.¹

A last issue is the dependence of the water surface tension on the size of the droplet. One would expect that as the droplet surface tension is the result of attractive forces between water molecules near the surface, a change in droplet diameter would change the number of molecules interacting with the molecules at the surface, thus changing the surface tension. However, because of the small range of molecular interaction, this dependence of σ_{wo} on size is significant only for extremely small drops, consisting merely of a few thousands of molecules, and the exact dependence is still a subject of debate (Pruppacher and Klett, 1980). The change is probably smaller than 1% for water drops as small as $0.1 \mu\text{m}$ and becomes significant only at drop sizes less than $0.01 \mu\text{m}$. Therefore the dependence of surface tension on droplet size can be neglected for atmospheric cloud applications.

¹Because solutes alter the surface tension of water, one would expect variations of the concentrations of these species near the droplet-air interface. For example, as nature tries to reach states of lower energies, if a solute increases the surface tension of water, this species at equilibrium should have lower concentrations at the interface than in the bulk solution. The opposite should happen for a surface-active compound that lowers the surface tension. One would expect higher concentrations of this species near the interface than in the bulk. For a 1 M NaCl solution this surface tension effect results in a NaCl deficiency at the interface of less than 1% (Pruppacher and Klett, 1980). The same authors suggested that for drops with diameters larger than $0.2 \mu\text{m}$ and NaCl concentrations lower than 1 M, this concentration gradient due to surface tension is less than 1% and can safely be ignored. The effect of solution inhomogeneity due to surface tension will therefore be neglected for our discussion of atmospheric droplet formation.

15.2 WATER EQUILIBRIUM IN THE ATMOSPHERE

Water in the atmosphere exists in the gas phase as water vapor and in the aqueous phase as water droplets and wet aerosol particles. In this section we will investigate the conditions for water equilibrium between the gas and aqueous phases. This equilibrium is complicated by two effects: the curvature of the particles and the formation of aqueous solutions. We will start from the simplest case—the equilibrium between a flat pure water surface and the atmosphere. Then the equilibrium of a pure water droplet will be investigated, followed by a flat water solution surface. Finally, these effects will be integrated, and the desired equilibrium conditions for an aqueous solution droplet will be derived.

15.2.1 Equilibrium of a Flat Pure Water Surface with the Atmosphere

When a pure substance is at equilibrium with its vapor, its gas-phase partial pressure is equal by definition to its saturation vapor pressure, p° . The gas-phase molar saturation concentration, $c^\circ = p^\circ/RT$, of a compound is determined by its chemical structure and for water at atmospheric conditions is, on a mass basis, the order of a few g m^{-3} (Figure 15.1).

The change of the saturation pressure with temperature can be calculated, as we showed in Chapter 9, by the Clausius–Clapeyron equation:

$$\frac{dp^\circ}{dT} = \frac{\Delta H_v(T)M_w}{T(v_v - v_w)} \quad (15.7)$$

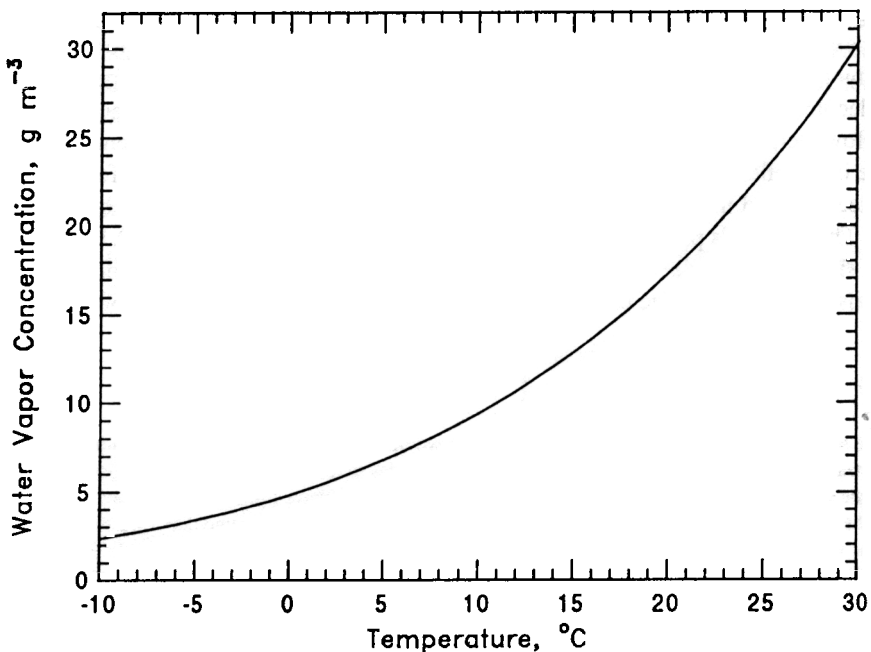


FIGURE 15.1 Saturation concentration of water over a flat water surface as a function of temperature. Values below 0°C correspond to supercooled (metastable) water.

TABLE 15.2 Saturation Vapor Pressure of Water Vapor Over a Flat Pure Water or Ice Surface

$$p^\circ(\text{mbar}) = a_0 + a_1T + a_2T^2 + a_3T^3 + a_4T^4 + a_5T^5 + a_6T^6 \quad (T \text{ is in } ^\circ\text{C})$$

Water (-50 to $+50^\circ\text{C}$) $a_0 = 6.107799961$ $a_1 = 4.436518521 \times 10^{-1}$ $a_2 = 1.428945805 \times 10^{-2}$ $a_3 = 2.650648471 \times 10^{-4}$ $a_4 = 3.031240396 \times 10^{-6}$ $a_5 = 2.034080948 \times 10^{-8}$ $a_6 = 6.136820929 \times 10^{-11}$	Ice (-50 to 0°C)
--	------------------------------------

Source: Lowe and Ficke (1974).

where ΔH_v is the specific heat for water evaporation, M_w is the molecular weight of water, and v_v and v_w are the molar volumes of water vapor and liquid water correspondingly. Assuming that $v_v \gg v_w$ and that water vapor satisfies the ideal gas law ($p^\circ v_v = RT$), then (15.7) becomes (9.68),

$$\frac{dp^\circ}{dT} \sim \frac{\Delta H_v(T) p^\circ M_w}{RT^2}$$

Replacing in the above equation a function describing the temperature dependence of the latent heat of evaporation (e.g., (15.3)), one can integrate and obtain an explicit expression for $p^\circ(T)$. A series of such expressions exist in the literature (see Problem 1.1), and that proposed by Lowe and Ficke (1974) is given in Table 15.2.

15.2.2 Equilibrium of a Pure Water Droplet

In Chapter 9 we showed that the vapor pressure over a curved interface always exceeds that of the same substance over a flat surface. The dependence of the water vapor pressure on the droplet diameter is given by the Kelvin equation (9.86) as

$$\frac{p_w(D_p)}{p^\circ} = \exp\left(\frac{4M_w\sigma_{wo}}{RT\rho_w D_p}\right)$$

where $p_w(D_p)$ is the water vapor pressure over the droplet of diameter D_p , p° is the water vapor pressure over a flat surface at the same temperature, M_w is the molecular weight of water, σ_{wo} is the air–water surface tension, and ρ_w is the water density. The equilibrium water vapor concentrations at 0°C and 20°C are shown in Figure 15.2 as a function of the droplet diameter. Note that the effect of curvature for water droplets becomes important only for $D_p < 0.1 \mu\text{m}$.

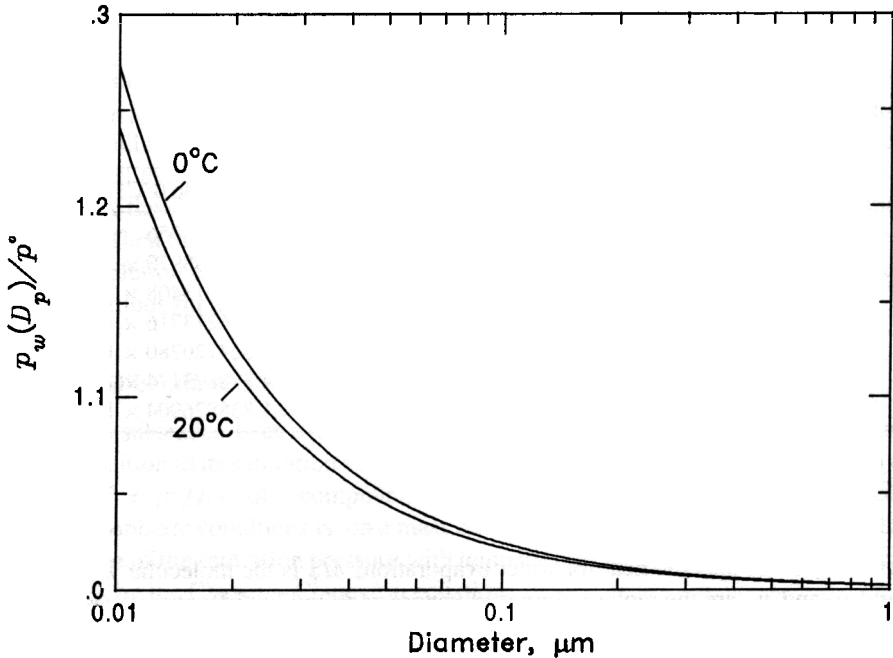


FIGURE 15.2 Ratio of the equilibrium vapor pressure of water over a droplet of diameter D_p , $p_w(D_p)$, to that over a flat surface, p^0 , as a function of droplet diameter for 0°C and 20°C .

Since $p_w(D_p) > p^0$, for equilibrium of a pure water droplet with the environment the air needs to be supersaturated with water vapor. For the equilibration of a large pure water droplet, a modest supersaturation is necessary, but a large supersaturation is necessary for a small droplet. Let us investigate the stability of such an equilibrium state. We assume that a droplet of pure water with diameter D_p is in equilibrium with the atmosphere. Maintaining the temperature constant at T , the atmosphere will have a water vapor partial pressure $p_w = p_w(D_p)$. Let us assume that a few molecules of water vapor collide with the droplet causing its diameter to increase infinitesimally to D'_p . This will cause a small decrease in the water vapor pressure required for the droplet equilibration to $p_w(D'_p)$. The water vapor concentration in the environment has not changed and therefore $p_w > p_w(D'_p)$, causing more water molecules to condense on the droplet and the droplet to grow even more. The opposite will happen if a few water molecules leave the droplet. The droplet diameter will decrease, the water vapor pressure at the droplet surface will exceed that of the environment, and the droplet will continue evaporating. These simple arguments indicate that *the equilibrium of a pure water droplet is unstable*. A minor perturbation is sufficient either for the complete evaporation of the droplet or for its uncontrollable growth.

Droplets in the atmosphere never consist exclusive of water; they always contain dissolved compounds. However, understanding the behavior of a pure water droplet is necessary for understanding the behavior of an aqueous droplet solution. •

15.2.3 Equilibrium of a Flat Water Solution

Let us consider a water solution (flat surface) at constant temperature T and pressure p in equilibrium with the atmosphere. Water equilibrium between the gas and aqueous phases requires equality of the corresponding water chemical potentials in the two phases (see Chapter 9):

$$\mu_w(\text{g}) = \mu_w(\text{aq}) \quad (15.10)$$

Water vapor behaves in the atmosphere as an ideal gas so its gas-phase chemical potential is

$$\mu_w(\text{g}) = \mu_w^\circ(T) + RT \ln p_s^\circ \quad (15.11)$$

where p_s° is the water vapor partial pressure over the solution. The chemical potential of liquid water will be given by

$$\mu_w(\text{aq}) = \mu_w^* + RT \ln \gamma_w x_w \quad (15.12)$$

where γ_w is the water activity coefficient and x_w the mole fraction of water in solution. Combining (15.10) to (15.12) we obtain

$$\frac{p_s^\circ}{\gamma_w x_w} = \exp\left(\frac{\mu_w^\circ - \mu_w^*}{RT}\right) = K(T) \quad (15.13)$$

The above equation describes the behavior of the system for any solution composition. Note that the right-hand side is a function of temperature only and therefore will be equal to a constant, K , for constant temperature. Considering the case of pure water (no solute) we note that when $x_w = 1$, $\gamma_w \rightarrow 1$ and $p_s^\circ = p^\circ = K(T)$, where p° is the vapor pressure of water over pure water. Therefore (15.13) can be rewritten as

$$p_s^\circ = \gamma_w x_w p^\circ \quad (15.14)$$

Equation (15.14) is applicable for any solution and does not assume ideal behavior. Nonideality is accounted for by the activity coefficient γ_w .

The mole fraction of water in a solution consisting of n_w water moles and n_s solute moles is given by

$$x_w = \frac{n_w}{n_w + n_s} \quad (15.15)$$

and therefore the vapor pressure of water over its solution is given by

$$p_s^\circ = \frac{n_w}{n_w + n_s} \gamma_w p^\circ \quad (15.16)$$

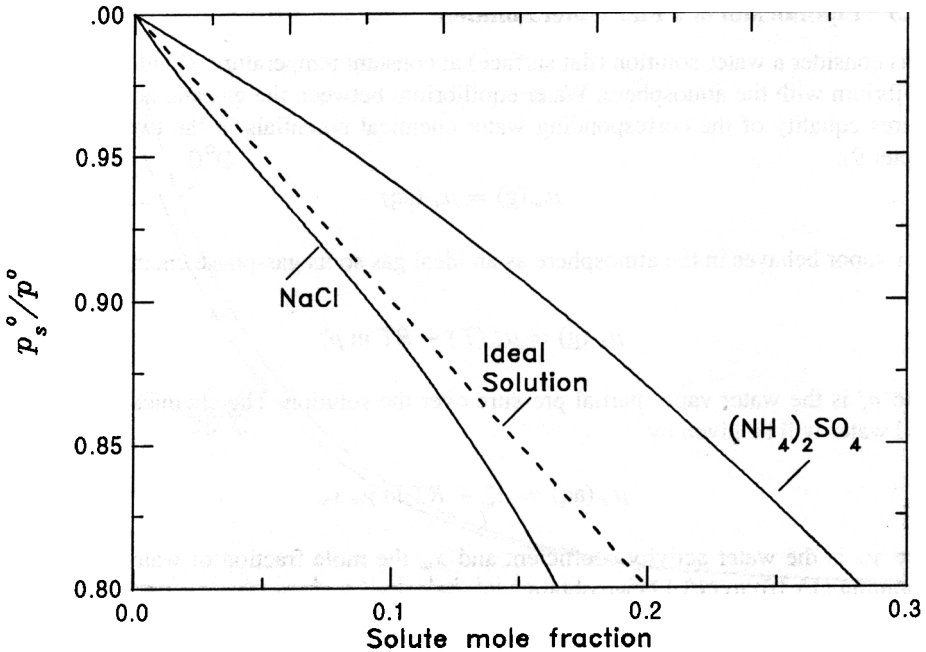


FIGURE 15.3 Variation of water vapor pressure ratio (p_s^o/p^o) as a function of the solute mole fraction at 25°C for solution of NaCl and $(\text{NH}_4)_2\text{SO}_4$ and an ideal solution. The mole fraction of the salts has been calculated taking into account their complete dissociation.

If the solution is dilute, then γ_w approaches its infinite dilution limit $\gamma_w \rightarrow 1$. Therefore, at high dilution, the vapor pressure of water is given by Raoult's law,

$$p_s^o = x_w p^o \quad (15.17)$$

and the solute causes a reduction of the water equilibrium vapor pressure over the solution.

The vapor pressure of water over NaCl and $(\text{NH}_4)_2\text{SO}_4$ solutions is shown in Figure 15.3. Also shown is the ideal solution behavior. Note that because NaCl dissociates into two ions, the number of equivalents in solution is twice the number of moles of NaCl. For $(\text{NH}_4)_2\text{SO}_4$, the number of ions in solution is three times the number of dissolved salt moles. In calculating the number of moles in solution, n_s , a dissociated molecule that has dissociated into i ions is treated as i molecules, whereas an undissociated molecule is counted only once. A similar diagram is given in Figure 15.4, using now the concentration of salt as the independent variable. Solutes that dissociate (e.g., salts) reduce the vapor pressure of water more than do solutes that do not dissociate, and this reduction depends strongly on the type of salt.

15.2.4 Atmospheric Equilibrium of an Aqueous Solution Drop

In the previous sections we developed expressions for the water vapor pressure over a pure water droplet and a flat solution. Atmospheric droplets virtually always contain dissolved solutes, so we need to combine these two previous results to treat this general case.

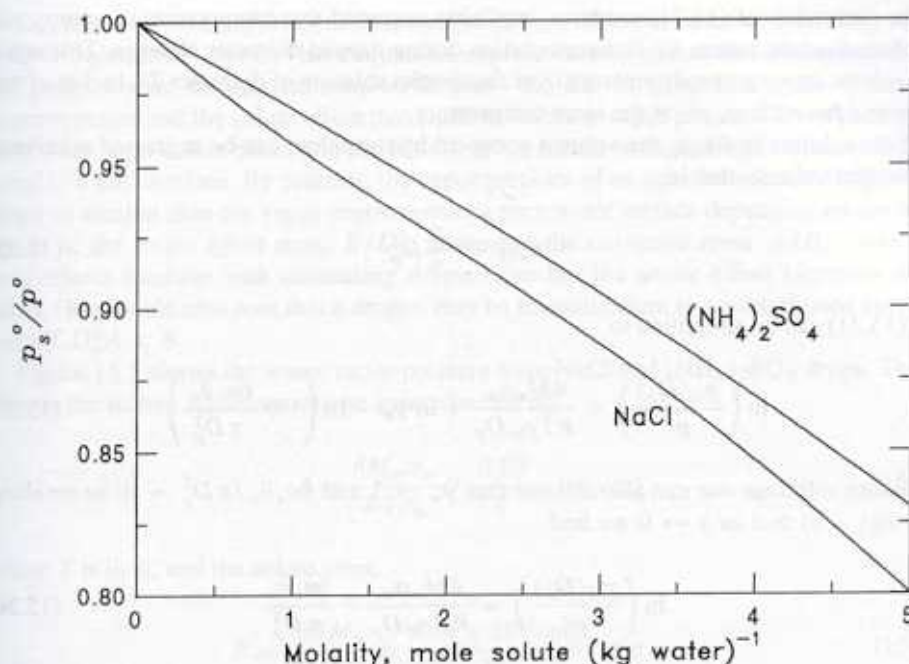


FIGURE 15.4 Variation of water vapor pressure ratio (p_s^o/p^o) as a function of the salt molality (mol of salt per kg of water) of NaCl and $(\text{NH}_4)_2\text{SO}_4$ at 25°C.

Let us consider a droplet of diameter D_p containing n_w moles of water and n_s moles of solute (e.g., a nonvolatile salt). If the solution were flat the water vapor pressure over it would satisfy (15.14). Substituting this expression into (15.9) one obtains

$$\frac{p_w(D_p)}{p^o \gamma_w x_w} = \exp\left(\frac{4M_w \sigma_w}{RT \rho_w D_p}\right) \quad (15.18)$$

Let \bar{v}_w and \bar{v}_s be the partial molar volumes of the two components in the solution and the total drop volume will satisfy

$$\frac{1}{6} \pi D_p^3 = n_w \bar{v}_w + n_s \bar{v}_s \quad (15.19)$$

Note that since we have assumed that the solute is nonvolatile, n_s is the same regardless of the value of D_p . Using (15.19) and (15.15), we find that

$$\frac{1}{x_w} = 1 + \frac{n_s}{n_w} = 1 + \frac{n_s \bar{v}_w}{(\pi/6) D_p^3 - n_s \bar{v}_s} \quad (15.20)$$

Replacing the water mole fraction appearing in (15.18) by (15.20) we obtain

$$\ln\left(\frac{p_w(D_p)}{p^o}\right) = \frac{4M_w \sigma_w}{RT \rho_w D_p} + \ln \gamma_w - \ln\left(1 + \frac{n_s \bar{v}_w}{(\pi/6) D_p^3 - n_s \bar{v}_s}\right) \quad (15.21)$$

In the derivation of (15.21) we have implicitly assumed that temperature, pressure, and number of solute moles, n_s , remain constant during droplet diameter changes. This equation relates the water vapor pressure over the droplet solution of diameter D_p to that of water over a flat surface, p° , at the same temperature.

If the solution is dilute, the volume occupied by the solute can be neglected relative to the droplet volume; that is,

$$n_s v_s \ll \frac{4}{3} \pi D_p^3 \quad (15.22)$$

and (15.21) can be simplified to

$$\ln \left(\frac{p_w(D_p)}{p^\circ} \right) = \frac{4M_w \sigma_w}{RT \rho_w D_p} + \ln \gamma_w - \ln \left(1 + \frac{6n_s v_w}{\pi D_p^3} \right) \quad (15.23)$$

For dilute solutions one can also assume that $\gamma_w \rightarrow 1$ and $6n_s \bar{v}_w / \pi D_p^3 \rightarrow 0$; so recalling that $\ln(1+x) \simeq x$ as $x \rightarrow 0$ we find

$$\ln \left(\frac{p_w(D_p)}{p^\circ} \right) = \frac{4M_w \sigma_w}{RT \rho_w D_p} - \frac{6n_s \bar{v}_w}{\pi D_p^3} \quad (15.24)$$

Recall that \bar{v}_w is the molar volume of water in the solution, which for a dilute solution is equal to the molar volume of pure water; that is,

$$\bar{v}_w \simeq \frac{M_w}{\rho_w} \quad (15.25)$$

where M_w is the molecular weight of water and ρ_w its density. Replacing (15.25) in (15.24),

$$\ln \left(\frac{p_w(D_p)}{p^\circ} \right) = \frac{4M_w \sigma_w}{RT \rho_w D_p} - \frac{6n_s M_w}{\pi \rho_w D_p^3} \quad (15.26)$$

It is customary to write

$$A = \frac{4M_w \sigma_w}{RT \rho_w} \quad B = \frac{6n_s M_w}{\pi \rho_w}$$

and (15.26) as

$$\ln \left(\frac{p_w(D_p)}{p^\circ} \right) = \frac{A}{D_p} - \frac{B}{D_p^3} \quad (15.27)$$

Equations (15.21), (15.24), (15.26), and (15.27) are different forms of the *Köhler equations* (Köhler, 1921, 1926). These equations express the two effects that determine the vapor pressure over an aqueous solution droplet—the Kelvin effect that tends to increase vapor pressure and the solute effect that tends to decrease vapor pressure. For a pure water drop there is no solute effect and the Kelvin effect results in higher vapor pressures compared to a flat interface. By contrast, the vapor pressure of an aqueous solution drop can be larger or smaller than the vapor pressure over a pure water surface depending on the magnitude of the *solute effect* term, B/D_p^3 , relative to the *curvature term*, A/D_p . Note that both effects increase with decreasing droplet size but the solute effect increases much faster. One should also note that a droplet may be in equilibrium in a subsaturated environment if $D_p^2 A < B$.

Figure 15.5 shows the water vapor pressure over NaCl and $(\text{NH}_4)_2\text{SO}_4$ drops. The A term in the Köhler equations can be approximated by

$$A = \frac{4M_w\sigma_w}{RT\rho_w} \simeq \frac{0.66}{T} \quad (\text{in } \mu\text{m}) \quad (15.28)$$

where T is in K, and the solute term,

$$B = \frac{6n_s M_w}{\pi \rho_w} \simeq \frac{3.44 \times 10^{13} \nu m_s}{M_s} \quad (\text{in } \mu\text{m}^3) \quad (15.29)$$

where m_s is the solute mass (in g) per particle, M_s the solute molecular weight (in g mol⁻¹), and ν is the number of ions resulting from the dissociation of one solute molecule. For example, $\nu = 2$ for NaCl and NaNO_3 , while $\nu = 3$ for $(\text{NH}_4)_2\text{SO}_4$.

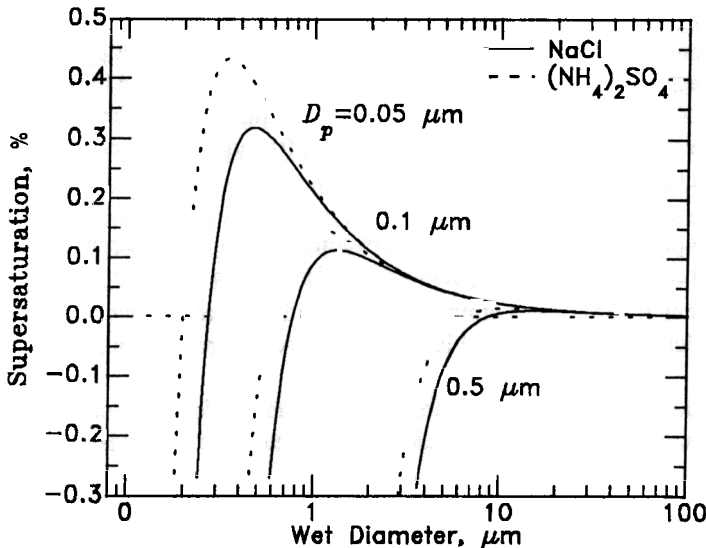


FIGURE 15.5 Köhler curves for NaCl and $(\text{NH}_4)_2\text{SO}_4$ particles with dry diameters 0.05, 0.1, and $0.5 \mu\text{m}$ at 293 K (assuming spherical dry particles). The supersaturation is defined as the saturation minus one. For example, a supersaturation of 1% corresponds to a relative humidity of 101%.

All the curves in Figure 15.5 pass through a maximum. These maxima occur at the *critical droplet diameter*, D_{pc} .

$$D_{pc} = \left(\frac{3B}{A} \right)^{1/2} \quad (15.30)$$

and at this diameter (denoted by the subscript c)

$$\left(\ln \frac{p_w}{p^\circ} \right)_c = \left(\frac{4A^3}{27B} \right)^{1/2} \quad (15.31)$$

The ratio p_w/p° is the saturation relative to a flat pure water surface required for droplet equilibrium and therefore at the critical diameter, the critical saturation, S_c , is

$$\ln S_c = \left(\frac{4A^3}{27B} \right)^{1/2} \quad (15.32)$$

The steeply rising portion of the Köhler curves represents a region where solute effects dominate. As the droplet diameter increases, the relative importance of the Kelvin effect over the solute effect increases, and finally beyond the critical diameter the domination of the Kelvin effect is evident. In this range all Köhler curves approach the Kelvin equation, represented by the equilibrium of a pure water droplet. Physically, the solute concentration is so small in this range (recall that each Köhler curve refers to fixed solute amount) that the droplet becomes similar to pure water.

The Köhler curves also represent the equilibrium size of a droplet for different ambient water vapor concentrations (or relative humidity values). If the water vapor partial pressure in the atmosphere is p_w , a droplet containing n_s moles of solute and having a diameter D_p satisfying the Köhler equations should be at equilibrium with its surroundings. Realizing that the Köhler curves can be viewed as size versus RH equilibrium curves poses a number of interesting questions:

What happens if the atmosphere is supersaturated with water vapor and the supersaturation exceeds the critical supersaturation for a given particle?

What happens if for a given atmospheric saturation there are two diameters for which the droplet can satisfy the Köhler equations? Are there two equilibrium states?

To answer these questions and understand the cloud and fog creation processes in the atmosphere, we need to investigate the stability of the equilibrium states given by the Köhler equation.

Stability of Atmospheric Droplets We have already seen in the previous section that a pure water droplet cannot be at stable equilibrium with its surroundings. A small perturbation of either the droplet itself or its surroundings causes spontaneous droplet growth or shrinkage.

Let us consider first a drop lying on the portion of the Köhler curve for which $D_p < D_{pc}$. We assume that the atmospheric saturation is fixed at S . A drop will constantly experience small perturbations caused by the gain or loss of a few molecules of water. Say that the drop grows slightly due to the addition of a few molecules of water. At its momentary larger size, its equilibrium vapor pressure is larger than the fixed ambient value and the drop will evaporate water, eventually returning to its original equilibrium state. The same phenomenon will be observed if the droplet loses a few molecules of water. Its equilibrium vapor pressure will decrease, become less than the ambient, and water will condense on the droplet returning it to its original size. Therefore drops in the rising part of the Köhler curve are in stable equilibrium with their environment.

Now consider a drop on the portion of the curve for which $D_p > D_{pc}$ that experiences a slight perturbation, causing it to grow by a few molecules of water. At its slightly larger size its equilibrium vapor pressure is lower than the ambient. Thus water molecules will continue to condense on the drop and it will grow even larger. Conversely, a slight shrinkage leads to a drop that has a higher equilibrium vapor pressure than the ambient so the drop continues to evaporate. If it is a drop of pure water, it will evaporate completely. If it contains a solute, it will diminish in size until it intersects the ascending branch of the Köhler curve that corresponds to stable equilibrium. In conclusion, the descending branches of the curves describe unstable equilibrium states.

If the ambient saturation ratio S is lower than the critical saturation S_c for a given particle, then the particle will be in equilibrium described by the ascending part of the curve. If $1 < S < S_c$, then there are two equilibrium states (two diameters corresponding to S). One of them is a stable state and the other is unstable. The particle can reach stable equilibrium only at the state corresponding to the smaller diameter.

If the ambient saturation ratio S happens to exceed the particle critical saturation S_c , there is no feasible equilibrium size for the particle. For any particle diameter the ambient saturation will exceed the saturation at the particle surface (equilibrium saturation), and the particle will grow indefinitely. In such a way a droplet can grow to a size much larger than the original size of the dry particle. It is, in fact, through this process that particles as small as $0.01 \mu\text{m}$ in diameter can grow one billion times in mass to become $10 \mu\text{m}$ cloud or fog droplets. Moreover, in cloud physics a particle is not considered to be a cloud droplet unless its diameter exceeds its critical diameter D_{pc} .

The critical saturation S_c of a particle is an important property. If the environment has reached a saturation larger than S_c , the particle is said to be *activated* and starts growing rapidly, becoming a cloud droplet. For a spherical aerosol particle of diameter d_s (dry diameter), density ρ_s , and molecular weight M_s , the number of moles (after complete dissociation) in the particle is given by

$$n_s = \frac{\nu\pi d_s^3 \rho_s}{6M_s} \tag{15.33}$$

and combining this result with (15.32) we find that

$$\ln S_c = \left(\frac{4A^3 \rho_w M_s}{27\nu\rho_s M_w d_s^3} \right)^{1/2} \tag{15.34}$$

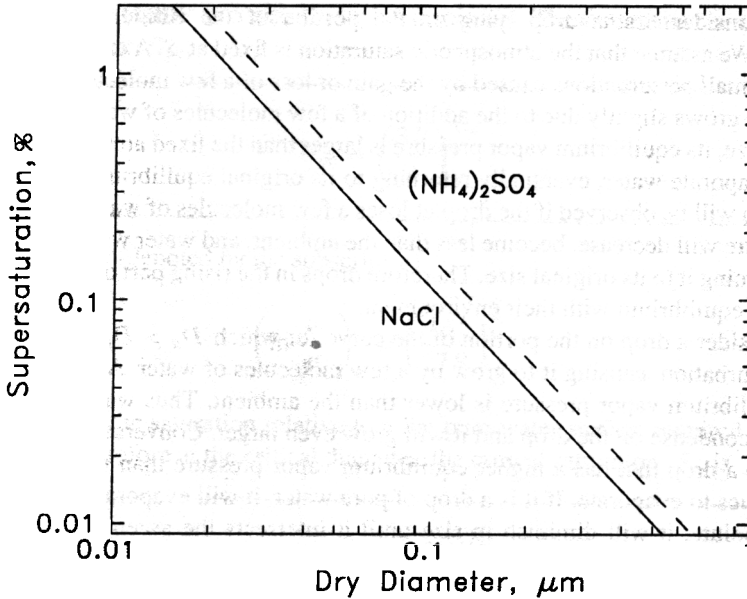


FIGURE 15.6 Critical supersaturation for activating aerosol particles composed of NaCl and $(\text{NH}_4)_2\text{SO}_4$ as function of the dry particle diameters (assuming spherical particles) at 293 K.

This equation gives the critical saturation for a dry particle of diameter d_s . Note that the smaller the particle the higher its critical saturation. When a fixed saturation S exists, all particles whose critical saturation, S_c , exceeds S come to a stable equilibrium size at the appropriate point on their Köhler curve. All particles whose S_c is below S become activated and grow indefinitely as long as $S > S_c$.

Figure 15.6 shows the critical supersaturation for spherical salt particles as a function of their diameters. One should note that critical saturations are always higher than unity and one often defines $s_c = S_c - 1$ as the critical supersaturation.

Figure 15.7 presents the Köhler curves for $(\text{NH}_4)_2\text{SO}_4$ for complete dissociation and no dissociation. Note that dissociation lowers the critical saturation ratio of the particle (the particle is activated more easily) and increases the drop critical diameter (the particle absorbs more water).

15.2.5 Atmospheric Equilibrium of an Aqueous Solution Drop Containing an Insoluble Substance

Our analysis so far has assumed that the aerosol particle consists of a soluble salt that dissociates completely as the RH exceeds 100%. Most atmospheric particles contain both water-soluble and water-insoluble substances (dust, elemental carbon, etc.). Our goal here is to extend the results of the previous section to account for the existence of insoluble material. Our assumption is that the original particle contains soluble material with mass fraction ϵ_m , and the rest is insoluble. We also assume that the insoluble portion does not interact at all with water or the salt ions.

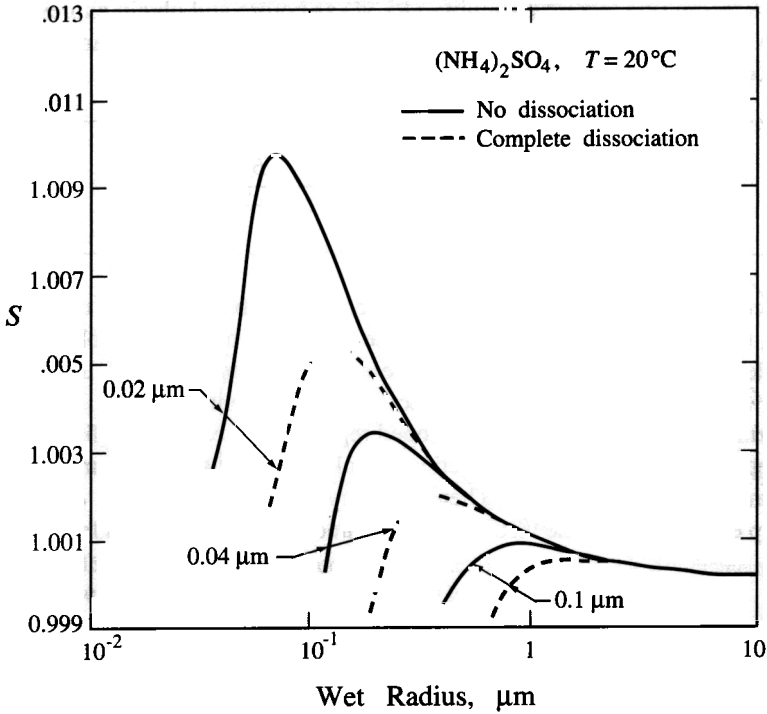


FIGURE 15.7 Köhler curves for $(\text{NH}_4)_2\text{SO}_4$ assuming complete dissociation and no dissociation of the salt in solution for dry radii of 0.02, 0.04, and 0.1 μm .

Our analysis follows exactly Section 15.2.4, until the derivation of the mole fraction of water x_w in (15.19) and (15.20). The existence of the insoluble material needs to be included in these equations. If the insoluble particle fraction is equivalent to a sphere of diameter d_u , then the droplet volume will be

$$\frac{1}{6} \pi D_p^3 = n_w \bar{v}_w + n_s \bar{v}_s + \frac{1}{6} \pi d_u^3 \tag{15.35}$$

and the mole fraction of water x_w in the solution will be given by

$$\frac{\bar{v}_w}{x_w} = \frac{n_s}{n_w} = \frac{n_s \bar{v}_w}{(\pi/6)(D_p^3 - d_u^3) - n_s \bar{v}_s} \tag{15.36}$$

Substituting this expression into (15.18) we find

$$\ln \left(\frac{p_w(D_p)}{p^0} \right) = \frac{4M_w \sigma_w}{RT \rho_w D_p} + \ln \gamma_w - \ln \left(1 + \frac{n_s \bar{v}_u}{(\pi/6)(D_p^3 - d_u^3) - n_s \bar{v}_s} \right) \tag{15.37}$$

For a dilute solution, we may simplify (15.37) as before and obtain expressions analogous to (15.26) and (15.27) with the same definitions of A and B . For example, in this case (15.27) becomes

$$\ln \left(\frac{p_w(D_p)}{p^\circ} \right) = \frac{A}{D_p} - \frac{B}{(D_p^3 - d_u^3)} \quad (15.38)$$

The effect of the insoluble material is to increase in absolute terms the solute effect. Physically, the insoluble material is responsible for part of the droplet volume, displacing the equivalent water. Therefore, for the same overall droplet diameter, the solution concentration will be higher and the solute effect more significant.

An alternative expression can be developed replacing the equivalent diameter of the insoluble material d_u with the mass fraction of soluble material ϵ_m , assuming that the insoluble material has a density ρ_u . Then for a dry particle of diameter d_s the following relationship exists between the insoluble core diameter d_u and the mass fraction ϵ_m :

$$d_u^3 = \frac{\epsilon_m d_s^3}{\left(\frac{\rho_u}{\rho_s} \epsilon_m + 1 \right)} \quad (15.39)$$

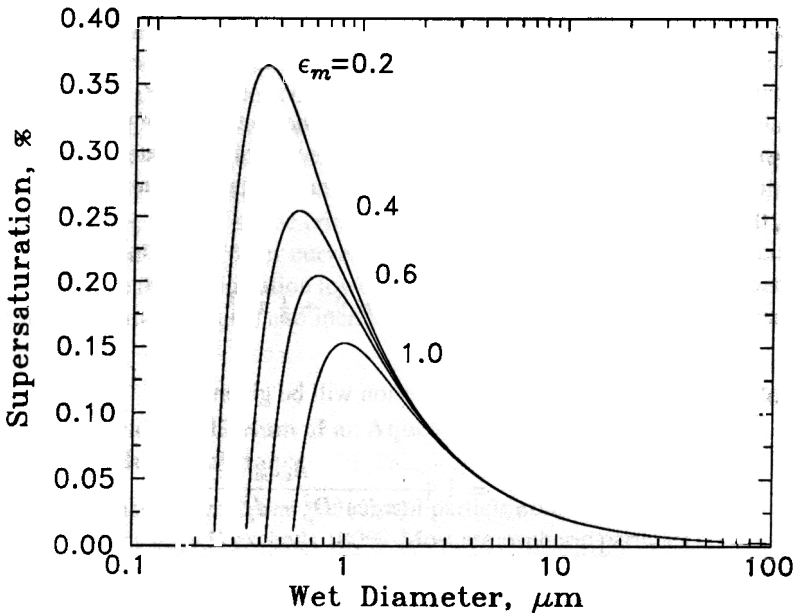


FIGURE 15.8 Variation of the equilibrium vapor pressure of an aqueous solution drop containing $(\text{NH}_4)_2\text{SO}_4$ and insoluble material for an initial dry particle diameter of $0.1 \mu\text{m}$ for soluble mass fractions 0.2, 0.4, 0.6, and 1.0 at 293 K.

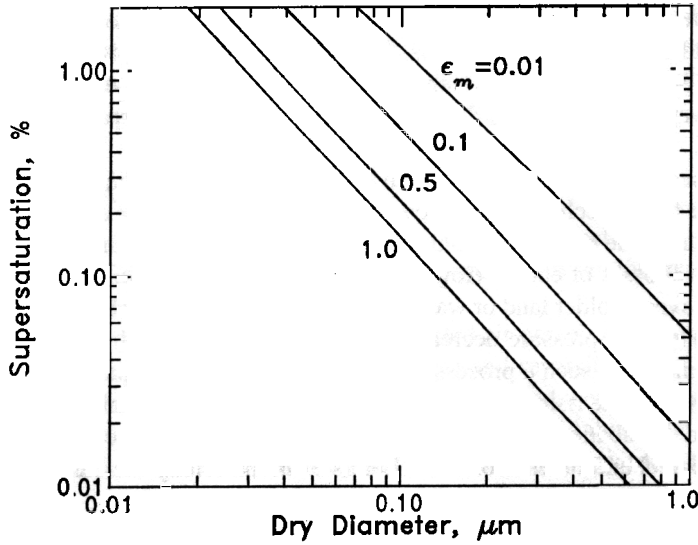


FIGURE 15.9 Critical supersaturation as a function of the particle dry diameter for different contents of insoluble material. The soluble material is $(\text{NH}_4)_2\text{SO}_4$.

and (15.38) can be rewritten as a function of the particle soluble fraction and the initial particle diameter provided that the densities of soluble and insoluble material are known. The number of moles of solute are in this case given not by (15.33) but by the following expression:

$$n_s = \frac{\epsilon_m}{\left(\frac{\epsilon_m}{\rho_s} + \frac{1 - \epsilon_m}{\rho_i}\right)} \frac{v\pi d_p^3}{6} \tag{15.40}$$

Köhler curves for a particle consisting of various combinations of $(\text{NH}_4)_2\text{SO}_4$ and insoluble material are given in Figure 15.8. We see that the smaller the water-soluble fraction the higher the supersaturation needed for activation of the same particle, and the lower the critical diameter. Critical supersaturation as a function of the dry particle diameter is given in Figure 15.9.

15.3 CLOUD AND FOG FORMATION

The ability of a given particle to become activated depends on its size and chemical composition and on the maximum supersaturation experienced by the particle. If, for example, the ambient RH does not exceed 100%, no particle will be activated and a cloud cannot be formed². In this section we will examine the mechanisms by which clouds are created in

²The classic Köhler formulation does not consider the cases of solutes that are not completely soluble or soluble gases, both of which influence the solute effect term in (15.27). In such cases cloud droplets can exist at $S < 1$ since $B/D_p^3 > A/D_p$.

the atmosphere. A necessary condition for this cloud formation is the increase in the RH of an air parcel to a value exceeding 100%. This RH increase is usually the result of cooling of a moist air parcel. Even if the water mass inside the air parcel does not change, its saturation water vapor concentration decreases as its temperature decreases, and therefore its RH increases.

There are several mechanisms by which air parcels can cool in the atmosphere. It is useful to separate these mechanisms into two groups: isobaric cooling and adiabatic cooling. Isobaric cooling is the cooling of an air parcel under constant pressure. It usually is the result of radiative losses of energy (fog and low stratus formation) or horizontal movement of an airmass over a colder land or water surface or colder airmass. If an air parcel ascends in the atmosphere, its pressure decreases, the parcel expands, and its temperature drops. The simplest model of such a process assumes that during this expansion there is no heat exchanged between the rising parcel of air and the environment. This idealized process is usually termed "adiabatic cooling." In reality there is always some heat and mass exchange between the parcel and its environment. Let us examine briefly the basic thermodynamic relations for these two mechanisms of cloud formation.

15.3.1 Isobaric Cooling

Let us consider a volume of moist air that is cooled isobarically. Assuming that we can neglect mass exchange between the air parcel and its surroundings, the water vapor partial pressure (p_w) will remain constant. A temperature decrease from an initial value T_0 to T_d will lead to a decrease of the saturation vapor pressure from $p^\circ(T_0)$ to $p^\circ(T_d)$.

We would like to calculate when the parcel will become saturated. In other words, if a parcel initially has a temperature T_0 and relative humidity RH (from 0 to 1), what is the temperature T_d at which it will become saturated (RH = 1)? The temperature T_d is called the *dew temperature* or *dew point*.

T_d can be calculated recognizing that by definition $\text{RH} = p_w/p^\circ(T_0)$ and that at the dew point $p_w = p^\circ(T_d)$. The dependence of the saturation vapor pressure on temperature is given by the Clausius–Clapeyron equation (15.8). Integration between T_0 , $p^\circ(T_0)$ and T_d , p_w yields

$$\int_{p^\circ(T_0)}^{p_w} d \ln p = \int_{T_0}^{T_d} \frac{\Delta H_v M_w}{RT^2} dT \quad (15.41)$$

Assuming that the latent heat ΔH_v is approximately constant from T_0 to T_d we get

$$\ln \left(\frac{p_w}{p^\circ(T_0)} \right) = \frac{\Delta H_v M_w}{R} \left(\frac{T_d - T_0}{T_0 T_d} \right) \quad (15.42)$$

Noting that the ratio on the left-hand side is equal to the initial relative humidity, and assuming that the temperature change is small enough so that $T_0 T_d \simeq T_0^2$, we get

$$T_d \simeq T_0 + \frac{RT_0^2}{\Delta H_v M_w} \ln(\text{RH}) \quad (15.43)$$

For an air parcel initially at 283 K with a relative humidity of 80% ($RH = 0.8$), a temperature reduction of 3.3 K is required to bring the parcel to saturation. The dew point of a subsaturated air parcel is always lower than its actual temperature (Figure 15.10). The two become equal only when the relative humidity reaches 100%.

15.3.2 Adiabatic Cooling

The thermodynamic behavior of a rising moist air parcel can be examined in two steps: the cooling of the air parcel from its initial condition to saturation followed by the cooling of the saturated air.

Let us consider first a moist unsaturated air parcel. Assuming that the rise is adiabatic (no heat exchange with its surroundings) and reversible, then it will also be isentropic. Recall that for a reversible process $dQ = T dS$ and therefore when $dQ = 0$, $dS = 0$ also. Under these conditions we have shown in Chapter 14 that if the air parcel is dry (no water vapor), its temperature will vary linearly with height according to (14.6),

$$\frac{dT}{dz} = -\Gamma \quad (15.44)$$

where $\Gamma = g/\hat{c}_p = 9.76^\circ\text{C km}^{-1}$ is the dry adiabatic lapse rate. If the air is moist, then, as we saw in Chapter 14, the heat capacity of the air parcel \hat{c}_p must be corrected. The changes are small as the water vapor mass fraction is usually less than 3%. Even at this rather extreme condition, the lapse rate of the moist parcel is $9.71^\circ\text{C km}^{-1}$, an essentially

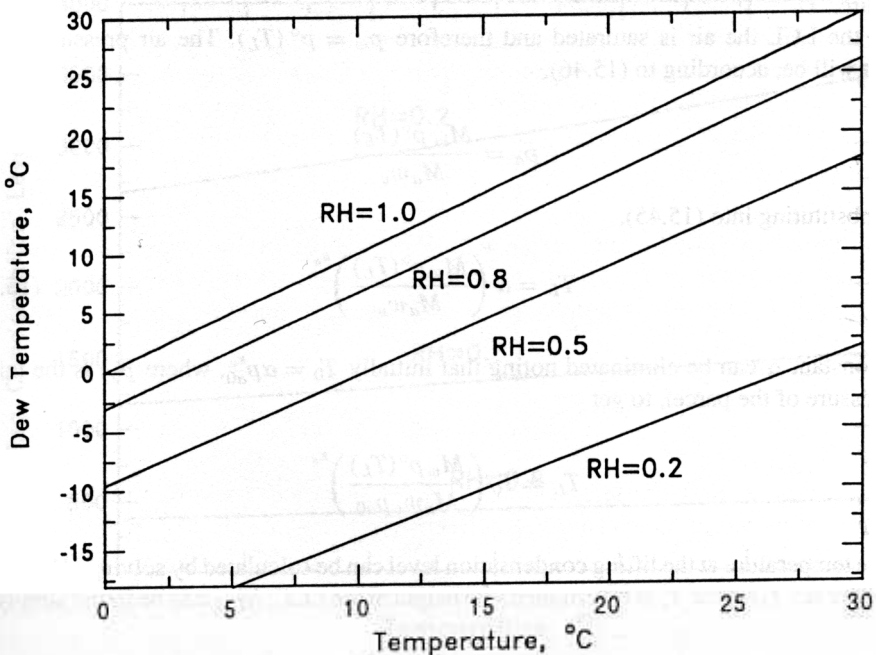


FIGURE 15.10 Dew temperature of an air parcel as a function of its temperature and relative humidity.

negligible change. Pruppacher and Klett (1980) note that setting the moist adiabatic lapse rate equal to the dry adiabatic lapse rate Γ results in negligible error for all practical purposes.

We can use the above information about temperature changes of a rising unsaturated air parcel to calculate the height at which the parcel will become saturated. This height is called the *lifting condensation level* (LCL) and is usually very close to the cloud base. To calculate the temperature T_L at the lifting condensation level, we need to recall (see (14.11)) that the temperature of an air parcel undergoing adiabatic cooling varies as function of pressure p_a according to

$$T = \alpha p_a^{\kappa_a} \quad (15.45)$$

where α is a constant and $\kappa_a = (\gamma - 1)/\gamma \simeq 0.286$ ($\gamma = \hat{c}_p/\hat{c}_v$ is the ratio of the air heat capacity under constant pressure to its heat capacity under constant volume). We also need to recall that because both the air and water vapor masses are conserved during the air parcel rise, the water vapor mass mixing ratio w_v will remain constant. Because both gases are ideal:

$$w_v = \frac{M_w p_w}{M_a p_a} \quad (15.46)$$

The water vapor and liquid water mixing ratios w_v and w_L are very useful quantities in cloud physics. They do not have units and can be defined on a molar, a volume, or a mass basis. The mass basis will be used in this chapter unless otherwise indicated. Several rather complicated expressions can be simplified considerably using these mixing ratios. If necessary, (15.46) can be used to convert the water vapor mixing ratio to water vapor partial pressure.

At the LCL the air is saturated and therefore $p_w = p^\circ(T_L)$. The air pressure at this height will be, according to (15.46),

$$p_a = \frac{M_w p^\circ(T_L)}{M_a w_v}$$

and substituting into (15.45),

$$T_L = \alpha \left(\frac{M_w p^\circ(T_L)}{M_a w_v} \right)^{\kappa_a} \quad (15.47)$$

The constant α can be eliminated noting that initially $T_0 = \alpha p_{a0}^{\kappa_a}$, where p_{a0} is the initial air pressure of the parcel, to get

$$T_L = T_0 \left(\frac{M_w p^\circ(T_L)}{M_a w_v p_{a0}} \right)^{\kappa_a} \quad (15.48)$$

The temperature at the lifting condensation level can be calculated by solving (15.48) numerically for T_L . Once T_L is determined, the height at the LCL, h_{LCL} can be found simply by

$$h_{\text{LCL}} = \frac{\bar{z}}{\Gamma} \quad (15.49)$$

The lifting condensation level h_{LCL} is shown in Figure 15.11 as a function of the initial temperature and relative humidity of the air parcel.

If the air parcel is lifted beyond the LCL, water will start condensing on the available particles, and latent heat of condensation ($-\Delta H_v$) will be released. The lapse rate Γ_s in this case can be calculated by an energy balance, assuming that the air parcel remains saturated. The cooling rate of the air parcel is balanced by the work necessary for the expansion of the air parcel and the condensation latent heat released. If the air parcel contains a water vapor mass mixing ratio w_{vs} (the subscript s is used to denote saturation of the atmosphere with water), where $w_{vs} = M_w p^s / M_a p_a$, then the energy change due to cooling will be $\hat{c}_p dT$ (\hat{c}_p is the heat capacity of air, which will be almost equal to the heat capacity of the air parcel including the water), the latent heat released will be $\Delta H_v dw_{vs}$, and the expansion work is $v dp = RT dp_a / p_a M_a$. Therefore the energy balance is

$$\hat{c}_p dT + \Delta H_v dw_{vs} - RT \frac{dp_a}{p_a M_a} = 0 \quad (15.50)$$

and dividing by dz leads to the expression

$$\Gamma_s = \left(-\frac{dT}{dz} \right) = \frac{\Delta H_v}{\hat{c}_p} \frac{dw_{vs}}{dz} - \frac{RT}{M_a p_a \hat{c}_p} \frac{dp_a}{dz} \quad (15.51)$$

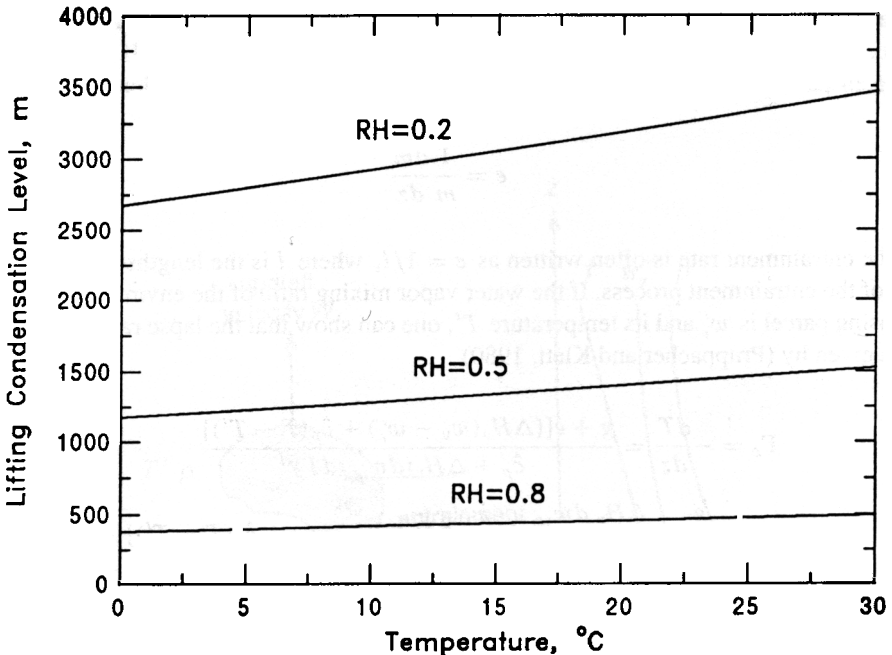


FIGURE 15.11 Lifting condensation level as a function of initial temperature and relative humidity of the air parcel assuming that the air parcel starts initially at the ground at $p = 1$ atm.

Using the fact that the pressure gradient is given by $dp_a/dz = -gM_a p_a/RT$ we get

$$\Gamma_s = \frac{g + \Delta H_v(dw_{vs}/dz)}{\hat{c}_p} \quad (15.52)$$

Since dw_{vs}/dz , the rate of change of the saturation water vapor mass fraction, will be negative during condensation of water, $\Gamma_s < \Gamma = g/\hat{c}_p$. Therefore the rate of cooling of saturated air is less than for dry air. For example, for 1000 mbar and 0°C a lapse rate of 5.8°C km⁻¹ is calculated, or about 60% of the dry adiabatic rate.

One can relate the derivative dw_{vs}/dz to dw_{vs}/dT to show that

$$\Gamma_s = \frac{g}{\hat{c}_p + \Delta H_v(dw_{vs}/dT)} \quad (15.53)$$

Since the saturation mixing ratio derivative (dw_{vs}/dT) is a strong function of temperature, the lapse rate Γ_s is not a constant, but rather a strong function of temperature. At the high temperatures of the tropics dw_{vs}/dT is high and Γ_s is only 30% of the dry lapse rate Γ_d . In cold polar regions (dw_{vs}/dT) is low and there is little difference between the two.

The latent heat release during cloud formation makes clouds warmer than the surrounding cloud-free air. This higher temperature enhances the buoyancy of clouds, as will have been noticed by anyone who has flown through clouds in an airplane.

15.3.3 Cooling with Entrainment

So far we have treated a rising air parcel as a closed system. This is rarely the case in real clouds, where air from the rising parcel is mixed with the surrounding air. If m is the mass of the air parcel one defines the *entrainment rate* e as (Pruppacher and Klett, 1980)

$$e = \frac{1}{m} \frac{dm}{dz} \quad (15.54)$$

The entrainment rate is often written as $e = 1/l$, where l is the lengthscale characteristic of the entrainment process. If the water vapor mixing ratio of the environment around the rising parcel is w'_v and its temperature T' , one can show that the lapse rate in the cloud Γ_c is given by (Pruppacher and Klett, 1980)

$$\begin{aligned} \Gamma_c &= -\frac{dT}{dz} = \frac{g + e[(\Delta H_v(w_v - w'_v) + \hat{c}_p(T - T'))]}{\hat{c}_p + \Delta H_v(dw_{vs}/dT)} \\ &= \frac{g}{\hat{c}_p} + \frac{\Delta H_v}{\hat{c}_p} \frac{dw_{vs}}{dz} + \frac{e}{\hat{c}_p} [\Delta H_v(w_v - w'_v) + \hat{c}_p(T - T')] \end{aligned} \quad (15.55)$$

Γ_c exceeds Γ_s because $e > 0$, $w_v > w'_v$, and $T > T'$. Observations show that use of (15.53) usually overestimates the temperature differences between updrafts in cumulus clouds and the environment. The correction for entrainment represented by (15.55) increases the lapse rate by 1 to 2°C and describes cloud formation much more realistically.

15.3.4 A Simplified Mathematical Description of Cloud Formation

Let us revisit the rising moist air parcel assuming that we are in a Lagrangian reference frame, moving with the air parcel. The air parcel is characterized by its temperature T , water vapor mixing ratio w_v , liquid water mixing ratio w_L , and velocity W . At the same time we need to know the temperature T' , pressure p , and water vapor saturation w'_v of the air around it (Figure 15.12). The pressure of the air parcel is assumed to be equal to its environment.

Let us assume that the air parcel has mass m and air density ρ (without including the liquid water). The velocity of the air parcel will be the result of buoyancy forces and the gravitational force due to liquid water. The buoyancy force is proportional to the volume of the air parcel, m/ρ , and the density difference between the air parcel and its surroundings, $\rho' - \rho$. The liquid water mass is mw_L and the corresponding gravitational force gmw_L . The equation for conservation of momentum is

$$\frac{d}{dt} (mW) = gm \left(\frac{\rho' - \rho}{\rho} - w_L \right) \tag{15.56}$$

where ρ' is the density of the surrounding air.

As the air parcel is moving, it causes the acceleration of surrounding airmasses, resulting in a decelerating force on the air parcel. The deceleration force is proportional to the mass of the displaced air, m' , and the corresponding deceleration, $-dW/dt$. Pruppacher and Klett (1980) show that this effect is actually equivalent to an acceleration of an "induced" mass $m/2$ and therefore a term $-\frac{1}{2}m dW/dt$ should be added on the right-hand side of (15.56). Using the ideal gas law $(\rho' - \rho)/\rho = (T - T')/T'$ and the modified (15.56) can be rewritten as

$$\frac{3}{2} \frac{dW}{dt} + \frac{W}{m} \frac{dm}{dt} = g \left(\frac{T - T'}{T'} - w_L \right) \tag{15.57}$$

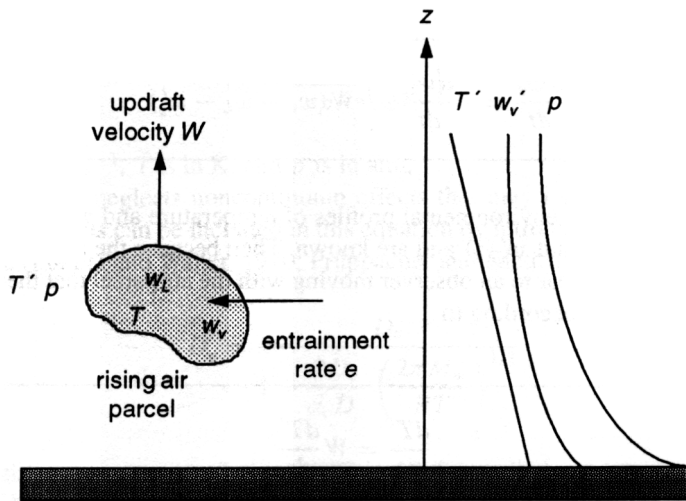


FIGURE 15.12 Schematic description of the cloud formation mathematical framework.

and by employing the definition of the entrainment rate, e ,

$$eW = \frac{1}{m} \frac{dm}{dt} \quad (15.58)$$

Therefore the velocity of the air parcel is described by

$$\frac{dW}{dt} = \frac{2}{3}g \left(\frac{T - T'}{T'} - w_L \right) - \frac{2}{3}eW^2 \quad (15.59)$$

The rate of change of temperature can be calculated using (15.55), noting that $dT/dt = WdT/dz$, and also that w_{vs} should be replaced by w_v to allow the creation of supersaturations. The final result is

$$-\frac{dT}{dt} = \frac{gW}{\hat{c}_p} + \frac{\Delta H_v}{\hat{c}_p} \frac{dw_v}{dt} + e \left[\frac{\Delta H_v}{\hat{c}_p} (w_v - w'_v) + (T - T') \right] W \quad (15.60)$$

The condensed water is related to w_v through the water mass balance for the entraining parcel. If air mass dm enters the parcel from the outside then the water vapor and liquid water mixing ratios will change according to

$$m(w_v + w_L) + w'_v dm = (w_v + dw_v + w_L + dw_L)(m + dm)$$

Neglecting products of differentials and dividing by dt we find that

$$\frac{dw_v}{dt} = -\frac{dw_L}{dt} - eW(w_v + w_L - w'_v) \quad (15.61)$$

Let us assume that the environmental profiles of temperature and water vapor are constant with time at $T'(z)$ and $w'_v(z)$ and are known. Then because the air parcel is moving with speed W , it will appear to an observer moving with the air parcel that the surrounding conditions are changing according to

$$\frac{dT'}{dt} = W \frac{dT'}{dz} \quad (15.62)$$

and

$$\frac{dw'_v}{dt} = W \frac{dw'_v}{dz} \quad (15.63)$$

For a given environment and given entrainment rate e , we need one more equation to close the system, namely, an equation describing the liquid water mixing ratio w_L of the drop population. This liquid water content can be calculated if the droplet size distribution is known, as a simple integral over the distribution. We thus need to derive differential equations for the droplet diameter rate of change dD_p/dt . These equations will link the cloud dynamics discussed here with the cloud microphysics discussed in the following sections.

15.4 GROWTH RATE OF INDIVIDUAL CLOUD DROPLETS

When cloud and fog droplets have diameters significantly larger than $1 \mu\text{m}$, mass transfer of water to a droplet can be expressed by the mass transfer equation for the continuum regime (see Chapter 11)

$$\frac{dm}{dt} = 2\pi D_p D_v (c_{w,\infty} - c_w^{\text{eq}}) \quad (15.64)$$

where m is the droplet mass, D_p its diameter, D_v the water vapor diffusivity, $c_{w,\infty}$ (in mass per volume of air) the concentration of water vapor far from the droplet, and c_w^{eq} (in mass per volume of air) the equilibrium water vapor concentration of the droplet.

The diffusivity of water vapor in air is given as a function of temperature and pressure by

$$D_v = \frac{0.211}{p} \left(\frac{T}{273} \right)^{.94} \quad (15.65)$$

where D_v is in $\text{cm}^2 \text{s}^{-1}$, T is in K, and p is in atm.

Equation (15.64) neglects noncontinuum effects that may influence very small cloud droplets. These effects can be included in this equation by introducing a modified diffusivity D'_v , where (Fukuta and Walter, 1970; Pruppacher and Klett, 1980)

$$D'_v = \frac{D_v}{1 + \frac{2D_v}{\alpha_c D_p} \left(\frac{2\pi M_w}{RT} \right)^{1/2}} \quad (15.66)$$

where α_c is the water accommodation coefficient (often called condensation coefficient). The corrected diffusivity is plotted as a function of droplet diameter in Figure 15.13. The

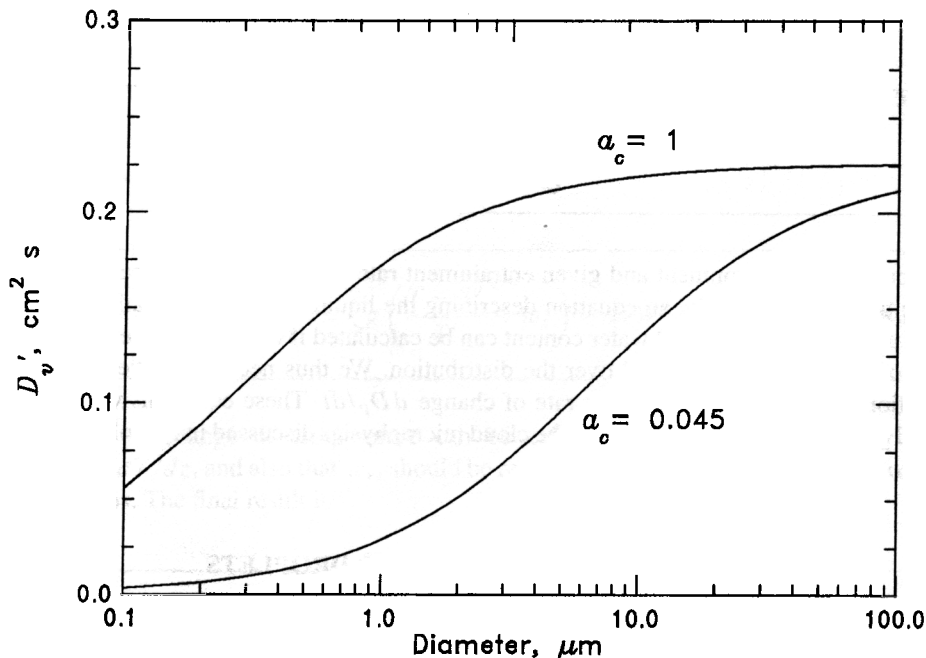


FIGURE 15.13 Water vapor diffusivity corrected for noncontinuum effects and imperfect accommodation as a function of the droplet diameter at $T = 283$ K and $p = 1$ atm.

magnitude of the correction depends strongly on the value of the water accommodation coefficient used. For a value equal to unity, the correction should be less than 25% for particles larger than $1 \mu\text{m}$ and less than 5% for droplet diameters larger than $5 \mu\text{m}$. However, the correction increases significantly if the α_c value is lower than unity. The value of α_c has been the subject of debate. A value of 0.045 was used by Pruppacher and Klett (1980), while ambient measurements seem to suggest a value closer to unity (Leaitch et al., 1986). However, this uncertainty appears to have little effect on the overall predictions of growth models for natural conditions (Pruppacher and Klett, 1980).

The equilibrium vapor concentration in (15.64) corresponds to the concentration at the droplet surface and has been derived in Section 15.2 as a function of temperature. However, during water condensation, heat is released at the droplet surface, and the droplet temperature is expected to be higher than the ambient temperature.

Let us calculate the droplet temperature by deriving an appropriate energy balance. If T_a is the temperature at the drop surface and T_∞ the temperature of the environment, an energy balance gives (see also (11.21))

$$2\pi D_p k'_a (T_\infty - T_a) = -\Delta H_v \left(\frac{dm}{dt} \right) \quad (15.67)$$

where k'_a is the effective thermal conductivity of air corrected for noncontinuum effects. Equation (15.67) simply states that at steady state the heat released during water condensation is equal to the heat released to the droplet surroundings. The temperature at the

droplet surface is then

$$T_s = T_\infty + \frac{\Delta H_v \rho_w}{4k'_a} D_p \frac{dD_p}{dt} = T_\infty (1 + \delta) \quad (15.68)$$

where we have used the mass balance

$$\frac{dm}{dt} = \frac{1}{2} \pi \rho_w D_p^2 \frac{dD_p}{dt} \quad (15.69)$$

and we have defined

$$\delta = \frac{\Delta H_v \rho_w}{4k'_a T_\infty} D_p \frac{dD_p}{dt} \quad (15.70)$$

For atmospheric cloud droplet growth $\delta \ll 1$; however, let us continue the derivation without assuming that $T_a = T_\infty$. Combining (15.64) and (15.69) and using the ideal gas law, we find that

$$D_p \frac{dD_p}{dt} = \frac{4D'_v M_w p^\circ(T_\infty)}{\rho_w RT} \left(S_{v,\infty} \frac{p_w(D_p, T_a)}{p^\circ(T_\infty)} \right) \quad (15.71)$$

where $S_{v,\infty} = p_{w\infty}/p^\circ(T_\infty)$ is the environmental saturation ratio. Recall that for a relative humidity equal to 100% the partial pressure of water in the atmosphere $p_{w\infty}$ is equal to the saturation vapor pressure $p^\circ(T_\infty)$ and $S_{v,\infty}$ is equal to unity. The ratio of the water saturation pressures at T_a and T_∞ is given by the Clausius–Clapeyron equation as

$$\frac{p^\circ(T_a)}{p^\circ(T_\infty)} = \exp \left[\frac{\Delta H_v M_w}{R} \left(\frac{1}{T_\infty} - \frac{1}{T_a} \right) \right] \quad (15.72)$$

Combining (15.68), (15.71), (15.38), and (15.72) we finally get

$$D_p \frac{dD_p}{dt} = \frac{4D'_v M_w p^\circ(T_\infty)}{\rho_w RT_\infty} \left(S_{v,\infty} \frac{\exp \left[\frac{\Delta H_v M_w}{RT_\infty} \delta \right]}{1 + \delta} + \frac{4M_w \sigma_w}{RT \rho_w D_p (1 + \delta)} \left[\frac{6n_s M_w}{\pi \rho_w (D_p^3 - d_u^3)} \right] \right) \quad (15.73)$$

The above result can be simplified since $\delta \ll 1$ and

$$\exp \left[\frac{\Delta H_v M_w \delta}{RT_\infty} \right] \simeq 1 + \frac{\Delta H_v M_w \delta}{RT_\infty}$$

After some algebra the implicit dependence on δ can be resolved to obtain

$$D_p \frac{dD_p}{dt} = \frac{S_{v,\infty} - \exp \left(\frac{4M_w \sigma_w}{RT_\infty \rho_w D_p} - \frac{6n_s M_w}{\pi \rho_w (D_p^3 - d_u^3)} \right)}{\frac{\rho_w RT_\infty}{4p^\circ(T_\infty) D'_v M_w} + \frac{\Delta H_v \rho_w}{4k'_a T_\infty} \left(\frac{\Delta H_v M_w}{T_\infty R} - 1 \right)} \quad (15.74)$$

This equation describes the growth/evaporation rate of an atmospheric droplet. The numerator is the driving force for the mass transfer of water, namely, the difference between the ambient saturation $S_{v,\infty}$ and the equilibrium saturation for the droplet (or equivalently the water vapor saturation at the droplet surface). The equilibrium saturation includes, as we saw in Section 15.2.4, the contributions of the Kelvin effect (first term in the exponential) and the solute effect (second term in the exponential). When the ambient saturation exceeds the equilibrium saturation, the cloud droplets grow and vice versa. The numerator is qualitatively equivalent to the term $c_{w,\infty} - c_w^{eq}$ in (15.64). The first term in the denominator corresponds to the diffusivity of water vapor (compare with (15.64)), while the second accounts for the temperature difference between the droplet and its surroundings. Note that if no heat were released during condensation, $\Delta H_v = 0$, and this term would be zero.

The thermal conductivity of air k_a is given by

$$k_a = 10^{-3}(4.39 + 0.071 T) \tag{15.75}$$

where k_a is in $J m^{-1} s^{-1} K^{-1}$ and T is in K. The modified form for the thermal conductivity k'_a accounting for non-continuum effects is given by

$$k'_a = k_a / \left[1 + \frac{2k_a}{\alpha_T D_p \rho \hat{c}_p} \left(\frac{2\pi M_a}{RT_a} \right)^{1/2} \right] \tag{15.76}$$

where α_T is the thermal accommodation coefficient. The value of α_T is also uncertain and it is often set equal to the value of the mass accommodation coefficient α_c .

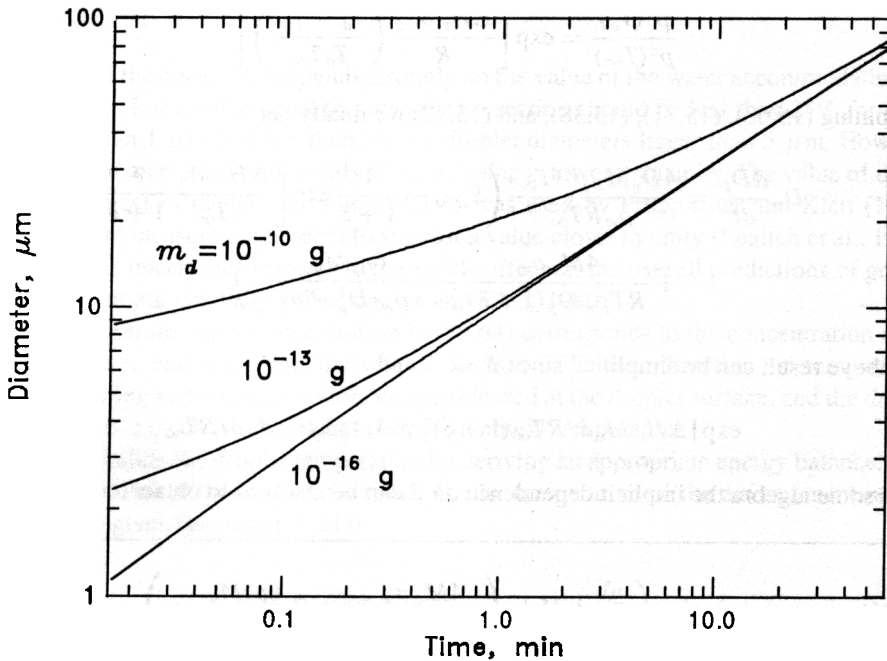


FIGURE 15.14 Diffusional growth of individual drops with different dry masses as a function of time. The drops are initially at equilibrium at 80% RH.

For a cloud droplet larger than 10 μm , using $\alpha_c = \alpha_T = 1$, at 283 K,

$$\frac{\rho_w RT_\infty}{\rho^\circ(T_\infty) D'_v M_w} = 4.85 \times 10^5 \text{ s cm}^{-2}$$

$$\frac{\Delta H_v \rho_w}{k'_v T_\infty} \left(\frac{\Delta H_v M_w}{T_\infty R} - 1 \right) = 6.4 \times 10^5 \text{ s cm}^{-2}$$

and defining $S_{v,\text{eq}}$ as the equilibrium saturation of the droplet, (15.74) can be rewritten as

$$D_p \frac{dD_p}{dt} = 3.5 \times 10^{-6} (S_{v,\infty} - S_{v,\text{eq}})$$

where D_p is in cm and t in s. The growth of an aerosol size distribution under constant supersaturation of 1% is shown in Figure 15.14. The rate of growth of droplets is inversely proportional to their diameters so smaller droplets grow faster than larger ones. As a result, small droplets catch up in size with larger ones during the growth stage of the cloud.

15.5 GROWTH OF A DROPLET POPULATION

The growth of an aerosol population to cloud droplets can be investigated using the growth equation derived in the previous section. In general, one would need to integrate simultaneously the differential equations derived in Section 15.3.4 for the air parcel updraft velocity, temperature, water vapor mixing ratio, and environmental temperature and water vapor mixing ratio, coupled with a set of droplet growth equations, one for each droplet size class. The liquid water mixing ratio of the population consisting of N_i droplets per volume of air of diameters D_{pi} will then be

$$w_L = \frac{\rho_w \pi}{\rho_a 6} \sum_{i=1}^n N_i D_{pi}^3 \quad (15.77)$$

where we have assumed that there are n groups of droplets.

It is instructive, before examining the interactions between cloud dynamics and microphysics, to focus our attention on the microphysics. Figure 15.15 presents the results of the integration of these equations for a polluted urban aerosol population (Pandis et al., 1990a) for an aerosol distribution consisting of seven size sections. At time zero the relative humidity is assumed to be 100%. At this time the particles have grown several times from their dry size as a result of water absorption and are assumed to be in equilibrium with the surrounding environment. The temperature of the air parcel is assumed to decrease with a constant rate of 2 K h⁻¹. As the temperature decreases, the saturation of the air parcel increases. The particles absorb water vapor, but the cooling rate is too rapid compared to mass transfer and the air parcel becomes supersaturated. After a few minutes the particles start becoming activated. The larger particles become activated first (Section 15.2) and the smaller soon follow. As particles become activated, they are able to grow much faster. Note that based on the Köhler curves as a particle grows the driving force for growth

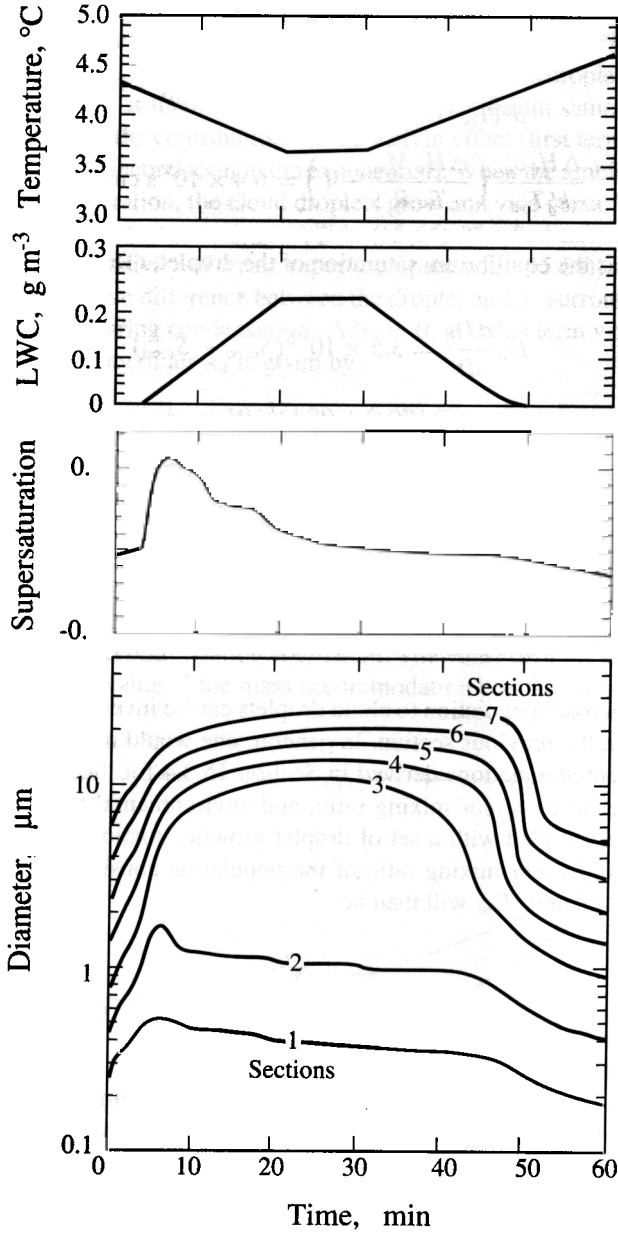


FIGURE 15.15 Simulated evolution of temperature, liquid water content, supersaturation, and particle diameters during the lifetime of a cloud (Pandis et al., 1990). The sections denote 7 sizes of initial particles.

$(c_{w,\infty} - c_w^{\text{eq}})$ becomes larger for almost constant $c_{w,\infty}$, because c_w^{eq} decreases rapidly with size. Therefore, as more and more particles get activated, the rate of transport of water from the vapor to the particulate phase increases, while the rate of supersaturation increase due to the cooling remains approximately constant. The result is that the supersaturation increase slows down and after 6 min reaches a maximum value of 0.1%.

Let us describe the above situation quantitatively, by deriving the equation for the rate of change of the supersaturation s_v . The water vapor mixing ratio w_v is related to the water vapor partial pressure p_w by (15.46), while by definition

$$+ s_v = \frac{p_w}{p^\circ}$$

Therefore combining these two relationships one gets

$$s_v = \frac{M_a p_a}{M_w p^\circ} w_v \quad (15.78)$$

Differentiating this expression with respect to time and rearranging the terms we obtain

$$\frac{ds_v}{dt} = \frac{M_a p_a}{M_w p^\circ} \frac{dw_v}{dt} - (1 + s_v) \left(\frac{1}{p^\circ} \frac{dp^\circ}{dt} - \frac{1}{p_a} \frac{dp_a}{dt} \right) \quad (15.79)$$

The change of the air pressure with time can be calculated assuming that the environment is in hydrostatic equilibrium so that

$$\frac{dp_a}{dt} = - \frac{g p_a M_a}{RT} W$$

where we have assumed that $T' \simeq T$. The change of the parcel saturation pressure with time can be calculated using the chain rule and the Clausius–Clapeyron equation,

$$\frac{dp^\circ}{dt} = \frac{dp^\circ}{dT} \frac{dT}{dt} = \frac{\Delta H_v M_w p^\circ}{RT^2} \frac{dT}{dt} \quad (15.81)$$

Substituting (15.80) and (15.81) into (15.79) one gets

$$\frac{ds_v}{dt} = \frac{M_a p_a}{M_w p^\circ} \frac{dw_v}{dt} - (1 + s_v) \left(\frac{\Delta H_v M_w}{RT^2} \frac{dT}{dt} + \frac{g M_a}{RT} W \right)$$

If we assume that there is no entrainment ($e = 0$) and substitute (15.60) and (15.61) into (15.82), we obtain

$$\frac{ds_v}{dt} = \left(\frac{\Delta H_v M_w g}{\hat{c}_p RT^2} - \frac{g M_a}{RT} \right) W - \left(\frac{p_a M_a}{p^\circ M_w} + \frac{\Delta H_v^2 M_w}{\hat{c}_p RT^2} \right) \frac{dw_L}{dt} \quad (15.83)$$

where we have assumed that $1 + s_v \simeq 1$, as $s_v \simeq 0.01$ in clouds. The above equation reveals that in the absence of condensation, the saturation varies linearly with the updraft velocity and is decreased by water condensation. One could replace in the above equation the updraft velocity with the cooling rate

$$W \simeq \frac{\hat{c}_p}{g} \left(\frac{dT}{dt} \right) \quad (15.84)$$

where we have assumed that the updraft velocity is almost constant, and therefore the air parcel cooling rate is also constant. Equation (15.83) is the mathematical representation of our previous qualitative theoretical arguments. It suggests that the supersaturation inside the cloud is the result of a balance between the cooling rate and the liquid water increase. The latter is limited by the mass transport to particles, which in turn depends on the particle size distribution and on their state of activation.

The maximum supersaturation reached inside a cloud/fog is an important parameter. Particles with critical supersaturations lower than this value will become activated and become cloud droplets. The rest remain close to equilibrium but never grow enough to be considered droplets and are called *interstitial aerosol*. The aerosol population inside a cloud is therefore separated into two groups, interstitial aerosols that contain significant amounts of water but are not activated (their sizes are usually smaller than $2 \mu\text{m}$) and cloud droplets, with size increases corresponding to mass changes of three orders of magnitude.

In our example, the maximum supersaturation of 0.1% was sufficient to activate aerosols with dry diameters larger than approximately $0.3 \mu\text{m}$, corresponding to size sections 3 to 7 in Figure 15.15. Note in Figure 15.15 that particles in section 1 (dry size $0.1 \mu\text{m}$) grow up to $0.5 \mu\text{m}$ for the maximum saturation and then evaporate slowly, following the relative humidity. These particles remain in equilibrium throughout the cloud lifetime. Particles in the second size section (dry diameter $0.2 \mu\text{m}$) exhibit a more interesting behavior. Their critical supersaturation is slightly lower than the maximum supersaturation, so they activate growing to a size of $1.5 \mu\text{m}$. However, as the supersaturation decreases, they deactivate after a few minutes and do not have the time to grow more in size. The rest of the particles (dry sizes larger than $0.3 \mu\text{m}$) all get activated and grow to droplets larger than $10 \mu\text{m}$ in size.

Direct measurements of ambient supersaturations in clouds have been extremely challenging. Not only does one try to measure a small deviation from saturation, but clouds are frequently patchy with supersaturated regions next to subsaturated ones corresponding to "dry" entrained masses. Previous measurements have indicated that ambient supersaturations are usually less than 1% and almost never exceed 2% (Warner, 1968). A median value of 0.1% was reported in these measurements. Most of our knowledge of these supersaturations is based on theoretical calculations using measurements of atmospheric conditions and are rather similar to that presented here as an example. Ranges of supersaturations expected in various cloud types are given in Table 15.3.

Note that supersaturations depend both on the macroscale cloud dynamics represented by the cloud updraft velocities (larger updrafts result in higher supersaturations) and on the microphysics (the details of the aerosol size distribution). Cleaner environments, with lower aerosol concentrations, usually result in higher supersaturations.

TABLE 15.3 Updraft Velocities and Maximum Supersaturations for Clouds and Fogs

Cloud Type	Updraft Velocity (m s ⁻¹)	Maximum Supersaturation (%)	Reference
		0.25–0.7	Pruppacher and Klett (1980)
		0.3–0.8	Pruppacher and Klett (1980)
			Mason (1971)
Stratiform	~ 0–	~0.05	Pruppacher and Klett (1980)
Fog	—	~0.1	Pandis and Seinfeld (1989)

15.6 CLOUD CONDENSATION NUCLEI

Supersaturations of several hundred percent are necessary for the formation of water droplets in particle free air (see Chapter 10). The need for such high supersaturations indicates the necessity of particles for cloud formation in the ambient atmosphere. The ability of a given particle to serve as a nucleus for water droplet formation, as we have seen in the previous sections, will depend on its size, chemical composition, and the local supersaturation.

Particles that can activate at a given supersaturation are defined as *cloud condensation nuclei* (CCN) for this supersaturation. In the cloud physics literature one often defines as *condensation nuclei* (CN) those particles that form droplets at supersaturations of $\geq 400\%$ and therefore CN include all the available particles. One can therefore assume that the CN concentration is equal to the total aerosol number concentration. This CN definition should be contrasted with the CCN definition where supersaturations often well less than 2% are used. Therefore CCN represent the particles that can form cloud droplets under reasonable atmospheric supersaturations. We caution the reader that CCN concentrations always refer to a specific supersaturation, for example, CCN(1%) or CCN(0.5%) and one should be careful when comparing CCN concentrations measured or estimated at different supersaturations.

The CCN concentration of a given supersaturation corresponds under ideal cloud formation conditions (e.g., spatial uniformity) to the number concentrations of droplets if the cloud had the same supersaturation. We will use the symbol CCN(s) for CCN at $s\%$ supersaturation.

For a given aerosol population CCN(s) depends on both the size and composition of the particles. In the simple case of an aerosol population that has uniform size-independent composition, by definition,

$$\text{CCN}(s) = \int_{D_s}^{\infty} n(D_p) dD_p \quad (15.85)$$

where $n(D_p)$ is the number distribution of the aerosol population, and D_s the activation diameter for $s\%$ supersaturation of these particles. Note that $\text{CN} = \text{CCN}(\infty)$ according to the above notation. Therefore, if all particles had the same composition, one needs to know only the activation diameter and the size distribution of these particles to estimate the cor-

responding CCN concentration (Figure 15.16a). However, for aerosol populations where chemical composition is size dependent, CCN concentration is a more complicated function,

$$\text{CCN}(s) = \int_0^{\infty} f_s(D_p)n(D_p) dD_p \quad (15.86)$$

where $f_s(D_p)$ is the fraction of the aerosol particles of diameter D_p that are activated at supersaturation $s\%$ (Figure 15.16b). Note that if the aerosol particles are internally mixed (all particles of the same diameter have the same chemical composition), $f_s(D_p)$ will be either zero or one. (We will return to the concept of internally mixed particles in Chapter 22.)

Because of the difficulties associated with measurement of the aerosol size composition distribution, and then calculating from that their CCN properties, a series of empirical parametrizations have been developed based on atmospheric measurements. One of the most popular relates CCN(s) concentration to atmospheric supersaturation s (percent) with a power law,

$$\text{CCN}(s) = cs^k \quad (15.87)$$

where CCN(s) is in particles cm^{-3} and s is the supersaturation expressed as a percentage (Twomey, 1959). The constant c corresponds to the CCN(1%), the particles active at 1% supersaturation. It should be noted that knowledge of the parameters c and k is often sufficient for many cloud microphysics applications. Information about the size/composition of the aerosol population is embedded in the empirical parameters c and k . Twomey (1959) suggested average values of $c = 310$ and $k = \frac{1}{3}$ for marine air and $c = 600$ and $k = \frac{2}{5}$ for continental air. Twomey and Wojcieckowski (1969) reported measurements indicating

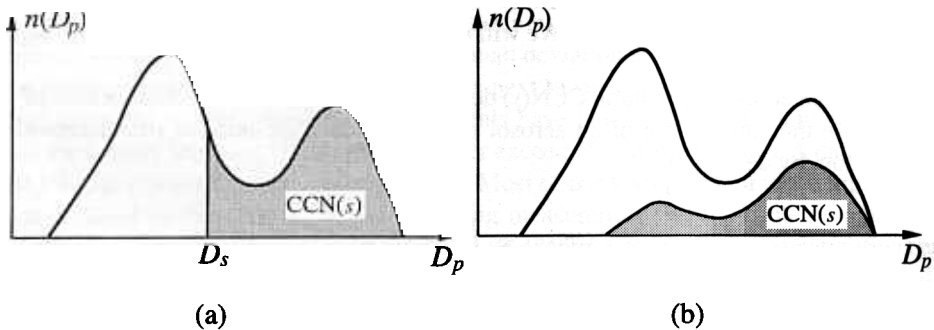


FIGURE 15.16 Schematic of an aerosol size distribution with the shaded area indicating the CCN for (a) uniform chemical composition and (b) a typical multicomponent aerosol population that is neither externally nor internally mixed and has a size-dependent composition.

$c = 600$ and $k = \frac{1}{2}$ for continental air. Hegg and Hobbs (1992) reviewed more recent measurements of marine CCN and suggested values of $c = 200$ and $k = \frac{1}{2}$. Other values for c and k based on ambient measurements are given in Table 15.4.

As expected, because of the variability of the aerosol size/composition both spatially and with time, the parameters c and k vary significantly, making the use of such empirical relationships rather questionable. Generally, CCN(1%) concentrations in maritime and modified maritime airmasses are around 100 cm^{-3} , while concentrations in excess of 1000 cm^{-3} are found in air that has been over land for several days.

The fraction of aerosol particles that are CCN(1%) is also quite variable. Over the oceans this fraction is roughly 0.5 (Hegg and Hobbs, 1992), but it does vary from 0.2 to 0.6. For polluted conditions the fraction is much lower, usually less than 1%. This is mainly due to the existence of thousands of ultrafine particles (less than 50 nm) that cannot get activated at this supersaturation regardless of their chemical composition.

Since ambient supersaturations rarely exceed 1%, the above CCN measurements indicate that cloud droplet concentrations should range from 200 to 1000 cm^{-3} over continents and from 10 to 200 cm^{-3} over oceans. These values agree well with the drop concentrations found in continental and maritime clouds.

The link between aerosol chemical composition and CCN behavior is still not completely understood. Whereas behavior of soluble inorganic aerosols is relatively well established, much less is known about the ability of organic aerosols (alone or mixed with inorganic components) to serve as CCN.

A series of studies have reported the activation efficiency of particles generated during fuel combustion. These results were summarized by Lammel and Novakov (1995) and are

TABLE 15.4 Empirical Parameters for the CCN Concentration Dependence on the Supersaturation s

$c(\text{cm}^{-3})$	k	Location
	0.3	Maritime (Australia)
	0.5–0.6	Maui (Hawaii)
	0.5	Atlantic, Pacific Oceans
	0.8	Pacific
	1.3–1.4	North Atlantic
	0.4–0.9	North Atlantic
	—	Arctic
	0.4	Cape Grim (Australia)
	0.5	North Atlantic
	0.4–0.6	North Pacific
	1.0	North Pacific
	0.3	Polluted North Pacific
	0.4	Equatorial Pacific
	0.5	Continental
	0.4	Continental (Australia)
	0.9	Continental (Buffalo, NY)

Source: Hegg and Hobbs (1992).

TABLE 15.5 Activated Fraction of Aerosol Particles at 1% Supersaturation and Their Content of Soluble Ions

fuel	Combustion Type	Fraction Activated	Soluble Ions (meq g ⁻¹)	
Low sulfur crude oil	Ignition, flaming	0.20	1.25	Rogers et al. (1991)
Wood smoke	Smoldering	0.24	1.3–3.8	Hallet et al. (1989)
Diesel	Diffusion flame	0.42	0.1	Lammel and Novakov (1995)
Acetylene gas	Welding torch	0.51	3.1	Hallet et al. (1989)
High sulfur crude oil	Ignition, flaming	0.58	1.2	Rogers et al. (1991)
Diesel	Engine motor, idling	0.8 ^a	1.0	Lammel and Novakov (1995)
Forest and brush fire	Flaming	0.8–1.0	1.3–3.8	Hallet et al. (1989), Roberts et al. (1991)

^aAt 0.8% supersaturation.

given in Table 15.5. These authors suggested that availability of soluble components is the major, but not the only, factor determining the activation of combustion particles. Cruz and Pandis (1997) showed that pure secondary organic aerosol can form CCN, and that its activation behavior can be described by the Köhler theory. The above studies demonstrate that one should not neglect the importance of particles containing a large organic fraction as CCN. For example, Hudson and Clark (1992) reported that roughly 70% of the particles ($D_p > 0.024 \mu\text{m}$) in the Kuwait oil fire plume were active CCN at 1% supersaturation. The majority of these particles were active even at supersaturations below 0.2%. The Kuwait oil fires contained high concentrations of salt (oil field brines) and sulfate and soot, no doubt facilitating activation of their smoke. Other studies (Rogers et al., 1991) have reported much lower levels of CCN activity for oil smoke. Forest fires produce many active CCN (Eagan et al., 1974; Hallett et al., 1989).

15.7 CLOUD PROCESSING OF AEROSOLS

During the processing of an air parcel by a nonraining cloud the aerosol size–composition distribution is transformed by a variety of processes. First, a fraction of the aerosol distribution is activated and becomes cloud droplets while the rest remains as interstitial particles. This process, often described as *nucleation scavenging* of aerosols, determines the initial composition of the cloud droplets. If this were the only process taking place, after cloud evaporation the aerosol distribution would return to its original form. However, a series of additional processes can modify the distribution, including chemical reaction in the aqueous phase, collisions between interstitial aerosols and cloud drops, and coalescence among cloud drops.

If the cloud is raining, there are additional interactions between the raindrops and the aerosols both in and around clouds, leading to removal of material from the atmosphere.

Finally, there are other processes that can occur around clouds that may lead to the formation of new particles.

15.7.1 Nucleation Scavenging of Aerosols by Clouds

Nucleation scavenging of aerosols in clouds refers to activation and subsequent growth of a fraction of the aerosol population to cloud droplets. This process is described by (15.74) and has been discussed in Section 15.5.

If $C_{i,0}$ is the concentration (in mass per volume of air) of an aerosol species in clear air before cloud formation (e.g., at the cloud base), and $C_{i,\text{cloud}}$ and $C_{i,\text{int}}$ are its concentrations again in mass per volume of air in the aqueous phase and in the interstitial aerosol, respectively, one can define the cloud *mass scavenging ratio* for species i , F_i , as

$$F_i = \frac{C_{i,0} - C_{i,\text{int}}}{C_{i,0}} \quad (15.88)$$

Note that if there is no production or removal of i in the cloud then $C_{i,0} = C_{i,\text{int}} + C_{i,\text{cloud}}$. The mass scavenging ratio defined above may vary from zero to unity. The number scavenging ratio F_N can be defined as

$$F_N = \frac{N_0 - N_{\text{int}}}{N_0} \quad (15.89)$$

where N_0 is the aerosol number concentration before cloud formation and N_{int} is the number concentration of interstitial aerosol.

Theoretically, as particles larger than $0.5 \mu\text{m}$ or so become cloud droplets in a typical cloud and these particles represent most of the aerosol mass, one would expect mass activation efficiencies close to unity. Junge (1963) predicted sulfate scavenging ratios from nucleation scavenging alone to range from 0.5 to 1.0. Since then all theoretical studies have predicted high mass nucleation scavenging efficiencies for all aerosol species. For example, Flossmann et al. (1985, 1987) reported calculated aerosol scavenging efficiencies exceeding 0.9 in typical cloud environments. Pandis et al. (1990a) estimated scavenging efficiencies of 0.7 for sulfate and 0.8 for nitrate and ammonia in polluted clouds. In other numerical studies, Flossmann (1991) reported mass scavenging efficiencies of 0.9 or higher for warm clouds over the Atlantic.

These theoretical estimates are in good agreement with the high mass scavenging efficiencies measured in the atmosphere. Ten Brink et al. (1987) observed nearly complete scavenging of aerosol sulfate in clouds. The data of Daum et al. (1984) also showed that the bulk of the sulfate mass is incorporated into cloud droplets. Hegg and Hobbs (1988) reported scavenging ratios for sulfate of 0.5 ± 0.2 .

On the contrary, low number scavenging efficiencies are expected in clouds influenced by anthropogenic sources because of the prevalence of fine aerosol particles; number scavenging efficiencies of a few percent or less are expected in most such situations. Only in clouds in the remote marine atmosphere does the total number scavenging efficiency exceed 0.1.

15.7.2 Chemical Composition of Cloud Droplets

During the droplet growth stage of a cloud, droplets of different sizes dilute at different rates, in particular, smaller droplets grow faster and therefore dilute faster than the larger ones. This can be shown by the following argument (Noone et al., 1988). Assume that the aerosol population consists of i particle groups of dry diameters $D_{s,i}$. These particles grow and become aqueous droplets of diameters D_i . Assuming for simplicity that the density of the dry particles is 1 g cm^{-3} , the solute mass fraction of droplets in section i is $X_i = (D_{s,i}/D_i)^3$. Defining the dilution rate DR_i of section i as the normalized rate of change of the solute mass fraction in the droplet,

$$DR_i = - \frac{1}{X_i} \frac{dX_i}{dt} \quad (15.90)$$

and assuming that the mass of scavenged aerosol in droplets of group i remains constant with time (i.e., neglecting processes like scavenging of gases, coagulation, etc.), then for two aerosol groups with $D_1 < D_2$

$$\frac{DR_1}{DR_2} = \frac{D_2}{D_1} \frac{dD_1/dt}{dD_2/dt} \quad (15.91)$$

For sufficiently large droplets the growth rate is approximately proportional to the inverse of the droplet diameter (see (15.74)) and

$$\frac{dD_i}{dt} \simeq \frac{K}{D_i} \quad (15.92)$$

where K is a constant that is only a very weak function of D_i . Then combining (15.91) and (15.92) one finds that

$$\frac{DR_1}{DR_2} \simeq \left(\frac{D_2}{D_1} \right)^2 > \quad (15.93)$$

and the smaller droplets, D_1 , are diluted at a faster rate than the larger D_2 ones if growth by water diffusion is the dominant process occurring.

The above argument suggests that, with time, the total solute concentrations of droplets for an aerosol population would tend to increase with particle size. These arguments are supported by calculations like those by Pandis et al. (1990a) shown in Figure 15.17. Note that initially, before cloud creation, solute concentration is high across the size spectrum and larger particles have slightly lower concentrations as they contain hydrophilic components such as NaCl. As aerosols become activated, their solute concentrations decrease. For a mature cloud solute concentration shows a minimum at around $10 \mu\text{m}$. This minimum is a result of existence of nonactivated particles for which solute concentration decreases with increasing size, and droplets for which the solute concentration increases with increasing size. Note that for a mature cloud droplets of diameter around $10 \mu\text{m}$ have a solute concentration of roughly 100 mg L^{-1} , whereas drops of diameter $24 \mu\text{m}$ have a solute con-

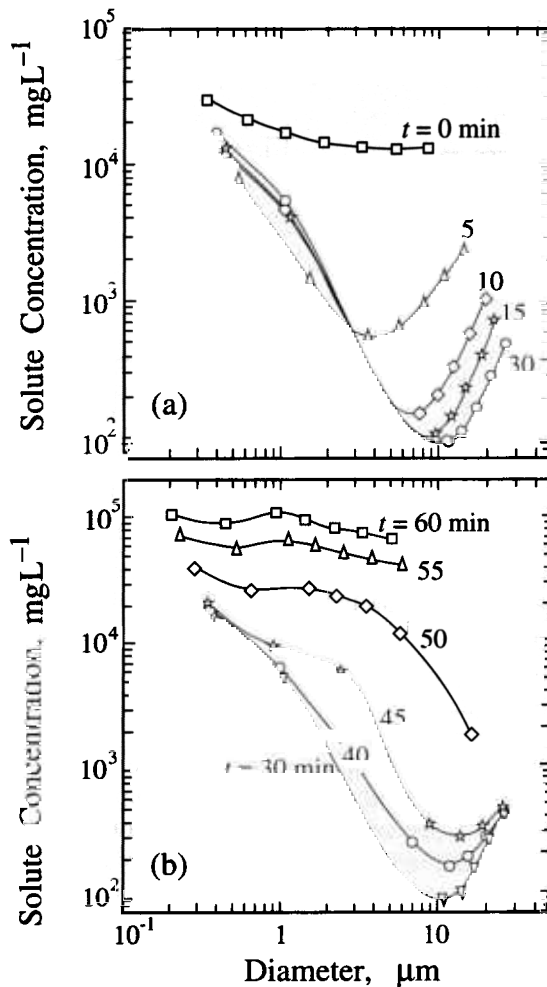


FIGURE 15.17 Predicted dependence of the total solute concentration on droplet diameter during the lifetime of a cloud (Pandis et al., 1990a).

centration that is 3.4 times higher. During the evaporation stage of a cloud, smaller droplets get deactivated and evaporate first (Figure 15.17b). Therefore the minimum gradually disappears and the system returns close to its original state.

The above predictions agree with measured concentration/size dependencies measured in clouds that are not heavily influenced by anthropogenic sources. Noone et al. (1988) sampled droplets from a marine stratus cloud and calculated that the volumetric mean solute concentration of the 9 to 18 μm droplets was a factor of 2.7 smaller than in the 18 to 23 μm droplets. Ogren et al. (1989) reported similar results for a cloud in Sweden. On the other hand, similar measurements for cloud and fog droplets in heavily polluted environments suggest that solute concentrations decrease with increasing droplet size (Munger et al., 1989; Ogren et al., 1992). No satisfactory explanation exists for such behavior.

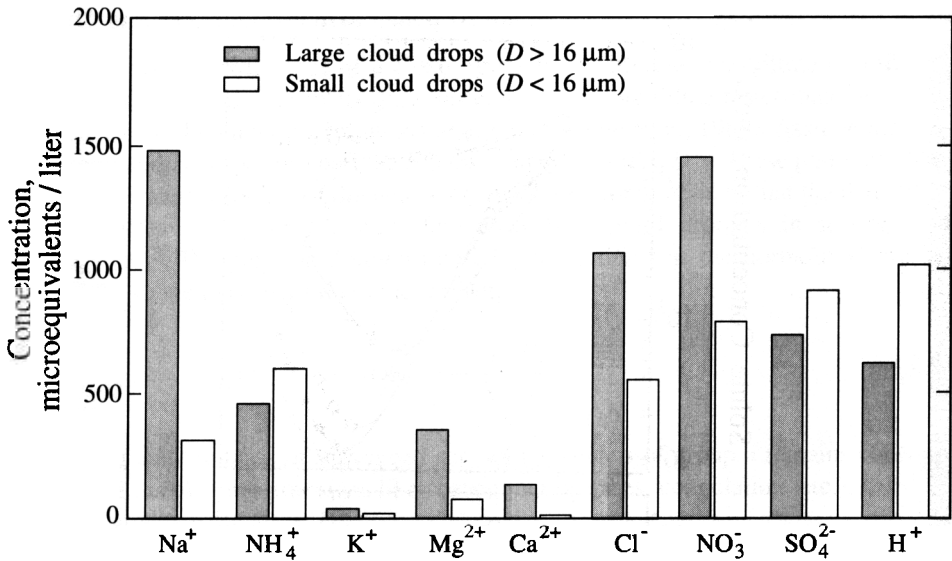


FIGURE 15.18 Measured composition of the small and large cloud droplets collected in coastal stratus clouds at La Jolla Peak, California, in July 1993 (Collett et al., 1994).

The above discussion concerns total solute concentration. For individual species, because their aerosol concentrations are also generally size dependent, there is an additional reason for size-dependent droplet concentrations. Concentrations of some major aerosol species measured in small and large droplets in a cloud are shown in Figure 15.18. The droplet population in these measurements was separated into only two samples with significant overlap and therefore the concentration deviations shown probably underestimate the actual differences.

The above differences in solute concentrations are accompanied by differences in acidity among droplets of different sizes. Figure 15.19 summarizes measurements of Collett et al. (1994) in a variety of environments. Significant pH differences are observed. Once more, because of significant mixing among droplets of different sizes during sampling, the actual differences are probably even higher than those depicted in Figure 15.19.

Measurements of bulk cloudwater concentrations have been presented by a number of investigators. These concentrations vary significantly because of both the aerosol loading (degree of anthropogenic influence) and the liquid water content of the cloud.

15.7.3 Nonraining Cloud Effects on Aerosol Concentrations

Significant production of sulfate has been detected and/or predicted in clouds and fogs in different environments (Hegg and Hobbs, 1987, 1988; Pandis and Seinfeld, 1989; Husain et al., 1991; Pandis et al., 1992; Swozdiak and Swozdiak, 1992; Develk, 1994; Liu et al., 1994). Detection of sulfate-producing reactions is often hindered by variability of cloud liquid water content and temporal instability and spatial variability in concentrations of reagents and product species (Kelly et al., 1989).

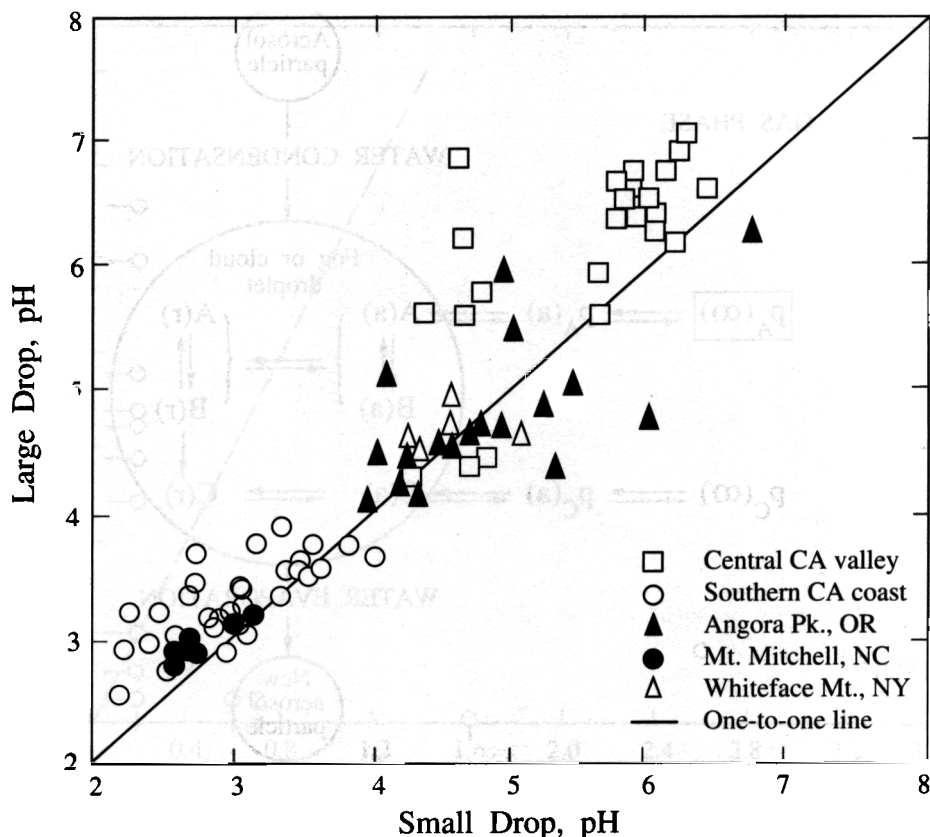


FIGURE 15.19 Measured pH of small and large droplets in a series of clouds and fogs in typical environments (Collett et al., 1994).

During cloud formation, aerosols that serve as cloud condensation nuclei (CCN) become activated and grow freely by vapor diffusion. Soluble gases such as nitric acid, ammonia, and sulfur dioxide dissolve into the droplets. The cloudwater serves as the reacting medium for a series of aqueous-phase reactions, most importantly the transformation of dissolved SO_2 , S(IV) , to sulfate, S(VI) . The sulfate formed is not volatile and remains in the particulate phase. Other reactions, for example, the oxidation of formaldehyde to formic acid, result in volatile products that return to the gas phase (Figure 15.20). During the cloud evaporation stage, several species that were dissolved in the cloudwater evaporate. Others, like sulfate, remain in the aerosol phase. Ammonia often accompanies the sulfate formed as the neutralizing cation. Species like nitrate or chloride that may have existed in the original particle can be displaced by the sulfate produced and forced to return to the gas phase. The result of these aqueous-phase processes is usually an overall increase in particle mass and size. Chemical composition of the particles may also change, with sulfate and ammonium concentrations generally increasing and nitrate and chloride decreasing (Pandis et al., 1990b).

Available evidence suggests that the single most important reaction during aerosol processing by clouds is the oxidation of HSO_3^- by H_2O_2 . This reaction, as we saw in Chapter

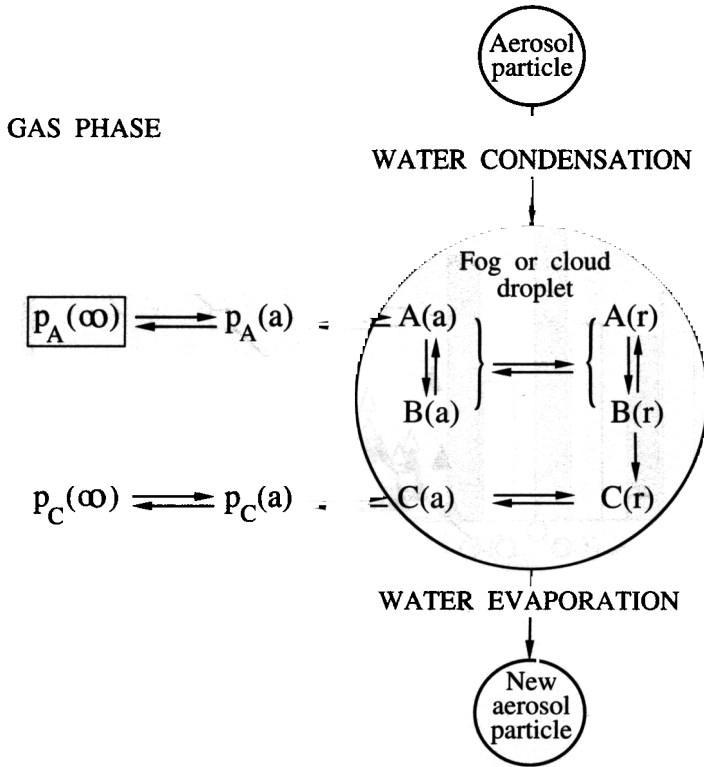


FIGURE 15.20 Schematic of the cloud processing of an aerosol particle.

6, is particularly fast with rates often exceeding $100\% \text{ SO}_2 \text{ h}^{-1}$. Daum et al. (1984) showed that SO_2 and H_2O_2 did not coexist in interstitial cloud air (Figure 15.21). If H_2O_2 was high then interstitial SO_2 was low and vice versa, a pattern consistent with the rapid and quantitative reaction of SO_2 with peroxide in which either SO_2 or peroxide acts as limiting reagent. Hydrogen peroxide has been reported to dominate aqueous sulfate formation in the northeastern United States. Measured H_2O_2 gas-phase mixing ratios over the northeastern and central United States vary from 0.2 to 6.7 ppb (Sakugawa et al., 1990) with the highest values during the summer and the lowest during the winter months. Availability of hydrogen peroxide is often limiting to sulfate formation in clouds, a limitation more pronounced near SO_2 sources and during winter months. The seasonal contribution of clouds to sulfate levels depends on both availability of oxidants and on cloud cover. In cases where sulfate production is oxidant limited, changes in aerosol sulfate levels will be less than proportional to SO_2 emission changes, with the relationship being more nonlinear in winter than in spring or summer (U.S. NAPAP, 1991).

Cloud processing is a major source of sulfate and aerosol mass in general on regional and global scales. Walcek et al. (1990) calculated that, during passage of a midlatitude storm system, over 65% of tropospheric sulfate over the northeastern United States was formed in cloud droplets via aqueous-phase reactions. The same authors estimated that,

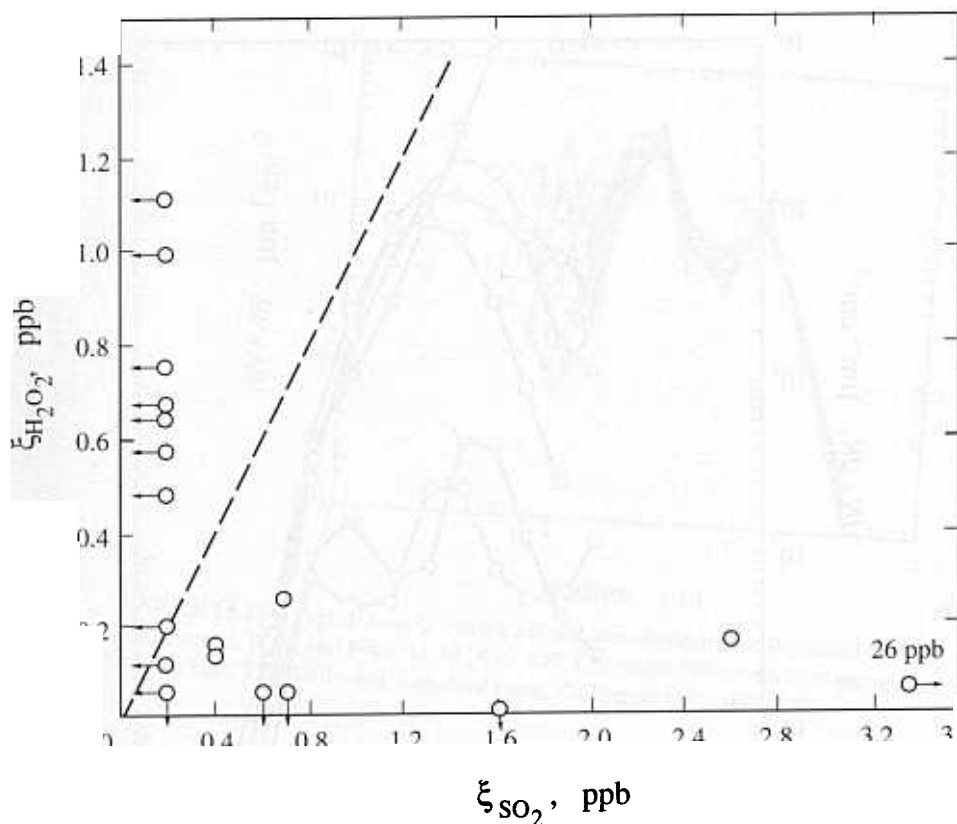


FIGURE 15.21 Measurements of the gas-phase partial pressures of H_2O_2 versus the SO_2 partial pressure for interstitial cloud air (Daum et al., 1984). Arrows signify that the mixing ratio was below the detection limit.

during a 3 day springtime period, chemical reactions in clouds occupying 1 to 2% of the tropospheric volume were responsible for sulfate production comparable to the gas-phase reactions throughout the entire tropospheric volume under consideration. McHenry and Dennis (1994) proposed that annually more than 60% of the ambient sulfate in central and eastern United States is produced in mostly nonprecipitating clouds. Similar conclusions were reached by Dennis et al. (1993) and Karamachandani and Venkatram (1992). Aqueous-phase SO_2 oxidation in clouds is predicted to be the most important pathway for the conversion of SO_2 to sulfate on a global scale (Hegg, 1985; Langner and Rodhe, 1991).

Effect of cloud processing of aerosols in the remote marine atmosphere has been demonstrated in a series of field studies (Hoppel et al., 1986; Frick and Hoppel, 1993). Figure 15.22 shows the formation of a second peak in the accumulation mode as an air-mass is advected off North America to the Atlantic and the Pacific Oceans. Note that the two modes observed in the number distribution should not be confused with modes of the mass distribution. Hoppel et al. (1986) proposed that cloud processing of aerosol is an efficient mechanism for accumulating mass in the 0.08 to $0.5 \mu\text{m}$ size range in the marine

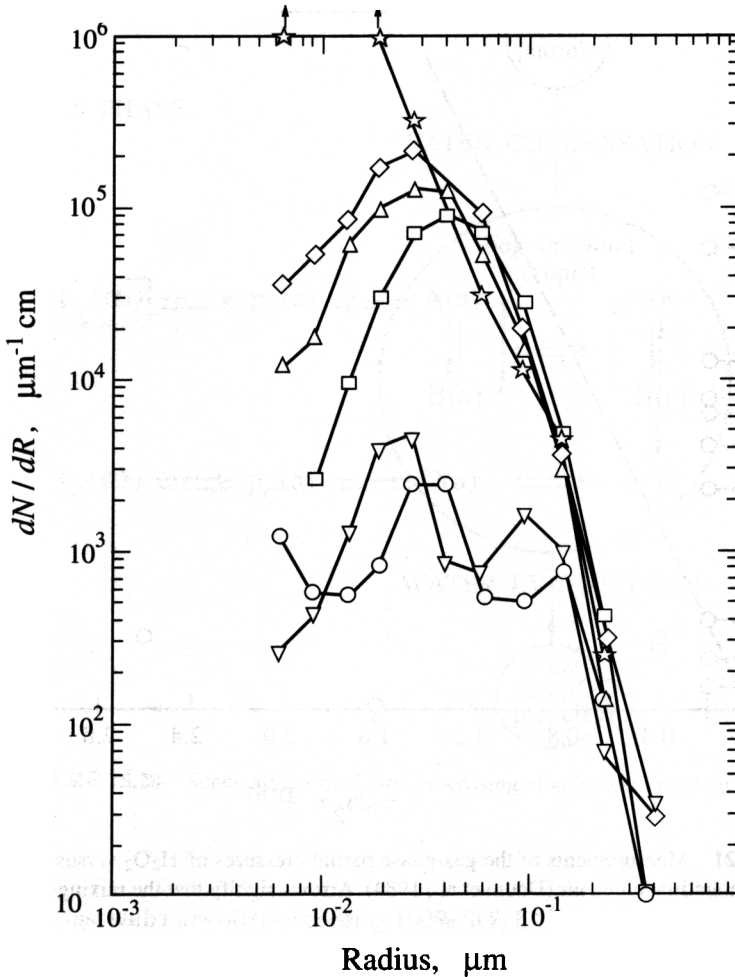


FIGURE 15.22 Size distribution measurements of remote marine aerosol indicating the formation of an additional peak as the air mass is advected off North America. Reprinted from *Atmos. Environ.*, **24A**, Hoppel, W. A. and Frick, G. M., 645–649, Copyright 1990, with kind permission from Elsevier Science Ltd., The Boulevard, Langford Lane, Kidlington OX5 1GB, UK.

atmosphere. The gap observed in most remote marine aerosol number distributions (Figure 15.23) is, as a result, often referred to as the “Hoppel gap.” These effects on the aerosol number distribution are expected to be important only in the remote atmosphere, where the number of CCN is a significant fraction of the total aerosol number. However, significant effects on the aerosol mass distribution are expected under all circumstances.

Measurements of the urban aerosol mass distribution have shown that two distinct modes often exist in the 0.1 to 1.0 μm diameter range (Hering and Friedlander, 1982; McMurry and Wilson, 1983; Wall et al., 1988; John et al., 1990). These are referred to as the condensation mode (approximate aerodynamic diameter 0.2 μm) and the droplet mode

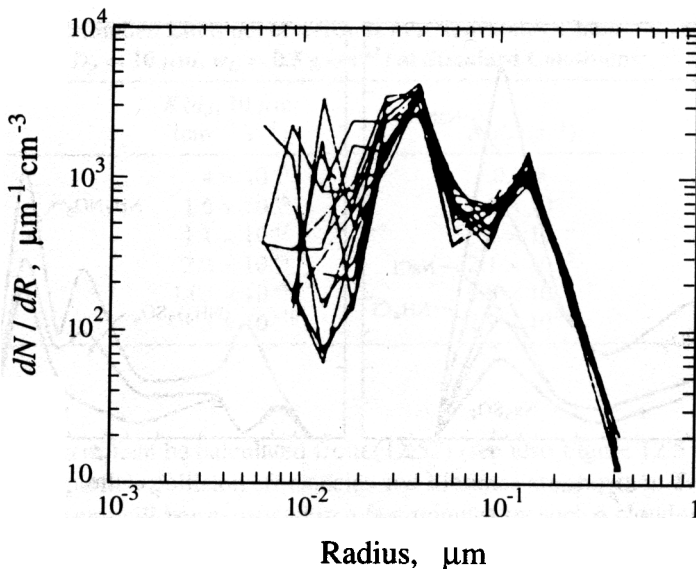


FIGURE 15.23 Typical remote marine aerosol size distributions. Reprinted from *Atmos. Environ.*, **24A**, Hoppel, W. A. and Frick, G. M., 645–649, Copyright 1990, with kind permission from Elsevier Science Ltd., The Boulevard, Langford Lane, Kidlington OX5 1GB, UK.

(aerodynamic diameter around $0.7 \mu\text{m}$). These two submicrometer mass distribution modes have also been observed in nonurban continental locations (McMurry and Wilson, 1983; Hobbs et al., 1985; Radke et al., 1989). Hering and Friedlander (1982) and John et al. (1990) proposed that the larger mode could be the result of aqueous-phase chemical reactions. Meng and Seinfeld (1994) showed that growth of condensation mode particles by accretion of water vapor or by gas-phase or aerosol-phase sulfate production cannot explain existence of the droplet mode. Activation of condensation mode particles, formation of cloud/fog drops, followed by aqueous-phase chemistry, and droplet evaporation were shown to be a plausible mechanism for formation of the aerosol droplet mode.

Simulations of the aerosol–cloud–aerosol cycle have shown that sulfate formed during cloud/fog processing of an air mass favors aerosol particles that have access to most of the cloud liquid water content, which are those with diameters in the 0.5 to $1.0 \mu\text{m}$ range (Pandis et al., 1990a). Figure 15.24 depicts simulation of fog processing of an urban aerosol population. Note that the shape of the aerosol distribution changes with the creation of an extra mode, resulting mainly from the formation of $(\text{NH}_4)_2\text{SO}_4$. Note also that there are significant changes in the aerosol chemical composition before and after the fog with sulfates replacing nitrate and chloride salts.

15.7.4 Interstitial Aerosol Scavenging by Cloud Droplets

Interstitial aerosol particles collide with cloud droplets and are removed from cloud interstitial air. The coagulation theory of Chapter 12 can be used to quantify the rate and effects of such removal. If $n(D_p, t)$ is the aerosol number distribution and $n_d(D_p, t)$ the droplet

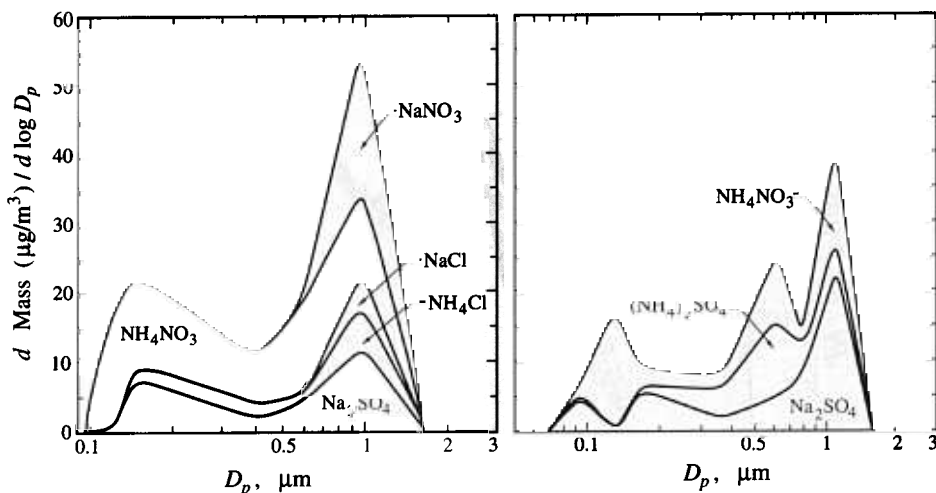


FIGURE 15.24 Predicted aerosol size-composition distributions before and after a fog episode (Pandis et al., 1990b).

size distribution at time t , the loss rate of aerosol particles per unit volume of air due to scavenging by cloud drops is governed by

$$-\frac{\partial n(D_p, t)}{\partial t} = n(D_p, t) \int_0^\infty K(D_p, x) n_d(x, t) dx \quad (15.94)$$

where $K(D_p, x)$ is the collection coefficient for collisions between an interstitial aerosol particle of diameter D_p and a droplet of diameter x . One can define the scavenging coefficient $\Lambda(D_p, t)$ for the full droplet population,

$$\Lambda(D_p, t) = -\frac{1}{n(D_p, t)} \frac{\partial n(D_p, t)}{\partial t} = \int_0^\infty K(D_p, x) n_d(x, t) dx \quad (15.95)$$

If the scavenging coefficient did not vary with time and were equal to $\Lambda(D_p)$, then the evolution of the number distribution would be given by

$$n(D_p, t) = n(D_p, 0) \exp[-\Lambda(D_p)t]$$

Assuming for the time being that cloud droplets are stationary, then particles are captured by Brownian diffusion. The collection of particles by a falling drop will be discussed when we consider wet deposition in Chapter 20. The collection coefficient $K(D_p, x)$ can then be estimated by (12.57). Let us estimate this collection rate assuming that the cloud has a liquid water content of 0.5 g m^{-3} and that all drops have diameters of $10 \text{ }\mu\text{m}$, resulting in a number concentration of $N_d = 955 \text{ cm}^{-3}$. For such a monodisperse droplet population (15.95) simplifies to

$$\Lambda(D_p) = N_d K(D_p, 10 \text{ }\mu\text{m}) \quad (15.96)$$

TABLE 15.6 Estimated Lifetimes of Aerosols in a Nonraining Cloud
 ($N = 955 \text{ cm}^{-3}$, $D_p = 10 \text{ } \mu\text{m}$, $w_L = 0.5 \text{ g cm}^{-3}$) at Standard Conditions

$d_p (\mu\text{m})$	$K(d_p, 10 \text{ } \mu\text{m})$ ($\text{cm}^{-3} \text{ s}^{-1}$)	$\Lambda(d_p) (\text{s}^{-1})$	Lifetime (= $1/\Lambda$)
	4×10^{-5}		
	1.6×10^{-6}		
	1.1×10^{-7}		
	2.2×10^{-8}		
	1.03×10^{-9}		
	3×10^{-10}		

and $K(D_p, 10 \text{ } \mu\text{m})$ can be calculated from (12.57) (see also Figure 12.5 and Table 12.3). Corresponding particle collision efficiencies and lifetimes are shown in Table 15.6. Nuclei smaller than 10 nm will be scavenged in a few minutes by such a cloud whereas particles larger than 0.1 μm will not be collected by droplets during the cloud lifetime.

The above results indicate that for average residence times of air parcels in clouds (on the order of an hour) only the very fine aerosol particles will be collected by cloud droplets. These particles often represent a significant fraction of the aerosol number, so the total number may be reduced significantly, and the shape of the aerosol number distribution may change drastically. However, these particles contain little of the mass and therefore the mass distribution effectively will not change. These qualitative conclusions are in agreement with detailed simulations of aerosol processing by clouds (Flossmann and Pruppacher, 1988; Flossmann, 1991).

15.7.5 Aerosol Nucleation Near Clouds

Clouds remove individual fine aerosol particles by scavenging. Even so, enhanced aerosol number concentrations in the vicinity of clouds have been observed (Saxena and Hendler, 1983; Hegg et al., 1990, 1991; Radke and Hobbs, 1991). Saxena and Hendler (1983) suggested that observed high aerosol number concentrations near clouds could be a result of shattering of rapidly evaporating droplets. Hudson and Frisbie (1991) suggested that these high particle concentrations may actually be an artifact due to droplet splashing. Hegg et al. (1991) proposed that the high actinic flux near cloud tops resulting from upward scattering of solar radiation could lead to high OH concentrations, rapid H_2SO_4 formation, and subsequent nucleation of new $\text{H}_2\text{SO}_4\text{-H}_2\text{O}$ particles. Kerminen and Wexler (1994) estimated a high nucleation probability associated with high relative humidity areas around clouds in relatively clean environments. Note that such a nucleation process in the vicinity of the clouds produces very little aerosol mass but a large number of particles and may influence significantly the shape of the aerosol number distribution, especially in remote regions.

15.8 OTHER FORMS OF WATER IN THE ATMOSPHERE

Our discussion in the preceding sections has focused on "warm" nonraining tropospheric clouds. Water in the atmosphere can also exist as ice, rain, snow, and so on. We summarize here aspects of the formation and removal of these water forms that are most associated

with atmospheric chemistry. The interested reader is referred for more information to Pruppacher and Klett (1980) and references therein.

15.8.1 Ice Clouds

Atmospheric observations indicate that water readily supercools, and water clouds are frequently found in the atmosphere at temperatures below 0°C. Figure 15.25 shows that supercooled clouds are quite common in the atmosphere, especially if cloud top temperature is warmer than -10°C. However, the likelihood of ice increases with decreasing temperature, and at -20°C only about 10% of clouds consist entirely of water drops. At these low temperatures, ice particles coexist with water drops in the same cloud.

The temperature dependence of the equilibrium between water vapor and ice can be described by the Clausius–Clapeyron equation. Following (15.7) one finds that

$$\frac{dp_{\text{sat},i}}{dT} = \frac{\Delta H_s}{T(v_v - v_i)} \tag{15.97}$$

where $p_{\text{sat},i}$ is the saturation vapor pressure of water over ice, ΔH_s is the molar enthalpy for ice sublimation, and v_i and v_v are the molar volumes of ice and water vapor. If we assume that $v_v \gg v_i$ and that water vapor behaves as an ideal gas, then

$$\frac{d \ln p_{\text{sat},i}}{dT} \approx \frac{\Delta H_s}{RT^2} \tag{15.98}$$

Note that (15.98) is similar to the Clausius–Clapeyron equation for water vapor–water equilibrium (15.8), with the enthalpy of sublimation replacing the enthalpy of evaporation.

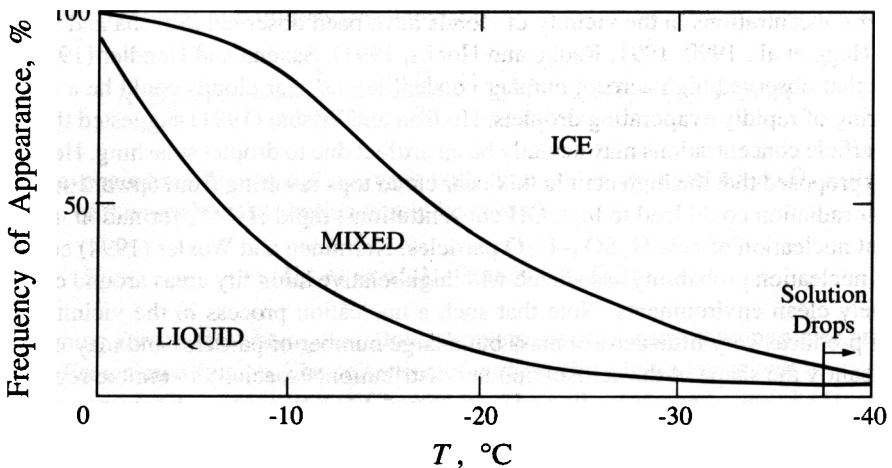


FIGURE 15.25 Average frequencies of appearance of supercooled water, mixed phase, and ice clouds as a function of temperature in layer clouds over Russia (Boronikov et al., 1963).

Finally, if the Clausius–Clapeyron equation is applied to the equilibrium between ice and water, we get

$$\frac{dp_m}{dT} = \frac{\Delta H_m}{v_w} \quad (15.99)$$

where p_m is the melting pressure of ice, ΔH_m the molar enthalpy of melting, and v_w the molar volume of water. Equations (9.66), (15.98), and (15.99) can be integrated and plotted to produce the p – T phase diagram for pure water shown in Figure 15.26. Note that there is only one point ($T = 0^\circ\text{C}$, $p = 6.1$ mbar), the *water triple point* for which all phases coexist. Another interesting observation is that for temperatures below 0°C the water vapor pressure over liquid water is higher than water vapor pressure over ice,

$$p_{\text{sat},w} > p_{\text{sat},i} \quad (T < 0^\circ\text{C})$$

So if air is saturated with respect to ice, it is subsaturated with respect to water. As a result, supercooled water droplets cannot coexist in equilibrium with ice crystals. Note that Figure 15.26 refers to the equilibrium of bulk water (curvature is neglected), without any impurities (zero solute concentration). Curvature and solute effects cause the behavior of water in

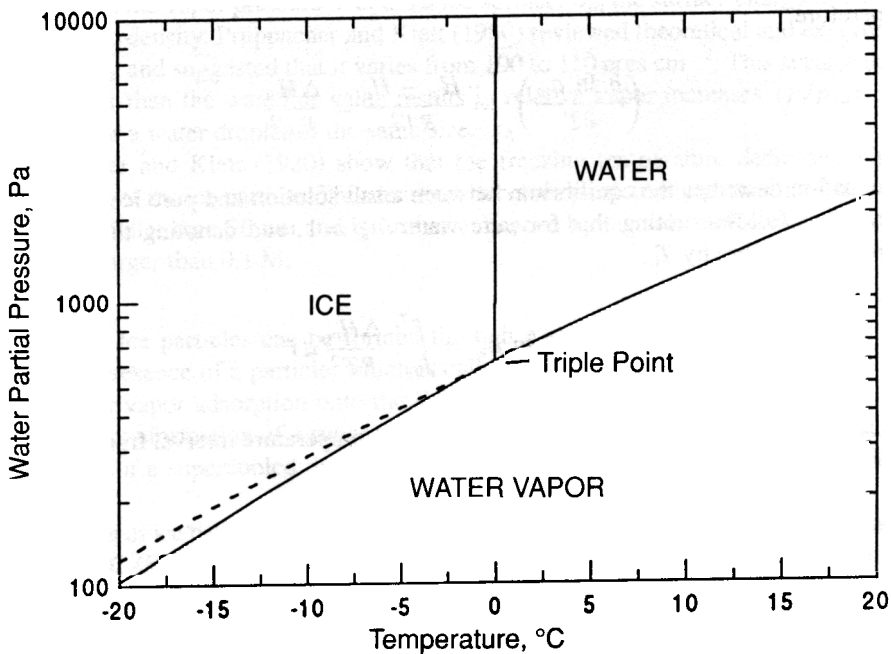


FIGURE 15.26 Pressure–temperature phase diagram for water. The dashed line corresponds to supercooled water and its metastable equilibrium with water vapor.

the atmosphere to deviate significantly from Figure 15.26. We discuss these effects briefly below.

Freezing Point Depression Dissolution of a salt in water lowers the vapor pressure over the solution. A direct result of this is the depression of the freezing point of water. In order to quantify this change, assume that our system has constant pressure and contains air and an aqueous salt solution in equilibrium with ice. According to thermodynamic equilibrium the chemical potential of water in the aqueous and ice phases will be the same, $\mu_i = \mu_w$. If a_w is the activity of water in solution then

$$\mu_i = \mu_w^\circ(T) + RT \ln a_w$$

Dividing by T and differentiating with respect to T under constant pressure p ,

$$\left(\frac{\partial(\mu_i/T)}{\partial T}\right)_p = \left(\frac{\partial(\mu_w^\circ/T)}{\partial T}\right)_p + R \left(\frac{\partial \ln a_w}{\partial T}\right)_p \quad (15.100)$$

But the chemical potential is related to the enthalpy by

$$\left(\frac{\partial(\mu_k/T)}{\partial T}\right)_p = -\frac{H_k}{T^2} \quad (15.101)$$

and therefore

$$\left(\frac{\partial \ln a_w}{\partial T}\right)_p = \frac{H_w - H_i}{RT^2} = \frac{\Delta H_m}{RT^2} \quad (15.102)$$

This equation describes the equilibrium between a salt solution and pure ice. This can be integrated as follows, noting that for pure water $a_w = 1$, and denoting the pure water freezing temperature by T_0 ,

$$\int_{a_w=1}^{a_w} d \ln a_w = \int_{T_0}^{T_e} \frac{\Delta H_m}{RT^2} dT \quad (15.103)$$

assuming that ΔH_m is approximately constant in the temperature interval from T_0 to T_e ,

$$T_0 - T_e = \frac{RT_0 T_e}{\Delta H_m} (-\ln a_w) \quad (15.104)$$

Because $a_w \leq 1$, $T_0 - T_e \geq 0$ and the new freezing temperature T_e is lower than the pure water freezing temperature. The difference $\Delta T_f = T_0 - T_e$ is the equilibrium freezing point depression. To get an estimate of this depression we can assume that the solution is ideal so that $a_w = x_w$ and that $T_0 T_e \simeq T_0^2$. Noting that $\ln a_w = \ln x_w \simeq -n_s/n_w$, we ob-

tain the estimate

$$\Delta T_f = \frac{RT_0^2 M_w}{1000 \Delta H_m} m \quad (15.105)$$

where m is the solution molarity. For ideal solutions this results in a depression of $1.86^\circ\text{C M}^{-1}$ of solute, and for a salt that dissociates into two ions this results in a depression of $3.72^\circ\text{C M}^{-1}$ of the salt. Due to the nonideality of real salts actual depression at 1 M concentration is 3.35°C for NaCl.

Curvature Effects Ice crystals in the atmosphere have a variety of shapes, with hexagonal prismatic being the basic one (Pruppacher and Klett, 1980). For instructive purposes let us ignore this complexity and concentrate on the behavior of a spherical ice particle of diameter D_p . Our analysis for water droplets and the Kelvin effect is directly applicable here and the vapor pressure of water over the ice particle surface, p_i , will be

$$p_i = p_{\text{sat},i} \exp\left(\frac{4M_w \sigma_{ia}}{RT \rho_i D_p}\right) \quad (15.106)$$

where $p_{\text{sat},i}$ is the vapor pressure over a flat ice surface, σ_{ia} the surface energy of ice in air, and ρ_i the ice density. Pruppacher and Klett (1980) reviewed theoretical and experimental values for σ_{ia} and suggested that it varies from 100 to 110 ergs cm^{-2} . This surface tension that is higher than the water/air value results in relative vapor increases (p/p_{sat}) higher than those for a water droplet of the same size.

Pruppacher and Klett (1980) show that the freezing temperature decreases with decreasing size of the ice particle. This decrease becomes particularly pronounced for crystal diameters smaller than 20 nm and is further enhanced by the solute effect for solute concentrations larger than 0.1 M.

Ice Nuclei Ice particles can be formed through a variety of mechanisms. All of these require the presence of a particle, which is called an *ice nucleus* (IN). These mechanisms are (1) water vapor adsorption onto the IN surface and transformation to ice (deposition mode), (2) transformation of a supercooled droplet to an ice particle (freezing mode), and (3) collision of a supercooled droplet with an IN and initiation of ice formation (contact mode).

Formation of ice particles in the absence of IN is possible only at very low temperatures, below -40°C (Hobbs, 1995). The presence of IN allows ice formation at higher temperatures. Aerosols that can serve as IN are rather different from those that serve as CCN. Ice-forming nuclei are usually insoluble in water and have chemical bonding and crystallographic structures similar to ice. Larger particles are more efficient than smaller ones. While our understanding of the ice nucleating abilities of aerosols remains incomplete, particles that are known to serve as IN include dust particles (especially clay particles such as

haolinite) and combustion particles (containing metal oxides). Experiments have shown that the ice nucleating active fraction of an aerosol population increases with decreasing temperature.

IN concentrations in the atmosphere are quite variable. A proposed empirical relation for their concentration as a function of temperature is (Pruppacher and Klett, 1980)

$$IN(L^{-1}) = \exp [0.6(253 - T)] \quad (15.107)$$

This relation suggests that ice nucleation in the atmosphere is a very selective process. For example, at temperatures as low as -20°C the atmosphere typically contains 1 IN L^{-1} and 10^6 particles L^{-1} . So, at most, one out of a million particles can serve as an IN.

Measurements of ice particle concentrations for cloud top temperatures below -10°C have given concentrations varying from 0.1 to 200 L^{-1} . For temperatures below -20°C , the concentrations vary from 10 to 300 L^{-1} . This number of ice crystals observed in clouds often exceeds by several orders of magnitude the IN concentration. The enhancement of ice particle concentration over the IN concentrations is still a matter of debate (Rangno and Hobbs, 1991). Proposed explanations include breakup of primary ice particles, ice splinter production during droplet freezing, and unusually high supersaturations. The reader is referred to Mason (1971), Pruppacher and Klett (1980), and Rogers and De Mott (1991) for further discussion of the nature, origins, and concentrations of atmospheric IN.

15.8.2 Rain

For a cloud to generate precipitation, some drops need to grow to precipitable size around 1 mm . Growth of droplets can proceed via a series of mechanisms: (1) water vapor condensation, (2) droplet coalescence, and (3) ice processes.

We have already examined the growth of droplets by water vapor condensation. While this is a very effective mechanism for the initial growth of aerosol particles from a fraction of a micrometer to $10 \mu\text{m}$ in a few minutes, further growth of a drop is a slow process. Figure 15.14 demonstrates that an hour is necessary under a constant supersaturation of 1% for drop growth to $100 \mu\text{m}$. After an entire hour the drop has collected only 0.1% of the water mass of an average raindrop.

For warm clouds (i.e., containing no ice), large drops can grow to precipitation size by collecting smaller droplets that lie in their fallpath. Therefore the largest drops in the cloud drop spectrum are of particular importance because they are the ones that initiate precipitation. The typical concentration of large drops required to initiate precipitation is one per liter of air, or only one out of a million cloud drops. These large drops form on giant particles, which are again the one in a million nuclei. The dramatic dependence of the precipitation on one out of a million droplets is indicative of the difficulty of quantitatively describing the overall process. Clearly a broad cloud drop size distribution is more conducive to precipitation development than a narrow distribution. Remote marine clouds tend to have broad size distribution and tend to produce precipitation more effectively than similar continental clouds.

Larger drops fall faster than smaller drops, resulting in the larger drops overtaking the smaller drops, colliding and coalescing with them. This process is growth by accretion, sometimes also called gravitational coagulation, coalescence, or collisional growth.

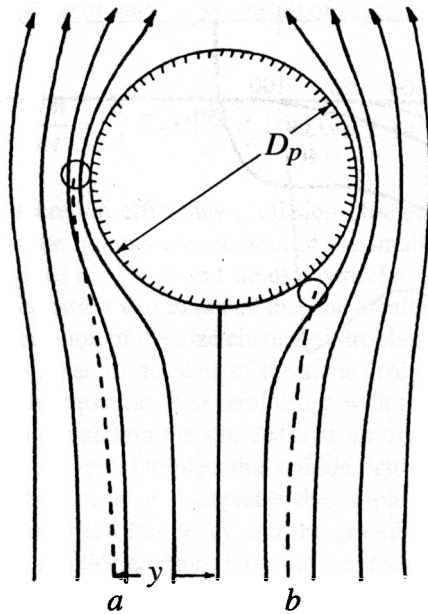


FIGURE 15.27 Schematic of the flow around a falling drop. The dashed lines are the trajectories of small drops considered as mass points. Trajectory *a* is a grazing trajectory, while *b* is a collision trajectory.

The collision process is illustrated in Figure 15.27 for viscous flow around a sphere of diameter D_p . As the large droplet approaches small drops of diameter d_p , the viscous forces exerted by the flow field around the large droplet push the droplets away from the center of flow, modifying their trajectories. In Figure 15.27 droplet *b* is collected by the raindrop while droplet *a* is not. Therefore the falling raindrop will in general collect fewer drops than those existing in the cylinder of diameter D_p below it. Droplets in the cylinder of diameter y will be collected. The distance y is defined by the grazing trajectory *a* and is a function of the raindrop size D_p and drop size d_p . One defines the collision efficiency E as the ratio of the actual collision cross section to the geometric cross section, or

$$E = \frac{y^2}{(D_p + d_p)^2} \quad (15.108)$$

Note that all drops of diameter d_p in the cylinder with diameter y , below the falling drop with diameter D_p , will be collected by it. Because small drops tend to move away from the falling raindrop, E is expected to be smaller than unity for most cases.

Figure 15.28 shows theoretically estimated collision efficiencies among drops as functions of the radii of the small and large drops. There is a rapid increase in collision efficiency as the two drops approach equal size. This is due to fluid mechanical interactions that accelerate the upper drop more than the lower one but have little importance for the atmosphere where the probability of collision of equal-sized drops is extremely small.

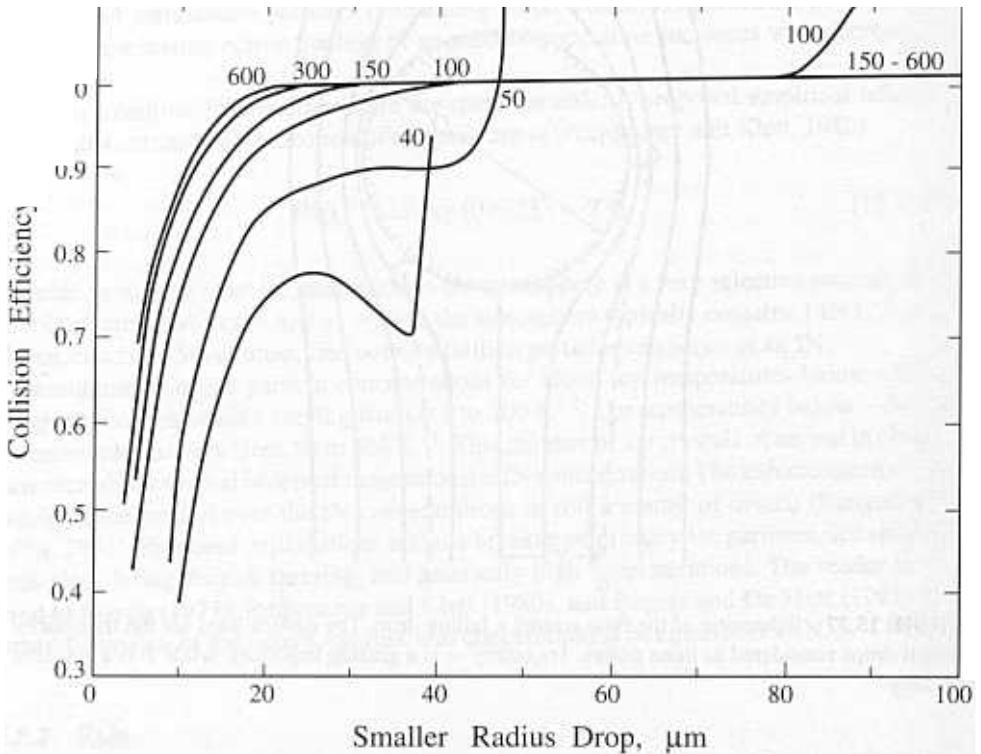


FIGURE 15.28 Theoretically estimated collision efficiencies among cloud droplets as functions of their radii. The radius of the smaller drop is on the x axis and the radius of the larger drop is on the curve. From H. G. Houghton, *Physical Meteorology* (Cambridge, MA: The MIT Press, 1985) p. 265.

Figure 15.28 shows that drops with diameters below $50 \mu\text{m}$ have a small collision efficiency and growth of drops to larger size is required for the acceleration of accretional growth.

Calculations for larger drops are complicated by phenomena such as shape deformation, wake oscillations, and eddy shedding, making theoretical estimates of E difficult. Unfortunately, experimental verification of these theoretical predictions is accompanied by similar uncertainties due to experimental difficulties (Pruppacher and Klett, 1980).

The overall process of rain formation is further complicated by the fact that drops on collision trajectories may not coalesce but bounce off each other. The principal barrier to coalescence is the cushion of air between the two drops that must be drained before they can come into contact. An empirical coalescence efficiency E_c suggested by Whelpdale and List (1971) to address droplet bounce-off is

$$E_c = \left(\frac{D_p}{D_p + d_p} \right)^2 \quad (15.109)$$

which is applicable for $D_p > 400 \mu\text{m}$. Equation (15.109) can probably be viewed as an upper limit for E_c . Note that while (15.108) describes the area swept by a falling drop, (15.109) quantifies the probability of coalescence of two colliding droplets.

The growth of a falling drop of mass m as a result of accretion of drops can be described by

$$\frac{dm}{dt} = \frac{\pi}{4} E_t (D_p + d_p)^2 w_L (v_D - v_d) \quad (15.110)$$

where E_t is the overall accretion efficiency (collision efficiency times coalescence efficiency, $E_t = EE_c$), w_L is the liquid water content of the small drops, and v_D and v_d are, respectively, the fall speeds of the larger and smaller particles. Equation (15.110) is called the continuous accretion equation and assumes that the smaller drops are uniformly distributed in space. The description of the size change of droplets falling through a cloud by (15.110) implicitly assumes that all droplets of the same size will grow in the same way. According to the continuous equation, if several drops with the same initial diameter fall through a cloud, they would maintain the same size at all times. In reality, each droplet-droplet collision is a discrete event. Droplets that collide first with others grow faster than droplets that had initially the same size. As a result, the simple continuous equation can seriously underestimate the collision frequency and the growth rate of falling drops, especially when the collector and collected drops have the same size. The coagulation equation (see (12.80)) is a better mathematical description of these discrete collisions. Equation (12.80) (often called the stochastic accretion equation in cloud microphysics) describes implicitly individual collisions and predicts that even if all falling droplets had initially the same size some will grow more than others.

The role of ice in rain formation was first proposed by Bergeron in 1933, based on the calculations of Wegener. Using thermodynamics, Wegener showed in 1911 that at temperatures below 0°C supercooled water drops and ice crystals cannot exist in equilibrium. Using this result, Bergeron proposed that in cold clouds the ice crystals grow by vapor diffusion at the expense of the water droplets until either all drops have been consumed or all ice crystals have fallen out of the cloud as precipitation. Findeisen later produced additional observations supporting the above mechanism, which is often called the Wegener-Bergeron-Findeisen mechanism. Mathematically the description of the mechanism requires solution of the growth equations by vapor diffusion for both ice crystals and water drops in a supersaturated environment (Pruppacher and Klett, 1980).

Raindrop Distributions A number of empirical formulas have been proposed for the raindrop spectrum. The distribution proposed by Best is often used to describe the fraction of rainwater comprised of raindrops smaller than D_p , $F(D_p)$:

$$F(D_p) = 1 - \exp \left[- \left(\frac{D_p}{1.3 p_0^{0.232}} \right)^{2.25} \right] \quad (15.111)$$

where p_0 is the rainfall intensity in (mm h^{-1}) and D_p is in mm.

Probably the most widely used is the Marshall-Palmer (MP) distribution, where

$$n(D_p) = n_0 \exp(-\psi D_p) \quad (15.112)$$

where $n(D_p) = dn/dD_p$ is the number distribution in drops $\text{m}^{-3} \text{mm}^{-1}$, $n_0 = 8000 \text{ m}^{-3} \text{mm}^{-1}$, and $\psi = 4.1 p_0^{-0.21} \text{ mm}^{-1}$. The MP distribution is often not sufficiently general to

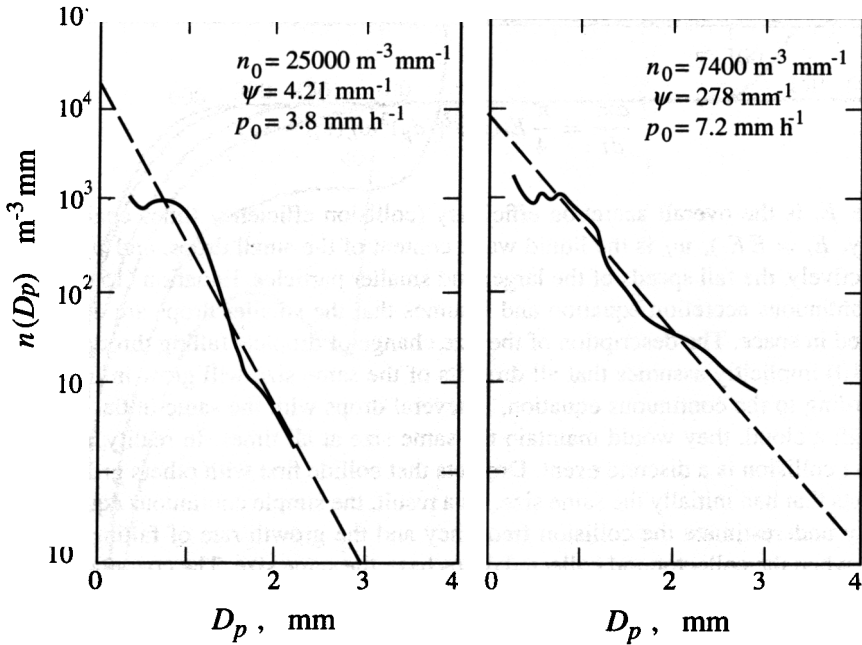


FIGURE 15.29 Raindrop spectra and fitted MP distributions. Reprinted from *Microphysics of Clouds and Precipitation*, Pruppacher, H. R., and Klett, J. D., 1980, with kind permission from Kluwer Academic Publishers.

describe observed rain spectra. Sekhon and Srivastava (1971) among others suggested that n_0 is not a constant but rather depends on the rainfall intensity. They suggested use of $n_0 = 7000p_0^{0.37} \text{ m}^{-3} \text{ mm}^{-1}$ and $\psi = 3.8p_0^{-0.14} \text{ mm}^{-1}$. A series of raindrop spectra and a fitted MP distribution with variable n_0 are shown in Figure 15.29. The MP distribution may overestimate by as much as 50% the number of small droplets in the 0.02 to 0.12 cm range and it is strictly applicable for $D_p \geq 0.12 \text{ cm}$.

15.9 CLOUD CLIMATOLOGY

Liquid water is one of the most important cloud characteristics for atmospheric chemistry. The liquid water content of an air parcel starts from almost zero during cloud formation, reaches a maximum for a mature cloud, and returns to zero during cloud evaporation.

Pruppacher and Klett (1980) note that the liquid water content field of clouds has four characteristic features:

1. It varies considerably horizontally due to variations in the vertical air velocity.
2. It increases with height above the cloud base, reaches a maximum value somewhere in the upper half of the cloud, and then decreases toward the cloud top.
3. It is determined to a large extent by drop size rather than drop number concentration.

TABLE 15.7 Microphysical Cloud Characteristics

Cloud Type	Droplet Concentration (cm^{-3})	Liquid Water (g m^{-3})	Mean Droplet Size (μm)
	< 500		< 19
	312		
	350		
	500		
	100–250	0.1–0.9	12 (base) 19 (top)
St (marine)	200–350	0.3	11
St (continental)	200–700	—	7
Sc (California)	25–125	0.1	18
Sc (California)		< 0.1	
Sc (U.K.)	200–500	0.15	10
Sc (Washington State)	302		
Sc (North Sea)	200	< 0.7	12–20
Sc (England)	200–400	< 0.5	8–14
As–Ac (Russia)		0.09–0.17	9–11
As–Ac (Alaska)	300	0.03–0.09	7–10
As–Ac	100	< 0.01	< 9
(Wisconsin)			
As–Ac	25	< 0.1	15–20
(Wisconsin)			
As–Ac	70–1000		
(Washington State)			
As–Ac (U.S.)	35–75	< 0.2	14–19

Source: Heymsfield (1993).

- It is less than the liquid water content calculated assuming adiabatic ascent of an air parcel due to entrainment of dry air. This deviation is on the order of 10% or so for the lower half of stratiform clouds and it increases with height.

Average droplet diameters are usually in the 10 to 20 μm range. Marine clouds are characterized by relatively smaller droplet concentration and larger diameters, where continental clouds tend to have smaller droplets (Table 15.7).

Minimum droplet diameters are a few micrometers, where large droplets exceed 100 μm . In general, droplet spectra are wider for orographic clouds, less wide for stratus, and rather narrow for cumulus cloud types. Continental cumuli drop sizes range only from a few micrometers to around 20 μm in diameter. Frequency distributions of the mean cloud droplet size for various cloud types are shown in Figure 15.30.

Squires' (1958) observations suggested that high drop concentrations are associated with narrow size spectra and small drop sizes for continental clouds. Bimodal droplet spectra are often encountered in the upper half of clouds. Lee and Pruppacher (1977) explained this bimodality by entrainment of fresh CCN into the cloud.

TABLE 15.7 Microphysical Cloud Characteristics

Cloud Type	Droplet Concentration (cm ⁻³)	Liquid Water (g m ⁻³)	Mean Droplet Size (μm)
	< 500	0.09–0.63	< 19
	312	—	—
	350	—	—
	500	—	—
	100–250	0.1–0.9	12 (base) 19 (top)
St (marine)	200–350	0.3	11
St (continental)	200–700	—	7
Sc (California)	25–125	0.1	18
Sc (California)	—	< 0.1	—
Sc (U.K.)	200–500	0.15	10
Sc (Washington State)	302	—	—
Sc (North Sea)	200	< 0.7	12–20
Sc (England)	200–400	< 0.5	8–14
As–Ac (Russia)	—	0.09–0.17	9–11
As–Ac (Alaska)	300	0.03–0.09	7–10
As–Ac	100	< 0.01	< 9
(Wisconsin)			
As–Ac	25	< 0.1	15–20
(Wisconsin)			
As–Ac	70–1000		
(Washington State)			
As–Ac (U.S.)	35–75	< 0.2	14–19

Source: Heymsfield (1993).

- It is less than the liquid water content calculated assuming adiabatic ascent of an air parcel due to entrainment of dry air. This deviation is on the order of 10% or so for the lower half of stratiform clouds and it increases with height.

Average droplet diameters are usually in the 10 to 20 μm range. Marine clouds are characterized by relatively smaller droplet concentration and larger diameters, where continental clouds tend to have smaller droplets (Table 15.7).

Minimum droplet diameters are a few micrometers, where large droplets exceed 100 μm. In general, droplet spectra are wider for orographic clouds, less wide for stratus, and rather narrow for cumulus cloud types. Continental cumuli drop sizes range only from a few micrometers to around 20 μm in diameter. Frequency distributions of the mean cloud droplet size for various cloud types are shown in Figure 15.30.

Squires' (1958) observations suggested that high drop concentrations are associated with narrow size spectra and small drop sizes for continental clouds. Bimodal droplet spectra are often encountered in the upper half of clouds. Lee and Pruppacher (1977) explained this bimodality by entrainment of fresh CCN into the cloud.

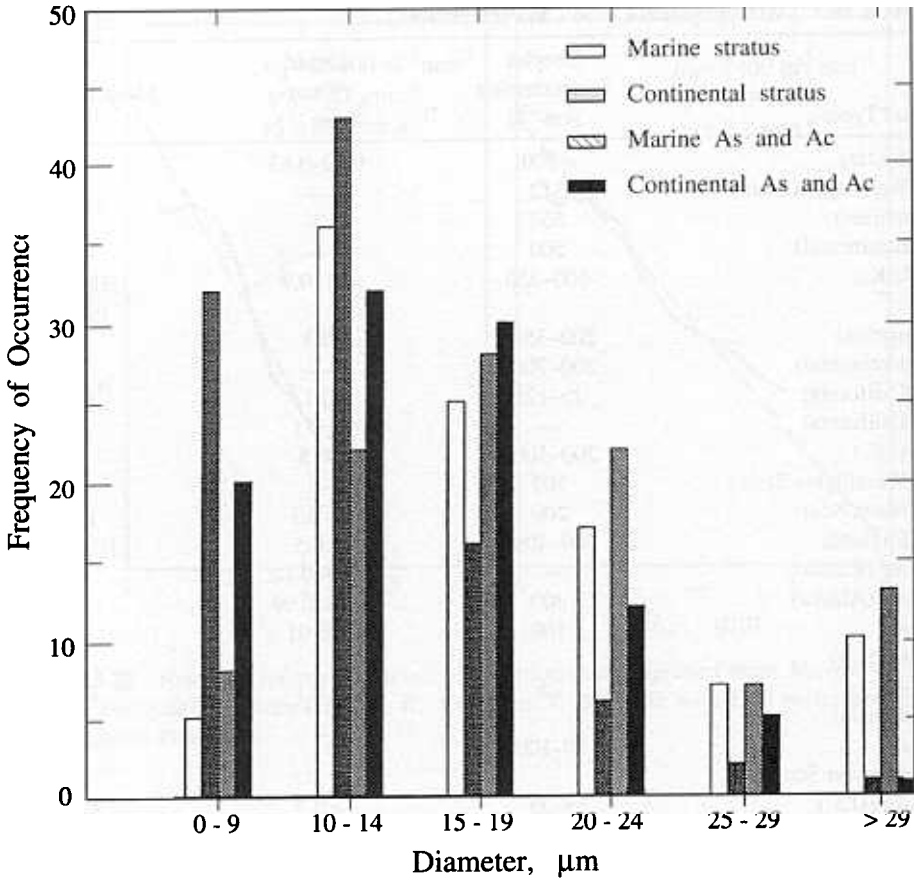


FIGURE 15.30 Frequency distributions of the mean cloud droplet size for various cloud types.

Figure 15.31 shows a zonally averaged climatology based on six cloud types: high clouds (Ci, Cs), middle clouds (As, Ac), low clouds (St, Sc), cumulus, cumulonimbus, and nimbostratus. The altitude, thickness, and cloud cover are shown with a 10° resolution. Note that the cirrus base heights vary with latitude but their thickness is fixed at 1.7 km due to limitations of the observations.

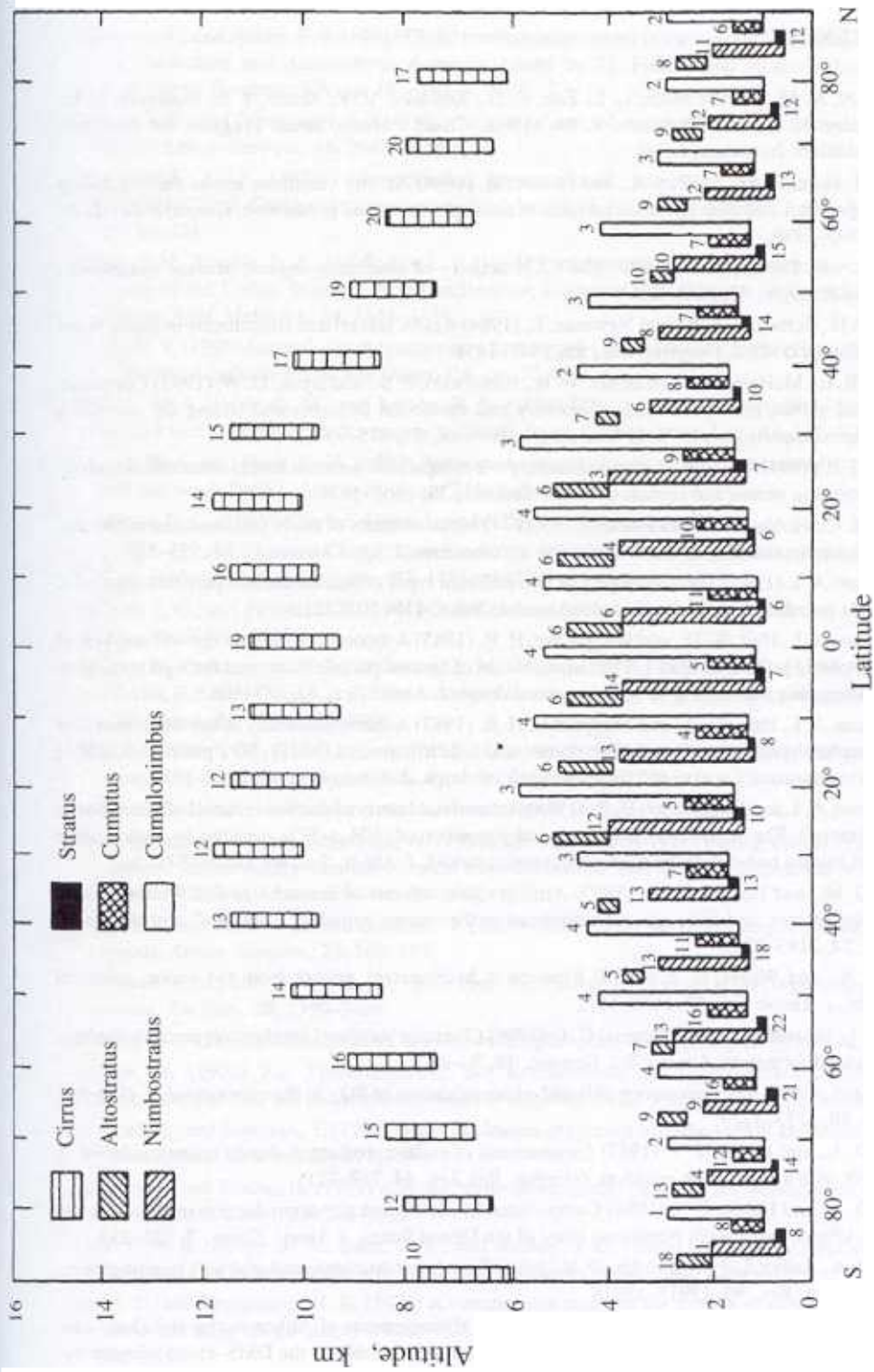


FIGURE 15.31 Zonally averaged climatology of cloud type, cover (number over bar indicates percent occurrence), and thickness for both Northern and Southern Hemispheres at 10° latitudinal intervals. Reprinted from K. N. Liou, *Radiation and Cloud Processes in the Atmosphere*, 1992, by permission of Oxford University Press

REFERENCES

- Boronikov, A. M., Gaivoronskii, L. I., Zak, E. G., Kostarev, V. V., Mazin, I. P., Minervin, V. E., Khrgian, A. K., and Shmeters, S. M. (1963) *Cloud Physics*, Israel Program for Scientific Translations, Jerusalem, Israel.
- Collett, J. L. Jr., Bator, A., Rao, X., and Demoz, B. (1994) Acidity variations across the cloud drop size spectrum and their influence on rates of atmospheric sulfate production, *Geophys. Res. Lett.*, **21**, 2393–2396.
- Cruz, C., and Pandis, S. N. (1997) The CCN activity of secondary organic aerosol compounds, *Atmos. Environ.*, **31**, 2205–2214.
- Daum, P. H., Schwartz, S. E., and Newman, L. (1984) Acidic and related constituents in liquid water stratiform clouds, *J. Geophys. Res.*, **89**, 1447–1458.
- Dennis, R. L., McHenry, J. N., Barchet, W. R., Binkowski, F. S., and Byun, D. W. (1993) Correcting RADM sulfate underprediction—discovery and correction of errors and testing the correction through comparisons with field data, *Atmos. Environ.*, **27**, 975–997.
- Develk, J. P. (1994) A model for cloud chemistry—a comparison between model simulations and observations in stratus and cumulus, *Atmos. Environ.*, **28**, 1665–1678.
- Eagan, R. C., Hobbs, P. V., and Radke, L. F. (1974) Measurements of cloud condensation nuclei and cloud droplet size distributions in vicinity of forest fires, *J. Appl. Meteorol.*, **13**, 553–557.
- Flossmann, A. I. (1991) The scavenging of two different types of marine aerosol particles calculated using a two dimensional detailed cloud model, *Tellus*, **43B**, 301–321.
- Flossmann, A. I., Hall, W. D., and Pruppacher, H. R. (1985) A theoretical study of the wet removal of atmospheric pollutants. Part I: The redistribution of aerosol particles captured through nucleation and impaction scavenging by growing cloud drops, *J. Atmos. Sci.*, **42**, 583–606.
- Flossmann, A. I., Hall, W. D., and Pruppacher, H. R. (1987) A theoretical study of the wet removal of atmospheric pollutants. Part II: The uptake and redistribution of $(\text{NH}_4)_2\text{SO}_4$ particles and SO_2 gas simultaneously scavenged by growing cloud drops, *J. Atmos. Sci.*, **44**, 2912–2923.
- Flossmann, A. I. and Pruppacher, H. R. (1988) A theoretical study of the wet removal of atmospheric pollutants 3. The uptake, redistribution, and deposition of $(\text{NH}_4)_2\text{SO}_4$ particles by a convective cloud using a two-dimensional cloud dynamics model, *J. Atmos. Sci.*, **45**, 1857–1871.
- Frick, G. M., and Hoppel, W. A. (1993) Airship measurements of aerosol size distributions, cloud droplet spectra, and trace gas concentrations in the marine boundary layer, *Bull. Am. Meteorol. Soc.*, **74**, 2195–2202.
- Fukuta, N., and Walter, L. A. (1970) Kinetics of hydrometeor growth from the vapor; spherical model, *J. Atmos. Sci.*, **27**, 1160–1172.
- Hallett, J., Hudson, J. G., and Rogers, C. F. (1989) Characterization of combustion aerosols for haze and cloud formation, *Aerosol Sci. Technol.*, **10**, 70–83.
- Hegg, D. A. (1985) The importance of liquid-phase oxidation of SO_2 in the troposphere, *J. Geophys. Res.*, **90**, 3773–3779.
- Hegg, D. A., and Hobbs, P. V. (1987) Comparisons of sulfate production due to ozone oxidation in clouds with a kinetic rate equation, *Geophys. Res. Lett.*, **14**, 719–721.
- Hegg, D. A., and Hobbs, P. V. (1988) Comparisons of sulfate and nitrate production in clouds on the mid-Atlantic and Pacific Northwest coast of the United States, *J. Atmos. Chem.*, **7**, 325–333.
- Hegg, D. A., Radke, L. F., and Hobbs, P. V. (1990) Particle production associated with marine clouds, *J. Geophys. Res.*, **95**, 13917–13926.
- Hegg, D. A., Radke, L. F., and Hobbs, P. V. (1991) Measurements of Aitken nuclei and cloud condensation nuclei in the marine atmosphere and their relationship to the DMS–cloud–climate hypothesis, *J. Geophys. Res.*, **96**, 18727–18733.

- Hegg, D. A., and Hobbs, P. V. (1992) Cloud condensation nuclei in the marine atmosphere: a review, in *Nucleation and Atmospheric Aerosols*, edited by N. Fukuta and P. E. Wagner. Deepak Publishing, Hampton, VA, pp. 181–192.
- Hering, S. V., and Friedlander, S. K. (1982) Origins of aerosol sulfur distributions in the Los Angeles basin, *Atmos. Environ.*, **16**, 2647–2656.
- Heymsfield, A. J. (1993) Microphysical structures of stratiform and cirrus clouds, in *Aerosol–Cloud–Climate Interactions*, edited by P. V. Hobbs, Academic Press, San Diego, pp. 97–121.
- Hobbs, P. V., Bowdle, D. A., and Radke, L. F. (1985) Particles in the lower troposphere over the high plains of the United States, 1. Size distributions, elemental compositions and morphologies, *J. Climat. Appl. Meteorol.*, **24**, 1344–1356.
- Hobbs, P. V. (1995) Aerosol–cloud interactions, in *Aerosol–Cloud–Climate Interactions*, edited by P. V. Hobbs. Academic Press, San Diego, CA, pp. 33–73.
- Hoppel, W. A., Frick, G. M., and Larson, R. E. (1986) Effects of non-precipitating clouds on the aerosol size distribution in the marine boundary layer, *Geophys. Res. Lett.*, **13**, 125–128.
- Hoppel, W. A., and Frick, G. M. (1990) Submicron aerosol size distributions measured over the tropical and south Pacific, *Atmos. Environ.*, **24A**, 645–659.
- Houghton H. G. (1985) *Physical Meteorology*, MIT Press, Cambridge, MA.
- Hudson, J. G., and Clark, A. D. (1992) Aerosol and cloud condensation nuclei measurements in the Kuwait plume, *J. Geophys. Res.*, **97**, 14533–14536.
- Hudson, J. G., and Frisbie, P. R. (1991) Cloud condensation nuclei near marine stratus, *J. Geophys. Res.*, **96**, 20795–20808.
- Husain, L., Dutkiewicz, V. A., Hussain, M. M., Khwaja, H. A., Burkhard, E. G., Mehmood, G., Parekh, P. P., and Canelli, E. (1991) A study of heterogeneous oxidation of SO₂ in summer clouds, *J. Geophys. Res.*, **96**, 8789–8805.
- John, W., Wall, S. M., Ondo, J. L., and Winklmayr, W. (1990) Modes in the size distributions of atmospheric inorganic aerosol, *Atmos. Environ.*, **24A**, 2349–2359.
- Junge, C. E. (1963) *Air Chemistry and Radioactivity*. Academic Press, New York.
- Karamachandani, P., and Venkatram, A. (1992) The role of non-precipitating clouds in producing ambient sulfate during summer—results from simulation with the Acid Deposition and Oxidant Model (ADOM), *Atmos. Environ.*, **26**, 1041–1052.
- Kelly, T. J., Schwartz, S. E., and Daum, P. H. (1989) Detection of acid producing reactions in natural clouds, *Atmos. Environ.*, **23**, 569–583.
- Kerminen, V. M., and Wexler, A. S. (1994) Post-fog nucleation of H₂SO₄–H₂O particles in smog, *Atmos. Environ.*, **28**, 2399–2406.
- Köhler, H. (1921) Zur Kondensation des Wasserdampfe in der Atmosphäre, *Geophys. Publ.*, **2**, 3–15.
- Köhler, H. (1926) Zur Thermodynamic der Kondensation an hygroskopischen Kernen und Bemerkungen über das Zusammenfließen der Tropfen, *Medd. Met. Hydr. Anst. Stockholm*, **3** (8).
- Lammel, G., and Novakov, T. (1995) Water nucleation properties of carbon black and diesel soot particles, *Atmos. Environ.*, **29**, 817–823.
- Langner, J., and Rodhe, H. (1991) A global three-dimensional model of the tropospheric sulfur cycle, *J. Atmos. Chem.*, **13**, 225–263.
- Leaitch, W. R., Strapp, J. W., Isaac, G. A., and Hudson, J. G. (1986) Cloud droplet nucleation and scavenging of aerosol sulphate in polluted atmospheres, *Tellus*, **38B**, 328–344.
- Lee, I. Y., and Pruppacher, H. R. (1977) A comparative study of the growth of cloud drops by condensation using an air parcel model with and without entrainment *Pure Appl. Geophys.*, **115**, 523–545.

- Liu, P. S. K., Leitch, W. R., McDonald, A. M., Isaac, G. A., Strapp, J. W., and Wiebe, H. A. (1994) Sulfate production in a summer cloud over Ontario, Canada, *Tellus*, **45B**, 368–389.
- Lowe, P. R., and Ficke, J. M. (1974) Technical Paper 4–74, Environmental Prediction Research Facility, Naval Postgraduate School, Monterey, California.
- Mason, B. J. (1971) *The Physics of Clouds*. Oxford Press, Oxford.
- McHenry, J. N., and Dennis, R. L. (1994) The relative importance of oxidation pathways and clouds to atmospheric ambient sulfate production as predicted by the regional acid deposition model, *J. Appl. Meteorol.*, **33**, 890–905.
- McMurry, P. H., and Wilson, J. C. (1983) Droplet phase (heterogeneous) and gas-phase (homogeneous) contributions to secondary ambient aerosol formation as functions of relative humidity, *J. Geophys. Res.*, **88**, 5101–5108.
- Meng, Z., and Seinfeld, J. H. (1994) On the source of the submicrometer droplet mode of urban and regional aerosols, *Aerosol Sci. Technol.*, **20**, 253–265.
- Munger, J. W., Collett, J. Jr., Daube, B., and Hoffmann, M. R. (1989) Chemical composition of coastal clouds: dependence on droplet size and distance from the coast, *Atmos. Environ.*, **23**, 2305–2320.
- Noone, K. J., Charlson, R. J., Covert, D. S., and Heintzenberg, J. (1988) Cloud droplets: solute concentration is size dependent, *J. Geophys. Res.*, **93**, 9477–9482.
- Ogren, J. A., Heintzenberg, J., Zuber, A., Noone, K. J., and Charlson, R. J. (1989) Measurements of the size-dependence of solute concentrations in cloud droplets, *Tellus*, **41B**, 24–31.
- Ogren, J. A., et al. (1992) Measurements of the size dependence of the concentration of non-volatile material in fog droplets, *Tellus*, **44B**, 570–580.
- Pandis, S.N., and Seinfeld, J. H. (1989) Mathematical modeling of acid deposition due to radiation fog, *J. Geophys. Res.*, **94**, 12156–12176.
- Pandis, S. N., Seinfeld, J. H., and Pilinis, C. (1990a) Chemical composition differences among droplets of different sizes, *Atmos. Environ*, **24A**, 1957–1969.
- Pandis, S. N., Seinfeld, J. H., and Pilinis, C. (1990b) The smog–fog–smog cycle and acid deposition, *J. Geophys. Res.*, **95**, 18489–18500.
- Pandis, S. N., Seinfeld, J. H., and Pilinis, C. (1992) Heterogeneous sulfate production in an urban fog, *Atmos. Environ*, **26A**, 2509–2522.
- Pruppacher, H. R., and Klett, J. D. (1980) *Microphysics of Clouds and Precipitation*. Reidel, Dordrecht, The Netherlands.
- Radke, L. F., Brock, C. A., Lyons, J. H., Hobbs, P. V., and Schnell, R. C. (1989) Aerosol and lidar measurements of hazes in mid-latitude and polar air masses, *Atmos. Environ*, **23**, 2417–2430.
- Radke, L. F., and Hobbs, P. V. (1991) Humidity and particle fields around some small cumulus clouds, *J. Atmos. Sci.*, **48**, 1190–1193.
- Rangno, A. L., and Hobbs, P. V. (1991) Ice particle concentrations and precipitation development in small polar maritime cumuliform clouds, *Q. J. R. Meteorol. Soc.*, **117**, 207–241.
- Rogers, D. C., and DeMott, P. J. (1991) Advances in laboratory cloud physics 1987–1990, *Rev. Geophys. Suppl.*, 80–87.
- Rogers, C. F., Hudson, J. G., Zielinska, B., Tanner, R. L., Hallet, J., and Watson, J. G. (1991) Cloud droplet nucleation by crude oil/wood smoke particles, *Atmos. Environ.*, **25A**, 2571–2580.
- Sakugawa, H., Kaplan, I. R., Tsai, W., and Cohen, Y. (1990) Atmospheric hydrogen peroxide, *Environ. Sci. Technol.*, **24**, 1452–1462.

- Saxena, V. K., and Hendler, A. H. (1983) In-cloud scavenging and resuspension of cloud active aerosols during winter storms over Lake Michigan, in *Precipitation Scavenging, Dry Deposition and Resuspension*, edited by H. R. Pruppacher, R. G. Semonin, and W. G. N. Slinn. Elsevier, New York, pp. 91–102.
- Sekhon, R. S., and Srivastava, R. C. (1971) Doppler observations of drop size distributions in a thunderstorm, *J. Atmos. Sci.*, **28**, 983–994.
- Squires, P. (1958) The microstructure and colloidal stability of warm clouds, *Tellus*, **10**, 256–261.
- Swozdziaik, J. W., and Swozdziaik, A. B. (1992) Sulfate aerosol production in the Sudely Range, Poland, *J. Aerosol Sci.*, S369–S372.
- Ten Brink, H. M., Schwartz, S. E., and Daum, P. H. (1987) Efficient scavenging of aerosol sulfate by liquid water clouds, *Atmos. Environ.*, **21**, 2035–2052.
- Twomey, S. (1959) The nuclei of natural clouds formation. Part II: The supersaturation in natural clouds and the variation of cloud droplet concentration, *Geofis. Pura Appl.*, **43**, 243–249.
- Twomey, S., and Wojciechowski, T. A. (1969) Observations of the geographical variation of cloud nuclei, *J. Atmos. Sci.*, **26**, 684–688.
- United States National Acid Precipitation Assessment Program (1991) *Acidic Deposition: State of Science and Technology, Vol. I Emissions, Atmospheric Processes and Deposition*, edited by P. M. Irving. U.S. Government Printing Office, Washington, DC.
- Walcek, C. J., Stockwell, W. R., and Chang, J. S. (1990) Theoretical estimates of the dynamic radiative and chemical effects of clouds on tropospheric gases, *Atmos. Res.*, **25**, 53–69.
- Wall, S. M., John, W., and Ondo, J. L. (1988) Measurements of aerosol size distributions for nitrate and major ionic species, *Atmos. Environ.*, **22**, 1649–1659.
- Warner, J. (1968) The supersaturation in natural clouds, *J. Appl. Meteorol.*, **7**, 233–237.
- Whelpdale, D. M., and List, R. (1971) The coalescence process in droplet growth, *J. Geophys. Res.*, **76**, 2836–2856.

PROBLEMS

- 15.1_A Show equations (15.39) and (15.40).
- 15.2_B Derive equation (15.53).
- 15.3_A You dissolve 5 g of NaCl in a glass containing 200 cm³ of water. The glass is in a room with constant temperature equal to 20°C and relative humidity 80%. Calculate the volume of water that will be left in the glass after several days of residence in this environment. Repeat the calculation for a relative humidity of 95%.
- 15.4_A Your grandmother and grandfather are upset, because it has just started raining. After listening to the weather prediction for a cloudy day but without rain, they planned to spend the day working in the garden. They have started criticizing the local weather forecaster who, despite the impressive gadgets (radar maps, 3D animated maps), still cannot reliably predict if it will rain tomorrow. They turn to you and ask why if we can send people to the Moon we still cannot tell if it is going to rain or not. Explain, avoiding scientific terminology.

- 15.5_B** What is the activation diameter at 0.3% supersaturation for particles consisting of 50% $(\text{NH}_4)_2\text{SO}_4$, 30% NH_4NO_3 , and 20% insoluble material?
- 15.6_C** A 100 nm diameter dry $(\text{NH}_4)_2\text{SO}_4$ particle is suddenly brought to an atmosphere with a 0.3% water supersaturation. How long will it take for the particle to reach a diameter of $5 \mu\text{m}$? Assume a unity accommodation coefficient.
- 15.7_C** Repeat Problem 15.6 neglecting the correction to the diffusion coefficients and thermal conductivities for noncontinuum effects (assume that $D'_v = D_v$, $k'_a = k_a$). Compare with Problem 15.6 and discuss your observations.
- 15.8_C** Repeat Problem 15.6 assuming that $\alpha_c = 0.045$. Compare with (15.4) and discuss your observations.
- 15.9_A** Dry activation diameters of roughly $0.5 \mu\text{m}$ have been observed in fogs in urban areas.
- If the particles consisted entirely of $(\text{NH}_4)_2\text{SO}_4$, what would be the maximum supersaturation inside the fog layer?
 - If the maximum supersaturation was 0.05% and the particles contained $(\text{NH}_4)_2\text{SO}_4$ and insoluble material, calculate the mass fraction of the insoluble material.